UNDERSTANDING CHEMICAL REACTIVITY

Solvent Effects and Chemical Reactivity

Orlando Tapia and Juan Bertrán (Eds.)

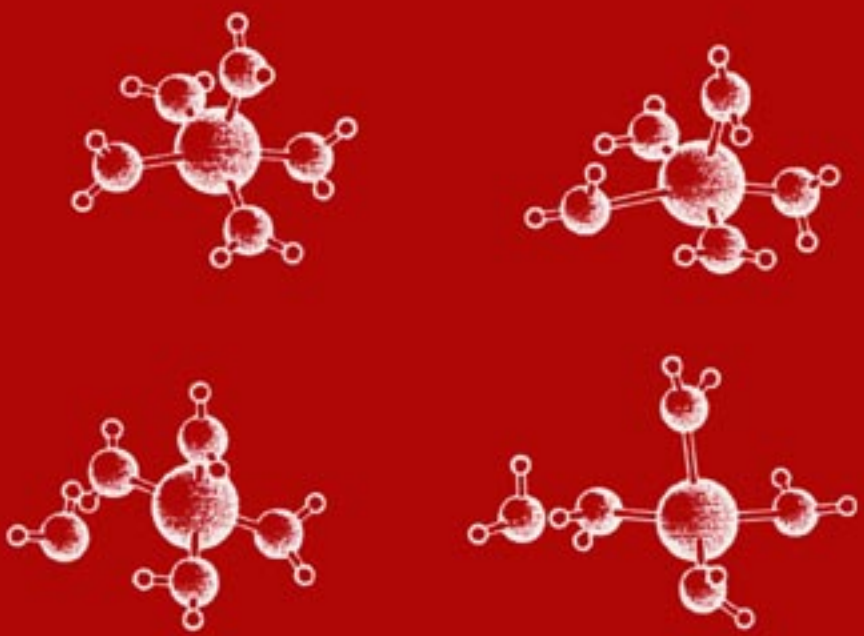

Kluwer Academic Publishers

SOLVENT EFFECTS AND CHEMICAL REACTIVITY

Understanding Chemical Reactivity

Volume 17

Series Editor

Paul G. Mezey, *University of Saskatchewan, Saskatoon, Canada*

Editorial Advisory Board

R. Stephen Berry, *University of Chicago, IL, USA*
John I. Brauman, *Stanford University, CA, USA*
A. Welford Castleman, Jr., *Pennsylvania State University, PA, USA*
Enrico Clementi, *Université Louis Pasteur, Strasbourg, France*
Stephen R. Langhoff, *NASA Ames Research Center, Moffett Field, CA, USA*
K. Morokuma, *Emory University, Atlanta, GA, USA*
Peter J. Rossky, *University of Texas at Austin, TX, USA*
Zdenek Slanina, *Czech Academy of Sciences, Prague, Czech Republic*
Donald G. Truhlar, *University of Minnesota, Minneapolis, MN, USA*
Ivar Ugi, *Technische Universität, München, Germany*

The titles published in this series are listed at the end of this volume.

Solvent Effects and Chemical Reactivity

edited by

Orlando Tapia

Department of Physical Chemistry,
University of Uppsala,
Uppsala, Sweden

and

Juan Bertrán

Department of Physical Chemistry,
Universitat Autònoma de Barcelona,
Bellaterra, Barcelona, Spain

KLUWER ACADEMIC PUBLISHERS
NEW YORK / BOSTON / DORDRECHT / LONDON / MOSCOW

eBook ISBN: 0-306-46931-6
Print ISBN: 0-792-33995-9

©2002 Kluwer Academic Publishers
New York, Boston, Dordrecht, London, Moscow

Print ©2000 Kluwer Academic Publishers
Dordrecht

All rights reserved

No part of this eBook may be reproduced or transmitted in any form or by any means, electronic, mechanical, recording, or otherwise, without written consent from the Publisher

Created in the United States of America

Visit Kluwer Online at: http://kluweronline.com
and Kluwer's eBookstore at: http://ebooks.kluweronline.com

TABLE OF CONTENTS

This page intentionally left blank.

PREFACE

This book gathers original contributions from a selected group of distinguished researchers that are actively working in the theory and practical applications of solvent effects and chemical reactions.

The importance of getting a good understanding of surrounding media effects on chemical reacting system is difficult to overestimate. Applications go from condensed phase chemistry, biochemical reactions in vitro to biological systems in vivo. Catalysis is a phenomenon produced by a particular system interacting with the reacting subsystem. The result may be an increment of the chemical rate or sometimes a decreased one. At the bottom, catalytic sources can be characterized as a special kind of surrounding medium effect. The materials involving in catalysis may range from inorganic components as in zeolites, homogenous components, enzymes, catalytic antibodies, and ceramic materials.

With the enormous progress achieved by computing technology, an increasing number of models and phenomenological approaches are being used to describe the effects of a given surrounding medium on the electronic properties of selected subsystem. A number of quantum chemical methods and programs, currently applied to calculate in vacuum systems, have been supplemented with a variety of model representations. With the increasing number of methodologies applied to this important field, it is becoming more and more difficult for non-specialist to cope with theoretical developments and extended applications. For this and other reasons, it is was deemed timely to produce a book where methodology and applications were analyzed and reviewed by leading experts in the field.

The scope of this book goes beyond the proper field of solvent effects on chemical reactions. It actually goes deeper in the analysis of solvent effects as such and of chemical reactions. It also addresses the problem of mimicking chemical reactions in condensed phases and bioenvironments. The authors have gone through the problems raised by the limitations found in the theoretical representations. In order to understand, it is not sufficient to have agreement with experiments, the schemes should meet the requirements put forward by well founded physical theories.

The book is structured about well defined themes. First stands the most methodologic contributions: continuum approach to the surrounding media (Chapter 1), density

functional theory within the reaction field approach (Chapter 2), Monte Carlo representations of solvent effects (Chapter 3), molecular dynamics simulation of surrounding medium within the ab initio density functional framework (Chapter 4). Dynamical aspects of chemical reactions and solvent effects occupies the central focus in Chapters 5 and 6. The last chapter contains a general quantum mechanical analysis of dynamical solvent effects and chemical reactions.

In chapter 1, Profs. Cramer and Truhlar provide an overview of the current status of continuum models of solvation. They examine available continuum models and computational techniques implementing such models for both electrostatic and non-electrostatic components of the free energy of solvation. They then consider a number of case studies with particular focus on the prediction of heterocyclic tautomeric equilibria. In the discussion of the latter they focus attention on the subtleties of actual chemical systems and some of the danger in applying continuum models uncritically. They hope the reader will emerge with a balanced appreciation of the power and limitations of these methods. In the last section they offer a brief overview of methods to extend continuum solvation modeling to account for dynamic effects in spectroscopy and kinetics. Their conclusion is that there has been tremendous progress in the development and practical implementation of useful continuum models in the last five years. These techniques are now poised to allow quantum chemistry to have the same revolutionary impact on condensed-phase chemistry as the last 25 years have witnessed for gas-phase chemistry.

In chapter 2, Profs. Contreras, Pérez and Aizman present the density functional (DF) theory in the framework of the reaction field (RF) approach to solvent effects. In spite of the fact that the electrostatic potentials for cations and anions display quite a different functional dependence with the radial variable, they show that it is possible in both cases to build up an unified procedure consistent with the Born model of ion solvation. The proposed procedure avoids the introduction of arbitrary ionic radii in the calculation of insertion energy. Especially interesting is the introduction of local indices in the solvation energy expression. the effect of the polarizable medium is directly expressed in terms of the natural reactivity indices of DF theory. The paper provides the theoretical basis for the treatment of chemical reactivity in solution.

In chapter 3, Profs. A. González-Lafont, Lluch and Bertrán present an overview of Monte Carlo simulations for chemical reactions in solution. First of all, the authors briefly review the main aspects of the Monte Carlo methodology when it is applied to the treatment of liquid state and solution. Special attention is paid to the calculations of the free energy differences and potential energy through pair potentials and many-body corrections. The applications of this methodology to different chemical reactions in solution are

checked.

In chapter 4, Profs. Corongiu, Estrin, Paglieri and Inquimae consider those systems they have analysed in the last few years, while indicating shortcomings and advantages in different approaches. In the methodological section they pay especial attention to the density functional theory implementation in their computer programs. Especially interesting is the presentation of DF theory and Molecular Dynamics method developed by Carr and Parrinello. Here, the electronic parameters as well as the nuclear coordinates are treated as dynamical variables.

In chapter 5, Prof Hynes reviews the Grote-Hynes (GH) approach to reaction rate constants in solution, together with simple models that give a deeper perspective on the reaction dynamics and various aspects of the generalized frictional influence on the rates. Both classical particle charge transfer and quantum particle charge transfer reactions are examined. The fact that the theory has always been found to agree with molecular dynamics computer simulations results for realistic models of many and varied reaction types gives confidence that it may be used to analyze real experimental results. Another interesting result in MD simulations of S_N2 reaction in solution is that a major portion of the solvent reorganization to a state appropiate to solvating the symmetric charge distribution of the reagents at the barrier top takes place well before the reagent charge distribution begins to change. This shows very clearly for the S_N2 system that one canot picture the progress of a chemical reaction as a calm progression along the potential of mean force curve (a chemical reaction is intrinsically a dynamic, and not an equilibrium event).

In chapter 6, Profs. Bianco and Hynes give some highlights of a theory which combines the familiar multistate valence bond (VB) picture of a molecular system with a dielectric continuum model for the solvent and includes a quantum model for the electronic solvent polarization. The different weights of the diabatic states going from gas phase to solution introduce easily the polarization of the solute by the reaction field. Non equilibrium effects are introducing dividing the solvent polarization in two components: the electronic polarization (fast) and the reorientation polarization (slow). In this way the theory is capable of describing both the regimes of equilibrium and non-equilibrium solvation. For the latter the authors have developed a framework of natural solvent coordinates. The non-equilbrium free energy surface obtained can be used to analyze reaction paths and to calculate reaction rates constants. Finally, the quantum model for the electronic solvent polarization allows to define two limits : self consistent (SC) and Born-Oppenheimer (BO). In the SC case, the electronic solvent frequency is much smaller than the frequency of interconversion of VB states. So, the solvent see the average charge distribution. In the BO case, it happens the contrary. Now the electronic solvent frequency is much faster than VB

interconversions. It means the solvation of localized states and, as a consequence, that the free energy from the solvent point of view is lower than the solvation of the delocalized self-consistent charge distribution.

In chapter 7, Profs. Tapia, Andrés and Stamato give an extended analysis of the quantum mechanics of solvent effects, chemical reactions and their reciprocal effects. The stand point is somewhat different from current pragmatic views. The quantum mechanics of n-electrons and m-nuclei is examined with special emphasis on possible shortcomings of the Born-Oppenheimer framework when it is applied to a chemical interconversion process. Time dependent phenomena is highligthed. The authors go a step beyond previous wave mechanical treatments of solvent effects by explicitly including a time-dependent approach to solvent dynamics and solute-solvent coupling. Solvent fluctuation effects on the solute reactive properties include now most of the 1-dimensional models currently available in the literature. Time dependent effects are also introduced in the discussion of the quantum mechanics of chemical interconversions. This perspective leads to a more general theory of chemical reactions incorporating the concept of quantum resonaces at the interconversion step. The theory of solvent effects on chemical reactions is then framed independently of current quantum chemical procedures. As the chapter unfolds, an extended overview is included of important work reported on solvent effects and chemical reaction.

A book on solvent effects today cannot claim completeness. The field is growing at a dazzling pace. Conspicuous by its absence is the integral equation description of correlation functions and, in particular, interaction-site model–RISM– by D. Chandler and H.C. Andersen and later extended for the treatment of polar and ionic systems by Rossky and coworkers. Path integral method is currently being employed in this field. By and large, we believe that the most important aspects of the theory and practice of solvent effects have been covered in this book and we apologize to those authors that may feel their work to have been inappropriately recognized.

Finally, the editors of this book would tend to agree with Cramer and Truhlar's statement that contemporary advances in the field of solvent effect representation would allow quantum chemistry to have the same revolutionary impact on condensed-phase chemistry as the last 25 years have witnessed for gas-phase chemistry. We hope this book will contribute to this end.

Continuum Solvation Models

Christopher J. Cramer and Donald G. Truhlar
Department of Chemistry and Supercomputer Institute, University of Minnesota, 207 Pleasant St. SE, Minneapolis, MN 55455-0431

June-1995

Abstract This chapter reviews the theoretical background for continuum models of solvation, recent advances in their implementation, and illustrative examples of their use. Continuum models are the most efficient way to include condensed-phase effects into quantum mechanical calculations, and this is typically accomplished by the using self-consistent reaction field (SCRF) approach for the electrostatic component. This approach does not automatically include the non-electrostatic component of solvation, and we review various approaches for including that aspect. The performance of various models is compared for a number of applications, with emphasis on heterocyclic tautomeric equilibria because they have been the subject of the widest variety of studies. For nonequilibrium applications, e.g., dynamics and spectroscopy, one must consider the various time scales of the solvation process and the dynamical process under consideration, and the final section of the review discusses these issues.

O. Tapia and J. Bertrán (eds.), Solvent Effects and Chemical Reactivity, 1–80.
© 1996 *Kluwer Academic Publishers. Printed in the Netherlands.*

1 Introduction

Accurate treatments of condensed-phase systems are particularly challenging for theoretical chemistry. The primary reason that condensed-phase problems are formidable is the intractability of solving the Schrödinger equation for large, non-periodic systems. Although the nuclear degrees of freedom may be rendered separable from the electronic ones by invocation of the Born-Oppenheimer approximation, the electronic degrees of freedom remain far too numerous to be handled practically, especially if a quantum mechanical approach is used without compromise. Therefore it is very common to replace the quantal problem by a classical one in which the electronic energy plus the coulombic interactions of the nuclei, taken together, are modeled by a classical force field—this approach is usually called molecular mechanics (MM). Another approach is to divide the system into two parts: (1) the primary subsystem consisting of solute and perhaps a few nearby solvent molecules and (2) the secondary subsystem consisting of the rest. The primary subsystem might be treated by quantum mechanics to retain the accuracy of that approach, whereas the secondary subsystem, for all practical purposes, is treated by MM to reduce the computational complexity. Such hybrids of quantum mechanics and classical mechanics, often abbreviated QM/MM, allow the prediction of properties dependent on the quantal nature of the solute, which is especially important for conformational equilibria dominated by stereoelectronic effects, open shell systems, bond rearrangements, and spectroscopy. At the same time, this approach permits the treatment of specific first-solvation-shell interactions.

The QM/MM methodology [1-7] has seen increasing application [8-16] and has been recently reviewed [17-19]. The classical solvent molecules may also be assigned classical polarizabiIity tensors, although this enhancement appears to have been used to date only for simulations in which the solute is also represented classically [20-30]. The treatment of the electronic problem, whether quantal, classical, or hybrid, eventually leads to a potential energy surface governing the nuclear coordinates.

The treatment of the nuclear coordinates also presents imposing challenges. The potential energy hypersurface for a condensed-phase system has numerous low-energy local minima. An accurate prediction of thermodynamic and quasi-thermodynamic properties thus requires wide sampling of the $6N$-dimensional energy/momentum phase space, where N is the number of particles [31, 32]. Both dynamical and probabilistic methods may be employed to accomplish this sampling [33-44], but it can be difficult to converge [42, 45-50], and it is expensive when long-range forces (e.g., Coulomb interactions) are

significant [48, 51-54]. Often local minima in the hypersurface have steep surrounding potentials due to intermolecular interactions or to solute molecules having multiple conformations separated by significant barriers [48, 55]; such situations are problematic for sampling approaches that are easily trapped in deep potential wells. The (impractical) fully quantal approach, and the QM/MM and fully MM methods that treat solvent molecules explicitly, share the disadvantage that they all require efficient techniques for the sampling of phase space. For the QM/MM and fully MM approaches, this sampling problem becomes the computational bottleneck.

When structural and dynamical information about the solvent molecules themselves is not of primary interest, the solute-solvent system may be made simpler by modeling the secondary subsystem as an infinite (usually isotropic) medium characterized by the same dielectric constant as the bulk solvent, i.e., a dielectric continuum. In most applications the continuum may be thought of as a configuration-averaged or time-averaged solvent environment, where the averaging is Boltzmann weighted at the temperature of interest. The dielectric continuum approach is thus also sometimes referred to as a "mean-field" approach. The model includes polarization of the dielectric continuum by the solute's electric field; that polarization and the energetics of the solute-continuum interaction are calculated by classical electrostatic formulas [56], in particular the Poisson equation or the Poisson-Boltzmann equation, the latter finding use in systems where the continuum is considered to have an ionic strength arising from dissolved salts.

Continuum models remove the difficulties associated with the statistical sampling of phase space, but they do so at the cost of losing molecular-level detail. In most continuum models, dynamical properties associated with the solvent and with solute-solvent interactions are replaced by equilibrium averages. Furthermore, the choice of where the primary subsystem "ends" and the dielectric continuum "begins", i.e., the boundary and the shape of the "cavity" containing the primary subsystem, is ambiguous (since such a boundary is intrinsically non-physical). Typically this boundary is placed on some sort of van der Waals envelope of either the solute or the solute plus a few key solvent molecules.

Continuum models have a long and honorable tradition in solvation modeling; they ultimately have their roots in the classical formulas of Mossotti (1850), Clausius (1879), Lorentz (1880), and Lorenz (1881), based on the polarization fields in condensed media [32, 57]. Chemical thermodynamics is based on free energies [58], and the modern theory of free energies in solution is traceable to Born's derivation (1920) of the electrostatic free energy of insertion of a monatomic ion in a continuum dielectric [59], and Kirkwood and Onsager's

closely related treatments [60-62] (1930s) of the electrostatic free energy of insertion of dipolar solutes. The seminal idea of a reaction field [32] was developed in this work. Nonelectrostatic contributions to solvation were originally treated by molecular models. However, Lee and Richards [63] and Hermann [64] introduced the concept of the solvent accessible surface area (SASA). When a proportionality is assumed between, on the one hand, the SASA and, on the other hand, non-bulk-type electrostatic effects and non-electrostatic effects in the first solvation shell (where they are largest), this augments the continuum approach in a rational way. The quasithermodynamic formulation of transition state theory extends all these concepts to the treatment of reaction rates by defining the condensed-phase free energy of activation [65-67]. The breakdown of transition state theory for dynamics, which is related to (if not identical to) the subject of nonequilibrium solvation, can also be discussed in terms of continuum models, as pioneered in Kramers' model involving solvent viscosity [67-69] and in Marcus' work involving nonequilibrium polarization fields [70].

The last thirty years have seen a flowering of simulation techniques based on explicit treatments of solvent molecules (some references are given above). Such methods provide new insight into the reasons why continuum methods work or don't work. However they have not and never will replace continuum models. In fact, continuum models are sometimes so strikingly successful that hubris may be the most serious danger facing their practitioners. One of the goals of this present chapter will be to diffuse (but not entirely deflate!) any possible overconfidence.

The present chapter thus provides an overview of the current status of continuum models of solvation. We review available continuum models and computational techniques implementing such models for both electrostatic and non-electrostatic components of the free energy of solvation. We then consider a number of case studies, with particular focus on the prediction of heterocyclic tautomeric equilibria. In the discussion of the latter we center attention on the subtleties of actual chemical systems and some of the dangers of applying continuum models uncritically. We hope the reader will emerge with a balanced appreciation of the power and limitations of these methods.

At this point we note the existence of several classic and recent reviews devoted to, or with considerable attention paid to, continuum models of solvation effects, and we direct the reader to these works [71-83] for other perspectives that we consider complementary to what is presented here.

Section 2 presents a review of the theory underlying self-consistent continuum models, with section 2.1 devoted to electrostatics and section 2.2 devoted to the incorporation of non-electrostatic effects into continuum solvation

modeling. Section 3 discusses the various algorithmic implementations extant. Section 4 reviews selected applications to various equilibrium properties and contrasts different approaches. Section 5 offers a brief overview of methods to extend continuum solvation modeling to account for dynamic effects in kinetics and spectroscopy, and Section 6 closes with some conclusions and remarks about future directions.

2 Theory

2.1 ELECTROSTATICS

A charged system has an electrical potential energy equal to the work that must be done to assemble it from separate components infinitely far apart and at rest. This energy resides in and can be calculated from the electric field. This electrostatic potential energy, when considered as a thermodynamic quantity, is a free energy because it is the maximum work obtainable from the system under isothermal conditions [84]. We have the option, therefore, of calculating it as an electrostatic potential energy or as the isothermal work in a charging process. Although the latter approach is very popular, dating back to its use by Born, the former approach seems to provide more insight into the quantum mechanical formulation, and so we adopt that approach here. Recognizing that the electrostatic potential energy is the free energy associated with the electric polarization of the dielectric medium, we will call it G_P.

In general the electrostatic potential energy of a charge distribution in a dielectric medium is [84, 85]

$$G_P = \frac{1}{2}\int d\mathbf{r}\left[\mathbf{E}^T(\mathbf{r})\mathbf{D}(\mathbf{r}) - 4\pi\mathbf{D}^T(\mathbf{r})\mathbf{D}(\mathbf{r})\right] \tag{1}$$

where the integration is over the whole dielectric medium (in the case of solvation this means an integration over all space except that occupied by the solute), **E** is the electric field, T denotes a transpose, **D** is the dielectric displacement, and the second term in the integrand references the energy to that for the same solute in a vacuum. Recall from electrostatics that

$$\nabla \cdot \mathbf{D} = \rho_{free} \tag{2}$$

where ρ_{free} is the charge density of the material inserted into the dielectric, i.e., of the solute, but

$$\nabla \cdot \mathbf{E} = 4\pi\rho_{\text{total}} \tag{3}$$

where

$$\rho_{\text{total}} = \rho_{\text{free}} + \rho_{\text{P}} \tag{4}$$

and ρ_{P} is the polarization charge density, i.e., the charge density induced in the dielectric medium by the solute (in classical electrostatics, ρ_{P} is often called ρ_{bound}). In an isotropic medium, assuming linear response of the solvent to the solute, it is generally the case that [84]

$$\mathbf{E}(\mathbf{r}) = \frac{4\pi}{\varepsilon(\mathbf{r})}\mathbf{D}(\mathbf{r}) \tag{5}$$

where $\varepsilon(\mathbf{r})$ is the dielectric constant (i.e., relative permittivity) of the solvent at position **r.**

Clearly, $\mathbf{D}(\mathbf{r})$ is a function of the solute charge density only, and we can write

$$\mathbf{D}(\mathbf{r}) = \langle\psi|\mathbf{d}(\mathbf{r})|\psi\rangle \tag{6}$$

where **d(r)** is the operator that generates the displacement at **r.** Then

$$G_{\text{P}} = \frac{1}{2}\int d\mathbf{r}\left[\mathbf{E}^{\text{T}}(\mathbf{r}) - 4\pi\mathbf{D}^{\text{T}}(\mathbf{r})\right]\langle\psi|\mathbf{d}(\mathbf{r})|\psi\rangle. \tag{7}$$

Using the linear response result (5), we then get

$$G_{\text{P}} = -2\pi\int d\mathbf{r}\left[1 - \frac{1}{\varepsilon(\mathbf{r})}\right]\langle\psi|\mathbf{d}^{\text{T}}(\mathbf{r})|\psi\rangle\langle\psi|\mathbf{d}(\mathbf{r})|\psi\rangle \tag{8a}$$

$$= \left\langle\psi\left|-2\pi\int d\mathbf{r}\left[1 - \frac{1}{\varepsilon(\mathbf{r})}\right]\mathbf{d}^{\text{T}}(\mathbf{r})\langle\psi|\mathbf{d}(\mathbf{r})|\psi\rangle\right|\psi\right\rangle \tag{8b}$$

$$= \langle\psi|G_{\text{P,op}}|\psi\rangle \tag{8c}$$

where

$$G_{\mathrm{P,op}}|\psi\rangle = -\frac{1}{2} K_{\mathrm{op}}\, \mathbf{d}^{\mathrm{T}}(\mathbf{r}) \langle \psi | \mathbf{d}(\mathbf{r}) | \psi \rangle | \psi \rangle \tag{9}$$

and we have defined the integral operator

$$K_{\mathrm{op}} f(\mathbf{r}) \equiv 4\pi \int d\mathbf{r}' \left(1 - \frac{1}{\varepsilon(\mathbf{r}')}\right) f(\mathbf{r}') \tag{10}$$

for any function $f(\mathbf{r})$. If the gas-phase Hamiltonian is H_0, then the solute's energy in the electrostatic field of the polarized solvent is

$$G_{\mathrm{ENP}} = \langle \psi | H_0 + G_{\mathrm{P,op}} | \psi \rangle \tag{11}$$

where G_{ENP} has the thermodynamic interpretation of the total internal energy of the solute (represented by H_0) plus the electric polarization free energy of the entire solute-solvent system.

We note that G_{ENP} is a complicated function of Ψ; in particular it is nonlinear. Recall that an operator L_{op} is linear if

$$L_{\mathrm{op}} | c_1 \psi_1 + c_2 \psi_2 \rangle = c_1 L_{\mathrm{op}} | \psi_1 \rangle + c_2 L_{\mathrm{op}} | \psi_2 \rangle . \tag{12}$$

However

$$G_{\mathrm{P,op}} | \psi_1 + \psi_2 \rangle = -\frac{1}{2} K_{\mathrm{op}}\, \mathbf{d}^{\mathrm{T}}(\mathbf{r}) \langle \psi_1 + \psi_2 | \mathbf{d}(\mathbf{r}) | \psi_1 + \psi_2 \rangle | \psi_1 \rangle$$

$$-\frac{1}{2} K_{\mathrm{op}}\, \mathbf{d}^{\mathrm{T}}(\mathbf{r}) \langle \psi_1 + \psi_2 | \mathbf{d}(\mathbf{r}) | \psi_1 + \psi_2 \rangle | \psi_2 \rangle \tag{13a}$$

$$\neq G_{\mathrm{P,op}} | \psi_1 \rangle + G_{\mathrm{P,op}} | \psi_2 \rangle . \tag{13b}$$

Hence $G_{\mathrm{P,op}}$ is nonlinear, and therefore the energy functional G_{ENP} of (11) is nonlinear.

Note that $G_{\mathrm{P,op}}$ of eq. (9) can be written in several equivalent but different looking forms, as is typical of electrostatic quantities in general. For example, it is often convenient to express the results in terms of the electrostatic scalar potential $\phi(\mathbf{r})$ instead of the electric vector field $\mathbf{E}(\mathbf{r})$. In the formulation above, the dielectric displacement vector field associated with the solute charge distribution induces an electric vector field, with which it interacts. In the electrostatic

potential formulation, the solute charge distribution induces an electrostatic scalar potential field, with which it interacts. The difference between *either* induced field in the presence of solvent compared to the absence of solvent may be called the reaction field, using the language mentioned above as introduced by Onsager. In any such formulation, $G_{P,op}$ will remain nonlinear. In particular it will have the form $A\,\mathrm{op}(\Psi^*\Psi)$ where A_{op} is some operator. Sanhueza et al. [86] have constructed variational functions representing general nonlinear Hamiltonians having the form $L_{op} + A_{op}(\Psi^*\Psi)^q$, where q is any positive number. The sense of the notation is simply that Ψ^* and Ψ each appear to the first power in one term of the operator. Thus, comparing to eq. (9), we see that their treatment reduces to our case when $q = 1$. The $q = 1$ case is of special interest since it arises any time a solute is immersed in a medium exhibiting linear response to it. Since this case is central to the work reviewed in this chapter, we present below a self-contained variational formulation for the $q = 1$ case. In particular we will consider the case of G_{ENP} as expressed above although the procedure is valid for any Hamiltonian whose nonlinearity may be written as $A_{op}(\Psi^*\Psi)^q$ with $q = 1$.

In order to motivate the quantum mechanical treatment of a system with the energy functional G_{ENP}, we first consider the functional

$$E = \langle \psi | H_0 | \psi \rangle \tag{14}$$

where H_0 is the gas-phase Hamiltonian. We use Euler-Lagrange theory to find a differential equation satisfied by the Ψ that extremizes the value of the integral functional E of Ψ. The Euler equation for an extremum of E subject to the constraint

$$\langle \psi | \psi \rangle = 1 \tag{15}$$

is

$$\delta\left[E + \lambda\langle \psi | \psi \rangle\right] = 0 \tag{16}$$

where λ is a Lagrange multiplier. Carrying out the variation gives

$$\langle \delta\psi | H_0 | \psi \rangle + \langle \psi | H_0 | \delta\psi \rangle + \lambda\left(\langle \delta\psi | \psi \rangle + \langle \psi | \delta\psi \rangle\right) = 0 \tag{17}$$

or

$$J = 0 \tag{18}$$

where

$$J = 2\Big(\langle \delta\psi | H_0 | \psi \rangle + \lambda \langle \delta\psi | \psi \rangle\Big). \tag{19}$$

For this to be valid for any variation $\delta\Psi$, it is required that

$$H_0\psi = -\lambda\psi \tag{20}$$

where λ is evaluated by using eq. (15). To use eq. (15), note that (20) implies that

$$\langle \psi | H_0 | \psi \rangle + \lambda \langle \psi | \psi \rangle = 0 \tag{21}$$

and using (15) then yields the interpretation of λ

$$\lambda = -\langle \psi | H_0 | \psi \rangle = -E. \tag{22}$$

Putting this in (20) yields

$$H_0\psi - E\psi = 0. \tag{23}$$

Thus, as expected, the Euler equation equivalent to extremizing E is the Schrödinger equation.

Now consider the functional

$$G_{\mathrm{ENP}} = \langle \psi | H_0 - \frac{1}{2} K_{\mathrm{op}} \mathbf{d}^{\mathrm{T}}(\mathbf{r}) \langle \psi | \mathbf{d}(\mathbf{r}) | \psi \rangle | \psi \rangle. \tag{24}$$

The Euler equation for an extremum of G_{ENP} subject to the constraint

$$\langle \psi | \psi \rangle = 1 \tag{25}$$

is

$$\delta\big[G_{\mathrm{ENP}} + \lambda \langle \psi | \psi \rangle\big] = 0 \tag{26}$$

where λ is a Lagrange multiplier. Carrying out the variation gives

$$\begin{aligned} J + 2\langle \delta\psi | - \frac{1}{2} K_{\mathrm{op}} \mathbf{d}^{\mathrm{T}}(\mathbf{r}) \langle \psi | \mathbf{d}(\mathbf{r}) | \psi \rangle | \psi \rangle \\ + 2\langle \psi | - \frac{1}{2} K_{\mathrm{op}} \mathbf{d}^{\mathrm{T}}(\mathbf{r}) \langle \delta\psi | \mathbf{d}(\mathbf{r}) | \psi \rangle | \psi \rangle = 0. \end{aligned} \tag{27}$$

For this is to be valid for arbitrary variations $\delta\Psi$, it is required that

$$H_0\psi + \lambda\psi - K_{op}\mathbf{d}^T(\mathbf{r})\langle\psi|\mathbf{d}(\mathbf{r})|\psi\rangle\psi = 0 \tag{28}$$

where λ is again to be evaluated from the constraint equation. Following the same procedure as before we find

$$\lambda = -\langle\psi|H_0 - K_{op}\mathbf{d}^T(\mathbf{r})\langle\psi|\mathbf{d}(\mathbf{r})|\psi\rangle|\psi\rangle. \tag{29}$$

It is conventional to rewrite eq. (28) as a nonlinear Schrödinger equation with eigenvalue E:

$$\left[H_0 - K_{op}\mathbf{d}^T(\mathbf{r})\langle\psi|\mathbf{d}(\mathbf{r})|\psi\rangle - E\right]|\psi\rangle = 0. \tag{30}$$

Comparison of (30) to (28) and (29) shows that

$$E = \langle\psi|H_0 - K_{op}\mathbf{d}^T(\mathbf{r})\langle\psi|\mathbf{d}(\mathbf{r})|\psi\rangle|\psi\rangle$$

$$= \langle\psi|H_0|\psi\rangle + 2G_P. \tag{31}$$

Solving the nonlinear Schrödinger equation yields E and Ψ and the desired physical quantity G_{ENP} may then be calculated directly from (11) or from

$$G_{ENP} = E + \frac{1}{2}K_{op}\mathbf{d}^T(\mathbf{r})\langle\psi|\mathbf{d}(\mathbf{r})|\psi\rangle$$

$$= E - Gp \tag{32}$$

which is easily derived by comparing eq. (8), (9), (24), and (31).

The fact that the eigenvalue E of the nonlinear effective Hamiltonian,

$$H_{eff} = H_0 - K_{op}\mathbf{d}^T(\mathbf{r})\langle\psi|\mathbf{d}(\mathbf{r})|\psi\rangle \tag{33}$$

does not equal the expectation value of the functional G_{ENP} that is extremized is sometimes a source of confusion for those unfamiliar with nonlinear Schrödinger equations. This is presumably because in the linear case the expectation value of the function extremized, e.g., eq. (14), and the eigenvalue, e.g., $-\lambda$ in eq. (20), are the same.

The second term of equation (33) may be called the self-consistent reaction field (SCRF) equation in that eq. (30) must be solved iteratively until the

|Ψ> obtained by solving the equation is consistent with the |Ψ> used to calculate the reaction field. Having established an effective nonlinear Hamiltonian, one may solve the Schrödinger equation by any standard (or nonstandard) manner. The common element is that the electrostatic free energy term G_P is combined with the gas-phase Hamiltonian H_0 to produce a nonlinear Schrödinger equation

$$(H_0 + 2G_P)\psi = E\psi \tag{34}$$

where Ψ is the solute wave function, and the reason that $2G_P$ appears in eq. (34) is explained above, namely that G_P depends on $\Psi^*\Psi$, and one can show that the variational solution of (34) yields the best approximation to

$$E_S \equiv \langle\psi|H_0 + G_P|\psi\rangle. \tag{35}$$

In most work reported so far, the solute is treated by the Hartree-Fock method (i.e., H_0 is expressed as a Fock operator), in which each electron moves in the self-consistent field (SCF) of the others. The term SCRF, which should refer to the treatment of the reaction field, is used by some workers to refer to a combination of the SCRF nonlinear Schrödinger equation (34) and SCF method to solve it, but in the future, as correlated treatments of the solute becomes more common, it will be necessary to more clearly distinguish the SCRF and SCF approximations. The SCRF method, with or without the additional SCF approximation, was first proposed by Rinaldi and Rivail [87, 88], Yomosa [89, 90], and Tapia and Goscinski [91]. A highly recommended review of the foundations of the field was given by Tapia [71].

When the SCRF method is employed in conjunction with Hartree-Fock theory for the solute, then the Fock operator is given by

$$F = F^{(0)} + 2G_{P,op} \tag{36}$$

where $F^{(0)}$ is the gas-phase Fock operator. Using eq. (9) we can also write this as

$$F = F^{(0)} - K_{op}\,\mathbf{d}^T(\mathbf{r})\langle\psi|\mathbf{d}(\mathbf{r})|\psi\rangle. \tag{37}$$

There is another widely used method of obtaining the Fock operator, namely to obtain its matrix elements $F_{\mu\nu}$ as the derivative of the energy functional with respect to the density. In our case that yields

$$F_{\mu\nu} = \frac{\partial G_{\mathrm{ENP}}}{\partial P_{\mu\nu}} \tag{38a}$$

$$= F_{\mu\nu}^{(0)} + \frac{\partial G_{\mathrm{P}}}{\partial P_{\mu\nu}} \tag{38b}$$

where $F_{\mu\nu}^{(0)}$ is the matrix element of the gas-phase Fock operator, and $P_{\mu\nu}$ is a matrix element of the density. This method bypasses the nonlinear Schrödinger equation and the nonlinear Hamiltonian, but a moment's reflection on the variational process of eqs. (24)–(30) shows that it yields the same results as eqs. (36) and (37). This too has caused confusion in the literature.

In conclusion, we note that there has recently been considerable interest in including intrasolute electron correlation energy in SCRF theory [77, 92-106]. Further progress in this area will be very important in improving the reliability of the predictions, at least for "small" solutes.

Next we discuss two aspects of the physical interpretation of the SCRF method that are well worth emphasizing: (i) the time scales and (ii) the assumption of linear response.

The natural time scale τ_{elec} of the electronic motion of the solute is $\vartheta(h/\Delta E_1)$ where ϑ denotes "order of", h is Planck's constant, and ΔE_1 is the lowest electronic excitation energy. Assuming a typical order of magnitude of 10^1 eV for ΔE_1 yields $\tau_{\mathrm{elec}} = \vartheta(10^{-16}\mathrm{s})$. The time scale for polarization of the solvent is more complicated. For a polar solvent, orientational polarization is the dominant effect, and it is usually considered to have a time scale of $\vartheta(10^{-12}\,\mathrm{s})$. Thus the electronic motion of the solute should adjust adiabatically to solvent orientational polarization, and the solvent should "see" the average charge distribution (i.e., the "mean field") of the solute. This argument provides a physical justification for the expectation value in (6) providing the field that induces the solvent polarization, resulting in a net electric field given by (5). We should not forget though that a part of the solvent polarization is electronic in origin. The time scale for solvent electronic polarization is comparable to that for electronic motions in the solute, and the SCRF method is not so applicable for this part. A correct treatment of this part of the polarization effect would require a treatment of electron correlation between solute electrons and solvent electrons, a daunting prospect. This correlation problem has also been discussed from other points of view [107-111].

Tapia, Colonna, and Ángyán [112-114] have presented an alternative justification for the appearance of average solute properties in the SCRF

equations. Their argument is based starting with a wave function for the entire solute-solvent system, then assuming a Hartree product wave function of the form $\Psi_{solute}\Psi_{solvent}$. This allows the "derivation" of a solute-only Schrödinger equation identical to the one derived here. The appearance of the Hartree approximation [115] in the derivation again makes it clear that solute-solvent electron correlation is neglected in the SCRF equations. It also raises the question of exchange repulsion, which is the short-range repulsion between two closed-shell systems due to the Pauli Exclusion Principle. (i.e., if the systems start to overlap, their orbitals must distort to remain orthogonal. This raises the energy, and hence it is a repulsive interaction.) Exchange repulsion between two systems is properly included in the Hartree-Fock approximation but not in the Hartree approximation. The neglect of exchange repulsion is a serious limitation of the SCRF model that prevents it from being systematically improvable with respect to the solute-solvent electron correlation.

The assumption of linear response played a prominent role in the derivation (given above) of the SCRF equations, and one aspect of the physics implied by this assumption is worthy of special emphasis. This aspect is the partitioning of G_P into a solute-solvent interaction part G_{sS} and a intrasolvent part G_{SS}. The partitioning is quite general since it follows entirely from the assumption of linear response. Since classical electrostatics with a constant permittivity is a special case of linear response, it can be derived by any number of classical electrostatic arguments. The result is [114, 116-119]

$$G_{SS} = -\frac{1}{2} G_{sS} \tag{39}$$

and hence

$$G_{sS} = 2G_P \tag{40}$$

and

$$G_{SS} = -G_P. \tag{41}$$

The physical interpretation of these equations is that when the solute polarizes the solvent to lower the solute-solvent interaction energy by an amount G_{sS}, half the gain in free energy is canceled by the work in polarizing the solvent, which raises its own internal energy.

Since these equations are general for a system exhibiting linear response, we can illustrate them by the simplest such system, a harmonic oscillator

(representing the solvent) linearly coupled to an external perturbation (representing the solute). The energy of the system (excluding the internal energy of the solute) is

$$V = \frac{1}{2} ky^2 + gys \tag{42}$$

where k is the oscillator force constant, y is the oscillator coordinate, which is a generalized solvent coordinate, g is the coupling force constant, and s is the solute coordinate. We identify

$$G_{\mathrm{P}} = V \tag{43}$$

$$G_{\mathrm{SS}} = \frac{1}{2} ky^2 \tag{44}$$

$$G_{\mathrm{sS}} = gys. \tag{45}$$

Now, at equilibrium

$$\frac{\partial V}{\partial y} = 0. \tag{46}$$

Therefore, from the derivative of (42):

$$s = -ky/g. \tag{47}$$

and putting this in (45) yields

$$G_{\mathrm{sS}} = -ky^2 \tag{48}$$

Comparison of (48) to (44) agrees with (39).

A subject *not* treated here is the use of distance-dependent effective dielectric constants as a way to take account of the structure in the dielectric medium when a solute is present. This subject has recently been reviewed [120]. In the approaches covered in the present chapter, deviations of the effective dielectric constant from the bulk value may be included in terms of physical effects in the first solvation shell, as discussed in Section 2.2.

As a final topic in this section, we briefly consider the effect of electrolyte concentration on the solvent properties. The linearized Poisson-Boltzmann equation [31,121] can be used instead of (2) and (3) when the dielectric medium

is a salt solution, and this equation can be solved analytically for the case of a single point charge Z at the center of a cavity of radius ρ in a solvent of dielectric constant ε. The resulting electric potential at a distance r from the center of the cavity is [122]

$$\phi(r) = \frac{Z}{\varepsilon r} D \frac{\exp\left[-(r-\rho)/r_D\right]}{1+\rho/r_D} \tag{49}$$

where r_D is the Debye screening length

$$r_D = 1/\kappa = \left[\varepsilon RT/(8\pi I)\right]^{1/2}, \tag{50}$$

R is the gas constant, T the temperature, and I is ionic strength. We may write this as

$$\phi(r) = \frac{Z}{\varepsilon_{\text{eff}}(r) r} \tag{51}$$

which yields [123]

$$\varepsilon_{\text{eff}}(r) = \varepsilon\left(1+\frac{\rho}{r_D}\right) e^{(r-\rho)/r_D} \tag{52}$$

For 0.1 M NaCl in water, this yields $\varepsilon_{\text{eff}}(\boldsymbol{r})$ values of about 105 and 130 at r equals 3 and 5 Å, respectively, as compared to ε = 78.5 for pure water. Since, however, for homogeneous ε, the dielectric constant enters the solvation free energy through the expression $(1 - \frac{1}{\varepsilon})$, the relative effect of such an increase will not be quantitatively large (whereas a decrease in ε could be more significant). In an organic biophase though, where ε is smaller, the relative effects of ions could be very significant, but they tend to be excluded from such phases. Even in aqueous solution and even when the relative change in the solvation free energy is small, the absolute effect of ions may be significant, especially for reactions involving ions [124] and electrostatics [125, 126], in both of which cases the magnitude of the total electrostatic free energy is large.

2.2 NON-ELECTROSTATIC CONTRIBUTIONS

It should be clear from the presentation in the previous section that the SCRF method is a model that by design focuses on only one physical effect accompanying the insertion of a solute in a solvent, namely the bulk polarization

of the solvent by the mean field of the solute. Thus the model admittedly neglects all other physical effects. One of these, electron correlation between the solute and the solvent, was mentioned explicitly already. This and other physical effects missing in the SCRF method are discussed in more detail in this section. As a shorthand we call these effects "non-electrostatic" (and abbreviate them *N*), but a more precise wording would be that used in Section 1, namely *and* "non-bulk-type electrostatic."

Electron correlation between the solute and solvent has an important quantitative effect on the solvation free energy. The most important qualitative manifestation of this correlation is the existence of dispersion interactions between solute and solvent (dispersion interactions are neglected in both the Hartree and Hartree-Fock approximations). The solute-solvent dispersion interactions are inseparable in practice from several other effects that are often grouped under the vague heading of cavitation. If we make a cavity in a solvent B to accommodate a solute A, the solvent molecules in the first solvation shell gain A–B dispersion and repulsive interactions, but at the expense of B–B ones. This tradeoff may have significant effects, both enthalpic and entropic, on solvent structural properties. The dispersion and solvent structural aspects of cavitation are two physical effects not accounted for in the treatment of the previous section, with its assumption of an uncorrelated, homogeneous dielectric medium with dielectric constant equal to the bulk value.

Certain aspects of the solvent structural changes in regions near to the solute have received specialized attention and even inspired their own nomenclature. Two examples, each with a long and distinguished theoretical history, are the "hydrophobic effect" and "dielectric saturation."

The hydrophobic effect refers to certain unfavorable components of the solvation free energy when a nonpolar solute is dissolved in water. The most generally accepted explanation (no explanation is universally accepted) starts from the premise that a typical cluster of water molecules in the bulk makes several hydrogen bonds and has several ways to do so. When a non-hydrogen-bonding solute is introduced, the neighboring water molecules will still make about the same average number of hydrogen bonds (although enthalpic components of hydrophobicity, when observed, may sometimes be ascribed to a reduced total number of hydrogen bonds), but they will have less ways to do so since the opportunities for maximum hydrogen bonding will restrict the orientation of solvent molecules in the first solvation shell, and flipping a hydrogen-bonded cluster will not provide the same possibilities for hydrogen bonding as it does in the bulk where the cluster is surrounded on all sides by

water. Thus the water structure in the first hydration shell is more "rigid," which is entropically unfavorable.

Dielectric saturation refers to the breakdown of linear response in the region near the solute. At high enough fields, the permittivity of a dielectric medium is not a constant; it depends on the field [116, 127]. The field in the vicinity of the solute may be high enough that this concern becomes a reality, and the solvent may fail to respond with the same susceptibility as bulk water responds to small applied fields. This will be especially likely to be a problem for multiply charged, small ions [128, 129]. Bucher and Porter [130] have analyzed the dielectric saturation effect quantitatively for ions in water, and they find that the effect of this saturation on the electrostatic contribution to the hydration energy comes primarily from the region within 3 Å of the atomic centers and hence only from the first hydration shell.

Another, related effect leading to non-bulk response in the first hydration shell is electrostriction [131], which is the change in solvent density due to the high electric fields in the first solvation shell of an ion.

A fourth solvent structural effect refers to the average properties of solvent molecules near the solute. These solvent molecules may have different bond lengths, bond angles, dipole moments, and polarizabilities than do bulk solvent molecules. For example, Wahlqvist [132] found a decrease in the magnitude of the dipole moment of water molecules near a hydrophobic wall from 2.8 D (in their model) to 2.55 D, and van Belle et al. [29] found a drop from 2.8 D to 2.6 D for first-hydration-shell water molecules around a methane molecule.

Dispersion is not the only short-range force that needs to be added to the electrostatic interactions. For example, hydrogen bonding is not 100% electrostatic but includes covalent aspects as well, and exchange repulsion is not included in classical electrostatics at all. An accurate model should take account of all the ways in which short-range forces differ from the electrostatic approximation with the bulk value for the dielectric constant.

All these overlapping effects, namely cavitation, solute-solvent dispersion interactions, other solute-solvent electron correlation effects, hydrophobic effects, dielectric saturation, and non-bulk properties of solvating solvent molecules, would be expected to be most significant in the first solvation shell, and numerous molecular dynamics simulations have borne this expectation out [133-137]. One might hope, in light of this, to treat such effects by treating all solvent molecules in the first solvation shell explicitly. In this section, however, we wish to make the point that continuum models need not be abandoned for treating such effects. In fact, continuum models have some significant advantages for such treatments, just as they do for treating bulk electrostatic effects.

The key to the continuum treatment of first solvation-shell effects is the concept of solvent-accessible surface area, introduced by Lee and Richards [63] and Hermann [64]. In a continuum treatment of the solvent, it is useful to define a non-integer "number" of solvent molecules in the first solvation shell so that in some sense this continuous number simulates the average of the integer number of discrete molecules in the first solvation shell in a treatment with explicit solvent molecules. If we imagine a continuous first hydration shell and pass a hypersurface through the middle of the shell, then the simplest assumption is that the average number of solvent molecules in the first solvation shell is proportional to the area of this hypersurface. This area is called the solvent-accessible surface area A. Other possible definitions of molecular surface area do not have this interpretation [138]. Because the surface tensions are empirical they can make up for many flaws in the model. For example, simulations have shown that, due to the dominance of water-water hydrogen bonding, hydrophobic crevices are not accessed by the solvent as much as would be predicted by the calculated solvent-accessible surface areas. Environment-dependent surface tensions can and do make up for such deficiencies in the model in an average way [139].

Since many of the effects that need to be added to the bulk electrostatics are localized in the first solvation shell, and since the solvent-accessible surface area is proportional to the number of solvent molecules in the first solvation shell, it is reasonable to assume that the component of the free energy of solvation, G_N^o, is proportional to the solvent-accessible surface area. A critical refinement of this idea is the recognition that the contribution per solvent molecule of the first-solvation shell in contact with one kind of atom is different from that in contact with another kind of solute atom. If we divide the local surface environment of a solute into several types of region, $\alpha = 1, 2, \ldots$ (e.g., $\alpha = 1$ might denote amine–like nitrogen surface, $\alpha = 2$ might denote nitrile-like nitrogen surfaces, $\alpha = 3$ might denote the surface of carbonyl oxygens, etc.), and if we partition A into parts A_α associated with the various environments of type α, then it is even more reasonable to write

$$G_N^o = \sum_\alpha \sigma_\alpha A_\alpha \tag{53}$$

where each σ_α is some proportionality constant with units of surface tension.

Although entropy cannot be strictly localized, some contributing factors to the solvent entropy change induced by the solute are localized in the first solvent shell, and contributions to the entropy of mixing that are proportional to the number of solvent molecules in the first solvation shell might sometimes

dominate σ_α as well. In assessing such entropic effects there has been considerable attention paid to the effects of size and shape. A nice overview of the current status of our understanding in this area, along with further original contributions, has been provided by Chan and Dill [140]. From a more empirical standpoint, we expect that these size effects, if and when present, may well scale with solvent-accessible surface area [141].

Clearly, since it includes so many effects (see above), σ_α can be positive or negative. Sometimes one effect will dominate, e.g., dispersion or solvent structural change. If the σ_α are determined empirically, they can also make up for fundamental limitations of the bulk electrostatic treatment (such as the intrinsically uncertain location of the solute/bulk boundary and also for systematic errors in the necessarily approximate model used for the solute.

We summarize this section by emphasizing that we have identified a host of effects, and we have seen that they are mainly short-range effects that are primarily associated with the first solvation shell. A reasonable way to model these effects quantitatively is to assume they are proportional to the number of solvent molecules in the first hydration shell with environment-dependent proportionality constants.

Some workers have attempted to treat particular effects more rigorously, e.g., by scaled-particle theory [142] or by extending [95, 103] Linder's theory [143] of dispersion interactions to the case of an SCRF treatment of solute-solvent interactions. We will not review these approaches here.

Finally, we note that we have mostly limited attention so far to the self-consistent reaction field limit of dynamical solvent polarization, which is the only one that has been generally implemented (see next Section). Nevertheless, there are problems where the solute-solvent dynamical correlation must be considered, and we will address that topic in Section 5.

3 Implementations

As reviewed above, when a solute is placed in a dielectric medium, it electrically polarizes that medium. The polarized medium produces a local electrostatic field at the site of the solute, this field polarizes the solute, and the polarized solute interacts with the polarized medium. The interaction is typically too large to be treated by perturbation theory, and some sort of self-consistent treatment of polarized solute and polarized medium is more appropriate. At this point several options present themselves. It promotes orderly discussion to classify these

options, but because there are many aspects, one needs several classification elements. The elements and the popular choices are as follows:

E. How to treat the electrostatics (*E*):
- E-A. Numerical or analytic solution of the classical electrostatic problem (e.g., Poisson equation) with homogeneous dielectric constant for solvent.
- E-B. A model solution to the electrostatic problem, e.g., the Generalized Born Approximation or a conductor-like screening solution.
- E-C. Electrostatics treated empirically, without reference to solute charge distribution.

S. What shape (*S*) to assume for the boundary between the solvent, considered as a continuum, and the solute:
- S-A. Taking account of molecular shape, e.g., treating the solute as a set of atom-centered spheres.
- S-B. Treating the solute as an ellipsoid.
- S-C. Treating the solute as a sphere.

L. At what level (*L*) to model the solute:
- L-A. With polarizable charges obtained by an approximate quantum mechanical method including electron correlation or by a Class IV charge model.
- L-B. With polarizable charges obtained by the *ab initio* Hartree-Fock method.
- L-C. With polarizable charges obtained by semiempirical molecular orbital theory.
- L-D. With polarizable charges obtained by A, B, or C combined with a truncated multipole expansion, including multipole moments up to some predetermined cutoff l, where $l > 1$ but not necessarily large enough for convergence.
- L-E. Like D but with only $l = 0$ and/or 1.
- L-F. By non-polarizable charges, e.g., as might be used in a molecular mechanics calculation, or an unpolarized charge

density on a grid. (Use of non-polarizable dipole moments, i.e., permanent rather than permanent plus induced, would also fit in here.)

N. Whether to augment the electrostatics terms by an estimate of non-electrostatic (*N*) contributions:
   N-A. Yes, including empirical elements to make up for the approximate character of the electrostatics as well as to include other identifiable effects.
   N-B. Yes, treating one or more non-electrostatic interactions non-empirically.
   N-C. Yes, by a single linear function of molecular surface area.
   N-D. No.

Although the list of choices is lengthy, we should also note some choices that are *not* present. With regard to the electrostatic (*E*) element, all models currently in general use assume a homogeneous dielectric constant for the solvent, thereby neglecting possible dielectric saturation in the first solvation shell and also neglecting the fact that solvent molecules near to the solute have different properties (average dipole moment, polarizability, geometry, size, and hence dielectric constant) than bulk solvent molecules. (Note, though, that Hoshi [144] and Tomasi and co-workers [145-148] have discussed algorithmic implementations of an inhomogeneous dielectric continuum in SCRF models, and note also that both dielectric saturation and the unique properties of the solvent molecules in the first solvation shell *are* included in models that make choice A for element *N*) With regard to the shape (*S*) element, all choices assume a well defined discontinuous change of dielectric properties at a fixed, sharp solute/solvent boundary. In reality of course, this boundary is a fluctuating, finite-width boundary *layer.* With regard to the level (*L*) element, we note that the ideal choice of "by converged quantum mechanics" is missing, for reasons of practicality. The missing choices have an important consequence for which combinations of the other choices seem most suitable. For example, one asks, given that the assumption of homogeneous dielectric constant, the assumption of a rigid, sharp solute/solvent boundary, the assumption of an approximate solute wave function, and the neglect of solute-solvent exchange repulsion all introduce significant approximations into the electrostatics, is it still worthwhile to solve the Poisson equation numerically, or would an approximate solution introduce errors smaller than those already inevitably present? Different workers have answered

such questions differently. We believe, in fact, that more than one answer to such questions is justifiable, and there is room in the computational toolbox for more than one tool, with the best choice depending on the application.

Tables 1 and 2 provide a list of recently proposed solvation models and classifies them according to the above scheme. For convenience, each row of the table is given a label. In some cases the label is based on a well established name or acronym (e.g., PCM, SM*x*), or an acronym to be used in this chapter. The acronyms to be used in labels are as follows:

SCME	single-center multipole expansion
DO	dipole only (SCME with $l \leq 1$)
DME	distributed multipole expansion
PCM	polarized continuum model
PE	Poisson equation (direct solution in physical space)
GB	generalized Born (approximation)
COSMO	conductor-like screening model
GCOSMO	generalized COSMO
/ST or /SA	plus surface tensions
SASA	solvent-accessible surface area
TBS	truncated basis set
SM*x*	Solvation model *x* (a name we give to our own parameterized GB/ST models)
AM1aq	Austin model 1 aqueous

In other cases we base the label on the author's initials. Next we comment on the methods in the tables and some aspects of the issues they raise.

The oldest methods are based on multipole expansions. Because these methods have been around for a long time, and because they lend themselves to appealing analytical solutions if further approximations are made, they have developed a history of sometimes being used with additional, unrealistic assumptions. The two most important of these further assumptions are truncating the multipole expansion at the dipole term (DO) and replacing the solute cavity by a sphere or ellipsoid. We now recognize, though, that these further approximations are usually unwarranted; indeed, we recommend that methods employing either or both of these approximations should be avoided for serious work.

TABLE I

Continuum models based on electrostatics only.

Label	Authors	Reference(s)	Elements			
			E	*S*	*L*	*N*
Models with *S* = B, C, and/or *L* = D, F						
PE1	Honig group	[149-151]	A	A	F	D
PE2	Rashin	[152]	A	A	F	D
PE3	McCammon group	[153]	A	A	F	D
PE4	Lim, Chan, Tole	[154]	A	A	F	D
DO	Kirkwood, Onsager	[61, 155]	A	C	F	D
DO1	Tapia, Goscinski	[91]	A	C	E	D
DO2	Szafran, Karelson, Katritzky, Zerner	[156, 157]	A	C	E	D
DO3	Wong, Wiberg, Frisch	[99, 158]	A	C	E	D
DO4	Freitas, Longo, Simas	[159]	A	C	E	D
DO5	Adamo, Lelj	[160]	A	C	E	D
GB1	Tucker, Truhlar	[161]	B	A	F	D
SCME	Kirkwood, Onsager	[61, 155]	A	C	F	D
SCME1	Rivail, Rinaldi	[88]	A	C	D	D
SCME2	Rivail, Terryn	[162, 163]	A	B	D	D
SCME3	Chipot, Rinaldi, Rivail	[100]	A	B	D	D
SCME4	Dillet, Rinald, Rivail	[164, 165]	A	A	D	D
SCME5	Mikkelsen et al.	[93, 106]	A	C	D	D
SCME6	Ford, Wang	[166]	A	B	D	D
SCME7	Pappalardo, Reguero, Robb, Frisch	[167]	A	B	D	D
DME	Huron, Claverie	[168]	A	C	F	D
DME1	Friedman	[169]	A	C	D	D
DME2	Gersten, Sapse	[170]	A	B	F	D
DME3	Karlström	[171]	A	C	B	D
DME4	Karelson, Tamm, Zemer	[172]	A	C	C	D
TBS	Kim, Bianco, Gertner, Hynes	[173, 174]	B	C	F	D

TABLE I (continued)
Continuum models based on electrostatics only.

Label	Authors	Reference(s)	Elements *E*	*S*	*L*	*N*
Models with untruncated, polarizable charge distributions and shape sensitivity						
PCM	Miertus, Scrocco, Tomasi	[175]	A	A	B	D
PCM2	Hoshi et al.	[144,176, 177]	A	A	C	D
PCM3	Ford and Wang	[178,1791	A	A	C	D
PCM4	Fox, Rösch, Zauhar	[180, 181]	A	A	C	D
PCM5	Negre, Orozco, Luque	[182, 183]	A	A	C	D
PCM6	Rashin, Bukatin, Andzelm, Hagler	[184]	A	A	A	D
PE4	Baldridge, Fine, Hagler	[185]	A	A	A	D
PE5	Chen, Noodleman, Case, Bashford	[186]	A	A	A	D
GB2	Peradejordi	[187]	B	A	C	D
GB3	Kozaki, Morihasi, Kikuchi	[188, 189]	B	A	C	D
DME5	Tapia, Colonna, Angyan	[112]	A	A	B	D
DME6	Dillet, Rinaldi, Ágyán, Rivail	[164]	A	A	A	D
COSMO	Klamt, Schüürmann	[190]	B	A	C	D

TABLE II
Classification of continuum models that include both electrostatic and non-electrostatic contributions.

Label	Authors	Reference(s)	Elements *E*	*S*	*L*	*N*
Models with $S \leq$ B, C and/or L = D, F						
SASA	Hermann	[64]	C	A	F	A
SASA1	Eisenberg	[191]	C	A	F	A
SASA2	Ooi, Oobatake, Némethy, Scheraga	[192]	C	A	F	A
GB/SA	Still et al.	[193]	B	A	F	C
SCME/RCR	Rinaldi, Costa Cabral, Rivail	[194]	A	B	D	B
SCME/RRR	Rivail, Rinaldi, and Ruiz-López	[95]	A	A	D	B
SCME/YGHB	Young, Green, Hillier, Burton	[195]	A	B	D	A
SCME/TSB	Tuñón, Silla, Bertrán	[196]	A	B	D	A
DME/ST/LCCP	Langlet, Claverie, Caillet, Pullman	[197]	A	A	D	B
DME/ST/SK	Sato, Kato	[198]	A	C	B	B
PCM7	Purisima and Nilar	[199]	A	A	F	C
PCM8	Varnek et al.	[200]	A	A	F	A
KH	Karlström and Halle	[201]	B	C	D	B
BCN	Basilevsky, Chudinov, Newton	[110]	B	C	C	B
Models with untruncated, polarizable charge distributions and shape sensitivity						
PCM/ST/FTP	Floris, Tomasi, and Pascual-Ahuir	[202, 203]	A	A	B	B
PCM/ST/OAT	Olivares del Valle, Aguilar, Tomasi	[97, 103, 104]	A	A	A	B
PCM/ST/YGHB	Young, Green, Hillier, Burton	[195]	A	A	B	B
PCM/ST/A	Amovilli	[204]	A	A	B	B
PCM9/ST	Bachs, Luque, and Orozco	[205]	A	A	B	A
PCM10/ST	Orozco, Luque, coworkers	[205-209]	A	A	C	A
GB/ST/SM1-3.1	Cramer and Truhlar	[210-215]	B	A	C	A
GB/ST/SM4&5	Cramer and Truhlar	[213, 216-218]	B	A	A	A
PCM/D	Rauhut, Clark, Steinke	[219]	A	A	C	B
PE/ST/FGH	Friesner, Goddard, Honig	[220]	A	A	A	C
AM1aq	Dixon, Leonard, Hehre	[221]	B	A	C	A
GCOSMO	Truong and Stefanovich	[222, 223]	B	A	A	C

If the cavity is not simplified and terms are added to the multipole expansion until it converges, the result is exact and none of the unphysical consequences of a truncated multipole expansion remain. One difficulty with this approach though is that the multipole series is not necessarily convergent at small distances. A second is that for large molecules, a single-center expansion is a very unnatural way to represent the electrostatics. Even very small molecules may require large numbers of terms in the multipole expansion to converge it. For example, a treatment of electron scattering by acetylene that employed a single-center multipole expansion contained terms with l up to 44 in an attempt to converge the anisotropy of the electrostatics [224].

One way around the slow convergence of single-center expansions is a multi-center multipole expansion [225-229]. Several workers have explored the utility of DME within the SCRF framework [112, 164, 171]. Of course, when the multipoles do not reside at atomic positions, it is clear that calculation of such quantities as analytic energy derivatives will become more difficult.

Alternatively one can avoid multipole expansions altogether. There are two main approaches in use for solving the electrostatic problem without a multipole expansion. One of these solves the Poisson equation in terms of virtual charges on the surface of the primary subsystem. This is usually called the polarized continuum model (PCM) in quantum chemistry although it is called a boundary element method in the numerical analysis literature. The second approach solves the Poisson equation directly in the volume of the solvent, e.g., by finite differences. The latter approach will be called a Poisson equation (PE) approach. We should keep in mind, however, that SCME, DME, PCM, and PE methods will all lead to (the same) accurate electrostatics if the numerical methods are taken to convergence and there is no difference due to the handling of other “details.”. One such detail that might be mentioned is charge penetration outside the cavity. By construction in the PCM model, the small amount of electronic density outside the cavity is eliminated from the surface charge computations and as a result the solute bears a very small charge. Tomasi has emphasized the need to correct for this phenomenon [79], but his approach has yet to be adopted by other groups doing PCM calculations.

As mentioned above, the PCM is based on representing the electric polarization of the dielectric medium surrounding the solute by a polarization charge density at the solute/solvent boundary. This solvent polarization charge polarizes the solute, and the solute and solvent polarizations are obtained self-consistently by numerical solution of the Poisson equation with boundary conditions on the solute-solvent interface. The free energy of solvation is obtained from the interaction between the polarized solute charge distribution and the self-

consistent surface charge distribution [175]. The physics is the same for the PCM and PE approaches (and for the fully converged SCME or DME, for that matter), although the numerical methods are different.

The next question to be discussed was already mentioned in Section 2.1, namely, since the electrostatic problem, with its sharp boundary and its homogeneous solvent dielectric constant, already represents a somewhat unrealistic idealization of the true molecular situation, how important is it to solve that problem by exact electrostatics? We would answer that this is not essential. Although it presumably can't hurt to solve the electrostatics accurately, except perhaps by raising the computer time, it may be unnecessary to do so in order to represent the most essential physics, and a simpler model may be more manageable, more numerically stable, and even more interpretable. This is the motivation for the GB approximation and COSMO.

GB-like approximations [41, 71, 119, 161, 187, 189, 230-233] may be derived from eq (1) by using the concept of dielectric energy density, as in the work of Bucher and Porter [130], Ehrenson [131], and Schaefer and Froemmel [234]. As the GB methodology has been extensively reviewed in the recent past [81, 83, 213], we confine our presentation to a very brief discussion of the key aspects of the theory. The polarization free energy in the GB model is defined as

$$G_P(aq) = -\frac{1}{2}\left(1-\frac{1}{\varepsilon}\right)\sum_{k,k'} q_k q_{k'} \gamma_{kk'}, \qquad (54)$$

where ε is the solvent dielectric constant, q is the net atomic charge, k labels an atomic center, and $\gamma_{kk'}$ is a coulomb integral, which in atomic units is the reciprocal of an effective radius (monatomic diagonal terms) or effective distance (diatomic off-diagonal terms). The descreening of individual parts of the solute from the dielectric by other parts of the solute is accounted for in these effective quantities. In particular, in our work we use an empirical functional form for γ that was proposed by Still et al. for their GB/SA model [193]. The present authors modified that form in several ways, including making it a function of atomic partial charges, in the development of the SM1 [210], SM1a [210], SM2 [211], SM2.1 [214], SM2.2 [215], SM3 [212], SM3.1 [214], and SM4 [213, 216, 217] GB/ST solvation models. The SM5 solvation model [218] further modifies γ so that it may be expressed purely as a function of geometry, i.e., it has no explicit dependence on elements of the density matrix, thereby facilitating the calculation of analytic energy derivatives. The SM4 and SM5 solvation models are based on Class IV charge models [235], which provide the best available estimates of partial charges for electrostatics calculations.

The E, N, and P terms are then obtained from the density matrix **P** of the aqueous-phase SCF calculation as

$$G_{ENP} = \frac{1}{2}\sum_{\mu\nu} P_{\mu\nu}\left(H_{\mu\nu} + F_{\mu\nu}\right) + \frac{1}{2}\sum_{k,k'\neq k} \frac{Z_k Z_{k'}}{r_{kk'}} \tag{55}$$

where **H** and **F** are respectively the one-electron and Fock matrices, μ and ν run over valence atomic orbitals, and Z_k is the valence nuclear charge of atom k (equal to the nuclear change minus the number of core electrons). When the net atomic charge q in equation 54 is determined by Mulliken analysis of the NDDO wave function, the Fock matrix is simply given by [71, 210, 236]

$$F_{\mu\nu} = F^{(0)}_{\mu\nu} + \delta_{\mu\nu}\left(1-\frac{1}{\varepsilon}\right)\sum_{k',\mu'\in k'}\left(Z_{k'} - P_{\mu'\mu'}\right)\gamma_{kk'}, \quad \mu \in k \tag{56}$$

where $\delta_{\mu\nu}$ is the Kronecker delta function. This approach was used in the SM1, SM1a, SM2, and SM3 solvation models. The SM4 alkane models [216, 217] an interim SM4 water model specific for selected kinds of {C, H, O} compounds [213], and SM5 models, on the other hand, use Class IV Charge Model 1 (CM1) partial atomic charges [213, 235], which provide a more accurate representation of the electronic structure. This renders eq 56 somewhat more complex [216], but does not change its basic form. In all SM*x* models, the density matrix is determined self-consistently in the presence of solvent.

Values of G_{ENP} calculated from the GB approximation compare well to values obtained from numerical solution of the Poisson equation for similar collections of point charges [83, 237, 238]. A very promising extension of the GB methods is provided by a new scaled pairwise approximation to the dielectric screening integrals [215].

The COSMO method is a solution of the Poisson equation designed primarily for the case of very high ε [190]. It takes advantage of an analytic solution for the case of a conductor ($\varepsilon = \infty$). The difference between $(1-\frac{1}{\varepsilon})$ for the case of $\varepsilon = 80$ and $\varepsilon = \infty$ is only 1.3%, so this is a good approximation for water. Its use for the treatment of nonpolar solvents with $\varepsilon \approx 2$ depends on further approximations which have not yet been sufficiently tested to permit an evaluation of their efficacy.

Finally we address the issue of contributions. In our view it is unbalanced to concentrate on a converged treatment of electrostatics but to ignore other effects. As discussed in section 2.2, first-solvation-shell effects may be included in continuum models in terms of surface tensions. An alternative way to try to include some of them is by scaled particle theory and/or by some *ab initio* theory

of dispersion. Table 2 summarizes continuum models that attempt to treat both electrostatic and first-solvation-shell effects.

Some models carry the surface tension approach to extreme, and attempt to include even the electrostatic contributions in the surface tensions. These pure SASA models are obviously limited in their ability to account for such phenomenon as dielectric screening, but they have the virtue of being very easy to compute. Thus, they can be used to augment molecular mechanics calculations on very large molecules with a qualitative accounting for solvation.

Also within the molecular mechanics framework is the molecular-mechanics-type GB/SA model of Still et al. [193] In this instance, the electrostatics are handled by a Generalized Born model, but the atomic charges are parametric. They are chosen in such a way that Still et al. assign only a single surface tension to the entire molecular solvent-accessible surface area; this is also done in the PE/ST/FGH and PCM10 models. All these authors rationalize this by calling the ST part a hydrophobic term, but it is clear that other non-electrostatic effects must then be being absorbed into the cavity parameterization and, in Still et al's MM case, possibly into the partial atomic charges.

Many groups have chosen to specifically calculate cavitation and/or dispersion terms. The former typically are computed by the scaled particle theory, following Pierotti [142], while several different approaches have been formulated for the latter. Ultimately, however, there are non-electrostatic components of the solvation free energy remaining that do not lend themselves to ready analysis. Bearing that in mind, it is not clear that there is much point in spending resources calculating any one non-electrostatic component more rigorously than the others. Thus, the most general approach is to parameterize *all* non-electrostatic effects into atomic surface tensions (so as to reproduce experimental free energies of solvation after the electrostatic components have been removed). This is the philosophy guiding the SM*x*, AM1aq, PCM9/ST, PCM10/ST, and SCME/TSB models, and an increasing number of workers appear to be moving in this direction.

4 Solvation effects on equilibrium properties

As discussed in Section 2, one key assumption of reaction field models is that the polarization field of the solvent is fully equilibrated with the solute. Such a situation is most likely to occur when the solute is a long-lived, stable molecular structure, e.g., the electronic ground state for some local minimum on a Born-Oppenheimer potential energy surface. As a result, continuum solvation models

based on reaction fields should be especially useful for the prediction of solvent effects on equilibrium constants.

Equilibria may take a number of forms—constitutional, tautomeric, conformational, etc. For any equilibrium problem in solution, one may consider the free energy cycle depicted in the figure below, where A and B label different molecules or different isomers of the same molecule, depending on the type of equilibrium. The scheme below shows that the free energy change for a reaction or tautomerization on going from the gas phase into solution is equal to the difference in the free energies of solvation of the initial and final species (the figure depicts a unimolecular reaction, but this statement is true in the general case).

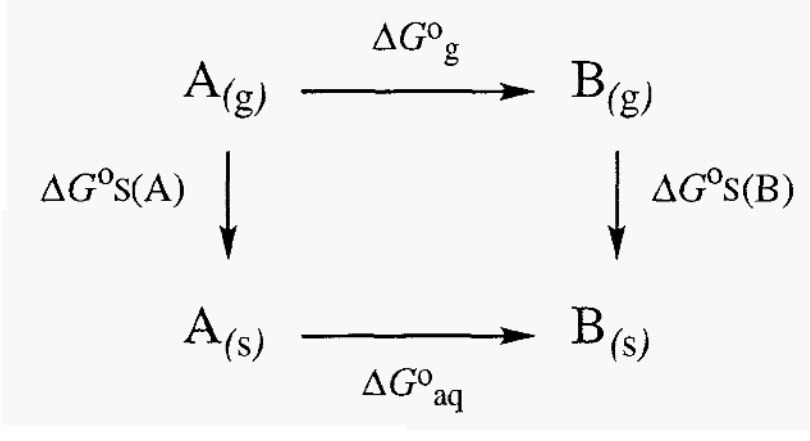

$$\Delta G^o_{aq} = \Delta G^o_g + \Delta G^o_S(B) - \Delta G^o_S(A)$$

Tautomeric equilibria involving populations of isomers that differ by bond connectivity are of special interest for the study of solvent effects, and such equilibria involving heterocycles have proven to be a favorite testing ground for developers of continuum solvation models. For protomeric heterocyclic equilibria, this is at least partly due to the very large changes in one-electron properties (e.g., the dipole moment) that affect the solvation free energy when the proton substitution pattern changes.

In this section we will consider only equilibria in which the number of moles of solute does not change. In such cases the population of a given contributor to the equilibrium may be calculated by using a standard Boltzmann formalism, i.e., the fraction of species A is

$$F(\mathrm{A}) = \frac{e^{-G^{\circ}_{\mathrm{A}}/RT}}{\sum_{\mathrm{B}} e^{-G^{\circ}_{\mathrm{B}}/RT}} \tag{57}$$

where G may be either a gas phase or a solution value, and the sum over B runs over all equilibrium contributors. In below discussion we will take %(A) ≡ 100 F(A). When free energies in both the gas phase and in solution are available, one may calculate [239] the absolute free energy of solvation, $\Delta G^{\circ}_{\mathrm{S}}$, as

$$\Delta G^{\circ}_{\mathrm{S}} = -RT \ln\left\{\sum_{\mathrm{A}}\left[\frac{e^{-G^{\circ}_{gas}(\mathrm{A})/RT}}{\sum_{\mathrm{B}} e^{-G^{\circ}_{gas}(\mathrm{B})/RT}}\right] e^{-\Delta G^{\circ}_{\mathrm{S}}(\mathrm{A})/RT}\right\} \tag{58}$$

where the sums over both B and A run over all contributors.

This section will focus on the application of dielectric continuum models to equilibria like those described above. A special effort will be made to highlight investigations that compared two or more solvation models. We emphasize that some care must be taken to distinguish the degree to which different continuum models have been extended to account for non-electrostatic effects, since these effects may certainly play a large role in some of the equilibria under discussion. Those continuum models that consider only electrostatics are of limited applicability unless non-electrostatic effects cancel for all equilibrium contributors.

We will begin with a discussion of reaction equilibria, including acid-base reactions and more complex bond-making/bond-breaking reactions. We will then move on to tautomeric equilibria. We note that Reichardt [240] has provided a thorough compilation of many equilibria, including most of those discussed below, where solvent effects had been studied experimentally and/or using some theoretical model, as of 1990. On the theoretical side, at least, the number of systems studied has greatly expanded since then.. Whereas Reichardt summarizes the use of linear free energy relationships for predicting such equilibria, a large amount of the recent work is based on SCRF models.

4.1 REACTION EQUILIBRIA

As one might expect, reactions that create, destroy, or separate charge tend to exhibit very large solvation effects. The most common examples of such reactions

are Brønsted acid-base equilibria. A particularly striking example is available for the special case of an *internal* acid-base proton transfer, which is also a special case of a tautomeric equilibrium. This occurs, for example, when amino acids are placed in water. Several continuum modeling studies have focused on this equilibrium for glycine, and they are summarized in section 4.1.1. Intermolecular proton transfers have also been the subject of several studies, particularly transfers between amine bases; these investigations are described in section 4.1.2.

4.1.1 Intramolecular proton transfer

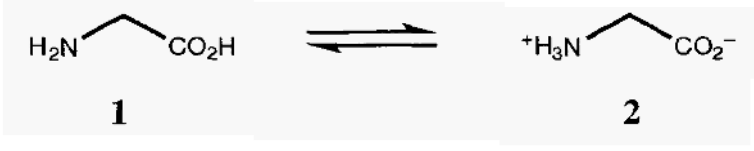

At biological pH, glycine exists exclusively in its zwitterionic form **2** [241], whereas in the gas phase, only the non-zwitterionic species **1** is observed [242]. In the absence of solvation, the zwitterion is not a stationary point, but instead undergoes spontaneous proton transfer back to the neutral form. In an early study, Bonaccorsi et al. [243], using the PCM model, showed that a continuum solvation model can account for the stability of the zwitterion in aqueous solution. Although they made some comparison to the experimental enthalpy for the transfer of **1** from the gas phase to **2** in aqueous solution (-19.2 ± 1 kcal/mol) [244], this particular study emphasized the sensitivity of the computational results to solute geometries (many of those discussed were unoptimized), basis set, and cavity size. Thus, the calculated gas-phase proton transfer energy ranges from 20 to 40 kcal/mol at the HF/4-31G [245] level, to 65 to 90 kcal/mol at the HF/STO-3G level. Different prescriptions for choosing the zwitterion cavity yielded solvation free energies varying from −36.2 kcal/mol to −57.3 kcal/mol. Since the zwitterion is not stationary in the gas phase, the experimental enthalpy of transfer cited above cannot be separated into proton transfer and solvation components (and the entropic aspects are similarly unclear, making comparison to reaction field free energies results difficult). Hehre et al. [246] used the AM1-SM2 model to study the solvation of neutral and zwitterionic glycine, and found the zwitterionic form to be better solvated by 25 kcal/mol in aqueous solution. Adding this differential free energy of solvation to the relative gas phase free energy difference (using a frozen zwitterion geometry) of 17.8 kcal/mol favoring the neutral form at the HF/3-21+G level, they predict the zwitterion to be the preferred form in aqueous solution by 7.6 kcal/mol.

4.1.2 Intermolecular proton transfer

In the gas phase, simple deprotonations tend to be barrierless reactions leading to a high-energy separated proton and anion, but solvation can change the situation even qualitatively. Pietro has emphasized the pedagogical utility of employing a continuum solvation model (in this case the SM1 model) in a computational study on the deprotonation of nitromethane [247]. When reaction field calculations are used to calculate standard state free energies of conjugate acids and bases in solution, this permits direct calculation of the acid dissociation constant (pK_a). Such calculations of the absolute pK_a are notoriously difficult, since very high levels of theory are required to accurately calculate the gas-phase component of proton affinities and since solvation energies of ions are very large, so that even relative errors in solvation energies can be large on an absolute scale. As a result, most methods for predicting pK_a values tend to be empirical in nature [248-250]. A simpler alternative to calculations of absolute pK_a's is to examine trends in pK_a values for related molecules. In this vein, Rajasekaran et al. [251] have used the finite difference Poisson-Boltzmann method to examine differences in pK_a values for aliphatic dicarboxylic acids. They identify the importance of solvent screening of charge-charge interactions internal to the solute. Urban et al. [252] have employed a similar approach in examining the relative pK_a values for phenol and *ortho-, meta-,* and *para*-fluorophenol, using the SM2 and SM3 quantum mechanical solvation models, and the physically similar molecular mechanics GB/SA model. They noted in particular the importance of accounting for non-electrostatic hydrophobic interactions of the fluorine atom. The QM models agree with experiment to within about 1 kcal/mol for the effect of solvation on the relative pK_a values. The MM model does similarly well when charges derived from fitting to the molecular electrostatic potential (ESP) are employed.

Other workers have considered proton transfer reactions between different bases and the effect of solvation on these processes. Terryn and Rivail [253], Galera et al. [254], Pascual-Ahuir et al. [255], Tuñón et al. [256], and Young et al. [195] have all focused on the interesting aqueous basicity trend of the series ammonia, methylamine, dimethylamine, and trimethylamine. In the gas phase, it is well established that the order of basicity for these amines is $Me_3N > Me_2NH > MeNH_2 > NH_3$ [257, 258]. This may be understood on the basis of simple polarizability arguments. However, in aqueous solution, the basicity ordering changes to $MeNH_2 \approx Me_2NH > Me_3N \approx NH_3$ [259]. All of these studies indicate that changes in basicity are dominated by the electrostatic component of the free energy of solvation of the relevant ammonium ions. In aqueous solution, the smaller ions are better solvated, and as a result have lower free energies. These

studies also emphasize, however, how sensitive the results are to choices of basis set and cavity size. In particular, Young et al. [195] compared an ellipsoidal cavity SCRF model with multipole expansions of $l = 1$ and $l = 6$ to the generalized-cavity PCM approach. The ellipsoidal cavity model predicts considerably larger differential solvation free energies between different members of the homologous amine series than does the PCM model, but these differences tend to cancel so that both PCM and the $l = 6$ expansion gave qualitatively correct answers (i.e., proper sign and within about 1 pK_a unit for ΔpK_a on going from the gas phase to aqueous solution). The $l = 1$ expansion, i.e., an ellipsoidal Kirkwood-Onsager model, was less satisfactory, and did particularly poorly when comparing ammonia and methylamine.

The present authors, using the SM*x* series of models, have considered aqueous solvation effects on proton transfer for these same amines, together with several other bases, and have arrived at similar conclusions to those detailed above [83, 236, 260].

Tuñón et al. have considered the inversion of the alcohol acidity scale on passing from the gas phase to solution [261]. They used gas-phase geometries, the PCM method for electrostatics (with a radius for O of 1.68 Å in the alcohol and 1.4 Å in the conjugate base), and separate estimates of dispersion and cavitation energies. They found that increasing the size of the alkyl group decreases the solvation energy of the conjugate base in solution and concluded that this is the primary source of the acidity order.

Finally, studies of proton transfer reactions in aqueous solution where an individual water molecule plays a role that distinguishes it from the bulk solvent have also recently appeared. Rivail et al. [105, 262] have examined the water-assisted ionization of HF and HCl in both nonpolar and polar solutions. Using a generalized multipole reaction field method (with multipoles up to $l = 6$) within an ellipsoidal cavity (to facilitate geometry optimization), they concluded that ionization of HCl requires the specific assistance of two water molecules, and that the resultant cation is better described as $H_5O_2^+$ than as $(H_3O^+)\bullet H_2O$. They also concluded that ionization of HF does not proceed in a polar continuum even with two explicit water molecules included in the cavity. This may be compared to a study by Ando and Hynes [263] in which the bulk water solvent is treated not within the framework of a reaction field formalism, but instead is represented as a generalized solvent coordinate [264]. The energetics associated with the solvent coordinate were determined from Monte Carlo simulations using explicit water molecules for various points along an assumed proton transfer reaction path. Ando and Hynes also included two explicit water molecules in their quantum mechanical treatment. Their key conclusions were that two proton transfer steps

occur adiabatically; the first has a negligible free energy barrier and proceeds with significant motion along the solvent coordinate (i.e., solvent structural rearrangement is required), while the second free energy barrier is about 0.9 kcal/mol and arises primarily from the requirement for nuclear reorganization of the two water molecules. The free energy change associated with this ionization was calculated to be −6.9 kcal/mol (an estimate of −7.5 kcal/mol was offered that includes complete separation of the ions), which may be compared with the experimental ionization free energy of −8 to −10 kcal/mol [265]. Ando and Hynes' findings agree with those of Rivail et al. in that the transferred proton is associated about equally strongly with both of the explicit water molecules; however Ando and Hynes observe this to be the case only after inclusion of zero point vibrational energy, while Rivail et al. find only a single equilibrium structure in the appropriate region of the $(Cl^-)\bullet H_5O_2^+$ potential energy surface.

4.2 TAUTOMERIC EQUILIBRIA

A tautomeric equilibrium is a unimolecular equilibrium in which the various contributors differ based upon bond connectivity. In the special case of a protomeric tautomeric equilibrium, they differ only in how many protons are attached to each heavy atom. In-text figures throughout this section illustrate molecules for which multiple tautomers exist. When the molecules of interest are heterocycles, different tautomers may exhibit very large differences in electronic properties [266]. In particular, they may span a wide range of polarities. That being the case, tautomeric equilibria can be quite sensitive to solvation effects, and they have thus proven to be attractive testing grounds for continuum solvation models.

In a recent review [83], the present authors discussed the tautomeric equilibria of 2-hydroxypyridine/2-pyridone and the 5-(2*H*)-isoxazolone system in considerable detail, focusing on the application of several different continuum solvation models. The following presentation will be somewhat more broad in terms of the different equilibria discussed and will not recapitulate all of the analysis previously presented for the above two systems.

Section 4.2.1 will be devoted to heterocycles, section 4.2.2 will cover other kinds of protomeric tautomeric equilibria (e.g., enol/ketone, formic acid, formamidine, etc.), and section 4.2.3 will discuss an example of a ring/chain tautomeric equilibrium. The order of presentation will be approximately by increasing molecular weight within each section. A review by Kwiatkowski et al. [267] covers work on formamide, pyridines, pyrimidines, purines, and nucleic

acid bases up to 1984, so for these systems our focus will predominantly be on more recent investigations.

We note one general point prior to addressing individual systems. Computational studies aimed at providing quantitative predictions of equilibrium populations in solution *must accurately predict total free energies in solution.* In particular, if the theory employed involves calculating solvation free energies to be added to a gas-phase potential energy surface with thermal rovibrational effects included (and essentially all calculations in solution may be viewed as conforming to this separation of components), then either the gas-phase free energies and the free energies of solvation must both be calculated accurately, or errors in one part of the calculation must be offset by errors in the other. Clearly, the former situation is the more desirable. Where possible, we will provide some analysis of the quality of the gas-phase portions of the following calculations as well. Naturally, when the point of the calculation is merely to provide qualitative indications of relative free energies of solvation for different tautomers, requirements on the accuracy of the levels of theory are less stringent.

4.2.1 Heterocycles

This section is divided into eight subsections, covering imidazoles, pyrazoles, isoxazoles, oxazoles, triazoles, tetrazoles, pyridines, and pyrimidines, purines, and nucleic acid bases respectively.

4.2.1.1 Imidazoles

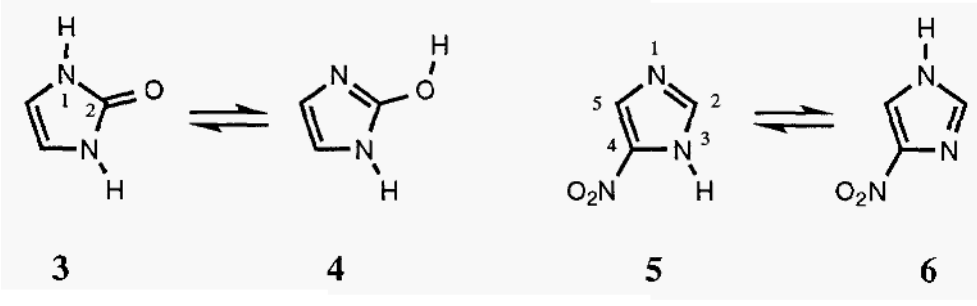

3 **4** **5** **6**

Two tautomeric equilibria have been considered for substituted imidazoles, that between 2-imidazolone **3** and its 2-hydroxyimidazole tautomer **4** [268] and also that between the 1*H* and 3*H* tautomers of 4-nitroimidazole, **6** and **5,** respectively [269, 270]. Karelson et al. used the DO2* model with a spherical cavity of 2.5 Å radius and found 2-imidazolone to be better solvated than its tautomer by 7.7 kcal/mol at the AM1 level. [The asterisk in DO2* indicates that the reaction field

was derived from solution of an incorrect non-linear Schrodinger equation, i.e., not eq 30 [157]. In the DO2* model, a factor of 0.5 precedes the operator K_{op} in eq 30; the result is reduced polarization of the wave function in response to solvation.] AM1 further predicts the gas phase energy difference to favor the oxo tautomer by about 8 kcal/mol. The observed tautomer in solution is the oxo tautomer [266].

Using the same theoretical model, Karelson et al. [269] and later Rzepa et al. [270] examined 4-nitroimidazole. The latter work corrected incomplete geometry optimizations present in the former study. In this instance, AM1 predicts **5** to be 1.4 kcal/mol lower in relative energy than **6.** However, the DO2* model predicts the aqueous solvation free energies to be –25.3 and –7.1 kcal/mol for **6** and **5,** respectively, rendering **6** considerably lower in energy than **5** in solution, which agrees with the experimental situation.

It is clear in both of these studies that the small cavity size (which fails to entirely contain all of the atoms given standard van der Waals radii) causes electrostatic solvation free energies to be seriously overestimated—the difference in the 4-nitroimidazole system seems much too large to be physically reasonable. This overestimation would be still *more* severe were a correct DO model to have been used (i.e., one which accounted self-consistently for the full solute polarization using eq 30). Nevertheless, the DO2* results may be considered qualitatively useful, to the extent that they identify trends in tautomer electrostatic solvation free energies.

One measure of the inaccuracy associated with the small cavity radius may be had from the calculations of Orozco et al. [207], who also studied the 4-nitroimidazole system using the PCM8/ST model. The general cavity in this case was constructed from atom-centered spheres having typical van der Waals radii [207]. At the AM1 level, the differential electrostatic free energy of hydration is predicted to be only 4.5 kcal/mol; this may be compared to the value of 18.2 kcal/mol noted above for the DO2* model. Orozco et al. [207] also included first-solvation-shell effects, which they found to favor **5** by 1.2 kcal/mol, leading to a net differential free energy in solution (AM1 + PCM8/ST) of 2.1 kcal/mol.

4.2.1.2 Pyrazoles

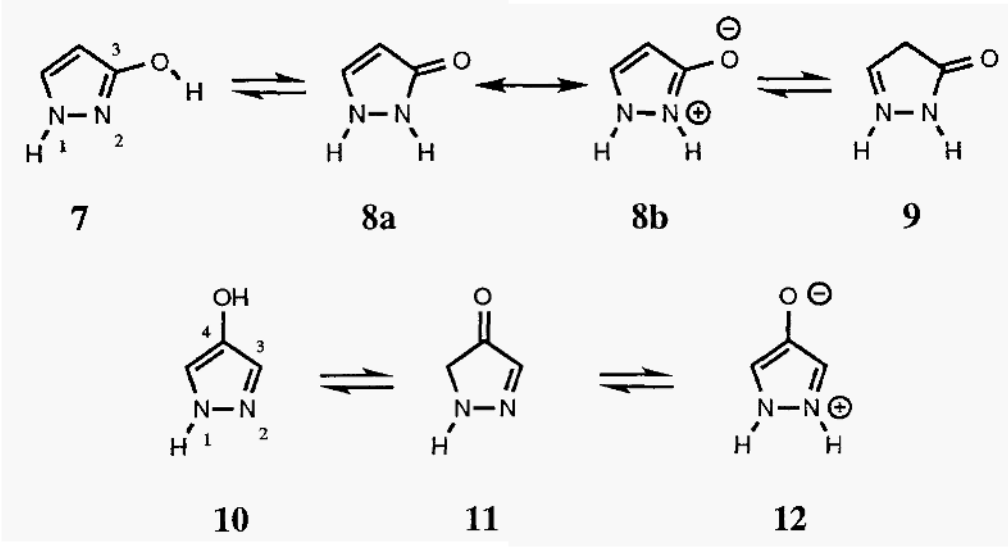

Karelson et al. [268] also used the AM1 DO2* method with a spherical cavity of 2.5 Å radius to study tautomeric equilibria in the 3- and 4-hydroxypyrazole systems, **7-9** and **10-12,** respectively. Rzepa et al. [270] later corrected the results for incomplete geometry optimization in the latter heterocycle. Although the observed [266] forms in aqueous solution are the oxo tautomer **8** (i.e., the pyrazolone) in the first case and the zwitterion **12** in the latter case, gas-phase AM1 calculations predict these tautomers to be much higher in relative energy than the corresponding hydroxy tautomers **7** and **10,** respectively. In each case, it was found that the DO2* method successfully predicted the observed aqueous tautomer. However, the DO2* electrostatic solvation free energy for **12** was predicted to be –57.3 kcal/mol! As for the nitroimidazole results discussed in the last section, this number is incredibly large, probably as a result of the small cavity radius chosen. However, so large a solvation free energy was required in order to overcome a very unfavorable gas-phase energy predicted by AM1 (about 40 kcal/mol higher than the other two tautomers). It seems likely that the AM1 relative energy is inaccurate, given the experimental situation and the very small likelihood of two tautomers differing in solvation free energy by so large an amount.

One qualitative result of particular interest arises in the study of 3-hydroxypyrazole. The electronic structure of the oxo tautomer **8** may be thought of as having two mesomeric (i.e., resonance) contributors **8a** and **8b,** as illustrated

above. In the gas phase, Karelson et al., using the DO2* model, found the C–O bond length in **8** increased by 0.098 Å on going from the gas phase into a solution with a dielectric constant ε of 78.4, which implies increased contribution from the zwitterionic mesomer.

Parchment et al. [271] have provided more recent calculations on the 3-hydroxypyrazole equilibrium at the ab initio level. They noted that tautomer **9,** which was not considered by Karelson et al. [268], is the lowest-energy tautomer in the gas phase at levels of theory (including AM1) up to MP4/6-31G**//HF/3-21G [271]. Although **8** is the dominant tautomer observed experimentally in aqueous solution, in the gas phase **8** is predicted to be nearly 9 kcal/mol less stable than **9** at the MP4 level [271]. Using a DO model with an unphysically small cavity radius of 2.5 Å, Parchment et al. [271] were able to reproduce at the ab initio level the AM1-DO prediction of Karelson et al. [268], namely that **8** is the most stable tautomer in aqueous solution. With this cavity, though, **8** is predicted to be better solvated than **9** by **–**22.2 kcal/mol [271]. This result is inconsistent with molecular dynamics simulations with explicit aqueous solvation [271], and with PCM and SCME calculations with more reasonable cavities [271]; these predict that **8** is only about 3 kcal/mol better solvated than **9.** In summary, the most complete models used by Parchment et al. do not lead to agreement with experiment

The comparisons made by Parchment et al. [271] illustrate the importance of combining electronic polarization effects with corrections for specific solvation effects. The latter are accounted for parametrically by the explicit simulation, but that procedure cannot explicitly account for the greater polarizability of tautomer **8.** The various SCRF models *do* indicate **8** to be more polarizable than any of the other tautomers, but polarization alone is not sufficient to shift the equilibrium to that experimentally observed. Were these two effects to be combined in a single theoretical model, a more accurate prediction of the experimental equilibrium would be expected.

4.2.1.3 Isoxazoles

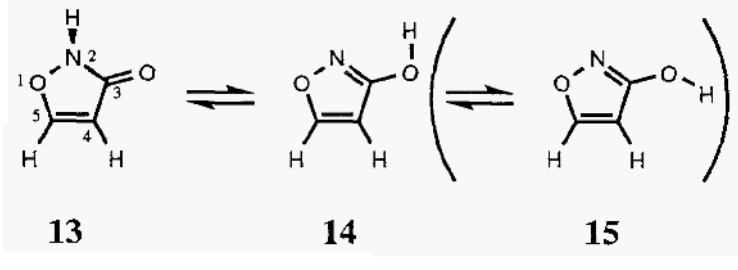

Karelson et al. [268] used the AM1 DO2* method with a spherical cavity of 2.5 Å, radius to study tautomeric equilibria in the 3-hydroxyisoxazole system (the keto tautomer **13** is referred to as an isoxazolone). AM1 predicts **13** to be 0.06 kcal/mol lower in energy than **14** in the gas phase. However, the AM1 dipole moments are 3.32 and 4.21 D for **13** and **14,** respectively. Hydroxy tautomer **14** is better solvated within the DO2* model, and is predicted to be 2.6 kcal/mol lower in energy than **13** in a continuum dielectric with $\varepsilon = 78.4$. Karelson et al. note, however, that the relative increase in dipole moment upon solvation is larger for **13** than for **14** (aqueous AM1 dipole moments of 5.05 and 5.39 D, respectively). This indicates that the relative magnitude of gas-phase dipole moments will not always be indicative of which tautomer will be better solvated within a DO solvation approach—the polarizability of the solutes must also be considered. In any case, the DO2* model is consistent with the experimental observation [266] of only the hydroxy tautomer in aqueous solution.

Woodcock et al. [272] also studied the 3-hydroxyisoxazole system, making several comparisons to the above work of Karelson et al. They noted in particular that the hydroxy tautomer has two possible rotamers about the C–O bond, one which places the hydroxyl proton syn to nitrogen (**14**) and one which places it anti (**15**). Karelson et al. considered only **14,** which is 4.3 kcal/mol lower in energy in the gas phase at the MP4/6-31G**//HF/3-21G level. Woodcock et al. also demonstrated that AM1 agrees poorly with this correlated ab initio level of theory for the relative energies of **13** and **14:** the MP4 calculations predict **13** to be 7.1 kcal/mol higher in energy than **14.** Finally, AM1 also disagrees with HF/6-31G**//HF/3-21G with respect to the molecular dipole moments. Tautomers **14** and **13** are predicted to have gas-phase dipole moments of 2.5 and 3.8 D respectively at the ab initio level, reversing the order found at the AM1 level. Moreover, the anti hydroxyl tautomer **15** has a gas-phase dipole moment of 6.2 D at the HF/6-31G**//HF/3-21G level! Thus, when Woodcock et al. considered the effects of solvation using a correct DO model (as opposed to DO2*) but continuing with the small spherical cavity radius of 2.5 Å used by Karelson et al., they find the relative energies in aqueous solution of **14,15,** and **13** to be 12.8, 0.0, and 1.8 kcal/mol respectively. Note the difference between AM1 and the ab initio level of theory with respect to **14** vs. **15:** the former predicts **15** to be the more stable tautomer by 2.6 kcal/mol while the latter predicts a reversal of this ordering by about 15 kcallmol. Note as well that the relative energies of the two hydroxyl rotamers differ by 12.8 kcal/mol—this is a very large difference in electrostatic solvation free energies for rotamers, and, if we recall that the DO model calculates the free energy of solvation as being proportional to the square of the molecular dipole moment and inversely proportional to the cube of the

cavity radius., we can reasonable conclude that this large difference reflects both the problems of truncating the multipole expansion at the dipole and of choosing unreasonably small cavity radii.

Woodcock et al. also examined a different continuum model, namely the PCM model with a solvent accessible surface area defined according to the prescription of Aguilar and Olivares del Valle [273] based on basis set and partial atomic charge. This much more realistic cavity still predicts **13** to be better solvated than **14,** but by only 2.4 kcal/mol at the HF/6-31G**//HF/3-21G level. When combined with the MP4 gas phase energies, **14** is predicted to predominate by 4.7 kcal/mol. This is remarkably consistent with molecular dynamics simulation studies carried out by Woodcock et al. using frozen ab initio geometries for the solutes, solute partial atomic charges derived from electrostatic potential fitting [274], and the Transferable Intermolecular Potential 3-Point (TIP3P) [275] water model with the AMBER [276] force field. The simulations predict **13** to be better solvated than **14** by 2.2 ± 0.4 kcal/mol. They also make the much more reasonable prediction that the difference in solvation free energies for the two hydroxyl rotamers is only 1.7 ± 0.5 kcal/mol, favoring the anti rotamer. When either the PCM or the MD solvation results are added to the MP4 relative gas-phase energies, **14** is predicted to be the most stable in aqueous solution.

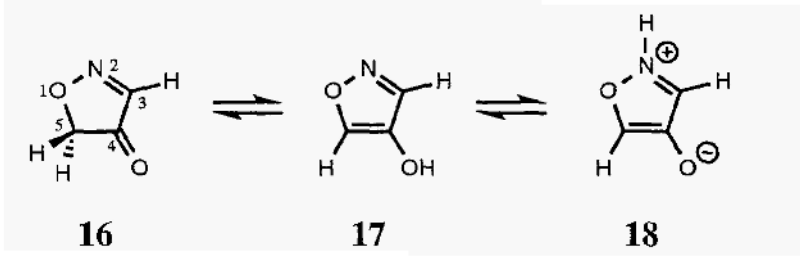

Karelson et al. [268] used the AM1 DO2* method with a spherical cavity of 2.5 Å radius to study tautomeric equilibria in the 4-hydroxyisoxazole system (they did not specify which hydroxyl rotamer they examined). Tautomer **17** predominates in aqueous solution. Although AM1 predicts **16** to be about 10 kcal/mol more stable in the gas-phase than **17,** its dipole moment is only predicted to be 0.68 D. Tautomer **17** has a predicted dipole moment of 2.83 D in the gas-phase. With the small cavity, the two dipole moments increase to 0.90 and 4.56 D, respectively, and this is sufficient to make **17** 0.3 kcal/mol more stable than **16** in solution. Zwitterion **18** is much better solvated than either of the other two tautomers, but AM1 predicts its gas-phase relative energy to be so high that it plays no equilibrium role in either the gas phase of solution.

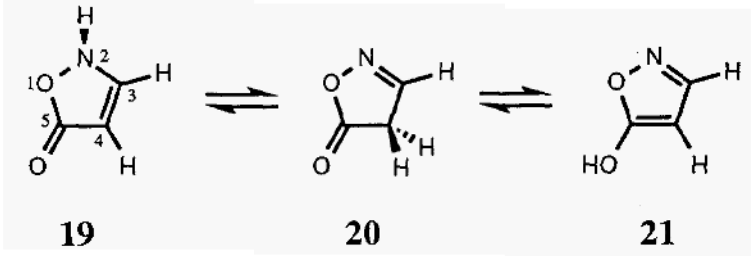

19 **20** **21**

The present authors have discussed the 5-hydroxyisoxazole tautomeric equilibrium at length in a previous review [83]. For the sake of completeness, we note that Karelson et al. [268] studied this equilibrium with the DO2* model and a spherical cavity radius of 2.5 Å and came to the conclusion that **19** should slightly predominate (hydroxyl rotation in **21** was not specified). Woodcock et al. [272] found that AM1 gas-phase energies differed from MP4/6-31G**//HF/3-21G energies by up to 5 kcal/mol, although predicted dipole moments were in better agreement between the two levels of theory than was the case for 3-hydroxyisoxazole (vide supra). Although Woodcock et al. found that adding solvation free energies from an ab initio DO model with a 2.5 Å spherical cavity radius also predicted that **19** should slightly predominate, this was not consistent with either PCM results or MD simulations, both of which suggested **20** to be lower in energy in aqueous solution. The present authors [277] employed ab initio levels of theory that effectively converged the gas-phase relative energies, noting, as had Rzepa et al. [270], that inaccurate geometries had been used for **19** in the earlier studies. When SM*x* solvation free energies were added to these gas-phase energies, the present authors predicted that both isoxazolone tautomers should be present with **20** slightly predominating. This is consistent with trends apparent in the tautomeric equilibria of the 3-methyl, 4-methyl, and 3,4-dimethyl homologs of this heterocyclic system, for which experimental equilibrium data are available [278, 279], and for which the SM*x* models are in good agreement with experiment [277]. Gould and Hillier [280] subsequentIy revisited this system and illustrated that the DO model was incapable of providing accurate predictions even when accurate geometries and a more reasonable cavity were employed. However, when higher solute multipole moments were included in the reaction field, the results were more consistent with the SM*x* predictions for the unsubstituted system. Finally, both the present authors as well as Gould and Hillier emphasized the importance of accounting for non-electrostatic components of the free energy of solvation.

4.2.1.4 Oxazoles

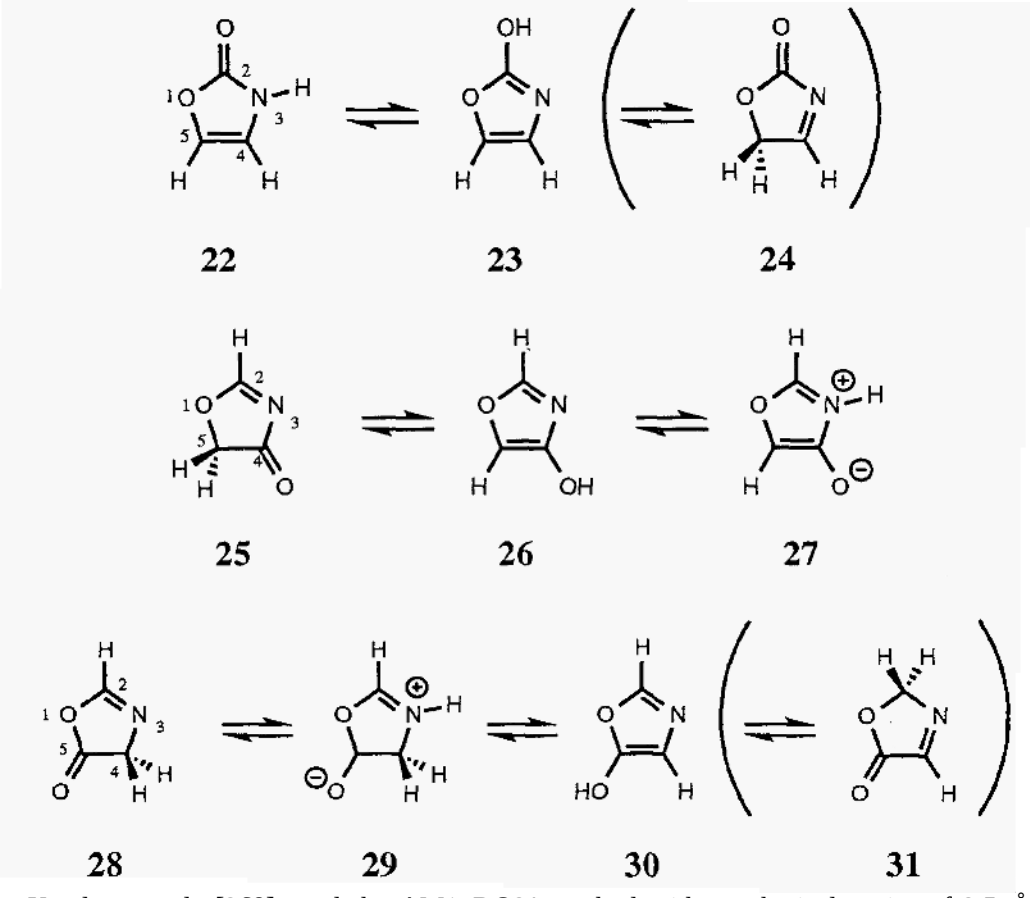

22 **23** **24**

25 **26** **27**

28 **29** **30** **31**

Karelson et al. [268] used the AM1 DO2* method with a spherical cavity of 2.5 Å radius to study tautomeric equilibria in the 2-, 4-, and 5-hydroxyoxazole systems (the keto tautomers are referred to as oxazolones). Tautomers illustrated above in parentheses were not considered and hydroxyl rotamers were not specified. In the first two systems, tautomers **22** and **25** are predicted by AM1 to be about 14 kcal/mol more stable than the nearest other tautomer in their respective equilibria. Differences in tautomer solvation free energies do not overcome this gas-phase preference in either case, and the oxazolones are predicted to dominate the aqueous equilibrium, as is observed experimentally [266].

In the 5-hydroxyoxazole system, AM1 predicts the 5-(4*H*)-oxazolone tautomer **28** to be the lowest in energy in the gas phase by 12.4 kcal/mol. This tautomer is experimentally observed in the solid state [266]. The employed DO2*

model, however, predicts that the zwitterionic tautomer **29** should predominate in aqueous solution by about 20 kcal/mol with a solvation free energy of nearly –40 kcal/mol; this is probably a large overestimation of the magnitude owing to the arbitrarily small size of the DO2* cavity employed. Experimental solution data are not available. The AM1 gas-phase energies are also not quantitative, suggesting that this might be an interesting system for which to make higher level predictions.

4.2.1.5 Triazoles

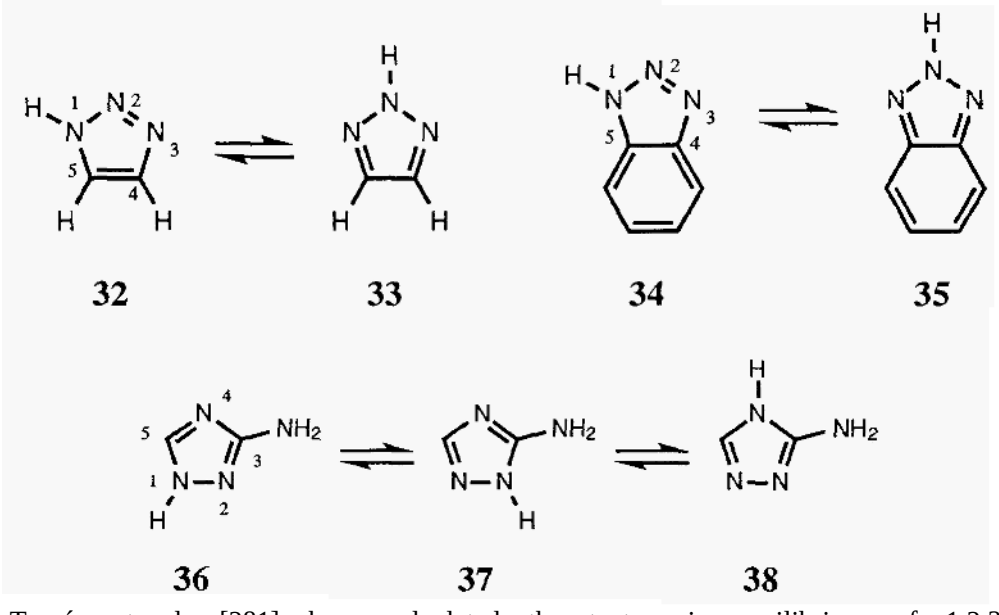

Tomás et al. [281] have calculated the tautomeric equilibrium of 1,2,3-benzotriazole in the gas phase and compared their results to experimental data [282] derived from ultraviolet spectroscopy. Experiment suggests that **35** is about 4 kcal/mol more stable than **34;** this result is consistent with calculations [281] at the MP2/6-31G* level, which predict **35** to be 2.5 kcal/mol more stable than **34.** The same level of theory predicts **33** to be 5.0 kcal/mol more stable than **32** in the parent triazole system. Although experimental data are available indicating **35** to be the dominant tautomer in $CDCl_3$ and d_6-dimethyl sulfoxide solutions [279, 283], this equilibrium does not appear to have been the subject of any modeling, continuum or otherwise. It may prove to be somewhat challenging, however. Tomás et al. point out that correlation effects favor **35** by about 5 kcal/mol at the MP2 level; AM1, PM3, and HF calculations with moderate basis sets all predict

34 to be the lowest in energy in the gas phase. Moreover, Fabian [284] has noted significant discrepancies between experimental tautomeric equilibria and predictions from both AM1 and PM3 when one or more tautomers has adjacent pyridine-like lone pairs, as is the case for **34.** This suggests that the electronic densities calculated at these levels may not be sufficiently accurate for solvation modeling.

In conjunction with the present review we have carried out AM1-SM4 calculations in solvent *n*-hexadecane (ε = 2.06) for the benzotriazole equilibrium. We find that **35** is better solvated than **34** by 0.9 kcal/mol, with all of the differential solvation being found in the ΔG_{ENP} term. Not surprisingly, PM3-SM4 results are very similar. This seems to be out of step with the data from $CDCl_3$, the most nonpolar solvent for which experimental results are available. It is not clear, however, whether this difference is attributable to (i) the smaller dielectric constant of *n*-hexadecane compared to $CDCl_3$ (for $CHCl_3$ ε = 4.8 at 293 K [240]), (ii) specific interactions between weakly acidic chloroform and the basic benzotriazole tautomers, (iii) inadequacies in the semiempirical electronic structure, (iv) inadequacies in the SM4 model, or (v) some combination of any or all of the above. When SM5 models are available for $CHCl_3$ and DMSO, it will be interesting to revisit this system.

Another challenging triazole system, 3-amino- 1,2,4-triazole, has been discussed by Parchment et al. [285]. In aqueous solution, ^{15}N-NMR indicates [286] a 2:1 mixture of **37:36,** with no detectable amounts of **38** present. Tautomer **38** is the least stable in the gas phase: at the CCSD/6-31G*//HF/6-3 1G* level, **36, 37,** and **38** are predicted to have relative energies of 0.0, 0.4, and 7.8 kcal/mol, respectively [285]. With a DO model using a cavity radius of 3.0 Å at the HF/6-31G** level, Parchment et al. [285] predicted the relative energies of **36, 37,** and **38** in aqueous solution to be 2.5, 0.0, and 1.4 kcal/mol, respectively; although the relative ordering of **36** and **37** is correct, **38** is too low in energy based on the above NMR data. PCM calculations at the same level of theory predicted the relative energies of **36, 37,** and **38** in aqueous solution to be 0.0, 1.8, and 5.0 kcal/mol, respectively. This prediction of the electrostatics is more consistent with the observed equilibrium, and it appears that correcting for specific solvation effects could easily reverse the relative energies of **36** and **37.** However, it may be that the proximity of the primary and secondary amino functionality in tautomer **37** requires inclusion of a specific water molecule in the continuum calculation as there is an opportunity for a unique hydrogen bonding pattern possible only for that tautomer (each amino group hydrogen bonding to one lone pair of a single water molecule).

4.2.1.6 Tetrazoles

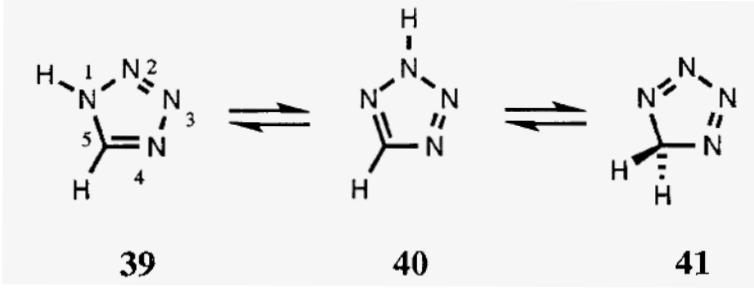

Tetrazole can exist as three tautomers, as illustrated above. Wong et al. [287] have summarized the experimental and theoretical data for the gas-phase equilibrium; there is general agreement that **40** is more stable than **39** by about 2 kcal/mol, while **41** is about 20 kcal/mol higher in free energy. Wong et al. also used the DO3 model to examine electrostatic solvation effects on the tetrazole equilibrium at the MP2/6-31 1+G**//HF/6-31G* level. At this level they predict the equilibrium to barely reverse in a continuum dielectric of $\varepsilon = 2$, so that **39** is favored over **40** by about 0.1 kcal/mol. For $\varepsilon = 40$, they predict **39** to be favored over **40** by about 3 kcal/mol. This ordering is consistent with the experimental observation [283] of only **39** in dimethylsulfoxide ($\varepsilon = 46.5$ at 298 K [240]). The possible differential effects of specific interactions between tetrazole tautomers acting as hydrogen-bond donors to DMSO were not considered. Tautomer **41** remained much higher in energy for both dielectric constants.

For comparison purposes, we have carried out for the present review AM1-SM4 calculations in *n*-hexadecane ($\varepsilon = 2.06$). We find the solvation free energies of **39** and **40** to be –3.5 and –2.7 kcal/mol, respectively. Thus, the two solvation models agree that **39** is better solvated than **40.** However, we calculate the differential solvation free energy, 0.8 kcal/mol, to be smaller than that found by Wong et al., 2.0 kcal/mol (in a hypothetical solvent with $\varepsilon = 2.0$). Moreover, we calculate ΔG_{ENP} for **39** and **40** to be –4.4 and –3.6 kcal/mol, respectively. These values may be compared to the DO3 (also electrostatics only) results of Wong et al., which were –2.4 and –0.4 kcal/mol. These differences, as noted above for the 5-hydroxyisoxazole system, are probably attributable to the failure of the DO model to take account of higher multipole moments. The net result is that the two models differ for $\varepsilon = 2$—the DO3 model predicts a very slight prevalence of **39,** while the SM4 model predicts about a 7:1 ratio of **40:39.** Unfortunately, limited solubility of tetrazole in solvents less polar than DMSO has not yet permitted an experimental measurement of this equilibrium.

4.2.1.7 Pyridines

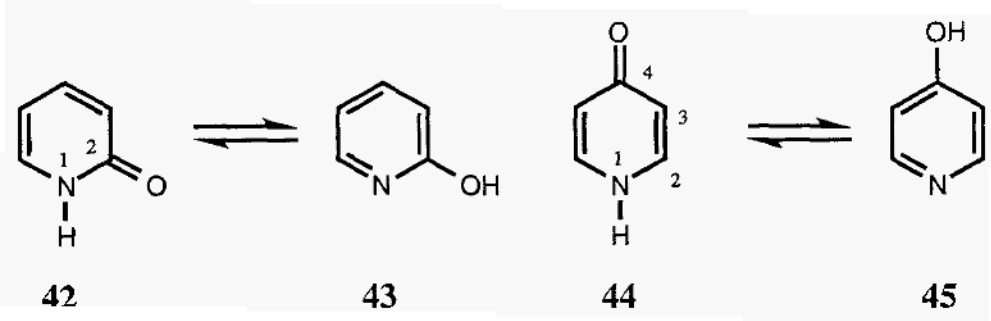

Hydroxypyridine/pyridone equilibria have been extensively studied. Numerous experimental [240, 266, 288, 289] and modeling studies of these systems in the gas phase [284, 290-293] and in solution [157, 159, 160, 195, 236, 260, 294-300] have appeared. An earlier review [83] by the present authors includes a summary of the literature through 1993. We briefly review that earlier work and include some more recent contributions.

The 2-substituted system has proven especially attractive to modelers because the experimental equilibrium constants are known both in the gas phase and in many different solutions. As a result, the focus of the modeling study can be on the straightforward calculation of the differential solvation free energy of the two tautomers, without any requirement to first accurately calculate the relative tautomeric free energies in the gas phase. However, in 1992 Les et al. [290] suggested that prior experimental data [240, 266, 288], primarily in the form of ultraviolet spectra in the gas phase and in low-temperature matrices, had been misinterpreted and that the reported equilibrium constants referred to homomeric dimers of tautomers (i.e., $\mathbf{(42)}_2 \rightleftharpoons \mathbf{(43)}_2$**).** Parchment et al. [291] contested this assertion and suggested an incomplete accounting for correlation in the modeling studies of Les et al. Simultaneously, a gas-phase microwave experiment appeared that unambiguously established the two tautomers to be monomeric in the gas phase [289].

Calculations on the differential solvation free energies of the two relevant tautomers are presented in the following table for several different models implemented at a number of levels of theory. The following discussion will focus on comparing specific calculations in the table.

We begin with a comparison of the various DO models to each other. Based on a parametric procedure that takes account of the molecular volume encompassed by the 0.001 a.u. electron density envelope, Wong et al. [297] suggested that an appropriate spherical cavity radius is 3.8 Å. Szafran et al. [157]

TABLE III

Differential free energies of solvation (kcal/mol) for 2-pyridone **42** and 2-hydroxypyridine **43** for different dielectric constants and solvent models.[a]

Model/Hamiltonian[b]	Dielectric Constant ε=2	ε=5	ε=36	ε=78	Cavity	Ref
DO2*/AM1				4.3	rad. 3.15 Å[c]	[295]
DO2*/AM1	0.8	1.5	2.0	2.1	rad. 3.8 Å	[157]
DO2*/PM3	0.7	1.3	1.8	1.9	rad. 3.8 Å	[157]
DO2*/AM 1[d]				1.5	rad. 3.8 Å	[157]
DO2*/PM3[d]				1.7	rad. 3.8 Å	[157]
DO/AM1				4.8	rad. 3.0 Å	[159]
DO/AM1	0.9	1.6	2.3	2.3	rad. 3.8 Å	[157]
DO/PM3	0.7	1.4	2.0	2.1	rad. 3.8 Å	[157]
DO/AM1[d]				2.7	rad. 3.8 Å	[157]
DO/PM3[d]				2.4	rad. 3.8 Å	[157]
DO/HF/3-21G				5.7	rad. 3.8 Å	[298]
DO/HF/6-31G**	1.1		3.0		sad. 3.8 Å	[297]
DO/HF/6-31+G**	1.2		3.4		rad. 3.8 Å	[297]
DO/MP2/6-31+G**	1.0		3.2		rad. 3.8 Å	[297]
DO/VWN/DZP				6.4	rad. 3.8 Å	[160]
DO/BP/DZP				6.2	rad. 3.8 Å	[160]
SCME(l= 6)/HF/6-31G**	1.5		4.2	4.3	rad. 3.8 Å	[195]
SCME(l= 6)/HF/6-31G**	3.3		4.5	4.6	ellipsoidal	[195]
PCM/AM1	1.6	3.3	4.8	5.0	van der Waals	[301]
PCM/HF/6-311G**	2.6		5.7	5.8	van der Waals	[195]
AM1-SM4 cyclohexane[e]	0.6				van der Waals	*f*
PM3-SM4 cyclohexane[e]	1.6				van der Waals	*f*
AM1-SM1 water[e]				4.4	van der Waals	[260]
AM1-SM2 water[e]				2.6	van der Waals	[236]
PM3-SM3 water[e]				4.3	van der Waals	[236]
PCM8/ST/AM1 water				4.1	van der Waals	[207]
PCM8/ST/PM3 water				3.0	van der Waals	[207]
Experiment	**1.1**	**1.8**	**3.8**	**4.3**		[288]

[a] In every case, 2-pyridone is the better solvated isomer by the amount indicated. [b] See text for description of Hamiltonians/acronyms. [c] rad. denotes radius of a spherical cavity. [d] Includes one explicit water of hydration. [e] The SMx and PCM8/ST models include non-electrostatic effects; the other models do not. [f] This work.

arrived at a similar cavity radius based on van der Waals volumes of the solutes. At the semiempirical level, Szafran et al. [157] compared the DO2* model to the normal DO approach. Although the DO2* model does not polarize the wave function as much as the full DO model, the effect on the differential solvation energy is fairly small at the AM1 and PM3 levels, amounting to only 0.2 kcal/mol at $\varepsilon = 78$. The agreement with experiment is good for the two smallest dielectric constants and rather poor for the two largest dielectric constants. When the cavity radius is treated as a free parameter, it is of course possible to improve the agreement with experiment for $\varepsilon = 78$. Karelson et al. [295] and Freitas et al. [159] chose unrealistically small cavity radii (2.5 Å) for their DO2* and DO calculations, respectively, at the AM1 level, and were able to increase the differential solvation free energy to more than 4 kcal/mol. Using the more reasonable cavity radius of 3.8 Å, Szafran et al. [157] considered the addition of one explicit water molecule. It is not clear, however, what the differential solvation energy of the monohydrates should be, since the tautomeric equilibrium constant for the monohydrates in the gas phase is not known (at the AM1 and PM3 levels, Szafran et al. found the monohydration energies to be identical for both tautomers—ab initio results focusing on the monohydrates in the gas phase have also appeared [293, 298-300]). What is noteworthy about the monohydrate calculations is that the difference between the DO2* and DO models becomes considerably more pronounced—the differential solvation energy differs by almost a factor of 2 at the AM1 level.

At ab initio levels of theory, Wong et al. [297] examined the effects of basis set and correlation (evaluated at the MP2 level) on the differential solvation free energy at $\varepsilon = 2$ and $\varepsilon = 36$. They did not calculate the $\varepsilon = 78$ case, noting that specific interactions not accounted for by the continuum model might be expected to be significant in aqueous solution. Within the DO model, however, the difference between $\varepsilon = 36$ and $\varepsilon = 78$ is almost negligible, as can be seen from many of the other calculations. In any case, Wong et al. achieve excellent agreement with experiment for $\varepsilon = 2$ and somewhat underestimate the differential solvation free energy for $\varepsilon = 36$. The effects of adding diffuse basis functions and taking account of electron correlation at the MP2 level are fairly small: each changes the differential solvation free energy by about 10%, albeit in opposite directions. Barone and Adamo [298] use the same cavity radius as Wong et al., (3.8 Å) but obtain a much larger differential solvation free energy at $\varepsilon = 78$, 5.7 kcal/mol, than would be expected based on the HF results of Wong et al. at $\varepsilon = 36$. The situation is not entirely clear, since the paper of Barone and Adamo states the calculation to be at the HF/3-21G level, while another paper by Adamo and Lelj [160] refers to this result as being at the HF/6-31G** level, which should

certainly agree closely with the results of Wong et al. at $\varepsilon = 36$. Assuming the calculations to be at the HF/3-21G level, it appears more likely that the discrepancy arises from the lack of polarization functions in the smaller basis set, since the reported geometries do not differ markedly. This seems to suggest a potentially important point, namely that at ab initio levels polarization basis functions appear to be crucial in permitting a realistic relaxation of the solute wave function in the presence of a reaction field. Adamo and Lelj [160] found a similarly large differential solvation free energy for $\varepsilon = 78$ using density functional theory (DFT). In this case, the local density approximation of Vosko, Wilks, and Nusair [302] (VWN) was used; the nonlocal corrections of Becke [303] and Perdew [304] for exchange and correlation energy, respectively (BP), were also employed. In both cases the results significantly overshoot the aqueous experimental values. Hall et al. [292] have found very similar density functional approaches to do poorly with respect to prediction of the gas-phase tautomeric equilibrium constant, so it appears that the DFT density for one (or both) of the two tautomers is inaccurate.

Young et al. [195] have provided a calculation in which they compared expanding the multipole series up to $l = 6$ in a spherical cavity of 3.8 Å. These results may be compared directly to those of Wong et al. [297] at the identical level of theory/basis set in order to assess the effect of including higher moments. In each case, the differential solvation free energy increases by about 40%. This illustrates nicely the relationship between cavity radius and model approximations—it is apparent that the prescription used by Wong et al. to calculate cavity radii may be useful when the effects of higher multipole moments are ignored (i.e., for a DO model) but it will *not* necessarily be useful for more general reaction field approaches. In this case, inclusion of higher order multipoles improves agreement with experiment for $\varepsilon = 36$ but agreement is now less good for $\varepsilon = 2$. As noted earlier, there is effectively no difference between the results for $\varepsilon = 78$ and $\varepsilon = 36$—for a cavity radius of 3.8 Å, the former are in quantitative agreement with experiment. Upon switching from a spherical cavity to an ellipsoidal one, however, the agreement with experiment is degraded [195], especially for $\varepsilon = 2$. This is in opposition to the general observation that ellipsoidal cavities are to be preferred over spherical ones (although both are inferior to more general cavities).

Results for continuum models having more general cavities are available. In particular, Wang and Ford [301] and Young et al. [195] have carried out PCM calculations at the AM1 and HF/6-311G** levels, respectively. Both sets of calculations significantly overestimate the differential solvation free energies. This may reflect a difficulty with charge penetration outside the cavity.

The GB/ST-type SM*x* models also employ a general cavity. Since they include non-electrostatic effects, they require parameterization on a solvent-by-solvent basis, and at present results for 2-pyridone are only available for $\varepsilon = 2$ (using the SM4 cyclohexane model [217]) and $\varepsilon = 78$ (using the SM1 [210], SM2 [211], and SM3 [212] water models). The cyclohexane solvation model brackets the experimental result depending on whether the AM1 or PM3 Hamiltonian is used. This is somewhat surprising, since the CM1 charge models should minimize differences between the two Hamiltonians. Indeed, for the pyridones the AM1-CM1 and PM3-CM1 atomic partial charges are very similar and the absolute solvation free energies agree closely (–6.7 and –6.9 kcal/mol for AM1-SM4 and PM3-SM4 cyclohexane, respectively). For 2-hydroxypyridine, the charges remain quite similar; the largest deviation is 0.06 charge units on the pyridine nitrogen (–0.53 with AM1-CM1 and –0.47 with PM3-CM1). Nevertheless, the solvation of this tautomer appears very sensitive to these small charge differences, and the absolute free energies of solvation are –6.1 and –5.3 kcal/mol for AM1-SM4 and PM3-SM4 cyclohexane, respectively. This effect is discussed in somewhat more detail for formamidic acid in section 4.2.2.1. Non-electrostatic contributions to the differential solvation free energy, as measured by G^{o}_{CDS} values, are less than 0.1 kcal/mol. This is intuitively reasonable and consistent with the assumptions of the electrostatics-only continuum studies.

The aqueous solvation results are in good agreement with experiment for the SM1 and SM3 models, but quantitatively too small for the SM2 model. The present authors have provided a detailed analysis of these results that emphasizes the importance of (i) relaxing the electronic wave function in the presence of the reaction field and (ii) reoptimizing the geometry in the presence of the reaction field [236]. The latter effect is small in terms of changes in bond lengths, angles, etc.; but, it permits additional electronic relaxation which contributes to the overall solvation free energy.

Using the PCM8/ST model, Orozco et al. [207] arrive at values similar to those found by the SM*x* models. Interestingly, in this case it is the AM1-based model that is more accurate than the PM3-based one. This illustrates the subtle balancing that goes into the parameterization of models that include electrostatic and non-electrostatic effects simultaneously.

One point of particular interest is that it is not clear from the electrostatics-only models whether non-electrostatic phenomena affect the *aqueous* tautomeric equilibria. For instance, the DO results of Wong et al. [297] would suggest there are differentiating non-electrostatic phenomena, while the results of Young et al. [195] for a multipole expansion in a spherical cavity suggest that there are not. Since the SM1, SM2, and SM3 GB/ST models use Mulliken charges rather than

CM1 charges in the calculation of ΔG_{ENP}, corrections for charge inadequacies appear in G^{o}_{CDS} and it is not possible to separate the electrostatic and non-electrostatic components of the free energy of solvation.

Finally, we note that Karelson et al. [295] have used the DO2* model with small cavity radii to consider aqueous solvation effects on other tautomeric equilibria of substituted pyridines. In particular, they examined methyllmethylene, amino/imino, hydroxy/oxo, and mercapto/thiono substitution at the 2-, 3, and 4-positions of pyridine. They observed methyl/methylene equilibria to be only slightly perturbed by aqueous solvation. Amino/imino equilibria were slightly more perturbed, followed by hydroxy/oxo equilibria. Mercapto/thiono equilibria were *very* significantly affected by aqueous solvation; Karelson et al. predicted pK shifts of up to 16 units. This sensitivity of the thiono group to solvation is also discussed in the next section. Overall, the tautomeric equilibria of 3- and 4-substituted pyridines were more sensitive to aqueous solvation than were those of 2-substituted pyridines.

4.2.1.8 Pyrimidines, Purines, and Nucleic Acid Bases

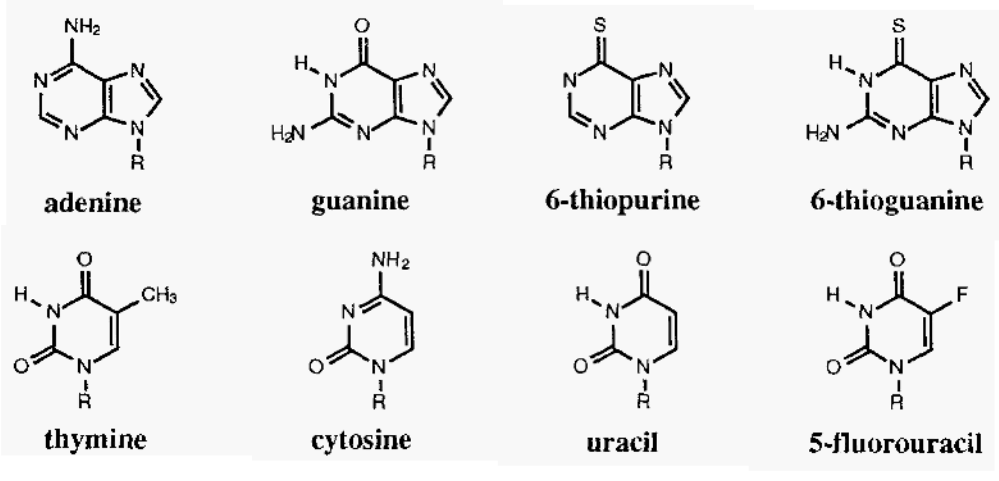

Some of the impetus for studying tautomeric equilibria in heterocycles arises because of the postulate that point mutations in genetic material may be introduced when a given base exists in a tautomeric form during replication [279, 305-307]. Cytosine, in particular, has imino and hydroxy tautomers that are within 3 kcal/mol of the global minimum illustrated above (because of the very large number of possible tautomers for the purines and pyrimidines, only the lowest energy tautomers are presented). This analysis has been made based on a

combination of matrix infrared spectroscopy [308] and theoretical [309-313] (gas phase) results. In the latter case, it is worth noting that Estrin et al. [314] found both local and gradient-corrected implementations of density functional theory to be effective in computing the relative tautomeric energies. This is in contrast to the observations of Hall et al. [292], discussed in the previous section, with respect to 2-pyridone. Even for the other nucleic acid bases, there has been interest in the possibility that solvation might influence the tautomeric equilibrium sufficiently to play a role in biological systems.

Continuum models have been employed by a number of groups in an effort to address this question. Scanlan and Hillier [309] considered the effect of aqueous solvation on uracil, thymine, 5-fluorouracil, and cytosine using a non-self-consistent DO reaction field model and HF/3-21G electronic structures. They observed that the model gave qualitative agreement with experimental results for solvation effects on the tautomeric equilibria, but that the predicted aqueous populations of non-standard tautomers were too small to be consistent with the observed rates of mutation in DNA replication. They concluded that other factors associated with the macromolecular system could not be ignored in this regard. Katritzky and Karelson [315] used the DO2* model with the AM1 and PM3 Hamiltonians to evaluate tautomeric equilibria for all of the nucleic acid bases, as well as for the 1-methylated pyrimidine bases. Cavity radii ranged from 3.45 to 3.83 Å for the pyrimidines, and the qualitative results were reported to be insensitive to 10% changes in these values; cavity radii were not reported for the purines. Katritzky and Karelson emphasized that the semiempirical dipole moments were in good agreement with experiment for uracil and thymine, and that the semiempirical structures also agreed well with higher level ab initio results. Similar points have been made by Fabian with respect to the success of semiempirical levels of theory in predicting the geometries and dipole moments for these and related heterocycles [284]. Katritzky and Karelson provide detailed comparisons between theory and experiment for the relative tautomeric energies of each base. Although uncertainties in some of the experimental relative free energies are quite large, nevertheless, the DO2* results were in quite reasonable qualitative agreement.

Young et al. [316] examined the cytosine tautomeric equilibrium using both the DO model (cavity radius of 3.54 Å) and a multipole expansion through $l = 6$ in both spherical and ellipsoidal cavities. They also employed the PCM model. All of their results were at the HF/6-31G** level. They observed that the absolute free energies of solvation were quite sensitive to choice of model, but that relative free energies were much less sensitive. They also noted that only the DO model gave good agreement with experimental estimates for the solvation

free energy of a high-energy oxo-amino tautomer. Finally, they noted that in some cases the AM1 results of Katritzky and Karelson benefited from a cancellation of errors in the gas phase and solvation energies. Ford and Wang [178] also examined the solvation of the three lowest energy tautomers of cytosine using an AM1 PCM model, and arrived at similar conclusions to those discussed above.

Orozco and Luque [317] have examined the tautomerism and protonation of 7-aminopyrazolopyrimidine (a drug component resembling adenine) using free energy perturbation and the SM2, PCM9/ST, and PCM10/ST continuum models. In this case, they note good agreement between the ab initio PCM9/ST model and their simulations with respect to which tautomer is the best solvated. This appears to be supported by experimental data. The AM1-based SM2 and PCM10/ST results, on the other hand, predict a different tautomer to be better solvated, apparently illustrating a case where the semiempirical wavefunction fails to provide an adequate representation of the solute electronic structure.

Lastly, some studies have recently appeared examining thiosubstituted purines (commonly used in the treatment of human leukemia) and thiopyrimidines. In particular, Contreras and Alderte [318] used the AM1-SM1 model to examine the tautomeric equilibrium of 6-thiopurine, and Alhambra et al. [319] used an HF/6-31G* PCM model to examine the tautomeric equilibrium of 6-thioguanine. Both studies noted very large polarization free energies associated with thiono tautomers, the net effect being a large shift of negative charge onto sulfur and a corresponding large gain in solvation free energy. These observations are consistent with the results of Karelson et al. [295] for thiosubstituted pyridines. In each case, aqueous solvation reversed the relative stability of the lowest energy thiol and thiono tautomers compared to the gas phase. Alhambra et al. also considered the solvation of protonated forms of 6-thioguanine [319]. Contreras and Alderete [320, 321] calculated free energies of solvation of prototropic tautomers of 2-thiopyrimidine using the SM2 and DO models. They found considerably larger solvation energies for the thione than the thiol by both approaches.

4.2.2 Non-heterocyclic Tautomeric Equilibria

In addition to heterocycles, other molecular systems have attracted theoretical attention with respect to prediction of tautomeric equilibria and solvation effects thereon. The most commonly studied example in this class is the equilibrium between formamide and formamidic acid, discussed in the next section. In addition, some continuum modeling of solvation effects on keto/enol equilibria have appeared; these are presented in section 4.2.2.2. We note that the equilibrium

between glycine and its zwitterionic form, discussed in section 4.1.1, is also formally a tautomeric equilibrium.

4.2.2.1 Formamide

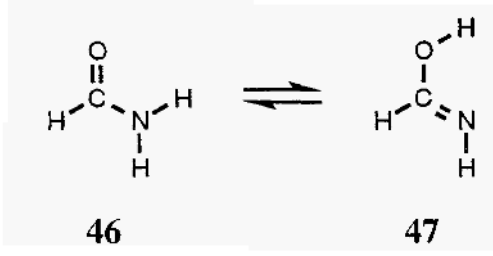

46 **47**

High-level gas-phase calculations unambiguously establish formamide **46** to be roughly 13 kcal/mol more stable than formamidic acid **47** [198, 297, 322]. It will be noted that these molecules represent the critical "fragment" of 2-pyridone involved in that molecule's tautomeric equilibrium. As such, it comes as no surprise that modeling of solvation effects indicates the amide form to be further stabilized in solution [198, 297]. As a result, no experimental data are available to which to compare. It remains instructive, however, to compare different theoretical studies. Wong et al. [297] used the DO model with a spherical cavity radius of 3.15 Å at the QCISD/6-31+G** level and concluded that the amide tautomer had the larger electrostatic free energy of solvation by 1.5 and 4.1 kcal/mol for dielectric constants of 2 and 36, respectively. Sato and Kato [198] also examined this system using a multicenter multipole expansion within a spherical cavity of radius 3.7 Å. These authors concluded that the amide tautomer had the larger electrostatic free energy of solvation by only 2.3 kcal/mol for a dielectric constant of 36 ($\varepsilon = 2$ was not examined). The reduction in magnitude of the differential solvation free energy may be a manifestation of either the more complete multipole expansion favoring the imine tautomer (which has a smaller dipole moment), or the considerably larger cavity radius employed, or both. The cavity radius is probably playing a significant role, since Wong et al. found ΔG_{ENP} ($\varepsilon = 36$) for formamide to be –4.3 kcal/mol, while Sato and Kato [198], with a more complete multipole expansion, obtained a value of only –2.8 kcal/mol.

For the present review we examined the $\varepsilon = 2$ case using the PM3-SM4 *n*-hexadecane model. This model is particularly appropriate because the PM3-CM1 dipole moments (3.4 and 1.2 D for formamide and formamidic acid, respectively) agree well with values obtained from MP2/6-31G** wave functions (3.9 and 1.2 D, respectively) [235]. The predicted differential free energy of

solvation is 1.9 kcal/mol, which is fairly close to the value obtained by Wong et al. [297]. However, the PM3-SM4 model predicts ΔG_{ENP} to be –4.4 kcal/mol at $\varepsilon = 2$; the DO model of Wong et al. [297] predicts a value of only –1.7 kcal/mol. Evidently, although solvation terms arising from multipole moments larger than the dipole and/or the approximation of a spherical cavity are not small, they appear to cancel in the differential free energy calculation. The PM3-SM4 results predict the change in G^{o}_{CDS} to be 0.3 kcal/mol on going from formamide to formamidic acid, a not entirely negligible change.

Finally, we note that the AM1-SM4 model is less satisfactory for this problem (predicted differential free energy of –0.2 kcal/mol in *n*-hexadecane), apparently because it overestimates the polarity of the functional groups in formamidic acid, especially the imine group (the AM1-CM1 dipole moment is 1.7 D and the atomic partial charges are up to 0.2 units larger than found for PM3-CM1). This deficiency is probably also reflected in the AM1-SM4 underestimation of solvation effects at $\varepsilon = 2$ for the 2-pyridone/hydroxypyridine tautomeric equilibrium discussed above. The greater generality of the PM3-CM1 model for nitrogen-containing systems has been previously noted [235].

4.2.2.2 Keto/enol equilibria

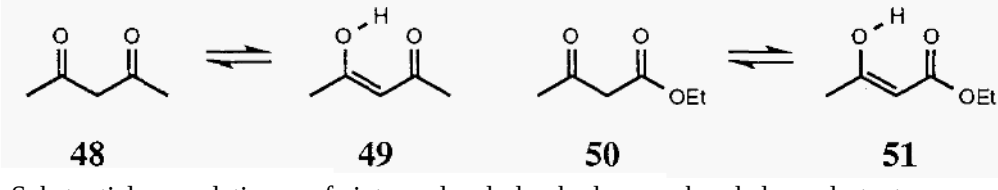

48 **49** **50** **51**

Substantial populations of intramolecularly hydrogen bonded enol tautomers of β-diketones and β-ketoesters are found in the gas-phase and in nonpolar solvents [240]. In water, on the other hand, the dione form is better solvated than the enol, causing the equilibrium to shift; for example, for ethyl 3-oxobutanoate **50,** the differential free energy of aqueous solvation for the two tautomers is 1.4 kcal/mol [323, 324]. The present authors examined this equilibrium with the SM1, SM2, and SM3 aqueous solvation models and found the differential free energies of solvation to be 1.1, –1.2, and 1.2 kcal/mol, respectively [236, 260]. The sizable difference between the predictions of the SM2 and SM3 models, with the latter being in much better agreement with experiment, arises from the ΔG_{ENP} term of the enol, which is very sensitive to the partial atomic charges on the oxygen atoms and on the hydroxyl proton. For 2,4-pentanedione, the differential free energy of aqueous solvation favors the dione tautomer **48** by 2.4 kcal/mol [323, 324] (note that a tabulation error occurred in our earlier work [236, 260]; our previously

tabulated experimental value of 1.0 kcal/mol is for gas to dimethylsulfoxide, *not* to water). The SM1, SM2, and SM3 aqueous solvation models predict differential free energies of solvation of 0.9, –1.6, and 0.6 kcal/mol, respectively [236, 260]. Again, the ΔG_{ENP} term of the enol **49** is very sensitive to variations in partial charges from the AM1 and PM3 Mulliken population analyses.

The 2,4-pentanedione system is interesting, since it seems to represent a challenge for the earlier generation SM*x* models. Moreover, data are also available for the tautomeric equilibrium constant in cyclohexane [324]. This allows us to explore the performance of the SM4 cyclohexane model, and the SM4-SRP water model (developed originally for hydrocarbons, ethers, and aldehydes [213], and later extended to include alcohols [325]; we observe that the performance of the SM4-SRP water model is about as good for ketones as for aldehydes). The situation is made particularly interesting because the direction of the equilibrium perturbation relative to the gas phase is opposite for the two solvents. In cyclohexane, the differential free energy of solvation for **48** and **49** is –0.7 kcal/mol i.e., favoring **49**) while in water it is 2.4 kcal/mol (i.e., favoring **48).** Obviously, the differential free energy of transfer from cyclohexane to water favors **48** by 3.1 kcal/mol.

This system is ideal for illustrating many issues associated with continuum solvation modeling, and we note several points that particularly merit discussion. Table IV provides the relevant details of the calculations.

To begin, the shift of the equilibrium constant in one direction in cyclohexane, and in the other direction in water (relative to the gas phase) could arise from several different phenomena. For instance, it could be that the enol is more polar than the dione in the gas phase, but the dione is more polarizable than the enol. In such a situation, the low dielectric medium would not induce sufficient polarization in the dione, and ΔG_{ENP} would be larger for the more polar enol; in water, the greater polarizability of the dione would permit a reversal of the relative magnitudes of the two ΔG_{ENP} terms. This does not appear to be the case, however. Instead, ΔG_{ENP} favors the dione slightly in cyclohexane, and by a still larger margin in water, i.e., it is both more polar and more polarizable than the enol. Instead, focusing on the AM1-SM4 models, specific solvation effects associated with $G^{\mathrm{o}}_{\mathrm{CDS}}$ sufficiently favor the enol in cyclohexane to overcome the small difference in ΔG_{ENP}. That preference is found entirely in the CD component; since the two tautomers are essentially equal in size, there is no distinction between them in the CS term. In the enol, there is a greater exposure of more polarizable (now in the sense of participating in favorable interactions

TABLE IV

Predicted solvation free energies and solvent-accessible surface areas (SASA) of 2,4-pentanedione tautomers in cyclohexane and water.[a,b]

	Dione **48**		Enol **49**	
	AM1	PM3	AM1	PM3
SM4 (cyclohexane)				
G_P	−3.0	−3.5	−2.4	−1.9
ΔE_{EN}	0.5	1.0	0.2	0.2
ΔG_{ENP}	−2.5	−2.5	−2.2	−1.7
G^o_{CD}	−17.0	−17.1	−17.5	−17.4
G^o_{CS}	14.8	14.8	14.8	14.7
G^o_{CDS}	−2.1	−2.3	−2.6	−2.7
ΔG^o_S	−4.6	−4.8	−4.8	−4.4
relative ΔG^{oc}_S	0.0	0.0	−0.2	0.4
SASA(CD)[d]	358.2	361.6	360.1	357.9
SASA(CS)[e]	596.0	593.9	596.7	591.6
SM4-SRP (water)				
G_P	−16.5	−16.1	−9.1	−7.7
ΔE_{EN}	7.8	6.9	2.2	1.7
ΔG_{ENP}	−8.7	−9.2	−6.9	−6.0
G^o_{CDS}	0.3	0.3	0.2	0.3
ΔG^o_S	−8.4	−8.9	−6.7	−5.7
relative ΔG^o_S	0.0	0.0	1.7	3.2
SASA[f]	304.6	304.8	300.8	298.2

[a] Free energies in kcal/mol. SASA in Å^2. [b] All geometries were fully optimized both in the gas phase and in solution. [c] Relative solvation free energy of dione and enol using the same NDDO Hamiltonian. [d] Solvent radius 2.0 Å for cavitation and dispersion. [e] Solvent radius 4.9 Å for cavitation and solvent structural rearrangement. [f] Solvent radius 1.4 Å.

associated with dispersion) hydrocarbon surface area at the expense of less polarizable oxygen surface area compared to the dione. This effect is worth about 0.4 kcal/mol favoring the enol in both of the SM4 models. In the AM1 case, that is sufficient to perturb the gas-phase equilibrium in the correct direction, although the magnitude of the perturbation is underestimated by about 0.5 kcal/mol. In the PM3 case, the difference in ΔG_{ENP} between the dione and the enol is larger, (apparently this term is quite sensitive to small charge variations in the enol—note that both SM4 models give much more consistent answers for the dione than the enol) and the net prediction is a very small shift of the gas-phase equilibrium in the wrong direction. Still, this is a fairly small quantitative error and the qualitative observation that these two terms are opposed remains unchanged.

While the PM3-SM4 model does appear to slightly underestimate the polarity of the enol component, there is some cancellation of errors upon considering the differential transfer free energies between cyclohexane and water. As noted above, experiment indicates that the differential free energy of transfer of the dione and the enol is 3.1 kcal/mol; the PM3-SM4 model predicts this value to be 2.8 kcal/mol, in excellent quantitative agreement. AM1-SM4 is less satisfactory in this regard, predicting only 1.9 kcal/mol.

Optimized 2,4-pentanedione geometries:

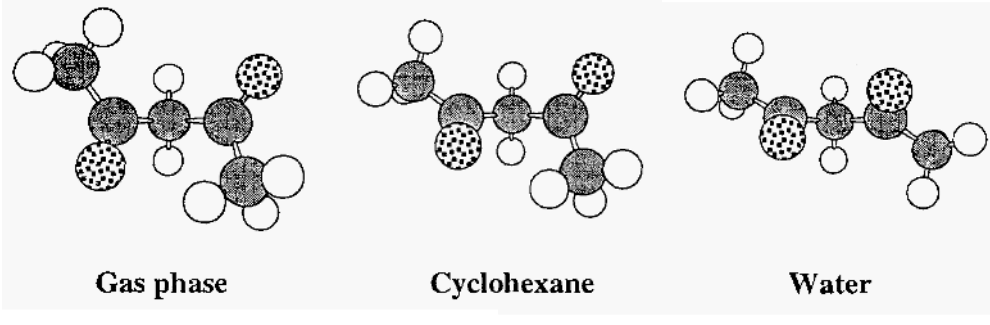

The analysis is complicated, however, because the dione undergoes a dramatic change in geometry upon optimization in aqueous solution. As illustrated above, the dihedral angle between the planes containing the two carbonyl groups and their respective substituents changes from 137° in the gas phase, to 113° in cyclohexane, to 59° in water. Reducing this dihedral angle aligns the carbonyl bond dipoles (1.36, 1.43, and 1.92 D in the gas phase, cyclohexane and water, respectively, using AM1-CM1A [235] charges) and improves the solvation of this tautomer. Note that G_P is increased dramatically in water compared to the twofold increase one would expect over cyclohexane due to

polarizability and geometric relaxation. That geometry change comes at the cost of an increase in solute internal energy, reflected in ΔE_{EN} being a very sizable 7 to 8 kcal/mol for the two models. The quantity ΔE_{EN} is the difference in the expectation values of the *gas phase* Hamiltonian operating on the optimized gas-phase and solvated wavefunctions. That is the complicating factor in the differential free energy of solvation analysis, because it brings the gas-phase potential energy surface back into the problem. It is not at all clear that the semiempirical levels accurately represent the gas-phase energetics of the observed change in geometry, and this may result in quantitative differences between experiment and the two SM4 models. In any case, the 2,4-pentanedione system should be interesting to study with ab initio solvation models that employ levels of theory adequate for the gas-phase torsional aspect of the problem. It would also be of interest to see how well this large change in geometry is reproduced by models that employ idealized cavities compared to ones that more accurately represent the solute's shape.

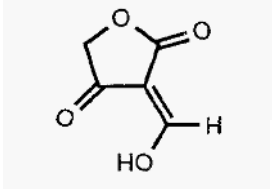

3-acetyltetronic acid

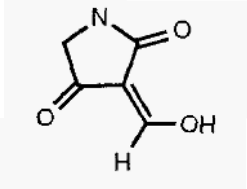

3-acetyltetramic acid

Finally, although they have not yet been the subject of any modeling study that has included solvation effects, 3-acetyltetronic and 3-acetyltetramic acid are very interesting solutes to consider. Each has more than 10 plausible tautomers—only the lowest-energy structures, as calculated at both the AM1 and MNDO levels by Broughton and Woodward [326], are shown above. The experimental situation in chloroform, as determined by NMR, remains unclear with respect to preferred structure. Gelin and Pollet [327] and Saito and Yamaguchi [328] have offered contrasting interpretations of the spectral data. Broughton and Woodward note that their semiempirical gas-phase calculations are in accord with the spectral interpretation of Gelin and Pollet, and as a consequence they suggest that solvation effects do not affect the tautomeric equilibrium. It seems evident that an investigation using a suitable chloroform continuum model would be worthwhile.

4.2.3 LACTOLIZATION

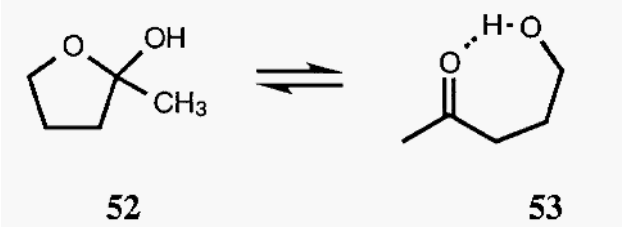

52 **53**

The present authors have examined the equilibrium between the lactol 2-hydroxy-2-methyltetrahydrofuran **52** and its corresponding open chain hydroxyketone **53** using the SM1, SM2, and SM3 models. The experimental situation indicates that the two structures are present in roughly equal proportions in non-polar media, while in water none of the lactol form is observed [329]. Making a reasonable assumption about detection limits, this sets a lower bound on the differential free energy of solvation for the two isomers of about 4 kcal/mol. Calculation of the differential free energy of transfer from the *gas phase* to aqueous solution using the SM1, SM2, and SM3 models gives values of 4.1, 3.6, and 4.4 kcal/mol, respectively. These results are probably somewhat too small since available experimental values are for the free energy of transfer from cyclohexane to water. Moreover, only one conformation of each tautomer was considered. For the hydroxyketone, the semiempirical models all predict the illustrated conformation having the intramolecular hydrogen bond to be lowest in energy, but this system should be revisited with an SM4 water model. Unfortunately, the gas-phase energies are required in order to calculate the free energy of transfer from one solvent to another when multiple conformations are involved, and this makes the problem somewhat more challenging.

5 Dynamic effects in kinetics and spectroscopy

The simplest generalization of free-energy-of-solvation concepts to dynamics in solution is provided by transition state theory. In conventional transition state theory, the rate constant of a chemical reaction at temperature T is given by

$$k(T) = \frac{k_B T}{h} K^{\neq,0} \exp[-\Delta G^{\neq,0}(T) / RT] \tag{59}$$

where k_B is Boltzmann's constant, h is Planck's constant, $K^{\neq,0}$ is unity for unimolecular reactions and the reciprocal of the standard state concentration for bimolecular reactions, and $\Delta G^{\neq,0}(T)$ is the standard-state free energy of

activation of the saddle point. For reactions in solution, $\Delta G^{\neq 0}(T)$ contains a solvation contribution which equals the free energy of solvation of the transition state minus the free energy of solvation of reactants [65-67]. To go beyond the conventional theory, we must define a reaction coordinate s and generalize the free energy of solvation to be a function of that coordinate; this is done by generalizing [330-333] the concept of potential of mean force [41, 82, 334-337] to treat generalized transition states defined at arbitrary locations along the reaction coordinate. The resulting standard-state free energy of activation as a function of s (called, for short, the free energy profile) is given by

$$\Delta G^{GT,0}(T,s) = \Delta G^{GT,0}_{solute}(T,s) + \Delta G^{0}_{S}(s,T) - \Delta G^{0}_{S}(R|T) \tag{60}$$

where all quantities are standard-state ones at temperature T, and the first term on the right-hand side is the internal standard-state free energy of the solute at s, the second term is the free energy of solvation at s, and the third term is the free energy of solvation of the reactant species. Note that the last term is an equilibrium quantity, but $\Delta G^{0}_{S}(s,T)$ is a generalized equilibrium quantity (sometimes called a quasiequilibrium quantity) for any choice of s, even the gas-phase saddle point, because both the conventional and generalized transition states have one less degree of freedom than equilibrium species.

Even at this level of dynamical theory, one is not restricted to considering equilibrium solvation of the gas-phase saddle point or of configurations along the gas-phase reaction path [109, 338-344], and to the extent that the solvent is allowed to affect the choice of the reaction path itself, dynamic (i.e., nonequilibrium) solvation effects begin to appear in the theory.

To more fully appreciate the equilibrium models, like SCRF theories, and their usefulness and limitations for dynamics calculations we must consider three relevant times, the solvent relaxation time, the characteristic time for solute nuclear motion in the absence of coupling to the solvent, and the characteristic time scale of electronic motion. We treat each of these in turn.

First, consider the solvent. The characterization of the solute-solvent coupling by a relaxation time is based on analogy to Brownian motion, and the relaxation time is called the frictional relaxational time τ_F. It is the relaxation time for momentum decay of a Brownian motion in the solute coordinate of interest when it interacts with the solvent under consideration. If we call the subject solute coordinate s, then the component of frictional force along this coordinate may be written as

$$F_s = -\mu\varsigma\frac{ds}{dt} \tag{61}$$

where μ is the reduced mass for motion along coordinate *s,* ζ is the frictional constant, and *t* is time. Then the momentum (or velocity) for Brownian motion in coordinate *s* decays as [32, 345, 346] $e^{-\zeta t}$.

Writing the momentum decay function as $e^{-t/\tau F}$ yields

$$\tau_F = \frac{1}{\varsigma}. \tag{62}$$

Even if we consider a single solvent, e.g., water, at a single temperature, say 298K, ζ depends on the solute and in fact on the coordinate of the solute which is under consideration, and we cannot take τ_F as a constant. Nevertheless, in the absence of a molecular dynamics simulation for the solute motion of interest, τ_F for polar solvents like water is often approximated by the Debye model. In this model, the dielectric polarization of the solvent relaxes as a single exponential with a relaxation time equal to the rotational (i.e., reorientational) relaxation time of a single molecule, which is called τ_D) or the Debye time [32, 347]. The Debye time may be associated with the relaxation of the transverse component of the polarization field. However the solvent fluctuations and frictional relaxation occur on a faster scale given by [348, 349]

$$\tau_L = (\varepsilon_\infty/\varepsilon_0)\tau_D \tag{63}$$

where ε_∞ is the infinite-frequency relative permittivity, and ε_0 is the static (i.e., zero-frequency) relative permittivity. (At constant temperature and pressure, the relative permittivity is the dielectric constant.) The quantity τ_L is called the longitudinal relaxation time [350, 351]. Dielectric dispersion measurements [352] on water yield ε_∞ = 1.8, ε_0 = 78.5, and τ_D = 8.5 ps, and hence τ_L = 0.2 ps. Thus $\tau_F \cong$ 0.2 ps.

Next consider the solute. We will again call the relevant solute nuclear coordinate *s* and the characteristic time now τ_s. For a thermally activated bamer crossing, where *s* is the reaction coordinate for passage over an effective potential $V_{eff}(s)$ at temperature *T,* a reasonable expression is

$$\tau_s = 1/\omega^{\ddagger} \tag{64}$$

where the barrier is written in the vicinity of its maximum as

$$V_{\mathrm{eff}}(s) = V_{\max} - \frac{1}{2}\mu\left(\omega^{\ddagger}\right)^2 s^2. \tag{65}$$

Note that the imaginary frequency associated with such a barrier is $i\omega^{\ddagger}$. For a bound mode with frequency ω_{vib}, an analogous approximation would be

$$\tau_s = 1/\omega_{\mathrm{vib}}. \tag{66}$$

The solute electronic time scale will be called τ_{elec}. It may be approximated as $h/\Delta E_1$, where ΔE_1 is the lowest (spin-allowed) electronic excitation energy of the solute.

A fully realistic picture of solvation would recognize that there is a distribution of solvent relaxation times (for several reasons, in particular because a second dispersion is often observable in the macroscopic dielectric loss spectra [353-355], because the friction constant for various types or modes of solute motion may be quite different, and because there is a fast electronic component to the solvent response along with the slower components due to vibration and reorientation of solvent molecules) and a distribution of solute electronic relaxation times (in the orbital picture, we recognize different lowest excitation energies for different orbitals). Nevertheless we can elucidate the essential physical issues by considering the three time scales τ_F, τ_s, and τ_{elec}.

The SCRF models assume that solvent response to the solute is dominated by motions that are slow on the solute electronic motion time scales, i.e., $\tau_F >> \tau_{\mathrm{elec}}$. Thus, as explained in Section 2.1, the solvent "sees" the solute electrons only in an averaged way. If, in addition to the SCRF approximation, we make the usual Born-Oppenheimer approximation for the solute, then we have $\tau_s >> \tau_{\mathrm{elect}}$. In this case the solute electronic motion is treated as adjusting adiabatically both to the solvent motion and to the solute nuclear motion.

For gas-phase molecules the assumption of electronic adiabaticity leads to the usual Born-Oppenheimer approximation, in which the electronic wave function is optimized for fixed nuclei. For solutes, the situation is more complicated because there are two types of heavy-body motion, the solute nuclear coordinates, which are treated mechanically, and the solvent, which is treated statistically. The SCRF procedures correspond to optimizing the electronic wave function in the presence of fixed solute nuclei and for a statistical distribution of solvent coordinates, which in turn are in equilibrium with the average electronic structure. The treatment of the solvent as a dielectric material by the laws of classical electrostatics and the treatment of the electronic charge distribution of the solute by the square of its wave function correctly embodies the result of

statistically averaging over a thermal solvent in equilibrium with an average (adiabatic) solute charge distribution. Because the self-consistent calculation of the adiabatic solute electronic distribution and the equilibrium polarization of the solvent is carried out at fixed solute atomic coordinates, the treatment corresponds most precisely to the case $\tau_s >> \tau_F >> \tau_{elec}$.

There are cases where the time scales do not satisfy these assumptions. Effects due to the violation of $\tau_s >> \tau_F$ are often called nonequilibrium solvation; and effects due to the violation of $\tau_F >> \tau_{elec}$ are often called nonadiabatic effects. The latter effects have been studied primarily in the context of electron transfer reactions. In electron transfer theory the interesting case of $\tau_{elec} >> \tau_F$ arises, and this is called nonadiabatic electron transfer. It occurs commonly for outer-sphere electron transfers in which ΔE_1 is very small in the critical configuration. For example ΔE_1 might be the energy difference of the symmetric and antisymmetric delocalized combinations of the two localized configurations $Fe^{3+}X_6...Fe^{2+}Y_6$ and $Fe^{2+}X_6...Fe^{3+}Y_6$, where X and Y are ligands, and ... indicates only weak interaction between the ferrous and ferric centers. In contrast, for typical chemical reactions involving the making and/or breaking of bonds, as well as for many inner-sphere electron transfers ("inner-sphere" electron transfer refers to the case in which a ligand is part of the coordination sphere of both the donor and the acceptor), we have $\tau_F >> \tau_{elec}$, which is called the adiabatic case. For adiabatic electron transfers it is often assumed that $\tau_s >> \tau_F$ in which case the rate constant decreases as τ_F decreases. This regime is variously called high-friction [67], overdamped [333], or solvent-controlled adiabatic [356]. In adiabatic bond rearrangements (i.e., ordinary chemical reactions) on the other hand, one typically finds $\tau_F = \vartheta(\tau_s)$, in which case frictional effects are small but not necessarily completely negligible [357-359]; if $\tau_F > \tau_s$, this might be called bond-coordinate-controlled adiabatic. The other adiabatic case, $\tau_F >> \tau_s >> \tau_{elec}$ is called the low-friction [67], energy diffusion [333], or strong adiabatic [356] limit. In this case reaction is controlled by the rate of activation of reactants to the transition state, which is not in equilibrium with the reactants. The scenario just sketched leads to a pattern of the rate constant increasing with increasing friction at low friction, then becoming independent of friction, then decreasing as friction increases further [67]. This pattern can also be observed in the nonadiabatic case, but in that case the friction-independent region is wider [360]. When quantum mechanical effects are important, nonequilibrium effects may be very large [361]—this regime needs further study.

The SCRF models should be useful for any of the adiabatic cases, but a more quantitative treatment would recognize at least three time scales for frictional coupling based on the three times scales for dielectric polarization,

namely electronic, $\tau_{F,\mathrm{elec}}$, vibrational, $\tau_{F,\mathrm{vib}}$, and Orientational, $\tau_{F,\mathrm{rot}}$, with $\tau_{F,\mathrm{rot}} >> \tau_{F,\mathrm{vib}} >> \tau_{F,\mathrm{elec}}$. The convenient adiabatic limit is never totally appropriate because $\tau_{F,\mathrm{elec}} = \vartheta(\tau_{\mathrm{elec}})$, even when $\tau_{F,\mathrm{vib}} >> \tau_{\mathrm{elec}}$.

One important phenomenon that sometimes occurs when $\tau_{\mathrm{elec}} \geq \tau_F$ is solvent-induced charge localization. Thus, even though the adiabatic states are delocalized, the solvent-induced states are not. Consider the system $Fe^{3+}X_6...Fe^{2+}X_6$, which is the reactant of the outer-sphere electron transfer reaction mentioned above when X = Y. Clearly the ground state involves a symmetric linear combination of a state with the electron on the right (as written) and one with the electron on the left. Thus we could create the localized states by using the SCRF method to calculate the symmetric and antisymmetric stationary states and taking plus and minus linear combinations. This is reasonable but does not take account of the fact that the orbitals for non-transferred electrons should be optimized for the case where the transferred electron is localized (in contrast to which, the SCRF orbitals are all optimized for the delocalized adiabatic structure). The role of solvent-induced charge localization has also been studied for ionic dissociation reactions [109].

Having obtained the charge-localized state, the dynamics of electron transfer can be treated as a time-dependent configuration interaction problem [356, 362-364]. In this case the two configurations would be taken as the left localized and right localized ones. A more general treatment, applicable in the regime [365] where electronic coupling is larger (i.e., τ_{elec} is smaller), but electronic motion is still not adiabatic, would involve a 3-state CI composed of the delocalized adiabatic state interacting with the two localized diabatic ones.

In electron transfer reactions one studies the conversion of an electron state localized on A to one localized on B. One can also consider the relaxation of a charge localized state to the adiabatic delocalized state [366].

The most general available treatment of solute electronic structure that does not make the SCRF assumption that solvent electronic motion is slow compared to solute electronic motion is provided by the coherent-state formulation introduced by Kim and Hynes [109] and generalized by Bianco et al. [111]. Hynes and coworkers denote the SCRF limit simply as SC. They call the opposite limit [109, 173], in which the solvent polarization is fast compared to the vacuum solute electronic time scale, the Born-Oppenheimer (BO) limit, which should not be confused with the usual Born-Oppenheimer approximation for separating the electronic and nuclear motions of a gas-phase molecule or of the solute. Kim and Hynes note that one might also call this an adiabatic limit, which, they correctly note, would introduce other possible confusions. [Adiabatic and sudden limits have a long history of introducing confusion in many fields since

the opposite of an adiabatic limit is always another adiabatic limit. Consider for example, the case where x has a time scale that is rapid compared to the controlled, slow motion of y; then x adjusts almost adiabatically to that motion, and one can treat x by an adiabatic approximation or y by a sudden approximation. But the opposite limit, where x moves slowly compared to the timescale of y is also an adiabatic limit with y adjusting almost adiabatically to x, and x may be treated by a sudden approximation. Furthermore, even under the same conditions x may be sudden with respect to y, but adiabatic with respect to z. To avoid ambiguity one must be specific about which two variables are under consideration *and* which one is considered to be fast and adiabatic. This may, of course, be obvious from context, but often it is more obvious to the author than to the reader!]

The effective frequencies that characterize solvent response can be characterized more quantitatively from several points of view, including generalized Langevin theory [367-372], Brownian osciIlators [373, 374], and instantaneous normal modes [375].

In addition to the intrinsic time scales of the system τ_F, τ_S, and τ_{elec}, one may introduce an additional time scale by the nature of the measurement. For example, electronic absorption spectroscopy may probe events on a time scale τ_{spect} that satisfies $\tau_{F,\mathrm{vib}} >> \tau_{\mathrm{spect}} >> \tau_{F,\mathrm{elec}}$. In this case the excitation would occur to a state with the electronic contribution to solvation operative but the nuclear solvation coordinates frozen in their initial state. A direct analog would be gas-phase ultraviolet or visible spectroscopy with $\tau_S >> \tau_{\mathrm{spect}} >> \tau_{\mathrm{elec}}$. This leads to the familiar Franck-Condon principle [115] according to which the electronic state is changed but the nuclear motion is frozen during the excitation. In solution, this leads to the general observation that emission is red-shifted relative to absorption, since the orientational components of solvation are optimal only for the initial (in this case, excited-state) configuration.

Because of the economic importance of dyes, the calculation of solvent effects on electronic spectroscopy using the SCRF methods has been a subject of significant interest. The interesting dynamical issue that arises in this context is the fact that solute electronic excitation may be viewed as occurring essentially instantaneously on the solute reorientational time scale, as discussed in the preceding paragraph. We refer the reader to the original source literature for further details [167, 180, 181, 219, 298, 299, 376-380].

The reader is referred to review articles concerned with dynamic solvent effects for further discussion of the interesting issues involved in applying continuum and explicit solvation models to dynamical situations [333, 381-385].

6 Concluding remarks

There has been tremendous progress in the development and practical implementation of useful continuum solvation models in the last five years. These techniques are now poised to allow quantum chemistry to have the same revolutionary impact on condensed-phase chemistry as the last 25 years have witnessed for gas-phase chemistry.

7 Acknowledgments

This work was supported in part by the NSF and the U. S. Army Research Office.

References

1. A. Warshel and M. Levitt, *J. Mol. Biol.,* **103,** 227 (1976).
2. S. J. Weiner, U. C. Singh, and P. A. Kollman, *J. Am Chem. Soc.,* **107,** 2219 (1985).
3. M. J. Field, P. A. Bash, and M. Karplus, *J. Comp. Chem.,* **11,** 700 (1990).
4. J. Gao, *J. Phys. Chem.,* **96,** 537 (1992).
5. V. V. Vasilyev, A. A. Bliznyuk, and A. A. Voityuk, *Int. J. Quant. Chem.,* **44,** 897 (1992).
6. R. V. Stanton, D. S. Hartsough, and K. M. Merz, *J. Phys. Chem.,* **97,** 11868 (1993).
7. V. Théry, D. Rinaldi, J.-L. Rivail, B. Maigret, and G. G. Ferenczy, *J. Comp. Chem.,* **15,** 269 (1994).
8. U. C. Singh and P. A. Kollman, *J. Comp. Chem.,* **7,** 718 (1986).
9. J. Gao, *J. Am. Chem. Soc.,* **115,** 2930 (1993).
10. J. L. Gao andX. F. Xia, *J. Am. Chem. Soc.,* **115,** 9667 (1993).
11. A. Warshel, T. Schewins, and M. Fothergill, *J. Am. Chem. Soc.,* **116,** 8437 (1994).
12. D. Wei and D. R. Salahub, *Chem. Phys. Lett.,* **224,** 291 (1994).
13. J. Gao, *J. Am. Chem. Soc.,* **116,** 1563 (1994).
14. J. Gao, *Proc Indian Acad. Sci. (Chem. Sci.),* **106,** 507 (1994).
15. T. J. Marrone, D. S. Hartsough, and K. M. Merz, *J. Phys. Chem.,* **98,** 1341 (1994).
16. J. Gao, *J. Am. Chem. Soc.,* **116,** 9324 (1994).
17. J. Åqvist and A. Warshel, *Chem. Rev.,* **93,** 2418 (1993).
18. A. Warshel and Z. T. Chu, in *Structure and Reactivity in Aqueous Solution,* C. J. Cramer and D. G. Truhlar, Eds., American Chemical Society, Washington, DC, 1994 p. 71.
19. J. Gao, in *Reviews in Computational Chemistry,* K. B. Lipkowitz and D. B. Boyd, Eds., VCH, New York, Vol. 7, in press.
20. M. Sprik and M. L. Klein, *J. Chem Phys.,* **89,** 7556 (1988).

21. U. Niesar, G. Corongiu, E. Clementi, G. R. Kneller, and D. K. Bhattacharya, *J. Chem. Phys.,* **94,** 7949 (1990).
22. L. X. Dang, J. E. Rice, J. Caldwell, and P. A. Kollman, *J. Am. Chem. Soc.,* **113,** 2481 (1991).
23. M. Sprik, *J. Chem. Phys.,* **95,** 6762 (1991).
24. L. X. Dang, *J. Chem. Phys.,* **97,** 2659 (1992).
25. S. W. Rick, S. J. Stuart, and B. J. Berne, *J. Chem. Phys.,* **101,** 6141 (1994).
26. S.-B. Zhu and C. F. Wong, *J. Phys. Chem.,* **98,** 4695 (1994).
27. I. Alkorta, M. Bachs, and J. J. Perez, *Chem. Phys. Lett.*, **224,** 160 (1994).
28. D. N. Bernardo, Y. Ding, K. Krogh-Jespersen, and R. M. Levy, *J. Phys. Chem,* **98,** 4180 (1994).
29. D. Van Belle, M. Prévost, G. Kippens, and S. J. Wodak, in *Structure and Reactivity in Aqueous Solution,* C. J. Cramer and D. G. Truhlar, Eds., American Chemical Society, Washington, DC, 1994 p. 318.
30. L. S. Sremeniak, L. Perera, and M. L. Berkowitz, *Chem. Phys. Lett.,* **218,** 377 (1994).
31. D. A. McQuarrie, *Statistical Mechanics.* Harper & Row, New York, 1976.
32. H. Eyring, D. Henderson, D. J. Stover, and E. M. Eyring, *Statistical Mechanics and Dynamics.* John Wiley & Sons, New York, 1982.
33. M. P. Allen and D. J. Tildesley, *Computer Simulations of Liquids.* Oxford University Press, London, 1987.
34. J. A, McCammon and S. C. Harvey, *Dynamics of Proteins and Nucleic Acids.* Cambridge University Press, Cambridge, 1987.
35. D. L. Beveridge and F. M. DiCapua, *Annu. Rev. Biophys. Biophys, Chem.,* **18,** 431 (1989).
36. W. L. Jorgensen, *Acc. Chem. Res.,* **22,** 184 (1989).
37. P. M. King, C. A. Reynolds, J. W. Essex, G. A. Worth, and W. G. Richards, *Mol. Sim.,* **5,** 262 (1990).
38. D. W. Heermann, *Computer Simulation Methods in Theoretical Physics.* Springer-Verlag, Berlin, 1990.
39. K. Binder and D. W. Heermann, *Monte Carlo Simulation in Statistical Physics.* Springer-Verlag, Berlin, 1992.
40. P. Kollman, *Chem. Rev.,* **93,** 2395 (1993).
41. P. M. King, in *Computer Simulation of Biomolecular Systems,* W. F. van Gunsteren, P. K. Weinger and A. J. Wilkinson, Eds., ESCOM, Leiden, 1993, Vol. 2, p. 267.
42. W. F. van Gunsteren, F. J. Luque, D. Timms, and A. E. Torda, *Annu. Rev. Biophys. Biomol. Struct.,* **23,** 847 (1994).
43. J. Åqvist, C. Medina, and J.-E. Samuelsson, *Protein Eng.,* **7,** 385 (1994).
44. T. J. A. Ewing and T. P. Lybrand, *J. Phys. Chem.,* **98,** 1748 (1994).
45. D. A. Pearlman and P. A. Kollman, *J. Chem. Phys.,* **94,** 4532 (1991).
46. M. Mazor and B. M. Pettitt, *Mol. Sim.,* **6,** 1 (1991).

47. M. J. Mitchell and J. A. McCammon, *J. Comp. Chem.,* **12,** 271 (1991).
48. A. Hodel, T. Simonson, R. O. Fox, and A. T. Brünger, *J. Phys. Chem.,* **97,** 3409 (1993).
49. D. A. Pearlman, *J. Phys. Chem.,* **98,** 1487 (1994).
50. M. E. Clamp, P. G. Baker, C. J. Stirling, and A. Brass, *J. Comp. Chem.,* **15,** 838 (1994).
51. F. S. Lee and A. Warshel, *J. Chem. Phys.,* **97,** 3100 (1992).
52. K. Tasaki, S. McDonald, and J. W. Brady, *J. Comp. Chem.,* **14,** 278 (1993).
53. B. M. Ladanyi andM. S. Skaf, *Annu. Rev. Phys. Chem.,* **44,** 335 (1993).
54. P. J. Steinbach and B. R. Brooks, *J. Comp. Chem.,* **15,** 667 (1994).
55. J. W. Brady and R. K. Schmidt, *J. Phys. Chem.,* **97,** 958 (1993).
56. N. H. Frank and W. Tobocman, in *Fundamental Formulas of Physics,* D. H. Menzel, Ed. Dover, New York, 1960,Vol. 1, p. 307.
57. J. B. Marion, *Classical Electromagnetic Radiation.* Academic, New York, 1965.
58. K. Denbigh, *The Principles of Chemical Equilibrium.* Cambridge University Press, London, 1981.
59. M. Born, Z. *Physik,* **1,** 45 (1920).
60. L. Onsager, *Chem. Rev.,* **13,** 73 (1933).
61. J. G. Kirkwood, *J. Chem. Phys.,* **2,** 351 (1934).
62. J. G. Kirkwood, *J. Chem. Phys.,* **7,** 911 (1939).
63. B. Lee and F. M. Richards, *J. Mol. Biol.,* **55,** 379 (1971).
64. R. B. Hermann, *J. Phys. Chem.,* **76,** 2754 (1972).
65. M. G. Evans and M. Polanyi, *Trans. Faraday Soc.,* **31,** 875 (1935).
66. H.Eyring and W. F. K. Wynne-Jones, *J. Chem. Phys.,* **3,** 492 (1935).
67. M. M. Kreevoy and D. G. Truhlar, in *Investigation of Rates and Mechanisms* of *Reactions, Part I,* C. F. Bernasconi, Ed. Wiley, New York, 1986 p. 13.
68. H. A. Kramers, *Physica (The Hague),* **7,** 284 (1940).
69. D. G. Truhlar, W. L. Hase, and J. T. Hynes, J. *Phys. Chem.,* **87,** 2664 (1983).
70. R. A. Marcus, *J. Chem. Phys.,* **24,** 979 (1956).
71. O. Tapia, in *Quantum Theory of Chemical Reactions,* R. Daudel, A. Pullman, L. Salem and A. Viellard, Eds., Reidel, Dordrecht, 1980, Vol. 2, p. 25.
72. O. Tapia, in *Molecular Interactions,* H. Rajaczak and W. J. Orville-Thomas, Eds., John Wiley & Sons, London, 1982, Vol. 3, p. 47.
73. M. L. J. Drummond, *Prog. Biophys. Mol. Biol.,* **47,** 1 (1986).
74. A. Rashin, *Int. J. Quant. Chem., Quant. Biol.,* **15,** 103 (1988).
75. M. E. Davis and J. A. McCammon, *Chem. Rev.,* **90,** 509 (1990).
76. J. Tomasi, R. Bonaccorsi, R. Cammi, and F. J. Olivares del Valle, *J. Mol. Struct. (Theochem),* **234,** 401 (1991).
77. J. G. Ángyán, *J. Math. Chem.,* **10,** 93 (1992).
78. J. Tomasi, in *Structure and Reactivity in Aqueous Solution,* C. J. Cramer and D. G. Truhlar, Eds., American Chemical Society, Washington, DC, 1994 p. 10.
79. J. Tomasi and M. Persico, *Chem. Rev.,* **94,** 2027 (1994).

80. A. A. Rashin and M. A. Bukatin, *Biophys. Chem.,* **51,** 167 (1994).
81. C. J. Cramer and D. G. Truhlar, in *Quantitative Treatments of Solute/Solvent Interactions,* P. Politzer and J. S. Murray, Eds., Elsevier, Amsterdam, 1994, Vol. 1, p. 9.
82. P. E. Smith and B. M. Pettitt, *J. Phys. Chem.,* **98,** 9700 (1994).
83. C. J. Cramer and D. G, Truhlar, in *Reviews in Computational Chemistry,* K. B. Lipkowitz and D. B. Boyd, Eds., VCH, New York, 1995, Vol. 6, p. 1.
84. W. K. H. Panofsky and M. Phillips, *Classical Electricity and Magnetism.* Addison-Wesley, Reading, MA, 1962.
85. D. R. Corson and P. Lorrain, *Introduction to Electromagnetic Fields and Waves.* W.H. Freeman, San Francisco, 1962.
86. J. E. Sanhueza, O. Tapia, W. G. Laidlaw, and M. Trsic, *J. Chem. Phys.,* **70,** 3096 (1979).
87. D. Rinaldi and J.-L. Rivail, *Theor. Chim. Acta,* **32,** 57 (1973).
88. J.-L. Rivail and D. Rinaldi, *Chem. Phys.,* **18,** 233 (1976).
89. S. Yomosa, *J. Phys. Soc. Japan,* **35,** 1738 (1973).
90. S. Yomosa, *J. Phys. Soc. Japan,* **36,** 1655 (1974).
91. O. Tapia and O. Goscinski, *Mol. Phys.,* **29,** 1653 (1975).
92. O. Tapia, E. Poulain, and F. Sussman, *Theor. Chim. Acta,* **47,** 171 (1978).
93. K. V. Mikkelsen, H. Agren, H. J. A. Jensen, and T. Helgaker, *J. Phys. Chem.,* **89,** 3086 (1988).
94. J.-L. Rivail, *Compt. Rend. Acad. Sci. Paris,* **311,** 307 (1990).
95. J.-L. Rivail, D. Rinaldi, and M. F. Ruiz-López, in *Theoretical and Computational Methods for Organic Chemistry,* S. J. Formosinho, I. G. Czismadia and L. G. Arnaut, Eds., Kluwer, Dordrecht, 1991 p. 79.
96. M. A. Aguilar, F. J. Olivares del Valle, and J. Tomasi, *J. Chem. Phys.,* **150,** 151 (1991).
97. F. J. Olivares del Valle and J. Tomasi, *Chem. Phys.,* **150,** 139 (1991).
98. F. J. Olivares del Valle, R. Bonaccorsi, R. Cammi, and J. Tomasi, *J. Mol. Struct. (Theochem),* **230,** 295 (1991).
99. M. W. Wong, M. J. Frisch, and K. B. Wiberg, *J. Am. Chem. Soc.,* **113,** 4776 (1991)
100. C. Chipot, D. Rinaldi, and J.-L. Rivail, *Chem. Phys. Lett.,* **191,** 287 (1992).
101. F. J. Olivares del Valle and M. A. Aguilar, *J. Comp. Chem.,* **13,** 115 (1992).
102. J. G. Ágyán, *Int. J. Quant. Chem.,* **47,** 469 (1993).
103. F. J. Olivares del Valle and M. A. Aguilar, *J. Mol. Struct. (Theochem),* **280,** 25 (1993).
104. F. J. Olivares del Valle, M. A. Aguilar, and S. Tolosa, *J. Mol. Struct. (Theochem),* **279,** 223 (1993).
105. C. Chipot, L. G. Gorb, and J.-L. Rivail, *J. Phys. Chem.,* **98,** 1601 (1994).
106. K. V. Mikkelsen, P. Jørgensen, and H. J. A. Jensen, *J. Chem. Phys.,* **100,** 6597 (1994).

107. J. Jortner, *Mol. Phys.,* **5,** 257 (1962).
108. J. Gehlen, D. Chandler, H. J. Kim, and J. T. Hynes, *J. Phys. Chem.,* **96,** 1748 (1992).
109. H. J. Kim and J. T. Hynes, *J. Am. Chem Soc.,* **114,** 10508 (1992).
110. M. V. Basilevsky, G. E. Chudinov, and M. D. Newton, *Chem. Phys.,* **179,** 263 (1994).
111. R. Bianco, J. J. I. Timoneda, and J. T. Hynes, *J. Phys. Chem.,* **98,** 12103 (1994).
112. O. Tapia, F. Colonna, and J. G. Angyan, J. *Chim. Phys.,* **87,** 875 (1990).
113. O. Tapia, *J. Mol. Struct. (Theochem),* **226,** 59 (1991).
114. J. G. Ángyán, *J. Math. Chem.,* **10,** 93 (1992).
115. B. A. Bransden and C. J. Joachain, *Physics* of *Atoms and Molecules.* Longman, London, 1983.
116. C. J. F. Böttcher, O. C. van Belle, P. Bordewijk, and A. Rip, in *Theory of Electric Polarization,* Elsevier, Amsterdam, 1973 pp. 94ff.
117. O. Tapia and B. Silvi, *J. Phys. Chem.,* **84,** 2646 (1980).
118. P. Claverie, in *Quantum Theory of Chemical Reactions,* R. Daudel, A. Pullman, L. Salem and A. Veillard, Eds., Reidel, Dordrecht, 1982, Vol. 3, p. 151.
119. R. Constanciel and R. Contreras, *Theor. Chim. Acta,* **65,** 1 (1984).
120. E. L. Mehler, *Adv. Comput. Biol.,* **2,** in press (1995).
121. D. F. Eggers, N. W. Gregory, G. D. Halsey, and B. S. Rabinovitch, *Physical Chemistry.* John Wiley & Sons, New York, 1964.
122. B. J. Yoon and A. M. Lenhoff, *J. Comp. Chem.,* **11,** 1080 (1990).
123. V. Frecer and S. Miertus, *Int. J. Quant. Chem,* **42,** 1449 (1992).
124. G. G. Hammes, *Principles of Chemical Kinetics.* Academic, New York, 1977.
125. M. Holst, R. E. Kozack, F. Saied, and S. Subramanian, *J. Biomol. Struct. Dynam.,* **11,** 1437 (1994).
126. S. P. Slagle, R. E. Kozack, and S. Subramanian, J. *Biomol. Struct. Dynam.,* **12,** 439 (1994).
127. P. Debye, *Polar Molecules.* Chemical Catalog Co., New York, 1929.
128. B. Roux, H.-A. Yu, and M. Karplus, *J. Phys. Chem.,* **94,** 4683 (1990).
129. F. Figueirido, G. S. Del Buono, and R. M. Levy, *Biophys. Chem.,* **51,** 235 (1994).
130. M. Bucher and T. L. Porter, *J. Phys. Chem.,* **90,** 3406 (1986).
131. **S.** Ehrenson, *J. Comp. Chem.,* **10,** 77 (1989).
132. A. Wallqvist, *Chem. Phys. Lett.,* **165,** 437 (1990).
133. N. Matubayasi, L. H. Reed, and R. M. Levy, *J. Phys. Chem.,* **98,** 10640 (1994).
134. A. A. Rashin and M. A. Bukatin, *J. Phys. Chem.,* **98,** 386 (1994).
135. P. Jungwirth and R. Zahradnik, *Chem. Phys. Lett.,* **217,** 319 (1994).
136. T. Lazaridis and M. E. Paulaitis, *J. Phys. Chem.,* **98,** 635 (1994).
137. I. I. Vaisman, F. K. Brown, and A. Tropsha, *J. Phys. Chem.,* **98,** 5559 (1994).
138. I. Tuñón, E. Silla, and J. L. Pascual-Ahuir, *Protein Eng.,* **5,** 715 (1992).
139. R. M. Lynden-Bell, *J. Phys. Chem.,* **97,** 2991 (1993).
140. H. S. Chan and K. A. Dill, *J. Chem. Phys.,* **101,** 7007 (1994).

141. D. J. Giesen, C. J. Cramer, and D. G. Truhlar, *J. Phys. Chem,* **98,** 4141 (1994).
142. R. A. Pierotti, *J. Phys. Chem.,* **67,** 1840 (1963).
143. B. Linder, *Adv. Chem. Phys.,* **12,** 225 (1967).
144. H. Hoshi, M. Sakurai, Y. Inouye, and R. Chûjô, *J. Chem. Phys.,* **87,** 1107 (1987).
145. R. Bonaccorsi, E. Ojalvo, and J. Tomasi, *Coll. Czech. Chem. Comm.,* **53,** 2320 (1988).
146. R. Bonaccorsi, F. Floris, P. Palla, and J. Tomasi, *Theor. Chim. Acta,* **162,** 213 (1990).
147. R. Bonaccorsi, E. Ojalvo, P. Palla, and J. Tomasi, *Chem. Phys.,* **143,** 245 (1990).
148. M. Cossi, B. Mennucci, and J. Tomasi, *Chem Phys. Lett.,* **228,** 165 (1994).
149. K. A. Sharp and B. Honig, *Annu. Rev. Biophys. Biophys. Chem.,* **19,** 301 (1990).
150. K. Sharp, A. Jean-Charles, and B. Honig, *J. Phys. Chem.,* **96,** 3822 (1992).
151. D. Sitkoff, K. A. Sharp, and B. Honig; *J. Phys. Chem.,* **98,** 1978 (1994).
152. A. Rashin, *J. Phys. Chem.,* **94,** 1725 (1990).
153. V. Mohan, M. E. Davis, J. A. McCammon, and B. M. Pettitt, *J. Phys. Chem.,* **96,** 6428 (1992).
154. C. Lim, S. L. Chan, and P. Tole, in *Structure and Reactivity in Aqueous Solution,* C. J. Cramer and D. G. Truhlar, Eds., American Chemical Society, Washington, DC, 1994, Vol. 568, p. 50.
155. L. Onsager, *J. Am. Chem. Soc.,* **58,** 1486 (1936).
156. A. Dega-Szafran, M. Gdaniec, M. Grunwald-Wyspianska, Z. Kosturkiewicz, J. Koput, P. Krzyzanowski, and M. Szafran, *J. Mol. Struct.,* **270,** 99 (1992).
157. M. Szafran, M. M. Karelson, A. R. Katritzky, J. Koput, and M. C. Zerner, *J. Comp. Chem.,* **14,** 371 (1993).
158. M. W. Wong, K. B. Wiberg, and M. J. Frisch, *J. Chem. Phys.,* **95,** 8991 (1991).
159. L. C. G. Freitas, R. L. Longo, and A. M. Simas, *J. Chem. Soc., Faraday Trans.,* **88,** 189 (1992).
160. C. Adamo and F. Lelj, *Chem. Phys. Lett.,* **223,** 54 (1994).
161. S. C. Tucker and D. G. Truhlar, *Chem Phys. Lett.,* **157,** 164 (1989).
162. J. L. Rivail and B. Terryn, *J. Chem. Phys.,* **79,** 1 (1982).
163. D. Rinaldi, M. F. Ruiz-Lopez, and J.-L. Rivail, *J. Chem. Phys.,* **78,** 834 (1983).
164. V. Dillet, D. Rinaldi, J. G. Angyán, and J.-L. Rivail, *Chem. Phys. Lett.,* **202,** 18 (1993).
165. V. Dillet, D. Rinaldi, and J.-L. Rivail, *J. Phys. Chem.,* **98,** 5034 (1994).
166. G. P. Ford and B. Wang, *J. Comp. Chem.,* **13,** 229 (1992).
167. R. R. Pappalardo, M. Reguero, and M. A. Robb, *Chem. Phys. Lett.,* **212,** 12 (1993).
168. M. J. Huron and P. Claverie, *J. Phys. Chem.,* **76,** 2123 (1972).
169. H. L. Friedman, *Mol. Phys.,* **29,** 29 (1975).
170. J. I. Gersten and A. M. Sapse, *J. Am. Chem. Soc.,* **107,** 3786 (1985).
171. G. Karlstrom, *J. Phys. Chem.,* **92,** 1315 (1988).
172. M. Karelson, T. Tamm, and M. C. Zerner, *J. Phys. Chem.,* **97,** 11901 (1993).

173. H. J. Kim, R. Bianco, B. J. Gertner, and J. T. Hynes, *J. Phys. Chem.,* **97,** 1723 (1993).
174. J. T. Hynes, H. J. Kim, J. R. Mathis, and J. Juanos i Timoneda, *J. Mol. Liquids,* **57,** 53 (1993).
175. S. Miertus, E. Scrocco, and J. Tomasi, *Chem. Phys.,* **55,** 117 (1981).
176. H. Hoshi, M. Sakurai, Y. Inoue, and R. Chûjô, *J. Mol. Struct. (Theochem),* **180,** 267 (1988).
177. T. Furuki, A. Umeda, M. Sakurai, Y. Inoue, and R. Chûjô, *J. Comp. Chem.,* **15,** 90 (1994).
178. G. P. Ford and B. Wang, *J. Am. Chem Soc.,* **114,** 10563 (1992).
179. B. Wang and G. P. Ford, *J. Chem. Phys.,* **97,** 4162 (1992).
180. T. Fox and N. Rosch, *J. Mol. Struct. (Theochem),* **276,** 279 (1992).
181. T. Fox, N. Rosch, and R. J. Zauhar, *J. Comp. Chem.,* **14,** 253 (1993).
182. M. Negre, M. Orozco, and F. J. Luque, *Chem. Phys. Lett.,* **196,** 27 (1992).
183. F. J. Luque, M. J. Negre, and M. Orozco, *J. Phys. Chem.,* **97,** 4386 (1993).
184. A. A. Rashin, M. A. Bukatin, J. Andzelm, and A. T. Hagler, *Biophys. Chem,* **51,** 375 (1994).
185. K. Baldridge, R. Fine, and A. Hagler, *J. Comp. Chem.,* **15,** 1217 (1994).
186. Y. Chen, L. Noodleman, D. A. Case, and D. Bashford, *J. Phys. Chem.,* **98,** 11059 (1994).
187. F. Peradejordi, *Cahiers Phys.,* **17,** 343 (1963).
188. T. Kozaki, K. Morihashi, and O. Kikuchi, *J. Mol. Struct. (Theochem),* **168,** 265 (1988).
189. T. Kozaki, M. Morihashi, and O. Kikuchi, *J. Am. Chem. Soc.,* **111,** 1547 (1989). 190. A. Klamt and G. Schüürmann, *J. Chem Soc., Perkin Trans.* 2, 799 (1993).
191. D. Eisenberg and A. D. McLachlan, *Nature,* **319,** 199 (1986).
192. T. Ooi, M. Oobatake, G. Nemethy, and H. A. Scheraga, *Proc. Natl. Acad. Sci., USA,* **84,** 3086 (1987).
193. W. C. Still, A. Tempczyk, R. C. Hawley, and T. Hendrickson, *J. Am. Chem. Soc.,* **112,** 6127 (1990).
194. D. Rinaldi, B. J. Costa Cabral, and J.-L. Rivail, *Chem Phys. Lett.,* **125,** 495 (1986).
195. P. Young, D. V. S. Green, I. H. Hillier, and N. A. Burton, *Mol. Phys.,* **80,** 503 (1993).
196. I. Tuñón, E. Silla, and J. Bertrán, *J. Phys. Chem.,* **97,** 5547 (1993).
197. J. Langlet, P. Claverie, J. Caillet, and A. Pullman, *J. Phys. Chem.,* **92,** 1617 (1988).
198. H. Sato and S. Kato, *J. Mol. Struct. (Theochem),* **310,** 67 (1994).
199. E. O. Purisima and S. H. Nilar, *J. Comp. Chem.,* **16,** 681 (1995).
200. A. Varnek, G. Wipff, A. S. Glebov, and D. Feil, *J. Comp. Chem.,* **16,** 1 (1995).
201. G. Karlström and B. Halle, *J. Chem. Phys.,* **99,** 8056 (1993).
202. F. Floris and J. Tomasi, *J. Comp. Chem.,* **10,** 616 (1989).
203. F. M. Floris, J. Tomasi, and J. L. Pascual-Ahuir, *J. Comp. Chem.,* **39,** 784 (1991).
204. C. Amovilli, *Chem. Phys. Lett.,* **229,** 244 (1994).

205. M. Bachs, F. J. Luque, and M. Orozco, *J. Comp. Chem.,* **15,** 446 (1994).
206. F. J. Luque, M. Bachs, and M. Orozco, *J. Comp. Chem.,* **15,** 847 (1994).
207. M. Orozco, M. Bachs, and F. J. Luque, *J. Comp. Chem*., **16,** 563 (1995).
208. F. J. Luque, C. Alemán, M. Bachs, and M. Orozco, preprint
209. F. J. Luque, C. Alemán, and M. Orozco, preprint
210. C. J. Cramer and D. G. Truhlar, *J. Am. Chem Soc.,* **113,** 8305 (1991).
211. C. J. Cramer and D. G. Truhlar, *Science,* **256,** 213 (1992).
212. C. J. Cramer and D. G. Truhlar, *J. Comp. Chem.,* **13,** 1089 (1992).
213, J. W. Storer, D. J. Giesen, G. D. Hawkins, G. C. Lynch, C. J. Cramer, D. G. Truhlar, and D. A. Liotard, in *Structure and Reactivity in Aqueous Solution,* C. J. Cramer and D. G. Truhlar, Eds., American Chemical Society, Washington, DC, 1994 p. 24.
214. D. A. Liotard, G. D. Hawkins, G. C.. Lynch, C. J. Cramer, and D. G. Truhlar, *J. Comp. Chem.,* **16,** 422 (1995).
215. G. D. Hawkins, C. J. Cramer, and D. G. Truhlar, *Chem Phys. Lett.,* submitted for publication
216. D. J. Giesen, J. W. Storer, C. J. Cramer, and D. G. Truhlar, *J. Am. Chem. Soc*., **117,** 1057 (1995).
217. D. J. Giesen, C. J. Cramer, and D. G. Truhlar, *J. Phys. Chem.,* **99,** 7137 (1995).
218. C. C. Chambers, D. J. Giesen, C. J. Cramer, and D. G. Truhlar, to be published
219. G. Rauhut, T. Clark, and T. Steinke, *J. Am. Chem. Soc.,* **115,** 9174 (1993).
220. D. J. Tannor, B. Marten, R. Murphy, R. A. Friesner, D. Sitkoff, A. Nicholls, M. Ringnalda, W. A. Goddard, and B. Honig, *J. Am. Chem. Soc.,* **116,** 11875 (1994).
221. R. W. Dixon, J. M. Leonard, and W. J. Hehre, *Israel J. Chem.,* **33,** 427 (1993).
222. T. N. Truong and E. V. Stefanovich, *Chem. Phys. Lett.,* **240,** 253 (1995).
223. T. N. Truong and E. V. Stefanovich, *J. Chem. Phys.,* in press.
224. D. Thirumalai, K. Onda, and D. G. Truhlar, *J. Chem. Phys.,* **74,** 526 (1981).
225. A. J. Stone, *Chem. Phys. Lett.,* **83,** 233 (1981).
226. A. J. Stone and M. Alderton, *Mol. Phys.,* **56,** 1047 (1985).
227. W. A. Sokalski, D. A. Keller, R. L. Ornstein, and R. Rein, *J. Comp. Chem.,* **14,** 970 (1993).
228. C. Chipot, J. G. Angyán, G. G. Ferenczy, and H. A. Scheraga, *J. Phys. Chem.,* **97,** 6628 (1993).
229. D. E. Williams, *J. Comp. Chem.,* **15,** 719 (1994).
230. G. J. Hoijtink, E. de Boer, P. H. Van der Meij, and W. P. Weijland, *Recl. Trav. Chim. Pays-Bas,* **75,** 487 (1956).
231. I. Jano, *Compt. Rend. Acad. Sci. Paris,* **261,** 103 (1965).
232. G. Klopman, *Chem Phys. Lett.,* **1,** 200 (1967).
233. R. Contreras and A. Aizman, *Int. J. Quant. Chem.,* **27,** 293 (1985).
234. M. Schaefer and C. Froemmel, *J.* Mol. *Biol.,* **216,** 1045 (1990).
235. J. W. Storer, D. J. Giesen, C. J. Cramer, and D. G. Truhlar, *J. Comput.-Aid. Mol. Des*., **9,** 87(1995).

236. C. J. Cramer and D. G. Truhlar, *J. Comput.-Aid. Mol. Des.,* **6,** 629 (1992).
237. I. Alkorta, H. O. Villar, and J. J. Perez, *J. Comp. Chem.,* **14,** 620 (1993).
238. C. J. Cramer, G. D. Hawkins, and D. G. Truhlar, *J. Chem. Soc., Faraday Trans.,* **90,** 1802 (1994).
239. A. Ben-Naim, *Statistical Thermodynamics for Chemists and Biochemists.* Plenum, New York, 1992.
240. C. Reichardt, *Solvents and Solvent Effects in Organic Chemistry.* VCH, New York, 1990.
241. L. Streyer, *Biochemistry.* W. H. Freeman and Co., New York, 1981.
242. K. Ijima, K. Tanaka, and S. Onuma, *J. Mol. Struct.,* **246,** 257 (1991).
243. R. Bonaccorsi, P. Palla, and J. Tomasi, *J. Am. Chem. Soc.,* **106,** 1945 (1984).
244. J. S. Gaffney, R. C. Pierce, and L. Friedman, *J. Am. Chem. Soc.,* **99,** 4293 (1977).
245. W. J. Hehre, L. Radom, P. v. R. Schleyer, and J. A. Pople, *Ab Initio Molecular Orbital Theory.* Wiley, New York, 1986.
246. W. J. Hehre, L. D. Burke, A. J. Shusterman, and W. J. Pietro, *Experiments in Computational Organic Chemistry.* Wavefunction Inc., Irvine, CA, 1993.
247. W. J. Pietro, *J. Chem. Ed.,* **71,** 416 (1994).
248. S. Inouye, *Chem. Pharm. Bull.,* **16,** 1134 (1968).
249. W. C. Herndon, *J. Phys. Org. Chem.,* **6,** 634 (1993).
250. S. H. Hilal, L. A. Carreira, G. L. Baughman, S. W. Karickhoff, and C. M. Melton, *J. Phys. Org. Chem.,* **7,** 122 (1994).
251. E. Rajasekaran, B. Jayaram, and B. Honig, *J. Am. Chem. Soc.,* **116,** 8238 (1994).
252. J. J. Urban, R. L. Vontersch, and G. R. Famini, *J. Org. Chem.,* **59,** 5239 (1994).
253. B. Terryn, J.-L. Rivail, and D. Rinaldi, *J. Chem. Res.* (S), 141 (1981).
254. S. Galera, A. Oliva, J. M. Lluch, and J. Bertrán, *J. Mol. Struct. (Theochem),* **110,** 15 (1984).
255. J. L. Pascual-Ahuir, J. Andres, and E. Silla, *Chem Phys. Lett.,* **169,** 297 (1990).
256. I. Tuñón, E. Silla, and J. Tomas, *J. Phys. Chem.,* **96,** 9043 (1992).
257. D. H. Aue, H. M. Webb, and M. T. Bowers, *J. Am. Chem. Soc.,* **98,** 311 (1976).
258. M. Meot-Ner and L. W. Sieck, *J. Am. Chem. Soc.,* **113,** 4448 (1991).
259. R. C. Weast, Ed., *CRC Handbook* of *Chemistry and Physics* CRC Press, Boca Raton, FL, 1980.
260. C. J. Cramer and D. G. Truhlar, *J. Am. Chem. Soc.,* **113,** 8552 9901(E) (1991).
261. I. Tuñón, E. Silla, and J.-L. Pascual-Ahuir, *J. Am. Chem. Soc.,* **115,** 2226 (1993).
262. J.-L. Rivail, S. Antoczak, C. Chipot, M. F. Ruiz-López, and L. G. Gorb, in *Structure and Reactivity in Aqueous Solution, C.* J. Cramer and D. G. Truhlar, Eds., American Chemical Society, Washington, DC, 1994, Vol. 568, p. 154.
263. K. Ando and J. T. Hynes, in *Structure and Reactivity in Aqueous Solution,* C. J. Cramer and D. G. Truhlar, Eds., American Chemical Society, Washington, DC, 1994, Vol. 568, p. 143.
264. R. A. Marcus, *Annu. Rev. Phys. Chem.,* **15,** 155 (1964).
265. R. A. Robertson, *Trans. Faraday Soc.,* **32,** 743 (1936).

266. A. R. Katritzky, *Handbook of Heterocyclic Chemistry.* Pergamon, Oxford, 1985.
267. J. S. Kwiatkowski, T. J. Zielinski, and R. Rein, *Adv. Quantum Chem.,* **18,** 85 (1986).
268. M. M. Karelson, A. R. Katritzky, M. Szafran, and M. C. Zerner, J. *Chem. Soc., Perkin Trans. 2*, 195 (1990).
269. M. M. Karelson, T. Tamm, A. R. Katritzky, S. J. Cato, and M. C. Zerner, *Tetrahedron Comput. Methodol.,* **2,** 295 (1989).
270. H. S. Rzepa, M. Y. Yi, M. M. Karelson, and M. C. Zerner, *J. Chem. Soc., Perkin Trans.* 2,635 (1991).
271. O. G. Parchment, D. V. S. Green, P. J. Taylor, and I. H. Hillier, *J. Am. Chem. Soc.,* **115,** 2352 (1993).
272. S. Woodcock, D. V. S. Green, M. A. Vincent, I. H. Hillier, M. F. Guest, and P. Shenvood, *J. Chem Soc., Perkin Trans.* 2, 2151 (1992).
273. M. A. Aguilar and F. J. Olivares del Valle, *Chem. Phys.,* **129,** 439 (1989).
274. U. C. Singh and P. A. Kollman, *J. Comp. Chem,* **5,** 129 (1984).
275. W. L. Jorgensen, J. Chandrasekhar, J. D. Madura, R. W. Impey, and M. L. Klein, *J. Chem. Phys.,* **79,** 926 (1983).
276. S. J. Weiner, P. A. Kollman, D. T. Nguyen, and D. A. Case, *J. Comp. Chem.,* **7,** 230 (1986).
277. C, J. Cramer and D. G. Truhlar, *J. Am. Chem. Soc.,* **115,** 8810 (1993).
278. A. R. Katritzky and J. M. Lagowski, *Adv. Heterocycl. Chem.,* **6,** 1 (1963).
279. J. Elguero, C. Marzin, A. R. Katritzky, and P. Linda, *The Tautomerism of Heterocycles.* Academic, New York, 1976.
280. I. R. Gould and I. H. Hillier, *J. Chem. Soc., Perkin Trans. 2,* 1771 (1993).
281. F. Tomás, J. Catalán, P. Pérez, and J. Elguero, *J. Org. Chem.,* **59,** 2799 (1994).
282. J. Catalán, P. Pérez, and J. Elguero, *J. Org. Chem.,* **58,** 5276 (1993).
283. D. S. Wofford, D. M. Forkey, and J. G. Russell, *J. Org. Chem.,* **47,** 5132 (1982).
284. W. M. F. Fabian, *J. Comp. Chem,* **12,** 17 (1991).
285. O. G. Parchment, I. H. Hillier, D. V. S. Green, N. A. Burton, J. O. Morley, and H. F. Schaefer, *J. Chem. Soc., Perkin Trans. 2*, 1681 (1992).
286. H. Fritz, *Bull. Soc. Chim. Belg.,* **93,** 559 (1984).
287. M. W. Wong, R. Leung-Toung, and C. Wentrup, *J. Am. Chem. Soc.,* **115,** 2465 (1993).
288. P. Beak, *Acc. Chem. Res.,* **10,** 186 (1977).
289. L. D. Hatherley, R. D. Brown, P. D. Godfrey, A. P. Pierlot, W. Caminati, D. Damiani, S. Melandri, and L. B. Favero, *J. Phys. Chem.,* **97,** 46 (1993).
290. A. Les, L. Adamowicz, M. J. Nowak, and L. Lapinski, *J. Mol. Struct. (Theochem),* **277,** 313 (1992).
291. O. G. Parchment, N. A. Burton, and I. H. Hillier, *Chem. Phys. Lett.,* **203,** 46 (1993).
292. R. J. Hall, N. A. Burton, I. H. Hillier, and P. E. Young, *Chem. Phys. Lett.,* **220,** 129 (1994).
293. V. Barone and C. Adamo, *Chem. Phys. Lett.,* **226,** 399 (1994).

294. J. S. Kwiatkowski and A. Tempczyk, *Chem. Phys.,* **85,** 397 (1984).
295. M. M. Karelson, A. R. Katritzky, M. Szafran, and M. C. Zerner, *J. Org. Chem.,* **54,** 6030 (1989).
296. H. S. Rzepa and M. Y. Yi, *J. Chem. Soc., Perkin Trans.* 2, 531 (1991).
297. M. W. Wong, K. B. Wiberg, and M. J. Frisch, *J. Am. Chem. Soc.,* **114,** 1645 (1992).
298. V. Barone and C. Adamo, *J. Comp. Chem,* **15,** 395 (1994).
299. V. Barone and C. Adamo, *J. Photochem. Photobiol. A: Chem.,* **80,** 211 (1994).
300. J. E. Del Bene, *J. Phys. Chem.,* **98,** 5902 (1994).
301. B. Wang and G. P. Ford, personal communication.
302. S. H. Vosko, L. Wilks, and M. Nussair, *Can. J. Phys.,* **58,** 1200 (1980).
303. A. D. Becke, *Phys. Rev. A,* **38,** 3098 (1988).
304. J. P. Perdew, *Physical Reviews B*, **33;** 8822 (1986).
305. P. O. Löwdin, *Adv. Quantum Chem.,* **2,** 213 (1965).
306. B. Pullman and A. Pullman, *Adv. Heterocycl. Chem.,* **13,**77 (1971).
307. M. D. Topal and J. R. Fresco, *Nature,* **263,** 285 (1976).
308. M. Szczeniak, K. Szczepaniak, J. S. Kwiatkowski, K. KuBulat, and W. B. Person, *J. Am. Chem. Soc.,* **110,** 8319 (1988).
309. M. Scanlan and I. H. Hillier, *J. Am. Chem. Soc.,* **106,** 3737 (1984).
310. J. S. Kwiatkowski, R. J. Bartlett, and W. B. Person, *J. Am. Chem. Soc.,* **110,** 2353 (1988).
311. A. Les, L. Adamowicz, and R. J. Bartlett, *J. Phys. Chem.,* **93,** 4001 (1989).
312. J. Leszcynski, *J. Phys. Chem.,* **96,** 1649 (1992).
313. J. W. Boughton and P. Pulay, *Int. J. Quant. Chem.,* **47,**49 (1993).
314. D. A. Estrin, L. Paglieri, and G. Corongiu, *J. Phys. Chem.,* **98,** 5653 (1994).
315. A. R. Katritzky and M. Karelson, *J. Am. Chem Soc.,* **113,** 1561 (1991).
316. P. E. Young and I. H. Hillier, *Chem Phys. Lett.,* **215,** 405 (1993).
317. M. Orozco and F. J. Luque, *J. Am Chem. Soc.,* **117,** 1378 (1995).
318. J. G. Contreras and J. B. Alderete, *J. Mol. Struct. (Theochem),* **309,** 137 (1994).
319. C. Alhambra, F. J. Luque, J. Estelrich, and M. Orozco, *J. Org. Chem.,* **60,** 969 (1995).
320. J. G. Contreras and I. B. Alderte, *Bol. Sci. Chil. Quim.,* **39,** 17 (1994).
321. J. G. Contreras and J. B. Alderete, *Chem. Phys. Lett.,* **232,** 61 (1995).
322. X.-C. Wang, J. Nichols, M. Feyereisen, M. Gutowski, J. Boatz, A. D. J. Haymet, and J. Simons, *J. Phys. Chem.,* **95,** 10419 (1991).
323. G. Briegleb and W. Strohmeier, *Angew. Chem.,* **64,** 409 (1952).
324. S. G. Mills and P. Beak, *J. Org. Chem.,* **50,** 1216 (1985).
325. S. E. Barrows, F. J. Dulles, C. J. Cramer, D. G. Truhlar, and A. D. French, *Carbohydr. Res.,* in press
326. H. B. Broughton and P. R. Woodward, *J. Comput.-Aid. Mol. Des.,* **4,** 147 (1990).
327. S. Gelin and P. Pollet, *Tetrahedron Lett.,* **21,** 4491 (1980).
328. K. Saito and T. Yamaguchi, *J. Chem. Soc., Perkin Trans.* 2, 1605 (1979).

329. J. Whiting and J. T. Edward, *Can. J. Chem.,* **49,** 3799 (1971).
330. D. Chandler and L. R. Pratt, *J. Chem. Phys.,* **65,** 2925 (1976).
331. L. R. Pratt and D. C. Chandler, *J. Chem. Phys.,* **67,** 3683 (1977).
332. D. Chandler, *J. Chem. Phys.,* **68,** 2959 (1978).
333. J. T. Hynes, in *Theory of Chemical Reaction Dynamics,* M. Baer, Ed. CRC Press, Boca Raton, 1985, Vol. 4, p. 171.
334. T. L. Hill, *Statistical Mechanics: Principles and Selected Applications.* McGraw-Hill, New York, 1956.
335. D. J. Tobias, S. F. Sneddon, and C. L. Brooks, *J. Mol. Biol.,* **216,** 783 (1990).
336. G. J. Tawa and L. R. Pratt, in *Structure and Reactivity in Aqueous Solution,* C. J. Cramer and D. G. Truhlar, Eds., American Chemical Society, Washington, DC, 1994, Vol. 568, p. 60.
337. T. C. Beutler and W. F. van Gunsteren, *Chem. Phys. Lett.,* **237,** 308 (1995).
338. C. Ritchie, *Pure Appl. Chem.,* **51,** 153 (1979).
339. J. Jaume, J. M. Lluch, A. Oliva, and J. Bertrán, *Chem. Phys. Lett.,* **106,** 232 (1984).
340. S. C. Tucker and D. G. Truhlar, *J. Am. Chem. Soc.,* **112,** 3347 (1990).
341. C. J. Cramer and D. G. Truhlar, *J. Am. Chem. Soc.,* **114,** 8794 (1992).
342. I. Tuñón, E. Silla, and J. Bertrán, *J. Chem. Soc,, Faraday Trans.,* **90,** 1757 (1994).
343. J. Frau, J. Donoso, F. Muñoz, and F. G. Blanco, *Helv. Chim. Acta,* **77,** 1557 (1994).
344. J. Bertrán, J. M. Lluch, A. Gonzalez-Lafont, V. Dillet, and V. Pérez, in *Structure and Reactivity in Aqueous Solution,* C. J. Cramer and D. G. Truhlar, Eds., American Chemical Society, Washington, DC, 1994, Vol. 568, p. 168.
345. P. M. Morse, *Thermal Physics.* W. A. Benjamin, New York, 1969.
346. C. V. Heer, *Statistical Mechanics, Kinetic Theory, and Stochastic Processes,* Academic, New York, 1972.
347. J. McConnell, *Rotational Brownian Motion and Dielectric Theory.* Academic, New York, 1980.
348. L. D. Zusman, *Soviet Phys. JETP,* **42,** 794 (1976).
349. I. Rips and J. Jortner, *J. Chem. Phys.,* **87,** 2090 (1987).
350. J. Hubbard and L. Onsager, *J. Chem. Phys.,* **67,** 4850 (1977).
351. D. Kivelson and H. Friedman, *J. Chem Phys.,* **93,** 7026 (1989).
352. R. Saxton, *Proc. R. Soc. London,* **A213,** 473 (1952).
353. S. K. Garg and C. P. Smyth, *J. Phys. Chem.,* **69,** 1294 (1965).
354. J. Crossley, *Adv. Molec. Relax. Processes,* **2,** 69 (1970).
355. L. D. Zusman, *Chem. Phys.,* **119,** 51 (1988).
356. Z. Wang, J. Tang, and J. R. Noms, *J. Chem. Phys.,* **97,** 7251 (1992).
357. S. Lee and J. T. Hynes, *J. Chem. Phys.,* **88,** 6863 (1988).
358. M. V. Basilevsky, G. E. Chudinov, and D. W. Napolov, *J. Phys. Chem.,* **97,** 3270 (1993).
359. D. G. Truhlar, G. K. Schenter, and B. C. Garrett, *J. Chem. Phys.,* **98,** 5756 (1993).
360. A. I. Burshtein and A. A. Zharikov, *Chem. Phys.,* **152,** 23 (1956).

361. B. C. Garrett and G. K. Schenter, in *Structure and Reactivity in Aqueous Solution,* C. J. Cramer and D. G. Truhlar, Eds., American Chemical Society, Washington, DC, 1994, Vol. 568, p. 122.
362. L. D. Zusman, *Chem. Phys.,* **49,** 265 (1980).
363. A. Garg, J. N. Onuchic, and V. Ambegaokar, *J. Chem. Phys.,* **83,** 4491 (1985).
364. M. V. Basilevsky and G. E. Chudinov, *Chem. Phys.,* **157,** 345 (1991).
365. H. J. Kim and J. T. Hynes, *J. Chem. Phys.,* **93,** 5211 (1990).
366. I. V. Alexandrov, *Chem. Phys.,* **51,** 449 (1980).
367. R. Zwanzig, *J. Stat. Phys.,* **9,** 215 (1973).
368. S. A. Adelman and J. D. Dull, *J. Chem Phys.,* **64,** 2375 (1976).
369. S. A. Adelman, *Adv. Chem. Phys.,* **44,** 143 (1980).
370. S. A. Adelman and C. L. Brooks, *J. Phys. Chem.,* **86,** 1511 (1982).
371. R. F. Grote and J. T. Hynes, *J. Chem. Phys.,* **73,** 2715 (1980).
372. G. van der Zwan and J. T. Hynes, *J. Chem. Phys.,* **78,** 4174 (1983).
373. **S.** Mukamel, *Annu. Rev. Phys. Chem.,* **41,** 647 (1990).
374. L.E. Fried and S. Mukamel, *Adv. Chem. Phys.,* **84,** 435 (1993).
375. R. M. Stratt, *Acc. Chem. Res.,* **28,** 201 (1995).
376. M. Karelson and M. C. Zerner, *J. Am. Chem. Soc.,* **112,** 9405 (1990).
377. M. M. Karelson and M. C. Zemer, *J. Phys. Chem.,* **96,** 6949 (1992).
378. T. Fox and N. Rösch, *Chem. Phys. Lett.,* **191,** 33 (1992).
379. N. Rosch and M. C. Zemer, *J. Phys. Chem.,* **98,** 5817 (1994).
380. A. Klamt, preprint
381. D. Chandler, in *Liquids, Freezing, and Glass Transition,* J. P. Hansen, D. Levesque and J. Zinn-Justin, Eds., Elsevier, Amsterdam, 1991 p. 193.
382. M. J. Weaver, *Chem. Rev.,* **92,** 463 (1992).
383. B. C. Garrett and G. K. Schenter, *Int. Rev. Phys. Chem.,* **13,** 263 (1994).
384. P. J. Rossky and J. D. Simon, *Nature,* **370,** 263 (1994).
385. S. C. Tucker, in *New Trends in Kramer's Reaction Rate Theory,* P. Talkner and P. Hänggi, Eds., Kluwer, Dordrecht, 1995 p. *5.*

THEORETICAL BASIS FOR THE TREATMENT OF SOLVENT EFFECTS IN THE CONTEXT OF DENSITY FUNCTIONAL THEORY

RENATO CONTRERAS and PATRICIA PÉREZ

Departamento de Quimica, Centro de Mecanica Cuantica Aplicada, Facultad de Ciencias, Universidad de Chile, Casilla 653- *Santiago, Chile.*

ARIE AIZMAN

Departamento de Quimica, Facultad de Ciencias, Universidad Tecnica Federico Santa Maria, Casilla 110 — *V, Valparaiso, Chile.*

Abstract.

Theoretical considerations leading to a density functional theory (DFT) formulation of the reaction field (RF) approach to solvent effects are discussed. The first model is based upon isolelectronic processes that take place at the nucleus of the host system. The energy variations are derived from the nuclear transition state (ZTS) model. The solvation energy is expressed in terms of the electrostatic potential at the nucleus of a *pseudo atom* having a fractional nuclear charge. This procedure avoids the introduction of arbitrary ionic radii in the calculation of insertion energy, since all integrations involved are performed over $[0,\infty]$. The quality of the approximations made are discussed within the frame of the Kohn-Sham formulation of density functional theory.

Introduction of the static density response function for a system with a constant number of electrons yields the *RF – DFT* model. This second approach is expected to be more useful in the analysis of chemical reactivity in condensed phases.

O. Tapia and J. Bertrán (eds.), Solvent Effects and Chemical Reactivity, 81–123.
© 1996 *Kluwer Academic Publishers. Printed in the Netherlands.*

1. Introduction.

The physical properties of atoms and molecules embedded in polar liquids have usually been described in the frame of the *effective medium* approximation. Within this model, the solute-solvent interactions are accounted for by means of the RF theory [1-3]. The basic quantity of this formalism is the RF potential. It is usually variationally derived from a model energy functional describing the effective energy of the solute in the field of an external eIectrostatic perturbation. For instance, if a singly negative or positive charged atomic system is considered, the RF potential is simply given by

$$\Phi_R(\vec{r}) = \alpha(\epsilon)\left(\frac{Z}{r_A} - \int d\vec{r'}\frac{\rho(\vec{r'})}{|\vec{r}-\vec{r'}|}\right) \quad (1)$$

In Eq (1), $\alpha(\varepsilon)$ is the RF response factor depending on an effective dielectric constant ε [4,5], and the quantity in brackets is the electrostatic potential of the ion $\Phi(\vec{r})$, expressed in terms of the nuclear charge Z, the ionic radius r_A and the one particle electron density $\rho(\vec{r})$.

If we introduce the following definition for the net charge of the ion :

$$Q = Z - \int d\vec{r'}\rho(\vec{r'}) \quad (2)$$

then, the electrostatic solute-solvent interaction energy is simply given by [6]:

$$\Delta E_{int} = Q\Phi_R(\vec{r}) = \alpha(\epsilon)Q\Phi(\vec{r}) \quad (3)$$

Using statistical thermodynamic arguments [5,7], it may be easily shown that the Born solvation free energy may be written as [8]:

$$\Delta E_{solv} = \frac{1}{2}\Delta E_{int} = \frac{1}{2}Q\Phi_R(\vec{r}) \quad (4)$$

Equations (1)- (4) have been generalized to molecules [2,3,10-13], in the context of the self consistent reaction field (SCRF) theory [14].

In the Born like approaches to solvation energy, the electrostatic potential of the ion appears as the basic variable of the theory. From Eq (1), it may be seen that if we have accurate electron densities at hand, the electrostatic potential strongly depends on the ionic radius r_A. The choice of suitable ionic radii usually introduces some arbitrariness in the calculation of ΔE_{solv} : there is no a physical criterium to justify the use of empirical r_A values coming from different sources [15-16].

Physically meaningful ionic radii may be obtained from Poisson equation for anions, and from electrostatic potentials defined in the the context of DFT for cations [17,18]. However, there remains the problem of being forced to use different mathematical criteria in both cases, because the electrostatic potential of anions and cations display a different functional behaviour with respect to the radial variable.

However, if we consider a model of ion solvation that uses the electrostatic potential at nucleus :

$$V_o = -\int d\vec{r}' \frac{\rho(\vec{r}')}{|\vec{r}-\vec{r}'|_{\vec{r}=0}} \qquad (5)$$

as the basic variable, anions and cations may be treated within a unified formalism. This procedure also avoids the problem of introducing empirically adjustable ionic radii, since all integrations are performed over $[0,\infty]$.

In this review we discuss the theoretical frame which may serve as a basis for a DFT formulation of solvent effects for atoms and molecules embedded in polar liquid environments. The emphasis is focused on the calculation of solvation energies in the context of the RF model, including the derivation of an effective energy functional for the atomic and molecular systems coupled to an electrostatic external field.

The article is organized as follows: in Section 2, a general discussion concerning the definition of electrostatic potentials in the frame of DFT is presented. In Section 3, the solvation energy is reformulated from a model based on isoelectronic processes at nucleus. The variational formulation of the insertion energy naturally leads to an energy functional, which is expressed in terms of the variation of the electron density with respect to

the variation of the external potential, for a fixed number of electrons. In Section 4, the resulting expression of the electrostatic solvation energy is discussed in the context of the nuclear transition state (ZTS) model. The quality of the approximations made are tested and discussed within the Kohn-Sham formulation of density functional theory. In Section 5, the RF model is reformulated on the basis of the static linear response function of DFT. The SCF version of the DFT-RF model is derived. In Section 6, a general discussion of the ZTS-RF and DFT-RF models is presented Our conclusions and future developments are included in Section 7.

2. Electrostatic Potential and Reaction Field Theory.

For a spherically symmetric charge distribution, an exact relationship between the electrostatic potential and the electron density is the Poisson equation :

$$\frac{\partial^2\Phi(r)}{\partial r^2} + \frac{2}{r}\frac{\partial\Phi(r)}{\partial r} = 4\pi\rho(r) \qquad (6)$$

Because $\rho(r) > 0$ everywhere, in the critical point defined by $\frac{\partial\Phi(r)}{\partial r} = 0$, we have $\frac{\partial^2\Phi(r)}{\partial r^2} > 0$, suggesting the existence of a minimum for a finite distance r^*, $(0 < r^* < \infty)$, from the nucleus. Sen and Politzer [19], shown that $\Phi(r)$ for anions displays a nonmonotonic behaviour with a characteristic minimum at r^*. Taking into account spherical symmetry, these authors proposed the following normalization condition for the electron density in the region $0 < r < r^*$:

$$Z = 4\pi \int_0^{r^*} dr' r'^2 \rho(r') \qquad (7)$$

Equation (7) guarantees that the minimum in the electrostatic potential is attained at the critical point r^* defining a sphere $S(0, r^*)$, which contains an electron density amount equal to the atomic number Z. From eq (7) we may conclude that the charge normalization condition for neutral atoms may only be satisfied for $r \to \infty$, whereas for cations it is never satisfied.

2.1. ELECTROSTATIC POTENTIAL FOR ANIONS.

For singly negative charged atoms, the electrostatic potential at the surface of $S(0,r^*)$ is given by [19] :

$$\Phi(r^*) = -4\pi \int_r^\infty dr' r' \rho(r') \qquad (8)$$

Equation (8) shows that $\Phi(r^*)$ for anions, is exclusively due to the electron density beyond the surface of $S(0,r^*)$. In other words, the electrostatic potential at the surface of $S(0, r^*)$ is due to the excess charge of the anion. Furthermore, because $\Phi(r^*)$ is a minimum, we may conclude that it represents the interaction of the anion with a positive charge *in vacuum.* In solution, after multiplying $\Phi(r^*)$ by the RF response factor according to eq (1), we may conclude that $\Phi_R(r^*)$ represents the interaction of the anion with a *polarization charge* distributed on the surface of $S(0,r^*)$ which, according to RF theory, displays an opposite sign to that of the source charge distribution. The solute-solvent electrostatic interaction energy is then readily obtained from eq (3), and the Born solvation energy *via* eq (4).

2.2. ELECTROSTATIC POTENTIAL FOR CATIONS.

From eq (7) it may be concluded that the charge normalization condition is never satisfied for cations. As a result, the functional dependence of $\Phi(r)$ with the radial variable is quite different in this case. For instance, it may be easily shown that $\Phi(r)$ displays a monotonic decreasing behavior without extrema points along the complete domain of the r variable. As a result, expression (8) for $\Phi(r)$ is not longer valid for singly positive charged atomic systems.

It is however possible to obtain a physically meaningful representation of $\Phi(r)$ for cations, in the context of density functional theory. The basic expression here is the fundamental stationary principle of DFT, which relates the electronic chemical potential μ, with the electrostatic potential and the functional derivatives of the kinetic and exchange-correlation contributions [20]:

$$\mu = \frac{\delta T}{\delta \rho(\vec{r})} - \Phi(\vec{r}) + \frac{\delta E_x}{\delta \rho(\vec{r})} + \frac{\delta E_c}{\delta \rho(\vec{r})}, \qquad (9)$$

where $T[\rho(\vec{r}]$, $E_x[\rho(\vec{r}]$ and $E_c[\rho(\vec{r}]$ are the kinetic, exchange and correlation energy functionals, respectively. Politzer et al [20] showed that Eq (9) may provide physically meaningful electrostatic potentials and atomic radii in the frame of the simple Thomas-Fermi-Dirac (TFD) theory. For this model, analytic simple expression for the kinetic, exchange and correlation energy functionals are available and it becomes possible to find a critical density $\rho^*(\vec{r})$ for which the chemical potential μ does exactly equal the negative of the electrostatic potential. This critical point is determined by :

$$\frac{\delta T}{\delta \rho(\vec{r})} = -\frac{\delta(E_x + E_c)}{\delta \rho(\vec{r})} \qquad (10)$$

Equation (10) is satisfied within TFD model, for a critical value $\rho^*(r)$ = 0.00872 [20]. Use of accurate atomic Hartree-Fock wavefunctions [21] to evaluate the electron density allowed the authors to obtain a set of critical radii for neutral atoms r_μ, associated to $\rho^*(r)$, which resulted in a remarkable good agreement with the covalent atomic radii. Application of this procedure to a series of singly charged monoatomic ions also produced a good agreement between r_μ and ionic radii [17]. In the case of doubly charged atomic cations however, such a good correlation was not found [17,18].

With physically meaningful ionic radii at hand, it is a rather simple task to evaluate the electrostatic properties of solvated cations in the frame of Born formalism. For instance, we may redefine the net charge of the ion given in Eq (2) as follows :

$$Q = Z - 4\pi \int_0^{r_\mu} dr' r'^2 \rho(r') \qquad (11)$$

Physically, Q represents the amount of charge inside the sphere $S(0, r_\mu)$ of radius r_μ centered at the nucleus. We may then associate to this net charge Q, the electrostatic potential $\Phi_Q(r_\mu) = Q/r_\mu$ which is the electrostatic potential at any point $r \geq r_\mu$, that is created by the nucleus and the electronic

charge within S(0, r_μ). Moreover, Eq (11) guarantees that the electrostatic potential at $r \geq r_\mu$ is the same as if the charge was concentrated at the nucleus. This feature is very important because it allows, within the Born formalism of ion solvation, the central charge Q to be considered as the limit of an ideal dipole centered at the origin of a spherical cavity represented by $S(0, r_\mu)$.

According to the above argument, the *central electrostatic potential* $\Phi_Q(r_\mu)$ of an atomic ion in the field of a polarizable environment, will be given by :

$$\Phi_Q(\epsilon, r_\mu) = \frac{Q}{\epsilon r_\mu} \qquad (12)$$

where ϵ is an affective dielectric constant of the medium.

According to the virtual charge model of Constanciel and Tapia [2], the same potential may be reproduced at the same point *in vacuum,* if we introduce the polarization charge $Q^{pol}(\epsilon)$, distributed on the surface of $S(0, r_\mu)$, such that

$$\frac{(Q + Q^{pol})}{r_\mu} = \frac{Q}{\epsilon r_\mu} \qquad (13)$$

Equation (13) entails the following definition of the polarization charges [2,3] :

$$Q^{pol}(\epsilon) = -\left(1 - \frac{1}{\epsilon}\right) Q \qquad (14)$$

with Q the central charge defined by Eq (2).

From Eq (14), the RF potential produced by $Q^{pol}(\epsilon)$ is

$$\Phi_Q^{pol}(\epsilon, r_\mu) = \frac{Q^{pol}}{r_\mu} = -\left(1 - \frac{1}{\epsilon}\right) \Phi_Q(r_\mu) \qquad (15)$$

The electrostatic interaction energy between the solute (represented by the charge distribution Q) and the polarizable medium represented by the induced charge distribution $Q^{pol}(\in)$ becomes :

$$E_{int}(\epsilon) = \Phi_Q^{pol}(\epsilon, r_\mu)Q = -\left(1 - \frac{1}{\epsilon}\right)\frac{Q^2}{r_\mu} \qquad (16)$$

and the electrostatic free energy of solvation is obtained from

$$\delta E_{solv}^{el} = \frac{1}{2}\Phi_Q^{pol}(\epsilon, r_\mu)Q = -\frac{1}{2}\left(1 - \frac{1}{\epsilon}\right)\frac{Q^2}{r_\mu} \qquad (17)$$

which is the well known Born formula, expressed as a function of the central charge Q, and the critical radius r_μ.

For calculational purposes, the basic quantities r_μ, Q and $\Phi_Q(r_\mu)$ are obtained as follows : a) From accurate atomic wavefunctions, the electron density is obtained by numerical integration; (b) with the electron density at any point at hand, the r_μ values are obtained by the simple reading of the distance at which $\rho(r)$ attains the critical value of 0.00872 electron units and (c) the central charge and the RF potential are readily obtained in terms of r_μ and $\Phi_Q(r_\mu)$ *via* Eqs (11) and (15), respectively.

In spite of the fact that the electrostatic solvation free energy for cations was derived for an homogeneuos electron gas with a positive background charge distribution, i.e. without specifying the sign of the total charge, it is found that this formalism is not applicable to negatively charged monoatomic ions. For instance, in the case of the fluorine ion, even though the critical r_μ value is very close to the crystalline ionic radius, we have found that the corresponding sphere $S(0,r_\mu)$ only contains about 50% of the electronic charge and as a consequence, only 25% of the electrostatic solvation free energy would be accounted for in the fluorine ion within the central charge and central potential model. However, if the fluorine ion is treated on the basis of the electrostatic potential derived from Poisson equation, a good correlation with the experimental value is obtained.

TABLE 1. - Electrostatic properties of solvated ions[a].

Ion	r^*	r_i	Q	$\Phi_R(r^*)$	δF_s^{el}	δF_s^{exp}
Li^+	1.38	1.31	1.110	-0.354	-123.3	-122.1
Na^+	1.93	1.79	1.129	-0.321	-117.6	-98.4
K^+	2.69	2.51	1.200	-0.288	-108.4	-80.5
Rb^+	3.18	2.80	1.228	-0.270	-103.8	-75.5
F^-	2.04	2.17	-1.00	0.350	-109.7	-89.5
Cl^-	3.08	3.15	-1.00	0.248	-77.9	-76.1
Br^-	3.38	3.44	-1.00	0.226	-71.3	-69.2
I^-	3.88	3.89	-1.00	0.204	-64.1	-60.3

[a]*Predicted ionic radii r*, experimental ionic radii r_i, central charge Q and RF potential Φ_R in atomic units. Electrostatic free energies of solvation, δF^{el}, in kcal/mol. Experimental values from reference [16]. Electrostatic potential for anions from reference [19]. For all calculations done, the effective dielectric constant reported in [16] was used.*

Table 1 summarizes the results obtained for the electrostatic properties of solvated anions and cations using the different electrostatic potential models discussed above. For cations, a remarkable good agreement between the predicted ionic radii with those reported in reference [22]. The Q values suggest that the major part of the electron density (about 90% for Li^+ and Na^+ and 80% K^+ and Rb^+) is confined within the corresponding sphere $S(0,r_\mu)$. The quality of the corresponding predicted values of the solvation free energy, strongly depends on the quality of the representation of the electron density inside the sphere $S(0,r_\mu)$: overall, the central charge model does reproduce the correct trend in the observed solvation energies for the series of cations selected. It is also interesting to note that deviations from experimental values increases with increasing number of electrons in the system. This fact may be associated with the quality of the atomic wavefunctions used to build up the electron density : Hartree-Fock wavefunctions do incorporate exchange exactly, whereas correlation effects are completely ignored. Improvements in the predictions of solvation free energies are expected by incorporating correlation effects within a Khon-Sham like scheme of calculation of the electron density.

For anions, the charge normalization condition given in Eq (7) guaran-

tees that 100% of the excess electron density is out of the corresponding sphere $S(0, r^*)$, so that $Q = -1.00$ for all the series. This fact is consistently reflected in the δF_S^{el} values reported in Table 1, which compares better with the experimental values as compared to the cation series.

In summary, density functional theory provides reliable and physically meaningful ionic radii to be used in the calculation of electrostatic solvation free energies, for singly positive and negative charged atomic ions. Perhaps the most serious shortcoming of this approach lies in the impossibility of treating cations and anions within a unic electrostatic effective potential model. In spite of this fact, we have shown that in both cases it is possible to describe the electrostatic solvation energy within a Born like formulation.

3. Solvation Energy from Isoelectronic Processes at Nucleus.

3.1 THE CHARGING MODEL.

It is possible to develop a unified model of solvation for anions and cations, if the classical Born charging process [8] is replaced by a Noyes like charging process [16]. This last model represents the inmersion of a charged atom into a liquid solution through a three step hypothetical cycle : a) in gas phase, an ion is converted into a neutral isoelectronic species by removing or adding a nuclear charge unity, (b) the resulting neutral system is added to the liquid solution and (c) the original charged atomic system is restored by the opposite process described in (a). If the non electrostatic (cavitation) energy contribution (step b) is neglected, the electrostatic solvation energy reduces to the sum of the contributions (a) and (c).

These succesive isoelectronic processes may be represented, for the inmersion of a charged monoatomic ion A^+ say, by the cycle described in *Figure* 1. Where X is an auxiliary isoelectronic neutral system. According to the cycle shown in *Figure* 1, we may write the insertion energy variation as follows:

$$\Delta E_{ins}(Z+1, Z+1) = \Delta E_a^{\circ}(Z+1, Z) + \Delta E_b(Z, Z) + \Delta E_c(Z, Z+1) \quad (18)$$

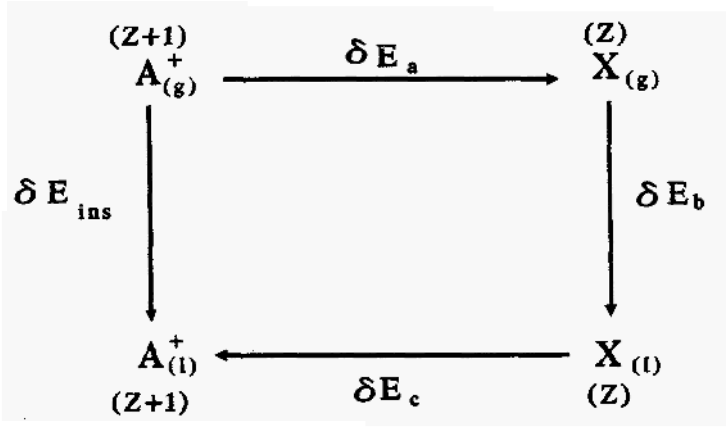

Figure 1. Thermodynamic cycle to achieve the insertion of an arbitrary ion into a continuum dielectric medium.

Where ΔE_a^o (Z + 1, Z) represents the total energy variation for the isoelectronic change *in vaccum,* $\Delta E_b(Z, Z)$ represents the total energy variation associated to the insertion of the neutral isoelectronic species into the polar liquid and $\Delta E_c(Z, Z + 1)$ denotes the total energy variation for the opposite isoelectronic process to step (a), in the presence of the polarizable medium. This last quantity does not only differ by an opposite sign to that of $\Delta E_a^o(Z + 1, Z)$ but also contains the polarization effect due to the electrostatic interaction with the medium. Moreover, if we are interested only in the electrostatic contributions to $\Delta E_{ins}(Z + 1, Z + 1)$, the quantity $\Delta E_b(Z, Z)$ representing the work required to form the hole in the polarizable host where the ion will be embedded, may be neglected to give

$$\Delta E_{ins}(Z+1, Z+1) = \Delta E_a^{\circ}(Z+1, Z) + \Delta E_c(Z, Z+1) \qquad (19)$$

in the sense that hereafter ΔE_{ins} will be considered as an electrostatic energy variation.

It is then possible, within a Noyes like charging model, to obtain the electrostatic component of the insertion energy expressed as a sum of two contribution coming from two opposite isoelectronic processes that takes

place *in vacuum,* and in the presence of an external field respectively. Since the energy variations associated to these isoelectronic processes are formulated in terms of a varying nuclear charge, keeping the number of electrons fixed, it seems then natural to obtain the expressions for $\Delta E_a^o(Z+1, Z)$ and $\Delta Ec(Z, Z+1)$ *via* the differential *Hellman – Feynman* (HF) theorem [32] as follows : consider the charged atomic ion as a system containing N electrons moving in a local external potential $\upsilon(\vec{r})$. The hamiltonian for such a system is :

$$\hat{H(Z)} = \hat{T} + \hat{V_{ee}} - \sum_{i=1}^{N} \hat{v}(\vec{r}_i, Z) \qquad (20)$$

where T and V_{ee} are the kinetic energy and the electron repulsion potential operators, respectively, and $\upsilon(\vec{r}) = \Sigma\ \hat{\upsilon}(\vec{r}_i, Z)$ the external potential representing here the nuclear-electron attraction operator. Application of the HF theorem gives :

$$\frac{dE(Z)}{dZ} = \langle \psi(Z) \mid \frac{d\hat{H}(Z)}{dZ} \mid \psi(Z) \rangle = -\langle \psi(Z) \mid \sum \frac{1}{r_i} \mid \psi(Z) \rangle = V_o(Z) \qquad (21)$$

with $V_o(Z)$ the electrostatic potential at nucleus, defined in Eq (5). For any arbitrary variation in the Z variable, Eq (21) may be integrated to give :

$$\Delta E(\Delta Z) = E(Z_X - Z_A) = \int_{Z_A}^{Z_X} dZ V_o(Z) \qquad (22)$$

Using Eq (22) the contributions $\Delta E_a^o(Z+1, Z)$ and $\Delta E_c(Z, Z+1)$ to solvation energy may be easily evaluated for a model potential $V_o(Z)$. For instance, for moderated changes in the Z variable (*i.e.* for $Z_X = Z_A \pm 1$), Davis [23] has shown that a linear potential model for $V_o(Z)$:

$$V_o = \alpha + \beta Z \qquad (23)$$

provides a reasonably good approximation for the energy variations associated to the isoelectronic changes in atoms. It is worth mentioning however, that the contribution ΔE_c $(Z, Z + 1)$ is not simply the opposite of $\Delta E_a^o(Z + 1, Z)$, but it further contains an electronic polarization contribution due to coupling of the whole system with the electrostatic external perturbation. We will show that such a contribution may be variationally incorporated into the calculation of ΔE_{ins}.

3.2. VARIATIONAL FORMULATION OF THE INSERTION ENERGY.

Consider the isoelectronic pair (A^+, X) *in vaccum,* with hamiltonians $\hat{H}_A^o$ and $\hat{H}_B^o$ which differ in external potentials $\hat{v}^o(\vec{r})$. In this particular case (step (a) of Noyes Cycle in *Figure* 1), $\hat{H}_A^o$ and $\hat{H}_B^o$ differ in nuclear charges.

For such isoelectronic changes in atoms, Levy [24,25] has proposed the approximate relationship :

$$\Delta E_a^\circ = E_X^\circ - E_A^\circ = \int d\vec{r}\delta\hat{v}^\circ(\vec{r})\rho_{av}^\circ(\vec{r}) \qquad (24)$$

where

$$\rho_{av}^\circ(\vec{r}) = \frac{1}{2}[\rho_X^\circ(\vec{r}) + \rho_A^\circ(\vec{r})] \qquad (25)$$

is Levy's average electron density [24], defined in terms of the one electron densities $\rho_X^o(\vec{r})$ and $\rho_A^o(\vec{r})$; $\delta\hat{v}^o(\vec{r})$ represents the difference between the electron-nuclear attraction operators of the isoelectronic pair (A^+, X) *in vaccum.*

Since Levy's expression (24) was derived for an isolated atomic system, we can inmediately identify it with the first term of Eq (19).

Consider now the systems A^+ and X in the field of a polarizable medium, with hamiltonians

$$\hat{H}_X = \hat{H}_X^\circ + \hat{H}_X^{int} \qquad (26)$$

and

$$\hat{H}_A = \hat{H}_A^\circ + \hat{H}_A^{int} \qquad (27)$$

where $\hat{H}_A^o$ and $\hat{H}_X^o$ are the hamiltonians of the isoelectronic pair (A^+, X) *in vaccum* and $\hat{H}_A^{int}$, $\hat{H}_X^{int}$, the corresponding interaction hamiltonians representing the electrostatic interaction with the polarizable environment. Using the fact, that $\hat{H}_A^o$ and $\hat{H}_X^o$ differ in external potentials (i.e.$\Delta\hat{H}^\circ = \delta\hat{v}^o(\vec{r})$), substraction of Eqs (26) and (27) yields:

$$\hat{H}_X = \hat{H}_A + \delta\hat{v}^\circ(\vec{r}) + \Delta\hat{H}^{int} \qquad (28)$$

and

$$\hat{H}_A = \hat{H}_X - \delta\hat{v}^\circ(\vec{r}) - \Delta\hat{H}^{int} \qquad (29)$$

with

$$\Delta\hat{H}^{int} = \hat{H}_X^{int} - \hat{H}_A^{int} \qquad (30)$$

If Ψ_X and Ψ_A are eigenstates of $\hat{H}_X$ and $\hat{H}_A$ respectively, then by the variational theorem we obtain from Eqs (28) and (29) :

$$E_X < \langle \Psi_A \mid \hat{H}_A + \delta\hat{v}^\circ(\vec{r}) + \Delta\hat{H}^{int} \mid \Psi_A \rangle \qquad (31)$$

and

$$E_A < \langle \Psi_X \mid \hat{H}_X - \delta\hat{v}^\circ(\vec{r}) - \Delta\hat{H}^{int} \mid \Psi_X \rangle \qquad (32)$$

If we neglect, consistently with Eq (19), the interaction of the neutral species X with the polarizable environment (i.e $< \Psi_X \mid \Delta\hat{H}^{int} \mid \Psi_X > = 0$), we obtain the following approximate relationships:

$$E_A \approx E_X - \int d\vec{r}\delta\hat{v}^\circ(\vec{r})\rho_A(\vec{r}) - \langle \Psi_A \mid \Delta\hat{H}^{int} \mid \Psi_A \rangle \qquad (33)$$

and

$$E_X \approx E_A + \int d\vec{r}\delta\hat{v}^\circ(\vec{r})\rho_X(\vec{r}) \qquad (34)$$

An additional comment with regard to Eqs (33) and (34) is worth making. These equations are not exact because in addition to the neglect of the interaction contribution of the neutral X system with the polarizable environment, there are the variational errors δ_A and δ_X associated with the expectation values E_A and E_X, respectively. Since we are interested in the energy difference $\Delta E = E_A - E_X$ and because the error δ_A and δ_X are

always positive, it follows that the errors in the energy difference will in general compensate.

Addition of Eqs (33) and (34) yields:

$$\langle \Psi_A \mid \Delta\hat{H}^{int} \mid \Psi_A \rangle = -\int d\vec{r}\delta\hat{v}^{\circ}(\vec{r})\delta\rho(\vec{r}) \qquad (35)$$

where

$$\delta\rho(\vec{r}) = [\rho_A(\vec{r}) - \rho_X(\vec{r})] \qquad (36)$$

According to Hohenberg-Kohn theorem, $\delta\rho(\vec{r})$ given in Eq (36) does never vanishes because $\rho_A(\vec{r})$ and $\rho_X(\vec{r})$ are determined by different external potentials [26]. Moreover, $\delta\rho(\vec{r})$ represents the electronic polarization contribution due to the isoelectronic change under the influence of the external electrostatic field.

On the other hand, substraction of Eqs (33) and (34) yields

$$[E_A - E_X] = -\int d\vec{r}\delta\hat{v}^{\circ}(\vec{r})\rho_{av}(\vec{r}) - \frac{1}{2}\langle \Psi_A \mid \Delta\hat{H}^{int} \mid \Psi_A \rangle \qquad (37)$$

where $\rho_{av}(\vec{r})$ is an average electron density equivalent to that introduced in Eq (25), but this time defined in terms of the one electron densities of the isoelectronic pair (A^+, X), in the presence of an external electrostatic field.

Substitution of Eq (35) into Eq (37) yields :

$$[E_A - E_X] = \Delta E_c(Z, Z+1) = -\int d\vec{r}\delta\hat{v}^{\circ}(\vec{r})\rho_{av}(\vec{r}) + \frac{1}{2}\int d\vec{r}\delta\hat{v}^{\circ}(\vec{r})\delta\rho(\vec{r}) \qquad (38)$$

Finally, combination of Eqs (19), (24) and (38) yields the desired general expression [27]. Namely,

$$\begin{aligned}\Delta E_{ins}(Z+1, Z+1) \;=\; & \int d\vec{r}\delta\hat{v}^{\circ}(\vec{r})[\rho^{\circ}_{av}(\vec{r}) - \rho_{av}(\vec{r})] \\ & + \frac{1}{2}\int d\vec{r}\delta\hat{v}^{\circ}(\vec{r})\delta\rho(\vec{r})\end{aligned} \qquad (39)$$

4. Formulation of the insertion energy within the Nuclear Transition State (ZTS) Model.

4.1. DERIVATION OF THE RF EQUATIONS.

It is interesting to note that Eq (39) may be easily interpreted within the frame of reaction field theory [1]. For instance, the second term of Eq (39) represents the electronic polarization contribution accounting for the solute screening cloud induced by the external (reaction) field: it may be interpreted as the response of electrons moving under the influence of an effective potential including the reaction field effect [26]. A completely equivalent interpretation has been established by Norskov and Lang [28] with regard to the second term of Eq (18), from a second order perturbation theory approach, in the study of atomic impurities in solids. To reinforce the above argument, we must show that the first term of Eq (39) corresponds to the ion-solvent electrostatic interaction energy.

We shall develop here a simple methodology for the computation of ΔE_{ins}, in terms of the electrostatic potential at nucleus V_o. Within this frame, we will show that the first term of Eq (18) represents, in the context of the reaction field theory, the ion-solvent interaction energy.

We start by reminding that the insertion of an atomic ion into a polar liquid is being described in terms of succesive isoelectronic processes that take place *in vaccum* and in the presence of a polarizable environment. Within this model, the energy changes are written as a function of a varying nuclear charge. It seems then natural to express the energy associated to the isoelectronic changes using the Hellmann-Feynman (HF) theorem. Consider for instance the energy change from Z_A to Z_X. Using the integrated form of the HF theorem we obtain [27] :

$$\Delta E(Z_A, Z_X) = \int_{Z_A}^{Z_X} \int d\vec{r}' dZ \frac{\rho(\vec{r}', Z)}{|\vec{r} - \vec{r}'|} \qquad (40)$$

Application of the mean value theorem yields :

$$\int_{Z_A}^{Z_X} \int d\vec{r}' dZ \frac{\rho(\vec{r}')}{|\vec{r} - \vec{r}'|} = [Z_X - Z_A] \int d\vec{r}' \frac{\rho(\vec{r}', Z^*)}{|\vec{r} - \vec{r}'|} = [Z_A - Z_X] V_o^* \quad (41)$$

where $\rho(\vec{r}, Z^*)$ is the electron density for some nuclear charge Z^* such that $Z_X < Z^* < Z_A$, and

$$V_o^* = - \int d\vec{r}' \frac{\rho(\vec{r}', Z^*)}{|\vec{r} - \vec{r}'|_{\vec{r}=0}} \quad (42)$$

is the electrostatic potential at a nucleus with an intermediate charge between Z_A and Z_X. This method for calculating $\Delta E(Z_A, Z_X)$ is called the ZTS model [29]. Within this model, the energy variation associated to the work of removing a nuclear charge unity in an isoelectronic process may be directly obtained for atoms, from a SCF wave function computed for the atomic charge $Z^* = \frac{1}{2}(Z_A + Z_X)$ [30].

Within this frame, it is possible to show that the first term of Eq (39) represents the electrostatic ion-solvent interaction energy, in terms of the ZTS potential at nucleus V_o^* Under the approximation :

$$\rho(\vec{r}, Z^*) \approx \rho_{av}(\vec{r}), \quad (43)$$

use of definition given in Eq (25) together with Eqs (39), (41) and (42) allow us to write the first term of Eq (39) in terms of V_o^* as follows :

$$\int d\vec{r} \delta\hat{v}^\circ(\vec{r})[\rho_{av}^\circ(\vec{r}) - \rho_{av}(\vec{r})] = [Z_X - Z_A][V_o^* - \bar{V}_o^*] = \Delta E_{int}[\delta\rho(\vec{r})] \quad (44)$$

which is the reaction field expression of the ion-solvent electrostatic interaction energy [27]. It is expressed in terms of V_o^* and $\bar{V}_o^*$, the electrostatic potential at nucleus of a pseudoatom having a fractional nuclear charge, *in*

vaccum and in the presence of the external electrostatic field, respectively. As expected, the interaction energy is a functional of the induced electron density $\delta\rho(\vec{r})$.

We shall now show that the insertion energy may be cast into a form completely equivalent to Born formula. This may be easily done by using the well known relationship between the electrostatic ion-solvent interaction energy and the electronic polarization energy [3,14]. Namely

$$\Delta E^{pol}[\delta\rho(\vec{r})] = -\frac{1}{2}\Delta E_{int}[\delta\rho(\vec{r})] \qquad (45)$$

From Eqs (44) and (45) we get :

$$\frac{1}{2}\int d\vec{r}\delta\hat{v}^{\circ}(\vec{r})\delta\rho(\vec{r}) = -\frac{1}{2}[Z_X - Z_A][V_o^* - \bar{V}_o^*] \qquad (46)$$

Finally, combination of Eqs (39), (44), (45) and (46) yields the desired find result. Namely,

$$\Delta E_{ins}(Z+1, Z+1) = \frac{1}{2}[Z_X - Z_A][V_o^* - \bar{V}_o^*] \qquad (47)$$

If we define the ZTS reaction field potential :

$$\Phi_R^*[\delta\rho(\vec{r})] \equiv [V_o^* - \bar{V}_o^*] \qquad (48)$$

then, the agreement of ΔE_{ins} with the classical RF expression of Born solvation energy is complete. Namely,

$$\Delta E_{ins}(Z+1, Z+1) = \frac{1}{2}\Delta Z\Phi_R^*[\delta\rho(\vec{r})] \qquad (49)$$

In summary, a general expression giving the solvation energy of singly positive or negative charged atomic ions has been presented. The formulation introduces the electrostatic potential at nucleus, of a nuclear transition state system having a fractional nuclear charge Z^*. Expression (49) giving

the solvation energy, is completely equivalent to the reaction field version of Born formula. However, in the present approach, ΔE_{ins} appears completely independent of the ionic radii. This aspect of the model is really important and very promising, since it permits the calculation of the insertion energy without making any reference to the partition of the space into a quantum region containing the solute, and a classical region representing the solvent. The absence of boundaries in the representation of the solute-solvent system leads directly to integration over $[0,\infty]$, thereby avoiding the introduction of empirical ionic radii in the calculation of solvation energies. In other words, the polarization of the environment appears naturally into the formalism, as a response to the coupling between the solute electron density and the external electrostatic perturbation.

4.2. ZTS ELECTRON DENSITY IN THE PRESENCE OF AN EXTERNAL FIELD.

4.2.1. *The Kohn – Sham Equations.*

The basic assumption leading to Eq (49) is represented by approximation (43), which relates Levy's average electron density with the corresponding ZTS electron density. It is important to emphasize that the average electron density approximates the transition density in the integral HF theorem, which is an exact expression for isoelectronic changes *in vacuum* [24]. However, it is not obvious that such approximation still holds for ions in the presence of a perturbing external electrostatic field. In order to test the quality of approximation (43) for isoelectronic changes in atomic ions coupled to an external field, it is necessary to determine the corresponding electron density. The Kohn-Sham (KS) formulation of density functional theory [31] appears as a suitable procedure to achieve this objective.

When an atomic ion is under the influence of an additional external spin-independent potential $v_{ext}(\vec{r})$, produced for instance by a polarizable environment, the effective energy of the atomic ion becomes:

$$E[\rho(\vec{r})] = E[\rho^{\circ}(\vec{r})] + \int d\vec{r}\rho(\vec{r})v_{ext}(\vec{r}) \qquad (50)$$

The $E[\rho^{\circ}(\vec{r})]$ functional is minimized by the ground state density of the isolated system $\rho^{\circ}(\vec{r})$. The $E[\rho(\vec{r})]$ functional is minimized by a new density

$\rho(\vec{r})$ which differs from $\rho^{\circ}(\vec{r})$ by an amount $\delta\rho(\vec{r})$:

$$\rho(\vec{r}) = \rho^{\circ}(\vec{r}) + \delta\rho(\vec{r})$$

Following the KS prescription, the density $\rho(\vec{r})$ may be obtained from a set of electronic orbitals $\phi_i(\vec{r})$ as :

$$\rho(\vec{r}) = \sum_{\epsilon_i < \mu} | \phi_i(\vec{r}) |^2 \qquad (52)$$

where the summation is done over all the bound states having monoelectronic energies ϵ_i lower than the chemical potential μ. The $\phi_i(\vec{r})$ orbitals are solution of the eigenvalue equation (in atomic units) :

$$[-\frac{1}{2} \nabla_i^2 + v_{eff}(\vec{r})]\phi_i(\vec{r}) = \epsilon_i \phi_i(\vec{r}) \qquad (53)$$

where the effective potential $v_{eff}(\vec{r})$ is also a functional of the density and is given by :

$$v_{eff}(\vec{r}) = v_{ext}(\vec{r}) + v(\vec{r}) + \int d\vec{r'} \frac{\rho(\vec{r'})}{| \vec{r} - \vec{r'} |} + \frac{\delta\epsilon_{xc}[\rho]}{\delta\rho(\vec{r})} \qquad (54)$$

The third term of Eq (54) is the electronic Hartree potential, whereas the fourth one represents the exchange-correlation potential. This last term is usually obtained from a model exchange-correlation energy functional $\epsilon_{xc}[\rho]$. To a first order approximation, the effective KS potential compatible with the electron density $\rho(\vec{r})$ given in Eq (51) may be written as :

$$v_{eff}(\vec{r}) = v^{o}_{eff}(\vec{r}) + \delta v_{eff}(\vec{r}) \qquad (55)$$

where $v^{o}_{eff}(\vec{r})$ is the sum of the external potential $\upsilon(\vec{r})$, the electronic Hartree potential and the exchange-correlation potential. The quantity $\delta v_{eff}(\vec{r})$ may be obtained from a RF model, and it will depend, to a first order approximation, on the induced electron density $\delta\rho(\vec{r}) = \rho(\vec{r}) - \rho^{\circ}(\vec{r})$. If a linear response model [32] is assumed for simplicity, the reaction field induced electron density becomes :

$$\delta\rho(\vec{r}) = [\epsilon^{-1} - 1]\rho^{\circ}(\vec{r}) \quad (56)$$

This simplified model of electronic polarization may be used within a KS like formalism to determine the electron density $\rho(\vec{r})$. For instance, if we place the model within the Hartree-Fock-Slater $X - \alpha$ approximation [33], the exchange-correlation potential reduces to :

$$\frac{\delta\epsilon_{xc}[\rho]}{\delta\rho(\vec{r})} = v^{\circ}_{X\alpha}(\vec{r}) \quad (57)$$

with

$$v^{\circ}_{X\alpha}(\vec{r}) = -\frac{3}{2}\alpha[\frac{3}{\pi}\rho(\vec{r})]^{\frac{1}{3}} = C(\alpha)[\rho(\vec{r})]^{\frac{1}{3}} \quad (58)$$

Combination of Eqs (42) and (54)-(58) yields :

$$\delta v_{eff}(\vec{r}) = \Phi^{*}_{R}(\vec{r}) + \delta v^{\circ}_{X\alpha}(\vec{r}) \quad (59)$$

with

$$\Phi^{*}_{R}(\vec{r}) = [1 - \epsilon^{-1}]V^{*}_{o} \quad (60)$$

and

$$\delta v_{X\alpha}(\vec{r}) = [1 - \epsilon^{\frac{1}{3}}]v^{\circ}_{X\alpha}(\vec{r}) \quad (61)$$

The effective KS like potential , within the $X - \alpha$ approximation, becomes

$$v_{eff}(\vec{r}) = v_{KS}(\vec{r}) + [1 - \epsilon^{-1}]V^{*}_{o} + [1 - \epsilon^{\frac{1}{3}}]v^{\circ}_{X\alpha}(\vec{r}) \quad (62)$$

Substitution of Eq (62) into Eq (53) yields the set of KS orbitals $\phi_i(\vec{r})$, which are then used to build up the electron density *via* Eq (52).

The procedure to obtain the ZTS electron density in the presence of an external electrostatic field, implemented within the $X - \alpha$ approximation, was used to test the quality of approximation (43). The comparison of the ZTS and Levy's average electron density was done for the following

systems, using a low dielectric constant value, ε = 2.0, consistent with an electronic polarization model : the $(H^{-}, Li^{+})_{He}$ isoelectronic pair which involves He as the neutral reference system (*Figure 2a*) and the $(F^{-}, Na^{+})_{Ne}$ isoelectronic pair, involving Ne as the neutral reference sytem (*Figure 2b*).

It may be seen that in all the systems studied, the ZTS electron density is located midpoint between the corresponding reference densities $\rho_A(\vec{r})$ and $\rho_X(\vec{r})$. In other words, the nuclear transition state approximation provides a rather simple protocole to estimate the electron density for atomic systems coupled to an external electrostatic field, in a form completely equivalent to that proposed for isolated atoms. With this electron density at hand, estimates of solvation energies for atomic ions may be obtained within a unified reaction field like formalism.

Another advantage of the present formulation is that the electrostatic potential at nucleus is in general described more accurately than total energies for atoms . As a result, anions and cations may be treated within a unified formalism. The present model may be easily implemented within a DFT formulation for the self consistent calculation of the ion-solvent interactions. Despite the fact that correlations effects are not included, the method is not dependent on this approximation, and may be extended to include correlation effects upon solvation. On the other hand the limitation of considering the polarization of the solute as being completely electronic in nature, allowed us to adopt a simple linear response model for the representation of the induced electronic polarization. In summary, the model considers the polarization of an electron gas, under the influence of an effective potential including the reaction field effects. This induced electron density may be interpreted as the response of electrons moving independently under the influence of an external electrostatic perturbation which is added to the external potential of the isolated system. The generalization of the ZTS model follows from the approximate formulae for the total energy in terms of the electrostatic potential at nucleus. The key quantity of the ZTS-RF model is the induced electron density. At the ZTS-RF level, it has been represented through a simple linear model shown in Eq (56). More refined representations for $\delta\rho(\vec{r})$ are possible. They will be discused in detail in Section 5.

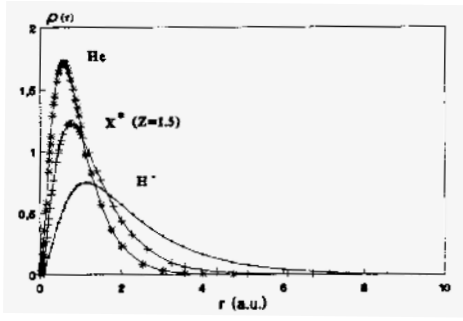

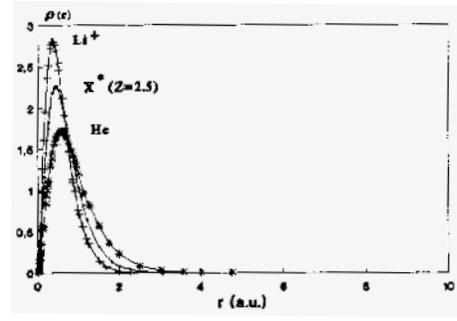

(a)

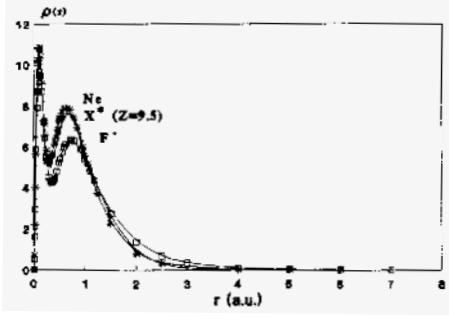

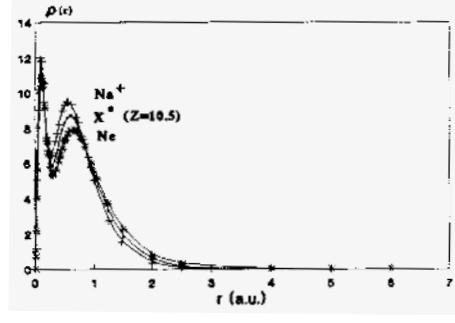

(b)

Figure 2. ZTS electron densities for the isoelectronic pairs (a) (H^-, Li^+) *and* (*b*) (F^-, Na^+).

5. Introduction of Local Indices in the Solvation Energy Expression.

5.1. THE STATIC DENSITY RESPONSE FUNCTION OF DFT.

In the preceding section, a simple model to compute solvation energies has been discussed. The basic quantity of this approach is the ZTS reaction field potential $\Phi_R^*[\delta\rho(\vec{r})]$ which, according to Eqs (46) and (48), is a functional of the induced electron density $\delta\rho(\vec{r})$. In this formulation, a simple model represented by Eq (56) for $\delta\rho(\vec{r})$ was adopted, allowing for an approximate expression of insertion energy. Despite the fact that Eq (49) may be easily generalized for molecules using approximate electrostatic potential at nucleus [27], there is an interesting alternative which uses the natural reactivity indices of DFT. The most popular ones are the *chemical potential* μ, the *global hardness* and *softness,* η and *S,* and the *molecular electronegativity* χ. All these reactivity indices are formally defined as first and second derivatives of the electronic energies with respect to the number of electrons in the system. They are called *global,* because they display an uniform value in every region of the molecular system [34]. On the other hand, the analysis of the variation of these global quantities when the system is under the influence of an electrostatic external field induced in the surrounding medium, still remains as an open problem. Recently, Pearson has proposed a methodology to obtain estimates of ionization potentials and electron affinities in solution from free energy of solvation and redox potentials data [35]. The most relevant results reported by Pearson were that electronegativity remained invariant upon solvation, and that the corresponding hardness displayed very little variation upon transfer from gas to solution phase, making these global quantities unuseful for the analysis of chemical reactivity in the liquid phase. These empirical observations may be tested by using approximate expression of the global DFT indices. For instance, within the Molecular Orbital (MO) theory they are expressed in terms of the one-electron energy differences involving the frontier *MO/s* [47]. In *Figure* 3 , gas phase and solution electronegativities as well as global hardness, obtained from approximated electron densities (CNDO/2 and CNDO-SCRF, respectively) are shown.

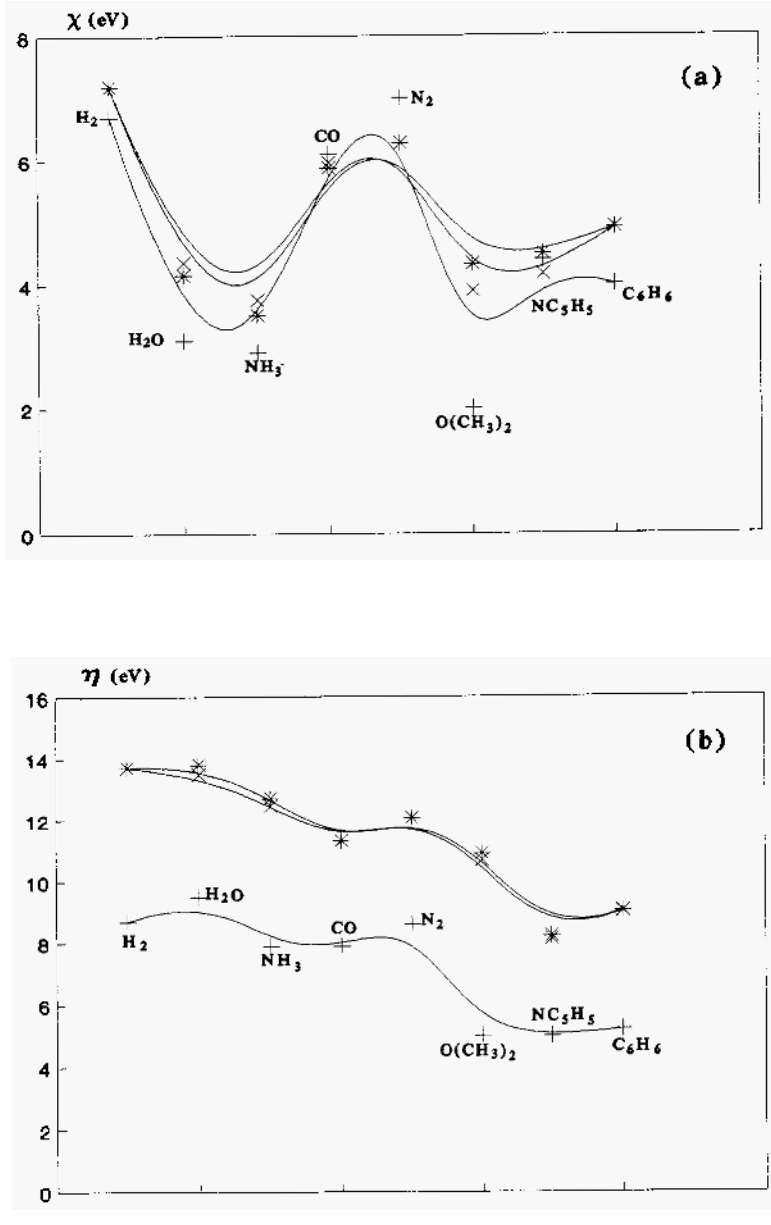

Figure 3. Comparison between gas and solution phase molecular electronegativities (a), and global hardness (b). Experimental values (+) rom reference [35]. Gas phase values (X) from CNDO/2 calculations and solution values (*), from SCRF calculations.

It may be seen that in both cases, the predicted values follow the experimental order. Also, it may be seen that the variation of χ and η with the reaction field strength is negligeable. Therefore, the introduction of solution global DFT indices have little utility in the study of solution chemical reactivity.

In order to better understand the RF model in terms of the local DFT indices, let us first consider some fundamental equations for the energy change from one ground state to another. Let the first ground state be characterized by $\rho_o(\vec{r})$, $\upsilon_o(\vec{r})$, N^o and $E°$ (e.g. the ground state associated to the isolated solute), whereas the other will be defined by the quantities $\rho(\vec{r})$, $\upsilon(\vec{r})$, N and E; and will be considered as the ground state of the solute in the field of the solvent. According to the class of problem we are dealing with, the most suitable representation for the description of the RF model is that containing $\{N, \upsilon(\vec{r})\}$ as fundamental variables. For such a representation, Vela and Gázquez [36] have reported the following relationship for the energy change :

$$\begin{aligned}\Delta E = E - E° &= \mu°\Delta N + \int d\vec{r}\rho°(\vec{r})\delta v(\vec{r}) + \frac{1}{2}\frac{1}{S°}(\Delta N)^2 \\ &+\Delta N \int d\vec{r} f°\delta v(\vec{r}) + \frac{1}{2}\int d\vec{r}\delta\rho(\vec{r})\delta v(\vec{r})\end{aligned} \quad (63)$$

where [2] :

$$\mu° = v°(\vec{r}) + \frac{\delta F°[\rho\circ]}{\delta\rho°(\vec{r})} \quad (64)$$

is the electronic chemical potential for the isolated solute, $s^o(\vec{r})$ its local softness defined by [34] :

$$s°(\vec{r}) = \left[\frac{\partial\rho°(\vec{r})}{\partial\mu°}\right]_N, \quad (65)$$

which upon integration over space coordinates yields the global softness :

$$S^\circ = \int d\vec{r} s^\circ(\vec{r}) \qquad (66)$$

The Fukui function $f^\circ(\vec{r})$ is defined by:

$$f^\circ(\vec{r}) = \left[\frac{\partial \rho^\circ(\vec{r})}{\partial N^\circ}\right]_{v(\vec{r})} = \frac{s^\circ(\vec{r})}{S^\circ}, \qquad (67)$$

and it is a normalized local softness in the sense that :

$$\int d\vec{r} f^\circ(\vec{r}) = \frac{1}{S^\circ}\int d\vec{r} s^\circ(\vec{r}) = 1 \qquad (68)$$

Equation (63) was obtained after performing a Taylor series functional expansion of $F[\rho]$ around $F^\circ[\rho^\circ]$ and retaining terms up to second order [36].

The first approximation we shall introduce in our developments is related to the fact that *within the continuum RF model,* the change in energy associated with inserting the solute into the solvent given by Eq(63) is being considered as an *isoelectronic process* (i.e., $\Delta N = N - N^\circ = 0$). As a result we obtain :

$$\Delta E = \int d\vec{r} \rho^\circ(\vec{r}) \delta v(\vec{r}) + \frac{1}{2}\int d\vec{r} \delta\rho(\vec{r}) \delta v(\vec{r}), \qquad (69)$$

where $\delta v(\vec{r})$ is the change in the external potential associated to the insertion process and $\delta\rho(\vec{r}) = \rho(\vec{r}) - \rho^\circ(\vec{r})$ is the induced electron density due to the coupling with the reaction field. It is also worth mentioning that $\delta\rho(\vec{r})$ will never vanishes because according to the HK theorem, $\rho(\vec{r})$ and $\rho^\circ(\vec{r})$ are determined by different external potentials. Another relevant aspect concerning Eq (69) is that it will remain valid within the *effective medium* representation of the solvent. It will certainly be no longer valid in a different model of solvation such as, for instance, the supermolecule approach where partial electron transfer between the solute and the solvent may occur [37].

We may now proceed to transform Eq (69) into a form closer to the more familiar RF picture. Let us first introduce the effective electrostatic potential of the solute in the field of the polarized solvent as follows :

$$\Phi(\vec{r}) = v(\vec{r}) + \int d\vec{r}\prime \frac{\rho(\vec{r}\prime)}{|\vec{r} - \vec{r}\prime|} = v^{\circ}(\vec{r}) + \delta\vartheta_{ext}(\vec{r})] + \int d\vec{r}\prime \frac{\rho(\vec{r}\prime)}{|\vec{r} - \vec{r}\prime|} \quad (70)$$

where $\delta\vartheta_{ext}(\vec{r})$ is an external spin-independent electrostatic perturbation produced by the reaction field. The corresponding total electrostatic potential of the isolated solute is :

$$\Phi^{\circ}(\vec{r}) = v^{\circ}(\vec{r}) + \int d\vec{r}\prime \frac{\rho^{\circ}(\vec{r}\prime)}{|\vec{r} - \vec{r}\prime|} \quad (71)$$

Substraction of Eqs (70) and (71) yields :

$$\delta\Phi(\vec{r}) = \Phi(\vec{r}) - \Phi^{\circ}(\vec{r}) = \delta\vartheta_{ext}(\vec{r}) + \int d\vec{r}\prime \frac{\delta\rho(\vec{r}\prime)}{|\vec{r} - \vec{r}\prime|} \quad (72)$$

From relationship (72), the following identities hold :

$$\int\int d\vec{r}d\vec{r}\prime \frac{\rho^{\circ}(\vec{r})\delta\rho(\vec{r}\prime)}{|\vec{r} - \vec{r}\prime|} = \int d\vec{r}\rho^{\circ}(\vec{r})[\delta\Phi(\vec{r}) - \delta\vartheta_{ext}(\vec{r})] \quad (73)$$

and

$$\int\int d\vec{r}d\vec{r}\prime \frac{\delta\rho(\vec{r})\delta\rho(\vec{r}\prime)}{|\vec{r} - \vec{r}\prime|} = \int d\vec{r}\delta\rho(\vec{r})[\delta\Phi(\vec{r}) - \delta\vartheta_{ext}(\vec{r})] \quad (74)$$

Combination of Eqs (69) - (74) gives :

$$\Delta E = \int d\vec{r}\rho^{\circ}(\vec{r})\delta\vartheta_{ext}(\vec{r}) + \frac{1}{2}\int d\vec{r}\delta\rho(\vec{r})\delta\vartheta_{ext}(\vec{r}) \quad (75)$$

The following relevant remark concerning Eq (75) is pertinent : the first term may be easily recognized as the electrostatic solute-solvent interaction energy, as defined in the context of RF theory. Formally speaking, the electrostatic solute-solvent interaction energy as given in the present approach, corresponds to a first order perturbation theory correction to $E^{\circ}[\rho^{\circ}]$. The physical meaning of the second contribution may be easily established after transforming Eq (75) as follows : addition and substraction of the second term in the righ hand side yields :

$$E[\rho] - E^{\circ}[\rho^{\circ}] = \int d\vec{r}\rho(\vec{r})\delta\vartheta_{ext}(\vec{r}) - \frac{1}{2}\int d\vec{r}\delta\rho(\vec{r})\delta\vartheta_{ext}(\vec{r}) \qquad (76)$$

On the other hand, when the solute is under the influence of the external perturbation, the effective energy functional is minimized by a new electron density $\rho(\vec{r})$, which differs from the ground state electron density of the isolated solute $\rho^{\circ}(\vec{r})$ by an amount $\delta\rho(\vec{r})$. In other words, the effective energy functional $E[\rho]$ may be written as [38] :

$$E[\rho] = E^{\circ}[\rho] + \int d\vec{r}\rho(\vec{r})\delta\vartheta_{ext}(\vec{r}) \qquad (77)$$

Substracting $E^{\circ}[\rho^{\circ}]$ from both sides of Eq (77), and using Eq (76) we obtain :

$$\Delta E_{\Sigma}^{pol}[\delta\rho] = (E^{\circ}[\rho] - E^{\circ}[\rho^{\circ}]) = -\frac{1}{2}\int d\vec{r}\delta\rho(\vec{r})\delta\vartheta_{ext}(\vec{r}), \qquad (78)$$

the solute electronic polarization contribution to δE. Since both Eqs (75) and (76) are equivalent expresions for δE, we may write using Eq (78) the following physically meaningful expression for the energy variation :

$$\Delta E = \Delta E_{int}^{el}[\delta\rho] + \Delta E_{\Sigma}^{pol}[\delta\rho] \qquad (79)$$

Where

$$\Delta E_{int}^{el}[\delta\rho] = \int d\vec{r}\rho(\vec{r})\delta\vartheta_{ext}(\vec{r}), \tag{80}$$

is an effective electrostatic solute solvent interaction energy. According to the RF theory, the solvation energy is obtained after adding to the electrostatic solute solvent interaction contribution and the solute self-polarization term, the contribution due to the solvent polarization $\Delta E_S^{pol}[\delta\rho]$ [2,3,7,14]. Namely,

$$\Delta E_{solv} = \Delta E_{int}^{el}[\delta\rho] + \delta E_{\Sigma}^{pol}[\delta\rho] + \Delta E_S^{pol}[\delta\rho] \tag{81}$$

The solvent polarization contribution (third term of Eq (81)), may be obtained from the fundamental theorem of the RF theory, relating the electrostatic solute-solvent interaction energy and the solvent polarization contribution [2,3,7,14] :

$$\Delta E_S^{pol}[\delta\rho] = -\frac{1}{2}\Delta E_{int}^{el}[\,\delta\rho] \tag{82}$$

Substitution of Eqs (78)- (80) and (82) into Eq (81) yields :

$$\begin{aligned}\Delta E_{solv} &= \frac{1}{2}\int d\vec{r}\rho(\vec{r})\delta\vartheta_{ext}(\vec{r}) - \frac{1}{2}\int d\vec{r}\delta\rho(\vec{r})\delta\vartheta_{ext}(\vec{r}) \\ &= \frac{1}{2}\int d\vec{r}\rho(\vec{r})\delta\vartheta_{ext}(\vec{r}) + \Delta E_{\Sigma}^{pol}[\delta\rho].\end{aligned} \tag{83}$$

The quantity $\Delta E_{\Sigma}^{pol}[\delta\rho]$ is usually implicitly considered in the variational calculation of ΔE_{solv}, when the effect of the RF is self-consistently incorporated into the effective hamiltonian of the solute system in the field of the solvent.

Local density functional theory may be introduced within the RF model of solvent effects thorugh the induced electron density. The basic quantity for such a development is the linear density response function [39] :

$$\chi(\vec{r},\vec{r\prime}) = \left[\frac{\delta\rho(\vec{r})}{\delta\vartheta(\vec{r\prime})}\right]_N \qquad (84)$$

Physically, the quantity $\chi(\vec{r},\vec{r\prime})$ represents the change of the electron density at any point $\vec{r}$ produced by the variation of an spin independent external perturbation $\delta\vartheta(\vec{r\prime})$ (for instance, and external applied electric field) at a different point $\vec{r\prime}$. In the present case, the linear response function $\chi(\vec{r},\vec{r\prime})$ would represent the variation of the electron density at any point $\vec{r}$ produced by the *RF* potential at $\vec{r\prime}$. Specifically, the induced electron density $\delta\rho(\vec{r})$ required for the calculation of the DFT-RF potential Φ_R^* may be obtained from [40] :

$$\delta\rho(\vec{r}) = \int d\vec{r\prime}\left[\frac{\delta\rho(\vec{r})}{\delta\vartheta(\vec{r\prime})}\right]_N \delta\vartheta(\vec{r\prime}) \qquad (85)$$

The calculation of the induced electron density may be done in the context of the Kohn-Sham approach to density functional theory, because the response of a KS system to a change in the one particle effective potential $\delta\vartheta_{eff}(\vec{r})$ corresponds to that of a system of non-interacting electrons. Moreover, Berkowitz and Parr [39] have shown that the static density response may be expressed in terms of the *softness kernel* $s(\vec{r},\vec{r\prime})$, the *global softness* S and the *Fukui functions* $f(\vec{r})$ as follows :

$$\left[\frac{\delta\rho(\vec{r})}{\delta\vartheta(\vec{r\prime})}\right]_N = -s(\vec{r},\vec{r\prime}) + Sf(\vec{r})f(\vec{r\prime}). \qquad (86)$$

Equation (86) is an exact relationship between the static density response and the DFT indices.

Within a local approximation, the electron density is just a function of the modified potential and the induced electron density $\delta\rho(\vec{r})$ given by Eq (85) reduces to [36] :

$$\delta\rho(\vec{r}) = Sf(\vec{r})\left[\int d\vec{r\prime} f(\vec{r\prime})\delta\vartheta(\vec{r\prime}) - \delta\vartheta(\vec{r})\right] \qquad (87)$$

Using this expression for the induced electron density, expression (83) giving the solvation energy may be transformed as follows : from Eqs (71) and (72), the first term of Eq (83) may be rewritten as :

$$\frac{1}{2}\int d\vec{r}\rho(\vec{r})\delta\vartheta_{ext}(\vec{r}) = \frac{1}{2}\left(\frac{1}{\epsilon_r}-1\right)\left[\int d\vec{r}v^{\circ}(\vec{r})\rho(\vec{r}) + \int d\vec{r}\rho(\vec{r})\phi^{\circ}(\vec{r})\right] \quad (88)$$

where $\phi^{\circ}(\vec{r})$ is the classical electrostatic potential at $\vec{r}$ due to the entire electron density. The first term of Eq (88) simply give us the nuclear component of the solvation energy ΔE^{N}_{solv}. For a fixed nuclear configuration, this term will be a constant contribution to ΔE_{solv}. The second term of Eq (88) may be however transformed to a more interesting form, by introducing the *local hardness* concept $\bar{\eta}(\vec{r})$ of Parr *et al* [41]. These authors showed that, within the local density version of the KS theory, the following approximate relationship holds [10] :

$$\bar{\eta}(\vec{r}) \simeq \frac{1}{2N}\phi(\vec{r}) \quad (89)$$

Substitution of Eq (89) into Eq (88) yields :

$$\frac{1}{2}\int d\vec{r}\rho(\vec{r})\delta\vartheta_{ext}(\vec{r}) = \Delta E^{N}_{solv} + N\left(\frac{1}{\epsilon_r}-1\right)\int d\vec{r}\rho(\vec{r})\bar{\eta}(\vec{r}). \quad (90)$$

We may now proceed to transform the second term of Eq (83). Based on the fact that within the RF theory, the external spinless electrostatic perturbation $\delta\vartheta_{ext}(\vec{r})$ may be identified with the RF potential $\Phi_R(\vec{r})$, substitution of Eqs (87) and (90) into Eq (83) yields the desired result. Namely,

$$\begin{aligned}\Delta E_{solv} &= \Delta E^{N}_{solv} + N\left(\frac{1}{\epsilon_r}-1\right)\int d\vec{r}\rho(\vec{r})\bar{\eta}(\vec{r}) \\ &\quad -\frac{1}{2}S\left[\left(\int d\vec{r}f(\vec{r})\Phi_R(\vec{r})\right)^2 - \int d\vec{r}f(\vec{r})(\Phi_R(\vec{r}))^2\right]\end{aligned} \quad (91)$$

Equation (91) has a quite interesting structure : the first two terms remain as a long-range electrostatic contribution to the solvation energy, whereas the third one introduces the local softness as a multiplicative factor of the fluctuation of the RF potential. This last term is expected to strongly depend upon the solute polarizability, since the global softness does [34,36]. On the other hand, Equation (91) may be easily used in conexion with an orbital theory with the electron density and the electrostatic potential obtained from a standard SCRF wavefunction. The third term may be also evaluated from finite difference approximation formula. The charm of Eq (91) comes from the fact that it introduces for the first time, the natural reactivity indices of DFT in the expression of the solvation energy. This feature should be of great importance for the study of solvation effects in chemical reactivity in solution phase. Finally, it is also worth noting that Eq (91) is also reminiscent of the well known Frontier Molecular Orbital equation of chemical reactivity : the first two terms may be associated to the long-range electrostatic [charge control) effects, whereas the third one may be associated with short-range (orbital) effects.

5.2. SELF CONSISTENT FIELD FORMULATION OF THE RF-DFT MODEL.

According to the HK theorem, the ground state energy of an interacting inhomogeneus electron gas in a static external potential $\upsilon(\vec{r})$ is given by [26] :

$$E[\rho] = \int d\vec{r}\rho(\vec{r})v(\vec{r}) + \frac{1}{2}\int\int d\vec{r}d\vec{r}\prime\frac{\rho(\vec{r})\rho(\vec{r}\prime)}{|\vec{r}-\vec{r}\prime|} + G[\rho] \qquad (92)$$

which simply means that the classical electrostatic part of $V_{ee}[\rho]$ has been extracted from the universal funtional $F[\rho]$, thereby defining a new universal functional $G[\rho]$. This is very convenient for our purposes, since it will allow us to treat the long range electrostatic part of the energy functional, including the effect of the external perturbation explicitly. The remaining term $G[\rho]$ is then assumed to contain the kinetic energy contribution and the exchange- correlation term, which are expected to be short-ranged.

Our problem is now to obtain $\rho(\vec{r})$, to estimate solvation energies via Eq (83) in a self consistent way. As implicitly assumed in Section 3, $\rho(\vec{r})$ may differ from the ground state electron density of the isolated solute $\rho^{o}(\vec{r})$, by an amount $\delta\rho(\vec{r})$:

$$\rho(\vec{r}) = \rho^{\circ}(\vec{r}) + \delta\rho(\vec{r}) \tag{93}$$

Following the KS formalism [31], the density $\rho(\vec{r})$ may be obtained from a set of electronic orbitals $\phi_i(\vec{r})$ for an effective *KS* potential similar to that discussed in Section 4.2.

On the other hand, the effective KS potential $\delta\upsilon_{eff}(\vec{r})$ compatible with the induced electron density $\delta\rho(\vec{r})$ defined in Eq (93) may be also written as :

$$\delta v_{eff}(\vec{r}) = \delta\vartheta_{ext}(\vec{r}) + \int d\vec{r}\prime \frac{\delta\rho(\vec{r}\prime)}{|\vec{r} - \vec{r}\prime|} + \int d\vec{r}\prime v\prime_{xc}(\vec{r}, \vec{r}\prime)\delta\rho(\vec{r}\prime) \tag{94}$$

with

$$v\prime_{xc}(\vec{r}, \vec{r}\prime) = \left.\frac{\delta^2 E_{xc}[\rho]}{\delta\rho(\vec{r})\delta\rho(\vec{r}\prime)}\right|_{\rho=\rho^{\circ}(\vec{r})}, \tag{95}$$

which yields again (see Section 4.2) :

$$\delta v_{eff}(\vec{r}) = \Phi_R(\vec{r}) + \delta v_{xc}(\vec{r}) \tag{96}$$

where $\Phi_R(\vec{r}) = \Phi(\vec{r}) - \Phi^{o}(\vec{r})$ is the RF potential introduced in Section 4. If we set $\Phi(\vec{r}) = \Phi^{o}(\vec{r}) /\epsilon_r$, we obtain :

$$\Phi_R(\vec{r}) = \left(\frac{1}{\epsilon_r} - 1\right)\left[v^{\circ}(\vec{r}) + \int d\vec{r}\prime \frac{\rho^{\circ}(\vec{r}\prime)}{|\vec{r} - \vec{r}\prime|}\right] \tag{97}$$

Equation (96) shows that the effective KS potential may be simply obtained by adding to the standard KS potential of the isolated solute , an electrostatic correction which turns out to be the RF potential Φ_R, and the exchange- correlation correction δv_{xc}. It is worth mentioning here, that Eq (96) is formally equivalent to the effective Fock operator correction $\delta\vartheta_{eff}$, defined in the context of the self consistent reaction field (SCRF) theory [2,3,14] : within the HF theory, the exchange contribution is exactly self-contained in Φ_R, whereas correlation effects are completely neglected. As a result, within the HF theory $\delta v_{eff}^{HF} = \Phi_R$, as expected.

On the other hand, the second term of Eq (96) :

$$\delta v_{xc}(\vec{r}) = \int d\vec{r}\prime \frac{\delta^2 E_{xc}[\rho]}{\delta\rho(\vec{r})\delta\rho(\vec{r}\prime)}\delta\rho(\vec{r}\prime), \qquad (98)$$

representing the variation in the exchange-correlation potential upon solvation may be further simplified if we place the model within the local density approximation (LDA). In that case, v_{xc} becomes simply a function of the density and Eq (95) reduces to :

$$v\prime_{xc}(\vec{r},\vec{r}\prime)_{LDA} = \left.\frac{dv_{xc}[\rho]}{d\rho}\right|_{\rho=\rho^\circ} \delta(\vec{r}-\vec{r}\prime) \qquad (99)$$

The simplest linear response model for the RF induced electron density compatible with expression (97) of Φ_R is :

$$\delta\rho(\vec{r}) = \left[\frac{1}{\epsilon_r} - 1\right]\rho^\circ(\vec{r}) \qquad (100)$$

which allows the exchange-correlation potential variation to be cast into a very simple form.

6. General Discussion.

In the preceeding section, we have shown that density functional theory provides a natural framework to discuss solvent effects in the context of the RF model. The approach was derived from a second order perturbation theory approximation, giving the energy change from one ground state representing the isolated solute, to another one describing the ground state of the solute under the influence of the electrostatic spin-independent external potential due to the solvent. Within this simplified approach, Eq (83) giving the insertion energy was derived. It was shown that within the perturbational approach used, the solvation energy expression contains the basic ingredients of the classical RF formula. Namely, the electrostatic solute-solvent interaction energy, the solvent polarization term and the solute self-polarization energy. This last quantity appears as a second order correction in the perturbational formula.

The complete treatment of solvation effects, including the solute self-polarization contribution was developed in the frame of the DFT-KS formalism. Within this self consistent field like formulation, the fundamental expressions (96) and (97) provide an appropriate scheme for the variational treatment of solvent effects in the context of the KS theory. The effective KS potential naturally appears as a sum of three contributions : the effective KS potential of the isolated solute, the electrostatic correction which is identified with the RF potential and an exchange-correlation correction. Simple formulae for these quantities have been presented within the LDA approximation. There is however, another alternative to express the solvation energy in a more simple and useful form.

We start from the first line of Eq (83), and substitute Eq (87) with $\delta\vartheta(\vec{r})$ replaced by the RF potential. We obtain [42]:

$$\begin{aligned}\Delta E_{solv} &= \frac{1}{2}\int d\vec{r}\rho(\vec{r})\Phi_R(\vec{r}) \\ &\quad -\frac{1}{2}S\left[\left(\int d\vec{r}f(\vec{r})\Phi_R(\vec{r})\right)^2 - \int d\vec{r}f(\vec{r})(\Phi_R(\vec{r}))^2\right] \end{aligned} \quad (101)$$

Next, introduce definition (67) of the Fukui function to obtain :

$$\Delta E_{solv} = \frac{1}{2}\langle \Phi_R(\vec{r})\rangle - \frac{1}{2}S\left[\left(\frac{\partial}{\partial N}\langle \Phi_R(\vec{r})\rangle\right)^2 - \frac{\partial}{\partial N}\left\langle \Phi_R(\vec{r})^2\right\rangle\right] \quad (102)$$

Where the following definitions have been used :

$$\int d\vec{r}\rho(\vec{r})A(\vec{r}) = \langle A(\vec{r})\rangle \quad (103)$$

$$\left(\int d\vec{r}f(\vec{r})\Phi_R(\vec{r})\right)^2 = \left(\frac{\partial}{\partial N}\langle \Phi_R(\vec{r})\rangle\right)^2 \quad (104)$$

and

$$\int d\vec{r}f(\vec{r})\left(\Phi_R(\vec{r})\right)^2 = \frac{\partial}{\partial N}\left\langle \Phi_R(\vec{r})^2\right\rangle \quad (105)$$

Equation (102), although equivalent to Eq (91), offers the advantage of being more useful for the discussion of chemical reactivity in solution. The main difference between both expression of the solvation energy, is contained in the second order contribution, which represents the electronic polarization of the solute through the effective global softness *S*, and the *fluctuation* of the RFP, as electrons are added to the solute system. This term is expected to be particularly useful in the study of the solvation energy variation along a series of atomic and molecular systems, with increasing number of electrons. On the other hand, this second term is expected to have a low contribution within an isoelectronic series of solutes. As a result, use of Eq (102) may be of great utility when we are interested in the partition of the effective energy in terms of electrostatic and non electrostatic contributions. Preliminary applications of Eq (102) to the calculation of

solvation energies in the aliphatic amines series reveal a linear dependence between ΔE_{solv} and the global softness [42]. This important result was reported by Geerlings *et al* [43], on the basis of a multivariate regression analysis. Eq(102) is however an *analytical* relationship between this two quantities .

7. Concluding Remarks.

The use of electrostatic potentials, defined in the context of DFT, for the calculation of ion solvation energies has been reviewed. It has been shown that physically meaningful ionic radii may be obtained from this methodology. In spite of the fact that the electrostatic potentials for cations and anions display a quite different functional dependence with the radial variable, we have shown that it is still possible in both cases to build up a procedure consistent with the Born model of ion solvation.

The use of electrostatic potential at nucleus provides the basis for a unified theory of ion solvation for singly positive and negative charged atomic ions. The polarizable host has been modeled through an effective medium, and the ion-solvent interactions treated within the reaction field theory. The most relevant aspects of the proposed ZTS-RF model are the following : (i) the formalism uses the eletrostatic potential at nucleus as the basic property for the description of the ion-solvent interactions. This quantity is in general described more accurately than total energies for atoms. As a result, anions and cations may be treated within a unified formalism and the problem of introducing arbitrary empirical ionic radii is avoided and replaced by integration in $[0,\infty]$. (ii) The present model may be easily implemented within a density functional theory formulation for the self consistent treatment of the ion-solvent interactions.

On the other hand, some limitations are present in the proposed formalism. For instance, all the solute polarization is assumed to be electronic in nature. Orientational (temperature dependent) effects are not introduced in the present formulation of solvation effects. However, this limitation allowed us to adopt a simple linear response model for the representation of the induced electronic polarization through the polarization of an electron

gas under the effect of an electrostatic external field, This induced electron density is to be interpreted as the response of electrons moving independently under the influence of an effective potential, including the reaction field effect.

Finally, an alternative derivation of ΔE_{ins} that introduces the static density response function was outlined. This model offers several advantages with respect to the ZTS-RF formalism. For instance, the effect of the polarizable medium is directly expressed in terms of the reactivity indices of DFT which may be determined either from an orbital theory or directly from the KS formalism. This aspect of the proposed model is really relevant and very promising since it provides the theoretical basis for the treatment of chemical reactivity in solution, within the framework of a modern methodology comparable in quality to the conventional *ab initio* methods, but at a considerably lower computational cost.

In summary, density functional theory provides a natural framework to discuss solvent effects in the context of RF theory. A general expression giving the insertion energy of an atom or molecule into a polarizable medium was derived. This expression given in Eq (83), when treated within a first order perturbation theory approach (i.e. when the solute self-polarization contribution is neglected), directly leads to the well known Born formula of the solvation energy. Within this framework, accurate solvation energies for singly positive and negatively charged atomic ions may be obtained. A complete treatment, including the solute self-polarization contribution, may be developped in the context of the KS theory. It was shown that within the LDA approximation, simple expressions for the effective KS potential may be obtained.

However, the most promising aspect of the DFT-RF model of solvent effects presented here is represented by Eq (102). This expression, derived from a model induced electron density, based on the static-density response function of DFT, allowed us to obtain a useful expression for the solvation energy in terms of the natural reactivity indices of DFT. This aspect of the DFT-RF model is really interesting if we consider its potential aplication to the study of chemical reactivity in solution.

Acknowledgments.

This work was supported by FONDECYT, under grant *N*°1146-91. One of us (R.C.) is deeply indebted to the Commission of European Communities for providing support through a *Marie Curie* Fellowship *N*° 93-0188, that permitted to complete this work at Universita Degli Studi di Pisa, Pisa, Italy. The warm hospitality and helpful suggestions of Professor J. Tomasi are also very much appreciated. P. Pérez is a CONICYT Graduate Program fellow.

References.

1. Bottcher, C.J.F. (1973) **Theory of Electric Polarization,** Elsevier Publishing Company, Amsterdam, London, New York, p. 129.
2. Constanciel, R. and Tapia, O. (1978) Theoret. Chim. Acta **48,** 75.
3. Constanciel, R. and Contreras, R. (1984) Theoret. Chim. Acta **65,** 1.
4. Contreras, R. and Aizman, A. (1985) Int. J. Quantum Chem. **27,** 293.
5. Contreras, R. and Aizman, A. (1989) Bol. Soc. Chil. Quim. **34,** 93.
6. Duran, E. (1964) **Electrostatique,** Masson et Cie (Eds.), Paris.
7. Constanciel, R. (1986) Theoret. Chim. Acta **69,** 505.
8. Born, M. (1920) Physik. Z. **1,** 45.
9. Jano, O. (1965) C.R. Acad. Sc. (Paris) **261,** 103.
10. Germer Jr., H.A. (1974) Theoret. Chim. Acta **35,** 27.
11. Miertus, S. and Kyesel, O. (1977) Chem. Phys. **21,** 27.
12. Miertus, S., Scrocco, E. and Tomasi, J. (1981) Chem. Phys. **55,** 117.
13. Cramer, C.J. and Truhlar, D. (1992) Science **256,** 213.
14. Tapia, O. and Goscinsky, O. (1975) Mol. Phys. **29,** 1653.
15. Stokes, R.H. (1964) J. Am. Chem. Soc. **86,** 979.
16. Noyes, R. (1964) J. Am. Chem. Soc. **86,** 971.
17. Contreras, R. and Aizman, A. (1991) Int. J. Quantum Chem. **S25,** 281.
18. Contreras, R. and Aizman, A. (1993) J. Mol. Struct. (Theochem) **282,** 143.

19. Sen, K.D. and Politzer, P. (1979) J. Chem. Phys. **71,** 4218.

20. Politzer, P., Parr, R.G. and Murphy, D.R. (1983) J. Chem. Phys. **79,** 3859.

21. Clementi, E. and Roetti, C. (1974) At. Data Nucl. Data Tables **14,** 1.

22. Morris, D.F.C. (1968) Structure and Bonding **4,** 1.

23. Davis, D. W. (1982) Chem. Phys. Lett. **91,** 459.

24. Levy, M. (1978) J. Chem. Phys. **68,** 5298.

25. Levy, M. (1979) J. Chem. Phys. **70,** 1573.

26. Hohenberg, P. and Kohn, W. (1964) Phys. Rev. **136,** B864.

27. Contreras, R., Mendizabal, F. and Aizman, A. (1994) Phys. Rev. A **49,** 3439.

28. Norskov, J. K. and Lang, N. D. (1980) Phys. Rev. **B21,** 2131.

29. Sen, K. D. (1979) J. Chem. Phys. **70,** 5334.

30. Sen, K. D., Seminario, J. and Politzer, P. (1989) J. Chem. Phys. **90,** 4374.

31. Kohn, W. and Sham, L. J. (1965) Phys. Rev. **140,** A1133.

32. Puska, M. J. and Nieminen, R. M. (1984) Phys. Rev. **B29,** 5382.

33. Slater, J. C. (1974) **The Self Consistent Field For Molecules and Solids 4,** McGraw-Hill.

34. Parr, R. G. and Yang, W. (1989) **Density Functional Theory of Atoms and Molecules,** Oxford Press, New York, Oxford.

35. Pearson, R. G. (1986) J. Am. Chem. Soc. **108,** 6109.

36. Vela, A. and Gasquez, J. L. (1990) J. Am. Chem. Soc. **112,** 1490.

37. Claverie, P., Daudey, J. P., Langlet, B., Pullman, B., Piazzola, D. and Huron, M. J. (1978) J. Phys. Chem. **82,** 405.

38. Stott, M. and Zaremba, E. (1980) Phys. Rev. **A21,** 12.

39. Berkowitz, M. and Parr, R. G. (1988) J. Chem. Phys. **88,** 2254.

40. Contreras, R., Perez, P. and Aizman, A. (1995) Int. J. Quantum Chem., in press.

41. Berkowitz, M., Ghosh, S. K. and Parr, R. G. (1985) J. Am. Chem. Soc. **107,** 6811.

42. Perez, P. and Contreras, R., to be submitted.

43. Baeten, A., De Proft, F., Langenaeker, W. and Geerlings, P. (1994) J. Mol. Struct. (Theochem) **306,** 203.

This page intentionally left blank.

MONTE CARLO SIMULATIONS OF CHEMICAL REACTIONS IN SOLUTION

ANGELS GONZÁLEZ-LAFONT
JOSÉ M. LLUCH
JUAN BERTRÁN
Departament de Química
Universitat Autònoma de Barcelona
08193 Bellaterra (Barcelona)
Spain

1. Introduction

Theoretical interpretation of chemical reaction rates has a long history already. Until recently, however, only the chemical reactions of systems containing a few atoms in the gas phase could be studied using molecular quantum mechanics due to the computational expense. So, understanding the effect of the environment on the behaviour of chemical reactions in solution has been an outstanding problem. Fortunately, the past ten years have seen very important advances in the power of computer simulation techniques for chemical reactions in the condensed phase, accompanied by an impressive progress in computer speed. Consequently, a clear microscopical picture of how solvent influences the rate of chemical reactions is now beginning to emerge. Anyway, calculations in this area are still quite difficult and are not at all a straightforward extension of the gas-phase methodology to systems containing a huge number of degrees of freedom. The goal of this chapter is to present a critical discussion of the current state of theoretical methods to microscopically simulate chemical reactions in solution and to calculate their rates. Before entering on the heart of this topic it is useful to briefly review the habitual treatment applied to gas-phase systems.

Transition State Theory [1,4] is the most frequently used theory to calculate rate constants for reactions in the gas phase. The two most basic assumptions of this theory are the separation of the electronic and nuclear motions (stemming from the Born-Oppenheimer approximation [5]), and that the reactant internal states are in thermal equilibrium with each other (that is, the reactant molecules are distributed among their states in accordance with the Maxwell-Boltzmann distribution). In addition, the fundamental hypothesis [6] of the Transition State Theory is that the net rate of forward reaction at equilibrium is given by the flux of trajectories across a suitable phase space surface (rather a hypersurface) in the product direction. This surface divides reactants from products and it is called the dividing surface. Wigner [6] showed long time ago that for reactants in thermal equilibrium, the Transition State expression gives the exact

O. Tapia and J. Bertrán (eds.), Solvent Effects and Chemical Reactivity, 125–177.
© 1996 *Kluwer Academic Publishers. Printed in the Netherlands.*

classical rate provided that trajectories that pass through the dividing surface never return. In Conventional Transition State Theory [7] the dividing surface is chosen to be a configuration-space hypersurface (this way the momenta not being considered) centered at the saddle point of the potential energy hypersurface. This fact leads to the definition of the transition state structure as the point that fulfils the following four conditions [8]: a) it is a stationary point, that is, of zero gradient: b) the force constant matrix at the point must have only one negative eigenvalue; c) it must be the highest energy point on a continuous line connecting reactants and products: d) it must be the lowest energy point that satisfies the above three conditions. The two first mathematical conditions characterize the transition state structure as a mathematical saddle point. The dividing surface is generally constructed perpendicular to the minimum energy path (MEP), which is the path of steepest-descent from the saddle point into the reactant and product valleys [9-11]. From now on in this paper we will use the term transition state as equivalent to the entire dividing surface, in contrast with the term transition state structure that is just a particular point (the saddle point) of the dividing surface. Really the rate constant depends on the difference between the free energy corresponding to the ensemble of configurations that belongs to the dividing surface and the free energy associated to reactants.

As the non-recrossing assumption is not certain, the one-way equilibrium flux through the dividing surface exceeds the equilibrium net forward reaction rate, the Transition State Theory leading to an overestimation of the true classical rate constant. Then, beyond the Conventional Transition State procedure, in Variational Transition State Theory [7,12,13] a set of dividing surfaces is constructed, searching for the one that maximizes the free energy barrier, what is equivalent to minimize the one-way equilibrium flux through it. Consequently, the variational transition state is a dividing surface not necessarily passing through the saddle point.

The location of transition state structures is the first step to calculate gas-phase reaction rate constants. Then, the MEP is built up. The next step is to perform a generalized normal-mode analysis at a sequence of points along the MEP, to obtain the free energy increments corresponding to the set of dividing surfaces, as provided by the statistical thermodynamic formulae within the ideal gas, rigid rotor and harmonic oscillator models (anharmonicity effects can also be incorporated). The maximum value of the free energy change determines the variational transition state.

It is also useful in this point to dedicate a few words to outline the case of the clusters, which represent a bridge between the gas phase and the solution situations. In clusters, the transition state structure should be rigorously characterized as a point with zero gradient, all the coordinates of the system being simultaneously considered. However, a cheaper way to treat solvation effects is to suppose that solvent molecules always remain in equilibrium with the solute. Then it is assumed that for each fixed solute coordinates (particularly, for the gas-phase MEP and, evidently, for the gas-phase transition state structure forming part of it) all the solvent coordinates are at a minimum energy point, with all the solvent gradient components being zero. As no force is acting on the solvent in this case, this approximation is known as the solvent equilibrium hypothesis [14] (which involves a conceptual partition of the system into two sets of degrees of freedom, the solute plus the solvent surrounding it). It has to be emphasized

that this hypothesis is not related at all with the above mentioned thermal equilibrium basic assumption of the Transition State Theory, which implies equilibrium among the states of the whole system.

As a matter of fact, from a strict point of view, the solvent equilibrium hypothesis is always false for a chemical reaction. Although in some cases it can be employed as a practical assumption that provides a good enough approximation, for others it is not acceptable. So, for instance, in several papers [15-17] we have shown that in an S_N2 reaction with reactants solvated by a small number of water molecules, the solvent coordinates are significant components of the transition vector. Therefore, the motion of the solvent molecules is an important part of the motion of the whole system along the reaction coordinate in this case, the solvent equilibrium hypothesis not being valid. At this point it should be noted that the whole gradient is zero at a transition state structure and, as a consequence, the solvent gradient components are zero too. This fact, however, does not imply the solvent equilibrium hypothesis if the solvent coordtnates are significant components of the transition vector: the motion of the solvent along the reaction coordinate going down from the transition state structure would produce a diminution of the potential energy, the solvent coordinates not actually satisfying therefore the conditions of a minimum energy point in the complete system.

As Tucker and Truhlar [14] have emphasized, the Conventional Transition State Theory is not unambiguously defined in the context of the solvent equilibrium hypothesis. They have built up the so-called equilibrium solvated path (ESP) by taking the same values as on the gas-phase MEP for the solute coordinates, and optimizing the solvent coordinates, for fixed solute coordinates, at each point on that reaction path. The problem lies on the fact that there is no true saddle point on the ESP, and, in addition, the point on the ESP which corresponds to the gas-phase transition state structure will not necessarily be the point of highest potential energy on the ESP. Conversely, Variational Transition State Theory can be applied by constructing a set of dividing surfaces that intersects the ESP, provided that the dividing surface orientations are conveniently chosen. Thus, in the microsolvated reaction $Cl^-(H_2O) + CH_3Cl$, Tucker and Truhlar [14] have shown that the solvent equilibrium hypothesis is a good approximation to be used in the frame of Variational Transition State Theory. Although the validity of this conclusion will probably depend on each particular chemical reaction, it seems clear that the inaccuracy introduced by the solvent equilibrium hypothesis is lesser when Variational Transition State Theory is used.

Beyond the clusters, to microscopically model a reaction in solution, we need to include a very big number of solvent molecules in the system to represent the bulk. The problem stems from the fact that it is computationally impossible, with our current capabilities, to locate the transition state structure of the reaction on the complete quantum mechanical potential energy hypersurface, if all the degrees of freedom are explicitly included. Moreover, the effect of thermal statistical averaging should be incorporated. Then, classical mechanical computer simulation techniques (Monte Carlo or Molecular Dynamics) appear to be the most suitable procedures to attack the above problems. In short, and applied to the computer simulation of chemical reactions in solution, the Monte Carlo [18-21] technique is a numerical method in the frame of the classical Statistical Mechanics, which allows to generate a set of system configurations

with a given probability distribution function, for instance, the canonical Boltzmann distribution function. Consequently, the Monte Carlo method is quite well adapted to reproduce the thermal equilibrium that is assumed within the Transition State Theory. Equilibrium properties are obtained by averaging over millions of geometrical configurations of the system that are conveniently selected along the simulation. As a matter of fact, a Molecular Dynamics [21] simulation can be used for the same purpose. In this case, the classical equations of motion (for instance, Newton's equations) for the system are integrated numerically in the phase space. From the solution of these equations, the atomic positions and velocities as a function of time are obtained, and the equilibrium properties are determined by performing time averages.

In this chapter we will focus on the Monte Carlo simulations, although many of the described points would also be applicable to Molecular Dynamics simulations. We begin, in section 2, with a summary of the basic methodological features of the Monte Carlo method. This is followed, in section 3, by a discussion of the meaning of the solvation of the gas-phase stationary points. In section 4, we outline the main methods to calculate free energy changes. In section 5, Variational Transition State Theory is applied to a chemical reaction in solution. In section 6, we discuss how the potential energy of each configuration can be calculated. We conclude, in section 7, with a survey of the most recent theoretical developments, and a list of the most promising perspectives for further advances.

2. Basis of the Monte Carlo Method

In this chapter we will briefly review the main aspects of the Monte Carlo methodology when it is applied to the treatement of liquid state and solutions. In this kind of studies the Monte Carlo method [18-21] consists of an algorithm to perform a random walk through the configuration space, in such a way that after a given number of equilibration steps, the generated configurations are distributed according with a previously chosen probability density $\Pi(\vec{q}^{(N)})$ where:

$$\vec{q}^{(N)} = (\vec{q}_1 , ..., \vec{q}_N) \qquad (1)$$

is the position of the vector of a point in the configurational space for a N-particle system, being $\vec{q}_\gamma$ the configurational coordinates of the particle γ.

Presently Monte Carlo calculations are based on the technique proposed by Metropolis [22] in 1953 which involves selecting the successive configurations in such a way that they build up a Markov chain [23]. The one-step transition probabilities p_{ij} are defined as the probability that beginning from the i configuration with $\vec{q}_i^{(N)}$, the configuration j with $\vec{q}_j^{(N)}$ is reached in one step. These probabilities are the elements of the one-step probability matrix associated to the Markov chain and they must fulfill the following conditions:

$$p_{ij} \geq 0 , \quad \forall\, i,j \tag{2}$$

$$\sum_j p_{ij} = 1 , \quad \forall\, i \quad (\textit{normalization condition})$$

If the n-steps transition probability elements are defined as the probability to reach the configuration j in n steps beginning from the configuration i and $\Pi_j = \Pi(\vec{q}_j^{(N)})$, then it can be demonstrated that if the Markov chain is ergodic (the ergodicity condition states that if i and j are two possible configurations with $\Pi_i \neq 0$ and $\Pi_j \neq 0$, for some finite n, $p_{ij}^{(n)} \neq 0$) and aperiodic (the chain of configurations do not form a sequence of events that repeats itself), the limits

$$\lim_{n \to \infty} p_{ij}^{(n)} = \Pi_j , \quad \forall\, i,j \tag{3}$$

do exist, they are independent of the configuration i and they are uniquely given as the solution of the steady-state equations

$$\sum_i \Pi_i p_{ij} = \Pi_j , \quad \forall\, j \tag{4}$$

subject to the conditions:

$$\Pi_i \geq 0 , \quad \forall\, i \tag{5}$$

$$\sum_i \Pi_i = 1$$

The existence of the limit (3) guarantees that, after a large enough number of steps, the different configurations are generated following a probability density Π. Then it is said that a distribution of stationary probability or situation of static equilibrium has been reached. If Π has been previously chosen, the method consists of selecting p_{ij} so that the conditions (2) and (4) are fulfilled. We must stress the fact that the condition of microscopic reversibility:

$$\Pi_i p_{ij} = \Pi_j p_{ji} , \quad \forall\, i,j \tag{6}$$

plus the normalization condition are sufficient for (4) to be satisfied.

Usually when closed, isothermal systems (N,V,T) are studied, the canonical distribution function is chosen:

$$\Pi(\vec{q}^{(N)}) = \frac{e^{-U(\vec{q}^{(N)})/kT}}{Z(N,V,T)} \tag{7}$$

where $U(\vec{q}^{(N)})$ is the potential energy of the system, k the Boltzmann constant , T the absolute temperature and Z(N,V,T) the configuration integral:

$$Z(N,V,T) = \int e^{-U(\vec{q}^{(N)})/kT}\, d\vec{q}^{(N)} \tag{8}$$

In this case, once the statistical equilibrium has been reached, the Markov chain generates a trajectory through configuration space that samples configurations in accord with the canonical Boltzmann distribution of configurations. Averages over these statistical trajectories correspond to equilibrium canonical ensemble averages In this way the mean value of any mechanical property M of the system, which depends only on the configuration coordinates,

$$\langle M \rangle = \int M(\vec{q}^{(N)})\, \frac{e^{-U(\vec{q}^{(N)})/kT}}{Z(N,V,T)}\, d\vec{q}^{(N)} \tag{9}$$

simply reduces to the sum:

$$\langle M \rangle = \lim_{n \to \infty} \frac{1}{n} \sum_{i=1}^{n} M(\vec{q}_i^{(N)}) \tag{10}$$

which is calculated only over the configurations obtained from the situation of statistical equilibrium.

Any selection of p_{ij} that fulfills conditions (2) and (6) leads through an infinitely long chain to the stationary distribution given by (3). Actually the chain must be of finite size so that one of the main difficulties in the Monte Carlo method consists of, by using a reasonable amount of computer time, to guarantee the convergence to the equilibrium situation given by (3) and to achieve a run over the configurational space

large enough so that $\langle M \rangle$ can be evaluated with sufficient accuracy using the expression (10) with n finite.

The convergence and statistical error bounds of the calculations are usually monitored [24,25] by partitioning the chain into several nonoverlapping blocks of equal lenght. Then the mean value $\langle M \rangle_b$ of a magnitude M (usually the potential energy) over each block b of configurations is calculated. It is considered that the statistical equilibrium has been reached when these mean values $\langle M \rangle_b$ fluctuate around a stable mean value $\langle M \rangle$. When the simulation has ended, supposing that the mean values $\langle M \rangle_b$ are independent and are normally distributed, and that the Markov chain is ergodic, the error bound for the property M within a 95% of confidence are $\pm 2\sigma$ where:

$$\sigma^2 = \frac{1}{K(K-1)} \sum_{b=1}^{K} \{ \langle M^2 \rangle_b - \langle M \rangle_b^2 \} \qquad (11)$$

and the sum is over K blocks.

The problem with convergence is particularly important when dealing with solutions [24,26]. The configurational means in a pure liquid are calculated by averaging over all the configurations and also, given the fact that all the particles are identical, by averaging over the N particles of the system. However, in simulating a solution there is one solute particle and N-1 solvent molecules. In the evaluation of configurational means with respect to the solute, such as the solute-solvent radial distribution functions, the statistics is reduced by a factor of 1/N with respect to the pure liquid. Thus, longer chains must be generated or, alternatively, methods that accelerate the convergence have to be devised so that the study of solutions can reach a degree of accuracy similar to the one obtained for pure liquids. The latter point can be achieved by conveniently choosing the p_{ij} elements of the transition matrix. This way, in section 2.1 the Metropolis algorithm is described whereas section 2.2 presents an example of alternative method suggested in order to accelerate the convergence of the Monte Carlo calculations.

Once the statistical equilibrium has been reached, the numerical data corresponding to the successive Markov chain configurations must be stored on a magnetic tape or disk. There are millions of real numbers, generally stored within a binary code that need a considerable volume of memory and contain a huge mount of information about the solution properties. The process to extract these data is quite complex and the kind and quantity of structural and energetic properties depend on the studied systems as well as on the imagination and the skill of the programmer. We must take into account that the program that produces the configurations as well as the ones that analyze them must be rewritten or, at least, adjusted for each studied system. A portion of the information obtained from the simulation can be readily compared with experimental data whereas another part consists of results not experimentally attainable.

Up to this point and in the following sections and as long as the contrary is not specified, all the discussion will refer to the study of closed, isothermal systems (N,V,T). Though in the applications of Monte Carlo method to the study of solutions

it is customary to make use of the canonical ensemble, the Markov chains can be similary generated for any ensemble. Monte Carlo calculations in the isothermal-isobaric ensemble are discussed in section 2.3.

The difference between the canonical (N,V,T) and the isothermal-isobaric ensemble (N,P,T) is that in the latter the thermodynamic pressure is kept constant throughout the simulation instead of the volume of the system. In both ensembles though, simulations at different temperatures are carried out in order to analyze the effect of thermal agitation on the energetic and structural characteristics of the generated configurations. In both ensembles too, the number of solvent molecules that can be explicitly simulated by means of the Monte Carlo method is obviously quite superior to what can be done with any quantum discrete methodology like the supermolecule approach. In any case, that statistical number is still too small compared with the Avogadro number. The attempt to infer the behaviour for large systems from calculations with a few hundred molecules clearly constitutes one of the most serious approximations involved in the application of the Monte Carlo method, and one which needs careful consideration.

In order to simulate as closely as possible the behaviour of an infinite system, it is customary to use the so-called "periodic boundary conditions". The mathematical treatement of those "periodic boundary conditions" was due to Metropolis. Basically, the method consists in locating the N-particle system under study in a central box (basic cell) that is surrounded by translational symmetry by an infinite set of identical boxes. The volume V of the system is chosen to have a shape which by the usual translational replication fills ν-dimensional space completely (ν = 3 in physical systems). Computationally it is usually convenient to choose V as a cube or a rectangular parallelepiped. With each configuration of the N molecules in V is associated the same configuration in each replica of V, thereby obtaining for each such configuration a corresponding periodic configuration of an infinite system. Molecules from different boxes may interact in such a way that surface effects are eliminated.

As it will be explained in section 6, the usual way to evaluate the potential energy of a system simulated by Monte Carlo techniques, makes use of the pair potential approximation (although, as it will also be reviewed, several works have already appeared where nonadditivity corrections to the interaction potential have been included). In the pair potential approximation only two body interactions are taken into account. We will briefly explain here how to apply this approximation for the calculation of the potential energy, to the periodic system just described. The interaction potential energy under the pair potential approximation can be written as:

$$U(\vec{q}^{(N)}) = \sum_{\alpha<\beta}^{N} V^{(2)}(\vec{q}_\alpha, \vec{q}_\beta) \qquad (12)$$

where the indexes α, β refer to the different molecules of the system and the summation extends over all the possible doublets (α , β) . $V^{(2)}$ is the so-called pair potential, the interaction energy of a pair of molecules.

In a periodic system the expression of the interaction energy under the pair potential approach would be the following (assuming, for instance, the special case in which the

pair potential depends only upon the distance between any pair of particles):

$$U(\vec{q}^{(N)}) = \sum_{\alpha<\beta}^{N} V^{(2)}(q_{\alpha\beta}) + \sum_{v}' \sum_{\alpha}^{N} \sum_{\beta}^{N} V^{(2)}(|L\vec{v} + \vec{q}_{\alpha\beta}|) \qquad (13)$$

where $V^{(2)}$ depends only upon the distance $\vec{q}_{\alpha\beta} = |\vec{q}_{\beta} - \vec{q}_{\alpha}|$ between particles α and β, the prime on the first summation of the second term of equation indicates that the addition is done over all boxes except the central one, L is the edge of the cubic box, and $\vec{v}$ stands for the position vector of a box versus the origin (0,0,0) where the basic cell is usually centered.

The infinite summation represented by equation (13) cannot be performed except if the interaction potential between pairs of particles cancels further on some particular distance, like it happens, for instance, with the hard-sphere potential. Then, some kind of approximation must be done in those systems that interact by means of a soft and continuum potential when trying to evaluate the potential energy of an infinite system from calculations on configurations with a small number of particles. Several approximations based on the methodology of truncated intermolecular forces have appeared in the literature. One of the most popular is the minimum image convention. According to this methodology, a molecule of the central box only interacts with the closest periodic image of each one of the other N-1 molecules in the same box. This is equivalent to truncate the intermolecular potential at the limits of a box identical to the original one but now centered at the particle for which interactions are being evaluated.

2.1. THE METROPOLIS ALGORITHM

The p_{ij} elements of the transition matrix can be written as a product of two terms

$$p_{ij} = t_{ij} \cdot \alpha_{ij} \qquad (14)$$

t_{ij} depends on how the attempted new configuration j is generated from the i configuration in only one step. α_{ij} is the probability that the trial move is accepted. In the Metropolis algorithm:

$$\alpha_{ij} = Min(1, \Pi_j t_{ji} / \Pi_i t_{ij}) \qquad (15)$$

So that:

$$p_{ij} = t_{ij} Min(1, \Pi_j t_{ji} / \Pi_i t_{ij}), \quad i \neq j \qquad (16)$$

It is clear that the p_{ij} elements defined by (16) fulfil the conditions (2) and (6).

Although theoretically it would be possible to go from one configuration to another through the global motion of the N system particles, actually the probability that

$$p_{ii} = 1 - \sum_{i \neq j} p_{ij}$$

it were accepted would be very small. Therefore motions are normally restricted to only one particle per step, randomly or sequentially chosen. This way the configuration coordinates i and j are related by:

$$\vec{q}_j^{(N)} = \vec{q}_i^{(N)} + \vec{\delta}^{(N)} \tag{17}$$

where:

$$\vec{\delta}^{(N)} = (0,0,\ldots,\vec{\delta}_\gamma,0,\ldots,0) \tag{18}$$

and $\vec{\delta}_\gamma$ is a displacement vector for the particle γ selected for the move. In the case of polyatomic rigid molecules:

$$\vec{\delta}_\gamma = (\delta_{XCM},\delta_{YCM},\delta_{ZCM},\delta_\phi,\xi) \tag{19}$$

where δ_{XCM}, δ_{YCM} , δ_{ZCM}, are the displacements of the center of mass and δ_ϕ is the rotation around a chosen axis ξ passing through the center of mass of the molecule γ.

In the Metropolis algorithm the components of the displacement vector $\vec{\delta}_\gamma$ are obtained by uniformly sampling from the domain D, centered in the coordinates of the molecule γ in the i configuration, and defined by the maximum allowed displacement δ^{MAX} and maximum allowed rotation $\delta_\phi{}^{MAX}$ parameters (convergence celerity greatly depends on the values used for these two parameters). That is, all the positions inside domain D have the same probability to be chosen as new trial configurations. Thus:

$$\begin{aligned} t_{ij} &= constant \quad , \quad \vec{q}_j^{(N)} \in \vec{q}_i^{(N)} + D \\ t_{ij} &= 0 \qquad\quad , \quad \vec{q}_j^{(N)} \notin \vec{q}_i^{(N)} + D \\ t_{ij} &= t_{ji} \end{aligned} \tag{20}$$

Two methods are commonly used in order to select the rotation axis ξ. In the method of Barker and Watts [27,28] ξ is chosen by uniformly sampling between the axis x,y and z in a fixed frame of reference. The second method makes use of the Euler angles [29].

From the expressions (20), equation (16) for the Metropolis algorithm can be written as :

$$\begin{aligned} p_{ij} &= constant \cdot Min(1, \Pi_j / \Pi_i) \;,\; i \neq j \;,\; \vec{q}_j^{(N)} \in \vec{q}_i^{(N)} + D \\ p_{ij} &= 0 \qquad\qquad\qquad\qquad\quad ,\; i \neq j \;,\; \vec{q}_j^{(N)} \notin \vec{q}_i^{(N)} + D \end{aligned} \tag{21}$$

Expression (21) tells us that if Π is the canonical distribution function (7), given that p_{ij} depends on the quotient Π_j / Π_i, the calculation of the configurational integral Z(N,V,T) is avoided. The change in potential energy of the system due to the trial move determines if the attempted new configuration is accepted.

2.2. CONVERGENCE ACCELERATION: PREFERENTIAL SAMPLING

This method [24,26,30] is specifically suited for simulating solutions. A great deal of the more interesting properties of solutions are essentially determined by the solute-solvent and solvent-solvent interactions close the solute. This fact suggests that the convergence of many solution properties can be accelerated by mainly sampling in the vicinity of the solute in contrast with the Metropolis method that samples among all the solvent molecules with identical probability.

The main idea of the method is to assign a weight function $w_i(\gamma)$ to each solvent molecule γ of the configuration i so that the probability that a given γ is chosen for the trial move is:

$$W_i(\gamma) = \frac{w_i(\gamma)}{\sum_\gamma w_i(\gamma)} \tag{22}$$

This manner, if γ is the solvent molecule selected for the move:

$$\begin{aligned} t_{ij} &= constant \cdot W_i(\gamma) , \quad \vec{q}_j^{(N)} \in \vec{q}_i^{(N)} + D \\ t_{ij} &= 0 , \quad \vec{q}_j^{(N)} \notin \vec{q}_i^{(N)} + D \end{aligned} \tag{23}$$

obviously now $t_{ij} \neq t_{ij}$ because

$$\begin{aligned} t_{ji} &= constant \cdot W_j(\gamma) , \quad \vec{q}_i^{(N)} \in \vec{q}_j^{(N)} + D \\ t_{ji} &= 0 , \quad \vec{q}_i^{(N)} \notin \vec{q}_j^{(N)} + D \end{aligned} \tag{24}$$

In order the microscopic reversibility condition (6) be fulfilled, p_{ij} must be expressed as:

$$\begin{aligned} p_{ij} &= constant \cdot W_i(\gamma) \cdot Min(1, \Pi_j W_j(\gamma) / \Pi_i W_i(\gamma)), \; i \neq j, \; \vec{q}_j^{(N)} \in \vec{q}_i^{(N)} + D \\ p_{ij} &= 0, \; i \neq j, \; \vec{q}_j^{(N)} \notin \vec{q}_i^{(N)} + D \end{aligned} \tag{25}$$

$w_i(\gamma)$ can be a function of the solute-solvent interaction energy, the orientation, the distance, etc. $w_i(\gamma)$ is usually chosen as an inverted power of the distance r between the solute and the g solvent molecule: $1/r$, $1/r^2$ or even $1/(r^2 + C)$, C being a given constant [31].

Solute motions follow a quite different pattern. The solute is perturbed after a given number of motions of the solvent. Hypothetically, the solute could remain motionless, which would correspond to place the system of coordinates in the solute molecule. However, from a statistical point of view it is better to allow some motion given the fact that if a solvent molecule is displaced, only one solute-solvent interaction is perturbed whereas if it is the solute that moves all the solute solvent interactions are modified.

2.3. ISOTHERMAL-ISOBARIC MONTE CARLO

The isothermal-isobaric ensemble (N,P,T) allows the simulation of chemical systems at a constant temperature and pressure, such as 298 K and 1 at. which are the most usual experimental conditions. At a given set of (N,P,T) the probability density is not only dependent of $\vec{q}^{(N)}$ but also of the volume V:

$$\Pi(\vec{q}^{(N)}, V) = \frac{e^{-[U(\vec{q}^{(N)}) + PV] / kT}}{Z(N,P,T)} \tag{26}$$

where P is the pressure of the system and Z(N,P,T) the configuration integral in this ensemble

$$\begin{aligned} Z(N,P,T) &= \int_0^\infty Z(N,V,T)\, e^{-PV/kT} dV = \\ &= \int_0^\infty \int e^{-[U(\vec{q}^{(N)}) + PV]/kT} d\vec{q}^{(N)} dV \end{aligned} \tag{27}$$

The essential changes with respect to the canonical ensemble is the substitution of the internal energy U by the enthalpy H = U + PV in equations (7) and (8).

The mean value of a mechanic magnitude M which is only function of $\vec{q}^{(N)}$ and V is given by:

$$\langle M \rangle = \int_0^\infty \int M(\vec{q}^{(N)}, V) \frac{e^{-[U(\vec{q}^{(N)}) + PV]/kT}}{Z(N,P,T)} d\vec{q}^{(N)} dV \tag{28}$$

Monte Carlo method within this ensemble [29,30,32,33] differs from the canonical ensemble (N,V,T) in that the configuration variables are $\vec{q}^{(N)}$ and V so that in the successive steps of the Markov chain not only $\vec{q}^{(N)}$ must be perturbed but also the volume. For computational reasons it is convenient to introduce scaled coordinates:

$$\vec{y}_\gamma = \frac{\vec{q}_\gamma}{L} \tag{29}$$

where L is the cell side length of the cubic lattice, being the coordinates $\vec{y}_\gamma$ dimensionless. Then, the sampling must be done over the variables $(\vec{y}^{(N)}, L)$. When one step of the Markov chain involves a change of L (and so of V) all the inter-particle distances are scaled. Volume is not changed at every step. The more convenient frequency is empirically calculated. If it is too high, it is too much time consuming; if it is too low, a poor convergence of magnitudes related to V is found.

The main drawback with the application of Monte Carlo method in this ensemble lies in the fact that, due to the perturbation [34] that must be applied to the volume, it takes approximately 15% more of computing time than in the canonical (N,V,T) ensemble. Another possible problem is that some interaction potentials may lead to unreasonable densities in the calculation.

3. Solvation of the Gas-Phase Stationary Points

In order to apply the Monte Carlo method to a chemical reaction in solution, two general problems immediately appear. Firstly, how do the configurational space have to be sampled? That is, which configurations are considered and what kind of chemical information can be extracted from them. Second, how is the potential energy of each configuration evaluated? The discussion of this last point will be delayed until section 6.

Regarding the first problem, the most elemental treatment consists of focusing on a few points on the gas-phase potential energy hypersurface, namely, the reactants, transition state structures and products. As an example, we will mention the work [35,36] that was done on the Meyer-Schuster reaction, an acid catalyzed rearrangement of α-acetylenic secondary and tertiary alcohols to α,β-unsaturated carbonyl compounds, in which the solvent plays an active role. This reaction comprises four steps. In the first, a rapid protonation takes place at the hydroxyl group. The second, which is the rate limiting step, is an apparent 1 ,3-shift of the protonated hydroxyl group from carbon C_1 to carbon C_3. The third step is presumably a rapid allenol deprotonation, followed by a keto-enol equilibrium that leads to the final product.

For the rate limiting step in an aqueous acid medium, the intermolecular mechanism of Edens et al. [37] postulated a reaction path through a transition state structure involving the attack of one solvent water to the C_3 center, while the protonated hydroxyl group leaves the C_1 center and becomes a free water solvent. Such a transition state structure was found on the 4-31G potential energy hypersurface, along with the corresponding reactant and product, for a gas-phase system consisting of an oxygen-protonated methylbutynol plus one water molecule. Those gas-phase stationary structures were then taken as rigid solutes, and Monte Carlo (with the canonical distribution function) simulations at 300 K including 125 water molecules as solvent were carried out to reproduce the solvation effects.

Because such a treatment implies that the solvent configurations are generated around frozen gas-phase geometries of the solute, it is evident that the solvent equilibrium hypothesis has been used, although in a way slightly different from the case of the clusters. In clusters, it is first assumed that solvent coordinates are at a minimum energy point for each fixed solute coordinates. Then, if necessary, the contribution of the remaining structures (arising from quantized vibrations) of each dividing surface (defined in a suitable orientation) is implicitly taken into account by means of the above mentioned statistical thermodynamic formulae. On the other hand, in a Monte Carlo simulation of a chemical reaction in solution the different classical configurations belonging to each dividing surface are explicitly generated.

If only the solvation of the gas-phase stationary points are studied, we are working within the frame of the Conventional Transition State Theory, whose problems when used along with the solvent equilibrium hypothesis have already been explained above. Thus, the set of Monte Carlo solvent configurations generated around the gas-phase transition state structure does not probably contain the real saddle point of the whole system, this way not being a correct representation of the conventional transition state of the chemical reaction in solution. However, in spite of that this elemental treatment

is not able to afford a quantitative estimation of the reaction rate, the detailed analysis of the solvent configurations can supply a lot of interesting qualitative information about the reaction mechanism.

Turning back to the rate limiting step of the Meyer-Schuster reaction, a close look of the inner solvation shells shows water arrangements that provide an useful molecular knowledge about the mechanism. At the reactant, the oxygen radial distribution function around the C_3 center presents a very large peak. This fact, along with the characterization of the more significant structures, indicates that there are several water molecules in the solution correctly oriented so as to initiate a nucleophilic attack onto C_3. The bulk supports these water molecules in the adequate position to produce the reaction, this way giving rise to a solvent caging effect. On the other hand, the solvation structure around the gas-phase transition state structure reveals the existence of some configurations in which "holes" (water occupation defaults) appear in the neighbourhood of the protonated hydroxyl group attached to the C_1 center. These holes in the solvation shell make possible an outgoing channel to eject the water molecule bonded to C_1, thus aiding the progress of the reaction. Finally, the protonated hydroxyl groups for the three gas-phase stationary points are seen to be fully solvated. The solvent water molecules in their neighbourhood are so orientated as to make possible hydrogen bondings with them. Networks of hydrogen bonds are found which connect the reactive sites of the solutes.

4. Calculation of free energy differences

Free energy is the key quantity that is required to determine the rate of a chemical reaction. Within the Conventional Transition State Theory, the rate constant depends on the free energy barrier imposed by the conventional transition state. On the other hand, in the frame of the Variational Transition State Theory, the free energy is the magnitude that allows the location of the variational transition state. Then, it is clear that the evaluation of the free energy is a cornerstone (and an important challenge) in the simulation of the chemical reactions in solution.

In order to fix ideas, we will consider in this section a canonical ensemble [38]. In this ensemble, the Helmholtz free energy is straightforwardly related with the canonical partition function through

$$F(N,V,T) = -kT \ln Q(N,V,T) \tag{30}$$

For a classical system of N point particles enclosed in a volume V, at a temperature T, the canonical partition function can be decomposed in two factors. The first one (Q_t) comes from the integration over the space of momenta of the kinetic term of the classical Hamiltonian, which represents the free motion of noninteracting particles. The second one, which introduces the interactions between the particles and involves integration over the positions, is the configuration integral. This way, equation (30)

gives

$$F(N,V,T) = -kT \ln [Q_t \, Z(N,V,T)] \tag{31}$$

The difficulty arises from the fact that the one-step transition probabilities of the Markov chain involve only ratios of probability densities, in which Z(N,V,T) cancels out. This way, the Metropolis Markov chain procedure intentionally avoids the calculation of the configurational integral, the Monte Carlo method not being able to directly apply equation (31).

As a matter of fact, we are rather interested in free energy differences between dividing surfaces. Then, if $S^{\#}$ and S_R stand for the dividing surfaces associated to the transition state and the reactants, respectively, taking into account that Q_t is not dependent of the dividing surface, the free energy barrier ($\Delta F^{\#}$) is written as

$$\Delta F^{\ddagger} = F^{\ddagger} - F_R = -kT \ln \frac{\int e^{-U(S^{\ddagger})/kT} \, dS^{\ddagger}}{\int e^{-U(S_R)/kT} \, dS_R} \tag{32}$$

where each integral is just spanned over the set of configurations belonging to each dividing surface, respectively. The problem lies again on the fact that both integrals are just configuration integrals, although now they are confined in particular zones of the configurational space, their calculation not being possible in a Monte Carlo simulation.

An equivalent way to envisage this problem is through the consideration that the probability of appearance of a configuration belonging to a S dividing surface is proportional to the corresponding configurational integral extended just over S. Thus, the free energy barrier could be obtained by means of

$$\Delta F^{\ddagger} = -kT \ln \frac{n(S^{\ddagger})}{n(S_R)} \tag{33}$$

where $n(S^{\#})$ and $n(S_R)$ represent the number of times a configuration belonging to $S^{\#}$ or S_R, respectively, appears along a Monte Carlo run. In a straightforward Monte Carlo simulation, one would count the number of times configurations of a given dividing surface ($S^{\#}$ in the present case) are visited during the course of a Monte Carlo run, in comparison with the number of times S_R is populated. The quotient between both numbers yields a good estimation of the free energy barrier, provided that the run is long enough.

However an important difficulty immediately arises when one realizes that we are

interested in a relatively rare event. The free energy barriers for chemical reactions in solution typically range from a few to many tens of kilocalories per mol. For example, if $\Delta F^{\#} \approx 20$ kcal/mol, at T = 298 K on average the transition state is reached only once for each 10^{15} configurations corresponding to the reactants. The generation of such a number of configurations is completely impractical because it would require thousands of years of computer time in a very fast machine. Even in this scale of time, a relatively poor statistics would be acquired for the transition state. Then, how are we to obtain meaningful statistics for these very infrequent events without wasting time populating irrelevant though accessible configurations?

To circumvent this problem avoiding such inefficient exploration of the configurational space, several methods have emerged. Two particularly useful approaches are the Umbrella Sampling and the Statistical Perturbation Theory. Both methods can be used either with Monte Carlo or with Molecular Dynamics simulations.

4.1. UMBRELLA SAMPLING

Let us suppose that a transformation path along a suitable reaction coordinate r connecting S_R and $S^{\#}$ is defined. This is equivalent to define a set of dividing surfaces, each one formed by the ensemble of configurations that has a particular value of r. If the r coordinate is allowed to vary during the Monte Carlo simulation just like any other variable, the most straightforward (although quite inefficient) procedure is direct sampling of r according a Boltzmann distribution. The frequency of occurrence of different values of r during the simulation can be accumulated in the distribution function g(r), which is simply related to the relative free energy (or potential of mean force) of the system as a function of r by

$$W(r) = -kT \ln g(r) \tag{34}$$

This way, the free energy barrier is given by

$$\Delta F^{\ddagger} = W(r^{\ddagger}) - W(r_R) \tag{35}$$

where $r^{\#}$ and r_R are, respectively, the values of the reaction coordinate that define $S^{\#}$ and S_R.

Unfortunately, as it has been above emphasized, the range of r values that can be reasonably sampled along a simulation is very limited. Umbrella Sampling [39-42] can sometimes provide a solution by using an artificial biasing potential energy function which is added to the potential energy U. It can constrain the simulation to sample a particular range of r values or flatten the energy barriers. Then, the Monte Carlo random walk is generated in the usual manner, but the configurations are selected with a non-Boltzmann probability density

$$\Pi(\vec{q}^{(N)}) = \frac{e^{-[U(\vec{q}^{(N)}) + U'(r)]/kT}}{\int e^{-[U(\vec{q}^{(N)}) + U'(r)]/kT} d\vec{q}^{(N)}} \tag{36}$$

where U'(r) is the biasing umbrella potential. After such simulations, the effects of non-Boltzmann sampling can be removed. Thus, the true distribution function, g(r), is recovered through

$$g(r) = \frac{g'(r)\, e^{U'(r)/kT}}{\langle e^{U'(r)/kT} \rangle_{U+U'}} \tag{37}$$

where g'(r) is the biased distribution function and $< >_{U+U'}$ refers to a canonical average in the biased system (that is, taking equation (36) as the probability density of the configurations).

If the entire range of the r reaction coordinate is still not spanned in a single simulation, importance sampling has to be used. That is, multiple simulations are performed with biasing umbrella potentials that center the sampling in different, overlapping regions of r (windows). The number of windows is chosen in order to cover the total range of r. Within each window the configurations are scanned to determine g(r). After the full range of r is studied in this way, the full g(r), and thus W(r), are found by requiring that these functions are continuous functions from one window to the next. Actually, the W(r) mean force potential is determined in each window to within an additive constant, which is a consequence of the fact that the g(r) distribution function is obtained in each window to within a normalization constant. Since windows are chosen in such a way that they have points in common with their neighbours, the g(r) values for each window have to be spliced together (i.e. the normalization constant must be adjusted from one window to the next) to obtain the overall g(r).

The main difficulties of Umbrella Sampling are the choice of the biasing umbrella potentials and the verification of complete sampling for each window.

4.2. STATISTICAL, PERTURBATION THEORY

Free energy perturbation calculations [38,43-47] are based on a relationship easily derived from equation (31)

$$\Delta F = -kT \ln \left\langle \exp\left[-\frac{(U_1 - U_o)}{kT} \right] \right\rangle_o \tag{38}$$

Here the free energy difference, ΔF, between states 1 (the perturbed state, with the U, potential energy) and 0 (the unperturbed state, with the U_0 potential energy) is obtained by a canonical average, $< >_0$, evaluated by sampling based on the unperturbed state. If the perturbation is large, the average in equation (38) will converge very slowly. Therefore, some care must be exercised to avoid overly large perturbations. In these cases the total change has to be broken into a series of small changes, in such a way that multiple simulations over intermediate states between 0 and 1 are carried out. Then, the total free energy difference between the fully perturbed state, 1, and the unperturbed state, 0, is obtained as the sum of the partial differences between two consecutive intermediate states.

Many times it is convenient to define a coupling parameter, λ, that allows the smooth conversion of system 0 to 1. Then for many possible features ξ of the states, including geometrical and potential function parameters, equation (37) can be used to represent the mutation of state 0 to 1 as λ goes from 0 to 1

$$\xi(\lambda) = \xi_o + \lambda (\xi_1 - \xi_o) \tag{39}$$

The λ coupling parameter defines a set of intermediate hybrid states between the unperturbed and the fully perturbed states. Then, the total change in the free energy is

$$\Delta F(\lambda = 0 \rightarrow \lambda = 1) = -kT \sum_{\lambda_i = 0}^{\lambda_{i+1} = 1} \ln \left\langle \exp \left[- \frac{U(\lambda_{i+1}) - U(\lambda_i)}{kT} \right] \right\rangle_{U(\lambda_i)} \tag{40}$$

where $U(\lambda_i)$ is the potential energy associated with the state defined by $\lambda = \lambda_i$, and $< >_{u(\lambda i)}$ indicates a canonical average evaluated by sampling over the intermediate state λ_i.

The main advantages over umbrella sampling are the lack of need for biasing functions and the complete control in choosing the sampled regime via the λ values. However, the choice of λ values for optimal convergence of ΔF values requires some testing. Depending on the way in which λ is changed, several implementations of the free energy perturbation method are possible [48,49]:

a) Window growth. In this procedure, the range $0 \rightarrow 1$ of λ is divided up into several equally spaced intervals (windows), i.e., $\delta\lambda_i = \lambda_{i+1} - \lambda_i$ = constant. For each value of λ, a Monte Carlo simulation is run firstly to equilibrate the system using the potential appropriate for that value of λ, and then additional configurations are generated to evaluate the corresponding ensemble average.

In order to check the self-consistency, the simulations can be run in both directions, i.e., $\lambda_i \rightarrow \lambda_{i+1}$ and $\lambda_{i+1} \rightarrow \lambda_i$ except at the two end points. This is known as double-ended sampling [50]. It is facilitated by using double wide sampling, i.e., the free energy

differences for $\lambda_i \rightarrow \lambda_{i+1}$ and $\lambda_i \rightarrow \lambda_{i-1}$ can be obtained simultaneously since both require sampling based on the λ_i state. It is known [51] that the errors tend to cancel out when the results of the two λ paths in opposite directions are averaged.

b) Slow growth. This procedure is the limiting case of window growth when $\delta\lambda$ is very small. It is assumed that if $\delta\lambda$ is very small, at each window the system remains in near equilibrium and the ensemble average can be approximated by its instantaneous value. Thus, equation (40) leads to

$$\Delta F(\lambda = 0 \rightarrow \lambda = 1) = \sum_{\lambda_i = 0}^{\lambda_{i+1} = 1} [\, U(\lambda_{i+1}) - U(\lambda_i) \,] \qquad (41)$$

each λ_i intermediate state being changed an infinitesimal amount over each step of the simulation.

c) Dynamically modified windows. This method is similar to window growth, except that the width of each window $\delta\lambda_i$ is determined by the slope of the free energy versus λ for recent windows.

5. Variational Transition State Simulations for Chemical Reactions in Solution

The first microscopical computation of a free energy curve for a chemical reaction in solution was performed by the Jorgensen's group [41,52,53] ten years ago. They studied the degenerate S_N2 reaction of chloride anion with methyl chloride in gas phase, in aqueous solution and in dimethylformamide (DMF):

$$Cl^- + CH_3Cl' \rightarrow ClCH_3 + Cl'^-$$

where C1' stands for the leaving chlorine. The interest for this kind of reactions arises from the fact that the rates of S_N2 reactions involving anions and polar molecules diminish up to 20 orders of magnitude on going from the gas phase to polar, specially protic, solvents.

The basic procedure of the Jorgensen's approach (that we will outline along with the S_N2 results) involves the following three steps:

a) Determination of the gas-phase reaction path.

6-31G(d) ab initio calculations were carried out to obtain the energies and geometries of the $[ClCH_3Cl']^-$ cluster at a number of representative points on the gas-phase potential energy surface. Both chloride anions and the methyl carbon were assumed to remain collinear throughout the reaction. For fixed values of the CCl distance (r_{CCl}), the remaining geometric parameters were optimized in C_{3v} symmetry. After the corresponding structures had been obtained, the reaction coordinate was defined as

$$r_C = r_{CCl'} - r_{CCl}$$

which reflects the symmetry of the reaction (this way, the gas-phase transition state

structure appears at $r_c = 0$). The typical gas-phase double-well energy profile was obtained, in which the two minima corresponding to stable ion-dipole complexes (C1- ... CH_3CI' or $ClCH_3$ ... Cl^{1-}) flanks the central barrier imposed by the symmetric transition state structure. The calculated energy of the ion-dipole complex relative to the reactants (-10.3 kcal/mol) as well as the energy of the transition state structure relative to the ion-dipole complex (13.9 kcal/mol) are in accord with the experimental complexation enthalpy (8.6 kcal/mol) and the estimated intrinsic barrier (11.6 kcal/mol ± 1.8 kcal/mol).

Since the statistical mechanics simulation requires a knowledge of the features of the solute along the reaction coordinate, the calculated geometric parameters and the energy were fitted into analytical functions of r_c. However, the absolute magnitude of the variation of r_{CH} was so small that this parameter was held constant in the simulations.

b) Development of the intermolecular potential energy functions.

The potential energy of each configuration is obtained by adding three kinds of pairwise additive potential energy functions: the solute internal potential energy (i.e. the potential corresponding to the gas-phase reaction), the solvent-solvent interaction and the solute-solvent interaction. These last two kinds of interactions were described through Coulomb (r^{-1}) and Lennard-Jones (r^{-6} and r^{-12}) terms, acting between various sites on the monomers. For water, the TIP4P model [54] was chosen. The interaction sites for the solute were located on its atoms. It has to be emphasized that the charges and Lennard-Jones terms for the solute atoms vary along the reaction coordinate. These parameters and their dependence on r_c were determined from 6-31G(d) ab initio calculations on a large number of geometries of the $ClCH_3Cl'^-$ ... H_2O cluster spanning the reaction coordinate. For the simulation in DMF, the same solute parameters as in the case of water, and the parameters previously obtained for DMF were adopted.

c) Monte Carlo simulations of the reaction in solution.

Monte Carlo simulations were carried out to determine the free energy curve for the reaction in solution. The simulations were executed for the solute surrounded by 250 water molecules (or 180 DMF molecules) in the isothermal-isobaric ensemble at 25 °C and 1 atm, including periodic boundary conditions. As a consequence, the Gibbs free energy is obtained in this case. There is sufficient solvent to adequately represent the bulk participation in the chemical reaction.

Umbrella Sampling simulations were carried out over six windows for water (seven for DMF), corresponding to biasing umbrella potentials centered at different ri values of the reaction coordinate (r_c)

$$U_i'(r_c) = -25\, e^{-r_c^2} + \frac{1}{2} k_i (r_c - r_i)^2 \qquad (42)$$

The system is constrained within limited ranges of r_c by imposing a harmonic force. The force constants, k_i were chosen to be progressively smaller when going from the gas-phase transition state structure region to the reactants region, reflecting the expected steepness of the energy profile. The exponential function is added to ensure uniform

sampling, specially near the gas-phase transition state structure.

Once the mean force potential was obtained, the free energy curve was built up, and the free energy barrier and the variational transition state were identified. The most striking feature of the results was the almost unimodal nature of the free energy curve in water in contrast to the double-well profile in the gas phase. This is a consequence of the flattening of the ion-dipole minima, due to the partial desolvation of the chloride anion. The calculated free energy barrier in water (26.3 ± 0.5 kcal/mol) is in quantitative agreement with the experimental value (26.6 kcal/mol), the enhancement of the free energy barrier in aqueous solution being due to the fact that the transition state with a disperse charge distribution forms weaker hydrogen bonds to water than the reactants. On the other hand, when the solvent is DMF, whose anion solvating ability is slower than that of water, the free energy curve was found to be intermediate between those for the reaction in gas phase and in aqueous solution, with the ion-dipole complexes still appearing as free energy minima. The calculated free energy barrier in DMF turns out to be 19.3 ± 0.5 kcal/mol, the corresponding experimental value being 22.7 kcal/mol.

In both solvents, the variational transition state (associated with the free energy maximum) corresponds, within the numerical errors, to the dividing surface located at $r_c = 0$. It has to be underlined that this fact is not a previous hypothesis (which would rather correspond to the Conventional Transition State Theory), but it arises, in this particular case, from the Umbrella Sampling calculations. However, there is no information about which is the location of the actual transition state structure in solution. Anyway, the definition of this saddle point has no relevance at all, because the Monte Carlo simulation provides directly the free energy barrier, the determination of the transition state structure requiring additional work and being unnecessary and unuseful.

Since for each dividing surface characterized by a particular value of r_c the remaining solute degrees of freedom are kept frozen (they take the values coming from the analytical functions), some kind of solute-solvent separation is still introduced. Then, solvent equilibrium hypothesis is used again. Only when the free motion of all degrees of freedom (excepting the one that defines the reaction coordinate) is allowed within each dividing surface, we can assure that no partition of the system is considered, the thermal equilibrium basic assumption of the Transition State Theory then being the unique hypothesis adopted.

A similar methodology was applied by Madura and Jorgensen [55] to the nucleophilic addition of hydroxide anion (OH^-) to formaldehyde ($H_2C{=}O$) in aqueous solution. In this case, the reaction coordinate was defined as the distance between the hydroxyl oxygen and the carbonyl carbon (r_{co}). At each value of the reaction coordinate, complete 6-31+G(d) ab initio optimization was carried out for all other geometrical variables within C_s symmetry. The energy and the geometrical variations along the reaction path were fitted into continuous functions through the use of cubic spline interpolations [56]. In short, this procedure involves calculating the coefficients for a cubic polynomial for an interval between two points, at the same time smoothly splicing the intervals together, giving as the final result a continuous function. The reaction proceeds without energy barrier (there is no transition state structure) into a

deep well (35.2 kcal/mol) for the tetrahedral complex (r_{CO} = 1.47 Å) in the gas phase. Conversely, Umbrella Sampling (including the solute plus 269 water molecules at 25 ºC and 1 atm) shows that an important free energy barrier (24-28 kcal/mol) is introduced by hydration with the transition state occurring at r_{CO} = 2.05 Å. In contrast to the S_N2 reaction, the free energy barrier for the nucleophilic addition reaction in solution is nearly entirely solvent-induced. For both reactions, the principal source of this solvent-induced free energy barriers in water was found to be weakening of solute-water hydrogen bonds on going from the charge-localized reactants to the more charge delocalized transition states. It is noteworthy that for this nucleophilic reaction a variational transition state appears in aqueous solution despite that no gas-phase saddle point exists.

In the recent few years Statistical Perturbation Theory has become the most used method to calculate free energy changes. Thus, Jorgensen et al. began with the study of the effect of the hydration on the transition state for the S_N2 chloride exchange reaction $Cl^- + CH_3CI$ [57], and the S_N1 reaction of t-ButCl in water to yield t-butyl cation and chloride anion [45]. The free energy for this last system, including the solute plus 250 water molecules at 25 ºC and 1 atm, was determined as a function of the central carbon-chlorine distance, with the chloride anion maintained on the C_3 axis of the t-butyl cation. The Statistical Perturbation Theory was applied by sequentially perturbing along the C-CI reaction coordinate in steps of 0.125 or 0.25 Å. In all 15 Monte Carlo simulations were carried out to cover C-CI distances between 2.5 and 8.0 Å. Each value of the C-CI reaction coordinate defines the corresponding dividing surface. The difference in the ion pair-water interaction potential energies through equation (40) (taking into account that this simulation is done in the isothermal-isobaric ensemble, the volume has to be periodically changed and the Gibbs free energy is obtained) gives the changes in free energy of hydration, ΔG_{hyd}. The total free energy change, ΔG_{tot}, is then given by the sum of ΔG_{hyd} and the difference in interionic energies (i.e., the solute internal potential energies) for the perturbation. The latter quantity is constant for a given perturbation since the chloride anion was kept on the C_3 axis of the t-butyl cation. The Monte Carlo simulations predict the occurrence of a contact ion pair at a C-CI distance of 2.9 Å, and the onset of the solvent-separated ion-pair regime near 5.5 Å, the free energy barrier for conversion of the contact to the solvent-separated ion pair being 2.1 kcal/mol.

Very recently the Jorgensen's group has updated his methodology in order to investigate the solvent effect in several pericyclic reactions [58]. The experimental problem stems from the observation that simple Diels-Alder reactions could show rate accelerations by factors of 10^2 to 10^4 in aqueous solution over hydrocarbon solvents. Comparable solvent dependence for the rates of Claisen rearrangements is reflected in the literature. Firstly, they have calculated the changes in free energy of solvation, ΔG_{sol}, during the reaction of cyclopentadiene with methyl vinyl ketone in liquid propane, methanol and water [59]. The gas-phase ab initio MEP (that is, the intrinsic reaction path) was determined going downhill from the transition state structure to reactants and product. A movie containing 65 frames (or solute structures) was obtained covering reaction coordinate (defined as the average of the lengths of the two forming C-C bonds) values from 1.5 to 8.2 Å. The Monte Carlo simulations were carried out in cells

containing 260 propane, 260 methanol or 500 water molecules plus the solute in the isothermal-isobaric ensemble. The system was perturbed between adjacent frames (43 of the 65 frames were used, spaced roughly 0.15 Å apart) and the changes in free energy of solvation were computed via Statistical Perturbation Theory. A similar procedure was applied to the Claisen rearrangement of allyl vinyl ether [60], for which 143 frames along the gas-phase MEP were generated. In this case, 59 of the 143 frames were used along the perturbation procedure, and 838 water molecules were introduced around the solute. From the analysis of the results of the simulations, it can be concluded that the enhanced rate for the Claisen rearrangement in water comes from both an increase in the strength and number of hydrogen bonds on progressing to the transition state, while for the Diels-Alder reaction of cyclopentadiene with methyl vinyl ketone the acceleration comes primarily from just an increase in hydrogen-bond strengths.

Using the sequence of gas-phase MEP frames each dividing surface is defined by the set of solvent configurations that are generated around the frozen solute structure of each frame. Then, some kind of solute-solvent separation is assumed again.

A case that deserves special attention is the corresponding to electron transfer reactions. These kind of reactions are processes of fundamental importance in physics, chemistry and biology. Computer simulations of a variety of electron transfer systems are of considemble current interest. Assuming a classical frame [61-63], the radiationless electron transfer occurs when a structure in which the precursor and successor diabatic potential energies are equal (the intersection region), is reached as a result of random thermal fluctuations in the nuclear configurations (involving both the solute and the solvent coordinates) of the precursor complex. The appearance of the proper fluctuations costs free energy. It is this free energy that determines the rate of the reaction. The electronic coupling integral between both diabatic states is supposed to be large enough for the reactants to be converted into products with unit probability in the intersection region, but small enough to be neglected in calculating the amount of internal energy required to arrive to that region.

Several authors [64-71] have shown that a convenient microscopic level choice of reaction coordinate for the computer simulations of electron transfer reactions is the nongeometrical parameter $\Delta E=H_{ss}-H_{pp}$, that is, the difference between the diabatic potential energy hypersurfaces corresponding to the successor (H_{ss}) and the precursor (H_{pp}) complexes, respectively. Using this nongeometrical variable, the transition state of the electron transfer reaction is considered to be the ensemble of isoenergetic structures, that is, the S* intersection region of the two diabatic potential energy hypersurfaces. However, this is a point of view corresponding to Conventional Transition State Theory. Within the frame of the Variational Transition State Theory, it is not obvious that S* is the best choice to define the transition state. Then, in order to study electron transfer reactions in solution, two main questions emerge. Firstly, is the ΔE parameter the most convenient choice to define the reaction path and, therefore, the set of dividing surfaces? Secondly, if ΔE is used as reaction coordinate, is S* the bottleneck of the reaction? To illustrate these points we will focus [72,73] on the electrochemical reduction of methyl chloride in water, to give methyl radical and chloride anion, a dissociative electron transfer reaction.

To describe the electron transfer we have used a diabatic two-state model consisting of the methyl chloride surrounded by the solvent plus an electron inside an electrode (precursor complex), and the methyl chloride anion immersed in the solvent, once the electron has already shifted from the electrode (successor complex). For the sake of simplicity, the methyl group has been modeled by a unique interaction center, in such a way that the $d_{C\text{-}Cl}$ parameter is enough to specify the solute geometry. The energies of the H_{pp} and H_{ss} diabatic potential energy hypersurfaces have been obtained by adding three kinds of pairwise additive potential energy functions: the solute internal potential energy (which only depends on the d_{CCl} parameter), the solute-water interaction, and the water-water interaction. The first one is the potential corresponding to the gas phase reaction and merits some comments. In the absence of the solvent, the precursor complex consists of the methyl chloride plus an electron inside an electrode. Its energy is calculated as the sum of the methyl chloride energy and a constant value that represents the Fermi's energy level of the electrode. This Fermi's energy level has been chosen as the value that makes the reaction energy equal to zero in gas phase. As for the successor complex in gas phase, it is considered to be the methyl chloride anion in the electronic state that leads to the diabatic dissociation in chloride anion and methyl radical.

Thermal fluctuations have been generated [72] by means of the Monte Carlo method in a canonical system that includes the solute and 200 water molecules at T = 298 K. For each generated configuration the value $\Delta E=H_{ss} - H_{pp}$ has been calculated. The configuration space was partitioned in different subsets S, each one being associated with a particular ΔE_S value of the reaction coordinate ΔE (that is, each value of ΔE_s defines the corresponding S dividing surface). For practical purposes, the criterion $|\Delta E-\Delta E_S| \leq 5$ kJ/mol has been adopted in order to classify a given configuration as belonging to a S dividing surface. We have identified the reactants' region (S_R) with the most populated interval when the H_{pp} potential is used. Conversely, the products' region (S_p) is the most populated interval corresponding to the H_{ss} potential. The intersection region S* corresponds to the interval centred at the value of ΔE_s =0 kJ/mol. Thus, the free energy barrier $\Delta F^{\#}$ corresponds to the evolution from S_R to S* .

Due to the high value of $\Delta F^{\#}$ for our reactions, the complete sampling of the configuration space in order to obtain the diabatic free energy curves as a function of ΔE_s would require an extremely long simulation. unless Statistical Perturbation Theory is used. However, there is no way to generate only configurations associated with a particular ΔE_s value in each perturbational step. Then, a modification of the standard Statistical Perturbation Theory due to Warshel's group [74-76] has to be used. A mapping potential energy hypersurface of the form $H_m=(1-\lambda_m)H_{pp}+\lambda_m H_{ss}$ is defined, H_{pp} and H_{ss} being calculated from the potential energy functions above mentioned. The parameter lm changes from 0 to 1 on movement from the precursor to the successor states. With the H_m potential corresponding to $\lambda_m=0$ the most populated subspace is S_R. As λ_m increases, the system is forced to evolve towards the intersection region S*. With the H_m potential corresponding to $\lambda_m=1$ the most populated subspace is S_p. Now the diabatic free energies corresponding to the precursor and the successor complexes along the reaction coordinate are obtained by using the following expressions [72,74] as a

function of ΔE_s:

$$\Delta F_{pp}(\Delta E_S) = \Delta F_{0 \rightarrow m} - \lambda_m \Delta E_S - kT \ln \left[\frac{q_m^{(S)}}{Q_m} \frac{Q_{pp}}{q_{pp}^{(S_R)}} \right] \quad (43)$$

$$\Delta F_{ss}(\Delta E_S) = \Delta F_{1 \rightarrow m} + (1 - \lambda_m) \Delta E_S - kT \ln \left[\frac{q_m^{(S)}}{Q_m} \frac{Q_{ss}}{q_{ss}^{(S_P)}} \right] \quad (44)$$

The last term of equations (43) and (44) involves ratios of partition functions. So, the factor $q_m^{(S)}/Q_m$ is the probability that, using the H_m potential, the configurations generated belong to the S dividing surface. The ratio $q_{pp}^{(S_R)}/Q_{pp}$ in the equation (43) represents the probability that, using the H_{pp} diabatic potential, the configurations generated belong to the reactants' dividing surface, S_R. Analogously, the factor $q_{ss}^{(Sp)}/Q_{ss}$ in the equation (44) represents the probability that, using the H_{ss} diabatic potential, the configurations generated belong to the products' dividing surface, S_p.

The values $\Delta F_{0\rightarrow m}$ and $\Delta F_{1\rightarrow m}$ have been calculated by using standard Statistical Perturbation Theory. Thus, equation (45) expresses the free energy difference between systems with mapping potentials H_j and H_j by

$$\Delta F(\lambda_j \rightarrow \lambda_{j'}) = -kT \ln \left\langle \exp -\frac{(H_{j'} - H_j)}{kT} \right\rangle_{H_j} \quad (45)$$

The average is for sampling based on the potential H_j, so the H_j potential corresponds to a perturbed system. Therefore

$$\Delta F_{0 \rightarrow m} = \Delta F(\lambda_0 = 0 \rightarrow \lambda_m) = \sum_{j=0}^{m-1} \Delta F(\lambda_j \rightarrow \lambda_{j+1}) \quad (46)$$

To transform the potential smoothly and to avoid large perturbations, λ_j has been increased in small steps from 0 to 1. To evaluate numerically $\Delta F(\Delta E_s)$ with equations (43) and (44), we have used in each case the mapping potential H_m for which the most populated S subset is the one centred at ΔE_s. Following this procedure, each calculation converges very fast.

On the other hand, the unique solute internal coordinate of the system, that is, the

carbon-chlorine distance ($d_{C\text{-}Cl}$), can be adopted [73] as an alternative choice to define the reaction coordinate. This is a logical choice, because it corresponds to the geometrical parameter that will be broken during the process. In this case each dividing surface along the reaction path consists of the set of configurations associated with a given value of the $d_{C\text{-}Cl}$ parameter. Two configurations belonging to the same dividing surface only differ on the solvent coordinates. Thus, with $d_{C\text{-}Cl} = d_i$, water molecules have been moved to generate the configurations corresponding to the i dividing surface. For each generated configuration the potential energy has been evaluated as the min $\{H_{pp},H_{ss}\}$. The standard Statistical Perturbation Theory has been used to obtain the free energy change between the dividing surfaces, by sequentially perturbing along the reaction coordinate in small steps of $d_{C\text{-}Cl}$.

Note that the definition of the dividing surface (and even the definition of reactants and products) depends on the choice of the reaction coordinate. If ΔE is taken as a reaction coordinate, each dividing surface consists of the set of configurations that has the same value of ΔE. This way, two configurations belonging to a given dividing surface differ on the value of the $d_{C\text{-}Cl}$ parameter and/or the solvent coordinates, but all of them correspond either to the precursor or to the successor complexes. The S* intersection region is a special case of this kind of dividing surfaces. On the other hand, if the reaction coordinate is $d_{C\text{-}Cl}$ each dividing surface contains the ensemble of configurations that has the same value of $d_{C\text{-}Cl}$, but different solvent coordinates. This way, in principle, some configurations of a given dividing surface could be associated with the precursor complex and other configurations in the same dividing surface could correspond to the successor complex.

Analysis of the both kinds of Monte Carlo simulations shows some differences between the two reaction coordinates. The $d_{C\text{-}Cl}$ transition state (in the variational sense, that is, the dividing surface that maximizes the free energy) appears at $d_{C\text{-}Cl}$=2.11 Å, imposing a free energy barrier of $\Delta F^{\#}$ = 91.4 kJ/mol, and involving a wide dispersion of ΔE_s values. It has to be mentioned that the gas phase transition state structure, obtained as the crossing point between the two diabatic solute internal potential energy curves, appears at $d_{C\text{-}Cl}$=2.28 Å. It is clear that the transition state in water had to appear at lower $d_{C\text{-}Cl}$ values than the gas phasc transition state structure, because in water the successor diabatic solute internal potential energy curve (that is derived from a charged species) is noticeably stabilized due to the interaction with the polar solvent.

On the other hand, when the parameter ΔE is taken to define the reaction coordinate, the variational ΔE transition state that maximizes the free energy change turns out to be the S* dividing surface, that is, the same transition state that would be expected within the Conventional Transition State Theory. Anyway, it has to be noted that the statistical noise is probably much too large for slight displacement away from S* of the transition state along the ΔE reaction coordinate being detected. A scanning of the configurations belonging to the S* transition state shows a spread of C-Cl distances (centred about 1.90 Å) that clearly appears at lower $d_{C\text{-}Cl}$ values than the gas phase transition state structure and the $d_{C\text{-}Cl}$ transition state as well. The first fact, due to the solvent effect, was expected, but the second one rather introduces a discrepancy between the two simulations. It has to be remarked that the important dispersion of ΔE_s values and the $d_{C\text{-}Cl}$ values at the $d_{C\text{-}Cl}$ transition state and the ΔE transition state,

respectively, in solution is completely analogous to the appearance of many structures of the dividing surface arising from vibrations orthogonal to the Minimum Energy Path for a normal reaction in gas phase.

The transition states arising from each reaction coordinate are a logical consequence of different ways to cut (or classify) the configuration space. The ΔE parameter as a reaction coordinate provides a free energy barrier of 82.2 kJ/mol, a value 10% lower than the one that arises from the $d_{C\text{-}Cl}$ reaction coordinate. Although the relative difference in free energy is not excessively big, it is clear that each reaction coordinate leads to a distinct kinetic description of the reaction. We feel that the nongeometrical parameter ΔE, which involves a suitable combination of the $d_{C\text{-}Cl}$ and the solvent coordinates, is the best choice as reaction coordinate for dissociative electron transfer reactions in solution and, probably, for whatever kind of electron transfer reactions in solution, because permits a best sampling within each dividing surface defined in the configurational space.

6. Potential Energy Calculation

In this section we will briefly review some of the main different approaches that have been used up to now in order to evaluate the potential energy of each configuration in a Monte Carlo run. As we have already stated, the force fields that describe intra- and intermolecular interactions are at the heart of such statistical calculations because the free energy differences that we want to evaluate are directly dependent on the changes of those interactions. In fact, the important advances of the last ten years in the power of computer techniques for chemical reactions in the condensed phase, that we have mentioned in the Introduction, have been due, to a great extent, to the continual evolution in force fields, with added complexity and improved performance.

Most usually, the performance of those potential energy functions has been carefully tested at the same time that the new force fields were coming up and their applications were being published. It can be said that testing the functions in the prediction of well characterized experimental observables can never be overdone; however, it may receive inadequate attention in the rush toward the latest challenging application on complex molecular systems. The statistical mechanical equations that are the basis for the evaluation of the free energy differences (Section 2) are exact and the source of any errors that result from the computational implementation of these is due to the description of the Hamiltonian (reduced to the potential energy in a Monte Carlo calculation) and the ability to sufficiently sample the relevant microstates. Since the latter is also related to accuracies in the Hamiltonian, the success of the free energy methods, in general, and their broader application is dependent of accurate descriptions of the potential energy functions.

A rigourous way to evaluate the total interaction potential energy, $U(\vec{q}^{(N)})$, would be the formulation and resolution of the Schrodinger equation for the whole system at each configuration. However, given the size of the samples where the statistical simulations are performed, this method is impracticable.

Alternatively, for a system of N interacting molecules, $U(\vec{q}^{(N)})$ in a given

configuration, defined as the difference between the energy of the system and that of the separate components at infinite distance:

$$U(\vec{q}^{(N)}) = E(\vec{q}^{(N)}) - \sum_{\alpha=1}^{N} E(\vec{q}_\alpha) \tag{47}$$

can be expanded in a series of n-body separate terms [77,78]

$$U(\vec{q}^{(N)}) = \sum_{\alpha<\beta}^{N} V^{(2)}(\vec{q}_\alpha,\vec{q}_\beta) + \sum_{\alpha<\beta<\gamma}^{N} V^{(3)}(\vec{q}_\alpha,\vec{q}_\beta,\vec{q}_\gamma) + \ldots + V^{(N)}(\vec{q}_1,\ldots,\vec{q}_N) \tag{48}$$

where the indexes α, β, γ refer to the different molecules of the system and the summation extends over all the possible doublets (α, β), triplets (α, β, γ), and so on.

We have already introduced, in Section 2 , the pair potential function $V^{(2)}$ as the interaction energy of a pair of molecules

$$V^{(2)}(\vec{q}_\alpha,\vec{q}_\beta) = U(\vec{q}_\alpha,\vec{q}_\beta) \tag{49}$$

The higher order n-body functions $V^{(3)}$, $V^{(4)}$,... can be obtained recursively considering sets of three, four, ... molecules and applying equation (48) successively. Thus, one can write

$$\begin{aligned} V^{(3)}(\vec{q}_\alpha,\vec{q}_\beta,\vec{q}_\gamma) = {} & U(\vec{q}_\alpha,\vec{q}_\beta,\vec{q}_\gamma) - V^{(2)}(\vec{q}_\alpha,\vec{q}_\beta) \\ & - V^{(2)}(\vec{q}_\alpha,\vec{q}_\gamma) - V^{(2)}(\vec{q}_\beta,\vec{q}_\gamma) \end{aligned} \tag{50}$$

$$\begin{aligned} V^{(4)}(\vec{q}_\alpha,\vec{q}_\beta,\vec{q}_\gamma,\vec{q}_\delta) = {} & U(\vec{q}_\alpha,\vec{q}_\beta,\vec{q}_\gamma,\vec{q}_\delta) - V^{(2)}(\vec{q}_\alpha,\vec{q}_\beta) \\ & - V^{(2)}(\vec{q}_\alpha,\vec{q}_\gamma) - V^{(2)}(\vec{q}_\alpha,\vec{q}_\delta) - V^{(2)}(\vec{q}_\beta,\vec{q}_\gamma) \\ & - V^{(2)}(\vec{q}_\beta,\vec{q}_\delta) - V^{(2)}(\vec{q}_\gamma,\vec{q}_\delta) - V^{(3)}(\vec{q}_\alpha,\vec{q}_\beta,\vec{q}_\gamma) \\ & - V^{(3)}(\vec{q}_\alpha,\vec{q}_\beta,\vec{q}_\delta) - V^{(3)}(\vec{q}_\alpha,\vec{q}_\gamma,\vec{q}_\delta) - V^{(3)}(\vec{q}_\beta,\vec{q}_\gamma,\vec{q}_\delta) \end{aligned}$$

The U values are always calculated according to equation (47) (taking the adequate N value in each case) and the required energies E can be obtained from standard quantum

mechanical methods.

Most of statistical-mechanical computer simulations are based upon the assumption of pairwise additivity for the total interaction energy, what means to truncate the right side of equation (48) up to the two-body term. The remaining terms of the series, which are neglected in this approach, are often known as the nonadditive corrections.

Assuming the hypothesis of additivity of the interaction energies, inter- and intra-molecular pair potentials $V^{(2)}$ have to be developed in order to obtain values of $U(\vec{q}^{(N)})$ through equation (12).

In a statistical Monte Carlo simulation the pair potentials are introduced by means of analytical functions. In the election of that analytical form for the pair potential, it must be considered that when a Monte Carlo calculation is performed, the more time consuming step is the evaluation of the energy for the different configurations. Given that this calculation must be done millions of times, the chosen analytic functions must be of enough accuracy and flexibility but also they must be fastly computed. In this way it is wise to avoid exponential terms and to minimize the number of interatomic distances to be calculated at each configuration which depends on the quantity of interaction centers chosen for each molecule. A very commonly used function consists of a sum of r^{-n} terms, r being the distance between the different interaction centers, usually. situated at the nuclei. In particular, non-bonded interactions are usually represented by an atom-atom centered monopole expression (Coulomb term) plus a Lennard-Jones 6-12 term, as indicated in equation (51).

$$U(\alpha,\beta) = \sum_i^{on\ \alpha} \sum_j^{on\ \beta} \left(\frac{q_i q_j e^2}{r_{ij}} + \frac{A_{ij}}{r_{ij}^{12}} - \frac{C_{ij}}{r_{ij}^{6}} \right) \qquad (51)$$

In this expression, i and j are the interaction centers in α and β molecules, respectively, A_{ij} and C_{ij} are adjustable parameters that describe the interaction between i and j, q_j and q_j are the charges associated with centers i and j and, finally, r_{ij} is the distance between i and j. The parameters, of whom pair potentials depend on, can be fitted to reproduce theoretical results, experimental data or a combination of both.

The first option involves the obtainement of an analytic function that reproduces the interaction energy between couples of molecules which has been calculated by solving the Schrodinger equation usually by means of an ab initio method. The advantge of this possibility is that information about any potential energy hypersurface point can be obtained from the calculation whereas experimentally this is not always possible. The practical procedure in order to build up an ab initio pair potential for the interaction between two molecules α and β can be divided in four steps.

a) By keeping fixed the α molecule, a wide span of orientations and distances of the β molecule with respect to the α molecule, have to be selected so that all the configurational space for the (α, β) pair is represented. It is of special importance to well decribe the low energy zones of the hypersurface. As α and β become bigger and have less symmetry more configurations will be needed in order to consider the

whole space.

b) Evaluation of the interaction energy U for each configuration. When choosing the level of calculation it must be taken into account that it will be usually necessary to compute a huge number of configurations. If a very extended basis set is used and a Configuration Interaction scheme (CI) is performed in order to incorporate the correlation energy, the computation time needed can be unattainable. On the other hand a minimal basis set may not be enough and require corrections due to the superposition basis set error.

c) Election of an analytic form for the pair potential. We have already mentioned the most widely used analytical expression (Coulomb + Lennard-Jones terms). However, a great deal of examples of other type of potentials can be found in the literature [79-90].

d) The potential parameters are fitted, in the best possible way,to the interaction energies calculated for the different configurations. Normally the least square method is used. Once the function has been obtained some additional tests must be run in order to guarantee the reliability of the potential. Sometimes it is convenient to introduce a weight function in the fitting process so that the role of some regions of the hypersurface-those of low energy in particular-is enforced [91,92].

The obtainment of pair potentials through the fitting to theoretical results have some drawbacks: a) the computer time needed if a relatively high level calculation is used; b) the difficulty to correctly evaluate the dispersion energy; c) obviously, the obtained pair potentials do not include any n-body corrections.

The question of the importance of nonadditive corrections has been largely discussed and a growing body of results shows that many body effects can affect properties (specially for solutions of multivalent ions) in non-negligible ways [93- 104].

In fact, in the failure of pairwise additivity for cation-water potentials, there are two aspects of the problem to be considered. The first one concerns the long-range behaviour of the ground state potential of $M(H_2O)^{q+}$ systems, with $q \geq 2$. In most cases (exceptions are M^{q+}= Ca^{2+},Sr^{2+},Ba^{2+}) the electron affinity of M^{q+}, i.e. the qth ionization potential (IP) of M, is larger than the first IP of water. Therefore, at large M - (H_2O) distances, the ground state of the system is represented by the charge-transfer (CT) configuration $M^{(q-1)+}$ (H_2O)+ and the long-range potential is repulsive. The presence of an avoided crossing between CT and non-CT states can be important in vacuo but it is quite irrelevant in solution because the +q charge of the cation is strongly stabilised by the solvent. This problem is not considered when constructing ab initio potentials for simulations. In fact, the restricted Hartree-Fock cation-water wave functions yield necessarily the M^{q+} - (H_2O) dissociation, at least for closed shell cations. This is qualitatively adequate for the study of the liquid phase although not correct in vacuo. In this sense some ab initio potentials should be considered as "effective" potentials. The second problem concerns the strength of the binding between a cation and the second, third and following water molecules in a complex. Induction and charge-transfer energy terms, important at short distances, are clearly nonadditive. Simulations based on uncorrected pair potentials that do not incorporate such effects, have consistently overestimated the binding properties of cation-water complexes. For that reason, hydration numbers estracted from Monte Carlo or Molecular Dynamics correlation

functions are often greater than experimental results and enthalpies and free energies of hydration are clearly overestimated for monocations as well as dications [51,84,99,103,105].

The problem of nonadditivity can be attacked in several ways. The most rigourous approach is to include the many-body terms in the potential energy function. The main practical difficulty in order to include the nonadditivity corrections is the calculation of energies E of equation (47). In addition, in some cases the series (48) slowly converges and the successive steps have alternate signs. When used, three body potentials have been found to reproduce correctly hydration numbers and free energies [106]. Other authors [107] have computed the interaction pair potential between a water molecule and the $M(H_2O)_n^{q+}$ complex as a whole. Those two approaches, though, increase the cost and complexity of the calculations. A different possibility, that we will further discuss, consists of defining "effective" pair potentials that represent the average interaction of a water molecule with a cation already solvated by other molecules. These "effective" pair potentials can be derived from experimental data or from calculations on cation-water clusters. Recently, Tomasi and col. [108] have presented an "effective" pair potential based on the Polarizable Continuum Model (PCM) of the solvent. Molecular Dynamics simulations performed with their effective potential were succesful in predicting the correct hydration number for Fe^{2+} and Fe^{3+}.

Nonadditivity corrections have also been shown to play a non-negligible role in the formation of hydrogen bonds in polar liquids such as water. In the development of pairwise additive energy functions, derived from quantum mechanical calculations, for describing water properties, the work of Clementi et al. [109] is one of the major recent efforts in this direction. Obviously, these potentials correctly describe the water dimer in the gas phase but the description of the liquid is rather poor from a quantitative point of view. In order to get accurate values for a wide spectrum of liquid water properties, it is essential to include many-body effects, which are mainly due to polarization and charge transfer. Three- and four-body corrections [97,110] to the MCY potential have been proposed by Clementi's group and applications of this potential have confirmed the previous conclusion for static and dynamics properties as well. Recently, a new potential, NCC [111], has been derived from the MCY potential which explicitly incorporates many-body effects due to polarization. Finally, other authors [112,113] have also proposed a model of polarizable molecules in which the induced dipole moment on each molecule is treated as a separate degree of freedom, fixing the permanent dipole moment at the gas phase.

The second option in the development of pair potentials is the use of "effective" two-body functions, whose parameters are derived by requiring a fit to a number of liquid properties. The key assumption in "effective" two-body potentials is that many-body interaction energies can be incorporated into the parameters that are evaluated as two-body interaction energies. For water, this leads to partial charges on the oxygen and hydrogen atoms that correspond to a dipole moment of the water molecule of about 2.4 D [54], considerably enhanced over the gas phase value of 1.85 D. Then the study of the water dimer using such "effective" potentials leads to equilibrium geometries with too short intermolecular distances and too overestimated stabilization energies. The classic work by Rahman and Stillinger [114] describes the first application of an

"effective" potential (ST2) to water using Molecular Dynamics, and the potentials SPC [115], TIPS3 [116], TIPS2 [117], TIP3P [54] and TIP4P [54] are refined versions of this approach. All of the potentials mentioned, assume a fixed geometry of the water molecule. The cooperative effect between water molecules implies the nonadditivity of the pairwise potentials because of the many-body effects but due to the strengthening of the hydrogen bonds it also implies modifications of the intramolecular OH distances. Two type of flexible water-water potentials, that go beyond the rigid water approximation, have been employed (the BJH [118] and the MCYL [119] potentials).

Jorgensen and col. extended their TIPS (Transferable Intermolecular Potentials for Simulations) [120- 122] to several organic liquids. More recently, they developed a new generation of "effective" potentials, which received the denomination of OPLS (Optimized Potentials for Liquid Simulations) [123-127]. The standard OPLS philosophy can be summarized in the following three points: 1) to keep the form of the potentials simply and easy to evaluate, 2) to include as few new parameters as possible, 3) to produce structural and thermodynamic properties in reasonable accord with experiment.

The OPLS model is an example of pair potential where non-bonded interactions are represented through Coulomb and Lennard-Jones terms interacting between sites centred on nuclei (equation (51). Within this model, each atomic nucleus has an interaction site, except CH_n groups that are treated as united atoms centered on the carbon. It is important to note that no special functions were found to be needed to describe hydrogen bonding and there are no additional interaction sites for lone pairs. Another important point is that standard combining rules are used for the Lennard-Jones interactions such that $A_{ij} = (A_{ii}\ A_{jj}\ )^{1/2}$ and $C_{ij} = (C_{ij}\ C_{ij})^{1/2}$. The A and C parameters may also be expressed in terms of Lennard-Jones σ's and ε's as $A_{ii} = 4\varepsilon_i\ \sigma_i^{12}$ and $C_{ii} = 4\varepsilon_i\ \sigma_i^{6}$.

The OPLS parameters (charges and Lennard-Jones terms) were obtained primarily via Monte Carlo simulations with particular emphasis on reproducing the experimental densities and heats of vaporization of liquids. Those simulations were performed iteratively as part of the parametrization, so better agreement with experiment is obtained than in previous studies where the simulations were usually carried out after the parametrization. Once the OPLS parametrization was completed, further simulations were also performed in order to test the new set of parameters in the calculation of other thermodynamic and structural properties of the system, besides its density and its heat of vaporization. Parameters have now been generated, among others, for water, alkanes, alkenes, alcohols, amides, alkyl chlorides, amines, carboxylic esters and acids, various sulfur and nitrogen compounds, and nitriles. A protein force field has been established as well.

In view of the simplicity of the functional form, the accord with the experimental data is remarkable. The average deviation between the experimental data and the theoretical results is less than 3%. For instance, average errors of 1-3 % are obtained [128] for the computed densities and heats of vaporization of alkyl ethers, including results for tetrahydrofuran at pressures up to 5000 atm. This last result provides further evidence of the robustness of the potential functions under a variety of conditions. In the same work, Jorgensen and col. show how the experimental trend of linearity of ΔH_{vap} with increasing length of the molecule for the acyclic series of ethers: dimethyl

ether, ethyl methyl ether, diethyl ether, and tetrahidrofuran, is reproduced by the OPLS potentials and that is primarily attributable to increasing Lennard-Jones attraction.

In Monte Carlo simulations carried out for parametrization, standard geometries, with fixed bond lengths and bond angles, were used for the different molecules although torsional motion was usually included. For instance [128], for ethyl methyl ether and diethyl ether, rotations were allowed around the central C-O bonds. The form of the torsional potential for ethyl methyl ether, which has only one dihedral angle, is given by a Fourier expansion. In general, then, the expression for the analytical function is augmented by a term of the form:

$$\sum_{dihedrals} \frac{V_n}{2} [1 + \cos(n\phi - \gamma)] \tag{52}$$

For molecules that have two dihedral angles, like diethyl ether, the Fourier series needs to be augmented by a Lennard-Jones potential. The coefficients of those Fourier expansions were obtained from a fit to molecular mechanics (MM2) calculations. The present torsional potential gives a gauche-trans energy difference of 1.51 kcal/mol for ethyl methyl ether, that compares well with a value of 1.5± 0.2 kcal/mol reported from an electron diffraction study. However, energy barriers evaluated from IR and Raman studies imply a gauche-trans energy difference of 1.13 kcal/mol.

In order to provide a complete energetic description of biomolecular systems, the intramolecular terms for bond length and bond angle variations as well as the torsions and non-bonded terms need to be included. Since substantial work had been done on the former items by others, Jorgensen et al. [127] decided to merge the OPLS non-bonded potential functions and the local vibration and torsional functions from another force field. AMBER [129] was chosen because it is widely used and because its documented success in comparison with other force fields. The resulting potential was called OPLS/AMBER model. The bond stretch an angle bend terms in AMBER are quadratic , while the torsional potentials consist of a cosine term plus the 1,4-non-bonded interaction, both Coulombic and Lennard-Jones. Jorgensen et al. [127] reported parameters for 25 peptide residues as well as the common neutral and charged terminal groups. The parameters were obtained and tested primarily in conjuction with Monte Carlo statistical mechanics simulations of 36 pure organic liquids and numerous aqueous solutions of organic ions representative of subunits in the side chains and backbones of proteins.

From a structural point of view the OPLS results for liquids have also shown to be in accord with available experimental data, including vibrational spectroscopy and diffraction data on, for Instance, formamide, dimethylformamide, methanol, ethanol, 1-propanol, 2-methyl-2-propanol, methane, ethane and neopentane. The hydrogen bonding in alcohols, thiols and amides is well represented by the OPLS potential functions. The average root-mean-square deviation from the X-ray structures of the crystals for four cyclic hexapeptides and a cyclic pentapeptide optimized with the OPLS/AMBER model, was only 0.17 Å for the atomic positions and 3% for the unit cell volumes.

As we have already noted, in the development of the OPLS potentials the introduction of new parameters has been kept to a minimum. For instance, only 12 different CH_n groups are used to describe all alkanes, alkenes, and benzene, and, for exemple, the parameters for the OH groups in all alcohols and the carbonyl groups in all amides are the same. Also, standard alkyl group parameters were used in ethers for those groups that are at least one atom removed from the ether oxygen. It has been established that Lennard-Jones parameters, ε and σ, are in general transferable to larger molecules from their components, while the choice of partial charges for a new molecule is the main problem. As we have already explained, the OPLS partial charges were optimized typically through iterative fluid simulations to reproduce experimental results. However, another remarkably simple approach was also considered and then supported by the subsequent simulations of aqueous systems and pure liquids. We refer to the study of substituted benzenes [130]. In that case the parameters for benzene and the substituents were simply merged. These intermolecular potential functions, besides their simplicity, have shown to exhibit good success in reproducing experimental densities and heats of vaporization of pure liquids. Although in the case of aniline some readjustement in the charge distribution had to be done.

The OPLS charge distributions and the adopted standard geometries can be combined to yield calculated dipole moments. For instance, the OPLS dipole moments for aliphatic ethers and alcohols are greater than experimental values for isolated molecules by 0.5 - 0.6 D [130]. For substituted benzenes those differences range from 0.12 D in toluene to 0.66 D in benzonitrile. For aromatic ethers and alcohols the OPLS dipole moments are higher than the experimental values, similar to the situation with the aliphatic analogs, while the OPLS dipole moments in the nitrogen-containing systems are lower than the experimental ones. The authors of the OPLS model assert that coincidence between experimental and OPLS dipole moments is not sought in view of the limitations of the partial point-charge model and the desire of the OPLS potentials to focus on reproducing liquid-state properties. An interesting test of the OPLS potentials was carried out by Jorgensen et al. [131] in calculating the *cis-trans* free energy difference for N-methylacetamide (NMA). The authors report ab initio 6-31G(d) calculations that predict the dipole moment for *cis*-NMA to be larger than that for *trans*-NMA, 4.21 vs 4.04 D. This order is, of course, interesting because, from classical electrostatics, the isomer with the larger dipole moment is expected to be better solvated, though this theory simplifies the solvent to structureless dielectric medium. These computed dipole moments are consistent with experimental results [132,133] for NMA, which range from 3.85 D in benzene to 4.22 D in 1,4-dioxane. However, by using the OPLS charge distribution derived for *trans*-NMA for both conformers (i.e., assuming that charges are independent of conformation) and standard geometries, Jorgensen et al. [131] obtained dipole moments of 3.86 and 4.23 D for *cis*- and *trans*-NMA, respectively. This incorrect order was also attributed by the authors to the inadequacies of computing dipole moments from point charge distributions, particularly when atoms, that formally have lone-pairs of electrons, lire present . However, it turns out that the order can be reversed by an all-atom model for the CH_3 group on nitrogen or by the use of slightly different charge distributions for the *cis* and *trans* form.

The parametrization of the OPLS potentials also entailed the careful consideration

of the interaction between organic molecules and a water molecule. The water model used in conjunction with the OPLS potentials was TIP4P, though the TP3P or SPC models yield very similar results. For most purposes these three alternatives may be interchangeable, though the slightly more complicated TIP4P model gives a better description of the angular variation of hydrogen bond energies. Complexes of a water molecule with amides, ethers, esters, alcohols, thiols, sulfides, azoles, and azines, for exemple, were studied with the OPLS potentials as well as ab initio molecular orbital calculations primarily with the 6-31G(d) basis set. The trends in the ab initio findings for the hydrogen bond strengths and geometries are well reproduced by the OPLS results [124,126,134,135]. For instance, Nagy et al carried out theoretical studies on the hydration of pyrrole, imidazole and protonated imidazole in the gas phase and in aqueous solution [136]. In this case, they found that the OPLS geometric parameters and relative energies for the monohydrates are closer to values obtained in the MP2/6-31G(d) calculations than the HF/6-31G(d) results. Gas phase monohydrates optimized at the HF level have hydrogen bond distances longer by about 0.18, than the MP2 values. Using the OPLS interaction potential the bond distances were shorter than the MP2 values by 0.02-0.17 Å, but follow the tendency found in the ab initio calculations. The hydrogen bond angles from all three methods are close. The only remarkable difference between the OPLS and MP2 results were found for the imidazole hydration at its N_3 site. The OPLS potential favors out-of-plane hydration over the in-plane one, in contrast to the ab initio results. Relative dimerization energies with the OPLS potential are close to the BSSE corrected MP2/6-31G(d) values. The only remarkable exception is again the hydration of the neutral imidazole at the N_3 site.

Furthermore, Monte Carlo simulations [125,130,137] were carried out for dilute aqueous solutions of formamide, NMA, dimethylformamide (DMF), methanol, seven alkanes, substituted benzenes, among others. For the amides, experimental structural data are limited; however, the computed numbers of amide - water hydrogen bonds are reasonable and the computed heats of hydration, ca. -20 kcal/mol, are in the correct range. Similarly, the hydration of methanol appears reasonable and the computed difference in free energies of hydration for methanol and ethane, 6.75 ± 0.2 kcal/mol, is in excellent accord with the experimental value 6.93 kcal/mol. Taking into account the uncertainties in the data, experimental as well as theoretical, the accord between the Monte Carlo and measured absolute free energies of hydration for substituted benzenes compared by Jorgensen et al., is nearly perfect. The accord is particularly notable given the simple origin of the OPLS parameters for the substituted benzenes and the significant range of free energies of hydration. The worst discrepancies are for hydroquinone (1.3± 0.5 kcal/mol) and possibly benzonitrile (1.3 ca ±1 kcal/mol). In general, then, the OPLS model has proven to be accurate in its calculation of solvation free energies. This is because the model is inherently well-balanced due to the kind of parametrization undertaken by their authors.

In the study of reactivity, Jorgensen and col. have normally used both, the OPLS model and potential functions derived from ab initio calculations. As we have already indicated, when intermolecular pair potentials are applied to the study of a chemical process, the evolution of charges, as well as the Lennard-Jones terms, along the reaction coordinate, has to be considered. For the S_N2 reaction in water between chloride anion

and methyl chloride, that we discussed in Section 5, Jorgensen and col. [41,52] used a simple functional form of the reaction coordinate for the potential function parameters describing the solute-solvent interaction. The TIP4P model was assumed for water monomers. Since all the geometric parameters showed the same qualitative variation along the reaction, Jorgensen and col. adopted the same kind of function for the *q, A* and *C* terms for the four distinct sites, Cl, Cl′, C and H, of the solute. Those parameters for reactants and the transition state structure were determined based on ab initio interaction energies and geometries of $Cl^-(H_2O)$, $CH_3Cl(H_2O)$ and several structures of the monohydrated transition state structure. The *q, A* and *C* parameters were determined from these data via non-linear least-squares procedure. The mean error in comparing the predicted interaction energies of 71 solvated structures with the corresponding 6-31G(d) values is only 0.78 kcal/mol for energies which cover a range of 22 kcal/mol. Further, the simple potential function correctly describes all the key features of the solute-solvent interaction in the system, in particular, hydrogen bonding. It may be noted that the Lennard-Jones terms for C and H as well as the *A* parameter for Cl were kept constant over the entire reaction, as they showed negligible variation. Also, the charge on the hydrogen atoms was forced to yield a net unit negative charge for the solute during the simulations.

As mentioned above, for the simulation in dimethylformamide (DMF) of the same reaction [53], the parameters for the substrate were not changed from the parametrization in water. For DMF the parameters were adopted from the OPLS parametrization of the pure liquid. The transferability was tested in part by performing a Monte Carlo simulation for CI^- plus 128 DMF molecules and evaluating the heat of solution for the chloride ion. The obtained value compares favorably with the experimental estimate. It is important to remark here that when potentials are used to simulate different solutions to the ones used in the parametrization process, they no longer are "effective" potentials. This fact becomes more evident in the simulation of solutions of small ions with localized charge that polarizes the neighboring solvent molecules. In this case it is convenient to consider the n-body corrections.

An interesting application of the OPLS potentials along areaction coordinate is the study by Jorgensen and col. of solvent effects on the barrier to isomerization for a tertiary amide as N,N-dimethylacetamide (DMA) [138]. Solute-solvent potential functions were refined by fitting to results of 6-31G(d) calculations for the ground and transition state structures interacting with a water molecule in 17 low energy orientations. The only parameters that were varied to reproduce the ab initio complex energies and structures were the partial charges for DMA. For a balanced fit to the 6-31G(d) data, minor variations to the OPLS charges for the ground states were made and one charge set sufficed for the transition state structures. These potentials were used in Monte Carlo simulations that yielded the changes in free energies of solvation in TIP4P water and the OPLS model of carbon tetrachloride. Two difficulties arose in the fitting. It was not possible to reproduce the 6-31G(d) ordering for two of the eight ground states considered. Thus, the ab initio calculations indicate a 0.7 kcal/mol preference for the complex with the water anti to the nitrogen, while the fitted potentials favor the water syn to the nitrogen by 0.8 kcal/mol. Many different charge distributions were tried with both united-atom and all-atom models without success in reproducing the ab initio

order. The authors [138] observe that it would be desirable to confirm the 6-31G(d) order with higher level optimizations including correlation corrections because the potential functions reflect some correlation effects through the Lennard-Jones terms. The only other notable discrepancy was for two ground states with the C=O...H—OH fragment collinear. The interaction is uniformly too attractive with the potential functions, probably owing to the inadequacies of the simple point charge description for the electron density on the oxygen. The geometrical results from the potential functions compare well with the 6-31G(d) predictions. The average difference for the bond angles is 11° and the intermolecular distances are uniformly 0.1-0.2 Å shorter from the potential functions. The latter feature is normal and comes from the use of Lennard-Jones s's that are appropiate for yielding correct liquid densities.

In the calculations [45] of the free energy profiles for the separation of *tert*-butyl cation and chloride anion in dilute aqueous solution, the necessary carbenium ion-water potential functions were obtained from ab initio molecular orbital calculations with the 6-31G(d) basis set. In fact, only the charge and the Lennard-Jones σ's were varied since the ε's were assigned from experience with other systems and are not very important in comparison with the dominant Coulombic interactions. The TIP4P model was assumed for water along with previously reported parameters for Cl' that had been tested in Monte Carlo simulations for Cl^- in TIP4P water. In these calculations for the ion pair region in the hydrolysis of *t*-BuC1, Jorgensen et al. assumed that complete ionization had occurred, i.e., *t*-Bu^+ and Cl^- have unit charges at all separations. Thus, the charge separation for the contact ion pair should be essentially complete since it is further along the reaction coordinate. This assumption simplified the potential functions since the charge distributions and Lennard-Jones parameters could be taken as invariant along the reaction coordinate. In the study of the effect of hydration on the $Cl^- + CH_3Cl$ S_N2 transition state structure, Jorgensen et al. [57] used again the TIP4P model to describe water-water interactions while the potential functions for the water-transition state structure interactions were derived from ab initio 6-31G(d) calculations on monohydrated complexes. The Lennard-Jones parameters for the transition state structure were kept fixed for all values of the reaction coordinate, the distance between C and Cl (r_{CCl}). The key item was then the alterations in the charges. 6-31G(d) calculations were executed for the transition state structure varying r_{ccl} and optimizing the remaining variable r_{CH}. A linear variation of the Mulliken populations with the reaction coordinate was observed over the entire range of C-Cl distances. This linear dependency was then analytically introduced in the statistical simulations by means of three equations that expressed the changes in q_C, q_H, and q_{cl} as a function of r_{CCl}. In the study of the S_N1 process as well as in this last work on a S_N2 reaction, Jorgensen et al. point out that the lack of polarization is especially a concern and probably the chief source of potential error in the last mentioned study. However, the authors also indicate that for the hydrolysis of *t*-BuCl the nature of the perturbation is such that some compensation of errors for the reference and perturbed system is probable and that the same seems to be true for small errors in the balance between the interionic and ion-solvent interactions. The results for the monohydrated transition state structure of the S_N2 chloride exchange reaction suggest that the effect of hydration on the charge distribution for the solute is comparatively minor. Nevertheless, the polarization of the

first shell water molecules appears to be of greater importance. This polarization is not accommodated in TIP4P potential function because, although being an "effective" pair potential, it maintains fixed charges. A more subtle point concerns the charge variations along the reaction coordinate, that we have mentioned above. Though the shifts are in accord with expectations for aqueous solution, the actual variations are undoubtedly affected by the use of a single determinant wave function.

In their study of the water dimer in liquid water, Bertran et al. [139] indicate that their results justify the use of a dipole moment value substantially higher than the gas phase value, in simulations of the liquid state by means of "effective" pair potentials. However, the authors state that allowing variation of both intramolecular and intermolecular geometry parameters and atomic charges (and, hence, multipole moments) would be necessary in order to get a more sophisticated description of water in the liquid state. This indicates the trends which should be considered for deriving a more sophisticated water-water potential to be used in liquid water simulations. From their study it appears that the minimum requirements for such a potential are an accurate description of the electrostatic and the induction energies. These requirements are quite realistic owing to the recent advances in these fields, such as the representation of a molecule by means of distributed multipoles and distributed polarizabilities. Nevertheless, when those potentials are introduced in a statistical simulation and in the interest of speed, truncated expansions must be employed and simple atom-centered monopole models are still the most widely used. The monopole model has the advantage that it provides an intuitive way to think about the charge distribution within a molecule. In order to improve then, the description of the electrostatic term, many techniques have been proposed over the years to accurately reproduce a molecular charge distribution. These techniques range from empirical approaches (i.e., fitting charges to experimental data, like in the OPLS model) or the determination of charges from experiment, to theoretical methodologies like fitting charges to reproduce quantum mechanical results, using Mulliken population analysis or using electrostatic potential surface (EPS) fitting by means of ab initio or semiempirical techniques.

As an aid in understanding the properties of a molecule, the concept of atomic charge is not a magnitude which can be directly determined from the Hartree-Fock wave function. Some scheme must be adopted to divide the total electronic charge among the atoms in a molecule.

The most widely used procedure is the population analysis proposed by Mulliken, the popularity of this method being due to its simplicity, but the poor performance of Mulliken charges to reproduce the essential features of electrostatic potential maps is well established. Mulliken populations often yield rather different multipole moments for the molecule than those calculated from the actual wave function. Such Mulliken populations are also very basis-set dependent, In recent years, though, a number of other methods have been developed which alocate charge to a molecule's atoms based on physical criterions rather than simply by the equal partitioning method of Mulliken population analysis. Electrostatic charges reported by those methodologies are obtained by fitting the rigourously defined quantum mechanical and the point-charge electrostatic potentials. Both Williams [140] and Cox and Williams [141] have described methods for calculating point-charge models from ab initio wavefunctions which use regular

grids of points in their fitting procedures, while Kollman and Singh [142] and Chirlian and Francl [143] use point selection routines which are based upon atom-centered shells of points. The CHELP (CHarges from Electrostatic Potentials) routine, by Chirlian and Francl [143], chooses 14 points for each concentric shell surrounding the molecule (±x,±y,±z, and in the center of each octant) and uses the method of Lagrange multipliers to fit the charges. The Lagrange multiplier technique has the advantage of being fast and noniterative. The public version of the CHELP program has a built-in 1.0 Å increment between concentric shells. All of the routines use approximately 200-400 points in each fit, with point spacings of 0.8-1.0 Å. When each of these methods are used with appropiate wave functions, they yield "atomic charges" which reproduce certain molecular properties, such as the dipole moment, reasonable well. However, Breneman and Wiberg [144] found that CHELP was inappropiate for use in conformational analysis because of its rotational variance. As a result of this random variation, CHELP analysis of internal rotation pathways is severely limited. The two authors developed then a new approach, called CHELPG (Charges form Electrostatic Potentials Grid-oriented), which has shown to be considerably less dependent upon molecular orientation. The principal difference between the CHELPG method and the older CHELP program is that the CHELPG procedure employs a point-selection algorithm based upon regularly spaced points. Following the point selection procedure, the electrostatic potential at each of the sample points is calculated analytically from the wave function and geometry data contained in the corresponding checkpoint files. These data are then used as input for the Lagrange least-squares routine, which has been constrained to fit the exact molecular charge. The computed best-fit charges reproduce the restricted Hartree-Fock molecular dipole moments reasonably well.

In the original work of Chirlian and Francl [143], a comparison of the electrostatic potentials and charges obtained with different basis sets was reported. Reasonable correlation was obtained for all basis sets when comparing results with 6-31G(d,p) calculations for a series of molecules at their experimental geometries. If the experimental geometry for a molecule is not available, good charges may still be obtained by using an optimized structure. For this case, calculations using the 6-31G(d) or 6-31G(d,p) basis sets and geometries optimized at the same level give results which reproduce the charges obtained with the experimental geometry and the 6-31G(d) basis set. The charges given by CHELP reproduce the dipole moments of the molecules calculated at the same level of theory while the Mulliken dipoles are notably erratic. The dipoles calculated at 6-31G(d,p) level have the best correlation with the expenmentiilly measured values.

More recently, studies carried out by several authors converged on partial charges obtained from fitting to the electrostatic potential surface of ab initio 6-31G(d) calculations as a de facto standard [145-148]. Support for this choice has noted: 1) Dipole moments are overestimated by 10-20 % with 6-31G(d) calculations, which is desirable to compensate for the neglect of polarization effects with fixed-charged models; 2) EPS charges are relatively insensitive to extension of the basis set beyond 6-31G(d) and inclusion of electron correlation; and 3) 6-31G(d) EPS charges correlate well (r=0.93) with OPLS charges for organic molecules, which have been derived to reproduce fluid properties.

Kollman and col. have long advocated the use of electrostatic potential derived charges as being simple to derive, transferable, and not subject to bias. In fact, they have validated their effectiveness in nucleic acid-base interactions and simple associations between crown ethers and polar molecules [149]. In a recent paper [147] they presented free energy perturbation calculations on the relative solvation free energy of *cis*- and *trans*-NMA, previously reported by Jorgensen et al. [131]. Experimentally, the solvation free energy difference has been found to be near zero. Using the 6-31G(d) charges derived for the *trans* conformation for both the *cis* and *trans* models leads to a solvation free energy difference of 0.9 ± 0.1 kcal/mol, compared to the value of 2.2 kcal/mol determined for the OPLS model for *trans*-NMA. Furthermore, when using the *trans* electrostatic potential based charges for *trans*-NMA and *cis* charges for the *cis*-NMA, the calculated solvation free energy difference of ca. 0.1 kcal/mol is in excellent agreement with experiment.

The viability of the 6-31G(d) EPS charges in fluid simulations was tested by Carlson et al. [150] by computing free energies of hydration for 13 diverse organic molecules. Both Mulliken charges and charges fit to the EPS were considered in conjunction with OPLS Lennard-Jones parameters for the organic molecules and the TIP4P model of water. Monte Carlo simulations with statistical perturbation theory yielded relative free energies of hydration. These were converted to absolute quantities through perturbations to reference molecules for which absolute free energies of hydration had been obtained previously in TlP4P water. The average errors in the computed absolute free energies of hydration are 1.1 kcal/mol for the 6-31G(d) EPS charges and 4.0 kcal/mol for the Mulliken charges. A principal problem was traced to the Mulliken charge distribution for methyl groups attached to hydrogen-bonding functionality, which could be largely relieved in a united-atom format. Aromatic C-H bonds are found to be too polarized with Mulliken charges. Further, EPS charges were found to yield reasonable predictions in the number of hydrogen bonds between the organic solutes and water. Though the results with the EPS charge are impressive, the authors advise on their use for biochemical applications in view of the individual errors of 3-4 kcal/mol for acetamide and 1-2 kcal/mol for ethane. The authors state that a combination of, for example, OPLS and 6-31G(d) EPS charges might be a viable alternative for rapid derivation of partial charges for new applications. Scaling of the 6-31G(d) EPS charges could also be an alternative, though uniform scaling is unlikely to be fruitful in view of the good accord that already exists between many of the predicted free energies of hydration and the experimental values.

The CHELPG model has been used by Jorgensen and col. in several of their reactivity studies. For instance, in the investigation of solvent effects in perycíclic reactions undertaken by the authors, the intermolecular interactions were represented by Coulomb and Lennard-Jones terms with all atoms explicit. The TIP4P was adopted for water, while standard OPLS Lennard-Jones parameters were adopted for the solute and scaled as the hybridation changed. The partial charges for the solute were obtained by fitting to the 6-31G(d) electrostatic potential surfaces via CHELPG calculations on several solute structures along the MEP. Namely, the 6-31G(d) CHELPG charges were used for the solutes in the dimerization of cyclopentadiene (CP) and in the dimerization of cyclopentadiene with methyl vinyl ketone (MVK) in water [58]. The stabilization by

water for the MVK + CP reaction was predicted to be of -3.2 ± 0.4 kcal/mol. This is somewhat less pronunced than the value of -4.2 kcal/mol that was obtained from the full energy profile for the MVK + CP reaction with the 6-31G(d) Mulliken charges [59]. In that previous study, Blake and Jorgensen still used Mulliken population analysis because, as they indicated, a better correlation (r=0.99) exists between 6-31G(d) Mulliken charges and the OPLS charges, for neutral molecules with first row atoms, than for 6-31G(d) EPS charges (r=0.93). The last results with the CHELPG charges suggest a more even balance between the contributions from the hydrogen bonding and hydrophobic effects to the acceleration of the MVK + CP reaction in water.

CHELPG charges were again used for a reacting system along with standard Lennard-Jones parameters for the Claisen rearrangement of allyl vinyl ether [60]. Mulliken charges were also considered; however, they showed more variation in going to the 6-31+G (d,p) basis set and computed dipole moments with the Mulliken charges deviated significantly (0.5 - 1.4 D) from the 6-31G(d) and the CHELPG values. In that work, the authors report results for the free energy of activation in water versus gas phase with several SCRF (Self Consistent Reaction Field) methods considered with the 6-31G(d) structures and the CHELPG charges. The SCRF results are all qualitatively correct; however, the predicted rate accelerations are all too small. With the Monte Carlo approach and the associated two-body potential functions with 6-31G(d) CHELPG charges, the obtained values, for the stabilization by water, are much closer to experiment. The realiability of the charges is undoubtedly the dominant element in getting correct relative free energies of hydration. This approach can be critized for ignoring solute polarization by the solvent since the partial charges are fixed from the CHELPG calculations. However, these results seem to confirm that polarization is included to some extent in an average way owing to overestimation of the polarity of molecules at the 6-31G(d) level.

Very recently, Jorgensen and col. [151] have studied the solvent effects on the ring opening of cyclopropanones to oxyallyls. Geometries for the cyclopropanones, the transition state structure for the rearrangement of cyclopropanone, and the oxyallyls were obtained from ab initio CASSCF calculations with the 6-31G(d) basis set. For each geometry, CHELPG and Mulliken charges were determined for the use in the fluid simulations. The modest computed solvent effects are in good accord with experimental data [152]. Their results support the intermediacy of oxyallyls in cyclopropanone stereomutations, indicate the proximity of the oxyallyls to the transition state structures for the ring openings, and confirm the principally diradical rather than zwitterionic nature of the oxyallyls. In this case, the results from the two charge models are quite similar; the somewhat larger effects from the Mulliken charges are consistent with the correspondingly larger changes in dipole moments. The authors state that this accord is rather surprising in view of the significantly poorer results that are obtained for free energies of hydration with 6-31G(d) Mulliken charges, though the previous comparisons [150] involved far more diverse structures than those represented by the present mutations. In order to assess to which extent the structures and charge distributions of the different molecules studied might be medium dependent with an anticipated tendency toward more zwitterionic character in more polar solvents, Jorgensen and col. [151] carried out calculations in the presence of a reaction field. SCRF theory was used

with a dielectric constant of 36 (acetonitrile) for calculations of cyclopropane, the transition state structure and oxyallyl to recompute Mulliken and CHELPG charges in the presence of the reaction field. Reoptimization of the geometry of the oxyallyl resulted in very small geometrical changes. The computed dipole moments for cyclopropanone and oxyallyl with the CHELPG charges are 2.79 and 3.47 D in the gas phase and 3.09 and 3.86 D for ε = 36 without geometry reoptimization. From these results, the authors conclude that use of SCRF charges would have little impact on the differences in free energies of solvation already obtained

7. Recent Theoretical Developments

As seen above, the evaluation of the potential energy of each generated configuration is a key point in the Monte Carlo (or Molecular Dynamics) simulation of a chemical reaction in solution. The understanding of chemical processes in solution depends on the availability of intermolecular potential energy functions that can properly describe the molecular interactions. So far, pairwise additive potentials whose parametrization process is very laborious have been employed. However, this kind of potential is not suited for describing polarization effects. An alternative approach is to use a combined quantum mechanical and classical procedure [153-157], in which the reacting system is treated explicitly by a quantum mechanical (QM) method, while the surrounding solvent (the most computational time-consuming part) is approximated by a standard molecular-mechanics (MM) force field. This recent strategy avoids the difficult development of the potential energy functions along the reaction path and is able to introduce the solute polarization effects.

In this hybrid QM/MM model the molecular system is divided into two parts: 1) a QM region consisting of 2N electrons (assuming closed-shell molecules) and M nuclei belonging to the reacting solute molecules, which is described by Hartree-Fock molecular orbital theory; 2) an interaction-site MM region containing the environmental solvent, which is described by molecular mechanical potential energy functions. This way, the total effective Hamiltonian of the whole system is

$$\hat{H}_{eff} = \hat{H}^{o}_{QM} + \hat{H}_{QM/MM} + \hat{H}_{MM} \tag{53}$$

where $\hat{H}^{0}_{QM}$ is the Hamiltonian for the isolated QM solute, $\hat{H}_{MM}$ is the molecular mechanical solvent-solvent interaction energy, and $\hat{H}_{QM/MM}$ is the solute-solvent interaction Hamiltonian, which depends on the partial charges and positions of the solvent interaction sites and is given by

$$\hat{H}_{QM/MM} = \hat{H}^{el}_{QM/MM} + \hat{H}^{vdw}_{QM/MM} = \left(- \sum_{s=1}^{S} \sum_{i=1}^{2N} \frac{eq_s}{r_{si}} + \sum_{s=1}^{S} \sum_{m=1}^{M} \frac{q_s Z_m}{R_{sm}} \right) + + \sum_{s=1}^{S} \sum_{m=1}^{M} 4 \epsilon_{sm} \left[\left(\frac{\sigma_{sm}}{R_{sm}} \right)^{12} - \left(\frac{\sigma_{sm}}{R_{sm}} \right)^{6} \right] \quad (54)$$

where e is the charge of electrons, q_s and Z_m are charges on the solvent and solute nuclei, S and M are the corresponding total numbers of interaction sites, and r_{si} and R_{sm} are the distances of the solute electrons and nuclei from the solvent sites, respectively. The Lennard-Jones term includes the dispersion interaction between the QM and MM regions, and contains the only adjustable parameters for the solute (ε_{sm} and σ_{sm}) in the present approach. It is noteworthy that the terms added to $\hat{H}^0_{QM}$ in equation (53) only affect the one-electron part in the Fock matrix.

The total potential energy of the system in the combined QM/MM force field is calculated from the expectation value of the wave function, ϕ, over $\hat{H}_{eff}$:

$$E_{tot} = \langle \Phi | \hat{H}_{eff} | \Phi \rangle = E_{QM} + E^{el}_{QM/MM} + E^{vdw}_{QM/MM} + E_{MM} \quad (55)$$

Here Φ is the Hartree-Fock wave function of the solute immersed in the solution, and the four energy terms of equation (55) come directly from the corresponding Hamiltonian operators of equations (53) and (54).

Within this scheme, the polarization energy of the solute, E_{pol}, due to its interaction with the solvent is given by

$$E_{pol} = \langle \Phi | \hat{H}^{o}_{QM} + \hat{H}^{el}_{QM/MM} | \Phi \rangle - \langle \Phi^{o} | \hat{H}^{o}_{QM} + \hat{H}^{el}_{QM/MM} | \Phi^{o} \rangle \quad (56)$$

where ϕ^0 is the Hartree-Fock wave function of the isolated solute (i.e. in gas phase). The polarization energy can be decomposed into two contributions

$$E_{pol} = E_{dist} + \Delta E_{QM/MM} \quad (57)$$

where the solute electronic distortion energy, E_{dist},

$$E_{dist} = \langle \Phi | \hat{H}^{o}_{QM} | \Phi \rangle - \langle \Phi^{o} | \hat{H}^{o}_{QM} | \Phi^{o} \rangle \quad (58)$$

is a positive value that gives the energy penalty for reorganizing (or polarizing) the solute electronic distribution in solution, and

$$\Delta E_{QM/MM} = \langle \Phi | \hat{H}^{el}_{QM/MM} | \Phi \rangle - \langle \Phi^o | \hat{H}^{el}_{QM/MM} | \Phi^o \rangle \quad (59)$$

is a net gain in interaction energy between the polarized solute and the bulk solvent over that of an unpolarized solute, which compensates the solute electronic distortion energy leading to the polarization energy.

On the other hand, electric dipolar moments of the solute molecules can be obtained with standard methods in ab initio molecular orbital calculations, whereas the induced dipole moments in solution are determined from differences between the values obtained in solution and in the gas phase.

Ab initio molecular orbital methodology or density functional theory [158-160] would be suited for this combined QM/MM approach. However, in order to be able to compute the QM energies along the Monte Carlo simulation, nowadays a semiempirical Hamiltonian, like AM1 [161], is a much more computationally efficient method. Before using AM1, the goodness of the semiempirical results in gas phase in comparison with the ab initio ones has to be tested. For systems in which the semiempirical results are poor, the relation

$$E_{QM} = \langle \Phi | \hat{H}^{o}_{QM} | \Phi \rangle - \langle \Phi^o | \hat{H}^{o}_{QM} | \Phi^o \rangle + \langle \Phi^o | \hat{H}^{o}_{QM} | \Phi^o \rangle = E_{dist} + E_{gas\ phase} \quad (60)$$

provides the way to use high-level ab initio results to replace AM1 gas-phase energies, thus the AM1 Hamiltonian being essentially employed to evaluate the effects of solvation.

The combined QM/MM model can be used along with Statistical Perturbation Theory to carry out a Monte Carlo simulation of a chemical reaction in solution, with the advantage of allowing solute electronic structure relaxation in solution. Particularly, the combined AM1/TIP3P force field has recently been applied to simulate several chemical processes in solution. We will refer here briefly to the Claisen rearrangement and to the Menshutkin reaction.

The Claisen rearrangement of allyl vinyl ether in aqueous solution was studied by Gao et al. [157] by using the gas-phase ab initio MEP determined previously by the Jorgensen's group [60]. In this case, 69 of the 143 frames were employed along the perturbation procedure in the isothermal-isobaric ensemble at 25 ºC and 1 atm. The

hydration effects were found to produce a rate acceleration by a factor of 368, in good agreement with both the Monte Carlo results of Jorgensen's group and the experimental data. The solvent effects were attributed to an enhancement of the polarization in going from the reactant to the transition state, what was mirrored by the behaviour of the induced dipole moments.

A specially interesting case is the Menshutkin reaction in aqueous solution, in which a neutral nucleophile attacks to a neutral substrate producing a large charge separation during the reaction. In gas phase this reaction is an extremely unfavoured process due to Coulombic interactions, with a huge energy barrier (coming from a transition state or the products if the transition state does not exist). As a matter of fact, Menshutkin reactions have never been reported in the gas phase. However, hydration very significantly reduces the energy barrier, the reaction becoming clearly exothermic. Furthermore, the solvent effect on the polarization of the reactants is expected to enhance the charge separation of the aqueous reaction over that of the gas-phase reaction. Then, the Menshutkin reaction in water is a very appropriate case to apply the combined quantum mechanical and molecular mechanical (QM/MM) Monte Carlo simulation approach. This way, Gao et al. [162] studied the Menshutkin reaction in aqueous solution

by using the AM1/TIP3P force field. Due to the symmetry of this reaction, the three heavy atoms were constrained to be collinear along the C_3 symmetry axis. Dihedral variations of H_3N and CH_3 groups about the C-H bond were allowed during the Monte Carlo simulation. The bond length and bond angles associated with the hydrogen atoms were optimized at a fixed H-N-C-H dihedral angle sampled in the calculation. Monte Carlo calculations were carried out in the isothermal-isobaric ensemble at 25 °C and 1 atm, in a box containing 265 water molecules.

To assess the effects of hydration a two-dimensional free energy surface was constructed through a grid search method. The two independent coordinates of the map were C-N distance ($R_{C\text{-}N}$) and C-Cl distance ($R_{C\text{-}Cl}$) and the Statistical Perturbation Theory was used to compute free energy differences between neighbouring grid points. First, at a given value of $R_{C\text{-}Cl}$ a series of perturbation calculations with $\Delta R_{C\text{-}N} = \pm 0.05$ Å were carried out to yield a free energy profile as a function of $R_{C\text{-}N}$. Then, the relative heights of two such neighbouring profiles (parallel to each other) at an interval of 0.10 Å were determined by another perturbation calculation with respect to $R_{C\text{-}Cl}$ at a fixed $R_{C\text{-}N}$ value. Finally, the free energy surface was anchored relative to the free energy at a value of the reaction coordinate (RC) of -2.0 Å. The reaction coordinate was defined by

$$RC = R_{C\text{-}CL} - R_{C\text{-}N} - RC_0$$

where RC_0 is the difference between the C-Cl and C-N separations at the gas-phase transition state structure.

Gao et al. located the saddle point of the two-dimensional free energy surface at $R_{C\text{-}N}$ = 1.96 Å and $R_{C\text{-}Cl}$ = 2.09 Å, and used this point to define the transition state in solution. This way, their most striking finding was that on going from the gas phase

into aqueous solution the transition state was shifted significantly toward the reactants, with a lengthening of the C-N bond by 0.30 Å and a shortening of the C-Cl bond by 0.15 Å (the AM1 gas-phase saddle point appears at $R_{C\text{-}N}$ = 1.66 Å and $R_{C\text{-}Cl}$ = 2.24 Å), in good accord with the expectation according to Hammond postulate. On the other hand, the results show that the solvent effects strongly stabilize the transition state and the products. The calculated free energy barrier in water derived from the free energy saddle point is 26.3 ± 0.3 kcal/mol, which is in accord with the experimental activation energy (23.5 kcal/mol) for a similar reaction between H_3N and CH_3I in water. Charge separation is promoted by the solvent effect, with a charge transfer of more than 65% complete at the transition state in water, whereas it is only about 50% in the gas-phase saddle point.

It is evident that the construction and detailed analysis of the two-dimensional free energy surface provide both qualitative and quantitative new insights into the solvent effects on the Menshutkin reaction in water, and promise a viable approach in other chemical reactions in solution. However, we have to note that the use of the saddle point of the two-dimensional free energy surface to characterize the transition state can be confusing and does not strictly correspond to the notion of transition state within the frame of the Transition State Theory, which defines the transition state for a system containing N atoms as a (3N-1)-dimensional configurational-space hypersurface (the dividing surface). Since that free energy saddle point is the result of the collection of the configurations submitted to two independent constraints ($R_{C\text{-}N}$ = 1.96 Å and $R_{C\text{-}C1}$ = 2.09 Å), it represents only a subset of configurations of an actual dividing surface (which only has one constraint).

Along this chapter we have reviewed the present theoretical methods to microscopically simulate chemical reactions in solution and we have discussed their limitations. Indeed there is a great potential of growth in methodology development. In the next years, with the impressive advances in computer speed, we expect to see a progressive development and application of new methodologies to simulate chemical reactions in solution. Several quite promising new approaches, some of which begin to be applied, could be the following:

1) Extension of the QM region to an increasing number of solvent molecules.

2) Use of high-level ab initio molecular orbital methods or density functional Hamiltonians to simulate the QM region through approximate solutions of the electronic Schrodinger equation.

3) Empirical Valence Bond (EVB) [163,164] simulations as an alternative to Molecular Orbital based methods.

4) The Statistical Perturbation Theory should be applied allowing a complete sampling of the solute coordinates (and, if possible, of the solvent coordinates). This way no solvent equilibrium hypothesis would be introduced at all.

5) Different prescriptions to choice the set of dividing surfaces in order to apply the Variational Transition State Theory, should be analyzed and compared.

6) Beyond Transition State Theory (and, therefore, beyond Monte Carlo simulations) dynamical effects coming from recrossings should be introduced. Furthermore, additional quantum mechanical aspects, like tunneling, should be taken into account in some chemical reactions.

8. References

[1] Eyring, H. *J. Chem. Phys.* **1935,** *3,* 107.

[2] Glasstone, S.; Laidler, K.J.; Eyring, H. *The Theory of Rate Processes;* Mc. Graw Hill: New York, **1941.**

[3] Laidler, KJ.; King, M.C. *J. Phys. Chem.* **1983,** *87,* 2657.

[4] Truhlar, D.G.; Hase, W.L.; Hynes, J.T. *J. Phys.Chem.* **1983,** *87,* 2664.

[5] Born, M.; Oppenheimer, J.R. *Ann. Physik.* **1927,** *84,* 457.

[6] Wigner, E.P. *Trans. Faraday Soc.* **1938,** *34,* 29.

[7] Truhlar, D.G.; Isaacson, A.D.; Garrett, B.C. *In Theory of Chemical Reaction Dynamics;* Baer, M., Ed.; CRC Press: Boca Raton, FL, **1985,** *Vol. IV,* Chap. 2, p. 65.

[8] Mc Iver, J.W.; Komornicki, A. *J. Am. Chem. Soc* **1974,** *94,* 2625.

[9] Fukui, K. *J. Phys. Chem.* **1970,** 74, 4161.

[10] Truhlar, D.G.; Kupperman, A. *J. Am. Chem. Soc.* **1971,** *93,* 1840.

[11] Fukui, K. *Pure Appl. Chem.* **1982,** *54,* 1825.

[12] Truhlar, D.G.; Garrett, B.C. *Acc.Chem.Res.* **1980,** *13,* 440.

[13] Truhlar. D.G.; Isaacson, A.D. *J.Chem.Phys.* **1982,** *76,* 1380.

[14] Tucker, S.C.; Truhlar, D.G. *J. Am. Chem. Soc.* **1990,** *112,* 3347.

[15] Alemany, C.; Maseras, F.; Lledós, A.; Duran, M.; Bertrán, J. *J. Phys. Org. Chem.* **1989,** *2,* 611.

[16] Jaume, J.; Lluch, J.M.; Oliva,A.; Bertrán, J. *Chem. Phys. Lett.* **1984,** *106,* 232.

[17] Bertrán, J. *In New Theoretical Concepts for Understanding Organic Reactions;* Csizmadia, I.G., Ed.; Kluwer Academic Press: Dordretch, **1989,** p.231.

[18] Wood, W.W. In *Physics of Simple Liquids;* Temperley, H.N.V.; Rushbrooke, G.S.; Rowlinson, J.S., Ed.; North-Holland: Amsterdam, **1968,** p.115.

[19] Wood, W.W. In *Fundamental Problems in Statistical Mechanics Ill;* Cohen, E.G.D., Ed.; North-Holland: Amsterdam, **1975,** p.331.

[20] Valleau, J.P.; Whittington, S.G. In *Statistical Mechanics. Part A: Equilibrium Techniques;* Berne, B.J., Ed.; Plenum Press: New York, **1977,** p.137.

[21] Allen, M.P.; Tildesley, D.J. *Computer Simulations of Liquids;* Clarendon Press: Oxford, **1987.**

[22] Metropolis, N.; Rosenbluth, A.W.; Rosenbluth, M.N.; Teller, A.H. Teller, E. *J. Chem. Phys.* **1953,** *21,* 1087.

[23] Hammersley, J.M.; Handscomb, D.C. *Monte Carlo Methods;* Chapman and Hall: London, **1979.**

[24] Mehrotra, P.K.; Mezei, M.; Beveridge, D.L. *J. Chem. Phys.* **1983,** *78,* 3156.

[25] Bishop, M.; Frinks, S. *J. Chem. Phys.* **1987,** *87,* 3675.

[26] Kincaid, R.H.; Scheraga, H.A. *J. Comp. Chem.* **1982,** *3,* 525.

[27] Barker, J.A.; Watts, R.O. *Chem. Phys. Lett.* **1969,** *3,* 144.

[28] Swaminathan, S.; Beveridge, D.L. *J. Am. Chem. Soc.* **1977,** *99,* 8392.

[29] Owicki, J.C.; Scheraga, H.A. *J. Am. Chem. Soc.* **1977,** *99,* 7403.

[30] Owicki, J.C.; Scheraga, H.A. *JAm.Chem.Soc.* **1977,** *99,* 7413.
[31] Jorgensen, W.L.; Gao, J. *J. Phys. Chem.* **1986,** *90,* 2174.
[32] Jorgensen, W.L.; Ibrahim, M. *J. Am. Chem. Soc.* **1981,** *103,* 3976.
[33] Jorgensen, W.L. *J. Am. Chem. Soc.* **1981,** *103,* 4721.
[34] Jorgensen, W.L.; Bigot, B.; Chandrasekhar, J. *J. Am. Chem. Soc.* **1982,** *104,* 4584.
[35] Tapia, O.; Lluch, J.M. *J. Chem. Phys.* **1985,** *83,* 3970.
[36] Tapia, O:; Lluch, J.M.; Cárdenas, R.; Andrés, J. *J. Am. Chem. Soc.* **1989,** *111,* 829.
[37] Edens, M.; Boerner, D.; Chase, C.R.; Nass, D.; Sciavelli, M.D. *J. Org. Chem.* **1977,** *42,* 3403.
[38] McQuarrie, D.A. *Statistical Mechanics;* Harper and Row: New York, **1976.**
[39] Valleau, J.P.; Torrie, G.M. In *Statistical Mechanics. Part A: Equilibrium Techniques;* Berne, B.J. Ed.; Plenum Press: New York, **1977,** p.169.
[40] Patey, G.N.; Valleau, J.P. *J. Chem. Phys.* **1975,** *63,* 2334.
[41] Chandrasekhar, J.; Smith, S.F.; Jorgensen, W.L. *J. Am. Chem. Soc.* **1985,** *107,* 154.
[42] Harvey, S.C.: Prabhakaran, M. *J. Phys. Chem.* **1987,** *91,* 4799.
[43] Zwanzig, R.W. *J. Chem. Phys.* **1954,** *22,* 1420.
[44] Jorgensen, W.L.; Ravimohan, C. *J. Chem. Phys.* **1985,** *83, 3050.*
[45] Jorgensen, W.L.; Buckner, J.K.; Huston, S.E.; Rossky, P.J. *J. Am. Chem. Soc.* **1987,** *109,* 1891.
[46] Jorgensen, W.L. *Acc. Chem. Res.* **1989,** *22,* 184.
[47] Kollman, P. *Chem.Rev.* **1993,** *93,* 2395.
[48] Pearlman, D.A.; Kollman, P.A. *J.Chem.Phys.* **1989,** *90,* 2460.
[49] Pearlman, D.A.; Kollman, P.A. *J.Chem.Phys.* **1989,** *91,* 7831.
[50] Bennett, C.H. *J. Comp. Phys.* **1976,** *22,* 245.
[51] Migliore, M.; Corongiu, G.; Clementi, E.: Lie, G.C. *J. Chem. Phys.* **1988,** *88,* 7766.
[52] Chandrasekhar, J.; Smith, S.F.; Jorgensen, W.L. *J. Am. Chem. Soc.* **1984,** *106,* 3049.
[53] Chandrasekhar, J.; Jorgensen, W.L. *J. Am. Chem. Soc.* **1985,** *107,* 2974.
[54] Jorgensen, W.L.; Chandrasekhar, J.; Madura, J.D.; Impey, R.W.; KLein, M.L. *J. Chem. Phys.* **1983,** *79,* 926.
[55] Madura, J.D.; Jorgensen, W.L. *J.Am.Chem.Soc.* **1986,** *108,* 2517.
[56] Gerald, C. *Applied Numerical Analysis;* Addison-Wesley: Reading, MA, **1980.**
[57] Jorgensen, W.L.; Buckner, J.K. *J. Phys. Chem.* **1986,** *90,* 4651.
[58] Jorgensen, W.L.; Blake, J.F.; Lim, D.; Severance, D.L. *J. Chem. Soc. Faraday Trans.* **1994,** *90,* 1727.
[59] Blake, J.F.; Jorgensen, W.L. *J. Am. Chem. Soc.* **1991,** *113,* 7430.
[60] Severance, D.L.; Jorgensen W.L. *J. Am. Chem. Soc.* **1992,** *114,* 10966.
[61] Marcus, R.A. *J. Chem. Phys.* **1965,** *43,* 679.
[62] Sutin, N. *Annu. Rev. Nucl. Sci.* **1962,** *12,* 285.
[63] Hush, N.S. *Trans. Faraday Soc.* **1965,** *57,* 155.

[64] Churg, A.K.; Weiss, R.M.; Warshel, A.; Takano, T. *J. Phys. Chem.* **1983,** *87,* 1683.
[65] Zichi, D.A.; Ciccotti, G.; Hynes, J.T.; Ferrario, M. *J. Phys. Chem.* **1989,** *93,* 6261.
[66] Tachiya, M. *J. Phys. Chem.* **1989,** *93,* 7050.
[67] González-Lafont, A.; Lluch, J.M.; Oliva, A.; Bertán, J. *J. Comput. Chem.* **1991,** *12,* 1165.
[68] Carter, E.A.; Hynes, J.T. *J. Phys. Chem.* **1989,** *93,* 2184.
[69] Warshel, A. *J. Phys. Chem.* **1982,** *86,* 2218.
[70] Yoshimori, A.; Kakitani, T.; Enomoto, Y.; Mataga, N. *J. Phys. Chem.* **1989,** *93,* 8316.
[71] Pérez, V.; Lluch, J.M.; Bertrán, J. *J. Comput. Chem.* **1992,** *13,* 1057.
[72] Pérez, V.; Lluch, J.M.; Bertrán J. *J. Am. Chem.* Soc. **1994,** *116,* 10117.
[73] Perez, V.: González-Lafont, A.; Lluch, J.M.; Bertrán, J. *J. Chem. Soc. Faraday Trans.* in press.
[74] King, G.M.; Warshel, A. *J. Chem. Phys.* **1990,** *93,* 8682.
[75] Hwang, J.K.; Warshel, A. *J. Am. Chem. Soc.* **1987,** *109,* 715.
[76] Hwang, J.K.; King, G.; Creighton, S.; Warshel, A. *J. Am. Chem. Soc.* **1988,** *110,* 5297.
[77] Clementi. E.; Kistenmacher, H.; Kolos, W.; Romano, S. *Theoret. Chim. Acta (Berl.)* **1980,** *55,* 257.
[78] Clementi, E. *Lectures Notes in Chemistry;* Vol. 19, Springer-Verlag: Berlin, **1980.**
[79] Kistenmacher, H.; Popkie, H.; Clementi, E. *J. Chem. Phys.* **1973,** *59,* 5842.
[80] Jorgensen, W.L.; Cumoyer, M.E. *J. Am. Chem. Soc.* **1978,** *100,* 4942.
[81] Karlström, G.; Linse, P.; Wallquist, A.; Jönsson, B. *J. Am. Chem. Soc.* **1983,** *105,* 3777.
[82] Nakanishi, K.; Ikari, K.; Okazaki, S. Touhara, H. J. *Chem. Phys.* **1984,** *80,* 1656.
[83] Sordo, J.A.; Klobukowski, M.; Fraga, S. *J. Am. Chem. Soc.* **1985,** *107,* 7569.
[84] González-Lafont, A.; Lluch, J.M.; Oliva, A.; Bertrán, J. *Int. J. Quantum Chem.* **1986,** *29,* 1373.
[85] González-Lafont, A.; Lluch, J.M.; Oliva, A.; Bertrán, J. *Int. J. Quantum Chem.* **1986,** *30,* 663.
[86] Portmann, P.; Marvizumi, T.; Welti, M.; Badertscher, M.; Neszmelyi, A.; Simon, W.; Pretsch, E. *J. Chem. Phys.* **1987,** *87,* 493.
[87] Kim, S.; Jhon, M.S.; Scheraga, H.A. J. *Phys. Chem.* 1988, *92*, 7216.
[88] González-Lafont, A.; Lluch, J.M.; Oliva, A.; Bertrán, J. *Int. J. Quantum Chem.* **1988,** *33,* 77.
[89] Cordeiro, M.N.D.S.; Gomes, J.A.N.F.; González-Lafont, A.; Lluch, J.M.; Oliva, A.: Bertrán, J. *J. Chem. Soc. Faraday Trans. 2* **1988,** *84,* 693.
[90] Wee, S.S.; Kim, S.; Jhon, M.S.; Scheraga, H.A. *J. Phys. Chem.* **1990,** *94,* 1656.
[91] Swaminathan, S.; Whitehead, R.J.; Guth, E.; Beveridge, D.L. *J. Am. Chem.*

Soc. **1977,** *99,* 7817.
[92] Curnoyer, M.E.; Jorgensen, W.L. *J. Am. Chem. Soc.* **1984,** *106,* 5104.
[93] Ortega-Blake, I.; Novaro, O.; Les, A.; Rybak, S. *J. Chem. Phys.* **1982,** *76,* 5405.
[94] Ortega-Blake, I.; Hernández, J.; Novaro, O. *J. Chem. Phys.* **1984,** *81,* 1894.
[95] Lybrand, T.P.; Kollman, P.A. *J. Chem. Phys.* **1985,** *83,* 2923.
[96] Kochanski, E. *J. Am. Chem. Soc.* **1985,** *107,* 7869.
[97] Detrich, J.; Corongiu, G.; Clementi, E. *Chem. Phys. Lett.* **1984,** *112,* 426.
[98] Kim, K.S.; Dupuis, M.; Lie, G.C.; Clementi, E. *Chem. Phys. Lett.* **1986,** *131,* 451.
[99] Curtiss, L.A.; Halley, J.W.; Hautman, J.; Rahman, A. *J. Chem. Phys.* **1987,** *86,* 2319.
[100] Corongiu, G.; Migliore, M.; Clementi, E. *J. Chem. Phys.* **1989,** *90,* 4629.
[101] Curtiss, L.A.; Halley, J.W.; Hautman, J. *Chem. Phys.* **1989,** *133,* 89.
[102] Cordeiro, M.N.D.S.; Gomes, J.A.N.F.; González-Lafont, A.; Lluch, J.M.; Bertrán, J. *Chem. Phys.* **1990,** *141,* 379.
[103] Cordeiro, M.N.D.S.; Gomes, J.A.N.F. *J. Comp. Chem.* **1993,** *14,* 629.
[104] Floris, F.; Persico, M.; Tani, A.; Tomasi, J. *Chem. Phys. Lett.* **1992,** *199,* 518.
[105] Bounds, D.G. *Mol. Phys.* **1985,** *54,* 1335.
[106] Probst, M.M.; Spohr, E.; Heinzinger, K. *Chem. Phys. Lett.* **1989,** *161,* 405.
[107] Pappalardo, R.R.; Sánchez Marcos, E. *J. Phys. Chem.* **1993,** *97,* 4500.
[108] Tomasi, J.; Bonaccorsi, R.; Cammi, R.; Olivares del Valle, F.J. *J. Mol. Struct. (Theochem)* **1991,** *234,* 401.
[109] Matsuoka, O.; Clementi, E.; Yoshimine, M. *J. Chem. Phys.* **1976,** *64,* 1351.
[110] Clementi, E.; Corongiu, G. *Int. J. Quantum Chem. Symp.* **1983,** *10,* 31.
[111] Niesar, U.; Corongiu, G.; Huang, M.J.; Dupuis, M.; Clementi, E. *Int. J. Quantum Chem.Symp.* **1989,** *23,* 421.
[112] Sprik, M. *J. Chem. Phys.* **1991,** *95,* 6762.
[113] Caldwell, J.; Dang, L.X.; Kollman, P.A. *J. Am. Chem. Soc.* **1990,** *112,* 9144.
[114] Stillinger, F.H.; Rahman, A. *J. Chem. Phys.* **1974,** *60,* 1545.
[115] Berendsen, H.J.; Grigera, J.; Shaatsma, T.P. *J. Phys. Chem.* **1987,** *91,* 6269.
[116] Jorgensen, W.L. *J. Am. Chem. Soc.* **1981,** *103,* 335.
[117] Jorgenscn, W.L. *J. Chem. Phys.* **1982,** *77,* 4156.
[118] Bopp, P.; Jausco, G.; Heinzinger, K. *Chem. Phys. Lett.* **1983,** *98,* 129.
[119] Lie, G.C.; Clementi, E. *Phys. Rev,* **1986,** *A33,* 2679.
[120] Jorgensen, W.L. *J. Am. Chem. Soc*. **1981,** *103,* 335.
[121] Jorgensen, W.L. *J. Am. Chem. Soc*. **1981,** *103,* 341.
[122] Jorgensen, W.L. *J. Am. Chem. Soc* . **1981,** *103,* 345.
[123] Jorgensen. W.L.; Madura, J.D.; Swenson, C.J. **1984,** *106,* 6638.
[124] Jorgensen, W.L.; Swenson, C.J. *J. Am. Chem. Soc.* **1985,** *107,* 569.
[125] Jorgensen, W.L.; Swenson, C.J. *J. Am. Chem. Soc.* **1985,** *107,* 1489.
[126] Jorgensen, W.L. *J. Phys. Chem.* **1986,** *90,* 6379.
[127] Jorgensen, W.L.; Tirado-Rives, J. **1988,** *110,* 1657.
[128] Briggs, J.M.; Matsui, T.; Jorgensen, W.L. *J. Comp. Chem.* **1990,** *11,* 958.

[129] Weiner, S.J.; Kollman, P.A.; Case, D.A.; Singh, U.C.; Ghio, C.; Alagona, G.; Profeta, S.; Weiner, P. *J. Am. Chem. Soc.* **1984,** *106,* 765.

[130] Jorgensen, W.L.; Nguyen, T.B. *J. Comput. Chem.* **1993,** *14,* 195.
[131] Jorgensen, W.L.; Gao, J. *J. Am. Chem. Soc.* **1988,** *110,* 4212.
[132] Pralat, K.; Jadzyn, J.; Balanicka, S. *J. Phys. Chem.* **1983,** *87,* 1385.
[133] Rodrigo, M.M.; Tarazona, M.P.; Saiz, E. *J. Phys. Chem.* **1986,** *90,* 2236.
[134] Jorgensen, W.L. *J. Phys. Chem.* **1986,** *90,* 1276.
[135] Francl, M.M.; Pietro, W.J.; Hehre, WJ.; Binkley, J.S.; Gordon, M.S.; De Frees, D.J.; Pople, J.A. *J. Chem. Phys.* **1983,** *77,* 3054.
[136] Nagy, P.I.; Durant, G.I.; Smith, D.A. *J. Am. Chem. Soc*. **1993,** *115,* 2912.
[137] Jorgensen, W.L.; Gao, J.; Ravimohan, C. *J. Phys. Chem.* **1985,** *89,* 3470.
[138] Duffy, E.M.; Severance, D.L.; Jorgensen, W.L. *J. Am. Chem. Soc*. **1992,** *114,* 7535.
[139] Bertrán, J.; Ruiz-López, M.F.; Rinaldi, D.; Rivail, J.L. *Theor. Chim. Acta* **1992,** *84,* 181.
[140] Williams, D.E.; *J. Comp. Chem.* **1988,** *9,* 745.
[141] Cox, S.R.; Williams, D.E. *J. Comp. Chem.* **1981,** *2,* 304.
[142] Singh, U.C.; Kollman, P.A. *J. Comp. Chem.* **1984,** *5,* 129.
[143] Chirlian, L.E.; Francl, M.M. *J. Comp. Chem.* **1987,** *8,* 894.
[144] Breneman, C.M.; Wiberg, K.B. *J. Comp. Chem.* **1990,** *11,* 361.
[145] Besler, B.H.; Merz, K.M.Jr.; Kollman, P.A. *J. Comp. Chem.* **1990,** *11,* 431.
[146] Orozco, M.; Luque, F.J. *J. Comp. Chem.* **1990,** *11,* 909.
[147] Cieplak, P.; Kollman, P.A. *J. Comp. Chem.* **1991,** *12,* 1232.
[148] Merz, K.M.Jr. *J. Comp. Chem.* **1992,** *13,* 749.
[149] Grootenhuis, P.D.J.; Kollman, P.A. *J. Am. Chem. Soc.* **1989,** *111,* 4046.
[150] Carlson, H.A.; Nguyen, T.B.; Orozco, M.; Jorgensen, W.L. *J. Comp. Chem.* **1993,** *14,* 1240.
[151] Lim, D.; Hrovat, D.A.; Borden, W.T.; Jorgensen, W.L. *J. Am. Chem. Soc.* **1994,** *116,* 3494.
[152] Sclove, D.B.; Pazos, J.F.; Camp, R.L.; Greene, F.D. *J. Am. Chem. Soc.* **1970,** *92,* 7488.
[153] Bash, P.A.; Field, M.J.; Karplus, M. *J. Am. Chem. Soc.* **1987,** *109,* 8092.
[154] Gao, J. *J. Phys. Chem.* **1992,** *96,* 537.
[155] Gao, J.; Pavelites, J.J. *J. Am. Chem. Soc.* **1992,** *114,* 1912.
[156] Gao, J. *J. Am. Chem. Soc.* **1993,** *115,* 2930.
[157] Gao, J.; Xia, X. *In Structure and Reactivity in Aqueous Solution;* Cramer, Ch.J.; Truhlar, D.G., Eds.; American Chemical Society: Washington, DC, **1994,** *568,* Chap. 15, p.212.
[158] Kohn, W.; Shom, L.J. *Phys. Rev.* **1965,** *140,* A1133.
[159] Hohenberg, P.; Kohn, W. *Phys. Rev.* **1964,** *136,* 864.
[160] Stanton, R.V.; Hartsough, D.S.; Merz, K.M. Jr. *J. Phys. Chem.* **1993,** *97,* 11868.
[161] Dewar, M.J.S.; Zoebisch, E.G.; Healy, E.F.; Stewart, J.J.P. *J. Am. Chem. Soc.* **1985,** *107,* 3902.

[162] Gao, J.; Xia, X. *J. Am. Chem. Soc.* **1993,** *115,* 9667.
[163] Åquist, J.; Warshel, A. *Chem. Rev.* **1993,** *93,* 2523.
[164] Warshel, A. *Computer Modeling of Chemical Reactions in Enzymes and Solutions;* Wiley: New York, **1991.**

This page intentionally left blank.

COMPUTER SIMULATION FOR CHEMICAL SYSTEMS: FROM VACUUM TO SOLUTION

G. CORONGIU*†, D.A. ESTRIN‡ , L. PAGLIERI*

* *CRS4 - Centre for Advanced Studies, Research and Development in Sardinia*
P.O. Box 1048 , 09100 Cagliari - Italy

† *Université Louis Pasteur*
3, rue de l'Université
67084 Strasbourg Cedex - France

‡ *INQUIMAE, Universidad de Buenos Aires*
Ciudad Universitaria - Pab. II
01428 Buenos Aires - Argentina

1. Introduction

The most abundant compound on our planet is water at the liquid state. Because of its diffusion and its solvating properties, a large number of chemical reactions, important in life and in industrial processes, take place in aqueous solution.

From a computational view point, chemical reactions in solution present a yet not solved challenge. On one hand, some of the solvent effects can be approximated as if the solute molecule would be in a continuum with a given dielectric characterization of the liquid, and this view point has been pioneered by Born [1], later by Kirkwood [2] and Onsager [3] and even later by many computational quantum chemists [4-9]. On the other hand, the continuum model fails totally when one is interested in the specific

O. Tapia and J. Bertrán (eds.), Solvent Effects and Chemical Reactivity, 179-229.
© 1996 *Kluwer Academic Publishers. Printed in the Netherlands.*

interactions of the first solvation shell with the solute; clearly if an hydrogen rather than an oxygen atom points towards a specific atom of the solute molecule, the energetics of the interaction is drastically different. This leads to the need to represent the first shell in a detailed way, recognizing explicitly the solvent molecules at the atomic level. An extreme case of this need is for reactions in acqueous solution, where one of the reactants is a molecule of water.

Unfortunately, as it is well known, in liquid water one water molecule, solute or solvent, is characterized by being connected to other molecules of water, creating a complex network. It is also known that this network is of two main types: clatrate-like or hydrophyllic type. The two have different characterizations in the first solvation shell, thus generate a different electric field on the solute.

From the above, it should be clear that the continuum model can simulate only those aspects of the solvent which are somewhat independent from hydrophobicity, hydrophyllicity, in general first solvation shell, and specific interactions with the solute. The physical problem is a general one; namely, it relates to the validity to use quantities, correctly described and defined at the macroscopic level, in the discrete description of matter at the atomic level. For such study, one needs explicit consideration of the solvent, for example the molecules of water. This can be done either at the quantum-mechanical level, as in cluster computations. We recall, in this regard, the pioneering ab initio work by E. Clementi and his group [10] for systems like water-water, water-ions, water-small molecules. We recall also the pioneering work at the semiempirical level presented by many, for example by Scheraga and his school. Another approach is to simulate the system at the Molecular Dynamics (or Monte Carlo) level; these techniques allow to consider very large systems and, if one assumes periodic boundary conditions, even infinitely large systems. The limitations of the Molecular Dynamics are in its classical nature and in the need to make use of force-fields. The latter can be obtained either semi-empirically, as it is done for example in the AMBER, GROMOS, CHARMm computer programs, or from ab-initio computations as is done in Clementi and co-workers codes.

The motions of a molecular system, for example a solution, occur on many time scales. There are very fast electronic motions, the basic mechanism in chemical reactions; then, the nuclear motions, vibrations, librations, rotations, and translations (diffusion). In the Born-Oppenheimer spirit, one can consider the electronic motion as separated from the nuclear motions, thus one can talk of micro-deformations to be treated quantum mechani-

cally and macro-deformations, which can be treated classically. This is the ab-initio approach proposed by Clementi and co-workers for the study of papain [11] in the late '70. More recently, Car and Parrinello [12] have suggested to compute the force field in Molecular Dynamics with approximated quantum mechanics techniques. Since the latter are still expensive computations, the Car-Parrinello method, and similar ones, can be used for systems of moderate size and for relative short simulation time (say no more than 100 molecules of water, for a few picoseconds at most, and using the best computational facilities today available. Alternatively, one can use semi-empirical approximations, which scale as n^2 rather than n^3, where n is the number of basis functions used to describe the electronic orbitals).

The two avenues above recalled, namely ab-initio computations on clusters and Molecular Dynamics on one hand and continuum model on the other, are somewhat bridged by those techniques where the solvent is included in the hamiltonian at the electrostatic level with a discrete representation [13,17]. It is important to stress that quantum-mechanical computations imply a temperature of zero K, whereas Molecular Dynamics computations do include temperature. As it is well known, this inclusion is of paramount importance and allows also the consideration of entropic effects and thus free-energy, essential parameters in any reaction.

In this paper we shall consider a few systems we have analysed in the last few years, attempting to indicate shortcomings and advantages in the above approaches. We start with the reaction NH_3+HCl $\leftrightarrow$ NH_4Cl, an example pioneered by Clementi in the mid 60's with all-electron ab-initio computations. This is a classical calculation, since not only is the first ab-initio work for a non trivial molecular system, but also because by computations it attempts to verify the R.S. Mulliken's hypothesis on the existence of two complexes: an inner-complex $H_3N \cdots H \cdots Cl$, and an outer-complex $NH_4^+ \cdots C1^-$. The computation by Clementi indicated the existence of only the inner complex. Since it was done at the HF level, the correlation errors were only estimated, but it was concluded that the overall reaction would occur on a surface with only one minimum corresponding to the H_3N - H - Cl complex. The binding energy of the complex was measured experimentally few years after the computation and resulted in substantial agreement with the spread of binding energies proposed by Clementi. Later, the energy surface of the reaction was analysed by many authors, and this narrowed down the predicted range of the binding energies, but left unaltered the conclusion of the one-minimum only in the reaction hypersurface. In this work, we shall include the reaction field model to the computation of the reaction hypersurface of the above process and we shall show that

we have two shallow minima, the deepest one corresponds to the outer-complex proposed by Mulliken. Thus, we can conclude that the solvent effect, even considered within the limitations of the continuum model, can bring about a different reaction product. Parenthetically, this points out once more the non transferability of reaction mechanism from gas phase to solution; unfortunately, many quantum chemical studies of reaction mechanism, in current literature, compare computations in the gas phase with experimental data in solution. It can be argued that when there is agreement between the two sets of data, there is reasonable doubt for assuming the latter is obtained somewhat accidentally.

The second example concerns the lithium ion, either considered in a cluster of water molecules or in aqueous solution. The idealized solution at infinite dilution of a lithium ion (without counter-ion) predicts six molecules of water in the first solvation shell if one uses pair-wise 2-body interactions, but the same type of computation predicts four molecules of water when 3-body effects are included. The computations were performed at room temperature. We have performed cluster computations for the $Li^+(H_2O)_n$ system, with n = 1,2,3,4,5 and 6, using a density functional program developed in our laboratory. When we compute the most stable configuration for the pentamer complex $Li^+(H_2O)_5$, starting from the most stable configuration obtained with the 2-body potential, we obtain an energy minimum for a conformation of 5 water molecules surrounding the Li^+ in a first solvation shell. However in a MD simulation of the same system, analysis of the trajectories indicated that one water molecule tends to abandon the first solvation shell, entering in the second solvation shell region. This example is given to stress that energy minimization for non trivial small systems must face the multi minima problem, since results are too heavily dependent on the initial condition. Further, recalling that many minima can occur on a very narrow energetic range, we must be aware that entropic effects, neglected in general in the energy minimization, can lead to incorrect conclusions.

In the third example we shall compare structural details of connectivity in water, either in clusters or in the liquid. This example is given to warn on transferring conclusions obtained from clusters to the liquid. Indeed, we shall show that, whereas in the clusters at zero K temperature, closed ring or 3D-type structures are the most stable ones, in the liquid, at finite temperature, three-dimensional networks are the predominant configurations.

In the last example, we move to the general problem of nucleic acid simulations. It is abundantly clear that simulations on DNA double helix

without considering the solvent are open to very serious criticism, since the double helix in vacuo is not stable. In our example we consider the stability of the base pairs (A-T and G-C) either in vacuo or with a reaction field, simulating the solvent. We have concluded that there is a decrease in the stability for the pair when the solvent is included. We have also performed vibrational analysis for both the separated bases and the base pairs (in vacuo and in solution). For the gas phase simulations, the computed IR frequencies are in agreement with available experimental data. Notable shifts are predicted for the IR frequencies of those atoms involved in the hydrogen bridges in the pairs. Laboratory results on the shifts are important since they provide an additional test on the predictive power of the simulation approaches we have experimented with.

2. Comments on the methods used in our simulations

The methods and the corresponding computer programs we have used, have been amply documented in the past literature. However, for the sake of completeness, we present a few comments, which might be useful to the general reader.

Concerning quantum chemical computations, we have used the MOLECOLE program [18a], for HF and MP2 type computations. The Molecular Dynamics simulations with analytical force fields have been performed with the DINAMICA program [18b]. The MOLECOLE-DFT program [18c] has been used for both the DFT energy minimization and for the DFT-Molecular Dynamics.

2.1 DENSITY FUNCTIONAL THEORY IMPLEMENTATION

Here, we discuss in some detail the DFT implementation in our computer program, since only in the last few years DFT is becoming more familiar to the chemists' community, as opposite to the physicists' community, where it was used routinely for the last thirty years for obtaining structural and electronic properties of bulk solids and surfaces [19].

For many problems in solid state physics, the computational efficiency of the computer programs is the result of using a planewave basis set and performing part of the calculation in momentum space through the use of Fast Fourier transforms. A planewave basis set is naturally applicable to systems with translational symmetry and this is the key of the success of

the applications of Density Functional Theory to crystalline solids and surfaces. However, the use of planewaves enforces a periodicity not present in most molecules and the so called "supercell approach" must be used in order to treat aperiodic systems [20]. In this method, the molecule is placed at the sites of a three dimensional lattice of points, thereby restoring periodicity. In the limit that the lattice points are very far apart, the molecule is treated accurately. An alternative formulation consists in using a basis set of localized functions. This approach offers a more natural way for simulation of molecular systems, which usually are non-periodic. Techniques using numerical basis sets [21-22], Slater type basis sets [23-24] and Gaussian basis sets [22-26] have been developed and used successfully in many chemical problems [27-29]. In particular the use of Gaussian type basis sets permits the utilization of the wealth of experience gained in standard ab-initio methods for the evaluation of two electron integrals, derivation of analytic gradients, etc. Approximate density functional theories for the correlation energy evaluation using the exact exchange have been proposed and used extensively for obtaining the dynamical correlation [30-31]. In cases in which the near-degeneracy correlation is important, a proper dissociation wave function should be employed [31]. A density functional for the exchange and correlation energies will be used in several examples discuss in the present chapter.

The Density Functional Theory is based on a theorem by Hohenberg and Kohn [32] which states that the total energy E is a functional of the charge density ρ. Essentially the problem of determining the wavefunction, a function of 3N dimensions, where N is the number of electrons, is reduced to finding the density, $\rho(\vec{r})$, a function of only 3 dimensions. However, there are no simple and unique prescriptions for the determination of this density. Applications of DFT became feasible with the work of Kohn and Sham (KS) [33]. Assuming that the wavefunction of a system can always be written as a single Slater-determinant, by minimizing the total energy with respect to the density

$$\rho = \sum_{\lambda} n_{\lambda} \Psi_{\lambda}^{*} \Psi_{\lambda} \tag{1}$$

a set of N one-electron equations is obtained

$$(-\frac{\nabla^2}{2} + v_{eff})\Psi_{\lambda} = \epsilon_{\lambda}\Psi_{\lambda} \tag{2}$$

with the effective potential,

$$v_{eff}(\vec{r}) = V_N(\vec{r}) + \int d\vec{r'} \frac{\rho(\vec{r'})}{|\vec{r} - \vec{r'}|} + \frac{\delta E_{xc}[\rho]}{\delta \rho} \tag{3}$$

where $n\lambda$ is the occupation number of the KS eigenstate whose eigenvector is denoted by $\Psi\lambda$ (Here, the equations are derived for the unpolarized spin case, an extension to the spin-polarized case is straightforward). In Eq. (3), $V_N(\vec{r})$ is the external potential, specifically the nuclear attraction potential, the second term is the Coulomb potential and the last term is the exchange-correlation potential, given by the functional derivative of the exchange-correlation energy with respect to the density.

It has been found that a reasonable approximation for the exchange-correlation energy can be taken from the solutions of the homogeneous electron gas (Local Density Approximation, LDA). The LDA provides a reasonable description of exchange-correlation effects when the density is a slowly varying function of position [34-35]. The correlation energy term for the homogeneous electron gas has been computed very accurately [36] and several fits of these results to analytical expressions can be found in literature [34,35,37]. The exchange-correlation energy in the LDA is written as:

$$E_{xc}[\rho] = \int d\vec{r}\,\rho(\vec{r})\epsilon_{xc}(\rho) \tag{4}$$

where $e_{xc}(\rho)$ represents the exchange-correlation energy per electron in a gas with density ρ. Since finite systems are often non-homogeneous, more sophisticated functionals were developed [38-40] containing also the gradient of the density which is clearly a measure for the inhomogeneity of the electronic density. This kind of approximation is usually called non-local density approximation (NLDA). The use of the NLDA has been shown to improve considerably the agreement with experiment in the evaluation of properties of chemical interest [41], for example bond energies, hydrogen bond interactions, etc. In our implementation the gradient corrections of Perdew and Wang [40] and Becke [42] are available for the exchange terms. For the correlation terms the gradient corrections given by Perdew [39] are used, with the Vosko parameterization of the local part.

In the present approach, the KS orbitals are expanded in a set of functions related to atomic orbitals (Linear Combination of Atomic Orbitals, LCAO). These functions usually are optimized in atomic calculations. In our implementation a basis set of contracted Gaussians $\{\Psi_j\}$ is used. The basis set is in general a truncated (finite) basis set "reasonably selected".

Following standard formalism, by expanding the orbitals and the density matrix in terms of the basis set :

$$\Psi_\lambda(\vec{r}) = \sum_j C_j^\lambda \psi_j(\vec{r}) \text{ and } P_{ij} = \sum_\lambda n_\lambda C_i^\lambda C_j^\lambda \tag{5}$$

the total energy can be written as

$$E = -\frac{1}{2}\sum_{\lambda} n_\lambda \int d\vec{r}\,\Psi_\lambda^* \nabla^2 \Psi_\lambda + \int d\vec{r}\, V(\vec{r})\rho(\vec{r}) + J[\rho] + E_{xc}[\rho] \quad (6)$$

with $J[\rho]$ term, the Coulomb term, given by

$$J[\rho] = \frac{1}{2}\int d\vec{r} \int d\vec{r'}\, \frac{\rho(\vec{r})\rho(\vec{r'})}{|\vec{r} - \vec{r'}|} \quad (7)$$

Besides the Gaussian basis set for the wavefunction, an additional set of nuclear centered Gaussians, $\{g_k\}$, can be used for expanding the electronic density [25], which can be written as

$$\rho(\vec{r}) \cong \tilde{\rho}(\vec{r}) = \sum_k a_k g_k(\vec{r}) \quad (8)$$

With this approximation, the evaluation of the Coulomb term scales as N^2M, in contrast to the standard way, which scales as N^4 (N and M are the number of primitive functions in the orbital and density basis sets, respectively). The expansion coefficients of the electronic density in Eq. (8) are chosen such as to minimize the error in the Coulomb term arising from the difference between the real density and the fitted density [25].

Unlike the expansion for the electrostatic density, the fitting of the exchange-correlation energy requires a least squares fit of the coefficients by evaluating an auxiliary set of basis functions, $\{h_k\}$, the exchange-correlation energy and the potential on a three dimensional grid [25,26,43]. After performing the least-squares fit, two sets of coefficients are obtained, $\{b_j\}$ and $\{d_j\}$, for the exchange-correlation energy density and potential, respectively.

$$\epsilon_{xc}(\rho) = \sum_j b_j h_j(\vec{r}) \text{ and } v_{xc}(\rho) = \sum_j d_j h_j(\vec{r}) \quad (9)$$

To perform the least-squares fit, the density (and its derivatives if a non-local density functional is used) has to be evaluated at all points of the grid, making this step very time consuming. Many different types of grids have been proposed for fitting the exchange-correlation energy and potential. In most of the cases these grids are based on the superposition of atomic centered grids [44-45]. In our program we implemented the adaptive nuclear centered grid proposed by Becke [46]. The auxiliary basis, $\{h_k\}$, needed for expanding the exchange-correlation energy density $\epsilon_{xc}(\rho)$, and potential $v_{xc}(\rho)$ (see Eq.(9)) is usually chosen as a new set of Gaussian functions [43]. We have implemented a different approach in order to use the same

set of two electron integrals for the Coulomb and the exchange-correlation terms, the set $\{h_k\}$ is related to the density basis set through the following expression :

$$h_k(\vec{r}) = \int d\vec{r'} \frac{g_k(\vec{r'})}{|\vec{r} - \vec{r'}|} \tag{10}$$

Once the coefficients for the expansion of the exchange-correlation term have been evaluated, all matrix elements can be calculated analytically. The Obara and Saika [47] recursive scheme has been used for the evaluation of the one and the two electron integrals. The total energy is therefore expressed in terms of the fitting coefficients for the electronic density and the exchange-correlation potential.

An alternative procedure consists in using a numerical integration scheme to evaluate the exchange-correlation contribution. In this case, no auxiliary basis set is needed for the exchange-correlation terms, and numerically more reliable results can be obtained.

In order to solve the electronic structure problem for a single geometry, the energy should be minimized with respect to the coefficients $\{C_i^\lambda\}$ (see Eq. (5)) subject to the orthogonality constraints. This leads to the eigenvalue equation :

$$\sum_j (T_{ij} + V_{ij}^N + V_{ij}^c + V_{ij}^{xc}) C_j^\lambda = \sum_j F_{ij} C_j^\lambda = \epsilon_\lambda \sum_j S_{ij} C_j^\lambda \tag{11}$$

where T_{ij} and V_{ij}^N are the standard one electron kinetic energy and nuclear attraction matrix elements, F_{ij} is the corresponding Fock matrix element and the V_{ij}^c and V_{ij}^{xc} are function of $\{a_k\}$ and $\{d_k\}$, the fitting coefficients for the electronic density and exchange-correlation potential respectively. As it is usual, the Fock matrix is a function of the matrix of coefficients $\{C_i^\lambda\}$, therefore the problem is solved iteratively. The matrix of coefficients $\{C_i^\lambda\}$ is obtained by solving Eq. (11), which in turn depends on the same set of coefficients through the Fock matrix dependence on the fitting sets $\{a_i\}$ and $\{d_i\}$.

The evaluation of the analytical gradients of the energy with respect to the nuclear coordinates is of importance for searching equilibrium geometries, reaction pathways and for performing first principles Molecular Dynamics simulations. In our approach, the evaluation of the nuclear gradients requires the computation of the derivatives of the one electron (two index) and two electron (three index) integrals. Since only nuclear centered cartesian Gaussian functions are being employed for both orbital and

auxiliary basis sets, we can use the property that the derivative of a cartesian Gaussian function is a combination of two different Cartesian Gaussian functions with angular momentum either lowered or raised by one, respectively.

The calculation of the harmonic vibrational frequencies is performed by evaluating the second derivatives of the energy with respect to the nuclear positions through a numerical differentiation of the gradients. By using a mass weighting procedure followed by a diagonalization, the harmonic frequencies and the normal modes are obtained. These frequencies can be used in the evaluation of the zero-point energies. Notice that the infrared absorption intensities can be calculated by taking the numerical derivatives of the dipole moment and by transforming them to the corresponding ones with respect to the normal modes [48].

2.2 DFT MOLECULAR DYNAMICS

Molecular dynamics simulations, with quantum-mechanically derived energy and forces, can provide valuable insights into the dynamics and structure of systems in which electronic excitations or bond breaking processes are important. In these cases, conventional techniques with classical analytical potentials, are not appropriate. Since the quantum mechanical calculation has to be performed many times, one at each time step, the choice of a computationally fast method is crucial. Moreover, the method should be able to simulate electronic excitations and breaking or forming of bonds, in order to provide a proper treatment of those properties for which classical potentials fail.

Once the energy and forces have been obtained, the nuclear equations of motion are integrated using standard methods [49]

$$M_I \ddot{R}_I^\alpha = -\frac{\partial E}{\partial R_I^\alpha} \tag{12}$$

Since the changes in geometry from one molecular dynamics step to the next one are small, usually a few iterations suffice for achieving self-consistency.

An alternative approach was introduced by Car and Parrinello [12], who developed a DFT-MD method to study periodic systems using a planewave expansion in which the electronic parameters, as well as the nuclear coordinates, are treated as dynamical variables. Following the Car and Parrinello

approach, in the LCAO implementation of DFT, a Lagrangian of the form:

$$L(\{\dot{C}_i^\lambda\},\{C_i^\lambda\},\{\dot{R}_I\},\{R_I\}) =$$

$$\tfrac{\mu}{2}\sum_\lambda^N \sum_{i=1}^{N_\lambda} \dot{C}_i^{\lambda 2} + \tfrac{1}{2}\sum_{I=1}^{N_A} M_I \dot{R}_I^2 - E[\{C_i^\lambda\},\{R_I\}] + \qquad (13)$$

$$\sum_{\mu\nu} \Lambda_{\mu\nu}[\sum_{ij} C_i^\mu C_j^\nu S_{ij}^{\mu\nu} - \delta_{\mu\nu}]$$

can be constructed for generating the equations of motion for the atomic nuclei and variational parameters. The N_λ is the number of contracted Gaussian functions in the expansion of the molecular orbitals, μ is a fictitious mass, associated with the expansion coefficients, and the $\Lambda_{\lambda\nu}$ are Lagrange multipliers, necessary to enforce orthogonality for the molecular orbitals.

In order to generate the equations of motion, one needs the gradients of the energy with respect to the nuclear coordinates and the variational parameters. The expression for the nuclear gradients are reported in Ref. [18c], and the derivation of the gradients with respect to the electronic coefficients is straightforward :

$$\frac{\partial E}{\partial C_i^\lambda} = 2\sum_j F_{ij} C_j^\lambda \qquad (14)$$

The nuclear equations of motion are given by Eq. (12) and the corresponding ones for the electronic coefficients are :

$$\mu \ddot{C}_i^\lambda = -\frac{\partial E}{\partial C_i^\lambda} + 2\sum_\nu^N \Lambda_{\lambda\nu} \sum_j^N C_j^\nu S_{ij}^{\lambda\nu} \qquad (15)$$

The technique can be used either to perform geometry optimization, by simultaneously annealing the wavefunction and the geometry, or to simulate real dynamics, if the temperature of the fictitious (electronic) parameters is kept close to zero. A drawback of the method is that small masses must be chosen for the electronic parameters in order to achieve an adiabatic separation of the nuclear and the fictitious parameter motions. As a consequence, time steps smaller than MD simulations involving only nuclear motion, are required.

In our approach, using a standard nuclear centered Gaussian basis set, we found that, in general, it is computationally more efficient to carry out

a full self consistent calculation at each time step than to use the Car-Parrinello approach, since we can use much larger time steps. However, the Car-Parrinello method offers a convenient and powerful alternative [50] for those cases in which the variational problem is non-linear, for example when using a floating Gaussian basis set, where it is not possible to solve the problem through self-consistent diagonalization.

2.3 THE SELF CONSISTENT REACTION FIELD, SCRF, METHOD

The Onsager's reaction field theory [3] has been incorporated into MO calculations by Tapia and Goscinski [6]. The model has been applied to different problems using either semiempirical [51] or ab-initio MO theory [52], or correlated ab-initio techniques [52].

In the Onsager's SCRF model, the solute is placed in a cavity immersed in a continuous medium with a dielectric constant ϵ. The molecular dipole of the solute induces a dipole in the solvent, which in turn interacts with the molecular dipole, leading to a net stabilization effect.

This electrostatic effect may be represented by an additional term in the one-electron operator:

$$H_1 = -\vec{\mu}.\vec{R} \text{ with } \vec{R} = g\vec{\mu} \tag{16}$$

The reaction field factor g depends on the geometry of the cavity and on the dielectric permittivity ϵ of the solvent.

When one uses a regularly shaped cavity, such an ellipsoid or a sphere, the reaction field factors are given by analytical expressions [53]. For a spherical cavity, g is given by:

$$g = \frac{2(\epsilon - 1)}{(2\epsilon + 1)a_0^3} \tag{17}$$

The reaction field effects are easily incorporated as an additional term in the Kohn-Sham matrix, given by :

$$F_{ij} = F_{ij}^0 - g\ \vec{\mu} < \Psi_i |\ \vec{\mu}\ | \Psi_j > \tag{18}$$

where F_{ij}^0 is the Kohn-Sham matrix eIement given in Eq. (11) and Ψ_i and Ψ_j are basis functions. After self-consistency is achieved, a solvent polarization energy

$$E_{pol} = -1/2\ \vec{\mu}.\vec{R} \tag{19}$$

is added to the total energy. The self-consistent reaction field procedure consists of iteratively solving for a consistent dipole moment $\vec{\mu}$ and reaction

field $\vec{R}$. This is done by evaluating the dipole moment $\vec{\mu}$ at each Kohn-Sham iteration, and iterating until both the density matrix and the reaction field are converged.

In the case of charged systems with a total charge Q, a term to account for the ion-dipole interaction should be added to the total energy. For a spherical cavity, this term is a constant, since it does not contribute variationally to the total energy.

$$E_{charge} = -0.5(1 - \frac{1}{\epsilon})\frac{Q^2}{a_0} \tag{20}$$

The dipole moment of a charged system is not translationally invariant, and it must be evaluated with the origin at the center of the electric charge, in order to be consistent with the spherical cavity assumption. The dipole moment is therefore computed according to:

$$\vec{\mu} = \vec{\mu}_{el}\frac{(Q+N)}{N} + \vec{\mu}_{nuc} \tag{21}$$

where $\vec{\mu}_{nuc}$ and $\vec{\mu}_{el}$ are the nuclear and electronic contributions to the total dipole moment, with respect to an arbitrary origin, and N is the total number of electrons in the molecule.

A related methodology that makes use of the calculated surface charges at the cavity surface to estimate the interaction with the solvent has been described in Ref. [54]; in addition, the reaction field model can be extended to include the effects of higher order multipoles [55]. In the present implementation, only dipole effects are considered.

Unfortunately, the shape of the cavity plays a major role in the model, and the polarization energy of Eq. (19) is a function of the assumed cavity's shape. In the case of relatively compact molecules the cavity can be approximated by a regularly shaped surface such as an ellipsoid, a spheroid or a sphere. However, more sophisticated approaches have been proposed, defining for example the cavity by an electronic isodensity surface enclosing a volume equal to the molecular volume, or to the molecule Van der Waals surface [54]. Whereas the reaction field factors, in the general case, are evaluated numerically by using electrostatic boundary conditions, for the simpler geometrical shapes, analytical expressions have been derived [53]. Given the approximations involved in the reaction field model, and in order to have an efficient program which allows the determination of optimized structures, normal modes and molecular dynamics, in our program we have implemented only the spherical cavity. This seems to be a reasonable choice for the study of relatively compact molecules avoiding the approximations involved in the definition of more complicated shapes for the cavity.

In our approach, to estimate the size of the cavity, the solute molecular volume (V_m) is needed. For a spherical cavity the radius is related to the molecular volume (which can be evaluated from the experimental density) according to:

$$a_0^3 = \frac{3V_m}{4\pi} \tag{22}$$

Alternative methods, at times very complicated, have been proposed for estimating the value of a_0.

Analytical first derivatives in presence of the reaction field are easily derived for a fixed cavity size. The expression for the gradients is the same as the one given in equation (33) of Ref. [18c], with an extra term for the reaction field :

$$-\frac{(Q+N)}{N}\, g \quad [\frac{\partial}{\partial R_I^\alpha} \sum P_{ij} < \Psi_i |\, \vec{\mu}\, | \Psi_j >] \qquad - g\, Z^\alpha\, \mu_I \tag{23}$$

where R_I^α is the I Cartesian coordinate of atom α, Q is the total charge of the system, N the number of electrons, P_{ij} a density matrix element, Ψ_i and Ψ_j basis functions, Z^α the charge on atom α and μ_I the I component of the molecular dipole moment.
The derivatives of the integrals $< \Psi_i |\, \vec{\mu}\, | \Psi_j >$ are evaluated by using the recursive scheme of Obara and Saika [47].
By adding the term given in Eq. (23), and keeping the value of a_0 fixed, geometry optimizations can be performed at very little additional cost, compared to isolated molecule calculations.
In addition, by numerically differentiating the analytical gradients, the harmonic vibrational frequencies can be obtained.

3. The NH_3 + HCl $\leftrightarrow$ NH_4Cl reaction in vacuo and in solution

The reaction of ammonia and hydrogen chloride in the gas phase has been the subject of several studies in the last 30 years [56-65]. The interest in this system is mainly that it represents a simple model for proton transfer reactions, which are important for many chemical and biological processes. Moreover, in the field of atmospheric sciences, this reaction has been considered as a prototype system for investigation of particle formation from volatile species [66,67]. Finally, it is the reaction chosen as a benchmark on the ability, of quantum chemical computer simulations, to realistically simulate a chemical process, its reaction path and, eventually, its kinetics.

Since the first theoretical ab-initio prediction of the existence of a stable gaseous complex between HCl and NH_3, $NH_3 + HCl \leftrightarrow NH_4Cl$ [56], the interest has been focused on the nature of the stabilization. A number of theoretical and experimental studies have been carried out in order to establish the geometry of the equilibrium structure (or structures) of the complex and hence to define the character of the interaction as either ion-pair-like or H-bonded-like [56-65].

In 1952, when there was still no experimental evidence of a stable NH_4Cl gaseous complex, Mulliken [68] suggested that two types of stable structures should exist: an *inner* complex and an *outer* one separated by an energy barrier. To test these hypotheses, in 1967 Clementi [56,57] performed SCF-MO calculations and thermodynamical analyses and showed that, within the Hartree-Fock approximation, a single bound complex characterizes the potential energy curve of the approaching HCl and NH_3 without any barrier between the separated fragments and the complex. The estimated equilibrium structure resulted to be an H-bonded specie with a limited charge transfer character. Although quite advanced for that time, the SCF-MO calculations suffered from basis set truncation and neglect of correlation effects. Energy estimates related to these limitations were provided, in the spirit of the Multi- Configuration-Self-Consistent-Field theory (MC- SCF), which at the time was being rediscovered; it was concluded that the conclusion on a single minimum will remain valid even with post-Hartree-Fock simulations.

In 1968, Verhaegen and Goldfinger obtained the first experimental evidence of the complex formation from mass spectroscopic studies [58] and proposed a D_0 value between 5 - 15 kcal/mol against the value of 10 - 14 kcal/mol derived by Clementi from the computed D_e and the zero-point energy estimates. Analysing the IR spectra performed at 15 K in a N_2 matrix, Pimentel confirmed the H-bonded nature of the complex and estimated a value for D_0 in the range of 10 - 20 kcal/mol [59]. A substantial improvement in the theoretical study of this system was presented about 12 years after Clementi's work [61,63-65], and the new value of D_0 calculated falls in the range 5 - 9 kcal/mol; the computed complex nature is H-bond like. Recently, we have computed [69] the potential energy surface for the collinear C_{3v} approach with ab-initio (SCF, MP2, CASSCF, MR-CASSCF, CC) and DFT methods. All calculations predict a single minimum for the complex, corresponding to the hydrogen bonded structure. Inclusion of correlation corrections strongly influences the geometrical results; the most affected geometrical parameter is the N-Cl distance that ranges from 6.41 a.u. (CASSCF and SCF) to 5.61 a.u. (DFT-LDA, local density approxima-

tion), while the binding energy varies from 5.2-5.5 kcal/mol (CASSCF and SCF) to 19.1 kcal/mol (DFT/LDA). The MP2 result provides intermediate values for both quantities, namely D_0 = 11.6 kcal/mol and 5.91 a.u. for the N-Cl distance. These data show that the inclusion of correlation corrections predicts a closer interaction between the fragments and a small lengthening of the H-Cl bond. Although the experimental uncertainty is quite large, it is still possible to obtain very reliable data from the theoretical predictions; for this reason we have carried out Coupled Cluster computations, likely a very accurate approach, unfortunately computationally too expensive for medium size and for large chemical systems. Indeed the NH_3-HCl system represents today nearly the upper limit for its size. The Coupled Cluster binding energy is D_0 = 8.0 kcal/mol and the minimum corresponds to a N-Cl distance of 5.91 a.u. and a H-Cl distance of 2.46 a.u..

The experimental data by Pimentel were carried out in a Nitrogen matrix, and this calls for an analyses of the reaction with inclusion of environment effects. In addition, the system can be present in acqueous solutions. To assess the influence of the environment on the reaction, we have performed DFT calculations, using the Onsager's reaction field approach described in Section 2, with a value of ϵ=78.5, which corresponds to the dielectric constant of water. We have determined the full potential energy surface and found that the ion pair system becomes more and more stable, the larger the N-Cl distance. For intermediate N-Cl distances (at R(N-Cl) $\cong$ 6 a.u.) the potential energy surface has two minima separated by a very small barrier. The new minimum corresponds to the Mulliken "inner complex", namely in solution, we have the stabilisation of two charged species NH_4^+ and Cl^- . The Mulliken gross population analysis confirms this picture. Fig. 1 reports the potential energy surfaces for the two simulations; each curve is a cut of the potential energy surface for a fixed distance R(N-Cl), and it is obtained by varying the position of the hydrogen atom lying between the N and Cl atoms (see the geometrical display given in Fig. 2).

The curves in Fig. 1 correspond to a distance R(N-Cl) of 9.41, 8.41, 7.41, 6.41, 5.91, 5.41, 4.41 a.u., in going, orderly, from right to left. From the Figure, it can be seen that in the "solvent" case, the minima for each fixed R(N-Cl) distance are obtained for values of the R(N-H) distance smaller than the "vacuum" case.

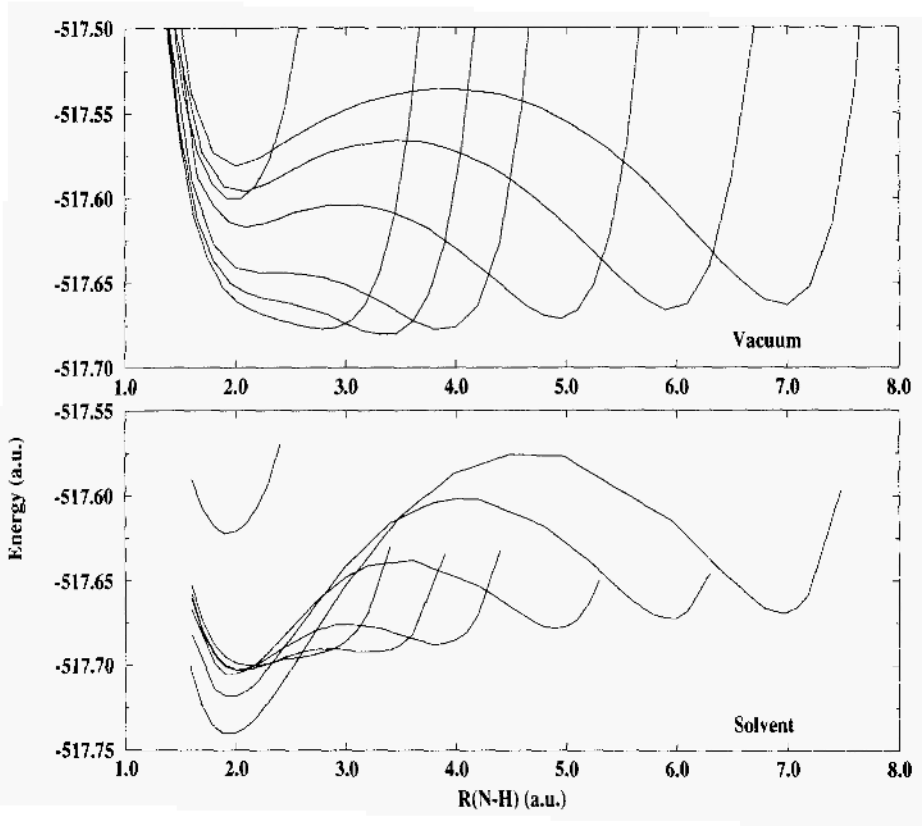

Figure 1. Potential energy curves for the reaction NH_3 + HCL ↔ NH_4C1. Each curve, corresponding to a fixed N-CI distance, is obtained by varying the position of the hydrogen atom lying between the N and Cl atoms. *Top:* calculations in vacuo. *Bottom:* calculations in solvent.

To mark clearly this behavior, in Fig. 2 we report the energy profile for a single N-Cl distance, fixed at R = 5.91 a.u.. From this figure, it is clear that for the "solvent" curve, the minimum occurs at about R(N-H) = 2.0 a.u., which corresponds to the complex $NH_4^+Cl^-$. The strong dependency from the surrounding of the potential energy surface for this system confirm a previous study [70] with MP2 reaction field; in that work it is shown that even a solvent with a low dielectric constant (ciclohexane, with ϵ =2), can alter substantially the energetics of the NH_4Cl system. We refer the reader to our NH_3-HCl paper for full details and for a study of the reaction for

$\in$ variation from $\in$=0 to $\in$ = 100 [69]. Here, we observe only that in the interval $\in$ = 0 to $\in$ = 10, the solvent effect is substantial, as discussed, whereas from $\in$ = 10 to $\in$ = 100 the effect varies more slowly that expected in passing from a solvent nearly non polar to a strongly polar one.

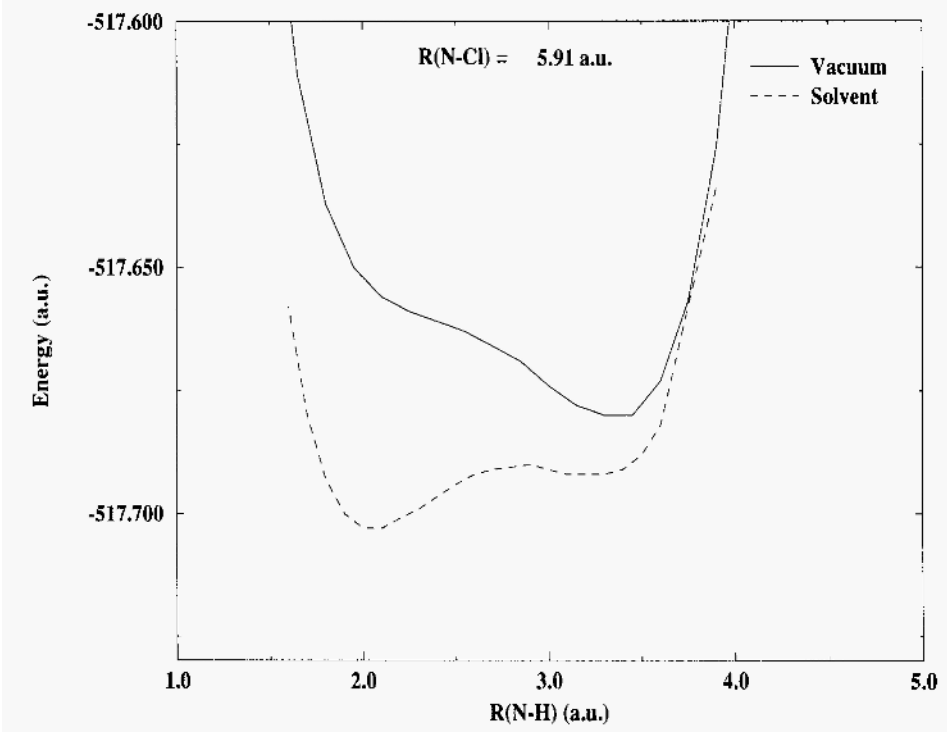

Figure 2. Potential energy curves for the reaction NH_3 + HCL $\leftrightarrow$ NH_4Cl. The curves are for fixed N-Cl distance, R(N-Cl) = 5.91 a.u., and variation of the H positions.

We have performed also a reaction field DFT/Molecular Dynamics simulation of this system. We found that after an initial time, when the complex oscillates within the cage at R(N-H) $\approx$ 2.0 a.u. and R(N-Cl) $\approx$ 6.0 a.u., a small temperature variation is enough for allowing the complex to overcome the small energetic barrier and, with time, the distance between Cl^- and the NH_4^+ fragments starts to increase. Extrapolating to a real solution environment, the two fragments will be completely surrounded by water molecules, i.e. in a solution at infinite dilution the two ions are fully solvated.

4. The Li^+ ion in solution and in water clusters

Accurate thermodynamical data for the gas phase reaction

$$Ion \cdot (H_2O)_{n-1} + H_2O \leftrightarrow Ion \cdot (H_2O)_n \tag{24}$$

have been determined experimentally for both positive [71] and negative [72] ions since 1970. The first effort to describe theoretically the gas phase hydration of ions [73] was phenomenological and ignored the detailed nature of molecular interactions by treating the water molecule as a continuous fluid with a uniform dielectric constant, following essentially the Born theory [1].

In order to account for the behavior of ion-water clusters at a molecular level, one can follow different strategies. One strategy would be to use, for the water-water and ion-water interactions, potential functions with parameters either empirically adjusted to fit the available experimental data or adjusted to fit ab-initio data. An alternative strategy would be to simulate directly the cluster at the ab-initio level. In 1972, the potential energy surface for a single water molecule interacting with a Li^+ cation was reported [74], and using those data the heat of formation of the ion-water complex was determined [75]; the computed value, 34.13 kcal/mol, was in good agreement with the experimental value [71] of 34.00 kcal/mol.

After this computer experiment, a great number of papers followed. Some of them attempted to simulate with the ab-initio data the properties of the ion in solution at room temperature [76,77], others [78] attempted to determine, via Monte Carlo simulations, the free energy, enthalpy and entropy for the reaction (24). The discrepancy between experimental and simulated data was rationalized in terms of the inadequacy of a two-body potential to represent correctly the n-body system. In addition, the radial distribution function for the $Li^+(H_2O)_6$ cluster showed [78] only one maximum, pointing out that the six water molecules are in the first hydration shell of the ion. The Monte Carlo simulation [77] for the system $Li^+(H_2O)_{200}$ predicted five water molecules in the first hydration shell. A subsequent MD simulation [79] of a system composed of one Li^+ ion and 343 water molecules at T=298 K, with periodic boundary conditions, yielded

the pair correlation functions reported in Fig. 3.

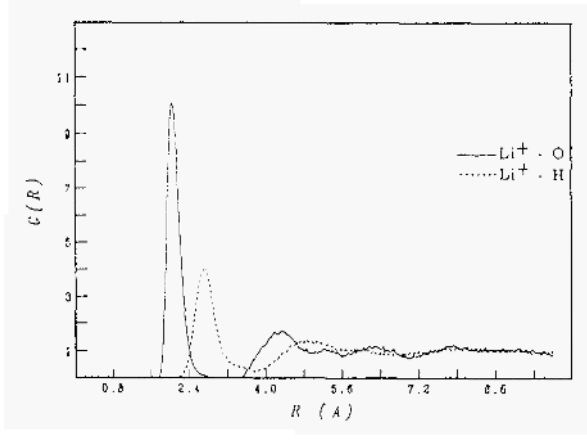

Figure 3. Li^+-O and Li^+-H pair correlation function determined from a MD simulation of a Li^+ surrounded by 343 water molecules, at T=298 K, using 2-body potentials.

Integration of the Li^+-O pair correlation function (see Fig. 4, curve labeled 2-body) shows that in the first hydration shell the Li^+ is surrounded by 6 water molecules.

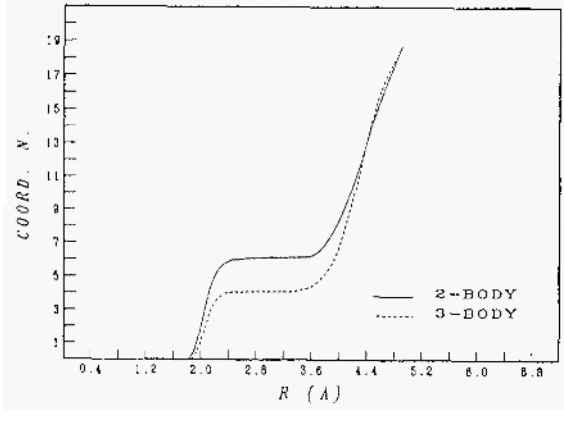

Figure 4. Coordination number for the Li^+-water solution obtained from a MD simulation using 2-body potentials (continuous line), and using 3-body potentials (dashed line).

The shortcoming of the pair-wise 2-body potential was eliminated by determining an analytical function which included 3-body corrections for both the interactions ion-water-water [80] and water-water-water [81]. A MD simulation at T=298 K of a Li^+ surrounded by 343 water molecules with periodic boundary conditions, with the 3-body corrections included yielded the pair correlation functions reported in Fig. 5. The integration of the Li^+-O pair correlation yields the curve labeled 3-body of Fig. 4, where it is evident that the ion has a coordination number of 4 in liquid water, in agreement with x-ray experimental data [82]. Recently, we have revisited once more the $Li^+(H_2O)_n$ clusters, with n from 1 to 6. Using the 2-body and the 3-body interaction potentials, we have performed Monte Carlo geometry optimizations for each cluster, constraining the bond lengths and bond angle of the water molecules at the gas phase experimental values. The results are summarized in Table I.

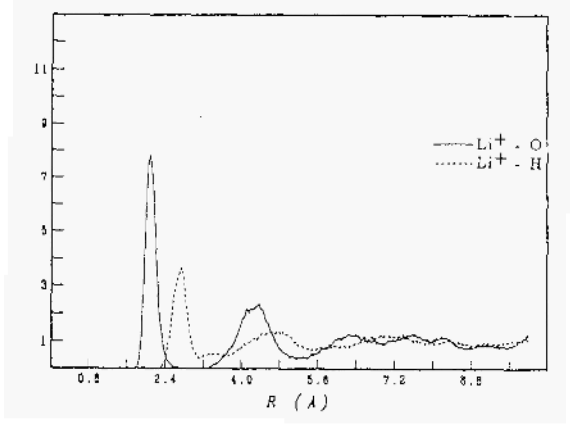

Figure 5. Li^+-O and Li^+-H pair correlation function, determined from a MD simulation of a Li^+ surrounded by 343 water molecules, at T=298 K, using 3-body potentials.

From the data in Table I it is clear that the potential with the 3-body corrections yields lower values for the interaction energies, and (not reported) larger ion-water distances. In addition, for n=5 and n=6 we find, respectively, one and two water molecules in the second solvation shell, whereas the 2-body potential gives one water molecule in the second shell

only for n=6.

TABLE I. Interaction energies (in kcal/mol) per water molecule for the clusters $Li^+(H_2O)_n$.

n	2-body	DFT	3-body	DFT
	ΔE	ΔE	ΔE	ΔE
1	-34.3	-33.9		
2	-32.2	-31.3	-31.4	-30.2
3	-30.6	-23.8	-27.9	-24.5
4	-28.5	-21.4	-24.9	-21.4
5	-27.8	-17.8	-22.9	-20.3
6	-25.3	-17.4	-21.0	-18.6

Starting from the Monte Carlo optimized geometries, we have performed geometry optimization at the DFT level. Now, by definition, the n-body corrections are fully taken into account and the systems are ”free” to relax to their closest minimum. Using as starting points the configurations obtained with the 2-body potential we obtain, per water molecule, the interaction energies reported in Table I, column 2, whereas, using as starting point the minimum configurations from the 3-body potential, we obtained the results of Table I, column 4.

Let us make a comment on the DFT results. As it is known, all minimization techniques are biased by the starting point. Starting from a given atomic arrangement, the closest minimum is reached, and this is generally a local minimum, not the absolute one, since for systems with many degrees of freedom it is difficult to overcome energy barriers. The DFT results of Table I, clearly point out this shortcomings. The results obtained using as starting point the 2-body potential configurations show almost an energy degeneracy for the clusters with n=5 and n=6, whereas those obtained using as starting point the 3-body potential configurations seem more realistic.

In Table II, we report the enthalpy of formation at T=298 K, for the reaction (24). The results obtained with the 3-body potential are in good agreement with the experimental data of Ref. [71], whereas those obtained with the 2-body potential are only in qualitative agreement (the trend is

correct). Notice that, for n=5, the 2-body yields the same enthalpy change as the 3-body potential, but as pointed out the two potentials do not agree with the number of water molecules in the first hydration shell.

TABLE II. Enthalpy changes for reaction (24) (in kcal/mol) at T=298K

n	2-body	3-body	DFT	Expt.
1	-33.5		-32.7	-34.0
2	-31.0	-26.5	-26.4	-25.8
3	-26.5	-18.9	-9.1	-20.7
4	-21.8	-14.2	-9.7	-16.4
5	-12.3	-12.4		-13.9
6	-11.0	-10.2		-12.1

The DFT results of Table II (which include the zero point energy correction) have been computed by considering the lowest values of the two sets of Table I. The results are clearly good for n=l and n=2, but wrong for higher n; a clear indication that the minima we have reached are far from being close to the absolute ones. Therefore, the question remains whether for n=5, one water molecule is in a second hydration shell.

Starting from a Li^+ surrounded by 5 water molecules (all in the first solvation shell), we have started a DFT Molecular Dynamics simulation, with a time step of 0.5 femtoseconds. In Fig. 6 we report a plot of the system at four different times. To better visualize the evolution of the cluster geometry, we have drawn, in Fig. 6, a fictitious bond between the ion and the water oxygen, if the distance is below 2.535 $\mathring{A}$.
Inset a) refers to the starting configuration, t=0 fs, with the 5 water molecules in the first hydration shell. Inset b) refers to t=70 fs; some rearrangement starts to occur, especially for the left most water molecule. At t=110 fs (inset c)) one ion-water distance is above the threshold value, the water starts to leave the first hydration shell. Finally, at t=210 fs, one water molecule is in the second hydration shell and the remaining four

water molecules assume a tetrahedrical configuration around the ion.

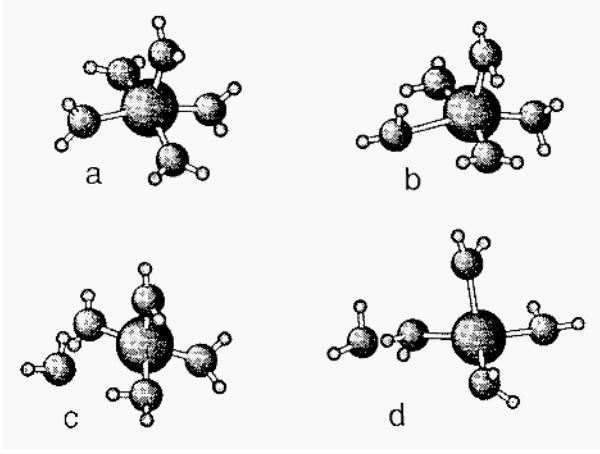

Figure 6. Four frames of a DFT Molecular Dynamics simulation for $Li^+(H_2O)_5$, showing the evolution in time of the system: a) The starting configuration at t = 0. b) The system at t = 70 fs. c) The system at t = 110 fs. d) The system at t = 210 fs.

5. The water clusters in vacuo and within the liquid

Small clusters of water molecules have been the subject of a large number of theoretical studies in the last 25 years [83-88]. Since the early ab-initio computations [83], it was clear that, the larger the cluster, the larger the number of energetically closely spaced energy minima. For clusters with up to six water molecules, the combination of Monte-Carlo minimizations and ab-initio computations with reliable basis sets, pointed out [83] the existence of cyclic structures, which were assumed to be either the lowest or near to the lowest energy. Later [84], the water clusters were revisited and it was confirmed that the cyclic structures correspond to the lowest energy minima for small clusters, whereas large clusters have 3-D characterization. Today, structural and vibrational determinations of water clusters are the object of studies, because of the importance of these systems for understanding hydrogen bonding, which in turn plays a key role on many chemical and biological problems. Furthermore, additional motivations are

either the existence of experimental information based on spectroscopic studies of clusters [89-91], which complements the theoretical calculations through experimental- theoretical feed-back, or the development of models of liquid water based on the existence of discrete clusters-like structures in the bulk [92-93].

As it is now very well known, accurate studies of the water-water interaction by means of ab-initio techniques require the use of larger and flexible basis sets and methods which consider correlation effects [85,94-96]. Since high level ab-initio post-Hartree-Fock calculations are unfeasible because of their high computational cost for systems with many degrees of freedom, Density Functional Theory, more economical from the computational point of view, is being more and more considered as a viable alternative. Recently, we have presented [97] results of structural parameters and vibrational frequencies for the water clusters $(H_2O)_n$, n=2 to 8, using the DFT method with gradient corrected density functionals.

The results obtained using the Perdew and Wang [40] functional for the exchange and that of Perdew [39] for the correlation, and a good size basis set (with three polarization functions on the oxygen and hydrogen atom), show good agreement with results obtained with high level ab-initio approaches, like MP2 and MP4. We have optimized 8 different structures for the clusters $(H_2O)_n$, with n=2 to n=8, obtaining local minima, i.e. each optimized structure is characterized by not having imaginary frequencies in the harmonic vibrational spectrum. For the systems with 1,2,3,4,5 water molecules we are confident to have obtained absolute minima. The final geometries are reported in Fig. 7.

We observe the following trends, in the cluster's geometrical parameters; the O-O distances decrease as the number of molecules increases, from a value of 2.907 *Å* in the dimer to a value of 2.705 Å in the hexamer. On the contrary, O-H bond lengths increase (if the H atom is hydrogen bonded) with increasing number of molecules, from 0.981 *Å* in the dimer to 1.000 *Å* in the hexamer. Both these trends appear to be very near to convergence for the hexamer, and thus we expect no further modifications for these parameters in larger cyclic water clusters. In all the clusters under consideration in this work, the O-H bond length has constantly the value

of 0.971 Å, if the H atom is not hydrogen bonded.

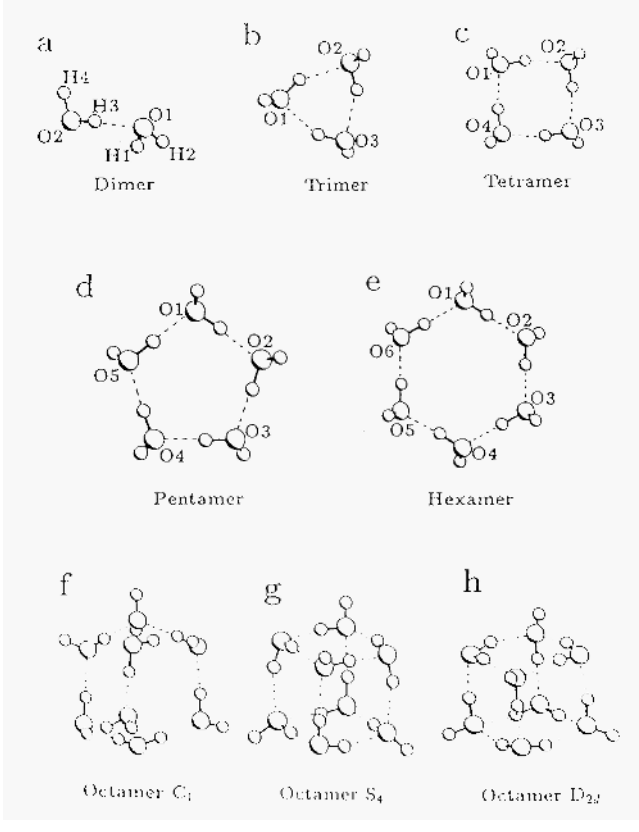

Figure 7. Minimum geometrical configurations for selected water clusters, as resulting from DFT calculations.

The binding energies, including BSSE and ZPE corrections for all the clusters studied, are collected in Table III, along with the average O-O distances. Since for the clusters with 8 water molecules, the number of h-bonds is not constant, information on this is also given.

As often pointed out, it is apparent from the results that non-additive effects are very important, since the results deviate strongly from linearity. The harmonic vibrational data compare well with experimental anharmonic results, when available (see Fig. 8).

TABLE III. For each water cluster we report in the first column the number of hydrogen bonds, in the second column the binding energies (in kcal/mol) including ZPE and BSSE corrections, and in the third column the average O-O distance (in $\AA$).

	h-bonds	ΔH^0	R(O-O)
$(H_2O)_2$	1	-3.53	2.91
$(H_2O)_3$	3	-12.71	2.78
$(H_2O)_4$	4	-24.18	2.73
$(H_2O)_5$	5	-32.13	2.71
$(H_2O)_6$	6	-39.88	2.70
$(H_2O)_8$ (C_1)	9	-55.18	2.64 - 2.79
$(H_2O)_8$ (S_4)	12	-64.06	2.68 - 2.79
$(H_2O)_8$ (D_{2d})	12	-63.51	2.67 - 2.83

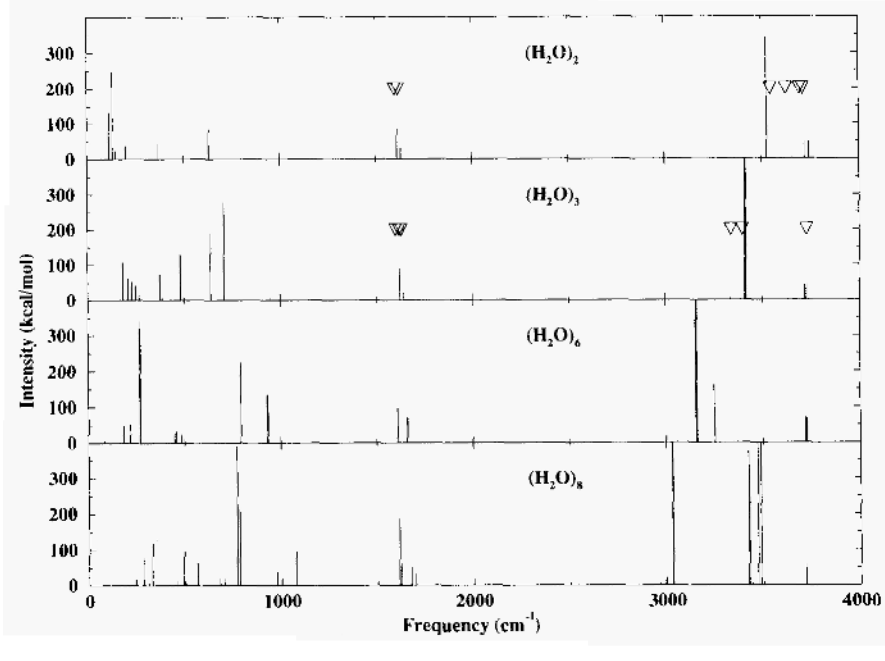

Figure 8. Computed IR frequencies for the some of the water clusters of Fig. 7. The ∇ symbol indicates the position of experimental frequencies.

Following the trends observed in some geometrical parameters, vibrational frequencies show themselves regular shifts, when passing from small to large clusters.

The asymmetric stretching mode, $\nu 3$, calculated to have a frequency equal to 3752 cm^{-1} for the isolated water molecule, shows an increasing red shift, with increasing number of molecules, and for the hexamer the average value of the six $\nu 3$ intramolecular modes is 3720 cm^{-1}. Furthermore, this mode looses, upon clusterization, the character of "asymmetric stretching", resulting in a more and more pronounced stretching of the $O\text{-}H_{free}$ bond solely. Analogously, the $\nu 1$ symmetric stretching mode transforms itself in a $O\text{-}H_{bonded}$ stretching, and reduces its frequency from the value of 3664 cm^{-1} for the water monomer, to an average value of 3180 cm^{-1} in the hexamer; differently from the $\nu 3$ modes, the values of the $\nu 1$ stretchings are spread over a large interval, while the $\nu 3$ frequencies are restricted to a much smaller range of values, indicating possibly a different degree of coupling between the vibrations. The bending modes, $\nu 2$, suffer, upon cyclic clusterization, a blue shift of several cm^{-1} and the values cover a range wider and wider, up to an interval of $\approx$ 70 cm^{-1} for the hexamer. Analogous modifications can be found in the octamers' vibrational frequencies; in addition, the frequencies corresponding to vibrational modes of the double hydrogen donor molecules appear.

Let us now compare with the situation in solution and let us start from a single water molecule. In Table IV we summarize gas phase and solution results. The DFT values show good agreement with the experimental data for the dipole moment [98] and frequencies [99-100] (if we compare computed harmonic values with experimental anharmonic values); regarding the geometry, the value of the bond angle is in excellent agreement with the experimental data [101], but the computed bond length is 0.015 *Å* longer. Let us now comment on the "solution" results, i.e. the water molecule within the liquid. If the liquid is simulated with the reaction field model, discussed in section 2, we obtain a water molecule which appears to be slightly different from the gas phase, but far from the experimental molecule in the liquid. Analogous results have been obtained in Ref. [102] using, however, the MP2 method. The changes with respect to the gas phase are in the DFT approach 0.001 *Å* for the bond length and -0.9 degree for the bond angle; the MP2 computations [102] report a corresponding value of 0.003 *Å* and -0.25 degree.

TABLE IV. Properties of the water monomer in gas phase and in solution. Distances in *Å*, angles in degrees, dipole moment, μ, in Debyes, frequencies in cm^{-1}.

	gas phase		liquid phase		
property	DFT	Expt.[a]	DFT solvent	MD[b] T = 305 K	Expt. T = 298 K
d(O-H)	0.972	0.9572	0.973	0.978	0.98[c] 0.97[d]
∠ HOH	104.7	104.52	103.8	101.1	105.5[c] 102.8[d]
μ	1.855	1.855	2.022	2.66	2.6[e]
Sym. Stretching $\nu 1$	3664	3657 3832[g]	3653	3626[f]	3400[f]
Asym. Stretching $\nu 3$	3752	3756 3942[g]	3732	3690[f]	
Bending $\nu 2$	1613	1595 1649[g]	1622	1750[f]	1650[f]

a) Ref. [98-102].
b) The same model potential gives, for the gas phase water molecule, d(O-H) = 0.9572, ∠ HOH = 104.59, $\nu 1$ = 3846, $\nu 3$ = 3955, $\nu 2$ = 1685 cm^{-1} (harmonic frequencies).
c) Ref. [103].
d) Ref. [104].
e) Ref. [105].
f) Ref. [106].
g) harmonic values from Ref. [99].

The results reported in the column MD have been obtained [107] from a Molecular Dynamics simulation at T=305 K using an analytical polarizable and flexible potential, parametrized against ab-initio computations. Regarding the water geometry in the liquid, two sets of experimental data have been proposed [103,104], both report a lengthening of the O-H bond length, but Ref. [103] proposes a widening of the bond angle and Ref. [104] a narrowing. Our MD simulation predicts a lengthening of the O-H bond (+0.021 *Å*) and a narrowing of the bond angle (-3.4 degrees), whereas

the DFT-solvent and MP2-solvent [102] results predict smaller changes for both quantities. The dipole moment of the water molecule within the liquid changes drastically, with respect to the gas phase. The MD simulation predicts a value in agreement with the experimental data, whereas the DFT-solvent computation predicts a too small change, but in the right direction, as the MP2 method [102], which however gives a too high value for the gas phase, an indication of basis set deficiency. Let us now consider the stretching and bending modes. Experimentally [106] has been found an up shift of 55 cm^{-1} for the bending mode (comparing the liquid with the gas phase) and a down shift of ≈ 300 cm^{-1} for the stretching modes (experimentally, $\nu 1$ and $\nu 3$ are not resolved). The MD simulation [108] predicts an up shift of ≈ 65 cm^{-1} for $\nu 2$ and down shifts of 220 cm^{-1} and 261 cm^{-1} for $\nu 1$ and $\nu 3$, respectively. The DFT-solvent model predicts modest down shift for the stretching frequencies (-11 and -20 cm^{-1} for $\nu 1$ and v3, respectively) and modest up shift (+9 cm^{-1}) for the bending. Again the qualitatively directions of the shifts are correct, but quantitatively the results are unsatisfactory.

We must warn on the fact that in Table IV, we have reported, for the liquid experimental and MD results, the frequencies corresponding to the maximum positions of the bending and stretching bands, which, because of thermal disorder, are quite broaden; in addition the two sets of data present also librational and translational modes, not discussed here.

Within the liquid, each water molecule is both a ”solvent molecule” and a ”solute molecule”; at the same time, each water molecule is part of a network. Indeed, we can view the solvation shell as a time-averaged representation, resulting by considering a given water molecule as fixed in space with its neighboring molecules librating around it; the librations are, however, motions which are transmitted through the network. In Ref. [109] we have focused our attention on specific pathways formed by hydrogen bridges, i.e. ”structures” which can be obtained by following a specific path once some predefined rules and constraints are selected. At each time step in our simulation, each water molecule belongs to a ”cyclic structure”, which is defined by the following rules: starting with one of the two OH bonds, one moves to the nearest hydrogen-bridged water, then to the next one, satisfying the condition that among different pathways one selects the one which will close the pathway on the starting water molecule. Notice that ”by construction” we search for ”cyclic structures” purely on geometrical grounds, neglecting both energetics and lifetime conditions (for

this reason, we have used the old notation ”hydrogen bridge” rather than ”hydrogen bond”). In the above selection rule, the operational definition for the existence of a hydrogen bridge is that a hydrogen atom must exist between two oxygen atoms. In the search and count of the polygons, we count *all* possible closed circuits, eliminating, however, those large polygons which contain all the atoms of small ones.

We have carried out a detailed analysis for studying the abundance and stability of the cyclic structures, in function of the temperature [109]. Our study predicts that at all temperatures, the five member rings are the most abundant, followed by the 6, 4, 7 and 3 member rings. The lifetime of these polygons is very short and with almost no temperature dependence. In addition, if we analyze for the cyclic polymers $(H_2O)n$ the average O-O distance as a function of temperature, we found that the trimers have the largest O-O distances, followed by the tetramers and then by larger polygons. Whereas for the trimers the distance remains almost constant for all the temperatures, the O-O distance of the larger polymers have a strong temperature dependence, which approaches the value of ice. Comparing these distances with those of the clusters in gas phase (see Table III), we find for the trimers in the liquid an average O-O distance of 2.90-2.92 $\AA$, of the same order than the gas phase. Larger differences are found for the other clusters: in the gas phase the distances are in the range 2.63-2.77 $\AA$, in the liquid phase 2.77-2.87 $\AA$.

Let us now analyze the vibrational spectrum. In Fig. 9 we report (for T=305 K) the density of states for the full liquid water sample (curve marked as total) and those belonging to three-, four-, five- and six-member polygons within the liquid. The dotted vertical lines in Fig. 9 refer to the stretching and bending of the gas phase water molecule. As evident from the figure, for all polygons there is a red shift for the stretching frequencies and a blue shift for the bending frequency, but no substantial difference from the total sample. In other words, within the liquid, the water molecules belonging to a polygon of a given size are equal to those belonging to a smaller or larger polygon. This is contrast to the findings of Fig. 8.

Let us now build up an imaginary liquid formed by the clusters of Fig. 7. The IR spectrum of such a system is reported in Fig. 10, where the vertical dotted lines refer to one single molecule for the gas phase. As for the data in Fig. 9, we observe a red shift for the stretching frequencies and

a blue shift for the bending. Notice that we cannot compare the absolute intensities of Figs. 9 and 10, since the former refers to the density of states in arbitrary units and the latter to the simulated IR spectrum; with this in mind we can only compare the frequency positions. In Fig. 10 a set of frequencies fall in the same region as the asymmetric stretching of the gas phase water molecule. This feature is absent in tha data of Fig. 9; namely, for the cluster in vacuo, there are free hydrogen atoms not present in the polygons within the liquid.

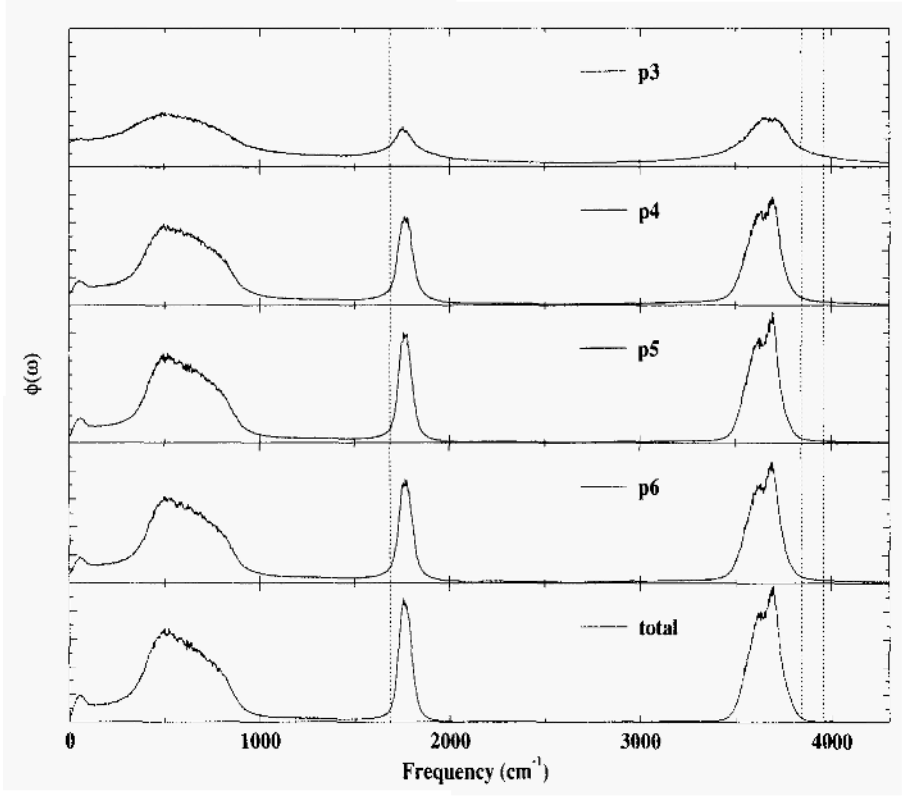

Figure 9. Density of states of a water sample, referring to three-, four-, five- and six-member polygons and to the total of the sample (from top to bottom), as resulting from MD simulation, T=305 K. Dotted lines indicate vibrational frequencies for a single water molecule in gas phase.

We have also analysed the liquid in terms of 3-D clusters, and we have found that the most abundant structures, for all the considered temperatures, are those in which one water molecule is hydrogen bonded to

four additional water molecules (tetra-coordination), followed by the three-coordination and penta coordination. The lifetime of the tetra-coordinated water molecules is the longest (on the order of the picosecond). For these 3D-clusters we report in Fig. 11 the density of states. Again, the curve labeled as total refers to the full sample and the vertical dotted lines to the water molecule in gas phase. The curves labelled as 2, 3, 4, and 5 belong to water molecules bi-, three-, tetra- and penta-coordinated. Notice that now we have differences in the stretching region of these spectra. In particular the bi- and three-coordinated water molecules show frequencies close to the gas phase value.

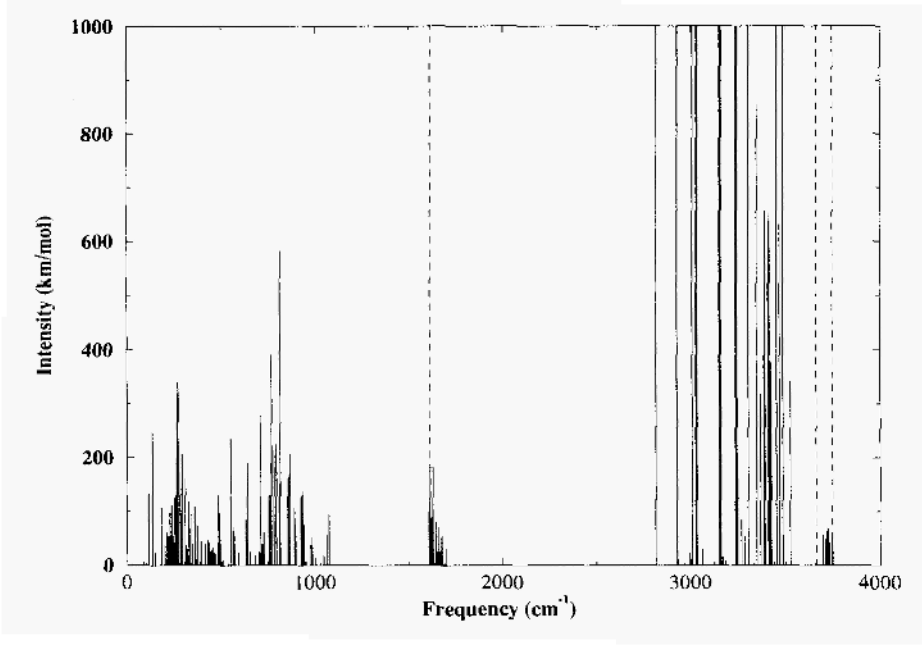

Figure 10. Simulated IR spectrum of a liquid formed by the water clusters of Fig. 7, as resulting from DFT calculations. Dashed lines indicate vibrational frequencies of an isolated water molecule.

The resulting overall picture of liquid water is that of a very dynamical "macromolecular" system, where clusters of different size and structure coexist in different subvolumes of the liquid and each has characteristic lifetimes and specific temperature dependences. In our opinion, if we would

regard the liquid as formed by polygons (equivalent to those most stable structures found in the gas phase), then we would have a liquid more static in time, the only freedom associated to the individual water molecules would be inter- and intra-molecular vibrations and librations, with limited translational possibilities. Therefore, by considering water as a liquid, one should favor the 3-D clusters, whereas water as a solvent can nicely make use of ”polymers” as building blocks, to build cages around the solute.

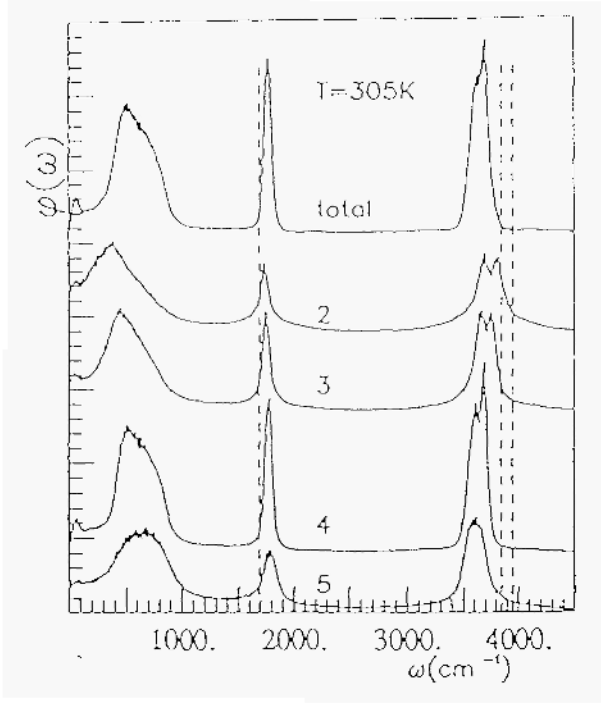

Figure 11. Density of states of a water sample, referring to two-, three-, tetra- and penta-coordinated 3D clusters and to the total of the sample, as resulting from MD simulation, T=305 K. Dotted lines indicate vibrational frequencies for a single water molecule in gas phase.

6. DNA bases and base-pairs

Intermolecular interactions play a dominant role in the structure and dynamics of DNA [110]. Among these intermolecular interactions, the hydrogen bonds between base pairs are of interest since represent an intermediate step between strong intramolecular bonds and typically weak intermolecular interactions. In addition, even if the stability of the DNA and RNA helixes is mainly due to steric, dispersive and electrostatic interactions, the hydrogen bonds provide the specificity needed to achieve high levels of fidelity during replication and transcription. Therefore, the understanding of these interactions is most important [111-113]. It is very well known that quantitative determination of the structure and binding energies of the pair bases are computationally very demanding [114-116], since high level electron correlation corrections, associated with basis sets of good quality, are required to obtain a proper description of both the structure and binding energies of these systems. The use of correlated methods has been often limited to single point calculations of structures optimized at a lower level of theory, i.e HF. However, it is well known that the Hartree-Fock geometries can deviate considerably from experimental results in gas phase; it is necessary to perform post-Hartree-Fock geometry optimizations to obtain niore satisfactory agreement with the experimental structures [117]. Here, we report simulations obtained with the DFT for the study of the structure, binding energy and infrared spectrum of the C-G and A-T DNA base pairs, and we compare these results with those obtained with ab-initio calculations (HF and MP2) and with available experimental data.

6.1 GEOMETRIES AND BINDING ENERGIES

Full geometry optimizations have been carried out for the 9-methyladenine (A), 1-methylthymine (T), 1-methylcytosine (C), and 9-methylguanine (G) bases at both the HF and the DFT levels, using double zeta quality basis sets augmented with polarization functions for all the atoms. The two methods yield similar results: the main difference is in the heteroatom-hydrogen bond lengths, which are systematically longer in the DFT calculations. In addition, computations with the reaction field method have been done at the DFT level. All the DFT calculations have been performed both with the Perdew and Wang exchange functional [40] and with the Becke

exchange functional [42], (in both case, the Perdew correlation functional [39] has been used). Since the two functionals yielded essentially the same range of values, in the Tables we report only the values obtained with the Becke exchange functional.

The geometry optimization of the complexes AT and CG (depicted in Fig. 12), reflects a more delicate issue than the single bases; a reliable determination requires performing the optimization with methods which take into account the correlation energy.

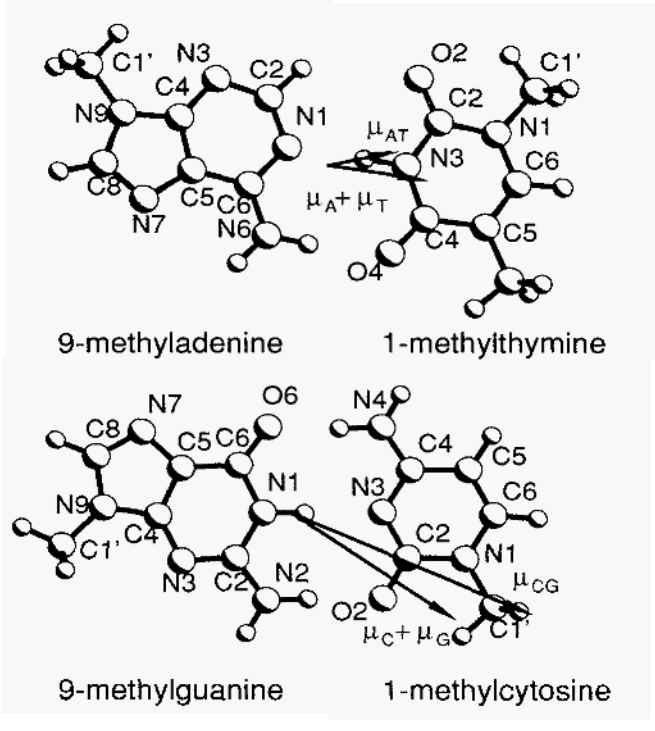

Figure 12. Methyladenine - Methylthymine (AT) and Methylcytosine - Methylguanine (CG) base pairs. The dipole moments of the isolated bases and of the base pairs are also shown.

A comparison of the hydrogen bond lengths obtained from the DFT and HF methods, and from X rays experimental data [118-119] is reported in Table V.

TABLE V. Optimized hydrogen bonds distances for the AT and CG complexes (Å)

Base pair	Bond length	HF	DFT	DFT-solvent	Expt.[a]
AT	r(N6O4)	3.08	3.00	3.01	2.95
	r(N1N3)	2.99	2.92	2.92	2.82
CG	r (O6N4)	2.92	2.83	2.84	2.91
	r(N1N3)	3.05	2.99	2.98	2.95
	r (N2O2)	3.00	2.91	2.90	2.86

[a] Ref. [118].

It can be seen that the DFT method, which includes the correlation energy contribution in the optimization processes, yields an optimized geometry closer to the experimental values than the HF optimization. The solvent effect has a minor influence on these geometrical parameters, at least in the reaction field approach; the computations do not evidence any significative effect on the hydrogen bond lengths, the only observable change is in a slight shortening of two hydrogen bonds in the CG pair.

The interaction energies for the AT and CG complexes have been evaluated at the HF level using the HF optimized geometry, at the MP2 level rising the HF and the DFT optimized geometry and at the DFT-reaction field optimized geometries. The interaction energy has been evaluated as the difference in the energies of the optimized complex and individual bases, i.e.

$$\Delta E = E(X...Y)_{op} - E(X)_{op} - E(Y)_{op} \tag{25}$$

The corrections for basis set superposition errors (BSSE) with the counterpoise correction are still a controversial issue [120-122]. However, some type of correction is needed for calculations on systems with weak interactions. It has been proved that only considering the BSSE meaningful results can be obtained on large systems [122]. Of course, by using good quality basis sets the BSSE is less troublesome and the results obtained can be accepted, readily, as reliable. The BSSE in DFT calculations is less important than in conventional ab-initio calculations. We compute the counterpoise correction as:

$$BSSE = E(X) + E(Y) - E[X(Y)] - E[Y(X)] \quad (26)$$

where $E(X)$ and $E[X(Y)]$ represent the energies of molecule X at the geometry of the optimized complex, computed with its own basis set and the basis set of the whole complex, respectively. The corrected interaction energy can be written as:

$$\Delta E_{bsse} = \Delta E + BSSE \quad (27)$$

In order to compare the computed results with those obtained from the experiment, the interaction enthalpy at 0 K has to be evaluated. The interaction enthalpy, ΔH, differs from the ΔE by the change in the zero point energies, ΔZPE, between the complex and the isolated subsystems.

$$\Delta H = \Delta E_{bsse} + \Delta ZPE \quad (28)$$

A summary of our results is given in Table VI. At the HF optimized geometries, the CG interaction energy corrected by BSSE and ΔZPE is close to the experimental value, while the AT result is too low. The MP2 results for both pairs are very good, however this must be considered a fortunate coincidence, since we found inconsistent intermediate results: a) negative reorganization energies for G and T (the reorganization energy is defined as the difference in energy between the base in the geometry of the base pair and of the isolated base) and b) energies at the DFT geometry lower than at the HF geometry, an indication that the HF geometry is not a minimum for MP2. These two observations indicate clearly that the MP2 lowest energy configurations are far from the HF ones and closer to the DFT geometries. Performing MP2 calculations at HF optimized geometries is a very common procedure, but in this case our calculations point out that even if the results appear as good, the validity of the whole procedure must be analyzed critically.

Let us now consider the reaction field results; it can be seen that the solvent effect on the energetics is to reduce the strength of the bonding, for both the base pairs. The binding energies for AT is reduced by 1.5 kcal/mol. More pronounced is the change for CG binding energy, which is

reduced by 7.5 kcal/mol. These changes are due to the different solvation energies exhibited by the isolated bases and by the pairs, that is, the solvation energy of a pair is smaller than the sum of the solvation energies of the isolated bases.

TABLE VI. Interaction energies for the AT and CG complexes evaluated with different techniques (in kcal/mol).

Method	AT	CG
HF/HF[a]	11.7	26.1
HF/HF[b]	9.5	23.5
HF/HF[c]	6.6	19.5
MP2/HF[a]	17.5	31.8
MP2/HF[b]	15.5	25.7
MP2/HF[C]	12.6	21.7
MP2/DFT[a]	17.8	32.1
MP2/DFT[b]	12.3	25.3
MP2/DFT[c]	9.4	21.3
DFT/DFT[a]	14.1	26.5
DFT/DFT[b]	13.1	26.4
DFT/DFT[c]	10.2	22.2
DFT solv/DFT solv[a]	12.6	19.0
Expt. [d]	13.0	21.0

[a] Results obtained using optimized fragment energies (Eq. 1).

[b] Results obtained including BSSE (Eq. 2).

[c] Results obtained including BSSE and the estimation of the change in zero point energies given in Ref. [114].

[d] Refs. [118-119].

Since one major component of the base pair interactions is of electrostatic nature, dipole moments were calculated at the HF and DFT levels for the isolated fragments and the complexes (Table VII). By proceeding from the isolated bases to the base pairs there is a change in the magnitude and direction of the resultant dipole moment. The HF results point out that for the CG pair, there is an increment of 1.42 D (27.6 %) and a rotation of 11.1º,

whereas for the AT pair, a decrement of 0.49 D (18.6 %) and a rotation of 20.5° are observed, The DFT computations yield equivalent magnitudes. The magnitude changes cannot be accounted by charge transfer effects. In fact the Mulliken population analysis shows that upon formation of the CG pair, there is a net charge transfer of only 0.024 e^- from cytosine to guanine. In the AT pair the charge transfer is 0.003 e^- from adenine to thymine. According to the differences in the dipole moment orientations (Fig. 12) from the individual bases to the complexes it can be seen that the binding energy is not determined simply by dipole-dipole interactions, but also by induced dipoles - induced dipoles interactions, therefore polarization effects seem to play an important role in the base pairing.

Inclusion of the reaction field method gives the same picture; indeed, the dipole moments are simply enhanced in magnitude, but their orientation is not changed, neither in the isolated bases nor in the pairs.

TABLE VII. Calculated dipole moments for the individual bases and the AT and CG complexes (in Debyes).

Molecule	HF	DFT	DFT-solvent
Adenine (A)	2.54	2.68	3.62
Thymine (T)	4.88	4.79	6.08
AT	2.15	1.61	2.31
Cytosine (C)	6.76	6.21	8.00
Guanine (G)	7.41	7.33	9.85
CG	6.55	6.34	9.63

6.2 VIBRATIONAL ANALYSIS

The harmonic vibrational infrared spectrum of the four bases, as well as of the two base pairs, has been calculated at the DFT and DFT-solvent level of theory by finite differentiation of the forces acting on atoms along the normal coordinates. In the following, we briefly analize the results, which

are partially sketched in Figs. 13-16.

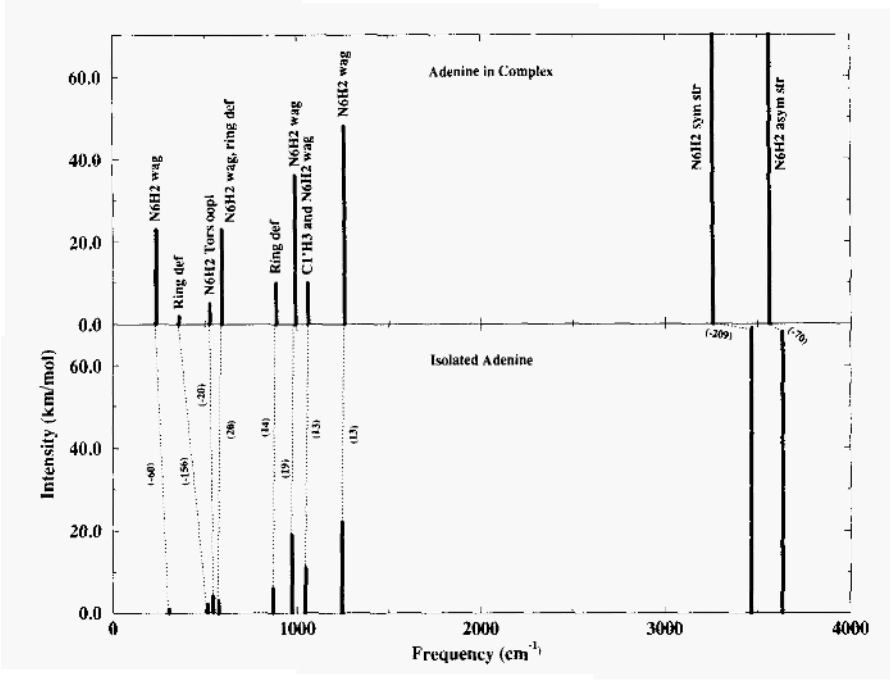

Figure 13. Selected frequency assignments for methyladenine, both in complex (top) and isolated (bottom). The values of the shift due to complexation are also given.

In general, we did found some difficulties in the assignments of the modes, particularly of the low-frequency ones.

For the isolated 9-methyladenine (see Fig. 13), largely recognizable are the stretching and bending modes of the amino group, while modes of the CH_3 group are usually coupled with other vibrations. The comparison with values obtained with spectroscopic measurements of infrared spectrum in Argon matrix [123] shows substantial agreement for all the frequencies. Major discrepancies between calculated and experimental values are found for the asymmetric stretching frequency of the amino group, 3636 cm^{-1} (calc.) vs. 3557 cm^{-1} (expt.), possibly due to matrix effects, and for some low frequency modes, whose assignment is particularly difficult and for which the harmonic approximation has a limited validity. Qualitative

agreement is found also for the relative intensities.

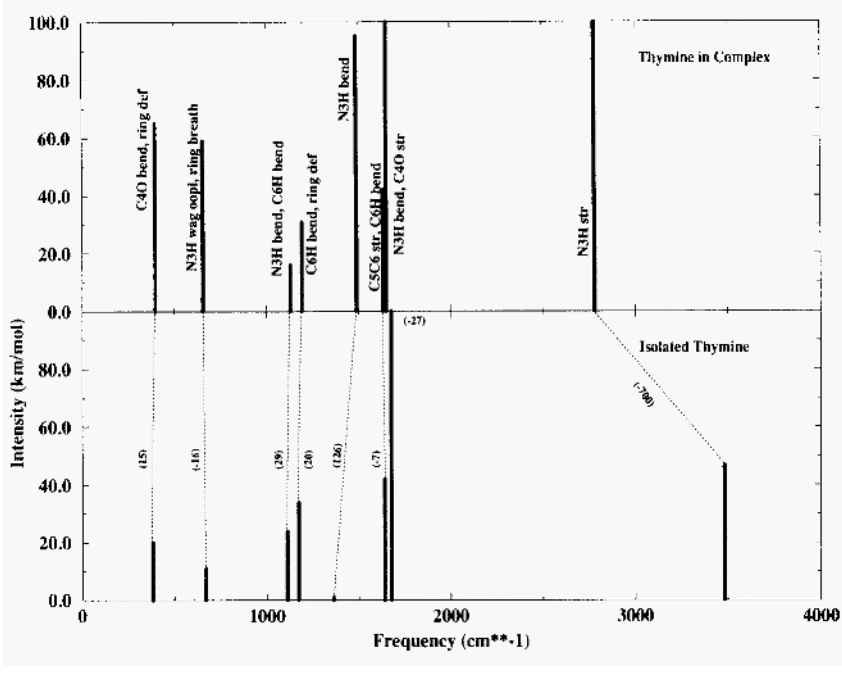

Figure 14. Selected frequency assignments for methylthymine, both in complex (top) and isolated (bottom). The values of the shift due to complexation are also given.

Also for the isolated 1-methylthymine (see Fig. 14) substantial agreement with experimental results [124,125] is found.

The vibrational spectrum of the methyladenine-methylthymine (AT) base-pair consists of 102 normal modes frequencies; many of the intramolecular modes of the two isolated molecules are recognizable in the complex. It is therefore easy to report the shifts suffered by these modes in the complex formation. Here we mention only some of the shifts of modes belonging to atoms involved in the h-bonding of the complex. The NH_2 stretching modes of adenine show a red shift and an increase in intensity, whereas the frequencies related to the NH_2 bendings change little both in position and intensity. As it is clear from Fig. 13, all the modes involving displacements of the amino-group are affected by complexation effects. A sharp red shift, from 515 cm^{-1} to 359 cm^{-1}, is evident for a ring deformation mode, which

clearly regards displacement of the N1 atom involved in h-bonding.

For thymine, the most pronounced shift belongs to the NH stretching mode, whose frequency position is lowered by 700 cm^{-1} upon complexation and whose intensity increases by a factor of 40. The C40 stretching (coupled with the NH bending) is red-shifted from 1678 to 1651 cm^{-1} while the NH bending is notably blue shifted (+126 cm^{-1}) with an increase in intensity; the same trend is evident whenever the NH bending is coupled with other modes. A pictorial view of these shifts is reported in Fig. 14.

Although very well resolved experimental infrared spectra are available for the methylguanine molecule, it is difficult to make a comparison with our calculations, since two different tautomers of 9-methylguanine exist, and their frequencies are mixed in the experimental spectra [126]. However, in general we can state that the agreement is good, even for the relative intensities. The spectrum is partially reported in Fig. 15.

The available experimental data [127] for the 1-methylcytosine base agree with our results. The spectrum of the isolated base is partially reported in Fig. 16.

The vibrational spectrum of methylguanine-methylcytosine (GC) complex consists of 99 normal modes frequencies. Differently from the AT base pair, in the GC complex the normal modes of the two bases are coupled together, thus an analysis of the shift relatively to the isolated bases is extremely complicated. This stronger coupling can possibly he ascribed to the presence of three h-bonds, rather than two as in AT. However, we tentatively discuss some significant shifts.

In guanine, the amino-group asymmetric and symmetric stretchings exhibit red shifts and increase in intensity. The shift is more pronounced for the symmetric stretching, which is coupled, as in in the isolated base, with the NH stretching. The CO stretching, which occurs at the same frequency as the NH bending, shows a moderate red shift, while the NH bending associated with NH_2 bending exhibit a blue shift.

Also for cytosine, red shifts are detected in the NH_2 stretching and bending modes. Ring stretchings and deformations, involving the CO vibration, suffer little changes with respect to the isolated base (see Fig. 16). In the overall, the computed frequency shifts are in agreement with the

available experimental [128] observations.

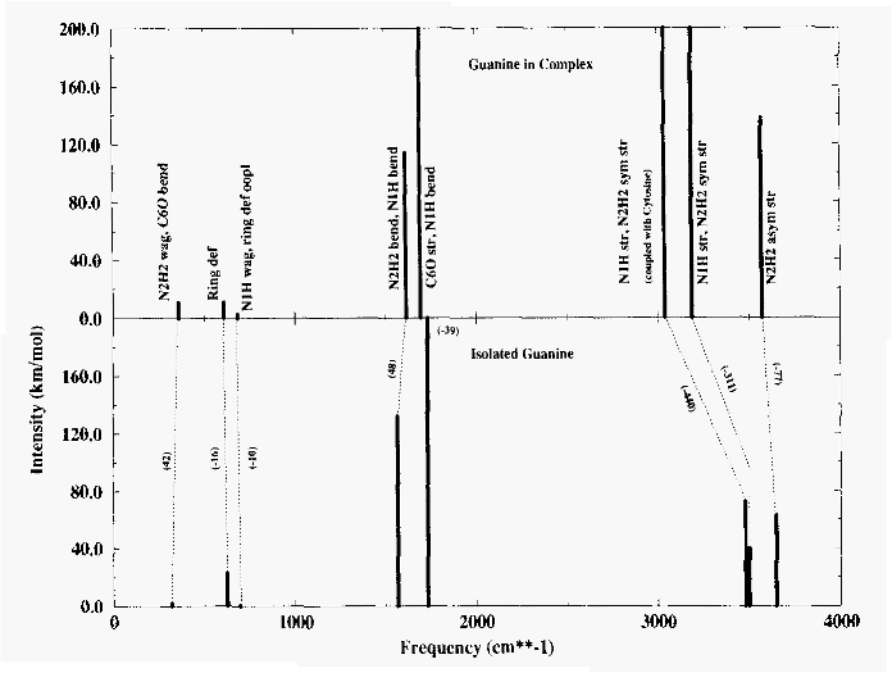

Figure 15. Selected frequency assignments for methylguanine, both in complex (top) and isolated (bottom). The values of the shift due to complexation are also given.

Let us now comment on the results obtained when including solvent effects. The geometrical arrangements of the isolated bases are not heavily affected upon solvation, thus we can expect a slight modification of the potential energy surface and therefore of the vibrational behavior for these systems. Indeed, it appears that only some stretching modes exhibit significant shifts, particularly when they involve movements of the peripheral atoms.

For the isolated methyladenine, we observe blue shifts for the stretching modes of the amino-group (+25 cm^{-1} for the asymmetric stretching, +46 cm^{-1} for the symmetric stretching), and also for the stretching mode of the C8O (+56 cm^{-1}) and for an asymmetric stretching mode of the methyl group (+89 cm^{-1}). For the isolated methylthimine, the changes are more modest than for methyladenine, resulting in a slight blue shift for some

stretching modes of the two methyl groups and of the C6H bond.

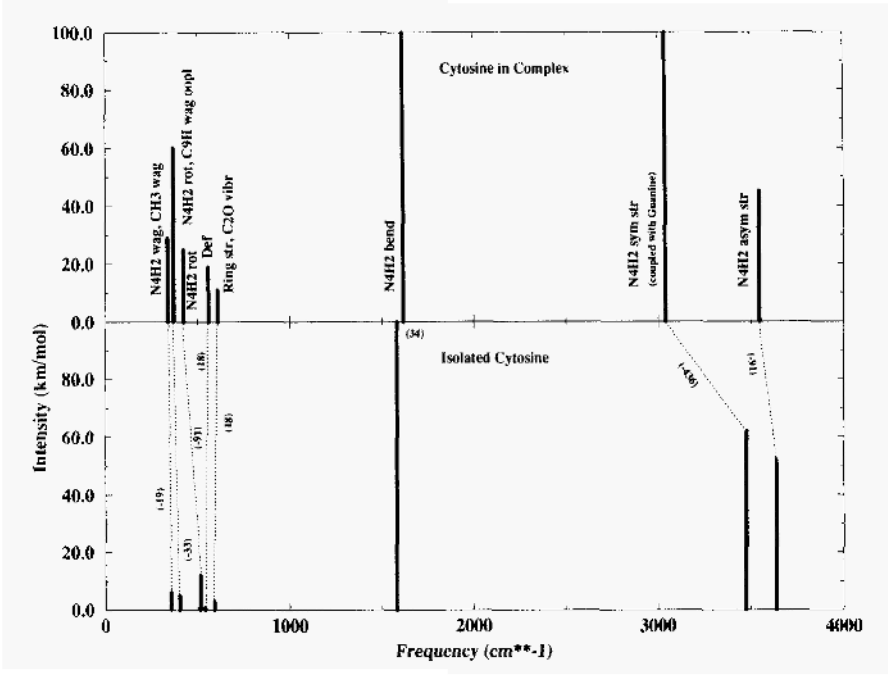

Figure 16. Selected frequency assignments for methylcytosine, both in complex (top) and isolated (bottom). The values of the shift due to complexation are also given.

Isolated methylguanine exhibits red shifts in the frequencies of some stretching modes, rather than blue shifts; the C8H stretching mode exhibit a red shift of 29 cm^{-1}, and the symmetric stretching mode of the methyl group is red shifted in frequencies by 18 cm^{-1}. A red shift is also evident for the C6O stretching and N1H bending, with its frequency lowered by 39 cm^{-1}. Methylcytosine differs from the other bases; indeed, the solvent effect induces strong modifications in the normal vibrational frequencies. The amino group symmetric stretching exhibit a blue shift of 90 cm^{-1}, and the C5H bond increases its stretching frequency of 100 cm^{-1}, while the methyl group shows a blue shift of 92 cm^{-1} in its symmetric stretching mode. A red shift of 32 cm^{-1} is suffered by the C2O stretching mode.

As previously noted, we are of the opinion that, in the overall, the shifts induced by the solvent are in the correct directions, but we must be cau-

tious in trying conclusions from their absolute values.

Acknowledgments

Financial support from ”Regione Autonoma della Sardegna” is kindly acknowledged. In addition, the authors wish to thank Prof. Enrico Clementi for inspiration, encouragement and continous advise in our research work.

References

1. Born, M.: *Z. Phys.* **1,** 45 (1920).
2. Kirkwood, G.: *J. Chem. Phys.* **2,** 351 (1934).
3. Onsager, L.: *J. Am. Chem. Soc.* **58,** 1486 (1936).
4. Rinaldi, D., and Rivail, J.L.: *Theor. Chimica Acta* **32,** 57 (1973).
5. Huron, M.J., and Claverie, P.: *J. Phys. Chem.* **78,** 1862 (1974).
6. Tapia, O., and Goscinski, O.*: Mol. Phys.* **29,** 1653 (1975).
7. Thole, B.T., and van Dujnen, P.Th.: *Theor. Chimica Acta* **55,** 307 (1980).
8. Miertus, S., Scrocco, E., and Tomasi, J.: *Chem. Phys.* **55,** 117 (1981).
9. Tucker, S.C., and Truhlar, D.G.: *Chem. Phys. Lett.* **157,** 164 (1989).
10. Clementi, E.: Determination of Liquid Water Structure, Coordination Numbers for Ions and Solvation for Biological Molecules, in *Lecture Notes in Chemistry,* Vol. 2, Springer-Verlag, Berlin, Heidelberg, New York, 1976.
11. Bolis, G., Ragazzi, M., Salvaderi, D., Ferro, D.R., and Clementi, E.: *Int. J. Quantum Chem.* **14,** 815 (1978).
12. Car R., and Parrinello, M.: *Phys. Rev. Letters* **55,** 2571 (1985).
13. Warshel, A., and Levitt, M.: *J. Mol. Biol.* **103,** 227 (1976).
14. Tapia, O., Lamborelle, C., and Johannin, G.: *Chem. Phys. Lett.* **72,** 334 (1980).
15. Tapia, O., and Johannin, G.: *J. Chem. Phys.* **75,** 3624 (1981).
16. Tapia, O., Colonna, F., and Angyan, J.: *J. Chem. Phys.* **87,** 875 (1990).
17. Field, M.J., Bash, P.A., and Karplus, M.: *J. Comp. Chem.* **11,** 700 (1990).
18. a) Hollauer, E., Hoffmann, D.W.M., and Clementi, E.: in *Methods and Techniques in Computational Chemistry: METECC-94,* Vol. B, Chapter 4, Clementi, E., ed., STEF, Cagliari, 1993; b) Corongiu, G., and Martorana, V.: *ibid.,* Vol. C, Chapter 3; c) Estrin, D.A., Corongiu, G., and Clementi, E.: *ibid,* Vol, B, Chapter 12.
19. See for example, Jones, R., and Gunnarsson, **O.:** *Rev. Mod. Phys.* **61,** 689 (1990); Parr, R.G., and Yang, W.: (1990), *Density Functional Theory of Atoms and Molecules* , Oxford University Press, New York ; Kryachko, E.S., and Ludeña, E.V.: *Energy Density Functional Theory of Many Electron Systems* Kluwer Academic Publishers, 1990 ; Callaway, J., and March, N.H.: *Solid State Phys.* **38,** 135 (1984).
20. Rappe, A.M., Joannopoulos, J.D., and Bash, P.A.: *J. Am. Chem. Soc.* **114,** 6466 (1992).
21. Ellis, D.E., and Painter, G.S.: *Phys.Rev.* **B2,** 2887 (1970).
22. Delley, B.: *J. Chem. Phys.* **92** , 508 (1990).
23. Baerends, E.J., Ellis, D.E., and Ros, P.: *Chem. Phys.* **2,** 41 (1973).
24. Boerrigter, P.M., te Velde, G., and Baerends, E.J.: *Int. J. Quant. Chem.* **33,** 87 (1988)
25. Sambe, H., and Felton, R.H.: *J. Chem. Phys.* **61,** 3862 (1974); *J. Chem. Phys.* **62,** 1122 (1975).

26. Dunlap, B.I., Connolly, J.W.D., and Sabin, J.R.: *J. Chem. Phys.* **71,** 3396 (1979).
27. Labanowski, J., and Andzelm, J.: Eds., *Density Functional Methods in Chemistry* , Springer, New York (1991); Fitzgerald, G., and Andzelm, J.: *J. Phys. Chem.* **95,** 10531 (1991).
28. St. Amant, A., and Salahub, D.R.; *Chem. Phys. Lett.* **169,** 387 (1990).
29. Sosa, C., Andzelm, J., Elkin, B., Wimmer, E., Dobbs, K., and Dixon, D.A.: *J. Phys. Chem.* **96,** 6630 (1992).
30. Wigner, E.P.: *Phys. Rev.* **46,** 1002 (1934); Wigner, E.P., and Seitz, F.: *Phys. Rev.* **43,** 804 (1933).
31. Lie, G.C., and Clementi, E.: *J. Chem. Phys.* **60,** 1275 (1974); *J. Chem. Phys.* **60** , 1288 (1974).
32. Hohenberg, P., and Kohn, W.: *Phys. Rev. A* **136,** 864 (1964).
33. Kohn, W., and Sham, L.J.: *Phys. Rev. A* **140,** 1133 (1965).
34. Gunnarsson, O., and Lundquist, I.: *Phys. Rev. B* **13,** 4274 (1976).
35. von Barth, U., and Hedin, L.: *Phys. Rev. A* **20,** 1693 (1979).
36. Ceperley, D.M., and Alder, B.J.: *Phys. Rev. Lett.* **45,** 566 (1980).
37. Vosko, S.H., Wilk, L., and Nusair, M.: *Can. J. Phys.* **58,** 1200 (1980).
38. Becke, A.D.: *J. Chem. Phys.* **88,** 1053 (1983).
39. Perdew, J.P.: *Phys. Rev. B* , **33,** 8822 (1986).
40. Perdew, J.P., and Wang, Y.: *Phys. Rev. B.* **33,** 8800 (1986).
41. a) Ziegler, T.: *Chem. Rev,* **91,** 651 (1991); b) Sim, F., St-Amaint, A., Papai, I., and Salahub, D.R.: *J. Am. Chem. Soc*. **114,** 4391 (1992); *c*) Sim, F., Salahub, D.R., Chin, S., and Dupuis, M.: *J. Chem. Phys.* **95,** 4317 (1991).
42. Becke, A.D.: *Phys. Rev. A* **38,** 3098 (1988).
43. Salahub, D.R.: *Adv. Chem. Phys.* **69,** 447 (1987).
44. Herman, F., and Skillman, S.: *Atomic Structure Calculations* , Prentice Hall, Englewood Cliffs NJ (1963).
45. Jones, R.S., Mintmire, J.W., and Dunlap, B.I.: *Int. J. Quant. Chem.* **S22,** 77 (1988).
46. Becke, A.D.: *J. Chem. Phys.* **88***,* 2547 (1988).
47. Obara, S., and Saika, A.: *J. Chem. Phys.* **84,** 3963 (1986).
48. Person, W.B., and Zerbi, G.: Eds., *Vibrational intensities in Infrared and Raman Spectroscopy* , Elsevier, Amsterdam (1982).
49. Allen, M.P., and Tildesley, D.J.: *Computer Simulation in Liquids.,* Clarendon Press, Oxford (1987).
50. Estrin, D.A., Tsoo, C., and Singer, S.J.: *J. Chem. Phys.* **93** , 7201 (1990).
51. Karelson, M., Katritzky, A.R., and Zerner, M.: *Int. J. Quant. Chem.* **S20,** 521 (1986).
52. (a) Wong, M.W., Frisch, M.J., and Wiberg, K.W.: *J. Am,. Chem. Soc.* **113,** 4476 (1991); (b) Wong, M.W., Wiberg, K.W., and Frisch, M.J.: *J. Am. Chem. Soc.* **114,** 523 (1992); (c) Wong, M.W., Wiberg, K.W., and Frisch, M.J.: *J. Am. Chem. Soc.* **114,** 1645 (1992).
53. Rivail, J.L., and Terryn, B.: *J. Chim. Phys.* **79,** 1 (1982).

54. Tomasi, J., Bonaccorsi, R., Cammi, R., Olivares del Valle, F.J .: *THEOCHEM,* **234,** 401 (1991);
55. Rinaldi, D., Ruiz-Lopez, M.F., and Rivail, J.L.: *J. Chem. Phys.* **78,** 834 (1983).
56. Ciementi, E., *J. Chem. Phys.* **46,** 3851 (1967); ibid. **47,** 2323 (1967).
57. Clementi, E., and Gayles, J.N.: *J. Chem. Phys.* **47,** 3837 (1967).
58. Goldfinger, P., and Verhaegen, G.: *J. Chem. Phys.* **50,** 1467 (1968).
59. Ault, B.S., and Pimentel, G.C.: *J. Phys. Chem.* **77,** 1649 (1973).
60. Kollman, P., Johansson, A., and Rothenberg, S.: *Chem. Phys. Lett.* **24,** 199 (1974); Kollman, P., McKelvey, J., Johansson, A., and Rothenberg, S.: *J. Am. Chem. Soc.* **97,** 955 (1975).
61. Raffenetti, R.C., and Phillips, D.H.: *J. Chem. Phys.* **71,** 4534 (1979).
62. Barnes, A.J., Beech, T.R., and Mielke, Z.: *J. Chem. Soc. Far. Trans.* II **80,** 455 (1984).
63. Brciz, A., Karpfen, A., Lischka, H., and Schuster, P.: *Chem. Phys.* **89,** 337 (1984).
64. Latajka, Z., and Scheiner, S.: *J. Chem. Phys.* **81,** 4014 (1984); Latajka, Z., Sakai, S., Morokuma, K., and Ratajczak, H.: *Chem. Phys. Lett.* **110,** 464 (1984); Latajka, Z., and Scheiner, S.: *J. Chem. Phys.* **82,** 4131 (1985).
65. Jasien, P.G., and Stevens, W.J.: *Chem. Phys. Lett.* **130,** 127 (1986).
66. Seinfeld, J.H.: *Atmospheric Chemistry and Physics of Air Pollution,* Wiley, New York, 1988.
67. Cronn, D.R., Charlson, R.J., Knights, R.L., Crittendon, A.L., and Appel, B.R.: *Atmos. Environ.* **11,** 929 (1977).
68. Mulliken, R.S.: *J. Phys. Chem.* **56,** 801 (1952).
69. Estrin, D., Murgia, G., Paglieri, L., Pisani, L., Suzzi Valli, G., Watts, J., and Clementi, E.: *Int. J. Quantum. Chem.,* submitted.
70. Chipot, C., Rinaldi, D., and Rivail, J.L.: *Chem. Phys. Letters* **191,** 287 (1992).
71. Dzidic, I., and Kebarle, P.: *J. Phys. Chem.* **74,** 1466 (1970).
72. Arshadi, M., Yamdagni, R., and Kebarle, P.: *J. Phys. Chem.* **74,** 1475 (1970).
73. Volmer, M.: *Kinetik der Phasenbiidung,* Theodor Steinkopff, Dresden, Germany (1939).
74. Clementi, E., and Popkie, H.: *J. Chem. Phys.* **57,** 1077 (1972).
75. Kistenmacher, H., Popkie, H., and Clementi, E.: *J. Chem. Phys.* **59,** 5842 (1973).
76. Watts, R.O., Clementi, E., and Fromm, J.: *J. Chem. Phys.* **61,** 2550 (1974); **62,** 1388 (1975).
77. Clementi, E., and Barsotti, R.: *Chem. Phys. Lett.* **59,** 21 (1978).
78. Mruzik, M.R., Abraham, F.F., and Schreiber, D.: *J. Chem. Phys.* **64,** 481 (1976).
79. Corongiu, G., and Clementi, E.: (unpublished results).
80. Clementi, E., Kistenmacher, H., Kolos W., and Romano, S.: *Theor. Chim. Acta* **55,** 257 (1980).

81. Clementi, E., and Corongiu, G.: *Int. J. Quantum Chem. Simp.* **10,** 31 (1983).
82. See for example *X-Ray Diffraction of Ions an Acqueous Solutions: Hydration and Complex Formation,* Mengini, M., Ed., CRC Press, Boca Raton, Florida (1988).
83. Kistenmacher, H., Lie, G.C., Popkie, H., and Clementi, E.: *J. Chem. Phys.* **61,** 546 (1974); see also Ref. [10].
84. Kim, K.S., Dupuis, M., Lie, G.C., and Clementi, E.: *Chem. Phys. Lett.* **131,** 451 (1986).
85. Matsuoka, O., Clementi, E., and Yoshimine, M.: *J. Chem. Phys.* **64,** 1351 (1976).
86. a) Dietrich, G., Corongiu, G., and Clementi, E.: *Chem. Phys. Lett.* **112,** 426 (1984); b) Niesar, U., Corongiu, G., and Clementi, E., Kneller, G.R., and Bhattacharya: *J. Phys. Chem.* **198,** 7949 (1990).
87. a) Newton, M.D., and Kestner, N.R.: *Chem. Phys. Lett.* **94,** 198 (1983); b) Dykstra, C.: *J. Chem. Phys.* **91,** 6472 (1989).
88. a) Reimers, J.R., and Watts, R.O.: *Chem. Phys.* **85** 83 (1984); b) Stillinger, F.H., and David, C.W.: *J. Chem. Phys.* **73,** 3384 (1980).
89. a) Pugliano, N., and Saykally, R.J.: *Science* **257,** 1937 (1992; b) *J. Chem. Phys.* **96,** 1832 (1992).
90. Wei, S., Shi, Z., and Castleman, A.W.: *J. Chem. Phys.* **94,** 3268 (1991).
91. Page, R.H., Vernon, M.F., Shen, Y.R., and Lee, Y.T.: *Chem. Phys. Lett.* **141,** l(1987).
92. a) Benson, S.W., and Siebert, E.D.: *J. Am. Chem. Soc.* **114,** 4269 (1992); b) Ferrari, A.M., Garrone, E., and Ugliengo, P.: *Chem. Phys. Lett.* **212,** 644 (1993).
93. Corongiu, G., and Clementi, E.: *J. Chem. Phys.* **98,** 2241 (1993), and references therein given.
94. a) Niesar, U., Corongiu, G., Huang, M.J., Dupuis, M., and Clementi, E.: *int. J. Quant. Chem. Symp.* **23,** 421 (1989); b) Corongiu, G., Aida, M., Pas, M.F., and Clementi, E.: in *MOTECC 91,* Modern Techniques in Computational Chemistry, E. Clementi Ed., ESCOM, Leiden (1991).
95. a) Schiiz, M., Biirgi, T., Leutwyler, S., and Bürgi, H.B.: *J. Chem. Phys.* **99,** 5229 (1993); b) Xantheas, S.S., and Dunning, T.H. Jr : *J. Chem. Phys.* **98,** 8037 (1993); c) Xantheas, S.S, and Dunning, T.H. Jr : *J. Chem. Phys.* **99,** 8774 (1993); d) Xantheas, S.S.: *J. Chem. Phys.* **100,** 7523 (1994).
96. Tsai, C.J., Jordan, K.D.: *Chem. Phys. Lett.* **213,** 181 (1993).
97. Estrin, D.A., Paglieri, L., Corongiu, G., and Clementi, E.: *J. Phys. Chem.,* (submitted).
98. Clough, S.A., Beers, Y., Klein, G.P., and Rothman, L.S.: *J. Chem. Phys.* **59,** 2254 (1973).
99. Mills, I.M.: *Theoretical Chemistry,* Dixon, R.N., Ed., Chemical Society; London (1974).
100. Kuchitsu, K., and Morino, Y.: *Bull. Chem. Soc. Jpn.,* **38,** 805 (1985).

101. Benedict, W.S., Gailar, N., and Plyler, E.K.: *J. Chem. Phys.* **24,** 1139 (1956).
102. Bertran, J., Ruiz-Lopez, M.F., Rinaldi, D., and Rivail, J.L.: *Theoret. Chimica Acta* **84,** 181 (1992).
103. Soper, A.K., and Phillips, M.G.: *Chem. Phys.* **107,** 47 (1986).
104. Thiessen, W.E., and Narten, A.H.: *J. Chem. Phys.* **77,** 2656 (1982).
105. Coulson, C.A., and Eisenberg, D.: *Proc. R. Soc. London,* Ser A **291,** 445 (1966).
106. Walrafen, G.E., Hokmadabi, M.S., and Yang, W.H.: *J. Chem. Phys.* **92,** 2433 (1988).
107. Corongiu, G., and Clementi, E.: *J. Chem. Phys.* **97**, 2030 (1992).
108. Corongiu, G., and Clementi, E.: *J. Chem. Phys.* **98,** 4984 (1993).
109. Corongiu, G., and Clementi, E., *J. Chem. Phys.* **98,** 2241 (1993).
110. Watson, J., and Crick, H.C.: *Nature* **171,** 753 (1953).
111. Clementi, E.:*Computational Aspects for Large Chemical Systems* Springer Verlag, Berlin, 1980.
112. Pearlman, D., and Kollman, P.: *J. Mol. Biol.* **220,** 457 (1991).
113. Trollope, K.I., Gould, I.R., and Hillier, I.H.: *Chem. Phys. Lett.* **209,** 113 (1993).
114. Hobza, P., and Sandorfy, C.: *J. Am. Chem. Soc.* **109,** 1302 (1987).
115. Hrouda, V., Florian, J., and Hobza, P.: *J. Phys. Chem.* **97,** 1542 (1993).
116. Colson, A.O., Besleri, B., and Sevilla, M.D.: *J. Phys. Chem.* **96,** 9787 (1992).
117. Hehre, W.J., Radom, L., Schleyer, P.V., and Pople, J.A.: *Ab Initio Molecular Orbital Theory,* Wiley, New York, 1986.
118. Saenger, W.: *Principles of Nucleic Acid Structure,* Springer-Verlag, New York, 1984.
119. Nerdal, W., Hare, D., and Reid, B.: *Nuc. Acids Res.* **28,** 10008 (1989).
120. Boys, S.F., and Bernardi, F.: *Mol. Phys.* **19,** 553 (1970).
121. Schwenke, D.W., and Truhlar, D.G.: *J. Chem. Phys.* **82**i, 2418 (1985).
122. Alagona, G., and Ghio, C.: *J. Comput. Chem.* **11,** 930 (1990).
123. Stepanian, S.G, Sheina, G.G., Radchenko, E.D., and Blagoi, Yu.P.: *J. Mol. Struct.* **131,** 333 (1985).
124. Susi, H., and Ard, J.S.: *Spectrochimica Acta* **30A,** 1843 (1974).
125. Nowak, M.J.: *J. Mol. Struct.* **193,** 35 (1589).
126. Szczepaniak, K., and Szcześniak, M.: *J. Mol. Struct.* **156,** 29 (1987).
127. Szcześniak, M., Nowak, M.J., and Szczepaniak, K.: *J. Mol. Struct.* **115,** 221 (1984).
128. Hartman, Lord, T.: in *Physicochemical Properties of Nucleic Acids,* Vol. II, Duchesne, J., Ed., Academic Press, London 1973.

This page intentionally left blank.

CROSSING THE TRANSITION STATE IN SOLUTION

JAMES T. HYNES*

Unitat de Química Fisica
Universitat Autònoma de Barcelona
08293 Bellaterra (Barcelona) SPAIN

and

Department of Chemistry and Biochemistry
University of Colorado
Boulder, CO 80309-0215 USA

* *IBERDROLA Foundation Invited*
Professor at UAB, May-August 1995

1. Introduction

In this chapter, we give a brief account of two related aspects of chemical reactions in solution: the so-called "stochastic" theoretical approach to the rates of reactions and related features, and Molecular Dynamics (MD) computer simulations designed to test such theories and to otherwise provide insight on the reaction dynamics.

By the term "stochastic" we mean here that the reaction description is at a reduced level, that is, in terms of a dynamical equation(s) of motion for only one variable – i.e., the solute reactive coordinate – or perhaps two – the solute reactive coordinate and a coupled, collective solvent coordinate. Such equations have a probabilistic or stochastic aspect due to the fluctuations arising from the remaining and not explicitly followed degrees of freedom (of the order of a multiple of Avogadro's number in number!), MD simulations, on the other hand, treat explicitly – albeit numerically – all the system degrees of freedom (classically) in full detail. The latter tells us all there is to know (with the very important caveats that the interaction forces are known – a focus of much of the rest of this book – and that classical mechanics is a sufficiently accurate description). The stochastic approach has the more modest goals of providing a simpler – and in favorable cases – analytic description of limited but critical aspects such as the reaction rate constant and reaction pathways; this is an especially attractive feature in connection with the interpretation of experiments and – more philosophically – in bringing order and generality into the vast and rich array of chemical reaction dynamics for specific reaction systems.

In the limited space available, we make no pretense of providing a compre-

O. Tapia and J. Bertrán (eds.). Solvent Effects and Chemical Reactivity, 231–258.
© 1996 *Kluwer Academic Publishers. Printed in the Netherlands.*

hensive coverage, and indeed we give a very focussed discussion, largely focussed on Grote-Hynes (GH) theory [1,2] and MD simulations connected with it. In addition to the obvious rationale of our familiarity with these topics, we can offer the justification that Grote-Hynes theory is the most successful theory for solution reaction rates, as judged objectively by its confirmation in a very considerable number of simulations for a very wide array of chemical reaction types and examples [3-12], with experimental support as well [13-16]. Those interested in a broader overview and alternate approaches may consult a number of reviews [1,3,17,18]. We also focus exclusively on charge transfer reactions, where there is often a strong electrostatic coupling between the reactering solute and the surrounding polar solvent.

Of course, GH theory has important antecedents. The first is the well known Transition State Theory for solution reaction rate constants k^{TST} [1,191. With its exponential activation free energy factor, k^{TST} is the starting point, and indeed is the *sine qua non,* of reaction rate theory – it gives most of the answer. GH theory addresses the proper prefactor for k^{TST}, or alternately stated, the transmission coefficient, which accounts for solvent dynamical effects responsible for reducing the actual rate constant from its k^{TST} approximation. The first – and for many years the only – stochastic approach to this factor is Kramers Theory [20], which employs a simple Langevin equation description involving a friction constant to account for the dynamical solvent rate influence. GH theory generalizes this to a Generalized Langevin Equation description, and is properly focussed on the key short molecular time scale in which the system is crossing the transition state. Another theme of this chapter is that of nonequilibrium solvation – the feature that the solvent is out of equilibrium with the reacting solute during the Transition State passage, an aspect not included in conventional Transition State Theory. Various model elaborations focussed on nonequilibrium solvation and related to GH theory have been developed [21,22] to more completely characterize important detailed aspects of what is happening to the solute and solvent during the reaction. These efforts received an important initial encouragement from the work of Kurz and Kurz [23].

The outline of the chapter is the following. In Sec. 2, we give an overview of GH theory and various important limits, as well as an overview of its applications to assorted charge transfer reaction classes. In Sec. 3, we sketch a model development that is quite useful in comprehending the meaning of GH theory. Various MD simulation studies on reaction dynamics are described in Sec. 4. from the perspective of the preceding sections. Sec. 5 sketches some other related developments, while concluding remarks are offered in Sec. 6.

The reader interested in a further discussion of connections of reaction rates to the topic of solvation dynamics – an arena of intense activity – is directed to Ref. 24, upon which the present chapter is partly based.

2. Stochastic Reaction Rate Formulation

2.1. CLASSICAL PARTICLE CHARGE TRANSFER–GROTE-HYNES THEORY

We begin by giving a brief account of Grote-Hynes Theory [1,2] for reaction rate constants. This theory has been verified for a very wide range of solution reactions via computer simulation [3-12] and has also proved useful in comparison

with experimental rate studies [13 - 16].

GH Theory was originally developed to describe chemical reactions in solution involving a classical nuclear solute reactive coordinate *x.* The identity of *x* will depend of course on the reaction type, i.e., it will be a separation coordinate in an S_N1 unimolecular ionization and an anS_N2 displacement reaction. To begin our considerations, we can picture a reaction free energy profile in the solute reactive coordinate *x* calculated via the potential of mean force $G_{eq}(x)$ – the system free energy when the system is equilibrated at each fixed value of *x,* which would be the output of e.g. equilibrium Monte Carlo or Molecular Dynamics calculations [25] or equilibrium integral equation methods [26]. Attention then focusses on the barrier top in this profile, located at $x^{\ddagger}$.

In the GH theory, it is assumed that the reaction barrier is parabolic in the neighborhood of $x^{\ddagger}$ and that the solute reactive coordinate satisfies a generalized Langevin equation (GLE),

$$\ddot{x}(t) = \omega_{beq}^2 \, x(t) - \int_0^t d\tau \zeta(t-\tau) \, \dot{x}(\tau) \, , \tag{2.1}$$

where a random force term which is not essential for our purposes has been ignored. It is convenient – and we have in fact already assumed this in (2.1) – to take the barrier top location $x^{\ddagger}$ to be $x^{\ddagger}=0$. The square equilibrium barrier frequency is governed by the mean potential curvature

$$\omega_{beq}^2 = - \mu^{-1} \left. \frac{\partial^2 G_{eq}(x)}{\partial x^2} \right|_{x^{\ddagger}} . \tag{2.2}$$

The time dependent friction coefficient, per solute mass μ, is related to the fluctuating forces exerted by the solvent on the solute coordinate *x* through their time correlation function:

$$\zeta(t) = (\mu k_B T)^{-1} \left. \langle \delta F \delta F(t) \rangle \right|_{x^{\ddagger}} . \tag{2.3}$$

The GLE accounts for the crucial fact that the time scale of these forces is finite, and in particular, finite on the relevant time scale for the barrier crossing. This is an important point to which we return presently.

We should stress that the friction in (2.3) is that relevant to the barrier top vicinity, and indeed the entire description is assumed to be valid in just that vicinity. This is not at all inconsistent with, and indeed it recognizes, the fact that this friction can be different from the corresponding frictions relevant for reactants and products; for charge transfer reactions, this is most obviously a consequence of the fact that the

solute charge distributions are different in the three locations.

With the assumptions detailed above, the reaction transmission coefficient,

$$\kappa = \frac{k}{k^{TST}} , \tag{2.4}$$

i.e., the ratio of the actual rate constant to its Transition State Theory (TST) value, is found to be the ratio of the reactive frequency λ and the mean barrier frequency [1,2]

This self-consistent equation has a simple message: the relevant friction for the reaction is determined by the (Laplace) frequency component of the time dependent friction at the reactive frequency λ. This frequency sets the basic time scale for the microscopic events affecting κ.

There is a simple route to the middle equation for λ in (2.5) which helps to understand λ We look for a solution to the GLE (2.1) of the form x(t) ~ exp (λt)

$$\kappa = \lambda/\omega_{beq} ;$$

$$\lambda = \omega_{beq}^2 \, [\lambda + \hat{\zeta}(\lambda)]^{-1} ;$$

$$\hat{\zeta}(\lambda) = \int_0^\infty dt \, \exp(-\lambda t) \, \zeta(t) . \tag{2.5}$$

reflecting the longer time divergence of a trajectory away from the unstable barrier top. Insertion of this into (2.1) gives just the desired result for asymptotic times.

The TST rate constant in (2.4) refers to the conventional solution application of TST in which it is imagined that – even if it is not explicity stated – *equilibrium* solvation conditions hold [1,2,21,22]. This is equivalent, although perhaps not obviously, to picturing the reaction as passage over the equilibrated barrier in *x,* without any recrossing. (2.1) indicates that these equilibrium conditions will apply when the *x* coordinate velocity is so low, and the generalized friction due to the coupling of *x* to the solvent is so small, that the solvent can adjust sufficiently rapidly, i.e., adiabatically, to the *x* motion to provide the equilibrium solvation that is incorporated in the equilibrium barrier frequency, but with no further effect. In the perspective of (2.5), the reactive frequency λ would then be the equilibrium barrier frequency w_{beq}. Whether these conditions are actually met, so that the relations k = k^{TST} and thus κ=1 will hold, will depend on the time scale of the solvation dynamics and the coupling of the solvent to the reactive solute coordinate *x.*

To appreciate this latter point, we consider four important limits for the GH theory [1,21,221. First, if the adjustment of the solvent is rapid on the time scale of λ^{-1}, then the frequency dependence of $\hat{\zeta}(\lambda)$ can be safely ignored, and the GH equations reduce to the famous Kramers Theory result [20]

$$\kappa_{GH} \rightarrow \kappa_{KR} = \frac{\omega_{beq}}{\omega_{beq}\,\kappa_{KR} + \zeta} , \tag{2.6}$$

in which the zero frequency friction, or simply the friction constant, is

$$\hat{\zeta}(0) = \zeta = (\mu k_B T)^{-1} \int_0^\infty dt\, \langle \delta F \delta F(t) \rangle . \tag{2.7}$$

If the magnitude of the solute coupling to the solvent is large, gauged in the Kramers picture by $\zeta / \omega_{beq} >> 1$, the transmission coefficient will be low – $K \sim \omega_{beq} / \zeta$. This is caused by extensive recrossing of the barrier induced by the solvent friction. Equivalently stated, there is extensive spatial nonequilibrium departure from equilibrium solvation conditions. In this limit, the reaction can be described as a spatial diffusion-controlled passage over the barrier – the Smoluchowski spatial diffusion limit – and the full zero frequency solvent dynamics are required for its accurate description. (One frequently sees in the literature the confusing terminology "spatial diffusion limit" instead applied to, e.g., (2.6). This is clearly wrong; for example, (2.6) contains the TST limit κ=1, where no spatial diffusion is involved).

A second important limit is attained if the solvent dynamics are slow on the reactive time scale λ^{-1}, that is to say there is *nonadiabatic* solvation. Then we can put $\hat{\zeta}(\lambda) = \lambda^{-1}\, \zeta(t=0)$ in (2.5), and the GH equations reduce to [21,22]

$$\kappa_{GH} \rightarrow \kappa_{na} = \frac{\omega_{bna}^2}{\omega_{beq}^2} ;$$
$$\omega_{bna}^2 = \omega_{beq}^2 - \zeta(t=0) > 0 . \tag{2.8}$$

In this nonadiabatic solvation limi – which is favored by a sharp reaction barrier – the reaction can be viewed as *x* motion on a nonadiabatic *barrier,* whose frequency is the nonadiabatic value ω_{bna}. (The situation when ω^2_{bna} is negative represents another limit, described below). This can be seen directly from the GLE (2.1) by ignoring the time dependence of $\zeta(\lambda)$, performing the time integral for short times, and remembering that x(t=0)=0. This frequency ω_{bna} is less then the corresponding equilibrium value ω_{beq}, since the passage is occuring for fixed solvent configurations, and the solvent cannot respond to provide the equilibrium solvation that is incorporated in ω_{beq}. Once again, there is no equilibrium solvation and κ<1. In the neighborhood of, but not exactly in, this limit, some information about the solvation dynamics is required, but is limited to the very early time behavior of $\zeta(\lambda)$.

One should take careful note of the fact that in the nonadiabatic solvation, or "frozen solvent" limit, it is the *absence* of solvation dynamics that is important. But is just this lack that is responsible for the deviation from equilibrium solvation, which instead assumes the dynamics are effective in always maintaining equilibrium.

We now consider the *polarization cage* limit favored by a more broad reaction barrier [1,21,22]

On short time scales where the solvent has not moved while the solute coordinate x crosses the barrier, (2.9) indicates, with (2.1), that the x motion is

$$\omega_{bna}^2 < 0 \; ; \qquad \omega_{beq}^2 < \zeta(t=0) \; . \tag{2.9}$$

temporarily trapped, or "caged". The initial friction $\zeta(t=0)$ is simply too great to allow the reaction to proceed. No net passage on to the product side of the barrier can occur unless and until there is solvent motion to relax this cage and free the motion along the reaction coordinate. Thus in this limit the solvent dynamics is absolutely *essential* for the reaction to occur; the transmission coefficient reflects this, decreasing more and more as the solvent relaxation time lengthens. The associated multiple recrossing of the reaction barrier is particularly pronounced when the x coordinate motion is overdamped as well [22]; an average trajectory can oscillate several times before ultimately passing to the product region.

The polarization cage limit just discussed will apply when there is a relatively broad barrier in the mean potential (small w_{beq}) and at the same time there is strong solute-solvent electrostatic coupling [(large $\zeta(t=0)$)]. If conditions are such that the reactive frequency is so low as to be small compared to the time scale of the friction, then the polarization cage regime predictions for κ will coincide with the Kramers limit. Otherwise, one must simply solve the GH (2.5). Here something more than the initial time behavior of $\zeta(t)$ will be required to characterize the influence of the solvation dynamics on the reaction rate.

One should appreciate that in all of these limits, both the solvent time scale and the magnitude of the coupling of the solvent to the x coordinate are critical in the consequences for the reaction rate of any nonequilibrium solvation conditions. The former will not lead to any departure from the TST equilibrium solvation rate if the solvent coupling is weak. For example, in the nonadiabatic limit, if the coupling is weak – as gauged by $\zeta(t=0)/\omega^2_{beq} << 1$, then $\kappa \rightarrow 1$ and $k \rightarrow k^{TST}$. It is certainly not the case that the equilibrium solvation conditions are satisfied – indeed they are not, since the slow solvent cannot equilibrate to the reactive solute motion. Instead, it is the case that the coupling is so weak that the barrier crossing in x and thus the transmission coefficient are largely insenstive to the surrounding solvent: it simply does not matter that the solvent is out of equilibrium. This is the fourth and final limit that we discuss here, the *weak solvation* limit [21,22].

2.2. QUANTUM PARTICLE CHARGE TRANSFER REACTIONS

We now turn to charge transfer reactions involving a quantum particle, an electron or a proton. At first glance, these might seem strange applications of GH theory, since the coordinate of the reactant is quantum, and not classical as in Sec. 2.1. But as described below, the actual reactive coordinate for these reaction classes is classical.

We first consider outer sphere transfer (ET) reactions, e.g. $D^- + A \rightarrow D + A^-$, a donor-acceptor electron transfer without significant coupled internal reorganization of the D and A species [27,29,30]. A hallmark of such reactions, which has been long appreciated [27], is that the reactive coordinate is itself a many-body collective solvent variable (and is not the coordinate of the electron itself). In particular, if R and P stand for the reactant and product, then the reactive coordinate is

$$\Delta E = V_{solv\text{-}R} - V_{solv\text{-}P} \ . \tag{2.10}$$

This is the difference in interaction energy, for the solvent molecules in given positions, of the solvent with the reactant and product [31]. In the simplest case of no geometric size changes accompanying the ET, ΔE will be exclusively determinated by the Coulombic interactions between the solute and the solvent molecules. We will assume this to be the case in all that follows. We make the further restriction that the solute intramolecular vibrations play no key role.

For electronically adiabatic ET, the electronic coupling between the R and P diabatic states is sufficiently large that there is a continuous change in electronic character in passage over a reaction barrier in the ΔE coordinate. Again, one can apply GH Theory to this by assuming a GLE in the barrier top neighborhood, but now for the solvent coordinate $\delta\Delta E(t) = \Delta E(t) - \Delta E^{\ddagger}$, where $\Delta E^{\ddagger}$ locates the reaction barrier top in the equilibrium free energy $G_{eq}(\Delta E)$:

$$\delta\Delta\ddot{E}(t) = (\omega_{beq}^{ET})^2 \ \delta\Delta E(t) - \int_0^t d\tau \zeta_{ET}(t-\tau) \ \delta\Delta\dot{E}(\tau). \tag{2.11}$$

Here ω_{beq}^{ET} and $\zeta_{ET}^{\ddagger}(t)$ refer to the equilibrium barrier frequency and the time dependent friction for the *solvent* coordinate $\delta\Delta E$; note the contrast with (2.1), which refers to the corresponding quantities for a *solute* reactive coordinate.

The TST rate constant for electronically adiabatic ET reactions is the well-known Marcus rate constant k_{ET}^{TST} [27-29]. In the language of this chapter, solvent dynamical effects can alter the actual rate from this limit due to the friction ζ_{ET} influence. The corresponding GH equations for $\kappa_{ET} = k_{ET} / k_{ET}^{TST}$ are strictly analogous to (2.4) and (2.5), and so we do not write them out explicitly here.

We should briefly mention the electronically nonadiabatic ET situation. Here the electronic coupling is sufficiently weak that the intrinsic electronic passage from

R to P is slow, even when the isoenergetic conditions in the solvent allow the ET via the Franck-Condon principle. The TST rate for this case contains in its prefactor an *electronic* transmission coefficient κ_{el}, which is proportional to the square of the small electronic coupling [28]. But as first described by Zusman [32], if the solvation dynamics are sufficiently slow, the passage up to (and down from [33]) the nonadiabatic curve intersection can influence the rate. This has to do with solvent dynamics in the solvent wells (this is opposed to the barrier top description given above). We say no more about this here [8,11,32-36].

The situation for quantum proton transfer (PT) e.g. $AH + B \rightarrow A^- + HB^+$ is more complicated than for ET, in part due to the importance of the A-B separation coordinate (which would play no important role in the analogous short range ET processes $D + A \rightarrow D^+ + A^-$). We do not dwell on this here though. There are two important regimes for PT. The first is the nonadiabatic regime [37,38] in which reaction occurs by quantum proton tunnelling under its potential barrier. That barrier is itself modulated by the solvent, and in analogy to ET, the reaction barrier is in the solvent coordinate. In the proton adiabatic regime [39-42], the rapid proton adiabatically follows the slower solvent, and at the transition state of the solvent coordinate, is described by a bound quantized vibration above the barrier in its own coordinate (this is nothing at all like the classical motion of the proton over its barrier). Again the reactive coordinate is in the solvent.

We will only consider the adiabatic PT case here. In this situation, the free energy in the solvent coordinate will have a barrier, and the GH-GLE discussion above for ET in the solvent coordinate ΔE will also apply to the PT case.

3. Analytical Model

Prior to addressing the results of simulations on the issues exposed in the last section, we will now develop in this section a simple model perspective [5c,21,22,43]. Its purpose is both to shed light on the interpretation in terms of solvation of those results and to emphasize the interconnections (and differences) that may exist. The development given below is suitable for charge transfer reaction systems, which have pronounced solute-solvent electrostatic coupling; it is not appropiate for, e.g., neutral reactions in which the solvent influence is mainly of a collisional character. (Although we do not pursue it here, the various frequencies that arise in the model can be easily evaluated by dielectric continuum methods [21,431).

We consider the reactive solute system with coordinate x and its associated mass μ, in the neighborhood of the barrier top, located at $x=x^{\ddagger}=0$, and in the presence of the solvent. We characterize the latter by the single coordinate **s,** with an associated mass μ_s. If the solvent were equilibrated to x in the barrier passage, so that there is equilibrium solvation and $s = s_{eq}(x)$, the potential for x is just $-1/2\ \mu\omega_{beq}^2X^2$, where ω_{beq} is the equilibrium barrier frequency [cf. (2.2)]. To this potential we add a locally harmonic restoring potential for the solvent coordinate to account for deviations from this equilibrium state of affairs:

$$\frac{1}{2}\,\mu_s\omega_s^2\,[\,s-s_{eq}(x)^2\,]\;=\;\frac{1}{2}\,\mu_s\omega_s^2\,(s-gx)^2\;. \tag{3.1}$$

Here ω_s is the solvent frequency and we have assumed the solvent's equilibrium position to vary linearly with the solute coordinate x in the neighborhood of the barrier top:

$$s_{eq}(x)\;=\;gx\;;\qquad\qquad g\;=\;\frac{ds_{eq}(x)}{dx}\Big|_{\ddagger}\;. \tag{3.2}$$

This dependence of $s_{eq}(x)$ on x has its origin most importantly in charge transfer problems from the variation of the solute charge distribution with x, e.g., in an S_N1 ionization of RX, the ionic character of RX depends on the internuclear RX separation since the solute electronic structure is changing [7,43]. Even in a simple dipolar isomerization involving no electronic structure change, there will be such a dependence because the solute's dipole moment is changing with orientation [22]. We emphasize that the linear behavior (3.2) is only being assumed in the neighborhood of the barrier top (in general, $s_{eq}(x)$ will have an S-shape in the full range from reactants to products). Note also that at this stage, the precise identity of the solvent coordinate has not been specified. We will return to this question in Section 4.

With the above description, the Hamiltonian becomes

$$H\;=\;H^{\ddagger}+\frac{1}{2}\mu\dot{x}^2+\frac{1}{2}\mu_s\dot{s}^2-\frac{1}{2}\mu\omega_{beq}^2x^2+\frac{1}{2}\mu_s\omega_s^2(s-gx)^2\;. \tag{3.3}$$

It is convenient to now convert to mass-weighted coordinates $x = \mu^{1/2}x$ and $s = \mu_s^{1/2}s$ (and then drop the overbars hereafter), so that the Hamiltonian is

$$H\;=\;H^{\ddagger}\;+\;\frac{1}{2}\dot{x}^2\;+\;\frac{1}{2}\dot{s}^2\;-\;\frac{1}{2}\omega_{bna}^2x^2\;+\;\frac{1}{2}\omega_s^2s^2-\omega_c^2xs\;. \tag{3.4}$$

Here the square nonadiabatic frequency is given by

$$\omega_{bna}^2 = \omega_{beq}^2 - \frac{\omega_c^4}{\omega_s^2} , \tag{3.5}$$

while the x - s coupling square frequency – which measures the coupling strength – has the definition

$$\omega_c^2 = \left(\frac{\mu_s}{\mu} \right)^{1/2} \omega_s^2 \, g \, . \tag{3.6}$$

The nonadiabatic frequency governs the initial force experienced by x when the solvent coordinate is frozen at its saddle point value $s = s_{eq}(x^{\ddagger}) = 0$. In general, the coupled equations of motion for the (x,s) system are

$$\begin{aligned} \ddot{x} &= \omega_{bna}^2 x + \omega_c^2 s \; ; \\ \ddot{s} &= -\omega_s^2 s + \omega_c^2 x \, . \end{aligned} \tag{3.7}$$

If the solvent were to adjust rapidly (adiabatically) and equilibrate to the solute coordinate x so that there is no force on s, then we would have the equilibrium condition

$$s = s_{eq}(x) = \left(\frac{\omega_c^2}{\omega_s^2} \right) x \, . \tag{3.8}$$

When this condition is inserted into the first member of (3.7), it gives the simple equation of motion

$$\ddot{x} = \omega_{beq}^2 x \, , \tag{3.9}$$

where we have used (3.5); this is just the description x motion on an equilibrated

We will later further analyze the members of (3.7) as they stand, but it is useful for our subsequent discussion to now simply add a generalized dissipative term to the solvent equation of motion to obtain the stochastic equation of motion set

$$\ddot{x} = \omega_{bna}^2 x + \omega_c^2 s \; ; \tag{3.10}$$

where $\zeta_s(t)$ is the *solvent* time dependent friction coefficient (per unit mass μ_s). These two equations can be cast into the form of a GLE (2.1) for the reactive solute coordinate by Laplace transformation and insertion of the formal solution of the second equation into the first. The Laplace transform of the *solute* time dependent friction coefficient (per unit mass μ) in the resulting GLE is found to be [22]

$$\hat{\zeta}(\varepsilon) = (\mu k_B T)^{-1} \langle \delta F \delta \hat{F}(\varepsilon) \rangle = \zeta(t=0) \frac{(\varepsilon + \hat{\zeta}_s)}{(\varepsilon^2 + \omega_s^2 + \varepsilon \hat{\zeta}_s)} \; , \tag{3.11}$$

where the initial time value of the friction is connected to the coupling and solvent frequencies by the relation

$$\zeta(t=0) = \frac{\omega_c^4}{\omega_s^2} \; . \tag{3.12}$$

The content of (3.11) can be clarified by considering the time correlation function of the solvent coordinate itself, when the solute coordinate is fixed at its Transition State value x=0. It is then a straighforward exercise to show from (3.10) that

$$\frac{\langle s \hat{s}(\varepsilon) \rangle_{\ddagger}}{\langle s^2 \rangle_{\ddagger}} = \frac{\varepsilon + \hat{\zeta}_s}{\varepsilon^2 + \omega_s^2 + \varepsilon \hat{\zeta}_s} \; ;$$

$$\langle s^2 \rangle = \frac{k_B T}{\omega_s^2} \; , \tag{3.13}$$

(recall that s is mass-weighted) from which we can deduce the relationships

$$\zeta(t) = \zeta(t=0)\Delta_{\ddagger}(t) \; ;$$

$$\hat{\zeta}(0) = \zeta(t=0)\ \hat{\Delta}_{\ddagger}(0) = \zeta(t=0)\tau_s \; , \tag{3.14}$$

where $\Delta_{\ddagger}(t)$ is the normalized equilibrium tcf of the solvent coordinate

$$\Delta(t) = \frac{\langle ss(t)\rangle}{\langle s^2\rangle} \tag{3.15}$$

(3.14) is a key relation which connects the time dependent friction on the reactive solute coordinate to the solvation dynamics.

It is useful, for later reference, to consider the friction (3.14) in several limits. The first example we consider is that when the frequency dependence of $\hat{\zeta}_s$ is ignored – $\hat{\zeta}(\varepsilon)\approx\zeta_s$ – and the solvent acceleration is ignored as well – i.e., an overdamped solvent; then one has

$$\hat{\Delta}_{\ddagger}(\varepsilon) \approx \left[\ \varepsilon + \frac{\omega_s^2}{\zeta_s}\ \right]^{-1} \tag{3.16}$$

or in time language there is exponential decay of the solute friction

$$\zeta(t) = \zeta(t=0)\ \exp\left(-\frac{t}{\tau_s}\right) \; ;$$

$$\tau_s = \frac{\zeta_s}{\omega_s^2} \; . \tag{3.17}$$

This approximation requires that $\zeta_s >> \omega_s$. This behavior in fact follows from a Debye dielectric continuum model of the solvent when it is coupled to the solute nuclear motion [21,22] and then τ_s would be proportional to the longitudinal dielectric relaxation time of the solvent; indeed, in the context of time dependent fluorescence (TDF), the Debye model leads to such an exponential dependence of the analogue

there of $\Delta_{\ddagger}(t)$ [44]. While (3.17) is a useful broad characterization and was used in initial studies [21,22], we will see in Sec. 4 that it often does not capture the critical microscopic aspects of the friction revealed in MD studies.

Another limit of interest is that when only short times are of importance. In this case, the time dependence of the solvent coordinate tcf $\Delta_{\ddagger}(t)$ can be ignored. Then one has $\zeta(t) = \zeta(t=0)$, which by (3.12), is a measure of the solute-solvent coupling frequency. This is particularly relevant for the nonadiabatic limit (2.8), where it is only the initial friction value that is relevant for the reaction.

So far, the solvent coordinate has not been defined. As noted at the beginning of this Section, the time dependent friction is to be found for the reacting solute fixed at the transition state value $x^{\ddagger}$ of *x*. By (3.14), its dynamics were related to those of an (unspecified) solvent coordinate *s*. One strategy to identify the solvent coordinate, its frequency, friction, etc., would be to derive an equation of motion for the relevant fluctuating force δF there. To this end, one can use a double-membered projection technique in terms of δF and $\delta \dot{F}$. In particular, we define the projection operator

$$P\theta = \delta F \, \langle (\delta F)^2 \rangle^{-1} \, \langle \delta F \theta \rangle + \delta \dot{F} \, \langle (\delta \dot{F})^2 \rangle^{-1} \, \langle \delta \dot{F} \theta \rangle \ . \tag{3.18}$$

which projects onto the fluctuating force and its "velocity". One quickly finds [54]

$$\delta \ddot{F}(t) = -\omega_{\delta F}^2 \delta F(t) - \int_0^t d\tau \, \zeta_{\delta F}(t-\tau) \, \delta \dot{F}(\tau) \ , \tag{3.19}$$

where the associated square frequency is

$$\omega_{\delta F}^2 = \frac{\langle (\delta \dot{F})^2 \rangle}{\langle (\delta F)^2 \rangle} = \frac{k_{\delta F}}{\mu_{\delta F}} \ , \tag{3.20}$$

and the time dependent friction for δF, per δF mass,

$$\mu_{\delta F} = \frac{k_B T}{\langle (\delta \dot{F})^2 \rangle} \ , \tag{3.21}$$

involves the projection operator (PO)-modified dynamical tcf of the generalized force

$$\delta f = \mu_{\delta f} \, [\delta \ddot{F} + \omega_{\delta F}^2 \delta F] \ . \tag{3.22}$$

Averages fixed at the transition state are to be understood in all of these equations.

Let us make some connections to the results which came from the previous model development. First, if we compare (3.19)-(3.22) with (3.11)-(3.15), a natural identification of the solvent coordinate s in Sec. 3 is in fact just the fluctuating force δF on x at the transition state. (Note especially that this choice associates the solvent coordinate with a direct measure of the relevant solute-solvent interaction.) The solvent mass, force constant and frequencies in Sec. 3 would then be given molecular expressions via (3.19)-(3.21), while the solvent friction $\zeta_s(t)$ of Sec. 3 would be the friction per mass for δf (3.22),

$$\zeta_{\delta F}(t) = (\mu_{\delta F} k_B T)^{-1} \langle \delta f \delta f(t) \rangle \ , \tag{3.23}$$

in which the dagger denotes PO-modified dynamics. The final conjunction of the two descriptions consists of the (consistent) identification of the square solute-solvent coupling frequency ω_c^2 in (3.6) by

$$\omega_c^4 = \omega_{\delta F}^2 \ \zeta(t=0) =$$

$$= (\mu k_B T)^{-1} \ \langle (\delta F)^2 \rangle \ [\langle (\delta \dot{F}^{\dagger})^2 \rangle \ / \ \langle (\delta F)^2 \rangle] =$$

$$= (\mu k_B T)^{-1} \ \langle (\delta \dot{F})^2 \rangle \ . \tag{3.24}$$

Thus, everything maps in a one to one fashion.

In fact, this sort of identification of the solvent coordinate s with the fluctuating force δF was first noticed in [5b], but its generality had not been pursued until Ref 45. It is important to remark that this force δF is a very highly *nonlinear* function of the coordinates of the solvent molecules, referenced to the solute location [5b]; one should not at all think (as some evidently do) that the intermolecular forces can be untenably linearized.

Even the simplest approximation to this system – that of totally ignoring the friction $\zeta_{\delta F}$ – gives a Gaussian behavior for the solute friction at short times [1,2],

$$\zeta(t) = \zeta(t=0) \ \exp\left[-\frac{\omega_{\delta F}^2 t^2}{2} \right] , \tag{3.25}$$

which at least captures the initial behavior we will find to be evident in the examples to be discussed in Sec. 4.1. Since, as noted there, only the short time behavior of the time dependent solute friction is often of importance for the rate, (3.25) could prove useful.

This model perspective can also be used to characterize the reaction coordinate, i.e., the appropriate combination of solute and solvent coordinates along which reactive trajectories move [1,5c,22,43]. This amounts to finding the two normal modes of the equations of motion (3.7). The reactive or unstable mode is the reaction coordinate, while the stable, transverse mode is the nonreactive coordinate. There is even a tcf expression for the reaction coordinate [22]. In this new, rotated coordinate system, TST is exact, for the given model description. Thus when such a simplified description is possible, the generalized frictional reduction of the transmission coefficient via GH theory can also be understood as a TST result in a *new* reaction coordinate that differs from the simple solute coordinate choice x – thus the rate constant is not the equilibrium solvation TST result. This observation has been subsequently made, and further developed, by others [46]. (We repeat, however, our note above that one *cannot* linearize the intermolecular forces themselves.) We also note that the simple model normal mode analysis is a special case of a more general solution reaction path analysis [43], which is the generalization to solution, of the gas phase Fukui approach [47]. We do not review this here, but simply give a few representative references on its development, applications and generalizations [43,48].

4. Simulation Studies

In this section, we give the highlights of a few case studies of the dynamics of chemical reactions. We begin with a brief survey of heavy particle charge transfer reactions, followed by a few words about electron transfer reactions and proton transfer reactions.

4.1. HEAVY PARTICLE CHARGE TRANSFER REACTIONS

For many chemical reactions with high sharp barriers, the required time dependent friction on the reactive coordinate can be usefully approximated as the tcf of the force with the reacting solute *fixed* at the transition state. That is to say, no motion of the reactive solute is permitted in the evaluation of (2.3). This restriction has its rationale in the physical idea [1,2] that recrossing trajectories which influence the rate and the transmission coefficient occur on a quite short time scale. The results of many MD simulations for a very wide variety of different reaction types [3-12] show that this condition is satisfied; it can be valid even where it is most suspect, i.e., for low barrier reactions of the ion pair interconversion class [6].

What does this time dependent friction look like? To answer this, we describe the MD calculated results [5c] for $\zeta(t)$ for the reactive asymmetric stretch coordinate for the $Cl^- + CH_3Cl$ S_N2 system in H_2O solvent, and its associated Fourier spectrum. The latter is particularly illuminating, since it displays peaks clearly identifiable from the spectrum of the same pure H_2O liquid. Thus contributions from the H_2O bends and

symmetric and antisymmetric stretches are apparent at frequencies above ~ 1,500 cm^{-1}. At the lower frequency range 300 cm^{-1} - 1,000 cm^{-1} appear the hindered rotational, i.e., librational, contributions of water. A further noteworthy point is that the higher frequency motions (bends, stretches) have a diminished amplitude in the friction as compared to the spectrum, i.e., they are not so strongly *coupled* to the reactive solute as are the water librations. This illustrates the simultaneous importance of the time scales of solvent motions and their coupling strength to the solute reaction coordinate. Turning the focus to the time perspective, a fairly rapid initial decay is apparent, followed by a substantial and much longer lived tail. The initial decay is well described by the Gaussian (3.25). The tail makes a significant contribution to the large friction constant, i.e., the zero frequency friction [cf.(2.7)]. A very similar sort of behavior of $\zeta(t)$, in time and in frequency, is observed in an MD simulation for a model of the S_N1 ionization of tert-butyl chloride in water [7]. If we exploit the perspective of the model (3.14), it is apparent that the solvation dynamics is decidedly nonexponential for these problems. It is simply *not* going to be very useful to describe the time dependence of $\zeta(t)$ for the reaction problem via the exponential Debye-type expression of Sec. 2. On the other hand, as discussed below, the S_N2 reaction is in the nonadiabatic limit, and the time dependence of $\zeta(t)$ is irrelevant.

A second example of $\zeta(t)$ is available for an ion pair fixed at the transition state separation in a model dipolar solvent [6a]. Here the unusual feature is a rapid initial drop to negative values, followed by a long positive tail. (Prior to this, an initial Gaussian time decay applies). Such quasi-oscillatory behavior is highly suggestive of some sort of collective solvent cage motion. Once again, the long tail is a significant contributor to the friction constant. This same overall behavior has been observed for various ion pair combinations for Na^+ and Cl^- in water solvent [6b], and appears to be fairly characteristic for ion pair systems. Again, if we exploit the perspective of (3.14), the solvation dynamics is decidedly nonexponential.

Typical chemical reactions are characterized by sharp reaction barriers, often arising in part from the existence of a reaction barrier in the gas phase. Thus, even though the magnitude of the reactive solute-solvent coupling is strong [large $\zeta(t=0)$], the intrinsic barrier is of such high frequency that the *nonadiabatic solvation* limit

$$\omega_{beq}^2 > \zeta(t=0) \; ; \qquad \omega_{bna}^2 > 0 \; , \tag{4.1}$$

discussed in Sec. 2.1 is often an excellent guide to the microscopic mechanism of the barrier passage. The Cl^- - CH_3CI S_N2 system in H_2O provides a clear illustration of this [7], for which the nonadiabatic frequency is very high, ~ 500 cm^{-1}, along the antisymmetric stretch solute reactive coordinate. GH theory is found to agree with the MD results for the basic reaction system, as well as for many variants of the system [5]. The reaction transmission coefficient is found to be accurately given by the nonadiabatic value (2.8). As mentioned in Sec. 2.1, in the nonadiabatic solvation

limit the solvent is effectively frozen during the short time scale during which the fate of a trajectory, reactive or otherwise, is decided – this time is ~ 20 fs in the S_N2 example, very short indeed. The solvation dynamics *per se* are then irrelevant on this short timescale. Instead, one can picture a static distribution of barriers in x faced by the reactive solute coordinate x, whose location and height depend on the solvent coordinate s. These barriers arise from the different solvation patterns that exist in equilibrium with the solute at its transition state configuration $x^{\ddagger} = 0$. The S_N2 solute transition state structure is symmetric – $Cl^{\delta-}CH_3^{\delta+}Cl^{\delta-}$, but the distribution of equilibrium solvent configurations has contributions in which there is asymmetric solvation, i.e., better solvation of one Cl or another by the water molecules. Indeed, the model Hamiltonian (3.4) can be rewritten [5c] in the form

$$H = \frac{1}{2}\dot{s}^2 + \frac{\omega_s^2 s^2}{2} + H_x^{\ddagger}(s) \; ;$$

$$H_s^{\ddagger}(s) = G_T + \frac{\dot{x}^2}{2} - \frac{1}{2}\omega_{bna}^2 [\Delta x(s)]^2 + \Delta V(s) \; ;$$

$$\Delta V(s) = (\omega_c^4 / 2\omega_{bna}^2) \, s^2 \; ;$$

$$\Delta x(s) = - (\omega_c^2 / \omega_{bna}^2) \, s \; , \qquad (4.2)$$

which is quite instructive. This gives a representation in terms of a sequence of solvation dependent barriers $\Delta V(s)$ for the x motion, located along the line $\Delta x(s)$. These barriers arise from precisely the asymmetric solvation patterns mentioned above [5a]. Calculation of the rate constant from this perspective gives [5b] just the nonadiabatic solvation result (2.8). Indeed, this model succeeds even in accounting for whether trajectories are or are not reactive, depending on the kinetic energy in the solute S_N2 coordinate, as follows. For given H_2O solvation configurations, there is a solvent barrier $\Delta V(x)$ along x, and a trajectory will be unsuccessful if the kinetic energy K_x in the antisymmetric stretch – the solute reactive coordinate – is less that $\Delta V(x)$, and it will be successful if it exceeds it. This picture is precisely confirmed in the simulation results. This kind of detail about the microscopic aspects of a reaction begins to approach that considered in state-resolved gas phase chemistry. Finally, the solvent coordinate s can in fact be identified for this system in terms of a microscopic force [5b]; this was referred to in Sec. 3.

In this nonadiabatic limit, the transmission coefficient is determined, via (2.8) by the ratio of the nonadiabatic and equilibrium barrier frequencies, and is in full agreement with the MD results [5a-5c]. (By contrast, the Kramers theory prediction based on the zero frequency friction constant is far too low. Recall that we emphasized for example the importance of the tail to the full time area of the S_N2 $\zeta(t)$. In the language of (3.14), the solvation time τ_s is not directly relevant in determining

κ.) In favorable cases, these frequencies can be calculated by solution phase integral equation technology [26]. This is important, since it provides a prediction route, via GH theory, which avoids an MD simulation.

Even for cases where the reaction transmission coefficient is independent of the solvent dynamics *per se,* those dynamics can still (and indeed must) play a crucial role in the overall reactive process. This can be illustrated by the results of an MD simulation of how the S_N2 system C1- + CH_3C1 in H_2O actually reaches (and leaves) the transition state [5d]. We first recall, from the discussion above, that the solute has a symmetric charge distribution $Cl^{\delta-}CH_3^{\delta+}Cl^{\delta-}$ in the transition state. Examination of the barrier climbing process, starting from an ion-dipole complex $C1^{-}\cdot\ CH_3Cl$, during the 500 fs of its duration reveals the following phenomena. The changes in the solvent energy and the solvent-reagent interchange potential energy are gradual over most of the 500 fs time span of relevance to the climb. These changes are smooth, implying that the corresponding change in the solvation of the reaction complex is also smooth and gradual. But the change of the charge distribution in the reagents is not at all gradual over this same 500 fs period. Instead, the transition from an ion-dipole to a symmetric charge distribution occurs almost entirely over the last 50 fs prior to the arrival of the system at the transition state [5d].

These results show that a major portion of the solvent reorganization to a state appropriate to solvating the symmetric charge distribution of the reagents at the barrier top takes place *well before* the reagent charge distribution begins to change. The solvation is unable to adiabatically follow the rapid change in the distribution of the negative charge among the reagents [5d]. (Actually, this is already implicit in the frozen solvent, nonadiabatic solvation results of Ref 5a-5c.) This prior solvent reorganization is a necessary condition for the reagents to reach the transition state; the requisite solvation at the transition state has begun to develop well before any change in the reagents charge distribution. Together with the results of [5a-5c], this shows very clearly for this S_N2 system that one cannot picture the progress of a chemical reaction as a calm progression along the potential of mean force curve – a chemical reaction is intrinsically a dynamic, and not an equilibrium event. (Incidentally, in our opinion it would be worthwhile to subject other reaction class examples to this kind of analysis.)

Of related interest are results for water response to an instantaneous change in the dipole of a solute [44a], for the time scale of the solvent response for several charge-transfer reactions in water, including the S_N2 reaction [49], and for a similar response for Fe^{2+} - Fe^{3+} in water [44b]. The time scales found in those studies for the water solvent relaxation - and that originally found in [5] for time-dependent friction on the S_N2 transition state - are similar to those observed for the prior reorganization of the solvent H_2O.

The polarization cage limit described in Sec. 2.1 will characterize the reaction when there is a relatively broad barrier in the mean potential (small ω_{beq}) and there is strong solute-solvent electrostatic coupling [large $\zeta(t=0)$]. This regime has been observed in an MD simulation of ion pair recombination dynamics in a polar solvent [6a], whose friction was described above. This reaction class is especially interesting, in that its reaction barrier is entirely solvent-induced; it does not exist in the vacuum. Again, agreement with GH theory predictions within the error bars of the simulation is found [6a]. The nature of the dynamics is involved in crossing the transition state is instructive, and we give some discussion of it. The contact ion pair (CIP), located

at a separation of ~ 3.3 Å, is characterized by an average solvation shell whose key feature is a ring of four solvent molecules, at ~ 4 Å from the CIP axis with their dipoles antiparallel to that of the CIP. For the solvent separated ion pair (SSIP), at separation ~ 7.5 Å, the average solvation shell is contracted to ~ 2.5 Å, due to the increased dipole moment of the SSIP, and contains only three solvent molecules. The solvation shell at the transition state, which is located at an ion pair separation of ~ 5.5 Å, has a structure intermediate between these. The solvation dynamics at the transition state which allow, e.g., the formation of the SSIP, consist of a solvation shell contraction, with inward motion of three of its members. For passage to the CIP on the other hand, an expansion of the solvation shell is necessary. Without the occurence of these motions, the system is trapped in the transition state neighborhood, the hallmark of the polarization cage regime. It is also instructive to note that the solvent molecule motions appear to be much more translational than reorientational in character. It is also difficult to conceive that the dielectric relaxation time of the solvent has much direct relevance for such dynamics.

4.2. ELECTRON AND PROTON TRANSFER REACTIONS

We now turn to the electronically adiabatic ET reaction problem (cf. Sec. 2.2). There has been a spate oftheoretical papers [8,11,,28,33,35,36,50] dealing with the possible role of solvent dynamics in causing departures from the standard Marcus TST rate theory [27,28] (although many of these deal with nonadiabatic reactions). The ET reaction considered is a simplified symmetric model, $A^{-1/2}$ $A^{1/2} \rightarrow A^{1/2}$ $A^{-1/2}$, in a model solvent similar to CH_3Cl. The technical and computational rationales for this somewhat artificial fractional charge model are given in [8]; however, the model is sufficiently realistic to explicitly address the key dynamical issues.

The MD reaction simulation is effected via the electronically adiabatic Hamiltonian [8]

$$H_{ad} = \frac{H_R + H_P}{2} - \frac{1}{2}\sqrt{(\Delta E)^2 + 4\beta^2}\ ;$$

$$\Delta E = H_R - H_P\ , \qquad (4.3)$$

where $H_{R(P)}$ is the system Hamiltonian when the solute has the R(P) charge distribution and β is the invariant electronic coupling. This is appropriate as representative for many adiabatic ET reactions; in addition, solvent dynamical effects are expected to be most pronounced in the electronically adiabatic limit [33]. With this Hamiltonian, the reacting solute is always in its ground elelctronic state whatever the configurations of the solvent molecules may be. The barrier is traversed as ΔE progresses from values appropriate to the neighborhood of equilibrium with R to those similary appropriate to P. The solute electronic charge evolves smoothly from that of R, through the transition state distribution A^0 A^0 – which is a neutral pair, on

to the P charge distribution.

The transmission coefficient $\kappa = k_{ET} / k_{ET}^{TST}$ measures the departure of the rate constant from its Marcus, TST value and can be directly computed, for different choices of the electronic coupling β, in an MD simulation for the ET reaction [8]. The first important point is that for β = 1 kcal/mol, κ is quite close to unity; there are few recrossings of the barrier and the Marcus TST Theory is thus an excellent approximation.

When the coupling is increased to β = 5 kcal/mol and the barrier becomes more rounded, the transmission coefficient is smaller ($\kappa_{ET} \approx 0.6$) and there are noticeable departures from the Marcus TST theory, although they are not enormous. The the barrier recrossings are found to be restricted to the immediate vicinity of the reaction barrier top.

The GH theory can be applied for such dynamical rate effects and the transmission coefficient is given by (2.5), rewritten here as

$$\kappa_{ET} = \frac{k^{ET}}{k_{ET}^{TST}} = [\ \lambda + \hat{\zeta}_{ET}^{\ddagger}(\lambda)\ ]^{-1}\ \omega_{beq}^{ET} \ . \tag{4.4}$$

In the present context, GH theory relies on the assumption that the GLE (cf. Sec. 2.2)

$$\delta\Delta\ddot{E}(t) = (\omega_{beq}^{ET})^2\ \delta\Delta E(t) - \int_0^t d\tau \zeta_{ET}^{\ddagger}(t-\tau)\ \delta\Delta\dot{E}(\tau) \tag{4.5}$$

holds in the vicinity of the barrier top $\Delta E = \Delta E^{\ddagger} = 0$ [8,33]. The barrier frequency ω_{beq}^{ET} can be estimated [8] from the fomuIa $\omega_{beq}^{ET} = \omega_R\ [(\ 2\Delta G^{\ddagger} / \beta) - 1\ ]^{1/2}$, where ω_R is the frequency of the reactant solvent well. The friction $z\ddagger(t)$ appropriate for the transition state can be approximated [8] by the time dependent friction for the reference situation of a *neutral* pair. This approximate identification follows from the observation, mentioned above, that in the ET reaction, the transition state charge distribution is that of a neutral pair. The neutral pair friction $\zeta_{NP}(t)$ can be extracted [8] from studies of time dependent flurorescence dynamics, and with the approximation $\zeta_{ET}(t) \approx \zeta_{NP}(t)$, κ_{GH} can be estimated via (4.4) for the ET reaction. The results agree to within the error bars with the MD simulation values [8,11].

Actually, all of the above results are in contradiction to the currently conventional view [32-35] that solvent dynamical effects for electronically adiabatic ET reactions are determined by solvent dynamics in the R and P wells, and not the barrier top region. This misses the correct picture, even for fairly cusped barrier. Instead, it is the solvent dynamics occurring near the barrier top, and the associated time dependent friction, that are the crucial aspects. It could however be thought possible that, for cusped barrier adiabatic ET reactions in much more slowly relaxing solvents, the well dynamics could begin to play a significant role. However, MD simulations have now been carried out for the same ET solute in a solvent where the

solvent molecule internuclear separation is increased [11b]. This lengthening slows down the solvent molecule motion and causes it to be quite strongly overdamped – the ratio of $\zeta_{\delta\Delta e}$ / 2 $\omega_{\delta\Delta E}$ is of order 10. Yet once again it is found [11b] that the transmission coefficient is determined by trajectories near the barrier top and that the conventional well relaxation picture for the reaction is not valid.

The above discussion was for ET reactions with modest ot high barriers, where the barrier frequency is reasonably high. A quite different situation can arise for reactions with low barriers; here there is no obvious intrinsic bias favoring short time solvent dynamical effects in influencing the reaction rate. Some striking illustrations of this are given in [50] where it is found that various portions of the solvation dynamics can influence the ET rate for several low barrier exothermic ET reactions in methanol, depending on the detailed character of the free energy surface. This underlines the important point that what solvation dynamics are relevant for a reaction is very much a function of the reaction being considered.

Finally, for the PT problem, dynamical friction effects have been examined for a model for a phenol-amine acid-base reaction in methyl chloride solvent [12]. With the quantization of the proton and the O-N vibration, the problem can be reduced to a one-dimensional solvent coordinate problem, similar to the ET case. Again, GH theory is found to agree with the MD results to within the error bars of the computer simulation.

5. Other Applications

Another arena for the application of stochastic frictional approaches is the influence of ionic atmosphere relaxation on the rates of reactions in electrolyte solutions [19]. To gain perspective on this, we first recall the early and often quoted triumph of TST for the prediction of salt effects, in connection with Debye-Hückel theory, for reaction rates: In k^{TST} varies linearly with the square root of the solution ionic strength I, with a sign depending on whether the charge distribution of the transition state is stabilized or destabilized by the ionic atmosphere compared to the reactants.

But the entire conception here is that of equilibrium solvation of the transition state by the Debye ionic atmosphere, and closer inspection [51] indicates that this assumption can hardly be justified; indeed, time scale considerations reveal that it will nearly always be violated. The characteristic time for the system to cross the reaction barrier is ω_{beq}^{-1} ~ 0.1 ps say. On the other hand, the time required for equilibration of the atmosphere is something like the time for an ion to diffuse over the atmosphere dimension, the Debye length κ^{-1}; this time is ≈ 1 ns for a salt concentration C= 0.1M and only drops to 10ps for C ≈ 1M. Thus the ionic atmosphere is perforce out of equilibrium during the barrier passage, and in analogy with ionic transport problems, there should be an ionic atmosphere friction operative on the reaction coordinate which can influence the reaction rate.

These aspects were examined in a study [51] which employed a generalized Debye-Falkenhagen description for the ionic atmosphere dynamical friction and GH theory for the rate. It was found that, while indeed the atmosphere is almost never equilibrated during the barrier passage and to a large extent is frozen on this time scale, the atmosphere frictional derivations from the equilibrium solvation TST result

is often small. The reason for this is that, during the critical transit over the barrier top, there will not be an enormous charge shift and the ensuing electrostatic interaction force with the diffuse atmosphere is not large. This is thus an example of the weak solvation regime discussed in Sec. 2.1: the environment of the reacting solute is completely out of equilibrium, but the coupling to the solute is sufficiently weak that the system reacts despite the nonequilibrium conditions, and negligible frictional impact on the equilibrium solvation k^{TST} result ensues.

Nonetheless, there can be nonnegligible atmosphere frictional reduction of the rate constant when the electrolyte concentration is sufficiently high that the coupling force magnitude is important [51] (this reduction requires GH theory for its description; the zero frequency friction Kramers prediction can give an order of magnitude too large a reduction in the rate).

These predictions await experimental and simulation confirmation. It is worth pointing out that the continuum ion atmosphere approach is being pushed to its limits at the electrolyte concentrations high enough to cause the predicted dynamical effects on the rate, and it may be that a more molecular description is required to provide an accurate account of dynamic salt effects on reaction rates [52]. For example, it is clear that ion pairing effects are paramount in low dielectric constant solvents [53], which were excluded in the study of Ref. 51, and these may prove to be important even in high polarity solvents. The entire area needs further study, as does for example the closely related area of charge transfer reactions at electrodes occuring in the presence of an electrical double layer [54]. We mention that frictional effects on rates are beginning to be examined in other interfacial problems [55]. Finally, we observe that GH theory could be extended to reactions in enzymes and in solids, but evidently this remains to be done.

6. Concluding Remarks

We have reviewed above the GH approach to reaction rate constants in solution, together with simple models that give a deeper perspective on the reaction dynamics and various aspects of the generalized frictional influence on the rates. The fact that the theory has always been found to agree with Molecular Dynamics computer simulation results for realistic models of many and varied reaction types gives confidence that it may be used to analyze real experimental results.

It may be that in the future some cases may show noticeable deviations from GH theory and some further generalizations [56] may be necessary. In our view, this is most likely to happen for broad, low barrier reactions, where one should probably use a generalized spatial diffusional Smoluchowski approach instead, However, it seems most profitable to instead now focus effort on constructing useful theories for the reaction barrier heights – which, after all, are the most important features in determining the reaction rate constant – and more generally, reaction free energy surfaces. For this goal, one must face the problem of describing solute electronic structure in solution, under the nonequilibrium solvation conditions that have been stressed throughout this chapter. Some aspects of this are described in the article with Roberto Bianco in this volume.

7. Acknowledgments

We gratefully acknowledge the collaborative efforts of our students and co-workers, indicated in the references. This work was supported in part by NSF grants CHE 88-07852 and CHE 93-12267 and an NIH Shannon Award. This chapter was completed at UAB under the tenure of an Iberdrola Foundation Invited Visiting Professorship, and we thank the Foundation for its support and various members of the Unitat de Quimica Físìca for their hospitality.

8. References

1. Hynes, J. T., in *The Theory of Chemical reaction Dynamics,* Vol. IV, M. Bear, ed. (CRC Press, Boca Raton, FL, 1985), p. 171.

2. Grote, R. F. and Hynes, J. T., *J Chem. Phys.* **76,** 2715 (1980). (For some recent discussion of the GH rate equation and especially the associated GLE from a theoretical point of view, see Tarjus, G. and Kivelson, D., *Chem. Phys.* **152,** 153 (1991) and Ref. 5c below.)

3. Whitnell, R. M. and Wilson, K. R., *Adv. Comp. Chem.* **4,** 67 (1993).

4. Bergsma, J. P., Reimers, J. R., Wilson, K. R., and Hynes, J. T., *J. Chem. Phys.* **85,** 5625 (1986).

5. (a) Bergsma, J. P., Gertner, B. J., Wilson, K. R., and Hynes, J. T., *J. Chem. Phys.* **86,** 1356 (1987); (b) Gertner, B. J., Bergsma, J. P., Wilson, K. R., Lee, S., and Hynes, J. T., *ibid.* **86,** 1377 (1987); (c) Gertner, B. J., Wilson, K. R., and Hynes, J. T., *ibid.* **90,** 3537 (1989); (d) Gertner, B. J., Whitnell, R. M.; Wilson, K. R., and Hynes, J. T., J. *Am. Chem. Soc.* **113,** 74 (1991).

6. (a) Ciccotti, G., Ferrario, M., Hynes, J. T., and Kapral, R., *J Chem. Phys.* **93,** 7137 (1990); (b) Rey, R., and Guàrdia, E., J. *Phys. Chem.* **96,** 4712 (1992).

7. Keirstead, W. P., Wilson, K. R., and Hynes, J. T., *J. Chem. Phys.* **95,** 5256 (1991).

8. Zichi, D. A., Ciccotti, G., Hynes, J. T., and Ferrario, M., *J. Phys. Chem.* **93,** 2184 (1989).

9. (a) Zhu, S. B., Lee, J., and Robinson, G. W., *J. Phys. Chem.* 92,2401 (1988); (b) Berne, B. J., Borkevec, M., and Straub, J. E., *ibid.* **92,** 3711 (1988); (c) Roux, B. and Karplus, M., *ibid.* **95,** 4845 (1991).

10. Tucker, S. and Truhlar, D., *J. Am. Chem. Soc.* **112,** 3347 (1990).

11. (a) Smith, B. B., Kim, H. J.; Borgis, D., and Hynes, J. T., in *Dynamics and Mechanisms of Photoinduced Electron Transfer and Related Phenomena,* N. Mataga, T. Okada, and H. Masuhara, eds., (Elsevier, Amsterdam, 1992), p. 39; (b) Smith, B. B., Staib, A., and Hynes, J. T., *Chem. Phys.* **176,** 521 (1993).

12. Staib, A., Borgis, D., and Hynes, J. T., *J. Chem. Phys.* **102,** 2487 (1995).

13. Bagchi, B. and Oxtoby, D. W., *J. Chem. Phys.* **78,** 2735 (1983).

14. Ashcroft, J., Besnard, M., Aquada, V., and Jonas, J., *Chem. Phys. Lett.* **110,** 430 (1984).

15. Zeglinski, D. M. and Waldeck, D. H., *J. Phys. Chem.* **92,** 692 (1988); Sivakumar, N.; Hoburg, E. A., and Waldeck, D. H., *ibid.* 93, 2305 (1989); Park, N.S. and Waldeck, D. H., *ibid.*

16. McManis, G. E. and Weaver, M. J., *J. Chem. Phys.* **90,** 1720 (1989).

17. For some general reviews, see Ref. 1 and Truhlar, D. G., Hase, W. L., and Hynes, J. T., *J. Phys. Chem.* **87,** 2664 (1983); Hynes, J. T., *Annu. Rev. Phys. Chem.* **36,** 573 (1985); Berne, J. B., Borkovec, M., and Straub, J. E., *J. Phys. Chem.* **92,** 3711 (1988); Hänngi, P., Talkner, P., and Borkovec, M., *Rev. Mod. Phys.* **62,** 251 (1990); Simon, J. D., *Acc. Chem. Res*. **21,** 128 (1988); Bagchi, B. *Annu. Rev. Phys. Chem.* **37,** 127 (1986). In adition, the special issue *Chem. Phys.* **152,** nos. 1 and 2 (1991) is devoted to friction in liquid state reactions.

18. (a) Fleming, G. and Hanggi, P., eds. *Activated Barrier Crossing* (World Scientific, New Jersey, 1993); (b) Warshel, A., *Computer Modeling of Chemical Reactions in Enzymes andSolutions* (Wiley, New York, 1991); (c) Adelman, S. A., *Rev. Chem. Intermediates* **8,** 321 (1987); (d) Nitzan, A., *Adv. Chem. Phys.* **70,** 489 (1988).

19. Lowry, T. H. and Richardson, K. S., *Mechanism and Theory in Organic Chemistry,* 3rd Edition (Harper and Row, New York, 1987); Reichardt, C. S., *Solvent Effects in Organic Chemistry* (Verlag Chemie, Weinheim, 1988).

20. Kramers, H. A., *Physica* **7,** 284 (1940).

21. van der Zwan, G. and Hynes, J. T., *J. Chem. Phys.* **76,** 2993 (1982).

22. van der Zwan, G. and Hynes, J. T., J. *Chem. Phys.* **76,** 4174 (1983); Chem. Phys. **90,** 21 (1984). For some recent related work, see Ben-Num, M.: and Levine, R.D., *Acc. Chem. Res.* **27,** 166 (1994).

23. Kurz, J. L. and Kurz, L.C., *J. Am. Chem. Soc.* **94,** 4451 (1972).

24. Hynes, J. T., in *Ultrafast Dynamics of Chemical Systems,* Simon, J. D., ed. (Kluwer, Dordrecht, 1994), p. 345.

25. Chandrasekhar, J., Smith, S. F., and Jorgensen, W. L., *J. Am. Chem. Soc.* 106, 3049 (1984); *ibid.* **107,** 154 (1985).

26. Houston, S. E., Rossky, P. J., and Zichi, D., *J. Am. Chem. Soc.* **111,** 5680 (1989).

27. Marcus, R. A., *J. Chem. Phys.* **24,** 966-979 (1956).

28. See, e.g., Newton, M. D. and Sutin, N., *Annu.Rev. Phys. Chem.* **35,** 437 (1984).

29. For recent developments, one may consult: *Dynamics and Mechanics of Photoinduced Electron Transfer and Related Phenomena,* Mataga, N., Okada, T., and Masuhara, H., eds. (Elsevier, Amsterdam, 1992), and Ref. 30.

30. Weaver, M., *J. Mol. Liq.* **60,** 57 (1994).

31. For an early example of the use of ΔE coordinates, see Warshel, A., *J. Phys. Chem.* **86,** 2218 (1982).

32. Zusman, L. D., *Chem. Phys.* **49,** 295 (1980).

33. Hynes, J. T., *J. Phys. Chem.* **90,** 370 (1986).

34. Rips, I. and Jortner, J., *J. Chem. Phys.* **87,** 2090 (1987).

35. (a) Alexandrov, I. V. and Gabrielyan, R. G., *Mol. Phys.* **37,** 1963 (1979); Friedman, H. L. and Newton, M. D., *Faraday Discuss. Chem. Soc.* **74,** 73 (1982); Calef, D. F. and Wolynes, P. F., *J. Phys. Chem.* **87,** 3387 (1983); Sumi, H. and Marcus, R. A., *J. Chem. Phys.* **84,** 4272 (1986); Sparpaglioni, M. and Mukamel, S., *J. Chem. Phys.* **88,** 3263 (1988); (b) Rips, I. and Jortner, J., *ibid.* **87,** 2090 (1987); (c) Dakhnovskii, Yu. I. and Ovchinikov, A. D., *Mol. Phys.* **58,** 237 (1986); Zusman, L. D., *Chem. Phys. 51,* 119 (1988); Murillo, M. and Cukier, R. I., *J. Chem. Phys.* **89,** 6736 (1988); Fonseca, T., *ibid* **92,** 2869 (1989); Zhou, Y., Friedman, H. L., and Stell, G., *Chem. Phys.* **152,** 185 (1991); McManis, G. E., Gochev, A., and Weaver, M. J., *ibid.* **152,** 107 (1991).

36. There are other simulations of aspects of electron transfer reactions, but they do *not* address the issues considered here. See, e.g., (a) Warshel, A., *J. Chem. Phys.* **86,** 2218 (1982); Hwang, J. and Warshel, A., *J. Am. Chem. Soc.* **109,** 715 (1987); (b) Halley, J. W. and Hautmann, J., *Phys. Rev.* **B38,** 11704 (1988); (c) Kuharski, R A., Bader, J. S., Chandler, D., Sprik, M., Klein, M. L., and Impey, R W., *J. Chem. Phys.* **89,** 3248 (1988); (d) Gonzalez-Lafonf A., Lluch, J. M., Oliva, A., and Bertran, J., in *Chemical Reactivity in Liquids,* M. Moreau and P. Turq, eds. (Plenum, New York, 1988), p. 197; (e) Hwang, J. K. Creighton, S., *King,* G., Whitney, D., and Warshel, A., *J. Chem. Phys.* **89,** 859 (1988).

37. Ulstrup, J., *Charge Transfer Processes in Condensed Media* (Springer, Berlin, 1979); Dogonadze, R. R., Kuznetzov, A. M., and Levich, V. G., *Electrochim. Acta* **13,** 1025 (1968).

38. Borgis, D., Lee, S., and Hynes, J. T., Ch*em*. *Phys. Lett.* **162,** 19 (1989); Borgis, D. and Hynes, J. T., *J. Chem. Phys.* **94,** 3619 (1991); *Chem. Phys.* **170,** 315 (1993). Cukier, R. I. and Murillo, M. *J. Chem. Phys.* **91,** 857 (1989); Makri, N. and Miller, W. H., *J. Chem. Phys.* **91,** 4026 (1989); Schenter, G. K., Messina, M., and Garrett B. C., *J. Chem. Phys.* **99,** 1674 (1993); Liu, Y. P., Lynch, G. C., Truong, T. N., Lu, D. H., Truhlar, D. G., and Garrett, B. C., *J. Am. Chem. Soc.* **115,** 2408 (1993); Suarez, A. and Silbey, R, *J. Chem. Phys.* **94,** 4809 (1991); Truong, T. N., McCammon, J. A., Kouri, D. J., and Hoffman, D. K., *J. Chem. Phys.* **96,** 8136 (1992); Bala, P., Leysyng, B., Truong, T. N., and McCammon, J. A., in *Molecular*

Aspects of Biotechnology: Computational Models and Theories, Bertrain J., ed. (Kluwer: Dordrecht, The Netherlands, 1992); Marvi, J. and Berendsen, H. J. C., *J. Phys. Chem.* **97,** 13464 (1993); *J. Mol. Struct.* **82,** 322 (1994); Lobaugh, J. and Voth, G. A., Chem. Phys. Lett. **198,** 311 (1992); *J. Chem. Phys.* **100,** 3039 (1994).

39. Ando, K. and Hynes, J. T., in *Structure, Energetics and Reactivity in Aqueous Solution,* Cramer, C. J. and Truhlar, D. G., eds. (ACS, Washington, DC., 1994). p 143.

40. German, E. D., Kuznetzov, A. M., and Dogonadze, R. R., *J. Chem. Soc. Faraday Trans. II* **76,** 1128 (1980).

41. Staib, A., Borgis, D., and Hynes, J. T., *J. Chem. Phys.* **102,** 2487 (1995).

42. Warshel, A., *J. Phys. Chem.* **86,** 2218 (1982); Hwang, J. K., Chu, Z. T., Yadav, A., and Warshel, A., *J. Phys. Chem.* **95,** 8445 (1991); Borgis, D., Tarjus, G., and Azzouz, H., *J. Phys. Chem.* **96,** 3188 (1992); *J. Chem. Phys.* **97,** 1290 (1992); Laria, D., Ciccotti, G., Ferrario, M., and Kapral, R, *J. Chem. Phys.* **97,** 378 (1992); Azzouz, J. and Borgis, D., *J. Chem. Phys.* **98,** 7361 (1993); *J. Mol. Liq,* **61,** 17 (1995); **63,** 89 (1995); Gillan, M., *J. Phys. Chem.* **20,** 3621 (1987); *Phys. Rev. Lett.* **58,** 563 (1987); Voth, G. A., Chandler, D., and Miller, W. H., *J. Phys. Chem.* **93,** 7009 (1989); J. Chem. Phys. 91, 7749 (1989); G. A. Voth, *J. Phys. Chem.* **97,** 8365 (1993); Li, D and Voth, G. A., *J. Phys. Chem.* **95,** 10425 (1991); Bhattacharya-Kodali, I. and Voth, G. A., *J. Phys. Chem.* **97,** 11253 (1993).

43. Lee, S., and Hynes, J. T., *J. Chem. Phys.* **88,** 6853, 6863 (1988); Zichi, D. A. and Hynes, J. T., *ibid,* **88,** 2513 (1988); Kim, H. J. and Hynes, J. T. *J. Am. Chem. Soc.* **114,** 10508, 10528 (1992), Mathis, J. R. and Hynes, J. T., *J. Phys. Chem.* **98,** 5445, 5460 (1994); Fonseca, T., Kim, H. T., and Hynes, J. T., J. *Mol. Liq.* **60,** 161 (1994); Gertner, B. J., Ando, K., Bianco, R., and Hynes, J. T., *Chem. Phys.* **183,** 309 (1994).

44. For reviews, see, e.g., Kosower, E. M. and Huppert, D., *Annu. Rev. Phys. Chem.* **37,** 127 (1986); Barbara, P. F. and Jarzeba, W., *Adv. Photochem.* **15** (1990); Maroncelli, M., MacInnis, J., and Fleming, G. R., *Science,* **243,** 1674 (1989); Maroncelli, M., Simon, J. D., *J. Phys. Chem.* **91,** 2693 (1987); *Chem. Phys. Lett.* **158,** 423 (1989); Maroncelli, M., *J. Molec. Liq.,* 57 (1993). Some representative experimental studies include Su, S.-G. and Simon, J. D., *J. Phys. Chem.* **91,** 2693 (1987); *Chem. Phys. Lett.* **158,** 423 (1989); Kahlow, M. A., Jarzeba, W., Kang, T. J., and Barbara, P. F., *ibid.* **90,** 151 (1988); Maroncelli, M. and Fleming, G. R., *ibid.* **86,** 6221 (1987); Castner Jr., E W., Maroncelli, M. and Fleming, G. R., *ibid.* **86,** 1090 (1987); Simon, J. D. and Su, S.-G., *Chem. Phys.* **152,** 143 (1991). Representative theoretical studies include (a)Maroncelli, M. and Fleming, G. R., *J. Chem. Phys.* **86,** 6221 (1987); 89, 5044 (1987); (b) Bader, J. S. and Chandler, D., *Chem. Phys. Lett.* **157,** 501 (1989); (c) i) Levy, R. M., Kitchen, D. B., Blair, J. T., and Krogh-Jespersen, K., *J. Phys. Chem.* **94,** 4470 (1990), Blair, J. T., Krogh-Jespersen, K., and Levy, R. M., *ibid.* **111,** 6948 (1989); ii) Benjamin, I. and Wilson, K. R., *ibid.* 95, 4068 (1992); (d) Maroncelli, M., *J. Chem. Phys.* **94,** 2084 (1991); (e) Fonseca, T., *J. Chem. Phys.* **91,** 2869 (1989); *Chem. Phys. Lett.* **162,** 491 (1989); (f)Carter, E. A. and Hynes, J. T., *J.*

Chem. Phys. **94,** 5961 (1991); (g) Carter, E. A. and Hynes, J. T., *J. Phys. Chem.* **93,** 2184 (1989); Fonseca, T., Ladanyi, B. M., and Hynes, J. T., *ibid.* **96,** 4085 (1992); Fonseca., T. and Ladanyi, B. M., *J.* Mol. *Liq.,* **60,** 1 (1994); King, G. and Warshel, A., *J. Chem. Phys.* **93,** 8682 (1990); (h) Fonseca, T. and Ladanyi, B. M., *J. Phys. Chem.* **95,** 2116 (1991); (i) van der Zwan, G. and Hynes, J. T., *J. Phys. Chem.* **89,** 4181 (1985).

45. Hynes, J. T., unpublished.

46. Pollak, E., *J. Chem. Phys.* **85,** 865 (1986); *Chem. Phys. Lett.* **127,** 178 (1986).

47. Fukui, K., J. Phys. Chem. **23,** 4161 (1970); *Acc. Chem. Res.* **14,** 363 (1981).

48. Schenter, G. K., McRae, R. P. and Garrett, B. C., *J. Chem,* Phys. **97,** 9116 (1992); Truhlar, D. G., Schenter, G. K., and Garrett, B. C., *ibid.* **98,** 5756 (1993); Schenter, G. K., Messina, M., and Garrett, B. C., **99,** 1674 (1993).

49. Hwang, J.-K., King, G., Creighton, S., and Warshel, A., *J.* Am. *Chem. Soc.* **110,** 5297 (1988).

50. Fonseca, T. and Ladanyi, B. M., in *Ultrafast Reactions and Solvent Effects,* Gaudel, *Y.* and Rossky, P. J., eds. (AIP, New York, 1994). The low barrier ET reaction case is generally, though not always, a more faithful adherent to the full spectrum of solvation dynamics: see also Tominaga, K., Walker, G. C., Kang, T. J., Barbara, P. F., and Fonseca, T., *J. Chem. Phys.* **95,** 10485 (1991); Kang, T. J., Jarzeba, W., Barbara, P. F., and Fonseca, T., *Chem. Phys.* 149, 81 (1990), in *Perspectives in Photosynthesis,* J. Jortner and B. Pullman, eds. (Kluwer, Dordrecht, 1990).

51. van der Zwan, G. and Hynes, J. T., *Chem. Phys.* **152,** 169 (1991).

52. Neria, E. and Nitzan, A., in *Ultrafast Reactions and Solvent Effects,* Gauduel, Y. and Rossky, P. J., eds. (AIP, New York, 1994).

53. Chapman, C. F. and Maroncelli, M., *J. Phys. Chem.* **95** ,9095 (1991); Ittah, V. and Huppert, D., *Chem. Phys. Lett.* **173,** 496 (1990); Huppert, D., Itah, V., and Kosower, E. M., *ibid.* **159,** 267 (1989),

54. Sebastian, K., *J. Chem. Phys.* **90,** 5056 (1989); Smith, B. B. and Hynes, J. T., ibid, **99,** 6517 (1993); Schmickler, W., *J. Electroanal. Chem.* **230,** 43 (1987); Morgan, J. D. and Wolynes, P. G., *J. Phys. Chem.* **91,** 874 (1987).

55. Benjamin, I., *J. Chem. Phys.* **95,** 874 (1987); *Acc. Chem. Res.* **28,** 233 (1995).

56. Voth, G. A., *J. Chem. Phys.* **97,** 5908 (1992); Haynes, G. R., Voth, G. A., and Pollak, E., *J. Chem. Phy.* **101** 7811 (1994), and references therein.

VALENCE BOND MULTISTATE APPROACH TO CHEMICAL REACTIONS IN SOLUTION

ROBERTO BIANCO AND JAMES T. BYNES
Department of Chemistry and Biochemistry
University of Colorado, Boulder, CO 80309-0215, USA

1. Introduction

In this contribution, we describe and illustrate the latest generalizations and developments[1]-[3] of a theory of recent formulation[4]-[6] for the study of chemical reactions in solution. This theory combines the powerful interpretive framework of Valence Bond (VB) theory[7] — so well known to chemists — with a dielectric continuum description of the solvent. The latter includes the quantization of the solvent electronic polarization[5, 6] and also accounts for nonequilibrium solvation effects. Compared to earlier, related efforts[4]-[6], [8]-[10], the theory [1]-[3] includes the boundary conditions on the solute cavity in a fashion related to that of Tomasi[11] for equilibrium problems, and can be applied to reaction systems which require more than two VB states for their description, namely: bimolecular S_N2 reactions[7],[8](b),[12],[13] $X^- + RY \rightarrow XR + Y^-$, acid ionizations[8](a),[14] $HA + B \rightarrow A^- + HB^+$, and Menschutkin reactions[7](b), among other reactions. Compared to the various reaction field theories in use[11],[15]-[21] (some of which are discussed in the present volume), the theory is distinguished by its quantization of the solvent electronic polarization (which in general leads to deviations from a Self-consistent limiting behavior), the inclusion of nonequilibrium solvation — so important for chemical reactions, and the VB perspective. Further historical perspective and discussion of connections to other work may be found in Ref.[1].

The outline of this review is as follows. In Sec.2, we highlight the fundamental equations and structure of the theory: Sec.2.1 motivates the choice for the functional form of the solute wave function; Sec.2.2 explains the equation for the free energy of the solute plus solvent system in the nonequilibrium solvation regime; Sec.2.3 discusses the corresponding Schrödinger

O. Tapia and J. Bertrán (eds.), Solvent Effects and Chemical Reactivity, 259–281.
© 1996 *Kluwer Academic Publishers. Printed in the Netherlands.*

equation. The details of the formulation can be found in Ref.[1] (hereafter referred to as BH-I). In Sec.3, guided by a flow chart which summarizes our computational strategy, we describe the application of this formalism to the dissociation of I_2^- in acetonitrile in a two VB state framework reported in Ref.[2] (hereafter referred to as BH-II), and focus on several practical aspects concerning the implementation procedure. To broaden the perspective, the possible applications of our formalism in a two and three VB state framework respectively are sketched for both the *tert*-butylchloride S_N1 reaction system (Sec.4) and the $Cl^- + CH_3Cl$ S_N2 reaction system (Sec.5). We offer concluding remarks in Sec.6.

2. Theory

2.1. SOLUTE WAVEFUNCTION

The system wave function ansatz is the linear combination

$$|\Phi\rangle = \sum_{i=1}^{N_s} c_i \,|\, i\rangle \,|P_e^{(i)}\rangle \quad , \tag{2.1}$$

where the orthonormal $\{|i\rangle\}$ are solute diabatic electronic states, and the $\{|P_e^{(i)}\rangle\}$ are coherent states for the solvent electronic polarization[6]. By taking the functional derivative of the system free energy with respect to the coherent states' eigenvalues $\{P_e^{(i)}\}$, one obtains the *effective* solute wave function with equilibrated solvent electronic polarization in the simpler form

$$|\Psi\rangle = \sum_{i=1}^{N_s} c_i \,|\, i\rangle \quad . \tag{2.2}$$

(Henceforth all summations of indices i and j span the range $[1, N_s]$.) The wave function (2.2) is normalized, i.e. $\langle\Psi|\Psi\rangle = \Sigma_i\, c_i^2 = 1$, and its configuration interaction (CI) functional form describes best the idea of a solute system represented by a set of VB resonance structures.

In this context, the term *diabatic* means that the character of the charge distribution of each state — representative of a well-defined solute resonance structure — is conserved throughout the reaction. Indeed, the electronic structure of the components $\{|i\rangle\}$ is assumed not to be changed by the interaction with the solvent: the solvent effects are exclusively reflected by the variation of the coefficients $\{c_i\}$, which is to say that the solvent can polarize the solute electronic structure over its VB states.

The advantage of the wave function (2.2) over e.g. the choice of a more familiar Hartree-Fock (HF) wave function is its ease of interpretability, as we now illustrate for the *tert*-butylchloride (BuCl) S_N1 reaction system[10].

The wave function for this system can be written as a linear combination of two VB states, which represent the ionic Bu^+Cl^- and the covalent Bu–C1 resonance structures, namely

$$|\Psi_{BuCl}\rangle = c_{ion}|\Psi_{Bu^+Cl^-}\rangle + c_{cov}|\Psi_{Bu-Cl}\rangle \quad . \tag{2.3}$$

The values of c_{ion} and c_{cov} determine the weights of the respective components, and reflect the relative stabilization of the VB states in solution: e.g. a polar solvent is expected to stabilize the ionic $|\Psi_{Bu^+Cl^-}\rangle$ relative to the covalent $|\Psi_{Bu-Cl}\rangle$. By contrast, the HF wave function for BuCl is the (normalized) Slater determinant[22]

$$|\Phi_{BuCl}\rangle = \frac{1}{\sqrt{N!}}|\,\psi_1\bar{\psi}_1 \ldots \psi_{N/2}\bar{\psi}_{N/2}\,| \quad , \tag{2.4}$$

where $N = 50$ is the number of electrons, $\psi_i = \phi_i^{MO}\alpha$ and $\bar{\psi}_i = \phi_i^{MO}\beta$ are molecular spinorbitals — α and β are the spin-up and spin-down functions, respectively — and $\phi_i^{MO} = \Sigma_{j=1}^{N/2}\, c_{ji}\chi_j^{AO}$ is a molecular orbital expressed as a linear combination of atomic orbitals $\{X_j^{AO}\}$. In this framework, the solvent would affect BuCl via the coefficients $\{c_{ji}\}$, $(N/2)^2$ in number, while the atomic orbitals $\{X_j^{AO}\}$. are frozen components corresponding to the $\{|i\rangle\}$ in (2.2). The interpretive simplicity of (2.2) compared to (2.4) is apparent. This occurs at the cost, however, of a relative lack of polarizability on the part of (2.2), since neither of $|\Psi_{Bu^+Cl^-}\rangle$ and $|\Psi_{Bu-Cl}\rangle$ can be internally polarized by the solvent. But in fact, the VB states are in general linear combinations of Slater determinants like (2.4), and their quality is thus higher than $|\Phi_{BuCl}\rangle$ — for the same choice of the orbital basis set — since account is given, to some degree, of electron correlation.

Here we do not concern ourselves with the array of methodologies for the calculation of diabatic states, and refer the reader to the recent review by Sidis[23]. We mention, however, a few procedures which seem especially apt to provide diabatic states in a form most suitable to our framework: the Diatomics-in-Molecules method [24, 25] — adopted in BH-II — where only few valence electrons need to be treated explicitly, due to the use of parametric core potentials; the unitary transformation of a set of *ab initio* adiabatic (ground plus excited) states — obtainable from current quantum chemistry packages — to a set of diabatic states with the required charge character to describe the reaction[26]-[29]; and finally, the straightforward (but computationally expensive) *ab initio* VB approach[30]. A complementary option for obtaining diabatic states via *ab initio* techniques is the use of the natural orbitals resulting from the analysis of the electronic charge density of a standard HF wave function[31]. Further references are provided in the brief survey in BH-I.

The solute charge distribution derived from (2.2), which governs the interaction with the solvent, is expressed as

$$\rho = \sum_{m=1}^{M} w_m \rho_m \quad ; \quad M = N_s(N_s+1)/2 \quad , \tag{2.5}$$

where the weights $\{\omega_m\}$ — henceforth all summations of indices *m, n,* and *p* span the range [1, *M*] — are calculated from the wave function coefficients according to the mapping

$$w_m = (2-\delta_{ij})c_i c_j \quad ; \quad m = N_s(i-1) - \frac{1}{2}i(i-1) + j \quad , \tag{2.6}$$

with $1 \le i \le N_s$, $i \le j \le N_s$, and δ_{ij} the Kronecker delta. The charge distribution components ρ_m are the matrix elements $\rho_m \equiv \langle i|\hat{\rho}|j\rangle$ of the charge density operator $\hat{\rho} \equiv \hat{\rho}_e + \rho_{nuc}$, with $\hat{\rho}_e$ and ρ_{nuc} the electronic and nuclear components, respectively (the scalar ρ_{nuc} only contributes for *i* equal to *j* because of the orthonormality of the $\{|i\rangle\}$ set). Derived quantities such as the solute electric potential ϕ_o and the electric field $E_o = -\nabla\phi_o$ are equivalently partitioned as

$$\phi_o = \sum_m w_m \phi_o^m \quad ; \quad \mathbf{E}_o = \sum_m w_m \mathbf{E}_o^m \quad , \tag{2.7}$$

with the obvious definition $\phi_o^m(\mathbf{r}) = \int d\mathbf{r}' \rho_m(\mathbf{r}')/|\mathbf{r}-\mathbf{r}'|$. For instance, in the two state description of BuCl, the solute charge distribution is

$$\begin{aligned} \rho_{BuCl} \;=\; & c_{ion}^2 \langle \Psi_{Bu^+Cl^-} | \hat{\rho} | \Psi_{Bu^+Cl^-} \rangle \\ & + 2 c_{ion} c_{cov} \langle \Psi_{Bu^+Cl^-} | \hat{\rho} | \Psi_{Bu-Cl} \rangle \\ & + c_{cov}^2 \langle \Psi_{Bu-Cl} | \hat{\rho} | \Psi_{Bu-Cl} \rangle \quad . \end{aligned}$$

To conclude this sub-section, we note that the CI form of the wave function (2.2) leads, via the mapping (2.6) from the coefficients $\{c_i\}$ to the charge distribution weights $\{w_m\}$, to a computationally advantageous matrix formulation of the free energy of the solute plus solvent system, which we present next.

2.2. REACTION SYSTEM NONEQUILIBRIUM FREE ENERGY

The solvent medium is characterized by its static and optical dielectric constants, ϵ and ϵ_∞, respectively, and its polarization is assumed to be the sum of two components

$$\mathbf{P} = \mathbf{P}_e + \mathbf{P}_{or} \quad , \tag{2.9}$$

where $\mathbf{P}_e$ is the electronic (fast) solvent polarization described in a quantum mechanical fashion[6], whereas $\mathbf{P}_{or}$ is the solvent polarization component

due to the nuclear (slow) motions of the solvent. The solute is embedded in a van der Waals cavity — a smooth assembly of spheres centered on the solute nuclei — carved into the dielectric continuum[11]. The cavity surface, closely matching the solute's molecular shape, constitutes a convenient two dimensional domain in which to recast the formulas which account for the solute-solvent interactions expressed in terms of three dimensional integrals. In this context, the solvent polarization **P** is enters via the surface charge density

$$\sigma \equiv \hat{\mathbf{n}} \cdot \mathbf{P} = \sigma_{e,\rho} + \tilde{\sigma}_{or} \quad , \tag{2.10}$$

where $\hat{\mathbf{n}}$ is the local inward normal to the cavity surface. In this partitioning, reminiscent of (2.9), $\sigma_{e\rho}$ is an electronic polarization contribution which depends solely on the bare solute electric field $\mathbf{E}_o$, whereas $\tilde{\sigma}_{or}$ comprises all the interactions of the orientational polarization with the solute charge distribution. Both $\sigma_{e,p}$ and σ_{or} are expressed, corresponding to the solute charge distribution partitioning (2.5), as

$$\sigma_{e,\rho} = \sum_m w_m \sigma^m_{e,\rho} \quad ; \quad \tilde{\sigma}_{or} = \sum_m p_m \tilde{\sigma}^m_{or,eq} \quad , \tag{2.11}$$

where the components $\sigma^m_{e,\rho}$ and $\tilde{\sigma}^m_{or,eq}$ are *equilibrium* quantities, in the sense that they are equilibrated to the corresponding solute charge distribution components ρ_m. For $\tilde{\sigma}_{or}$, this amounts to assuming that an arbitrary nonequilibrium orientational polarization $\mathbf{P}_{or}$ can be expressed as a linear combination of equilibrium components $\Sigma_m\, p_m\, \mathbf{P}_{or,eq}$ Consistent with the character of the frozen internal electronic structure for the diabatic states, once $\sigma^m_{e,\rho}$ and $\tilde{\sigma}^m_{or,eq}$ have been calculated for a given nuclear geometry, their values remain constant, both in the equilibrium and the nonequilibrium regimes of solvation: the $\{w_m\}$ reflect the changes in the solute electronic structure, while the $\{p_m\}$ — whose values are in principle arbitrary — carry the information about any deviation from equilibrium solvation. They only become equal to the $\{w_m\}$ when full equilibrium solvation holds; it is only then that the solvent orientational polarization is that appropriate for the solute electronic charge distribution.

Having defined the basic quantities, we can now quote the expression of the free energy in the nonequilibrium solvation regime:

$$\begin{aligned} G \;=\; & \mathbf{w}\cdot\mathbf{h} - \frac{1}{2}\left[\lambda \mathbf{w}\cdot\mathbf{I}^e\cdot\mathbf{w} + (1-\lambda)\mathbf{w}\cdot\mathbf{i}^e + \mathbf{w}\cdot\mathbf{\Lambda}^e\cdot\mathbf{w}\right] \\ & -\mathbf{w}\cdot\mathbf{s} + \frac{1}{2}\mathbf{s}\cdot\mathbf{K}^{or}\cdot\mathbf{s} \quad . \end{aligned} \tag{2.12}$$

The dimensions of the vectors (lower case) and matrices (upper case) are M and $M \times M$, respectively. The first term has the structure of the vacuum

Hamiltonian contribution $\langle\Psi|\hat{H}_o|\Psi\rangle$ — the energy of the solute in the gas phase, i.e. the usual output of a quantum chemistry calculation — since $\mathbf{w}\cdot\mathbf{h} = \Sigma_{ij}\, c_i c_j \langle i|\hat{H}_o|j\rangle$ [cf. (2.6) for the mapping of $\langle i|\hat{H}_o|j\rangle$ to h_m] with the weights $\mathbf{w}$ determined from the wave function coefficients modified by the solution environment. The final two, explicitly $\mathbf{s}$-dependent terms are related to the nonequilibrium solvation and the associated solvent coordinates $\mathbf{s}$, and will be discussed below. The second term, in brackets, is associated with the quantized solvent electronic polarization, and can describe the three possible situations where the time scale of the solvent electronic motions is (a) much longer than, (b) much shorter than, or (c) comparable to the time scale of the solute electronic motions[6]. Case (a) corresponds to the Self-Consistent (SC) limit, while case (b) corresponds to the Born-Oppenheimer (BO) limit[5, 6, 32], with the solvent electronic polarization equilibrated, respectively, to the average solute charge distribution ρ (SC) or to its components ρ_m (BO) [cf. (2.5)]. The relative measure of the time scales is gauged by λ[3], a function of the wave function coefficients and of the ratios $\rho_{ij} = -2H'_{ij}/\hbar\omega_{el}$, in which $H'_{ij} = \langle i|\hat{H}_o|j\rangle$ is the solvent renormalized electronic coupling matrix element. The ρ_{ij} compare the frequency of the resonant interconversion between the diabatic states $|i\rangle$ and $|j\rangle$, namely $2|H'_{ij}|/\hbar$, versus the frequency of the solvent electronic polarization ω_{el} (the peak frequency in the solvent UV absorption spectrum)[33]. It suffices here to say that when $\lambda \to 1$ in G(2.12), the SC limit free energy

$$G^{SC} = \mathbf{w}\cdot\mathbf{h} - \frac{1}{2}\,\mathbf{w}\cdot\mathbf{I}^e\cdot\mathbf{w} - \mathbf{w}\cdot\mathbf{s} + \frac{1}{2}\,\mathbf{s}\cdot\mathbf{K}^{or}\cdot\mathbf{s} \quad , \tag{2.13}$$

is recovered. On the other hand, for $\lambda \to 0$, G(2.12) tends to the BO limit free energy

$$G^{BO} = \mathbf{w}\cdot\mathbf{h} - \frac{1}{2}\,\mathbf{w}\cdot\mathbf{i}^e - \mathbf{w}\cdot\mathbf{s} + \frac{1}{2}\,\mathbf{s}\cdot\mathbf{K}^{or}\cdot\mathbf{s} \quad . \tag{2.14}$$

In its equilibrium form, G^{SC} is the free energy limit most frequently interfaced to *ab initio* quantum chemistry packages[34], while G^{BO} is more common in outer sphere electron transfer studies[35].

The difference between G^{BO} and G^{SC} resides in their second terms, which comprise the interaction free energy between the solute charge distribution and the solvent electronic polarization. In particular, the matrix elements of $\mathbf{I}^e$ are the cavity surface integrals

$$I^e_{mn} = -\oint_S d\mathbf{s}'\,\phi^m_o(\mathbf{s}')\,\sigma^n_{e,\rho}(\mathbf{s}') \equiv -(\,\phi^m_o \,||\, \sigma^n_{e,\rho}\,) \quad , \tag{2.15}$$

with the elements of the vector $\mathbf{i}^e$ defined in terms of (2.15) as

$$i^e_p \equiv \sum_{l=1}^{N_s} I^e_{mn} \quad . \tag{2.16}$$

The various M-space indices displayed here — and in the equations which follow — are calculated via the wave function charge distribution mapping (2.6) from the appropriate N_s-space indices (see BH-I for details). The regime intermediate between the SC and the BO limits requires the solvent electronic polarization matrix [cf. (2.12)]

$$\mathbf{\Lambda}^e = \frac{\epsilon_\infty}{2\chi_e} \sum_i \sum_{j \neq i} (\alpha_{ij} - \bar{\alpha})\, \mathbf{\Lambda}^e(ij) \quad , \tag{2.17}$$

where the elements of the second rank tensor $\mathbf{\Lambda}^e(ij)$ are defined as

$$\Lambda^e_{mn}(ij) = \delta_{ns} \left(I^e_{m'n''} + I^e_{m''n'} \right) - \delta_{nr}\, I^e_{m'n'} - \delta_{nt}\, I^e_{m''n''} \quad , \tag{2.18}$$

with the polarizability matrix elements α_{ij} and the term $\bar{\alpha}$ functions of both the factors p_{ij} and the coefficients $\{c_i\}$, and the solvent electronic susceptibility χ_e defined by $\epsilon_\infty = 1 + 4\pi\chi_e$ (BH-I should be consulted for a detailed discussion of α_{ij}, which connects orientational polarization and electric field components.)

Finally, the last two terms in G(2.12) account for the effects of the solvent orientational polarization in the nonequilibrium solvation. The matrix $\mathbf{K}^{or}$ is the inverse of the solvent orientational polarization interaction energy matrix $\mathbf{I}^{or}$ whose elements are defined, analogously to I^e_{mn}, by

$$I^{or}_{mn} \equiv -\left(\phi^m_o \,\|\, \tilde{\sigma}^n_{or,eq} \right) \quad . \tag{2.19}$$

(We note in passing that both $\mathbf{I}^e$ and $\mathbf{I}^{or}$ are symmetric.) The collective solvent coordinates s are defined by the scalar product

$$\mathrm{s} = \mathbf{I}^{or} . \mathbf{p} \quad , \tag{2.20}$$

such that each solvent coordinate has the form

$$s_n = -\sum_m p_m \left(\phi^n_o \,\|\, \tilde{\sigma}^m_{or,eq} \right) = -\left(\phi^n_o \,\|\, \tilde{\sigma}_{or} \right) \tag{2.21}$$

In words, s_n describes the interaction of the solute charge distribution component ρ_n with the arbitrary solvent orientational polarization mediated by the cavity surface. The arbitrary weights $\{p_m\}$, previously defined by (2.11), enter accordingly the definition of the solvent coordinates, and reduce, in the equilibrium solvation regime, to the weights $\{w_m\}$, such that the solvent coordinates are no longer arbitrary, but instead depend on the solute nuclear geometry and assume the form $s^{eq} = \mathbf{I}^{or} . \mathrm{w}^{eq}$. In equilibrium, the solvent coordinates are correlated to the actual electronic structure of the solute, while out of equilibrium they are not.

To calculate G (2.12), in addition to the various matrices and vectors we have described, we need the weights $\{w_m\}$ derived from the coefficients $\{c_i\}$ of the wave function *in solution:* the latter are obtained by solving the appropriate eigenvalue equation, discussed in the next Section.

2.3. SCHRÖDINGER EQUATION IN MATRIX FORM

The coefficients $\{c_i\}$ in solution correspond to the global minimum of the free energy (note that this is not the equilibrium solvation condition), and satisfy the system of equations

$$\frac{\partial}{\partial c_i}\left[G - E\left(\sum_j c_j^2 - 1\right)\right] = 0 \;\; ; \;\; i = 1, 2, \ldots, N_s \;\; , \tag{2.22}$$

with E the Lagrange multiplier for the wave function normalization condition, which leads to the eigenvalue equation

$$\mathbf{HC} = \mathbf{EC}, \tag{2.23}$$

where **H** is the Hamiltonian matrix obtained by taking the derivative of the nonequilibrium free energy (2.12) with respect to the wave function coefficients, **E** is the diagonal matrix of the energy eigenvalues of the system in solution, and **C** is the matrix of the eigenvectors. The lowest eigenvalue is the adiabatic ground state energy of the solvated solute — distinguished from the total free energy, since the self-interaction term of the solvent polarization is absent from **E.** The matrix elements of **H** are

$$H_{ij} = \lambda H_{ij}^{SC} + (1 - \lambda) H_{ij}^{BO} + H_{ij}^{\Delta} \;\; ;$$

$$H_{ij}^{SC} = h_m - \sum_{\cdots} I_{mn}^{e} w_n - s_m \;\; ; \;\; H_{ij}^{BO} = h_m - \frac{1}{2} i_m^e - s_m \tag{2.24}$$

— with the mapping $m \leftrightarrow (i,j)$. Here H_{ij}^{SC} and H_{ij}^{BO} are SC and BO Hamiltonian matrix elements, respectively, while H_{ij}^{Δ}, whose expression is somewhat complicated, originates from the derivative of the terms λ and $\mathbf{w} \cdot \Lambda^e \cdot \mathbf{w}$ in (2.12) with respect to the wave function coefficients. We trace the origin of the various terms in H_{ij}^{SC} and H_{ij}^{BO} by examining the expressions for G^{SC} (2.13) and G^{BO} (2.14): h_m derives from $\mathbf{w} \cdot \mathbf{h}$ and the arbitrary solvent coordinate s_m derives from the s-containing terms in the free energy. Finally, the terms containing I_{mn}^e and i_m^e derive from the solvent electronic polarization interaction, and are distinctive for the SC and BO limits, respectively. The limiting behavior of H_{ij} for either $\lambda \rightarrow 1$ or $\lambda \rightarrow 0$

mirrors that of G (2.12) [cf. (2.13) and (2.14)]. In general, the Schrödinger equation is nonlinear, since the interaction with the solute depends on the solute charge distribution, which itself depends on the solvent.

The solution procedure of the (generally nonlinear) eigenvalue equation (2.23) is similar to that for the HF equations *in vacuo:* at a chosen solute geometry, one fixes the values of the solvent coordinates $\{s_m\}$; assigns guess values for the $\{c_i\}$ and constructs the weights $\{\omega_m\}$; then uses $\mathbf{I}^e$, $\mathbf{i}^e$, etc., to calculate the inatrix elements H_{ij}^{SC}, H_{ij}^{BO}, and H_{ij}^{Δ}; and finally diagonalizes the matrix **H.** The eigenvector of coefficients $\{c_i\}$ corresponding to the lowest eigenvalue E is used as the new guess, and the cycle is repeated until convergence.

Although in principle one could choose a set of arbitrary values for the solvent coordinates $\{s_m\}$, solve the eigenvalue equation (2.23), and compute the free energy (2.12), in practice a preliminary aquaintance with the equilibrium solvation picture for the target reaction system serves as a computationally convenient doorway for the calculations in the nonequilibrium solvation regime. We show this below in the section dedicated to an illustration of the method for a two state case reported in BH-II.

3. $I_2^- \rightarrow I + I^-$ in acetonitrile

The I_2^- system has been investigated experimentally, theoretically, and computationally by several groups, as a prototype for the study of dissociation and recombination dynamics influenced by the interactions with a surrounding solvent or cluster of solvent molecules[9],[36]-[41]. The system can be effectively modelled by two VB states[9],[41], which allows a focus on several key aspects of the implementation of the theory, without being hindered by the complexity of a multistate calculation. The implementation steps are conveniently collected in the flow chart in Table 1, to which the reader is referred to for a comprehensive overview of our strategy. All the details of the calculation are reported in BH-II. The effective wave function for the I_2^- reaction system can be written as

$$|\Psi_{I_2^-}\rangle = c_1|\Psi_{II^-}\rangle + c_2|\Psi_{^-II}\rangle \quad , \tag{3.1}$$

which corresponds to representing I_2^- by the two resonance structures II^- and ^-II. For the sake of simplicity, we skip over the details of the calculation of the diabatic states energies and electronic resonance coupling, and consider here and henceforth both $|\Psi_{II^-}\rangle$ and $|\Psi_{^-II}\rangle$ as orthonormal diabatic states, by referring to them as $|1\rangle$ and $|2\rangle$, respectively. It suffices to say that their charge character is highly representative of the resonance structures II^- and ^-II.

TABLE 1. Algorithm flow chart

- GAS PHASE CALCULATION
  1. selection of the diabatic states $\{|\Phi_i\rangle\}$
  2. symmetric orthogonalization $\{|\Phi_i\rangle\} \rightarrow S^{-1/2} \rightarrow \{|i\rangle\}$; $S_{ij} = \langle\Phi_i|\Phi_j\rangle$
  3. Hamiltonian matrix in the orthogonalized basis $\langle i|\hat{H}|j\rangle$
  4. charge distribution components $\rho_m \equiv \langle i|\rho|j\rangle$, $m \leftrightarrow (i,j)$ mapping
- SOLUTE-SOLVENT INTERACTION ENERGY MATRICES
  5. surface charge density components $\sigma^m_{e,\rho}$, σ^m_{eq} , $\sigma^m_{or,eq} = \sigma^m_{eq} - \sigma^m_{e,\rho}$
  6. interaction energy matrices $\mathbf{I}^e$, $\mathbf{i}^e$, $\mathbf{I}^{or}$, $\mathbf{K}^{or}$
- EQUILIBRIUM SOLVATION REGIME
  7. equilibrium Schrödinger equation $\mathbf{H}^{eq}[\mathbf{R}]\mathbf{C}^{eq} = \mathbf{E}^{eq}[\mathbf{R}]\mathbf{C}^{eq} \rightarrow \mathbf{w}^{eq}$, s^{eq}
  8. equilibrium free energy surface $G_{eq}[\mathbf{R}]$
  9. natural solvent coordinates $\bar{s} = \mathbf{T} \cdot \bar{s}$
  10. harmonic approximation $G^h = G_{eq} + (\bar{s} - \bar{s}_{eq}) \cdot \bar{\mathbf{K}} \cdot (\bar{s} - \bar{s}_{eq})/2$
  11. combined analysis of $\{c_i\}$, $\{\bar{s}_m\}$, and $\{\bar{K}_{mm}\}$ along the ESP
  12. selection of the relevant natural solvent coordinates $\{\bar{s}_m\}$
- NONEQUILIBRIUM SOLVATION REGIME
  13. $\bar{s} \rightarrow s$
  14. nonequilibrium Schrödinger equation $\mathbf{H}[\mathbf{R}, s]\mathbf{C} = \mathbf{E}[\mathbf{R}, s]\mathbf{C}$
  15. $s \rightarrow \bar{s}$
  16. nonequilibrium free energy surface $G[\mathbf{R}, \bar{s}]$

Concerning the three charge distribution components resulting from $|1\rangle$ and $|2\rangle$, here we only need to recall that $\rho_1 = \langle 1|\hat{\rho}|1\rangle$ and $\rho_3 = \langle 2|\hat{\rho}|2\rangle$ are symmetrically related along the I_2 bond direction, and that the exchange charge distribution $\rho_2 = \langle 1|\hat{\rho}|2\rangle$ is on average much smallr in modulo than both ρ_1 and ρ_3. The electronic resonance coupling $\beta = -\langle 1|\hat{H}_o|2\rangle = -\langle 2|\hat{H}_o|1\rangle$ and the degenerate diabatic states' energy $\alpha = \langle 1|\hat{H}_o|1\rangle = \langle 2|\hat{H}_o|2\rangle$ are reported in Fig.1 together with the overlap $S = \langle\Phi_1|\Phi_2\rangle$ for the original, nonorthogonal, charge-localized VB states $|\Phi_1\rangle$ and $|\Phi_2\rangle$ — obtained by a semiempirical method[25] — from which $|1\rangle$ and $|2\rangle$ were derived. The vacuum adiabatic ground state energy for the wave function (3.1) is simply $E = \alpha - \beta$. The stabilization displayed by E with respect to α is due to the electron delocalizing effect of the resonance coupling β. As the nuclear separation R increases, β decreases, and $E \sim \alpha$. The quantities α, β, ρ_1, ρ_2, and ρ_3 provide all the necessary ingredients to initiate the

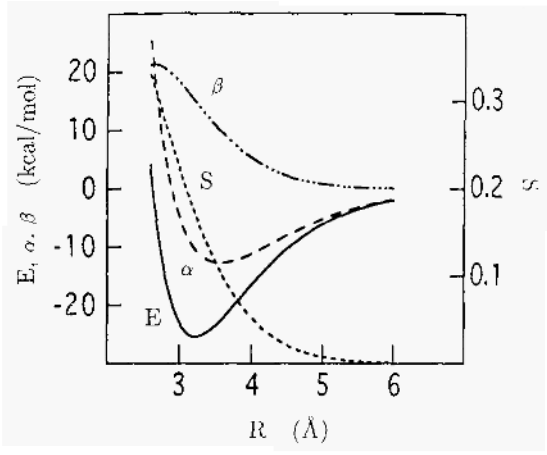

Figure 1. I_2^- vacuum energies, overlap and coupling. *E,* electronically adiabatic ground state energy; α, orthonormal diabatic states' energy; β, electronic resonance coupling; *S,* charge-localized, diabatic states' overlap, versus nuclear separation *R*

calculation in solution.

To calculate the surface charge densities $\sigma^m_{e,\rho}$ and $\tilde{\sigma}^m_{or,eq}$ [cf. (2.11)], one has to solve numerically the integral equations on the solute cavity surface domain[11]

$$\sigma^m(\mathbf{s}_j) = \sigma^m_o(\mathbf{s}_j) - \omega\,\hat{\mathbf{n}}\cdot\nabla\oint_S d\mathbf{s}'\frac{\sigma^m(\mathbf{s}')}{|\mathbf{s}_j-\mathbf{s}'|}\;\;;\;\; m=1,2,3$$
$$\sigma^m_o(\mathbf{s}_j) = \omega\,\hat{\mathbf{n}}\cdot\mathbf{E}^m_o(\mathbf{s}_j)\;\;;\;\; \omega=\frac{\chi_e}{\epsilon_\infty},\frac{\chi}{\epsilon}\;. \tag{3.2}$$

at the center s_j of each cavity tessera, with $\hat{\mathbf{n}}$ the inward normal in s_j to the cavity. While $\sigma^m_{e,\rho}$ results directly from the solution of the integral equation (3.2) with $\omega = \chi_e/\epsilon_\infty$, $\tilde{\sigma}^m_{or,eq}$ is not itself associated with a corresponding equilibrium condition, and is obtained by first solving (3.2) for the fully equilibrated component σ^m_{eq} ($\omega = \chi/\epsilon$), and then taking the difference $\sigma^m_{or,eq} = \sigma^m_{eq} - \sigma^m_{e,\rho}$. The surface integrals I^e_{mn} (2.15) and I^{or}_{mn} (2.19) are then numerically approximated by the summations

$$\begin{aligned} I^e_{mn} &\simeq -\sum_{j=1}^{N_\sigma} A_j\,\phi^m_o(\mathbf{s}_j)\,\sigma^n_{e,\rho}(\mathbf{s}_j) \\ I^{or}_{mn} &\simeq -\sum_{j=1}^{N_\sigma} A_j\,\phi^m_o(\mathbf{s}_j)\,\tilde{\sigma}^n_{or,eq}(\mathbf{s}_j) \end{aligned}\;, \tag{3.3}$$

where N_σ is the total number of tesserae tiling the cavity, and A_j is the area of the tessera centered in s_j. From $\mathbf{I}^e$ and $\mathbf{I}^{or}$ one then calculates $\mathbf{i}^e$

(2.16), Λ^e (2.17), and $\mathbf{K}^{or} = (\mathbf{I}^{\sigma})^{-1}$: *all the matrices and vectors need to be calculated only once at each nuclear geometry.*

In the equilibrium solvation regime, the M solvent coordinates are not arbitrary, but are functions of the solute nuclear geometry, since the solvent orientational polarization is equilibrated to the solute electronic structure at each such geometry. Our strategy is to exploit this property to gain an insight on the solvent coordinates' ability to couple to the solute electronic structure, and then select only the sensitive ones, in such a way to reduce the solvent coordinates' manifold for the nonequilibrium calculation without sacrifice of accuracy or content. Operationally, we approximate the free energy (2.12) in the neighborhood of the equilibrium solvation path (ESP) — along which $\mathbf{s} = s^{eq}$ — by its Taylor expansion

$$G \simeq G_{eq} + \frac{1}{2}(\mathbf{s} - \mathbf{s}_{eq}) \cdot \mathbf{K} \cdot (\mathbf{s} - \mathbf{s}_{eq}) \quad , \tag{3.4}$$

with the solvent force constant matrix $\mathbf{K}$ with elements

$$K_{mn} = K^{pol}_{mn} + K^{or}_{mn} \quad ; \quad K^{pol}_{mn} \equiv - \left. \frac{\partial w_m}{\partial s_n} \right|_{eq} \quad . \tag{3.5}$$

Due to the invariance of the free energy (3.4) — and also (2.12) — to an orthogonal transformation of its constituent matrices and vectors, we are allowed to carry out this analysis in a more convenient solvent coordinates framework.

The transformation $\mathbf{T}$ we adopt is induced by the wave function normalization condition which, in terms of the weights, reads $w_1 + w_3 = 1$. From (3.5), it is apparent that if $\mathbf{T}$ sends the $\{w_m\}$ set into a new set $\{\bar{w}_m\}$ with $\bar{w}_1 = w_1 + w_3 = 1$ as one of its elements, then both the first row and the first column of the transformed polarization component of the solvent force constant matrix $\bar{\mathbf{K}}^{pol} = \mathbf{T} \cdot \mathbf{K}^{pol} \cdot \tilde{\mathbf{T}}$. $\mathbf{T}$ ($\mathbf{T}^{-1} = \tilde{\mathbf{T}}$) are zero, since the derivatives of w_1 are zero. Given the normalization condition and the orthogonality requirement — with the latter conserving the original gauge of the solvent coordinates framework — one can calculate $\mathbf{T}$ for any number of diabatic states[42]. The transformation for the two state case is

$$\mathbf{T} = \begin{pmatrix} 1/\sqrt{2} & 0 & 1/\sqrt{2} \\ 0 & 1 & 0 \\ 1/\sqrt{2} & 0 & -1/\sqrt{2} \end{pmatrix} \quad ; \quad \mathbf{T} \cdot \tilde{\mathbf{T}} = \mathbf{1} \quad , \tag{3.6}$$

and it yields the *natural* solvent coordinates

$$\begin{aligned} \bar{s}_1 &= \tfrac{1}{\sqrt{2}}(s_1 + s_3) \\ \bar{s}_2 &= s_2 \\ \bar{s}_3 &= \tfrac{1}{\sqrt{2}}(s_1 - s_3) \end{aligned} \quad . \tag{3.7}$$

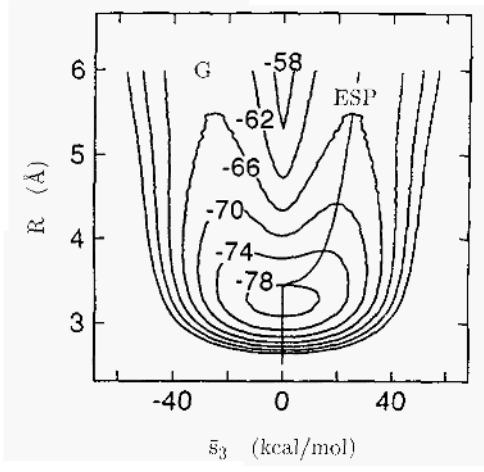

Figure 2. I_2^- in acetonitrile. Nonequilibrium free energy surface. Contours in kcal mol^{-1}, with the gas phase energy of the separated I and I^- species as a reference. The line cutting across the contours represents the ESP.

The terminology *natural* here and henceforth refers to the use of the wave function normalization condition inspiring the construction of the rotation matrix.

T combines only the solvent coordinates corresponding to the diagonal components of the charge distributions: in fact, the positions of the elements T_{mn} strictly match the labelling of the charge distribution components $\{\rho_m\}$. In general, the off-diagonal solvent coordinates are relatively less important, and can even he neglected in a first approximation[9]. The rationale for their exclusion is the minor contribution of the off-diagonal charge distribution components relative to the diagonal ones: the larger on average the charge distribution, the stronger the interaction with the solvent polarization, and the more important the corresponding solvent coordinate.

The next step is the analysis of the behaviour of the wave function coefficients $\{c_i\}$, the natural solvent coordinates $\bar{s}$ = **T.s**, and the corresponding diagonal elements of the transformed solvent force constant matrix $\{\bar{K}_{mm}\}$ along the ESP. For perspective, the ESP is reported in Fig.2, superimposed on the full nonequilibrium free energy surface for the I_2^- reaction system in acetonitrile (the justification for the coordinates' choice R and $\bar{s}_3$ will be given below).

We start by recalling that the framework of diahatic states depicts a competition in solution between the electronic resonance coupling β — which tends to delocalize the solute electronic charge — and the solvent polarization — which tries to localize it, to better solvate the reaction sys-

tem. Along the ESP, as the I_2^- internuclear separation increases from ca. 3.2 Å, the equilibrium bond length in the gas phase [cf. Fig.1], β decreases. The electronic structure remains delocalized ($c_1^{eq} = c_2^{eq}$) up to ca. 3.4 Å, when $|2\rangle$ starts being sharply stabilized, as indicated by the increase of the value of c_2^{eq} while the contribution of $|1\rangle$ to the wave function decreases together with the value of c_1^{eq} [Fig.3(a)]. (Obviously, the reverse picture is possible, due to the symmetry of the reaction, with states $|1\rangle$ and $|2\rangle$ exchanging their roles.) *At the same bond length,* the natural solvent coordinate $\bar{s}_3^{eq}$, related to $\bar{w}_3^{eq} \sim (c_1^{eq})^2 - (c_2^{eq})^2$, displays a sharp variation [Fig.3(b)] — while both $\bar{s}_1^{eq}$ and $\bar{s}_2^{eq}$ pass through that bifurcation point unaffected in their monotonic behaviour — and $\bar{K}_{33}$ reaches its minimum value [Fig.3(c)]. *It is this concurrent variation of* c_1^{eq}, c_2^{eq}, $\bar{s}_3^{eq}$, and $\bar{K}_{33}$ *that points out* $\bar{s}_3$ *as the sole important solvent coordinate, due to its sensitivity, to describe nonequilibrium solvation effects, and justifies the choice of coordinates for Fig.2.* The insensitive solvent coordinates $\bar{s}_1$ and $\bar{s}_2$ are fixed at their equilibrium values for each given *R.* (Of course, one might anticipate this conclusion ahead of time[9]. The present analysis provides a systematic basis for the decision, which will be indispensable for multiple VB state systems. But even for two state systems, the simplification possible for I_2^- will not always hold[6].)

We now give the rationales for the behavior of $\bar{s}_1^{eq}$, $\bar{s}_2^{eq}$, and $\bar{s}_3^{eq}$ and their associated solvent force constants $\bar{K}_{11}$, $\bar{K}_{22}$, and K_{33}.

and $\bar{K}_{11}$ turn out to be insensitive to the variations in c_1^{eq} and c_2^{eq} because **T** has removed every dependence on the charge distribution weights from the matrix elements $\bar{K}_{1m}$ and $\bar{K}_{m1}$; these then only carry the effects of the solute cavity geometry on the free energy via the $\mathbf{K}^{or}$ matrix elements at a fixed total charge, and this is not a strongly varying effect.

The reason for the insensitivity of $\bar{s}_2^{eq}$ and $\bar{K}_{22}$ apparent in Fig.3 is to be found in the weak interaction of the exchange charge distribution p_2 — vanishing for large internuclear separations — with the solvent polarization: this is also responsible for the very large value of $\bar{K}_{22}$, implying that the solute electronic structure cannot evolve along $\bar{s}_2$.

We now focus on the behaviour of $\bar{K}_{33}$. On approaching the internuclear separation of 3.4 Å, from below, the delocalizing electronic resonance coupling β is quickly decreasing, and is no longer able to prevent the localization of the extra electron by the solvent polarization, corresponding to the attainment of the minimum in $\bar{K}_{33}$, the indication that the evolution of the system along s_3 is no longer restrained by a restoring force. After the transition, the weights of the two VB states vary more steeply, and $\bar{s}_3^{eq}$ which is attuned to the difference charge distribution $\rho_1 - \rho_3$, varies accordingly. The increase in $\bar{K}_{33}$ past 3.4 Å is the indication that the electronic structure is being constrained in its new, charge-localized state II^-

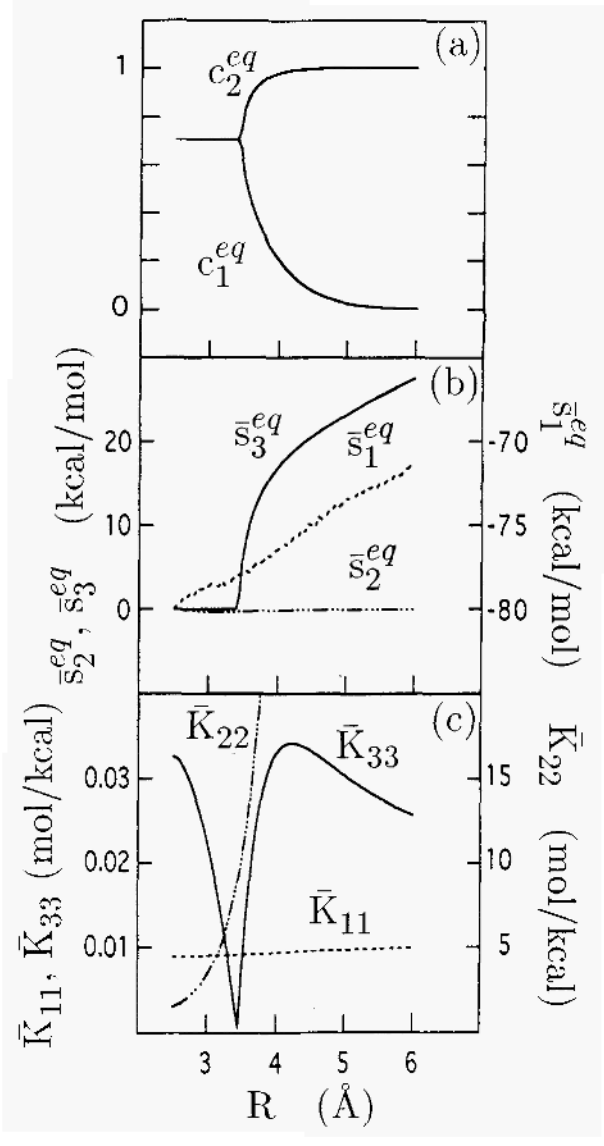

Figure 3. I_2^- in acetonitrile. ESP analysis for the selection of the solvent coordinates. (a) Wave function coefficients c_1^{eq} and c_2^{eq} (b) Natural solvent coordinates. (c) Diagonal elements of the solvent force constant tensor $\bar{\mathbf{K}}$.

by a restoring force. At about 4.5 Å, c_1^{eq}, c_2^{eq}, s_3^{eq}, and $\bar{K}_{33}$ attain an asymptotic behaviour, whose onset involves the quasi-completion of the charge localization on one of the iodines.

BH-II can he consulted for a discussion of the numerical importance of the quantum treatment of the solvent electronic polarization. It suffices to

note here that an SC treatment has the interesting qualitative failure that it incorrectly predicts that I_2^- has a localized electronic structure at the equilibrium geometry.

Finally, it is very important to stress that the ESP is different from the solution reaction path (SRP) for the I_2^- reaction system[9], which is a much more faithful indicator of the reaction dynamics. The SRP is for example critical in understanding the vibrational relaxation behavior of the system[9],[41]. The ESP only finds its use, illustrated above, in helping decide which solvent coordinates should be considered as independent variables in the nonequilibriurn calculation, and which solvent coordinates should instead be fixed at their equilibrium values.

4. The $(CH_3)_3C–Cl \rightarrow (CH_3)_3C^+ + Cl^-$ S_N1 reaction system

In this Section, we sketch how the methodology of the previous section could also be applied to the two state BuCl reaction system we introduced in Sec.2.1. (Ref.[10] should be consulted for a history of the problem and an account of the unconventional conclusions that result from a VB analysis.) The BuCl wave function can be written as the linear combination of orthonornial states [cf. (2.3)]

$$|\Psi_{BuCl}\rangle = c_1|\Psi_{Bu^+Cl^-}\rangle + c_2|\Psi_{Bu-Cl}\rangle \quad , \tag{4.1}$$

with the correspondence

$$|1\rangle \leftrightarrow |\Psi_{Bu^+Cl^-}\rangle \;\; ; \;\; |2\rangle \leftrightarrow |\Psi_{Bu-Cl}\rangle \tag{4.2}$$

For the gas phase part of the calculation, one has to calculate, at each solute nuclear geometry, three elements of the symmetric Hamiltonian matrix, namely $\langle 1|\hat{H}_o|1\rangle$, $\langle 1|\hat{H}_o|2\rangle$, and $\langle 2|\hat{H}_o|2\rangle$, with the diagonal elements corresponding to the diabatic energies of $|\Psi_{Bu^+Cl^-}\rangle$ and $|\Psi_{Bu-Cl}\rangle$, respectively, while the off-diagonal one to their electronic resonance coupling. Accordingly, the two states give rise to sets of three different charge distributions, weights, and solvent coordinates, reported below in array form to stress their association [cf. (2.6)]:

$$\begin{matrix} \langle 1|\hat{H}_o|1\rangle, \rho_1, w_1, s_1 & \langle 1|\hat{H}_o|2\rangle, \rho_2, w_2, s_2 \\ & \langle 2|\hat{H}_o|2\rangle, \rho_3, w_3, s_3 \end{matrix} \tag{4.3}$$

The calculation of the matrices $\mathbf{I}^e$ and $\mathbf{I}^{or}$ — and their derivatives — follows the procedure detailed in Sec.3, and is thus skipped here to dedicate more space to the natural solvent coordinates issue.

In the gas phase, BuCl would undergo acid elimination[10], but in polar solution the Bu^+ and Cl^- ions are produced in a heterolytic fashion. This reflects the strong solvent stabilization of the ionic state $|1\rangle$.

Hence, one should expect that, along the ESP at sufficiently large internuclear separation, the solvent will overcome the delocalizing effects of the electronic resonance coupling, and localize the solute charge distribution $\rho = w_1\rho_1 + w_2\rho_2 + w_3\rho_3$ to $\rho = \rho_1$

The two state orthogonal transformation (3.6) yields the natural solvent coordinates $\bar{s}_1 = (s_1+s_3)/\sqrt{2}$, $\bar{s}_2 = s_2$, $\bar{s}_3 = (s_1-s_3)/\sqrt{2}$. By assuming that the off-diagonal charge distribution component ρ_2 is far less important than the diagonal components ρ_1, and ρ_3, we disregard the off-diagonal, natural solvent coordinate $\bar{s}_2$, and focus instead on the diagonal ones, which we now discuss.

The transformed weight corresponding to s_1 is the wave function (4.1) normalization condition $\bar{w}_1 = w_1 + w_3 = 1$. Thus, the solvent force constant matrix elements $\bar{K}_{m1}$ and $\bar{K}_{1m}$, m = [1,3], bear no dependence on the solute electronic structure, since their components $\bar{K}^{pol}_{m1}$ and $\bar{K}^{pol}_{1m}$ are zero [cf. (3.5)]. Then, $\bar{s}_1$ cannot couple to the solute electronic structure, and is unable to monitor any rearrangement — due to the variation of the coefficients c_1 and c_2 — of the solute total charge distribution ρ. By contrast, $\bar{s}_3$ is associated with $\bar{K}^{pol}_{33} = -\partial\bar{s}_3$, $\bar{w}_3 \sim c_1^2 - c_2^2$, and is therefore sensitive to the relative change of the weights of the states $|1\rangle$ and $|2\rangle$.

With these insights on the meaning of $\bar{s}_3$, we now outline a possible outcome of the ESP analysis for the two VB state picture of the BuCl S_N1 dissociation. Let us imagine following the reaction from the solute equilibrium geometry, where the BuCl system is largely electronically localized in the covalent state $|2\rangle$. It is reasonable to expect that the product of the reaction will be well represented by the single resonance structure Bu^+C1^-. Thus we predict $|2\rangle \sim |\Psi_{Bu-Cl}\rangle$ to rise in energy — and its weight to decrease — as the dissociation progresses. In the neighborhood of the transition state, the system will be described by a resonance mixture of both $|2\rangle$ and the ionic state $|1\rangle \sim |\Psi_{Bu+Cl-}\rangle$. Subsequent to this, the solvent polarization should overcome, along the ESP, the delocalizing effect of the electronic coupling $\langle 1|\hat{H}_o|2\rangle$ — which ensures a contribution of $|2\rangle$ to the wave function, and the system will be described solely by the ionic state.

In view of the above discussion, there should be a dip in $\bar{K}_{33}$, and a sharp variation in $\bar{s}_3$, in the neighborhood of the transition state, where there is approximately, although not exactly, a 50-50 mixture of $|\Psi_{Bu+Cl-}\rangle$ and $|\Psi_{Bu-Cl}\rangle$ [10].

Hence, we conclude that the nonequilibrium solvation free energy surface for the BuCl S_N1 reaction system in a two VB state framework would be well described as a function of the bond length C-Cl (assuming the geometry of the Bu group is fixed) and of the natural solvent coordinates s_3. The natural solvent coordinates $\bar{s}_1$ and $\bar{s}_2$, on the other hand, would assume their equilibrium value at the given nuclear configuration. Indeed,

this was assumed in the empirical two VB state approach of Ref.[10].

5. The $Cl^- + CH_3Cl' \rightarrow ClCH_3 + Cl'^-$ S_N2 reaction system

In this section, we sketch the nature of the three VB state framework as a template to describe bimolecular nucleophilic substitutions (S_N2)[7, 12, 13]. Although it remains to be seen if three VB states are sufficient to describe the title reaction system in solution, this is still a useful additional exercise to expose the reasoning underlying the practical application of our theory. The wave function to describe the S_N2 reaction

$$Cl^- + CH_3Cl' \rightarrow ClCH_3 + Cl'^- \tag{5.1}$$

can be written as

$$|\Psi_{S_N2}\rangle = c_1|1\rangle + c_2|2\rangle + c_3|3\rangle \ , \tag{5.2}$$

with the association among the VB states, the resonance structures, and the other related quantities

$$\begin{array}{lcll} |1\rangle & \leftrightarrow & Cl^-/CH_3^+/Cl'^- & \leftrightarrow \langle 1|\hat{H}_o|1\rangle, \rho_1, w_1, s_1 \\ |2\rangle & \leftrightarrow & Cl^-/CH_3Cl' & \leftrightarrow \langle 2|\hat{H}_o|2\rangle, \rho_4, w_4, s_4 \\ |3\rangle & \leftrightarrow & ClCH_3/Cl'^- & \leftrightarrow \langle 3|\hat{H}_o|3\rangle, \rho_6, w_6, s_6 \end{array} \ , \tag{5.3}$$

where the bar means "no bond".

In Ref.[8](b), an approximate two state description of this S_N2 reaction was given, in which the triple ion state $|1\rangle$ was excluded (and incidentally, it was found that there could be quite large deviations from either an SC or BO picture of the ESP). As it was pointed out there, while it was not strictly necessary to invoke the involvement of state $|1\rangle$, available vacuum adiabatic calculations[44] of the evolving charge distribution pointed strongly to its involvement in the reaction transition state region, where the positive charge on the carbon is larger with respect to its value for the reactants.

The three state orthogonal transformation to the space of natural solvent coordinates is the 6×6 matrix (see BH-I)

$$\mathbf{T} = \begin{pmatrix} 3^{-1/2} & 0 & 0 & 3^{-1/2} & 0 & 3^{-1/2} \\ 0 & 1 & 0 & 0 & 0 & 0 \\ 0 & 0 & 1 & 0 & 0 & 0 \\ 0 & 0 & 0 & 2^{-1/2} & 0 & -2^{-1/2} \\ 0 & 0 & 0 & 0 & 1 & 0 \\ (2/3)^{1/2} & 0 & 0 & -6^{-1/2} & 0 & -6^{-1/2} \end{pmatrix} \tag{5.4}$$

By assuming that the off-diagonal charge distribution components ρ_2, ρ_3, and ρ_5 are far less important than the diagonal components ρ_1, ρ_4, and ρ_6, we disregard the off-diagonal, natural solvent coordinates $\bar{s}_2$, $\bar{s}_3$, and $\bar{s}_5$ — left equal by **T** to the starting solvent coordinates s_2, s_3, and s_5 — and focus instead on the diagonal ones, resulting in the linear combinations of the original solvent coordinates

$$\begin{aligned} \bar{s}_1 &= \frac{1}{\sqrt{3}}(s_1 + s_4 + s_6) \\ \bar{s}_4 &= \frac{1}{\sqrt{2}}(s_4 - s_6) \\ \bar{s}_6 &= \frac{1}{\sqrt{3}}\left[\frac{1}{\sqrt{2}}(s_1 - s_4) + \frac{1}{\sqrt{2}}(s_1 - s_6)\right] \end{aligned} , \qquad (5.5)$$

which we now discuss.

The natural solvent coordinate $\bar{s}_1$ corresponds to is the normalization condition $\bar{w}_1 = w_1 + w_4 + w_6 = 1$ for the wave function (5.2), and is unable to monitor variations in the solute electronic structure for the reasons discussed in the previous section. By contrast, $\bar{s}_4$ is associated with $K_{44}^{pol} = -\partial w_4/\partial s_4$, $w_4 \sim c_2^2 - c_3^2$, and is therefore sensitive to the relative change of the weights of the states $|2\rangle \sim Cl^- \,/\, CH_3Cl'$ and $|3\rangle \sim ClCH_3 \,/\, Cl'$. On the same basis, we can ascribe to s_6 the monitoring of the charge distribution rearrangements which involve the triple ion state $|1\rangle \sim Cl^- \,/\, CH^+_3 \,/\, Cl'^-$ via the weights' differences $w_1 - w_4$ and $w_1 - w_6$. It is important to notice that the assigned ordering of the VB states in (5.3) matches the symmetry of the natural solvent coordinates (5.5).

The first question to be answered in the above three state framework by an ESP analysis along the lines of that in Secs. 3 and 4 is the following. In the neighborhood of the reaction transition state, where by symmetry the contributions of the single ion states $|2\rangle$ and $|3\rangle$ must be equal, are the relative energies of $|1\rangle$, $|2\rangle$, and $|3\rangle$ and their mutual resonance couplings, such that there is a significant mixing of $|1\rangle$ into the transition state electronic structure ? The most extreme manifestation of this would arise in the event that at the transition state, where the VB states $|2\rangle$ and $|3\rangle$ are degenerate, the free energy of $|1\rangle$ lies below those degenerate values: then an intermediate well could arise. The answer to this and other questions should be available in the near future[13].

6. Concluding remarks

We have given some highlights of a theory which combines the familiar multistate VB picture of a molecular system with a dielectric continuum model for the solvent which accounts for the solute's boundary effects — due to the presence of a van der Waals cavity which displays the solute's shape — and includes a quantum model for the electronic solvent polarization.

The theory is capable of describing both the regimes of equilibrium and nonequilibrium solvation: for the latter we have developed a framework of natural solvent coordinates which greatly helps the analysis of the reaction system along the ESP, and displays the ability to reduce considerably the burden of the calculation of the free energy surface in the nonequilibrium solvation regime. While much remains to be done in practical implementations for various reactions, the theory should prove to be a very useful and practical description of reactions in solution.

The nonequilibrium free energy surface obtained along the lines described above can be used to analyze reaction paths and to calculate reaction rate constants[8]-[10],[43]. For this purpose, a further aspect has to be included: the provision of the kinetic energy of the system, encompassing the relevant solute nuclear coordinates and the solvent coordinates. In general, this is best accomplished by an appropriate scaling of the solvent coordinates so that the kinetic energy is diagonal, or nearly so. As a result, there is no kinetic coupling between the various momenta and the equations of motion are most simple[9],[10, 43, 45]. Together with the free energy hypersurface, this provides the Solution Reaction Path (SRP)[8]-[10],[43] — the solution phase generalization of the gas phase reaction path due to Fukui[46].

If one wishes instead to follow the explicit time dependent dynamics of a reaction system on the global multidimensional nonequilibrium free energy surface[47], an additional ingredient is necessary. This aspect derives from the fact that the present nonequilibrium free energy description is a nondissipative treatment of the solvent[6, 43]. That is to say that together with the kinetic energy mentioned above, (2.12) for G provides a *dynamic,* although nondissipative, Hamiltonian description for the solute nuclei and the solvent coordinates[43]; but no frictional damping of the solvent coorclinates is included. For many chemical reactions involving modest to high barriers, this is an excellent description for reaction rate constants[48], since reaction transmission coefficients depend only on short time dynamics and friction on the solvent coordinate does not contribute (see the contribution by Hynes in this volume). It is also a completely adequate description for obtaining the SRP referred to above. But for very low barrier reactions[49] and for examination of explicit dynamics over the entire surface, one requires explicit introduction of a generalized friction for each solvent coordinate[50] . This generally complex procedure is best discussed in the contest of specific reaction cases, and is a topic for future developments.

7. Acknowledgments

This work was supported in part by NSF grants CHE88-07852 and CHE93-12267, and by an NIH Shannon Award.

References

1. Bianco, R. and Hynes, J. T., (1995), *J. Chem. Phys.* **102,** 7864
2. Bianco, R. and Hynes, J. T., (1995), *J. Chem. Phys.* **102,** 7885.
3. Bianco, R., Juanos i Timoneda, J., and Hynes, J. T., (1994), *J. Phys. Chem.* **98,** 12103.
4. Kim, H. J. and Hynes, J. T., (1990), *J. Chem. Phys.* **93,** 5194, 5211.
5. Gehlen, J. N., Chandler, D., Kim, H. J., and Hynes, J. T., (1992), *J. Phys. Chem.* **96,** 1748.
6. Kim, H. J. and Hynes, J. T., (1992), *J. Chem. Phys.* **96,** 5088.
7. (a) Pross, A. and Shaik, S. S., (1982), *Tetrahedron Lett.* **23,** 5467; (1983), *Acc. Chem, Res.* **16,** 363; Shaik, S. S., (1985), *Prog. Phys. Org. Chem.* **15,** 197; Pross, A., (1985), *Adv. Phys. Org. Chem.* **21,** 99; Sini, G., Shaik, S., and Hiberty, P. C., (1992), *J. Chem. Soc. Perkin Trans.* **2,** 1019; Shaik, S. S., (1994), *J. Mol. Liq.* **61,** 49; (b) Shaik, S. S., Ioffe, A., Reddy, A. C., and Pross, A., (1994), *J. Am. Chem. Soc.* **116,** 262. (c) Shaik, S. S., Schlegel, H. B., and Wolfe, S. (1992) *Theoretical Aspects of Physical Organic Chemistry: The S_N2 Mechanism,* Wiley, New York, and references therein.
8. (a) Juanos i Timoneda, J. and Hynes, J. T., (1991), *J. Phys. Chem.* **95,** 10431; (b) Mathis, J. R., Bianco, R. and Hynes, J. T., (1994), *J. Mol. Liq.* **61,** 81; (c) Kim, H. J., Bianco, R., Gertner, B. J. and Hynes, J. T., (1993), *J. Phys. Chem.* **97,** 1723.; (d) Fonseca, T., Kim, H. J. and Hynes, J. T., (1994), *J. Photochem. Photobiol. A: Chem.* **82,** 67; (1994), *J. Mol. Liq,* **60,** 161.
9. Gertner, B. J., Ando, K., Bianco, R., and Hynes, J. T., (1994), *Chem. Phys.* **183,** 309.
10. Kim, H. J. and Hynes, J. T., (1992), *J. Am. Chem. Soc.* **114,** 10508, 10528; Mathis, J. R., Kim, H. J. and Hynes, J. T., (1993), *ibid.* **115,** 8248; Mathis, J. R. and Hynes, J. T., (1994), *J. Phys. Clzem.* **98,** 5445, 5460.
11. Ghio, C., Scrocco, E., and Tomasi, J. in (1976) *Environmental Effects on Molecular Structures and Properties,* Pullman, B., Ed., Reidel, Dordrecht; Miertus, S., Scrocco, E., and Tomasi, J., (1981), *Chem. Phys.* **55,** 117; Pascual-Ahuir, J. L., Silla, E., Tomasi, J., and Bonaccorsi, R., (1987), *J. Comput. Chem.* **8,** 778; Cammi, R., Olivares del Valle, F. J., and Tomasi, J., (1988), *J. Chem. Phys.* **122,** 63; Aguilar, M. A., Olivares del Valle, F. J., and Tomasi, J., (1993), *J. Chem. Phys.* **98,** 7375; Cammi, R. and Tomasi, J., (1994), *J. Chem. Phys.* **100,** 7495.
12. Basilevsky, M. V., Chudinov, G. E., and Napolov, D. V., (1993), *J. Phys. Chem.* **97,** 3270.
13. Mennucci, B., Bianco, R., Kim, H. J., and Hynes, J. T., *Valence Bond State Treatment of the $Cl^- + CH_3Cl$ S_N2 Reaction in Solution,* in preparation.
14. (a) Mulliken, R. S., (1952), *J. Phys. Chem.* **56,** 801; (1964), *J. Chim.* Phys. **20,** 20; Coulson, C. A., in (1959) *Hydrogen Bonding,* Hadži, D. and Thompson, H. W. Eds., Pergamon, London; Bratož, S., (1967), *Adv. Quant. Chem.* **3,** 209; Ilczyszyn, M., Ratajczak, II., and Skowronek, K., (1988), *Magn. Reson. Chem.* **26,** 445; Hasegawa, M., Daiyasu, K., and Yomosa, S., (1970), *J. Phys. Soc. Jpn,* **28,** 275, 1304; Warshel, A., and Russel, S. J., (1986), *J. Am. Chem. Soc.* **108,** 6569. (b) Ando, K. and Hynes, J. T. in (1994) *Structure and Reactivity in Aqueous Solution,* Cramer, C. J. and Truhlar, D. G. Eds., American Chemical Society, Washington, DC, p.143; Ando, K. and Hynes, J. T., *Molecular Mechanism of HCI Acid Ionization in Water: Ab Initio Potential Energy Surfaces and Monte Carlo Simulations,* submitted to J.

Phys. Chem.
15. (a) Beens, H. and Weller, A., (1969), *Chem. Phys. Lett.* **3,** 666; in (1975) *Organic Molecular Photophysics,* Birks, J.B., Ed., 2nd vol., Wiley, London; (b) Huron, M. J. and Claverie, P., (1972), *J. Phys. Chem.* **76,** 2123; (1974), *ibid.* **78,** 1853, 1862. (c) Newton, M. D., (1973), *J. Chem. Phys.* **58,** 5833; (1975), *J. Phys. Chem.* **79,** 2795. (d) Yomosa, S., (1973), *J. Phys. Soc. Jpn.* **35,** 1738; (1974), *ibid.* **36,** 1655; (1978), *ibid.* **44,** 602. (e) Tapia, O. and Goscinski, O., (1975), *Mol. Phys.* **29,** 1653; Tapia, O. in *Quantum Theory of Chemical Reactions,* Daudel, R., Pullman, A., Salem, L., Veillard, A., Eds., (1980) Reidel, Dordrecht; Tapia, O., (1991), *J. Mol. Struct.* (*Theochem.*) **226,** 59; Constanciel, R. and Tapia, O., (1978), *Theor. Chim. Acta* **48,** 75. (f) Rivail, J.-L. and Rinaldi, D., (1976), *Chem. Phys.* **18,** 233; Rivail, J.-L. in (1988) *Chemical Reactivity in Liquids,* Moreau, M. and Turq, P. , Eds., Plenum, New York; (g) Andres, J. L., Lledos, A., Bertran, J., (1994), *Chem. Phys. Lett.* **223,** 23.
16. (a) Furuki, T., Sakurai, M., Inoue, Y., Chûjô, R., and Harata, K., (1992), *Chem. Phys. Lett.* **188,** 584. (b) Ågren, H. and Mikkelsen, K. V., (1991), *J. Mol. Struct.* (*Theochem.*) **234,** 425. (c) Karlstrom, G., (1988), *J. Phys. Chem.* **92,** 1315. (d) Drummond, M. L. J., (1988), *J. Chem. Phys.* **88,** 5014, 5021. (e) Fox, T., Rosch, N., and Zauhar, R. J., (1993), *J. Comput. Chem.* **14,** 253. (f) Karelson, M. M. and Zerner, M. C., (1992), *J. Phys. Chem.* **96,** 6949. (g) Wong, M. W., Wiberg, K. B., and Frisch, M. J., (1992), *J. Am. Chem. Soc.* **114,** 523, 1645. (h) Ford, G. P. and Wang, B., (1992), *J. Comput. Chem.* **13,** 229; Wang, B. and Ford, G. P., (1992), *J. Ckem. Phys.* **97,** 4162; (i) Young, R. H., (1992), *J. Chem. Phys.* **97,** 8261.
17. Truhlar, D. G., Schenter, G. K., and Garrett, B. C., (1993), *J. Chem. Phys.* **98,** 5756; Cramer, C. J. and Truhlar, D. G. in *Reviews in Computational Chemistry,* vol. 6, Lipkowitz, K. B. and Boyd, D. B., Eds., VCH Publishers, New York, in press; (1992), *J. Am. Chem. Soc.* **113,** 8305, 8552; (1992), *Science* **256,** 213.
18. (a) Klopman, G. and Andreozzi, P., (1980), *Theor. Chim. Acta* **55,** 77. (b) Kihara, T. and Jhon, M. S., (1970), *Chem. Phys. Lett.* **7,** 559. (c) Germer, H. A., (1974), *Theor. Chim. Acta* **34,** 145; (1974), *ibid.* **35,** 273. (d) Miertus, S., Frecer, V., and Majekova, M., (1988), *J. Mol. Struct,* (*Theochem.*) **179,** 353; Frecer, V., Majekova, M., and Miertůs, S., (1989), *ibid.* **183,** 403. (e) Rashin, A. A., (1990), *J. Phys. Chem.* **94,** 1725. (f) Rzepa, H. S. and Yi, M. Y., (1991), *J, Chem. Soc. Perkin Trans.* **2,** 531. (g) Rauhut, G., Clark, T., and Steinke, T., (1993), *J. Am. Chem. Soc.* **115,** 9174.
19. Basilevsky, M. V. and Chudinov, G. E., (1992), *Chem. Phys.* **157,** 327, 345; Chudinov, G. E., Napolov, D. V., and Basilevsky, M. V., (1992), *ibid.* **160,** 41.
20. Tomasi, J. and Persico, M., (1994), *Chem. Rev.* **94,** 2027.
21. (a) Hylton-McCreery, J., Christoffersen, R. E. and Hall, G. G., (1976), *J. Am. Chem. Soc.* **98,** 7191, 7198. (b) Thole, B. P. and van Duijnen, P. T., (1980), *Theor. Chim. Acta* **55,** 307;
22. See e.g. McWeeny, R., (1989) *Methods of Molecular Quantum Mechanics,* 2nd Ed., Academic Press, San Diego.
23. Sidis, V., (1992), *Adv. Chem. Phys.* **82,** 73.
24. Ellison, F. O., (1963), *J. Am. Chem. Soc.* **85,** 3540.
25. Zeiri, Y. and Shapiro, M., (1978), *Chem. Phys.* **31,** 217; Shapiro, M. and Zeiri, Y., (1979), *J. Chem. Phys.* **70,** 5264; Zeiri, Y. and Shapiro, M., (1981), *ibid.* **75,** 1170.
26. Persico, M., in *Spectral Line Shapes,* Vol.3, Rostas, F., Ed., (1985) de Gruyter, Berlin, p. 587; Cimiraglia, R., Malrieu, J.-P., Persico, M., and Spiegelmann, F., (1985), *J. Phys. B: At. Mol. Phys.* **18,** 3073.
27. Ruedenberg, K. and Atchity, G. J., (1993), *J. Chem. Phys.* **99,** 3790, 3799.
28. Pacher, T., Cederbaum, L. S., and Köppel, H., (1993), *Adv. Chem. Phys.* **84,** 293.
29. Bernardi, F. and Robb, M. A., (1987), *Adv. Chem. Phys.* **67,** 155.
30. Cooper, D. L., Gerratt, J., and Raimondi, M., (1987), *Adv. Chem. Phys.* **67,** 319.

31. Reed, A. E., Curtis, L. A., and Weinhold, F. A., (1988), *Chem. Rev.* **88,** 899.
32. Basilevsky, M. V., Chudinov, G. E., and Newton, M. D., (1994), *Chem. Phys.* **179,** 263.
33. Grasselli, J. G. and Ritchey, W. M., Eds., (1975) *Atlas of Spectral Data and* Physical *Constants For Organic Compounds,* 2nd Ed., The Chemical Rubber Co., Cleveland.
34. See, for instance, the option for a self consistent reaction field in the popular quantum chemistry set of programs GAMESS by Schmidt, M. W., Baldridge, K. K., Boatz, J. A., Elbert, S. T., Gordon, M. S., Jensen, J. H., Koseki, S., Matsunaga, N., Nguyen, K. A., Su, S. J., and Windus, T. L., together with Dupuis, M., Montgomery, J. A., (1993), *J. Comput. Chem.* **14,** 1347.
35. For a review, see Newton, M. D. and Sutin, N., (1984), *Ann. Rev. Phys. Chem.* **35,** 437.
36. Papanikolas, J. M., Vorsa, V., Nadal, M. E., Campagnola, P. J., Gord, J. R., and Lineberger, W. C., (1992), *J. Chem. Phys.* **97,** 7002.
37. Kliner, D. A. V., Alfano, J. C., and Barbara , P. F., (1993), *J. Chem. Phys.* **98,** 5375.
38. U., Banin, A., Waldman, and S., Ruhman, (1992), *J. Chem. Phys.* **96,** 2416; U., Banin and S., Ruhman, (1993), *ibid.* **98,** 4391; (1993), ibid. **99,** 9318; U., Banin, R., Kosloff, and S., Ruhman, (1994), *Chem. Phys.* **183,** 289.
39. L., Perera and F. G., Amar, (1989), *J. Phys. Chem.* **90,** 7354; F. G., Amar and L., Perera, (1991), *Z. Phys. D* **20,** 173.
40. Papanikolas, J. M., Maslen, P. E., and Parson, R., (1995), *J. Chem. Phys.* **102,** 2452.
41. Benjamin, I., Barbara, P. F., Gertner, B. J., and Hynes, J. T., (1995), *J. Phys. Chem.* **99,** 7557.
42. Bianco, R. and Hynes, J. T., unpublished.
43. Lee, S. and Hynes, J. T., (1988), *J. Chem. Phys.* **88,** 6853, 6863.
44. See, for example, Chandrasekhar, J., Smith, S. F. and Jorgensen, W. L., (1985), *J. Am. Chem. Soc.* **107,** 154.
45. Borgis, D. and Hynes, J. T., (1993), *Chem. Phys.* **170,** 315; Kim, H. J., to be submitted; Kim, H. J., Lee, S., Gertner, B. J., Mathis, J. R., and Hynes, J. T., to be submitted; see also [10].
46. Fukui, K., (1970), *J. Phys. Chem.* **74,** 4161; (1981), *Acc. Chem. Res.* **14,** 363.
47. Gertner, B. J., Whitnell, R. M., Wilson, K. R., and Hynes, J. T., (1991), *J. Am. Chem. Soc.* **113,** 74.
45. Grote, R. F. and Hynes, J. T., (1980), *J. Chem. Phys.* **76,** 2715; Bergsma, J. P., Reimers, J. R., Wilson, K. R., and Hynes, J. T., (1986), *ibid.* **85,** 5625; Bergsma, J. P., Gertner, B. J., Wilson, K. R., and Hynes, J. T., (1987), *ibid.* **86,** 1356; Gertner, B. J., Bergsma, J. P., Wilson, K. R., Lee, S., and Hynes, J. T., (1987), *ibid.* **86,** 1377; Gertner, B. J., Wilson, K. R., and Hynes, J. T., (1989), *ibid.* **90,** 3537; Keirstead, W. P., Wilson, K. R., and Hynes, J. T., (1991), *ibid.* **95,** 5256; Zhu, S. B., Lee, J., and Robinson, G. W., (1988), ibid. **92,** 2401; Berne, B. J., Borkovec, M., and Straub, J. E., (1988), *ibid.* **92,** 3711; Roux, B. and Karplus, M., (1991), *ibid.* 95, 4845; Tucker, S. and Truhlar, D., (1990), *J. Am. Chem. Soc.* **112,** 3347; Smith, B. B., Staib, A., and Hynes, J. T., (1993), *Chem. Phys.* **176,** 521; Staib, A., Borgis, D., and Hynes, J. T., (1995), *J. Chem. Phys.* **102,** 2487.
49. Ciccotti, G., Ferrario, M., Hynes, J. T., and Kapral, R., (1990), *J. Chem. Phys.* **93,** 7137; Rey, R. and Guárdia, E., (1992), *J. Phys. Chem*. **96,** 4712; Zichi, D. A., Ciccotti, G., Hynes, J. T., and Ferrario, M., (1989), *J. Phys. Chem.* **93,** 2184; Fonseca, T. and Ladanyi, B. M., in (1994) *Ultrafast Reaction Dynamics and Solvent Effects: Experimental and Theoretical Aspects,* Gauduel, Y. and Rossky, P. J., Eds., AIP Press, New York, p.380.
50. See e.g. the discussion in Refs.[10].
51. See Ref.[8](b) for a survey of calculations which provide evidence in this sense.

This page intentionally left blank.

QUANTUM THEORY OF SOLVENT EFFECTS AND CHEMICAL REACTIONS

O.TAPIA, J.ANDRES* AND F.L.M.G.STAMATO
Department of Physical Chemistry. University of Uppsala,
Box 532, S-75121 UPPSALA,Sweden
** Department of Experimental Sciences. Universitat Jaume I*
Apartat 242, Castelló, Spain

1. Introduction

In this chapter a quantum mechanical approach encompassing solvent effects and chemical reactions is sketched and discussed. The theory of solvent effects on the electronic structure of a given solute leads to a representation of the sub-system embedded in a larger one with the help of effective Hamiltonians, wave functions and eigenvalues. Since the whole electronic system is quantum mechanical in nature, and in principle non-separable, the theory for the ground electronic state permits defining under which conditions the solute and solvent separability is an acceptable hypothesis. This problem has been extensively addressed in previous work from our group [1-6] and by many others [7-13]. In order to set up the stage for a quantum mechanical analysis of solvent effects and chemical reactions, in Section 2 is summarized the theory of n-electrons and m-nuclei with special emphasis on possible shortcomings of the Born-Oppenheimer framework. Time dependent phenomena is highligthed. In Section 3, we go a step beyond previous wave mechanical treatments of solvent effects by explicitly including a time-dependent approach to solvent dynamics and solute-solvent coupling. Solvent fluctuation effects on the solute reactive properties can thence be discussed in a more natural framework which includes, as especial cases, most of the 1-dimensional models currently available. The approach to thermal equilibrium is examined from this perspective. Time dependent effects are also introduced in Section 4 where a quantum mechanical theory of chemical interconversions is described.

The separation of a reactant system (solute) from its environment with the consequent concept of solvent or surrounding medium effect on the electronic properties of a given subsystem of interest as general as the quantum separability theorem can be. With its intrinsic limitations, the approach applies to the description of specific reacting subsystems in their particular active sites as they can be found in condensed phase and in media including the rather specific environments provided by enzymes, catalytic antibodies, zeolites, clusters or the less structured ones found in non-aqueous and mixed solvents [1, 3, 6, 8, 11, 12, 14-30].

Before considering the analysis of solvent effects on chemical reactions, some of the shortcomings of potential energy hypersurfaces as a tool to describe chemical process are

O. Tapia and J. Bertrán (eds.), Solvent Effects and Chemical Reactivity, 283-361.
© 1996 *Kluwer Academic Publishers. Printed in the Netherlands.*

discussed in section 4. A chemical reaction is viewed there as a fundamental quantum mechanical change of state. It is convenient to distinguish between the exact (global) Hamiltonian H and the molecular Hamiltonian Hc. The latter is obtained from the Born-Oppenheimer approach, which for a system having a minimum energy with respect to variations of the nuclear variables, leads to models for the electro-nuclear fluctuations around the stationary point. There are configurational points for which the electronuclear fluctuations sustain only excited states. These are saddle points of any index with respect to variations of nuclear coordinates. No ground state can be assigned to a saddle point of index n>0 (SPi-n). The overlooked fact is that all quantum states of Hc (with and without local ground states) are, in prnciple, eigen states of the global Hamiltonian H. It will be around this latter Hamiltonian that the theory is built, while the practical calculations are made with the molecular Hamiltonians Hc. The passage from the spectra of one molecular Hamiltonian to another may or may not be mediated by an intermediate molecular transition Hamiltonian (SPi-n), but the essence of the problem is the finite lifetime of the excited states of the molecular Hamiltonians where the quantum jumps are mediated by the photon field present in the reactant system. These matters are discussed in Section 4.

We distinguish passive from active solvent effects on chemical reactions. Passive solvent effects do not change the quantum nature of the interconversion step, while it may change the relative energies of the corresponding spectra. The active solvent effects involve a specific action of the solvent in the chemical interconversion step leading to a change of mechanism or to a surrogate mechanism. This may include general/specific acid or base catalysis by the solvent molecules. For a chemical reaction having different mechanism to accomplish the chemistry, a passive solvent may change the relative probabilities between channels but not the actual mechanisms. From the computational viewpoint, in the supermolecule approach, such a distintion is seldom retained. Small solvent clusters treated at any level of electronic theory cannot be expected to provide an adequate description of the characteristic many-body effects [31]. Active solvent effects can be treated as a passive one if by including a minimal (critical) number of solvent molecules the interconversion step is correctly described as a supermolecule, the remaining solvent can be considered as passive. It is to this type of system that the theory would apply.

A well defined theory of chemical reactions is required before analyzing solvent effects on this special type of solute. The transition state theory has had an enormous influence in the development of modern chemistry [32-37]. Quantum mechanical theories that go beyond the classical statistical mechanics theory of absolute rate have been developed by several authors [36, 38, 39]. However, there are still compelling motivations to formulate an alternate approach to the quantum theory that goes beyond a theory of reaction rates. In this paper, a particular theory of chemical reactions is elaborated. In this theoretical scheme, solvent effects at the thermodynamic and quantum mechanical level can be treated with a fair degree of generality. The theory can be related to modern versions of the Marcus theory of electron transfer [19,40,41] but there is no

reaction coodinate in the classical sense. The present theory gives a different definition of catalysis by separating necessary and sufficient conditions for the phenomenon to appear, and subsidiary conditions leading to an increase of the efficacy of the whole process. For interconversion steps going through an intermediate molecular Hamiltonian, the saddle points associated to the adiabatic solution of the electronic wave function define geometries to which the reactants should tend to adopt in order to open the interconversion channel. The invariance of such saddle point geometries is an essential element of the theory allowing for an understanding of catalysis in the sense given by Pauling[42], this time it has a general content in so far surrounding media are concerned. All these matters are discussed in Section 4, and for an early formulation of these ideas see ref.[43].

Contemporary computer assisted molecular simulation methods and modern computer technology have contributed to the actual numerical calculation of solvent effects on chemical reactions and molecular equilibria. Classical statistical mechanics and quantum mechanics are basic pillars on which practical approaches are based. On top of these, numerical methods borrowed from different fields of physics and engineering and computer graphics techniques have been integrated into computer programs running in graphics workstations and modern supercomputers. Recent results are overviewed in Section 6. In Section 7 a general discussion pointing towards recent trends is presented.

2. Theory

From a quantum mechanical perspective, physical and chemical processes can be described on equal basis. These processes are the result of changes among quantum states (discrete and/or continuum) and one of the tasks of the theory is to identify those states that are relevant to their description. A reactant system in a gas phase or in solution can be characterized as a set of electrons and nuclei. At a given temperature the system may change the populations od the quantum state via emission and absorption of energy quanta (photons, optical phonons). The system may change its quantum states if work is exerted on it (or exerted by the system on the surroundings) or it can change the population distribution (entropic change) via energy exchange with a thermal bath. Thermodynamic equilibrium is attained for a system weakly coupled to a thermal bath if the coupling has been on for a long time, and if all the fast processes have happened and all the slow ones not [44]. The first problem is the calculation of the relevant quantum states of the system. The chemical phenomena requires of an electrodynamics description [45, 46] as the charged particles constituting normal matter interacts via electromagnetic fields. The change of quantum states are prompted by the coupling between the matter and radiation fields. In the approach herein described the classical mechanical view of a chemical process taking place on an energy hypersurface fades away. The Born-Oppenheimer framework is thence used in a more restrictive fashion.

In what follows, standard quantum chemical approach is summarized. The modifications required to describe chemical processes by using an energy basis are

described and discussed.

2.1. TECHNICAL SEPARABILITY

The solute-solvent system, from the physical point of view, is nothing but a system that can be decomposed in a determined collection of electrons and nuclei. In the many-body representation, in principle, solving the global time-dependent Schrödinger equation with appropriate boundary conditions would yield a complete description for all measurable properties [47]. This equation requires a definition of the total Hamiltonian in coordinate representation $H(\mathbf{r},\mathbf{X})$, where $\mathbf{r}$ is the position vector operator for all electrons in the sample, and $\mathbf{X}$ is the position vector operator of the nuclei. In molecular quantum mechanics, as it is used in this section, $H(\mathbf{r},\mathbf{X})$ is the Coulomb Hamiltonian[46] . The global wave function $\Lambda(\mathbf{r},\mathbf{X},t)$ is obtained as a solution of the equation:

$$i\hbar\, \partial\Lambda(\mathbf{r},\mathbf{X},t)/\partial t = H(\mathbf{r},\mathbf{X})\, \Lambda(\mathbf{r},\mathbf{X},t) \tag{1}$$

To define the language and comment on some limitations usually overlooked in the theoretical chemical literature, let us outline the standard procedure leading to a formal solution for such an equation.

In the present analysis, the Hamiltonian does not explicitly depends upon time. The conditions defining a microcanonical ensemble are fulfilled [48], namely, one has a total constant energy E.

Applying the method of the separation of variables the total wave function can be cast as a product $\Lambda(\mathbf{r},\mathbf{X},t) = \Phi(\mathbf{r},\mathbf{X})\zeta(t)$ that, once introduced in Eq.(1), gives the customary separation of time from space coordinates:

$$i\hbar\partial\zeta(t)/\partial t = E\, \zeta(t) \qquad \text{and} \qquad H(\mathbf{r},\mathbf{X})\, \Phi(\mathbf{r},\mathbf{X}) = E\, \Phi(\mathbf{r},\mathbf{X}) \tag{2}$$

These are the equations on which a number of approximations are carried out to obtain approximate model solutions. In particular, the Born-Oppenheimer (BO) frame allows for a useful separation between nuclear and electronic motion [49-52]. See also Park's book where some interesting elementary examples are analyzed concerning electro-nuclear coupling effects[53].

Technically, the time-independent Schrodingcr equation (2) is solved for clamped nuclei. The Hamiltonian is broken into its electronic part, He, including the nuclear Coulomb repulsion energy, and the nuclear Hamiltonian HN. At this level, mass polarization effects are usually neglected. The wave function is therefore factorized as usual: $\Phi(\mathbf{r},\mathbf{X}) = \Psi(\mathbf{r};\mathbf{X})\xi(\mathbf{X})$. Formally, the electronic wave function $\Psi(\mathbf{r};\mathbf{X})$ and total electronic energy, $E(\mathbf{X})$, are obtained after solving the equation for each value of $\mathbf{X}$:

$$He\ \Psi_i(\mathbf{r};\mathbf{X}) = E_i(\mathbf{X})\ \Psi_i(\mathbf{r};\mathbf{X}) \tag{3}$$

Once this equation is solved for all relevant regions of the nuclear configuration space, in the BO framework, the nuclear motion can be treated either via a classical mechanical analysis with the help of computer simulations [6], or it can be treated quantum mechanically for simple models [54]. In the latter scheme, the nuclear Schrödinger equation must be solved:

$$(H_N + E_i(\mathbf{X}))\, \xi_{ik}(\mathbf{X}) = E_{ik}\, \xi_{ik}(\mathbf{X}) \tag{4}$$

Thus, the approximate total wave function $\Phi_{ik}(\mathbf{r},\mathbf{X}) = \Psi_i(\mathbf{r}_s,\mathbf{r}_m;\mathbf{X})\, \xi_{ik}(\mathbf{X})$ is taken as the solution of the time-independent equation (2) with energy levels E_{ik}. The time-dependent equation can be cast in terms of this energy so that: $\zeta_{ik}(t) = \exp(-iE_{ik}t/\hbar)$. An arbitrary quantum state can be expanded on the basis of the $\Phi_{ik}(\mathbf{r},\mathbf{X})\exp(-iE_{ik}t/\hbar)$ as:

$$\Psi(\mathbf{r},\mathbf{X},t) = \Sigma_{ik}\, C_{ik}(t)\, \Phi_{ik}(\mathbf{r},\mathbf{X}) \tag{5}$$

with $C_{ik}(t)=C_{ik}\exp(-iE_{ik}t/\hbar)$. For a recent analysis of time-dependent theoretical treatments of the dynamics of electrons and nuclei in molecular systems the reader is referred to Öhrn's and coworkers paper [55].

Before proceding ant further, it is worth reminding that general quantum mechanics is coordinate free. The wave function represented in (5), $\Psi(\mathbf{r},\mathbf{X},t) = \langle \mathbf{r},\mathbf{X}|\Psi\rangle$, corresponds to a general quantum state $|\Psi\rangle$ projected (modelled) on the coordinate basis $|\mathbf{r},\mathbf{X}\rangle$. The time evolution of this general quantum state is driven by a Schrödinger-like equation with a general (global) Hamiltonian operator [47]. A coordinate projection corresponds to the well known time dependent Schrödinger equation (1) with a model Coulomb Hamiltonian $H((\mathbf{r},\mathbf{X})$ representing the molecular system of interest. It is well known that the molecular systems have stationary $\mathbf{X}_o$ configurations in the sense that $E(\mathbf{X}_o)$ is stationary with respect to nuclear coordinate variations around $\mathbf{X}_o$. The Hamiltonian can now be expanded around this point. These will be the molecular Hamiltonians Hc. We consider then a general formulation of quantum mechanics, where H is the global Hamiltonian and use the coordinate-projected Hamiltonian as practical computing device to determine the Hc and thereby all the stationary states of the molecular system around a particular geometry in the nuclear configuration space. The approximate quantum states related to the stationary Hamiltonians are assumed to be models of the exact quantum states. This aspect of the quantum theory should be beared in mind when thinking about chemical reactions.

In coordinate representation, there exists alternative base representations, adiabatic and diabatic. Both representations are equivalent if the basis are complete. For a thorough discussion on adiabatic-diabatic electronic state transformations the reader is referred to the work by Baer [49, 50], see also the work by Chapuisat *et al.* [51] In this

section, the adiabatic approach is retained without loss of generality. The state wave function obtained in this frame is a model of the quantum state of a material system. Such a system is one of qualities, not an event or string of events. As the interest will be focussed on physical processes, their representation corresponds to changes of the quantum material state of the system under study.

All this ismore or less well known[55]. What is less well acknowledged is the fact that the coordinate type of approximation can be justified under relatively restrictive conditions. As is common practice, the nuclear Hamiltonian appearing in Eq.(4) can be further separated in order to treat the molecular rotation motion and spectra [50, 51, 56]. To illustrate such conditions, let us take a simple harmonic model for the fluctuation pattern of the particles, then $\omega = \sqrt{(k/m)}$, and k is the harmonic restitution (force) constant and m the reduced mass for that mode. After analysis, one gets the following relations for the ratio between electronic and vibrational (nuclear) energies: $E_v/E_e \approx \omega_n/\omega_e \approx \delta\mathbf{r}_n^2/\delta\mathbf{r}_e^2 \approx \sqrt{(m_e/m_n)} = \kappa^2$. Nuclear fluctuations are represented by $\delta\mathbf{r}_n$ with a similar form for the electron displacement. From the perturbation analysis carried out by Born and Oppenheimer, the separability of the nuclear and electronic fluctuations stems from the fact that $m_e << m_n$ and that $E_v \approx \kappa^2 E_e$. Although seldom emphasized, these relationships imply that the fluctuations are taken around stationary points of the (numerical) potential energy hypersurface $E_i(\mathbf{X})$. In what follows, the electronic Hamiltonian evaluated at a given stationary point of $E_i(\mathbf{X})$ is taken as a stationary Hamiltonian, and Taylor expansions in terms of fluctuation nuclear coordinates $\delta\mathbf{r}_n$ lead to different models allowing for practical calculation of models for the vibration and rotation spectra. The use of the numericaly calculated $E_i(\mathbf{X})$ in eq.(4) provides another model to practically obtain these spectra. For diatomics, the empirical method relating the vibrational levels to a classical anharmonic potential energy curve uses the Rees-Klein-Rydberg (RKR) method. This procedure provides a classical model for the nuclear fluctuation spectra which has been numerically reproduced by solving Eq.(3) with *ab initio* post Hartree-Fock methods to a high degree of numerical accuracy. The picture of a diatomic molecule as if it were a spring arose from this type of analysis. But, when describing physical changes of state, the quantum states and the associated quantum jumps of the molecular system are the physically meaningful elements of the theory. The classical picture acts as a language.

The scheme described above, reconforted by the post-HF calculations [57] where the coordinate representing the distance between the nuclei in the diatomic molecule (or any bond in polyatomic molecules), lead to the pervading picture of a diatom connected adiabatically with two non-interacting atoms at infinite distance. From a compuational point of view, this picture is quite useful and widely employed.

Quantum mechanically, however, the diatomic molecule and the separated atoms at infinite distance are two distinct quantum systems having their own quantum states. The physical dissociation cannot be seen as a continuous process of extending a classical spring as nearly all textbooks in chemistry, physical chemistry and quantum chemistry suggest. This is quite contrary to the fundamentals of quantum mechanics itself. Before

tackling this point in section 3, let us first examine the quantum physical picture and complete the decription of the quantum theory of solvent effects.

2.2. A QUANTUM PHYSICAL PICTURE

The technical picture described above must be supplemented with a photon field in order to enforce the quantum mechanical nature of the physical processes. The Coulomb Hamiltonian is useful to numerically calculate model quantum states. Charged systems interact among themselves via real and virtual photons [45]. A quantum system changes its state by quantum jumps and energy is conserved via absorption or emission of photons. For a system in equilibrium, the relative number of molecules per cubic centimeter in two quantum states having a frequency matching Bohr's rule (E_k-Ej) = $h\upsilon_{kj}$ = $\hbar\omega$ with $h=2\pi\hbar$), is given according to statistical mechanics by the Boltzmann ratio Nk/Nj = $\exp(-\hbar\omega/kT)$. Under these conditions, the number of molecules going from state j to k per unit time by absorption of photons $\hbar\omega$ must equal the number of photons emitted from k to j. If there are nw photons of frequency ω per cubic centimeter, then Nj n_ω = N_k (n_ω +1) and after introducing the Boltzmann ratio for Nk/Nj one gets the famous Planck's black-body distribution law: n_ω = 1/ [$\exp(+\hbar\omega$ kT) - 1]. The interaction between photons and matter causes the number of photons to change by ±1.

In a complete description, the photon and matter fields must be included with their interactions in the sense that charged particles interacts via the electromagnetic field. The Hamiltonian can be written in different gauges. Here, and as it is common practice in quantum chemistry, it is written in the Coulomb gauge [46, 58]. The Hamiltonian of equation (1) has an instantaneous Coulomb interaction between all charges, the quantum states of Eq.(2) are considered as non perturbed bound states that interact via perturbation terms coupling the charges with transverse waves representing the electromagnetic vector potential **A.** For example, putting the system in a box of volume V, the vector potential at a point **x** in the box is given by:

$$\mathbf{A}= \sqrt{(4\pi\,\hbar\,c^2/2\omega)}\;\hat{e}\;\{\exp[-i(\omega t-\mathbf{K}\cdot\mathbf{x}) + \exp[+i(\omega t-\mathbf{K}\cdot\mathbf{x})]\} \qquad (6)$$

where $\hat{e}$ is a polarization unit vector, and $\exp(+i\mathbf{K}\cdot\mathbf{x})$ is a plane running wave. The normalization was chosen so as to correspond to unit probability per cubic centimeter of finding the photon, and the average energy density becomes $\hbar\omega$. Under these conditions, the amplitude that an atomic system will absorb a photon during the process of jumping from one state to another has been made equivalent to the amplitude that the same transition will occur under the influence of a potential equal to that of a classical electromagnetic wave representing that photon (Eq.(6)) and provided that only first order terms in the potential act in perturbation [45].

The total Hamiltonian in the Coulomb gauge (Cf.sect.2.7) has the momentum

operators replaced by: **p**-(e/c)**A** for a particle of charge e. As the photon field is transversal and only first order terms in **A** should appear, one ends up with the Coulomb Hamiltonian form as the one appearing in Eq.(1) and a perturbation potential of the form U(**x**)=(e/mc) **A**(**x**,**t**).**p**. For further analysis see section 2.7. So that at the end, the probability of a transition per second depends upon the coupling between the molecular system and the radiation field:

$$P_{kj}\, d\Omega = (2\pi/\hbar)\, |\, U_{kj}\, |^2\, \omega^2\, d\Omega\, /(2\pi c)^3\, \hbar \tag{7}$$

After some algebra, the probability of jumping from one state to the other becomes proportional to the square modulus of the matrix element of the dipole moment between the bare quantum states k and j (if different from zero, or to any multipole moment having non-zero matrix elements between these two states).

With this digression closed, let us come back to the analysis and consequences derived from Eq.(3).

2.3. THE CLASSICAL MECHANICAL PICTURE

It is common practice to treat the nuclear configurational space **X** as a classical object. In this approach the forces on the nuclei are needed. The Hellman-Feynman formula for the force acting on the k-th nuclei (position coordinate $\mathbf{X}_k$) is given by:

$$\mathbf{F}_k = -\,\partial E_i(\mathbf{X})/\partial \mathbf{X}_k = -\,\langle \Psi_i(\mathbf{r}_s,\mathbf{r}_m;\mathbf{X})|\, \partial H_e/\partial \mathbf{X}_k\, |\Psi_i(\mathbf{r}_s,\mathbf{r}_m;\mathbf{X})\rangle \tag{8}$$

the total energy E_i playing the role of a potential energy function for the nuclei: $V(\mathbf{X})= E_i(\mathbf{X})$.

The equations of motion for the nuclei are obtained from Hamilton's least action principle. The nuclei total kinetic energy, K, is given by the sum of individual nucleus kinetic energy, $(1/2)M_k(d\mathbf{X}_k/dt)^2$. The time integral of the Lagrangian $L(\mathbf{X},d\mathbf{X}/dt,t) = K-V$ is the action S of the system. For different paths ($\mathbf{X}=\mathbf{X}(t)$) the action has different numerical values.

$$S[\mathbf{X}(t),\mathbf{X}(to),t,to] = \int L(\mathbf{X},d\mathbf{X}/dt,t)\, dt \tag{9}$$

For a family of trajectories all starting at the value **X**(to) and at t=t all arriving at **X**(t), there is one trajectory that renders the action stationary. The classical mechanical trajectory of a given dynamical system is the one for which δS=0, i.e. the action becomes stationary. The equation of motion is obtained from this variational principle [59]. The corresponding Euler-Lagrange equations are obtained: $d(\partial L/\partial \mathbf{v}_k)/dt = \partial \mathbf{L}/\partial \mathbf{X}_k$. In Cartesian coordinates these equations become Newton's equations of motion for each nucleus of mass M_k:

$$M_k d^2\mathbf{X}_k/dt^2 = \mathbf{F}_k = -\partial E(\mathbf{X})/\partial \mathbf{R}_k = -\langle \Psi_i(\mathbf{r}_s,\mathbf{r}_m;\mathbf{X})|\, \partial H_e/\partial \mathbf{X}_k \,|\Psi_i(\mathbf{r}_s,\mathbf{r}_m;\mathbf{X})\rangle \qquad (10)$$

This set of equations provides the basis for a number of so called combined quantum/classical mechanics methods [22, 60-62]. The force is calculated on the flight as the coordinates are updated by using the molecular dynamics algorithms. Periodic boundary conditions can be introduced in order to simulate the surrounding medium more accurately. However, in certain cases, the computing effort may be too high to be of a practical use. It is for this reason that the system has been simplified by projecting out the electronic components associated with the surrounding medium ($\mathbf{r}_m$-variables). This is done within the chemical picture to solvent effects.

2.4. POSSIBLE LIMITATIONS OF THE BO APPROXIMATION

The equation (3) generates the famous BO potential energy hypersurface. The practical power of this concept is well documented and it remains at the foundation of important domains in computational quantum chemistry. The theory of absolute reaction rates is entirely based upon it [32-34, 63] as well as all modern quantum theories of reaction rates [36, 39, 64-80].

A first insight into a different description of a chemical process can be obtained from an analysis of a (diatomic) dissociation process. Consider the standard treatment of a stable diatomic molecule. The word stable implies already the existence of a measurable characteristic size around which the electro-nuclear system fluctuates in its ground electronic state (i.e. a stationary molecular Hamiltonian with ground state). In standard quantum chemistry, this is the nuclear equilibrium distance.

The characteristic BO potential energy curve relates, in a continuous fashion, the bounded quantum diatomic state with a well defined electronic state of two atoms at infinite distance (which corresponds to a different molecular Hamiltonian, in this case an atomic one). Two atoms separated by a large distance and the associated diatomic molecule are two different molecular quantum systems. They have their characteristic quantum states. Two quantum states belonging to different classes cannot be adiabatically related without colliding with the quantum mechanical paradigm introduced by Planck at the beginning of this century. While the spectra of a quantum system can be adiabatically shifted by changes of external thermodynamic parameters, two different quantum states cannot be bridged with an adiabatic process. One cannot bring two hydrogen atoms, adiabatically, to form the hydrogen molecule without conflicting with the quantum mechanical nature of the systems. For processes carried out at constant temperature, the population of states must change, but the nature of the states is not modified.

Perusal of equation (3) shows that the existence of a quantum electronic state for each value of the configurational vector **X,** albeit computationally useful, is physically

untenable. In this connection, it is instructive to read Herring's critique to the Heitler-London method used to calculate spin couplings at large distances [81, 82]. The potential energy hypersurface $E_i(\mathbf{X})$ is an invaluable computing device, as is shown by the successful representation provided, for instance, by the RKR procedure of fitting vibrational levels to a potential energy curve.

The separability between electron and nuclear fluctuations makes theoretical sense for domains around the stationary points of $E_i(\mathbf{X})$ where the properties of the system can be characterized by computing high order derivatives that leads to a number of model representations for the nuclear dynamics [83]. At such a stationary point, non adiabatic effects on the vibrational spectra, for instance of the hydrogen molecule, are negligible. At saddle points of the BO potential energy, separability is conventionally agreed. The description of a chemical interconversion as a passage over this saddle point yields a computational device that help calculate the rate at which the model system moves away from the reactant valley entering the product valley. It is accepted that a passage through a given separating surface defines completion of that step. As early noted by Wigner, this is a classical mechanics picture [33]. Most, if not all, the computational quantum dynamical models are based, in one way or another, on potential energy hypersurfaces. Öhrn and coworkers [55] are among the first that have developed an electronuclear model avoiding the use of such hypersurfaces which, incidentally, shows that there is no exigency in using such a concept in describing quantum processes.

The usefulness of potential energy hypersurfaces in describing reaction dynamics and chemical reactivity is well illustrated by Levine and Bernstein [84] and Shaik *et al.* [85] books. See also the fundamental paper of Hase [86]. This success does not assure that the coordinate representation of quantum system is necessarily truthful. It goes without saying, the coordinate representation is an extremely useful mathematical model. However, from recent inelastic neutron scattering experiments on hydrogen bonded system, the idea that the BO approximation may be inadequate has been advanced by Kearley and coworkers[87].

The pictures derived from the adiabatic approach are certainly pedagogically useful but they are not necessarily a faithful view of quantum reactive systems. Now, since the adiabatic transition state theory provides the bottom line to describe reaction rates, it is necessary to implement some caveats in order to get a quantum mechanical theory of chemical reactions.

2.5. STATIONARY HAMILTONIANS

The theoretical view advocated here focus attention on the quantum states relevant to the description of particular phenomena. The concept of stationary Hamiltonians follows from the coordinate representation and leads to a numerical determination of relevant quantum states. Hc will denote this class of Hamiltonians. Thus, given a system that can be decomposed into n-electrons and m-nuclei in different dispositions, the set of $H_C = \Sigma_a(1/m_a)[\mathbf{p}_a]^2 + V_{Coul}$ are written in terms of fluctuation coordinates around particular

nuclear configurations: they may define a system having bound states (molecules, atoms and ions) with excited states having finite lifetimes, or they can display quantum states all having finite lifetimes. These latter are, on the BO hypersurface, saddle points of any index. It is now appropriate to label the stationary Hamiltonians as $H_C(i)$ where each label relates to a given catchment region in the sense defined by Mezey [88, 89]. Each one of them would be associated with a Schrodinger equation: $H_C(i)\ \Psi_{iv} = \varepsilon_{iv}\ \Psi_{iv}$.

Hc built in the coodinate representation is always an approximate model of the full Hamiltonian of the system. The exact Hamiltonian can be constructed if one knows the complete spectra, eqs.(53) or (68) illustrate the form of such Hamiltonians. In what follows we will refer to this type of Hamiltonian as Ho, that is, the exact molecular Hamiltonian for the system embedded in a radiation field. While the spectra of the full Hamiltonian Ho contains the spectra of the molecular Hamiltonians $\{H_C(i)]$, there is no reason to believe that the set formed by all these eigenfunctions may be complete with respect to the eigenfunctions of the global Hamiltonian, Ho. The very existence of entangled states [90, 91] will put a limitation to completeness. We observe that the general symmetries (invariances) of the total Hamitonian H can be spontaneously broken when the system is trapped in one of the states belonging to a molecular Hamiltonian Hc. Such is one of the origins of L and D isomers.

From the present stand point, the physical processes are described as quantum transitions among stationary states obtained from the adequate H_o. The coupling with the electromagnetic transversal field is the necessary cause producing changes among the states. Thus, seen from the viewpoint of the global system, the molecular system is not made of stationary states.

3. Solvent Effects

3.1. THE CHEMICAL PICTURE

In the chemical picture, the system is formed by molecules, atoms and/or ions. Each one of them has well defined properties. For such systems, a separability hypothesis is introduced in the physical picture. The different steps leading to effective equations for the subsystems have already been discussed by several authors. Here, we outline the important points; for detailed discussions we refer the reader to our original papers [1-3, 6].

3.1 .l. *Energy and Effective Schrödinger Equations for Separable Subsystems*

The total Coulomb Hamiltonian can always be written as a sum of terms describing arbitrary subsystems:

$$H(\mathbf{r}_s,\mathbf{r}_m, \mathbf{R}_s,\mathbf{R}_m) = H_s(\mathbf{r}_s,\mathbf{R}_s)+ H_m(\mathbf{r}_m,\mathbf{R}_m) + V_{sm} \tag{11}$$

with $\mathbf{X}=(\mathbf{R}_s,\mathbf{R}_m)$ representing the nuclear coordinates of the subsystems. The solute is designated by the subindex s; the surrounding medium or solvent is indicated with the

subindex m.

The interaction operator $V_{sm}= V(\mathbf{r}_s,\mathbf{r}_m,\mathbf{R}_s,\mathbf{R}_m)$is defined in terms of the Coulomb interaction operator $1/|\mathbf{r}-\mathbf{r}'| = T(\mathbf{r}-\mathbf{r}')$ and the charge density operators of the solute $W_s(\mathbf{r})$ and the surrounding medium $\Omega_m(\mathbf{r}')$:

$$V(\mathbf{r}_s,\mathbf{r}_m, \mathbf{R}_s,\mathbf{R}_m) = \int d\mathbf{r} \int d\mathbf{r}' \; \Omega_s(\mathbf{r}) T(\mathbf{r}-\mathbf{r}') \Omega_m(\mathbf{r}')$$

where

$$\Omega_s(\mathbf{r}) = -\sum_i \delta(\mathbf{r}-\mathbf{r}_i)+\sum_{si} Z_{si} \delta(\mathbf{r}-\mathbf{R}_{si})$$

with a similar expression for the solvent charge density operator $\Omega_m(\mathbf{r})$.

In the chemical approach it is assumed that the wave functions for the solute, $\Psi_s(\mathbf{r}_s;\mathbf{R}_s,\mathbf{R}_m)$, and surrounding medium, $\Psi_m(\mathbf{r}_m;\mathbf{R}_m,\mathbf{R}_s)$, are known at a given instant t and with a given nuclear configuration $\mathbf{X}(t)$, and that an approximation to the total wave function can be written down as an antisymmetrized product:

$$\Psi(\mathbf{r}_s,\mathbf{r}_m;\mathbf{X}) = A_{sm} \{\Psi_s(\mathbf{r}_s;\mathbf{R}_s,\mathbf{R}_m) \Psi_m(\mathbf{r}_m;\mathbf{R}_m,\mathbf{R}_s)\} \tag{14}$$

A_{sm} is an antisymmetrizer operator between electrons from these two groups s and m which is usually expressed as a sum of the identity operator (1) and normalized permuting operator P_{ms}: $A_{sm} =1+P_{ms}$. The total Hamiltonian is symmetric to any electron permutation. The interaction energy V_{sm} can be cast in terms of a direct Coulomb interaction and an exchange Coulomb interaction:

$$\begin{aligned} V_{sm}= & \int d\mathbf{r} \int d\mathbf{r}' \; <\Psi_s |\Omega_s(\mathbf{r})|\Psi_s> T(\mathbf{r}-\mathbf{r}')<\Psi_m |\Omega_m(\mathbf{r}')|\Psi_m> + \\ & \int d\mathbf{r} \int d\mathbf{r}' \; <\Psi_s \Psi_m |\Omega_s(\mathbf{r}) T(\mathbf{r}-\mathbf{r}')\Omega_m(\mathbf{r}')|P_{ms} \Psi_s \Psi_m> \end{aligned} \tag{15}$$

The ansatz used above for the wave function does not contain intergroup electron correlation and charge transfer effects among both subsystems. The former are second order effects that may or may not be included after solving for the effective subsystem, while the latter are of first order in perturbation theory language thereby deserving a special treatment if they are present. If inter group electron correlation is included, van der Waals forces result [7, 92]. In the construction of effective Schrödinger equations both are neglected [6], but they can be taken into account, for instance, with the use of a supermolecule scheme to allow for charge transfer effects if selected solvent molecules are included in the subsystem of interest. Charge transfer can be treated as a post local field effect.

3.1.1.1. *Effective Hamiltonian.* In this framework it is possible to define an effective

Hamiltonian H_S by neglecting the exchange interactions and intergroup electron correlations and by taking the quantum average over $\Psi_m(\mathbf{r}_m;\mathbf{R}_m,\mathbf{R}_S)$ of the total Hamiltonian H and neglecting the self energy of the surrounding medium:

$$H_S(\mathbf{r}_S;\mathbf{X}) = H_S(\mathbf{r}_S,\mathbf{R}_S) + \int d\mathbf{r} \int d\mathbf{r}' \; \Omega_S(\mathbf{r}) \, T(\mathbf{r}-\mathbf{r}') \langle \Psi_m | \Omega_m(\mathbf{r}') | \Psi_m \rangle \tag{16}$$

The interaction between both subsystems is cast into a form where the physical charge density of the surrounding medium $\Gamma_m(\mathbf{r}';\mathbf{X}) = \langle \Psi_m | \Omega_m(\mathbf{r}') | \Psi_m \rangle$ appears explicitly, and the interaction Hamiltonian describes now the coupling of the solute charge density operator with the electrostatic potential created by the surroundings at fixed X: $V_m(\mathbf{r};\mathbf{X}) = \int d\mathbf{r}' \langle \Psi_m | T(\mathbf{r}-\mathbf{r}') \; \Omega_m(\mathbf{r}') | \Psi_m \rangle = \int d\mathbf{r}' \; T(\mathbf{r}-\mathbf{r}') \Gamma_m(\mathbf{r}';\mathbf{X})$. The poitential $V_m(\mathbf{r};\mathbf{X})$ fulfils the classical electrostatic Poisson's equation [6]. For each nuclear configuration, the solute wave function Ψ_S and the effective energy $E_S(\mathbf{X})$ are obtained as a solution of the effective Schrödinger equation:

$$H_S(\mathbf{r}_S;\mathbf{X}) \, | \, \Psi_S \rangle = \varepsilon_S(\mathbf{X}) \, | \, \Psi_S \rangle \tag{17}$$

The surrounding medium system (the m-system) can also formally be represented with an effective Schrödinger equation having the same form as Eq.(17).

The Hamiltonian of eq.(17) contains the in vacuum Hamiltonian $\mathbf{H}_S(\mathbf{r}_S,\mathbf{R}_S)$. The stationary Hamiltonians of the in vacuum system usually go over the effective (solvated) system. We have calculated a number of cases related to saddle points of index one [93-98] as well as sadle points where the model system is increased in size, the invariance of the stationary point has been numerically established either with respect to models and in some other occassions with respect to the level of computing [99]. As the index of the saddle point can be obtained via the calculation of the Hessian in the BO scheme, if the solvent-solute off-diagonal matrix elements do not spoil the negative eigenvalue defined by the active subspace [100-102] one would expect a geometric and transition vector invariance when the in vacuum system is embedded in a pasive solvent. An analysis of the minimal subspace defining a SPi-1 has been given in references [101-103]. Note that the spectra of the composed system may be richer than the isolated species: solvent to solute and solute to solvent charge transfer states may appear in the spsctra. The more apparent effect of solvent in the spectra of stable solutes is the broadening of the spectra (band instead of line spectra) as well as changes in the transition moments.

3.1.1.2. *Electrostatic energy.* The calculation of the total electrostatic energy, starting from the effective energies, requires some qualification. It is not a simple sum of effective energies $\varepsilon_S(\mathbf{X})$ and $\varepsilon_m(\mathbf{X})$, for the simple reason that the interaction energy is counted twice. Thus, for each subsystem a "polarization work" has to be withdrawn in

order to get the correct final Coulomb energy. The Coulomb energy for each subsystem is given by:

$$Gc_s = \varepsilon_s(\mathbf{X}) - (1/2)\int d\mathbf{r}\int d\mathbf{r}' \langle \Psi_s |\Omega_s(\mathbf{r})|\Psi_s\rangle T(\mathbf{r}-\mathbf{r}')\langle\Psi_m |\Omega_m(\mathbf{r}')|\Psi_m\rangle \quad (18)$$

with a similar expression for the m-system:

$$Gc_m = \varepsilon_m(\mathbf{X}) - (1/2)\int d\mathbf{r}\int d\mathbf{r}' \langle \Psi_m |\Omega_m(\mathbf{r})|\Psi_m\rangle T(\mathbf{r}-\mathbf{r}')\langle\Psi_s |\Omega_s(\mathbf{r}')|\Psi_s\rangle \quad (19)$$

The interesting point with these definitions is that the total Coulomb energy is correctly obtained as the sum of two independent terms:

$$E_{s+m}(X) = Gc_s(X) + Gc_m(X) \quad (20)$$

These two quasi independent systems are, however, coupled via the quantum mechanical exchange effects. In fact, the expectation value of the total Hamiltonian with respect to the selfconsistent solution of the solute and solvent is given by:

$$Ecx_{ms}(\mathbf{X}) = \langle \Psi_s(\mathbf{r}_s;\mathbf{R}_s,\mathbf{R}_m)\Psi_m(\mathbf{r}_m;\mathbf{R}_m,\mathbf{R}_s)| H |A_{sm}\, \Psi_s(\mathbf{r}_s;\mathbf{R}_s,\mathbf{R}_m)\, \Psi_m(\mathbf{r}_m;\mathbf{R}_m,\mathbf{R}_s)\rangle \quad (21)$$

where one takes advantage of the fact that the total Hamiltonian commutes with the antisymmetrizer operator A_{sm}. Now, introducing the effective group Coulomb energies, the total energy can be written as:

$$Ecx_{ms}(\mathbf{X}) = Gc_m(\mathbf{X}) + Gc_s(\mathbf{X}) + \int d\mathbf{r}\int d\mathbf{r}' \langle \Psi_s\, \Psi_m |\Omega_s(\mathbf{r})T(\mathbf{r}-\mathbf{r}')\Omega_m(\mathbf{r}')|P_{ms}\, \Psi_s\, \Psi_m\rangle \quad (22)$$

The first two terms describe each subsystem dressed with the interaction of each other. It is now apparent that exchange forces between the two subsystems have to be included in order to get the total force acting on the nuclei. This latter force is usually mimicked with a repulsive short range potential. A pseudo potential method can also be used in a microscopic approach to the surrounding medium effects [104,105].

Now, one can proceed to define a functional form for each (coupled) subsystem, by dividing the exchange contribution among them, so that one obtains an effective energy functional for the subsystem of interest:

$$G_S = Gc_s(\mathbf{X}) + 1/2\int d\mathbf{r}\int d\mathbf{r}' \langle \Psi_s\, \Psi_m |\Omega_s(\mathbf{r})T(\mathbf{r}-\mathbf{r}')\Omega_m(\mathbf{r}')|P_{ms}\, \Psi_s\, \Psi_m\rangle \quad (23)$$

with a similar expression for the solvent functional.

The last term in eq(23) in the ground electronic state contributes with repulsive effects that results from the Pauli exclusion principle. It is common practice to include them in many approximate treatments via a $1/R^{12}$ repulsive term in the potential energy

function describing atom-atom interactions. In this case, there is no direct wave function modulation due to this exchange term. Formally, if the exchange effects can be mimicked, for instance, with a repulsive pseudopotential, the functional Gs depends upon the solute and the solvent wave functions as well as the global nuclear configuration.

It is worth noticing that a statistical mecjhanical averaging of eq.(23) would lead to a free energy formulation. This problem has been thoroughly discussed in refs.[1,3].

3.1.2. *Self consistent reaction field theory.* The objective of the generalized selfconsistent reaction field theories is to replace the solvent wave function dependency with a particular model of charge density representing it in the presence of the solute. The polarization charge density $\Gamma'(\mathbf{r}) = \nabla_r \cdot \mathbf{p}(\mathbf{r})$ is given by the divergence of the polarization vector $\mathbf{p}(\mathbf{r})$ so that in atomic units the total charge density of the solvent is given by:

$$\Gamma_m(\mathbf{r}) = \Gamma_m^{\circ}(\mathbf{r}) - \nabla_r \cdot \mathbf{p}(\mathbf{r}) \tag{24}$$

where $\nabla_{\mathbf{r}}$ is the gradient operator at $\mathbf{r}$. Note that the polarization density $\mathbf{p}$ at the boundaries and outside the macroscopic volume occupied by the solvent is zero. A great number of computational procedures only retain the first term in Eq.(24), namely $\Gamma_m^{o}(\mathbf{r})$ describing a surrounding medium charge density without polarization. The polarization density is set up by the solute electric field on the polarizable solvent or surrounding medium. This term may be extremely important when describing spatial charge separation processes such as hydride transfer and proton transfer reactions [2,73] or stabilization of carbonium ions in biological systems [14].

The polarization density is a functional of the solute charge density $\Gamma_S(\mathbf{r}) = \langle \Psi_S | \Omega_S(\mathbf{r}) | \Psi_S \rangle$. The effective Hamiltonian Eq.(16) acquires a non-linear structure via the polarization density term, i.e. the effective Hamiltonian a functional dependence of the wave function:

$$H_S = H_S + \int d\mathbf{r}\ \Omega_S(\mathbf{r}) \left(V_m^{\circ}(\mathbf{r}) + \int d\mathbf{r}'\ \nabla_{\mathbf{r}} T(\mathbf{r}-\mathbf{r}') \cdot \mathbf{p}(\mathbf{r}') \right) \tag{25}$$

where $\nabla_{\mathbf{r}} T(\mathbf{r}-\mathbf{r}')$ is a unit electric field at r' produced by a unit charge at $\mathbf{r}$.

The reaction field potential corresponds to the last term in Eq.(25) and will be designated by $\prod(\mathbf{r})$ in what follows. $V_m^{o}(\mathbf{r})$ is the electrostatic potential acting on the quantum system that is generated by the surrounding medium charge density, $\Gamma_m^{o}(\mathbf{r})$. For a recent overview on classical electrostatics in biology and chemistry see the paper written by Honig and Nicholls [106]. Note that the solute can be taken as a classical external electrostatic source to the surrounding medium. For this approximation to be accurate, the solute wave function must be fairly well localized in the volume assigned to the solute system; overlap with the surrounding medium must be minimal.

A Rayleigh-Schrödinger-type perturbation theory has recently been developed by Angyan [107]. The consideration of external perturbations, like electric fields, permits the calculation of response functions for solvated species.

3.2. PRACTICAL *AB INITIO* QUANTUM CHEMICAL APPROACHES

Note that the effective Schrodinger equation (17) is the Euler-Lagrange equation obtained from the variational principle applied to the functional Gc_s. The surrounding medium effect, in the present approximation, is a functional of the solute density. The operator appearing in Eq.(16) shows such a dependence in a clear manner. It is then a one-electron-type operator according to the definition given in Eq.(13). This property is important since, in the practical *ab initio* quantum chemical approach at post Hartree - Fock level of theory, the so called double and higher excitations do not couple to the ground state via this operator [108]. All the effects are included at the HF level via orbital polarization effects.

3.2.1. *Hartree-Fock level*

Let us consider the HF level of theory. The functional corresponding to Eq.(18) in conjunction with Eq.(16) or (25) and a one determinant wave function Ψ used for the solute can now be written as:

$$Gcs[\Psi] = \langle \Psi | \left(H_S(\mathbf{r}_S,\mathbf{R}_S) + (1/2)\int d\mathbf{r} \int d\mathbf{r}' \, \Omega_S(\mathbf{r}) T(\mathbf{r}-\mathbf{r}') \{ 2V_m^{\circ}(\mathbf{r}') + \int d\mathbf{r}' \, \nabla_r T(\mathbf{r}-\mathbf{r}') \cdot \mathbf{p}(\mathbf{r}';[\Gamma(\Psi)]) \} \right) | \Psi \rangle \tag{26}$$

where $\Gamma(\Psi)$ is the electronic density calculated with the one determinant wave function Ψ. $V_m^{\circ}(\mathbf{r}')$ is the external potential with which the solvent is represented; the factor 2 in front of it is due to the common practice consisting of carrying out the calculation of the solute system only. The first term, once the variational procedure is applied, leads to the standard Hartree-Fock equations for the orbitals used to construct the determinant for the system in vacuum. The orbitals are perturbed both by the potential $V_m^{\circ}(\mathbf{r}')$, which can be calculated if the solvent structure is known or a model is built to represent it, and by the reaction field potential which depends upon the density. Thus, the reaction field incorporates a second source of non-linearity in the orbital's HF equation besides the exchange term produced by the bi-electronic operator appearing in $H_S(\mathbf{r}_S,\mathbf{R}_S)$. For a closed shell system, for instance, one gets for the space orbitals $\phi_j(\mathbf{r})$ the Hartree-Fock one-electron equation:

$$\{-(1/2)\nabla^2 + V(\mathbf{r}) + \Sigma_i (2J_i(\mathbf{r}) - K_i(\mathbf{r})) + V_m^{\circ}(\mathbf{r}) + \Pi(\mathbf{r})\} \phi_j(\mathbf{r}) = \varepsilon_j \phi_j(\mathbf{r}) \tag{27}$$

where the first term is the one electron kinetic energy operator in atomic units, $\mathbf{V}(\mathbf{r})$ is

the electron-nuclei interaction operator for the solute system, $J_i(\mathbf{r})$ is the Coulomb operator created by the i-th orbital density at the configurational point $\mathbf{r}$, and $K_i(\mathbf{r})$ is the exchange operator that takes into account the fermion nature of the electron states; the sum is carried out from 1 to N/2. For a system of N electrons, the density $\Gamma(\Psi)$ is given by:

$$\Gamma(\Psi) = \langle\Psi|\Omega_S|\Psi\rangle = 2\,\Sigma_j\ \phi_j^*(\mathbf{r})\phi_j(\mathbf{r}) \tag{28}$$

and the sum is carried out over the HF manifold (occupied orbitals). In Eq.(27), it is the reaction field potential $\prod(\mathbf{r})$ which depends upon this density.

Computational studies with different solvent-solute coupling models continuously appear in the literature [13, 61, 109]. Solvent effects on molecular geometries and isomerization processes have been reported by Rivail and coworkers [110] as well as studies on the geometrical structures of hexahydrate metallic cations [111]. Jansen and coworkers have recently reported a mixed quantum-classical computer study on the water molecule in the liquid phase designed to examine the influence of a polarizable environment on its electronic properties [61]. This is the more advanced computer simulation carried out so far in the spirit of the selfconsistent reaction field theory. Solvent effects on the Menshutkin reaction have been studied by Karelson and coworkers [112] as well as the effects of solvation on chromophores, where a SCRF-SCF calculation was followed by configuration interaction to generate excited states in the presence of a dielectric continuum [113];the method was later extended to a multicavity reaction field and applied to study the effect of solvent on flexible molecular systems. The method presented by these authors is based on a gauge-independent partitioning of the molecule total reaction field in the polarizable medium into partial reaction fields which belong to the rotationally or inversionally groups in the molecule [114].

From the *ab initio* quantum chemistry coupled with a molecular dynamics treatment of the surrounding media, Zhao and Cuckier have reported a study of a proton coupled electron transfer reaction [115].

3.2.2. *Density functional approach*

The density functional model states that the total energy of a many-electron system can be cast as a functional $E[\Gamma]$ of the total electronic density $\Gamma(r)$ where the energy is a minimum for the ground-state density. Thus, minimizing the energy functional, subjected to charge normalization, would lead to the ground-state and energy of the system [116]. The method has been discussed in this book by R.Contreras. Here, we will make some comments in order to link the preceding treatment of solvent effects with the density functional model.

A simple way to connect Eq.(27) with a density functional approach is to make the exchange term a functional of $\Gamma(\Psi)$. Thus, integrating Eq.(27) and summing the orbital energies, it is not difficult to see that the energy appears as a functional of a density Γ such that the integral over the whole space available is equal to 2N. The solvent is in

some cases represented as a bare external potential $V_m°(\mathbf{r})$; in some other approaches, a reaction field potential $\prod(\mathbf{r})$ is added, which is, by its very nature, a functional of the electron density $\Gamma(\Psi)$. Thus, the solute-solvent coupling term can always be considered a functional of the density plus an external potential.

In the HF equation, the Coulomb term $\Sigma_i 2J_i(\mathbf{r})$ can be written with the help of eqs.(13) and (28) as:

$$<\Psi|\int d\mathbf{r}'\Omega_S/|\mathbf{r}-\mathbf{r}'||\Psi> = \int d\mathbf{r}'\Gamma(\mathbf{r}')/|\mathbf{r}-\mathbf{r}'| = \Sigma_i\ 2J_i(\mathbf{r}) \tag{29}$$

Thus, rewriting the exchange term $-\Sigma_i K_i(\mathbf{r})$ as a functional $G(\Gamma(\mathbf{r}'))$ of the density:

$$-\Sigma_i\ K_i(\mathbf{r})\ \text{->}\ V_{exch}(\mathbf{r}) = \int d\mathbf{r}\ G(\Gamma(\mathbf{r}'))/|\mathbf{r}-\mathbf{r}'| \tag{30}$$

one gets for an orbital equation the form:

$$\{-(1/2)\nabla^2+V(\mathbf{r})+\int d\mathbf{r}'\Gamma(\mathbf{r}')/|\mathbf{r}-\mathbf{r}'|+V_{exch}(\mathbf{r})+V_m°(\mathbf{r})+\Pi(\mathbf{r})\}\phi_j(\mathbf{r}) = \varepsilon_j\phi_j(\mathbf{r}) \tag{31}$$

where Eq.(31) is to be used to calculate all the density dependent terms. A more complete analysis should start from the functional form given by Eq.(22). Applying the process as a supermolecule to this functional one ends up with equations equivalent to the frozen density functional. If you want to use functional (23), then the exchange term must be approximated by a functional of the solvent density. The orbital equations (29) are now modified by adding to the existing exchange potential another term related to the solvent coupling. This latter approach corresponds, although it is not equivalent, to the frozen density functional developed by Warshel and coworkers [105].

The scheme analyzed so far is, in a way, a simplification of the Hartree-Fock scheme. As such, it is only a model approximation. The most serious drawback is the replacement of a fundamentally quantum mechanical term, whose very nature is to be non local, by a local approximation. Of course, when the system is in an electronic degenerate state, or when the BO approximation is no longer valid, the density functional method cannot be applied. For a discussion of this and other limitations the reader is referred to the paper by Bersuker [117].

The density functional (DF) method has been successful and quite useful in correlating experimental results when model densities are used in the calculations. In fact, the equations characteristic of the DF method can be derived from a variational approach as Kohn and Sham showed some time ago. In this approach, when model densities are introduced, it is not always possible to relate such densities to corresponding wave functions: this is the N-representability problem. Fortunately, for any normalized well behaved density there exists a Slater single determinant; this type of density is then N-representable. The problem of approximately N-representable density functional density matrices has been recently discussed by Soirat *et al.* [118]. In spite

of some theoretical limitations, the numerical procedures therefrom derived have been extremely useful. A couple of striking examples have recently been reported by Parrinello and coworkers [62,119]. For the protein superoxide dismutase, they present a theoretical description of the interactions between the copper(II) ion in the active site and the substrate of superoxide dismutase, using *ab initio* density functional theory calculations and model energy functional calculations. In the same spirit, an ab initio molecular dynamics method was used to study the solvation and dynamics of an excess proton and a proton hole in liquid water [120, 121]. The results obtained are extremely useful to understand proton transfer in solution. As pointed out by these authors, it would be the dynamic fluctuation between specific solvation complexes around the hydronium ion which result in a proton transfer, and the rate-limiting step for the migration of the excess proton appears to be the concerted dynamics of the second solvation shell hydrogen bonded to the ligand water molecules [120]. This is quite in agreement with the tenets of the structural diffusion model where it is the solvation structure that migrates rather than the particles themselves.

Notwithstanding the beatiful results obtained with the DF method, this one appears to be much less successful in calculating transition states and barriers for hydrogen exchange and abstraction reactions [122]. Parrinello and coworkers have voiced concerns about the accuracy of DF theory with respect to chemical reactions in solution [121].

The quantum/classical procedures recover the nuclear fluctuation properties of the surrounding medium via the Monte Carlo statistical approach or by using molecular dynamics simulations. In the following section we examine the problem of energy exchange between solute and solvent from a quantum dynamical viewpoint.

3.3. SOLUTE-SOLVENT NUCLEAR FLUCTUATION COUPLING

Once the quantum states for the effective solute have been determined with the self consistent reaction field equations, the next step to close the description of the complete system is to set up the equations driving the nuclear configuration dynamics. These equations are the translation of Eq.(4).

Computational procedures following a classical mechanical picture, as it was outlined in section 2.3, can be and have been implemented by a number of people. The quantum/classical schemes belong to this family [6,123]. At a semi empirical level of electronic theory, Warshel and coworkers' approach is the most complete from the statistical mechanical viewpoint. For early references and recent developments see ref.[31, 124]. Simplified schemes have been used to study chemical events in enzymes and solution [16, 60, 109, 125, 126].

The treatment of the solute-solvent system with the classical Generalized Langevin equation formalism [127], with especial attention to the present problem, has been examined by us [6]; a wealth of information can be found in references [128-131].

3.3.1 *Quantum Fluctuation Scheme*

The nuclear motion (fluctuations) have to be treated now even if at first sight such a task may appear hopeless. A relatively simple scheme can be worked out which describes some aspects of the dynamical coupling between solute and solvent subsystems. This is based on the idea of transient solvent structures around which the set of nuclei can be fluctuating. This idea, earlier suggested by Yomosa was extensively used by us in connection with the theory of solvent effects [3] where statistical mechanical aspects were analyzed. See also a recent review by Straat [132]. Here, we extend the study to the dynamical aspects introducing a second quantization approach. This formalism is useful to describe quantized energy exchange processes.

Let us consider the ground electronic state and transient structures represented by $\mathbf{R}s^{(n)}$ and $\mathbf{R}m^{(n)}$; this assumption means that the electro-nuclear system can be found fluctuating around such average global configurations with finite lifetimes. If we adopt as total energy Ei(**X**) the sum of terms expressed in Eq.(23) for the solute with a similar expression for the surrounding medium, the nuclear Hamiltonian (including the kinetic energy operator, $HN=\Sigma_a(1/2m_a)[pa]^2$) can be written as a sum of terms belonging to each separate subsystem:

$$(HNs + HNm + Gs(\mathbf{X}) + Gm(\mathbf{X}))\ \xi_{ik}(\mathbf{X}) = E_{ik}\ \xi_{ik}(\mathbf{X}) \tag{32}$$

Observe that separability is only formal as the potential energy terms, Gs(**X**)+Gm(**X**), depend upon the configuration of all nuclei in the sample (we have neglected exchange terms for the time being). To simplify notations, quantum index i in the potential energy terms is avoided. Unless otherwise stated, we assume that everything is occurring at the electronic ground state both of the solute and solvent. The analysis of this equation can be made by first expanding the energies around transient structure **R**s(n) and **R**m(n). Note that the time scale of the motions associated with these transient structures is significantly slower than the nuclear vibrations δ**R**s and δ**R**m around the molecular equilibrium configurations. In many situations, $\mathbf{R}s^{(n)}$ can be a stationary geometry obtained from a quantum chemical calculation. For the surrounding medium, $\mathbf{R}m^{(n)}$ may be one of the thermally accessible global geometric configurations for the set of rigid molecular solvent molecules (it can be a zeolite or a protein model). If the surrounding medium is provided by a protein, then the X-ray structure may be a good representative of **R**m(n). Thus, expanding Gs(**X**)=Gs(**R**s,**R**m) in a formal Taylor series of two vector variables, one gets an expression in terms of fluctuations for the solute:

$$\begin{aligned} Gs(\mathbf{X}) = {} & Gs(\mathbf{X}^{(n)}) + (\partial\, Gs(\mathbf{X})/\partial \mathbf{R}s)^{(n)} \cdot \delta\mathbf{R}s + (\partial\, Gs(\mathbf{X})/\partial \mathbf{R}m)^{(n)} \cdot \delta\mathbf{R}m + \\ & (1/2)(\partial^2\, Gs(\mathbf{X})/\partial \mathbf{R}s^2)^{(n)} : \delta\mathbf{R}s\ \delta\mathbf{R}s + (\partial^2\, Gs(\mathbf{X})/\partial \mathbf{R}s \partial \mathbf{R}m)^{(n)} : \delta\mathbf{R}s\ \delta\mathbf{R}m + \ldots \end{aligned} \tag{33}$$

with : indicating a tensor product between the dyad δ**R**s δ**R**s and the matrix of second derivatives. A similar equation holds for the solvent or surrounding medium,

$$G_m(\mathbf{X}) = G_m(X^{(n)}) + (\partial\, G_m(\mathbf{X})/\partial \mathbf{R}_m)^{(n)}\cdot \delta\mathbf{R}_m + (\partial\, G_m(\mathbf{X})/\partial \mathbf{R}_s)^{(n)}\cdot \delta\mathbf{R}_s + (1/2)(\partial^2 G_m(\mathbf{X})/\partial \mathbf{R}_m^2)^{(n)}\colon \delta\mathbf{R}_m\, \delta\mathbf{R}_m + (\partial^2 G_m(\mathbf{X})/\partial \mathbf{R}_s \partial \mathbf{R}_m)^{(n)}\colon \delta\mathbf{R}_s\, \delta\mathbf{R}_m + \ldots \quad (34)$$

The partial solution of Eq.(27) for the configurational space can be conceived as a stepwise process. The fluctuations around the transient configuration $\mathbf{X}(n) = (\mathbf{R}s(n), \mathbf{R}m\,(n))$ contain—pell-mell— vibrations driven by the intramolecular force field, librations and cage vibration modes of molecules as a whole. The transient configuration evolving in a different time scale contains diffusion terms for liquid environments.

In order to introduce some simplification we first look at solvent fluctuations. The linear term $(\partial G_m(\mathbf{X})/\partial \mathbf{R}_m)(n))\ \delta\mathbf{R}_m$ can be neglected. This would mean that the solvent molecules are at their (transient) equilibrium conformation in the solvent, while the cross linear term $(\partial G_m(\mathbf{X})/\partial \mathbf{R}_S)^{(n)}$, $d\mathbf{R}_S$ survives. The objective now is to construct a simple model for the vibration of the solvent molecules. This is done in the harmonic approximation. To construct such a simple model system, consider the quadratic term of the nuclear Hamiltonian, i.e. $(1/2)(\partial^2\, G_m(\mathbf{X})/\partial \mathbf{R}_m^2)^{(n)}\colon \delta\mathbf{R}m\ \delta\mathbf{R}m$ and the kinetic energy term, H_{Nm} of Eq.(32). Let us assume that the normal mode problem is solved so as to get a simple harmonic Hamiltonian. Using $\mathbf{x}_i$ to represent the fluctuation variable of the i-th mode (that for atomic solvents can be thought of as fluctuations of a solvent atom at its cage position) and $\mathbf{p}_i$ the canonically conjugated moment, one may write a model Hamiltonian operator for the solvent as:

$$H_m(n) = \Sigma_k\, \{(1/2\ \mu_{mk})\mathbf{p}_k^{\,2} + 1/2\ \mu_{mk} w^{o\,2}_{mk}\ \mathbf{x}_k^{\,2}\ \} \quad (35)$$

where $w^{o\,2}_{mk}$ is the square of the characteristic oscillation frequency of the k-th mode (atom) of the medium system and μ_{mk} is the effective mass of the given mode.

For the solute a similar expression can be worked out (note that for complex molecules it can be computed with present software technology):

$$H_s(n) = \Sigma j\, \{(1/2\ m_{sj})\pi_j^{\,2} + 1/2\ \mu_{sj} w^{o\,2}_{sj}\ \mathbf{q}_j^{\,2}\ \} \quad (36)$$

Implicit in the treatment is the existence of unitary transformations allowing for the diagonalization of the isolated quadratic Hamiltonians.

Now, let us consider the bilinear terms: $(\partial^2 Gm(\mathbf{X})/\partial \mathbf{R}s\partial \mathbf{R}m)(n)\colon \delta\mathbf{R}s\ \delta\mathbf{R}m$ and $(\partial^2 Gs(\mathbf{X})/\partial \mathbf{R}s\partial \mathbf{R}m)(n)\colon \delta\mathbf{R}s\ \delta\mathbf{R}m$. They have to be transformed to the fluctuation frame. The former term contributes to couple solvent modes with the solute, the latter describes the coupling of the solute modes with the bath. For the time being, we will only retain the solute-solvent coupling. Applying (in principle) the unitary transformations allowing for partial diagonalization of the solvent and solute quadratic models to the bilinear term, the following form obtains:

$$H = \{H_m(n) + Hs(n) + \Sigma_k\, (\,\mathbf{l}(s;m))_k\, \mathbf{q}_k + \Sigma_j\, \mathbf{x}_j\, \mathbf{G}(m;s)_{jk}\ \mathbf{q}_k\,)\} \tag{37}$$

As is shown below for the solute, the linear term can be included in the quadratic term by redefining the fluctuation operator. **G**(m;s) is a rectangular matrix obtained from the second cross-derivatives coupling the solute to the solvent; **l**(s;m) is a vector obtained by similar procedures from the $(\partial Gm(\mathbf{X})/\partial \mathbf{R}s)(n)$ linear coupling. How to actually perfonn such operation is not directly important now. We assume that, in principle, such operations are feasible.

The model Hamiltonian (37) obtained from Eq.(32) contains solute oscillators linearly perturbed by its coupling with the solvent as well as bilinear terms that break down a total separability between solute and solvent:

$$\begin{aligned} H = \quad & \Sigma_j\, \{(1/2\ m_{sj})\mathbf{p}_j^2 + 1/2\ \ m_{sj}w_{sj}^{o\,2}\ \ \mathbf{q}'_j{}^2\ \} + \Sigma_j\, \mathbf{l}(m;s)_j\, \mathbf{q}'_j \\ & + \Sigma_k\, \{(1/2\ m_{mk})\mathbf{p}_k^2 + 1/2\ \ m_{mk}w_{mk}^{o\,2}\ \mathbf{x}'_k{}^2\ \} \\ & + \Sigma_j\, \Sigma k\ \mathbf{q}'_k \mathbf{G}(s;m)_{kj}\ \mathbf{x}'_j \end{aligned} \tag{38}$$

The linear effect of the solvent on the solute —Σj **l**(m;s)j **q**′j— can be represented as a shift of the j-th mode origin by $(\mathbf{l}(m;s)j)^2/\ m_{sj}w_{sj}^{o\,2}$. This operation trivially consists of completing the square for the **q**′-variables. Defining the new shifted coordinate as: **q**j = **q**′j+**l**(m;s)j/$m_{sj}w_{sj}^{o\,2}$, the term (1/2)$(\mathbf{l}(m;s)j^2/\ m_{sj}w_{sj}^{o\,2}$ is to be substracted from the total Hamiltonian and included in an effective solute Hamiltonian H_{seff}.

$$H_{seff} = \Sigma j\, \{(1/2\ \mu_{sj})\mathbf{p}_j^2 + 1/2\ \mu_{sj}w_{sj}^{o\,2}\ \ \mathbf{q}_j^2 - (1/2)(\mathbf{l}(m;s)j)^2/\ \mu_{sj}w_{sj}^{o\,2}\ \} \tag{39}$$

The solvent oscillators could have been normalized in a similar manner which explains why the linear term was not incorporated from the beginning. Note that the terms added do not affect the dynamics; they are constant quantities that might be different for the different transient configurations. The linear term introduced by the solute on to the solvent can be altogether neglected. The model fluctuation Hamiltonian can be written now as:

$$\begin{aligned} H = H_{seff} \ & + \Sigma_k\, \{(1/2\ \mu_{mk})\mathbf{p}_k^2 + 1/2\ \ \mu_{mk}w_{mk}^{o\,2}\ \mathbf{x}_k^2\ \} + \\ & \Sigma k \Sigma j\ \ \mathbf{q}_k\ \mathbf{G}(s;m)_{kj}\ \mathbf{x}_j \end{aligned} \tag{40}$$

to within a constant. Using now a second quantization approach for the oscillators, namely [47]:

$$\mathbf{a}_j\dagger = \sqrt{(\mu_{sj} w_{sj}^\circ/2\hbar)}\ (\ \mathbf{q}_j - i\ \pi_j/\mu_{sj}\, w_{sj}^\circ\ )$$
$$\mathbf{a}_j = \sqrt{(\mu_{sj} w_{sj}^\circ/2\hbar)}\ (\ \mathbf{q}_j + i\ \pi_j/\mu_{sj}\, w_{sj}^\circ\ ) \qquad (41a)$$

for the creation and anhilation operators and for the solvent:

$$\mathbf{b}_k\dagger = \sqrt{(\mu_{mk} w_{mk}^\circ/2\hbar)}\ (\ \mathbf{x}_k - i\ \mathbf{p}_k/\mu_{mk}\, w_{mk}^\circ\ )$$
$$\mathbf{b}_k = \sqrt{(\mu_{mk} w_{mk}^\circ/2\hbar)}\ (\ \mathbf{x}_k + i\ \mathbf{p}_k/\mu_{sj}\, w_{mk}^\circ\ ) \qquad (41b)$$

the Hamiltonian (40) including Eq.(39) reads now for a solute and solvent (including the zero point enegy in H and other constant terms):

$$H = \Sigma_j \hbar\,\omega_{sj}\, \mathbf{a}_j\dagger\mathbf{a}_j + \Sigma_k\, \hbar\,\omega_{mk}\, \mathbf{b}_k\dagger\mathbf{b}_k + \Sigma_j\Sigma_k\, (\mathbf{a}+\mathbf{a}\dagger)_j \mathbf{G}_{jk} (\mathbf{b}+\mathbf{b}\dagger)_k \qquad (42)$$

ω_s and ω_m are diagonal matrices containing the frequencies of each mode for the solvent and medium, respectively. The operator $\mathbf{b_k}\dagger$ ($\mathbf{b_k}$) creates (destroys) a bath excitation of k-type and energy $\hbar\omega_{mk}$. Similarly, $\mathbf{a}$j ($\mathbf{a}$j$\dagger$) destroys (creates) an excitation in the solute. As excitations corresponds to vibration-like systems, they are called phonons. Note that for each transient configuration $\mathbf{X}^{(n)}$ there would be a Hamiltonian of this type so that a statistical average must also be carried out over the solvent spectra (although if computationally this is not an easy task). In what follows, we assume that the sums include all oscillators corresponding to independent transient configurations whenever statistical averages are involved. The commutation relation for these operators are: $[\mathbf{a}j,\mathbf{a}j'\dagger]=\delta jj'$. For solvent operators similar rules hold, and solute and solvent operators commute among them.

The Hamiltonian given by Eq.(42) corresponds to a fully coupled oscillator model [133]. The total Hamiltonian is cast then as a sum of a solute Hamiltonian, Hs, surrounding media Hamiltonian, Hm, and the bilinear coupling operator, Hms. A crystal environment is a limit case that is implicit in the present approach. Adopting the Ianguage used there, one may distinguish acoustic and optical modes. Note that phonons are not coupled with electron motion at this stage. The effective electron wave function would act as a sort of “vacuum”. Electron excitations have finite lifetimes which depend upon the interactions with the surrounding medium. It is at this level where dynamical aspects would enter the description of solute-solvent modulation. In crystals the anharmonic perturbation terms determine thermal expansion phenomena as well as equilibrium thermal distribution of phonons[134]. These excitation modes are responsible for thermal conductivity properties. Properties analogous to these are found in other surrounding media. For an interesting application to the phenomenon of proton transfer in benzoic acid crystals, the reader is referred to the paper by Skinner and Trommsdorf [135].

In the above sense, the system may be considered as a thermodynamically closed system that will attain equilibrium if a non-equilibrium fluctuation were produced by some external means.

It is worth noticing that energy exchange between quantum states belonging to the

solute and solvent are ensured in this framework by the bilinear terms (and all other terms deriving from the Taylor expansion eqs.(33) and (34). In this representation, the excited molecules act as sourcs of the electromagnetic field. Thus, for a system having a given amount of energy at disposal, all quantum states that are energetically accessible will be populated. The time required to do it would depend upon particular kinetic aspects.

In order to proceed now to a statistical mechanical description of the corresponding relaxation process, it is convenient to solve the equation of motion for the creation and destruction operators and cast them in a form ressembling a Generalized Langevin equation. We will only sketch the procedure.

The problem now is to find out the time evolution of these operators. The equation of motion for these operators are [47, 136]:

$$d\mathbf{a}(t)/dt = [\mathbf{H},\mathbf{a}] \qquad \text{and} \qquad d\mathbf{b}(t)/dt = [\mathbf{H},\mathbf{b}] \tag{43}$$

The components can be formally solved. For the present case one gets for the time evolution of the solute operators the equation:

$$d\mathbf{a}_j(t)/dt = i/\hbar\, [H,\mathbf{a}_j] = i/\hbar\, [Hs,\mathbf{a}_j] + i/\hbar\, [\, \Sigma_l(\mathbf{a}+\mathbf{a}\dagger)_l \mathbf{G}_{lk}(\mathbf{b}+\mathbf{b}\dagger)_k, \mathbf{a}_j] \tag{44}$$

The solute-solvent system is coupled via solvent operators $(\mathbf{b}+\mathbf{b}\dagger)_k$ so that the equation of motion for the solvent operator is to be solved first. Using the commutation relations one gets for the linear term components the equation :

$$\begin{aligned} \mathbf{b}_k\dagger(t)+\mathbf{b}_k(t) = \; & -\Sigma_j \{ \; (1/\hbar\omega_{mk})\{(\mathbf{a}(t)+\mathbf{a}\dagger(t))_j \, \mathbf{G}_{jk}\}+ \\ & [\mathbf{b}_k\dagger(0)+ (1/\hbar\omega_{mk})(\mathbf{a}(o)+\mathbf{a}\dagger(o))_j \, \mathbf{G}_{jk}] \exp+i\omega_{mk}\, t + \\ & [\, \mathbf{b}_k(0) + (1/\hbar\omega_{mk})(\mathbf{a}(o)+\mathbf{a}\dagger(o))_j \, \mathbf{G}_{jk}] \exp-i\omega_{mk}t \quad + \\ & (2/\hbar\omega_{mk})\int d\tau \cos(\omega_{mk}(t-\tau)) \{(d\,(\mathbf{a}(\tau)+\mathbf{a}\dagger(\tau))/d\tau)_j \, \mathbf{G}_{jk}) \; \} \end{aligned} \tag{45}$$

The matrix element $\mathbf{G}_{jk}$ (that can be taken as real) measures the coupling strength between the solute and the solvent modes. To get other formulations found in the literature, it is useful to introduce a real coupling parameter λ_j for each solute mode via the relationship: $\mathbf{G}_{jk} = -\lambda_j \, \mathbf{W}_{jk}$. With this convention one gets for the solute equations of motion:

$$\begin{aligned} & d\mathbf{a}_j(t)/dt = i/\hbar\, [H,\mathbf{a}_j] = i/\hbar\, [Hs,\mathbf{a}_j] - i\,(\lambda_j/\hbar)[\, \Sigma_k\Sigma_l\, (\mathbf{a}+\mathbf{a}\dagger)_l \mathbf{W}_{lk}(\mathbf{b}+\mathbf{b}\dagger)_k, \mathbf{a}_j] \quad = \\ & i/\hbar\, [H_{seff},\mathbf{a}_j] + i(\lambda_j/\hbar)\Sigma_k \, \{\mathbf{b}_k\dagger(0) - (\lambda_j/\hbar)(\mathbf{W}_{jk}/\omega_{mk})(\mathbf{a}(o)+\mathbf{a}\dagger(o))_j \, \} \exp+i\omega_{mk}t + \\ & \qquad i(\lambda_j/\hbar)\Sigma_k \, \{\mathbf{b}_k(0) - \lambda_j(\mathbf{W}_{jk}/\omega_{mk})(\mathbf{a}(o)+\mathbf{a}\dagger(o))_j\} \exp-i\omega_{mk}t + \\ & 2i(\lambda_j/\hbar)^2 \, \Sigma_k\Sigma_{j'}(\mathbf{W}_{jk}\mathbf{W}_{j'k})/\omega_{mk})\int d\tau \cos(\omega_{mk}(t-\tau)) \{(d\mathbf{a}(\tau)/d\tau + d\mathbf{a}\dagger(\tau)/d\tau))_{j'}\} \end{aligned} \tag{46}$$

where the effective solvent Hamiltonian appearing above is given by:

$$Hs_{eff} = Hs - \{ \sum_j \sum_l \lambda_j \lambda_l (\sum_k (W_{jk} W_{lk} / \hbar\omega_{mk}) \{ (\mathbf{a}(t)+\mathbf{a}^\dagger(t))_j (\mathbf{a}(t)+\mathbf{a}^\dagger(t))_l \}) \quad (47)$$

A more compact form can be given to Eq.(45) that would ressemble a Langevin equation and is obtained by introducing the kernel

$$K_{jj'}(t-\tau) = (1/\hbar) \sum_k ((W_{jk} W_{j'k}/\hbar^2 \omega_{mk}) \cos(\omega_k (t-\tau)) \quad (48)$$

and

$$F_j(t) = (1/\hbar)\{\sum_k \{ \mathbf{b}_k^\dagger(0) - (\lambda_j/\hbar)(W_{jk}/\omega_{mk})(\mathbf{a}(o)+\mathbf{a}^\dagger(o))_j \} \exp+i\omega_{mk} t + (1/\hbar)\{\sum_k \{ \mathbf{b}_k(0) - (\lambda_j/\hbar)(W_{jk}/\omega_{mk})(\mathbf{a}(o)+\mathbf{a}^\dagger(o))_j \} \exp-i\omega_{mk} t \}$$
$$= \sum_k (F_{jk}(t) + F_{jk}^\dagger(t)) = \sum_k f_{jk}(t)$$

Replacing in equation (45) one gets

$$d\mathbf{a}_j(t)/dt = i/\hbar [Hs_{eff}, \mathbf{a}_j] - i\lambda_j F_j(t) + i\hbar \int d\tau \sum_{j'} \lambda_j \lambda_{j'} (K_{jj'}(t-\tau)(d\mathbf{a}(\tau)/d\tau + d\mathbf{a}^\dagger(\tau)/d\tau))_{j'} \quad (50)$$

The set of equations (50) can be formally considered as generalized Langevin equations if the operator Fj(t) can be interpreted as a stochastic quantity in the statistical mechanical sense. If the memory function does not correlate different solute modes, namely, if $K_{jj'} = \delta_{jj'} K_j$, then a Langevin-type equation follows for each mode:

$$d\mathbf{a}_j(t)/dt = i/\hbar [Hs_{eff}, \mathbf{a}_j] - i\lambda_j F_j(t) + i\lambda_j^2 \hbar \int d\tau (K_j(t-\tau)(d\mathbf{a}(\tau)/d\tau + d\mathbf{a}^\dagger(\tau)/d\tau))_j \quad (51)$$

In absence of the operators Kj and Fj, the solute operator evolves under the action of the effective Hamiltonian Hs_{eff}. This is the type of equation analogous to the effective electronic functional Eq.(18).

The terms coupling to the bath in Eq.(51) allowing for energy exchange between both subsystems are given by the "friction" integral operator, while Fj would look like a random (possibly Gaussian) force. Note the similarity between this equation and equations (76 or 80) from our earlier paper [6], whilst the fundamental difference resides in the quantum nature of the exchange. See also our paper [4].

The next step is to introduce temperature by averaging out the bath operators appearing in the time dependent terms of Eq.(51) [137] over an adequate ensemble. To this end, the partial trace (or sum of the diagonal elements) over the surrounding subsystem has to be taken. For the system in interaction, the effective Hamiltonian of the solvent Hmeff must be defined in such a way that the sum of $Hs_{eff} + H_{meff}$ leads to the

starting (to within constant factors not affecting the dynamics). By defining scaled solvent operators in the following form:

$$\mathbf{B}_k\dagger = b_k\dagger - \Sigma_j' (\lambda_j' W_{j'k}^* / \hbar\omega_{mk})\{(\mathbf{a}(t)+\mathbf{a}\dagger(t))_{j'}\} \quad (52)$$

the effective solvent Hamiltonian is given now as:

$$H_{meff} = \Sigma_k \hbar\omega_{mk} \mathbf{B}k\dagger \mathbf{B}k \quad (53)$$

so that the adequate solvent statistical density matrix according to Lindenberg and coworkers [54,133] is given by:

$$\rho m = Q_m^{-1} \exp(-H_{meff}/kT) \quad (54)$$

where k is Boltzmann constant, T absolute temperature and Qm the partition function of the solvent medium: Qm = trace exp($-H_{meff}/kT$).

There are two mechanisms, at least, that couple the solute internal modes. One is represented by the last term in Eq.(50). For Eq.(51), since the cubic terms in the solute-solvent coupling terms were neglected in the Taylor expansion, the solute modes are uncoupled among themselves, and they are one by one coupled to the surrounding medium oscillators, so that such a mode coupling can be introduced by retaining cubic and quartic terms. Of course, one can assume that the exact vibration-rotation spectra of the solute has been previously determined and proceed the analysis with the "actual" quantum states. The couplings with the solvent are not changed in their essence.

3.3.2. Simple models

We have presented here the quasi harmonic approximation epitomized by Eq.(51) to show one way to represent the dynamics of nuclear motions in a quantum mechanical scheme. A general solution for these equations cannot be obtained. However, a number of particular cases exist for which solutions have been worked out in the literature.

For a solute single mode, Lindenberg and coworkers [54, 133] have presented a detailed analysis of the simplified resulting solution of Eq.(51). For two-level systems and a dimer in a heat bath, thorough analyses also exist [138].Model chemical reactions in condensed media using bilinear couplings have been discussed by Christov [139] using a two-level model to represent a reacting system, see also the interesting work by Pollak [70, 140]. The different forms of coupling operators used in this model are special cases of our general analysis. In fact, when the Taylor expansion is stopped at cubic terms, then solute solvent couplings of the form: Gijk(**a**+**a**†)i (**a**+**a**†)j (**b**+**b**†)k will appear in the solute-solvent couplings. Simplified forms have been used to model energy transfer in condensed media, exciton confined to a dimer and polaron formation in a deformable medium [44, 138, 141-143].

3.3.2.1. *Linear oscillator example.* The general equations can now be specialized to the case on one linear oscillator coupled to a thermal bath. We will closely follow the analysis given by Lindenberg and West so that the details and derivations can be consulted in that paper [133].

The total Hamiltonian of Eq.(42) contains one oscillator, j=1, with energy $E/\hbar = \omega_S$; the subindex j is dropped in all equations. The behavior of the quantum oscillator is characterized by: i) the natural frequency $E/\hbar = \omega_S$; ii) the coupling strength λE between the oscillator and the bath; iii) the memory time $\tau c = l/\gamma$ of the dissipation of oscillator energy by the heat bath; and iv) the bath's temperatute T. The equation of motion is given by Eq.(51) without subindex j.

The operators $F_k(t)$ defined in Eq.(49) are taken as fluctuations based on the idea that at t=0 the initial values of the bath operators are uncertain. Ensemble averages over initial conditions allow for a definite specification of statistical properties. The statistical average of the stochastic forces $F_k(t)$ is calculated over the solvent effective ensemble by taking the trace of the operator product $\rho_m F_k$ (this is equivalent to sum over the diagonal matrix elements of this product), so that $\langle F_k(t)\rangle = \mathrm{Trace}(\rho_m F_k)$ is identically zero (Fjk(t)=Fk(t) in this particular case). The non-zero correlation functions of the fluctuations are solvent statistical averages over products of operator forces,

$$\langle F_k^{\dagger}(t) F_{k'}(t')\rangle = n_k \exp(i\omega_{mk}(t-t'))\,\delta_{kk'}$$
$$\langle F_k(t) F_{k'}^{\dagger}(t')\rangle = (n_k+1)\exp(-i\omega_{mk}(t-t'))\,\delta_{kk'} \qquad (55)$$

with $n_k = 1/(\exp(\hbar\omega_{mk}/kT) - 1) = \mathrm{Tr}(\rho_m\, \mathbf{B}_k^{\dagger}\, B_k)$.

The kernel K(t-τ) is related to the dissipation process. The quantum fluctuation-dissipation relation yields

$$K(t-\tau) = \Sigma_k\ \lambda^2 \langle f_k(t) f_k(\tau) + f_k(\tau) f_k(t)\rangle\ (1/\hbar\omega_{mk})\ \tanh(\hbar\omega_{mk}/2kT) \qquad (56)$$

To get a classical limit, the symmetrized correlation function is represented by :

$$\Phi_k(t-\tau) = \lambda^2 \langle f_k(t) f_k(\tau) + f_k(\tau) f_k(t)\rangle \qquad (57)$$

By taking the limit $\hbar \to 0$ in Eq.(56) one gets the classical limit

$$K(t-\tau) = (1/2kT)\ \Sigma k\ \Phi\mathbf{k}(\mathbf{t}-\tau) = (1/2kT)\ \Phi(t-\tau) \qquad (58)$$

where the dissipation, represented by K and the fluctuations described by Φ are related via the classical fluctuation-dissipation theorem, whose mathematical expression is Eq.(58)[127].

To make the transition from the level of theory to experiment, the fluctuation-

dissipation relation is assumed to hold. For simple model systems, it was shown in [133] that the actual quantum relation has not the same form as the classical one. In the high-temperature limit the classical form obtains. This model can be derived from Eq.(51) by rewriting the sum over modes in Eq.(48) specialized to one solute mode as an integral over bath frequencies represented with a density of states D(ω). Note the correlation between this mode bands with the assumption made to derive the equations, namely, the existence of collective vibrations in the solvent. To go a step further, a particular model for the density of states can be introduced which amounts to take $D(\omega)\mathbf{W}^2(\omega)/\hbar^2\omega$ equal to the expression $(1/\pi)\ \gamma^2/(\gamma^2+\omega^2)$. Integrating from frequency zero up to infinite, one gets the empirical formula $K(t-\tau)= (\lambda/\hbar)\ \gamma\ \exp(-\gamma|t-\tau|)$. Here, $1/\gamma$ represents the memory time of the dissipation and is essentially the inverse of the phonon bandwidth of the heat bath excitations that can be coupled to the oscillator. It reduces to a delta function when y->infinite. The correlation function Φ(t-t), in this model is [133]

$$\Phi(t-t) = (\lambda\gamma^2/\pi) \int d\omega\ (\omega/(\gamma^2+\omega^2)(2\ n_\omega +1)\ \cos\omega(t-\tau) \tag{59}$$

using the same integration limits (0,∞) and $nw = 1/(\exp(\hbar\omega kT) -1)$.

Lindenberg and West conclude, after analysis of Eq.(59) at low temperatures where $kT<<\hbar\gamma$, that the correlation function decays on a time scale $\hbar / kT$ rather than $1/\gamma$. Thus, the bath can dissipate excitations whose energies lie in the range $(0,\hbar\gamma)$, while the spontaneous fluctuations occur only in the range (0,kT) if $kT<\hbar\gamma$. The correlation time of the fluctuations is therefore the longer of $\hbar/ kT$ and $1/\gamma$. The idea advanced by these authors is that fluctuations and dissipation can have quite distinct time scales [133]. This is important if the two quantum states of the system of interest correspond to chemical interconverting states [139, 144, 145].

To complete the description and get the connection with the solute emission and absorption spectra, there is need of the correlation functions of the dipole operator $\mu j= (\mathbf{a}(t)+\mathbf{a}\dagger(t))j$ and, consequently, the differential equation for the one solute mode has to be solved. The reader is referred to [133] for detailed analysis of this point as well as the equations controlling the relaxation to equilibrium population. The energy absorption and emission properties of the above model are determined by the two-time correlation functions:

$$\begin{aligned} Cabs(\tau) &= \lim_{t->\infty} < \mu(t)\mu(t+\tau)> \\ Cem(\tau) &= \lim_{t->\infty} < \mu(t+\tau)\mu(t)> \end{aligned} \tag{60}$$

The Fourier transform of the correlation functions Cem(τ) and Cabs(τ) are the emission (Sem) and absorption (Sabs) spectra, respectively: $Sem = \int d\tau C_{em}(\tau)\exp(-i\omega\tau)$;the integration limits are (-∞,+∞).

Experimental probing of the detailed solute-solvent dynamical mechanisms can be

obtained with contemporary femtosecond spectroscopy [146].

Femtosecond solvation dynamics experiments in water [147] clearly hint at the existence of a bimodal response of the solvent to a change in solute charge density that is produced by photon absorption for instance. Water appears to show an ultrafast component in the $\hbar / kT$ timescalc and a slow component due to diffusive motions whose timescale would be in the $1/\gamma$ range.

The need for quantum mechanical treatment of solute-solute and solute-solvent interactions is illustrated by recent NMR experiments of imaging with intermolecular multiple-quantum coherences in solution. Correlations between spins in different molecules were detected by magnetic-field gradient pulses [148]. The separation range can bc tuned from less than 10 μm to more than 1 mm. A theoretical analysis of these effects was reported by Warren and coworkers [149]. They noticed that the intermolecular cross peaks are not due to radiation damping but are induced by a mechanism that is local in nature. For chemically activated systems, Skrebkov [150] has developed a finite-difference equations of diffusional type to study vibrational relaxation processes in binary gas mixtures of quantum oscillators mimicking diatomic molecules. An interesting overview is given there of the Russian contributions to the theoretical study of electronic excitation and ionization, equilibrium approach to the molecular translational degrees of freedom, rotational-translational relaxation, etc.

The reader can see now that experimental conditions are progressing in such a way that would allow for verifications of the quantum theories of solvent effects. The important theoretical fact is the possibility of recasting the standard theory of solvent effects, based upon classical statistical mechanics, into a more complete quantum mechanical approach.

3.3.3. *Quantum Chemical Framework*

The analysis of the time dependent Schrödinger equation can bc made by using standard quantum chemical procedures in the Born-Oppenheimer approximation. Let us consider a system prepared in the n-th quantum state of a solute molecule which is coupled to a surrounding medium acting as an energy sink. The surrounding medium is represented by a set of quantum states whose energy bandwidth overlaps the discrete solute quantum level. The objective is the determination of the equation of motion for the probability amplitude of finding the system in the n-th state after a time t when at t=0 it was prcparcd in that state. Actually, one would be looking after the energy relaxation from the quantum n-state towards the m-states of the surrounding medium, a situation already analyzed with. second quantization formalism in the preceding section. The analysis can also be done by starting from equations (1) to (4). Instead of equation (5), the total wave function will be written as:

$$\Psi(\mathbf{r},\mathbf{X},t) = \Sigma_k \, \chi_k(\mathbf{X},t) \, \Phi_k(\mathbf{r},\mathbf{X}) \tag{61}$$

where $\Phi_k(\mathbf{r},\mathbf{X})$ fulfills Eq.(3) with eigenvalue $E_k(\mathbf{X})$ and $\chi_k(\mathbf{X},t)$ is a solution of the

time dependent Schrödinger equation:

$$i\hbar\,\partial\chi_n(\mathbf{X},t)/\partial t = (H_N + E_n(\mathbf{X}))\,\chi_n(\mathbf{X},t) + \Sigma_{m\neq n}\, H_{Nnm}\,\chi_m(\mathbf{X},t) \tag{62}$$

and a set of equations for the solvent states:

$$i\hbar\,\partial\chi_m(\mathbf{X},t)/\partial t = (H_N + E_m(\mathbf{X}))\,\chi_m(\mathbf{X},t) + \Sigma_{m'\neq m}\, H_{Nm'm}\,\chi_{m'}(\mathbf{X},t) \tag{63}$$

Bearing in mind how the system was prepared, namely, $\chi_m(\mathbf{X},0)=0$ for all $m\neq n$, one gets for the solvent modes:

$$\chi_m(\mathbf{X},t) = -(i/\hbar)\int d\tau\, \Sigma_{m'\neq m}\, H_{Nm'm}\exp[-i\,(H_N + E_m(\mathbf{X}))(t-\tau)/\hbar]\;\chi_{m'}(X,\tau) \tag{64}$$

Now, Eq.(64) is to be replaced in Eq.(62). Before doing this, it is convenient to extract the term $m'=n$ in the summation above. It is this term which will respond for a direct coupling between the solute quantum state and the states around it provided by the solvent. All other solvent states are not correlated, to first order, with the solute n-state. Thus, Eq.(62) can now be written as:

$$i\hbar\,\partial\chi_n(\mathbf{X},t)/\partial t = (H_N + E_n(\mathbf{X}))\,\chi_n(\mathbf{X},t) - (i/\hbar)\,\Sigma_{m\neq n}\, H_{Nnm}\,H_{Nnm}\int d\tau\exp[-i\,(H_N + E_n(\mathbf{X}) + E_m(\mathbf{X}) - E_n(\mathbf{X}))(t-\tau)/\hbar]\;\chi_n(X,\tau) \tag{65}$$

the exponential term becomes a slowly varying function if $(H_N + E_n(\mathbf{X}))\,\chi_n(X,\tau)$ is nearly always equal to $E_n(\mathbf{X})$, so that one can neglect the n-dependence in the exponential. Furthermore, assuming that the matrix elements H_{Nnm} are independent of m in the manifold coupled to the n-state, and defining an energy density of states $\rho(E)$ to ensure numerical equality, then Eq.(65) can be given the form:

$$i\hbar\,\partial\chi_n(\mathbf{X},t)/\partial t = (H_N + E_n(\mathbf{X}))\,\chi_n(\mathbf{X},t) - (i/\hbar)\,|H_{Nnm}|^2\;\rho(E)\int d\tau\,\Sigma_{m\neq n}\;\exp[-i\,(E_m)(t-\tau)/\hbar]\;\chi_n(X,\tau) \tag{66}$$

This equation has been used by Sundström and coworkers [151] and adapted to the analysis of femtosecond spectral evolution as monitored by the bond-twisting events in barrierless isomerization in solution. The theoretical derivation of Åberg et al. establishes a link between the Smoluchowski equation with a sink and the Schrödinger equation of a solute coupled to a thermal bath. The reader is referred to this important work for further theoretical details and a thorough description of the experimental set up. It is sufficient to say here that the classical link is established via the Hamilton-Jacobi equation formalism. By using the standard ansatz $\chi_n(\mathbf{X},t) = A(\mathbf{X},t)\exp(S(\mathbf{X},t)/i\hbar)$, where $S(\mathbf{X},t)$ is the action of the dynamical system, and neglecting terms in $\hbar^2$ once this

ansatz is entered in Eq.(66), the action must fulfil the Hamilton-Jacobi equation. The problem is now shifted to the calculation of those trajectories rendering stationary the action of the system. The Hamilton-equation for the classical variables [151] follows from this.

From the analyses presented in this section, it can be seen that, at least in principle, the enormous complexity of a solute surrounded by a solvent can be reduced to problems of smaller complexity. The interesting point is that these relatively simple model situations have been most useful to correlate experimental results derived from femtosecond spectroscopy.

3.4. MOLECULAR HAMILTONIAN IN AN ELECTROMAGNETIC FIELD

Physics and chemistry are carried out in laboratory frames using coordinate systems to set up experimental devices. Before discussing quantum mechanical processes let us recall the form of the total Hamiltonian for a set of particles having charges q_a and masses m_a interacting with an electromagnetic field **A.** This Hamiltonian is given by:

$$H= \Sigma_a (1/2m_a)[\mathbf{p}_a-q_a\mathbf{A}(\mathbf{r}_a)]^2 - \Sigma_a(g_a q_a/2m_a)\mathbf{S}_a\cdot\mathbf{B}(\mathbf{r}_a) + V_{Coul} + H_{rad} \qquad (67)$$

where $\mathbf{p}_a=(\hbar/i)\nabla_a$ and ra are the momentum and position vector operators of the particle a, **A(r)** is the vector potential in the Coulomb gauge (it has only transversal components Cf.[152]); **Sa** is the spin operator and **B(ra)** the magnetic field component of the radiation field evaluated at the position of the a-th particle, g_a is the Landé's factor; V_{Coul} represents the Coulomb energy of the set of charged particles including their self-energy ; finally, the radiation Hamiltonian Hrad is expressed in terms of transverse electric (**E**^) and magnetic (**B**) fields. The radiation Hamiltonian can be expressed in terms of destruction and creation **aj** and **aj†** operators of a photon in the j-th field mode defined by the wave vector **k**j, polarization **e**j and frequency $\omega_j = ck_j$ ($k_j=|k_j|$, c= speed of light) [45, 153, 154]:

$$H_{rad}= \Sigma_j \hbar\omega_j (\mathbf{a}_j^\dagger \mathbf{a}_j + 1/2) \qquad (68)$$

Note that $d\mathbf{r}_a(t)/dt = [H,\mathbf{r}_a]=(1/m_a)[\mathbf{p}_a-q_a\mathbf{A}(\mathbf{r}_a)]$ and, consequently, the first term in (69) represents the kinetic energy of the system of particles in the presence of the transverse electromagnetic field. Note the analogy between this representation and the dynamical solute-solvent coupling of section 2.6 where the optical phonons are equivalent to electromagnetic photons of low frequency (the acoustical phonons are related to sound waves).

It is now appropriate to cast Hamiltonian (53) as follows:

$$H = \Sigma_a (1/m_a)[\mathbf{p}_a]^2 + V_{Coul} + H_1(\mathbf{S},\mathbf{B}) + H_2(\mathbf{p},\mathbf{A}) + H_3(\mathbf{q},\mathbf{A}) + H_{rad} \quad (69)$$

where $H_1(\mathbf{S},\mathbf{B})$ describes the coupling of the molecular spin operator with the external magnetic field and H_k with k=2 or 3 corresponds to interactions between the charges and the electromagnetic field; H_2 is linear while H_3 is quadratic in **A.** Note that H_2 corresponds to $U(\mathbf{x})=(e/mc)\ \mathbf{A}(\mathbf{x},t).\mathbf{p}$ discussed in Section 2.2.

There are two ways the Hamiltonian (55) can be used to analyze physical problems. In one of them, the system does not have bound states and the zero-order Hamiltonian Ho is made of the $\mathbf{p}^2$-terms and H_{rad} describing the set of charged particles and a non-interacting radiation field. The couplings between the particles among themselves (V) and with the transverse field (any or all of the H_ks) are treated as perturbations. Compton scattering and bremsstrahlung radiation are phenomena treated in this framework [58, 153].

A second type of problems can be treated by defining a zero order Hamiltonian with the first two terms, $H_o = \Sigma_a\ (1/m_a)[p_a]^2 + V_{Coul}$. This corresponds to the Coulomb Hamiltonian in our equation (1) where the self energy is left out. This partitioning permits assembling the system into bound (sub)systems representing atoms, molecules, isomers, etc. These latter structures can numerically be identified via the coordinate representation of the Hamiltonian by calculating the stationary values with respect to the slow motion coordinates **X.** For the minima, this procedure leads to characteristic fluctuations around defined regions in configurational space for each bound quantum state (ground state), while for stationary Hamiltonians corresponding to saddle points along particular directions in the **X**-space one gets a reduced set of quantum states having all of them finite lifetimes in the the photon (phonon) field.

4. Quantum Theory of a Chemical Interconversion Step

A chemical reaction is a complex process. Besides thermodynamic factors, the process has two other distinct aspects: kinetic and molecular mechanistic ones. With the development of modern technology, more and more complex kinetic schemes can be determined by using sufficient experimental information and fairly general computer programs [155]. In order to proceed, it is useful to define what we mean by a theory of chemical reactions in the first place.

In a molecular mechanism there is always at least one step at which the system changes its initial identity, as it were, to acquire a different one. This is called here the chemical interconversion step. Following the viewpoint developed in our paper [43], the interconversion takes place unimolecular complex where the system jumps between quantum states having different stationary Hamiltonians. A simple reaction scheme is then one having only one such interconversion step. Chemical reactions proceeding with multiple interconversion steps can be treated along lines similar to the one step process as far as the quantum aspects are concerned.

It is worth noticing that the chemical interconversion step may not be the rate-

limiting step of the overall reaction. But, if this step does not happen, there would be no reaction at all. It is in this sense that a theory of reaction rates is seldom a general theory, and it is thereby preferable to talk of the theory of chemical interconversion.

Two classes of reactions are distinguished differing by the nature of the interconversion step. The first class contains those systems for which the change of spectra from Hc(i) to Hc(j) is carried out between two subsets of quantum states belonging to these Hamiltonians. The second class contains those system requiring an intermediate stationary Hamiltonian Hc(ij); this Hamiltonian does not have a ground state, namely, all its quantum states have finite lifetime and defines species related to an activated complex. To the first class belong the unimolecular reactions. To the second one belong, for instance, the bimolecular thermally activated as well as thermally non-activated processes.

4.1. A SIMPLE QUANTUM MODEL TO BOND DISSOCIATION PROCESSES

There is an alternative way of describing the simple bond dissociation process in a typical diatomic such as, for example, the hydrogen molecule. The interatomic parameter **r** makes sense for two colliding beams of hydrogen atoms. It is a laboratory controlled coordinate, since one can prepare two crossing atom jets. They have different electronuclear fluctuation regimes (for example, changes of these states can be sensed by the Balmer series for the atoms, electronic and vibrational spectra of H_2, etc.). The definition of an appropriate reference frame is required to plot different quantum fluctuation regimes that otherwise appear to cross in the standard plots using for instance **r.** The interconversion between these two systems may occur for an excited (vibrational) quantum state of H_2. In the present understanding, this state is (nearly) degenerated to a quantum state representing two entangled hydrogen atoms. This latter state is experimentally found to be unbound beyond a given energy threshold and could be measured as two spin correlated hydrogen atoms at large **r.**

Thus, to help discuss chemical reactions, it is advisable to define an auxiliary axis where the interconversion process is highlighted; this is graphically shown in Figure 1, This axis serves the purpose of differentiating the fluctuation regimes associated with the two quantum states when they are approximated as many-body wave functions. In the example above, both quantum states have different electronic fluctuation patterns. Following the pictorial description, the interconversion process of H_2 into $2H$ is decomposed in several moments: 1) excitation, from ground to excited ro-vibrational state of H_2 (eventually electronic excited state); this latter system may be in a defined quantum rotational state; 2) “horizontal” jump along the interconversion coordinate from the excited ro-vibrational state towards the virtual state (resonance) of two entangled hydrogen atoms with correlated spins. Such quantum states are always there since they belong to the spectra of the global Hamiltonian. This is a pure quantum mechanical property. A time-dependent field is required to couple the quasi degenerate states or to provide for an energy gap. This interconversion does not define, by itself, the rate since

3) the virtual state may either return to the ro-vibrational quantum state of the hydrogen molecule (which it does since a coherent quantum state can develop at the interconversion region) or 4) it may relax by its coupling to the translational continuum of two hydrogen atoms that will lead to products, i.e. it gets trapped into the quantum states of another stationary Hamiltonian. All these states are coupled by photon exchanges as in normal quantum electrodynamics processes [45, 46]. Thus, the chemical interconversion process can be seen as a fundamental quantum mechanical process. The motion at the saddle cannot be seen as a free translational motion, although crossings of the potential energy may provide a zero order description for the counting of events in a classical statistical mechanical frame.

The recombination process follows a similar pattern if the hydrogen atom states are spin correlated. In real situations this is not necessarily the case. They become correlated by forming an entangled state of two hydrogen atoms as they interact. Thereafter, there is a finite probability that, having formed the entangled state of two hydrogen atoms, this system jumps into one of the excited vibrational-rotationaI states of the hydrogen molecule. These states exist as states of the global Hamiltonian. The probability amplitude is related to the matrix element of the transition dipole between the two states. This type of phenomenon can be reflected as resonances in the scattering cross section [84]. Formation of H_2 would occur if relaxation channels are available to bring the system to a lower energy vibrational-rotational quantum state.

It is worth noticing that the energy range required to onset dissociation of H_2 into two atoms in the gas phase does not suffice to produce an heterolytic (di-ionic) break. The di-ionic form belongs to a different stationary Hamiltonian (proton plus hydride ion) and its energy is located at a much higher level than the energy required to break the covalent bond. In Figure 1, the coordinate on the interconversion axis of such a quantum state is just opposite to the one occupied by two hydrogen atoms. Solvent (cage) effects may change the energy of this highly polar state bringing it down on the energy scale. This is what we showed in 1974 for the di-ionic species in a water dimer [156]. If the effective Hamiltonians still represent the same species, albeit solvated, the discussion presented so far holds. In a polarizable medium, di-ionic states are energy stabilized to a great extent. In condensed (polarizable) phases, one would expect the di-ionic species to have resonance conditions with the excited vibrational states of the hydrogen molecule at nuclear distances larger than that which is characteristic of two entangled hydrogen atoms. Solvent effects are also expected to modulate the transition moment. Thus, for instance in solid molecular hydrogen, the di-ionic channel would be accessible if sufficient energy is provided, or if the packing put two H-atoms belonging to nearest neighbor molecules within a distance where the quantum dynamical process of jumping to the di-ionic state is made more likely to occur. Experimentally, such an effect has been detected albeit described along more quantum chemical lines (charge transfer) [157].

One can see the advantage of using the interconversion coordinate when describing different quantum states. This coordinate replaces the reaction coordinate which in this

theory has no place (the interconversion is not seen as a classical mechanics process in the sense that the motion of the system along the standard reaction coordinate is treated as free translational motion [37]). As with any other coordinate set, the interconversion coordinate is useful as a mediating language. While we can describe the processes as changes in the quantum fluctuations of the particles used to build the molecular model, what is physically meaningful is the quantum jump between states and what is physically measurable corresponds to the quantum transition probabilities [158].

4.1.1. *Quantum mechanics of the intercoversion step*

Let us consider a model case for a single bond dissociation process where there is no need to call for an intermediate Hamiltonian in the sense discussed above. The discussion presented in 2.8 applies. Here, some formal aspects are discussed.

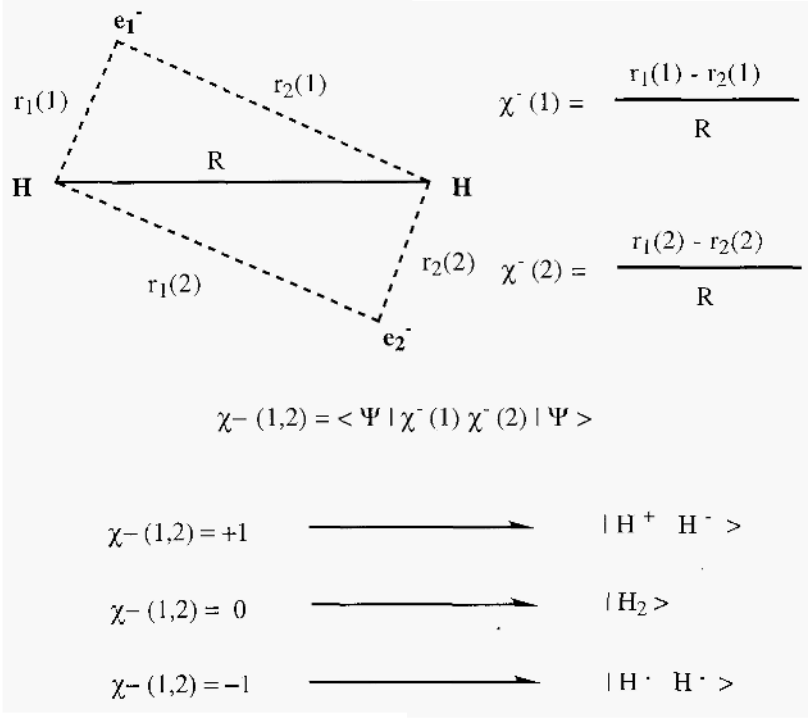

Figure 1. Definition of the quantum interconversion coordinate for a two-electron case epitomized by the hydrogen molecule. The quantum states are indicated in the kets with their corresponding collective χ- value.

The kets $|\Psi_{ik}>$ and $|\Psi_{jn}>$ are two eigenstates, one associated to the Hamiltonians $H_C(i)$ and the other related with $H_C(j)$. They describe different regimes of electro-nuclear fluctuations. The labels i and j are there to indicate that by spontaneous or/and induced emission processes, there is a subset of corresponding excited states that would relax

towards the (lower) energy bound states associated with the Hamiltonians H(i) and H(j), respectively. The former might be describing the vibrationally-rotationally excited state of the pseudo diatomics, while the other may be related to the electronic state of two fragments at infinite distance and each one in an electron spin doublet state. Such processes can be modeled with adiabatic methods. A second subset of quantum states can be found about at a given distance (call it R-region) which have finite matrix elements between i- and j-states for the radiation-molecule coupling operator. This can be called the activated state set. For complex molecules undergoing a dissociation process, the structure would certainly move into a critical configuration or activated precursor so that the R-region involves a particular geometric set up (see sect.4.2 for discussions).

Note that chemistry forces the introduction of two different Hamiltonians, while the total number of charged particles is invariant. In the case of a hydrogen molecule, operationally, one can identify the hydrogen molecule with all the required quantum numbers. It requires a different experiment to identify the hydrogen atoms with their set of quantum numbers. Two hydrogen atoms can be interconverted into one hydrogen molecule if the spin states are entangled into a global singlet state and an inter-conversion process takes place. In turn, a hydrogen molecule can be decomposed into an entangled state of two hydrogen atoms via the same interconversion process. The electro-nuclear fluctuation pattern, measured as the expectation value of the interconversion coordinate χ-(1,2) defined in Figure 1, is totally different for both states. For the R-region, about which there is energy degeneracy or quasi-degeneracy, the state of electronuclear fluctuation can jump into the electronuclear fluctuation of the other state, both being different but have finite transition dipole amplitudes to form coherent quantum states under an appropriate external electromagnetic excitation. This inter-conversion process can be formalized by using standard time dependent perturbation theory where the unperturbed Hamiltonian is Ho and the perturbing potential is for instance $H_2(\mathbf{p},\mathbf{A})$. Models for the quantum states oh Ho are obtained with the help of the stationary Hamiltonians Hc.

The system is prepared at t=0 in the quantum state $|\Psi_{ik}>$ and the question is: how to calculate the probability that at a later time t the system is in the state $|\Psi_{jn}>$. By construction, these quantum states are solutions of molecular Hamiltonian in absence of the radiation field, Hc->Ho: $H_o|\Psi_{ik}> = e_{ik}\,|\Psi_{ik}>$ and $H_o|\Psi_{jn}> = \varepsilon_{jn}\,|\Psi_{jn}>$. The states are orthogonal. The perturbation driving the jumps between these two states is taken to be $H_2(\mathbf{p},\mathbf{A})$= D exp(iωt), where ω is the frequency of the incoherent radiation field and D will be a time independent operator. From standard quantum mechanics, the time dependent quantum state is given by:

$$|\Psi(t)> = C_{ik}(t)\exp(i\,\varepsilon_{ik}\,t/\hbar)|\Psi_{ik}> + C_{jn}(t)\exp(i\,\varepsilon_{jn}\,t/\hbar)|\Psi_{jn}> \qquad (70)$$

then, for a system starting at t=0 in quantum state $|\Psi_{ik}>$, the probability of finding it at time t=t in the state $|\Psi_{jn}>$ for the case of near-resonant absorption is given by Rabi′s

equation [47, 154]:

$$|C_{jn}(t)|^2=[|\langle\Psi_{ik}|H_2(\mathbf{p},\mathbf{A})|\Psi_{jn}\rangle/\hbar|^2/\{(|\langle\Psi_{ik}|H_2(\mathbf{p},\mathbf{A})|\Psi_{jn}\rangle/\hbar|^2)+(\omega-\omega_{jn,ik})^2/4\}]\ x$$
$$\sin^2\{\sqrt{[(|\langle\Psi_{ik}|H_2(\mathbf{p},\mathbf{A})|\Psi_{jn}\rangle/\hbar|^2)+(\omega-\omega_{jn,ik})^2/4)]}\ t\} \qquad (71)$$

where $\omega_{jn,ik} = (\varepsilon_{jn} - \varepsilon_{ik})/\hbar$.

The probability of finding the system in the state $|\Psi_{jn}\rangle$ has an oscillatory time dependence. For off-resonance conditions, the system presents a line width at half maximum equal to 4 $|\langle\Psi_{ik}|H_2(\mathbf{p},\mathbf{A})|\Psi_{jn}\rangle/\hbar|$. This matrix element can be expanded in a multipolar expansion, the first term being the electric dipole approximation [45, 152, 154].

A chemical reaction is then described as a two-fold process. The fundamental one is the quantum mechanical interconverting process among the states, the second process is the interrelated population of the interconverting state and the relaxation process leading forward to products or backwards to reactants for a given step. These latter determine the rate at which one will measure the products. The standard quantum mechanical scattering theory of rate processes melds both aspects in one [21, 159-165]. A qualitative fine tuned analysis of the chemical mechanisms enforces a disjointed view (for further analysis see below).

The relaxation towards the product channel may take place via different processes. It is a common situation for bond dissociation that there might be a number of n-states along the j-channel where interconversion may be achieved. In some particular situations, the total probability is obtained after summing over the transition probabilities $\Sigma n\ |C_{jn}(t)|^2$. Introducing the concept of density of final states as the number of states $\rho(E)dE$, the sum is transformed into an integral. Then by taking the limit $t \rightarrow \infty$, one arrives at Fermi's golden rule when the time derivative of the total probability is sought. We have presented already a discussion of this type of process in ref.[43]. For a system at thermal equilibrium, Boltzman weight factors must be included for the different quantum states involved in order to get a mathematical expression for the rate.

The states in the R-region for which resonance is allowed are called active precursor and successor states (APS and ASS). At equilibrium, there is a symmetry between the interconversion viewed from the side of the successor and the precursor states, and this is the detailed balancing. The transition rate from the ik-state towards the set {jn} multiplied by the density of states for ik should be equal to the transition rate from the jn-state towards the set {ik} multiplied by the density of states for jn [47].

The basic ideas presented above correspond to an analysis of a typical unimolecular process, as for instance, SN1 mechanism where the solvent may have achieved the stabilization of the di-ionic quantum state and has favored ionic dissociation as opposed to homolytic dissociation. The chemical interconversion appears here to be a quantum mechanical change of state where the solvent fluctuations would play the role of

bringing the system to near resonance of the quantum subsystem. The theory differs in a fundamental way from a valence bond-like and a molecular orbital-like approaches. From their very approximate nature, these methods produce couplings between configurations that look as models for the exact quantum states. The theory herein discussed is based on an exact quantum mechanical approach. The approximate methods, that are adiabatic in nature are useful to construct models for reactants, precursor and activated precursor geometries entering in the general approach. The quantum interconversion process cannot be properly handled with such approximate methods. Notwithstanding, the geometries associated with the stationary Hamiltonians can be modelled with advanced quantum chemical techniques or semi empirical ones. Models of the spectra (vibrational) and relative total energies are also obtained with present day computing techniques.

4.2. PROCESSES MEDIATED BY INTERMEDIATE HAMILTONIANS

It is common knowledge that a chemical interconversion process can take place when two or more molecules come into a common region to form a complex. This is the region corresponding to the activated complex or quantum mechanical bottleneck [37, 67, 166]. For gas phase reactions, the reactants are tied up in a much smaller volume than predicted by random encounters. The problem lies in the proper identification of the activated complex [37, 167]. It has been assumed in some works that the molecules are either forming a relatively undistorted species or are in the form of strongly bound but decomposing complexes. This point is challenged here as complexes approaching the geometric arrangement of the stationary intermediating Hamiltonian are those actually opening the interconversion channel [101, 102].

A chemical interconversion requiring an intermediate stationary Hamiltonian means that the direct passage from states of a Hamiltonian Hc(i) to quantum states related to Hc(j) has zero probability. The intermediate stationary Hamiltonian Hc(ij) has no ground electronic state. All its quantum states have a finite lifetime in presence of an electromagnetic field. These levels can be accessed from particular molecular species referred to as active precursor and successor complexes (APC and ASC). All these states are accessible since they all belong to the spectra of the total Hamiltonian, so that as soon as those quantum states in the active precursor (successor) complex that have a non zero electric transition moment matrix element with a quantum state of Hc(ij) these latter states will necessarily be populated. The rate at which they are populated is another problem (see below).

It is worthwhile to emphasize that the intermediate Hamiltonian Hc(ij) defines a geometry that can be used to construct a model of an activated complex. A portrait of it can be obtained at the BO level of theory. For thermally activativated processes, the transition state is the analogous of the intermediate Hamiltonian, while for processes without thermal activation (a number of reactions taking place in gas phase, such as for example, the SN2 reaction between methyl halides and halides ions [168-171]) the quantum states of this Hamiltonian mediate the chemical interconversion. For particular

systems, calculated at the BO level, it has been noticed that from all the internal degrees of freedom fonning the system, only a few (control space) are essential for defining the index of saddle point. The remaining degrees of freedom form the complementary space and its stereochemistry is strongly determined by the geometry of the control space at the stationary point [43, 94, 100-102, 172-174]. It has also been computationally found that among the variables entering the transition vector, there is a minimal subset that is still able to produce a unique negative eigenvalue representing the reactive fluctuation at zero order. This is the so called active subspace. The invariance of the active subspace is an important property of stationary Hamiltonians without ground state.

Let us take a simple example, namely a generic S_N2 reaction mechanism and construct the state functions for the active precursor and successor complexes. To accomplish this task, it is useful to introduce a coordinate set where an interconversion coordinate (χ-) can again be defined. This is sketched in Figure 2. The reactant and product channels are labelled as Hc(i) and Hc(j), and the chemical interconversion step can usually be related to a stationary Hamiltonian Hc(ij) whose characterization, at the adiabatic level, corresponds to a saddle point of index one [89, 175]. The stationarity required for the interconversion Hamiltonian Hc(ij) defines a point (geometry) on the configurational space. We assume that the quantum states of the active precursor and successor complexes that have non zero transition matrix elements, if they exist, will be found in the neighborhood of this point.

The interconversion is defined here as the “tunneling” of the carbon atom along the coordinate χ^- , the stretching mode of the atoms bonded to carbon with the donor-acceptor distance frozen at the value found for the stationary Hamiltonian Hc(ij). Pictorially speaking, as soon as the C-atom moves away from the plane defined by the three atoms bound to it, the system would enter the active precursor (AP) in one direction and the active successor (AS) domain in the opposite direction. Note the difference with respect to the commonly defined interaction complex that sometimes is dubbed as precursor complex [176]. This latter is an ion-dipole complex, while in our case, a molding process would be required with the geometry of the stationary intermediate Hamiltonian as template. The two sets of quantum states for the AP an AS complexes can now be thought of as quantum jumping via the quantum states of the intermediate stationary Hamiltonian. The jump from the precursor to the intermediate states is done precisely in the same way as was described above for the bond-breaking process (see section 4.3 for further discussion). Thus, while the molding process can be modeled with an adiabatic procedure, the essential interconversion cannot.

To make the ideas sharper consider the case of two quasi degenerate quantum states of the active precursor and successor complexes. The discussion made around equation (57) holds true here too. The activated complex will be the place of a coherent electro-nuclear fluctuation that will go on forever, unless there are quantum states belonging to the relaxation channels of Hc(i) and Hc(j). Note that the mechanisms of excitation to get into the quantum activated complex and those required to relax therefrom are related to the actual rate, while the mechanism of interconversion is closely connected with an

electronuclear fluctuation with characteristic frequencies and represents the essence of the

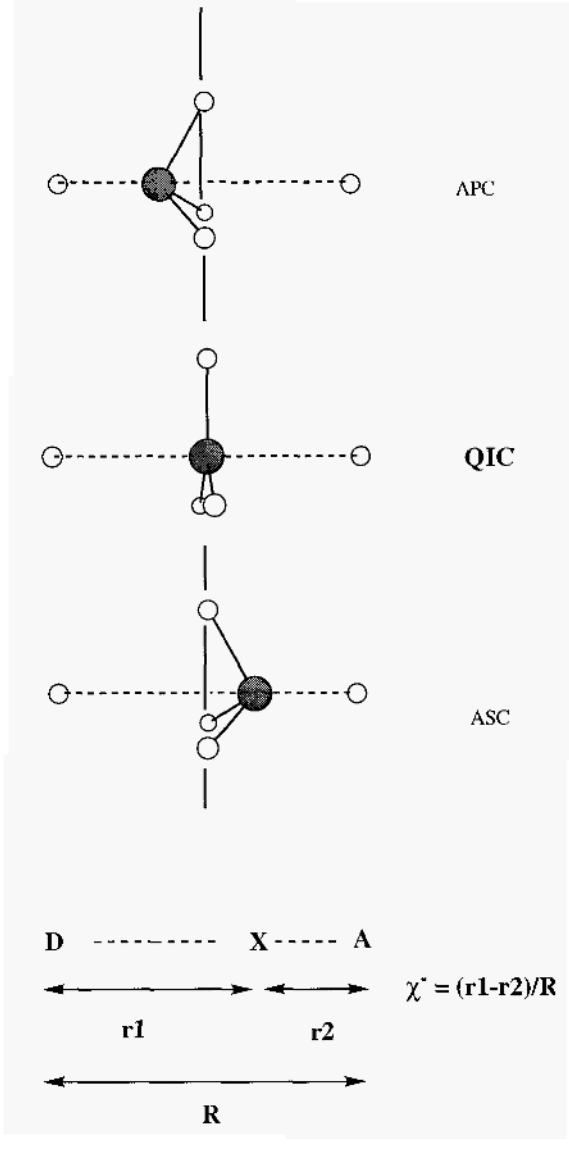

Figure 2. Interconversion coordinate used in generic group exchange reactions. In this case a S_N2 model is described. The donor and acceptor in the scheme above would correspond for instance to an halide ion Y- entering from the right in the APC and the leaving group is the halide ion Y-. The central carbon is shetched by the dark circle. The distance R is determined by the SPi-1, and the quantum states to the left and the right of the plane formed by the 3-substituents linked to the C-atom being different, they cannot physically be reached by an adiabatic process as implied in the BO-scheme if quantum mechanics must prevail (two different quantum states cannot be linked adiabatically).

molecular mechanism. The quantum fluctuations at the activated complex have been made evident with femtochemistry techniques [146, 177]. It is worth noting that the current explanation for those experimental results is different from the one developed here.

As noted above, the idea of quantum active precursor and successor states, or active complexes is rather different from the standard terms used in chemical reactivity. Here, these states are related to the stationary intermediate Hamiltonian Hc(ij). The geometry associated with this stationary point is usually quite different from the geometries of the molecules making the encounter complexes. These latter may or may not be specific stationary species in the quantum mechanical sense, namely, that they are quantum states characterizable by their spectroscopic or other measurable quantum properties. Stable charge transfer complexes provide a typical example. The set of complexes formed by gas phase reactants in S_N2 reactions is another example [168-170]. The gas-phase $X^- ... CH_3Y$ ion-molecule complex with X=Y=I has been carefully studied with extended basis set calculations by Hu and Truhlar [176]. The results show that the complex has not proceeded very far in the direction of products. The equilibrium I...C distance in the complex is 3.396Å and C-I distance 2.184Å [176] (both calculated at MP2/APDZ-level). These distances in the activated precursor complex must be nearly equal as the C-atom moves away the stationary Hamiltonian (SPi-1) value only a small fraction of an Angström. If the reaction starts from the ground state of the ion-molecule complex, the quantum active precursor states can be reached therefrom via excitations (produced by light or by interaction with a photon field due to surrounding medium effects). Pictorially speaking, the geometries of the collision or encounter species must be molded into an arrangement resembling the stationary Hamiltonian Hc(ij) geometry in order to populate the quantum interconversion states associated with the quantum interconversion complex (QIC). It is in this region where field-driven electronuclear fluctuations couple states belonging to different chemical Hamiltonians. What is essential now is not a wandering on an energy hypersurface (which is a pictorial way to describe things) but the population of the interconverting quantum states. For this particular class of reaction it is well acknowledged that they exhibit nonstatistical behavior in the sense that excitation of some internal modes are much more effective in driving the reaction than others [170,178-180]

The relationship between the geometry of the saddle point of index one (SPi-1) and the accessibility to the quantum transition states cannot be proved, but it can be postulated [43,172]. To some extent, invariance of the geometry associated with the SPi-1 would entail an invariance of the quantum states responsible for the interconversion. Thus, if a chemical process follows the same mechanism in different solvents, the invariance of the geometry of the SPi-1 to solvent effects would ensure the mechanistic invariance. This idea has been proposed by us based on computational evidence during the study of some enzyme catalyzed reactions [94, 96, 97, 100-102, 173, 174, 181-184].

A chemical interconversion step has assigned to it an invariant feature: the quantum

interconversion complex (quantum transition complex). One way to model this species is via the calculation of saddle points of index one. The name of quantum activated complex can also be used to refer to this special state.

Pictorially speaking, this property permits defining a (static-like) stereochemical disposition of the particles constituting the species, thereby providing an inter-conversion coordinate sufficiently general for a quantum mechanical characterization of the chemical reaction.

4.3. CHEMICAL REACTIONS: RATES AND MECHANISM

For the sake of simplicity, let us consider a reaction scheme where only one step corresponds to the chemical interconversion. From reactants R1 and R2 and the products that will be measured as species P1 and P2, the following mechanistic scheme covers a variety of possibilities:

$$\begin{array}{ccccccccccc} & & k1 & & k2 & & k+ & & k'-2 & & k'-1 & \\ R1+R2 & <----> & R1\text{-}R2 & <----> & APC & <----> & ASC & <----> & P1\text{-}P2 & <----> & P1+P2 \\ & & k-1 & & k-2 & & k- & & k'2 & & k'1 & \end{array} \tag{72}$$

This is a (minimal) model including the formation of the complex R1-R2, the active precursor complex APC that interconverts to those states belonging to the active successor complex ASC, as discussed in the previous section. The chemical reaction, in this model, ends up with the formation of the products P1 and P2. The kinetic parameters k+ and k- hide the effects of quantum interconversions via the intermediate Hamiltonian Hc(ij). Let us introduce this feature in the kinetic model, so that

$$\begin{array}{ccccc} & & k'+ & & k''+ & \\ APC & <----> & QIC & <----> & ASC \\ & & k'- & & k''- & \end{array} \tag{73}$$

If we solve the kinetic problem assuming stationary concentration of [QIC], one gets the following equations for k+ and k- in terms of the kinetic coefficients appearing in eq (73):

$$k_+ = (k'_+ * k''_+)/(k'_- + k''_+) \text{ and } k_- = (k'_- * k''_-)/(k'_- + k''_+) \tag{74}$$

Strictly speaking, all steps in the model (72) have a quantum mechanical nature. The measured rate is determined by the relative values of the kinetic parameters and a number of situations can be envisaged. The rate limiting step for the forward direction, defined from left to the right in Eq.(72), may be located at any level depending of course on the nature of the species. There is, however, a necessary and sufficient condition for the process to occur. This is related to the relaxation time of ASC into quantum states of P1-P2. This relaxation time must be finite.

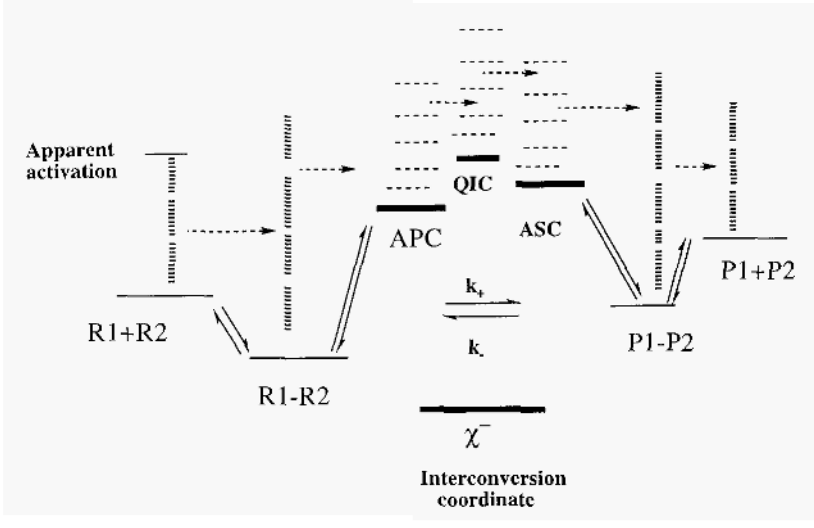

Figure 3. Schematic view related to eq.(72) acording to the quantum view discussed in the text. Observe that k+ and k- are kinetic parameters describing the passage from APC to the ASC. We have not indicated all other parameters included in this equation. In eq.(73) the quantum states of the QIC are explicitly taken into account. The arrows here indicate the forward reaction sense; For a reaction starting from R1+R2 the process going from P1-P2 towards ASC can be neglected as the concentration of P1+P2 and P1-P2 are negligible at initial time. In chemical equilibrium situation, arrows from right to left are implied. Note that the apparent activation may become negative for some very strong precursor complexes R1-R2, and the active precursor complex may well be below the energy for the reference reaction R1+R2.

The reactants in equation (72) may be a normal molecule or a photon field, e.g. R2=hv, where h is Planck's constant and v is the frequency of the photon. The complex made by the photon and the molecule may or may not activate the interconversion space for a given photodissociation process.

The Lindemann kinetics for unimolecular reactions [185] can be formally recovered if one subsumes the formation of a collision complex with the precursor complex steps {R1-R2 <---> APC) into one corresponding to the excited reactant R1*. The excited

molecule must redistribute its excess energy so as to populate the interconversion states. The fundamental interactions between molecular systems is carried out by virtual photons. This example is discussed in more detail below.

The reactant R2 can also be considered to be a solvent molecule. The global kinetics become pseudo first order in R1. For a S_N1 mechanism, the bond breaking in R1 can be solvent assisted in the sense that the ionic fluctuation state is stabilized by solvent polarization effects and the probability of having an interconversion via heterolytic decomposition is facilitated by the solvent. This is actually found when external and/or reaction field effects are introduced in the quantum chemical calculation of the energy of such species [2]. The kinetics, however, may depend on the process moving the system from the contact ionic-pair to a solvent-separated ionic pair, but the interconversion step takes place inside the contact ion-pair following the quantum mechanical mechanism described in section 4.1. Solvation then should ensure quantum resonance conditions.

To conclude this elementary discussion, it can be said that the quantum mechanical interconversion step is a necessary and sufficient condition for the reaction to happen, although the rate is not necessarily determined by this step. It is this aspect which leaves any general quantum theory of reaction rates devoid of substance. There can be a general quantum theory of the chemical interconversion step only. Thermally activated processes form a special category for which quantum theories exist [36, 39, 67, 76].

4.3.1 *Chemical Reaction Rate*

Let us consider now processes where intermediate stationary Hamiltonians are mediating the interconversion. In these processes, there is implicit the assumption that direct couplings between the quantum states of the precursor and successor species are forbidden. All the information required to accomplish the reaction is embodied in the quantum states of the corresponding intermediate Hamiltonian. It is in this sense that the transient geometric fluctuation around the saddle point define an invariant property.

Thermally activated processes belong to the category of mediated interconversion processes. It comes as a no surprise that the main factor required for the setting up of interconversion is molding the reactant complex into a geometry as proximal as possible to the geometry defined by the saddle point. It will be in this region where quantum jumps between states representig different electronuclear fluctuations with a minimal deformation of the global system become possible. Thus, if sufficient energy is available, such states will be populated. The rate of population is akin to the kinetics of the given process. It is customary to assume that once such states are populated things go fast. This may be so in the great majority of cases. However, one should not overlook the fundamental quantum mechanical nature of the processes involved.

The reaction channel is open as soon as quantum states of the intermediate Hamiltonian become populated. By hypothesis, such states have two possible different relaxation channels: One back to the reactants, the other forward to product via the quantum states of the successor complex.

Let us consider the non-stationary situation in the neigborhood of the intermediate

Hamiltonian quantum states. Two situations can be envisaged. In the first one, the system moves stepwise from the APC states to the interconversion complex. We assume that the i-th state of the active precursor is populated $|i\dagger\rangle$ at a given time to, and $|if\dagger\rangle$ is intermediate Hamiltonian state that are coupled by the electro-magnetic field.

Thus, having prepared the system at the initial time t=0 in the state $|i\dagger\rangle$, the probability of finding the system in the state $|f\dagger\rangle$ at time t is given, as usual, by $|C_f(t)|^2$. The Fermi Golden-rule expression (to first order in TDPT) has the form [47]

$$w(i \rightarrow if) = 2\pi/\hbar \; |\langle i\dagger|U|if\dagger\rangle|^2 \; \delta(\varepsilon_{if\dagger} - \varepsilon_{i\dagger}) \tag{75a}$$

where the i-th quantum state and energy of the active precursor complex are $|i\dagger\rangle$ and $\varepsilon_i\dagger$, respectively (Cf.Eq.(69)), and $U=H_2$. In case that the interconversion complex has a dense spectra in the region of $\varepsilon_i\dagger$, it is implied then in the equation a density of states. Then, the interconversion state can be coupled to the ASC states leading to w(if ->f) with a formulae similar to eq.(75a).

The second situation corresponds to an indirect coupling of the APC states with the ASC ones via the quantum states of the interconversion states (if). The largest contribution comes again from those state being quasi degenerate in the energy scale. Thus, to second order in TDPT one gets

$$w'(i \rightarrow f) = \frac{4\pi}{h} \left| \sum_{m \neq f} \frac{\overline{U_{fm}}\,\overline{U_{mi}}}{\varepsilon_i - \varepsilon_m} \right|^2 \delta(\varepsilon_i - \varepsilon_m) \tag{75b}$$

Thus, all those quantum states of the interconversion complex (QIC) that are quasi degenerate with the APC would contribute to the population rate of the ASC. Note that there is no first order contributionsin the present theory since the matrix elements of the dipole transition between quantum states belonging to APC and ASC are zero.

Now, let us discuss the rate equations embodied in eq.(74). To do this, there is need of a statistical analysis. If the system is kept coupled to a thermostat at absolute temperature T, and assuming that w(i ->if) contains effects to all orders in perturbation theory, the rate of this unimolecular process per unit (state) reactant concentration k'+ is obtained after summation over the if-index is carried out with Boltzman weight factors p(if,T):

$$k'_+(i) = \Sigma_{if}\, p(if,T) w(i \rightarrow if) \tag{76a}$$

and for the depletion of the intermediate quantum states towards the f-th state of the successor complex one gets:

$$k''_+(if) = \Sigma_f\, p(f,T) w(if \rightarrow f) \tag{76b}$$

Similar expressions can be written down for k'- and k"-. The rate of production of final products for the given interconversion step is determined by the different rates of energy relaxation.

Note that the equation (74) for k+ can be recast in terms of the probability P→ for the system to continue from the QIC towards products, namely, P→ = k"+ / (k'- + k''+), so that k+ = k'+*P→. This equation can be further worked out in order to include the concept of resonance in a more direct way. To get at the desired result, one has to calculate the rate at which $C_i(t)$ is changing. The differential equation fulfilled by this coefficient can bc obtained by using an adiabatic coupling method [47] that, in the limit η->0 it is given by

$$\dot{c}i/c_i = \left(\frac{-2\pi i}{h}\right)^2 \sum_{m\neq i} \frac{U_{im}U_{mi}}{\varepsilon_i-\varepsilon_m+i\eta h/2\pi} \qquad (77)$$

where the summation is done with m≠i and the dot indicates a time derivative. Note that the spectra over which one is performing the summation has two distinct components. One is the spectra of the precursor channel, the other is the spectra of the interconversion complex (QIC) which opens the way forward to products.

The solution to eq.(77) can be cast in the form $C_i(t) = \exp(-i\Delta_i\, t/\hbar)$, where Δ_i is the level shift produced by the perturbation coupling different quantum levels. Expanding Δ_i in terms of first $\Delta_i^{(1)}$ and second $\Delta_i^{(2)}$ order contributions, the imaginary part of $\Delta_i^{(2)}$ is equal to-(ħ /2) $\Sigma_{m\neq i} w(i \to m)$ and, after defining $\Gamma i/\hbar = -(1/\hbar)$ Im (Δ_i), one gets $|C_i|2 = \exp(1\mathrm{Im}(\Delta_i^{(2)})t/\hbar) = \exp(-\Gamma_i t /2\hbar)$. So that the imaginary part of the energy shift is related to the decay width of f-state belonging to the activated successor complex. In summary, one can write the rate associated to the i-th quantum of the active precursor complex as:

$$\Sigma_{m\neq i}\, w(i \to m) = \Gamma_i/ 2\hbar \qquad (78a)$$

Reducing now the spectra to terms found only in the QIC one gets

$$\Sigma_{if\neq i}\, w(i \to if) = \Gamma_i'/ 2\hbar \qquad (78b)$$

and, assuming the existence of only one resonance at ε_{if} one gets the equation:

$$k_+ = k'_+ * P\to = p(if,T) * \Gamma_i'/ 2\hbar * P\to \qquad (79)$$

where $p(if,T) = \exp(-ß\ \varepsilon_{if}) / Z$, with Z representing the partition function of the QIC and $ß=1/k_BT$ (k_B stands for the Boltzman constant). A form similar to equation (79) has

been used by Lefebvre in a recent treatment of rates as resonance [165]. The resonace state approach to quantum transition state theory has been advocated by Zhao and Rice [186], and Truhlar and Garret [187]. The approach considered here is not based on a classical reaction coordinate idea, neither on a BO scheme. The interesting point suggested by the present work refers to the equivalence of treating the interconversion process as a mechanistic quantum mechanical effect with the more widespread and elegant quantum scattering approaches. The present theory goes beyond the standard transition state theory of reaction rates for thermally activated processess. Even if $P\rightarrow =1$ which would correspond to one of the hypothesis founding the whole TS theory, eq.(79) puts in evidence the quantum mechanical nature of the chemical interconversion.

From the analysis presented above it follows that the chemical interconversion step is essentially quantum mechanical. It is not the passage over a barrier the determining factor, but the population and coupling of the ingoing channel with the virtual quantum mechanical interconversion states. The process is being mediated by the quantum states of the intermediate stationary Hamiltonian.

In the gas phase, the formation of the precursor complex is determined by the collision pattern among the reactants [188-190], however, these do not correspond to the activated precursor complex (APC) in the present theory. Trajectory simulations of SN2 reactions compared with experimental data strongly suggest the existence of non-RRKM (Rice-Ramsperger-Kassel-Marcus) and nontransition state theory effects [191, 192]. Hase and coworkers observe two types of central barrier recrossings, for intermediate recrossings the trajectory appears to linger near the top of the central barrier in what they call two variational transition states, while complex recrossings occur when a trajectory temporarily trapped in the $Cl^{-}+CH_3C1$ complex returns to the central barrier [192]. Experimentally, it is not yet a clearly established the nonstatistical nature of the SN2 reaction [193, 194]. It is worth noticing that from the perspective presented here, the APC, QIC and ASC quantum states would accomplish, when viewed from a classical dynamics perspective, what is called intermediate recrossings, while a relaxation and reactivation would lead to complex recrossings. To solve the problem of "non-statiscality" would require a clear time resolution. It is quite possible that it may depend upon the particular reactant partners.

5. Surrounding Medium Effects on Chemical Reactions: Catalysis

At the beginning of this decade, Zewail and coworkers reported a fundamental work of solvation effect on a proton transfer reaction [195]. α-naphthol and n-ammonia molecules were studied in real-time for the reaction dynamics on the number of solvent molecules involved in the proton transfer reaction from alcohol towards the ammonia base. Nanosecond dynamics was observed for n=l and 2, while no evidence for proton transfer was found. For n=3 and 4, proton transfer reaction was measured at pisosecond time scale. The nanosecond dynamics appears to be related to the global cluster behavior. The idea of a critical solvation number required to onset proton transfer

dynamics has emerged from this and other studies reported by Zewail′s group and others [146, 177].

5.1 .SOLVENT EFFECTS

From a quantum mechanical perspective, the invariance of the quantum transition states is only natural. A carbonyl group, a guanidinium, a nicotinamide fragment, etc., have their characteristic absorption bands. Solvent effects may shift them, they can be broadened, but they are an invariant feature allowing for their identification with analytical tools. These spectral characteristics are pictorially associated with stationary Hamiltonians (in the sense defined above) leading to geometric characteristic parameters: bond lengths, angles, polarizabilities, etc. Solvent effects produce variations in these properties, of course, but they continue to be assigned as properties of the corresponding functional group or chromophore. Being related to a stationary Hamiltonian, the saddle point of index one (SPi-1)defines a geometry around which a particular quantum fluctuation takes place. From a BO view, the system is unstable. But we are working at a general quantum mechanical level, and accordingly, the fluctuations between precursor and successor quantum states may become a quantum coherent state whose lifetime is determined, via its coupling with the electromagnetic field, by its coupling with relaxation channels leading, in the last resort, to products or back to reactants.

The existence of critical solvation numbers for a given process to happen is an important concept. Quantum chemical calculations using ancillary solvent molecules usually produce drastic changes on the electronic nature of saddle points of index one (SPi-1) when comparisons are made with those that have been determined in absence of such solvent molecules. Such results can not be used to show the lack of invariance of a given quantum transition structure without further ado. Solvent cluster calculations must be carefully matched with experimental information on such species, they cannot be used to represent solvation effects in condensed phases.

The reactive fluctuations of the activated complex defined by the precursor and active successor complexes define the chemical interconversion step. The geometries of these complexes are closely related to the geometry of a SPi-1. If we take a simple case for the interconversion step, the solvent may affect the process in different manners. One of the effects that the condensed medium may have on the QIC is to modulate its lifetime. If the solvent fully damps down the fluctuation inside the gas-phase activated complex, the reaction cannot proceed any further. Since we are interested in reactions actually taking place, we assume that reactive fluctuations are modulated by the solvent but not wiped out. A second effect is related to the energy of the QIC with respect to the ingoing reactants and the associated molecular complexes. Inside the QIC, the quantum states corresponding to the active precursor and successor states may be differentially shifted in the energy scale. This would modify the characteristic frequency for the set up of the quantum jumps. Another effect would manifest itself in the strength of the transition matrix element <i‡|H2|f‡>. This effect is a pure quantum mechanical effect.

The quantum mechanical rate k_+ depends upon interactions with the solvent. Statistically averaged interaction effects, including reaction field effects [6] usually result in a shift in the equilibrium distances r1° and r2° with a change in the vibrational spectra due to a renormalization of the force constants. The reactive fluctuations of the activated complex can be coupled with the field fluctuations of the solvent around their static average configurations. Model systems describing such a situation have been proposed and studied in the literature [54, 70, 196-200]. These effects may probably affect the rate by a factor probably less than ten, while the thermodynamic factor K_r can change the situation by order of magnitudes (see below).

Another important solvent effect involves the equilibrium between solvated reactants and solvated active precursor and successor complexes. A solvent favoring the formation of a precursor complex will increase the reaction rate, all other things being equal. In the present view of a chemical reaction in solution, one has to form first a complex having a geometry not too far away from the one characterizing the transition structure in vacuum. If we call E the environment, S the reactants in chemical equilibrium, and $E\text{-}\tilde{S}$ the reactants solvated and having a structure similar the one characterizing the generic QIC without solvent, the following kinetic scheme describes the chemistry:

$$E+S \underset{k_2}{\overset{k_1}{\longleftrightarrow}} E\text{-}\tilde{S} \qquad K_r = [E\text{-}\tilde{S}]/[E][S] = k_1/k_2 \tag{80}$$

The interconversion step with $\tilde{S}i$ and $\tilde{S}f$ standing for the active precursor and successor complexes reads now:

$$E\text{-}\tilde{S}i \underset{k-}{\overset{k+}{\longleftrightarrow}} E\text{-}\tilde{S}f \tag{81}$$

and the relaxation towards products is characterized by the kinetic parameter k_3

$$E\text{-}\tilde{S}f \xrightarrow{k_3} E + P \tag{82}$$

The scheme is valid when products are at zero concentration, since back reaction is negligible. Note that k_+ and k_- are given by eq.(74) including eqs.(76a,b) and related expressions for k'- and k"-. So that the spectra responsible for the interconversion remains invariant, although shifted in the energy scale.

A steady state analysis of these equations produces an expression of the observed rate constant k_{obs} :

$$1/k_{obs} = 1/k_1 + (1/K_r k_+)\{1 + k_- / k_3\} \tag{83}$$

From this equation it can be seen that quantum mechanical effects on the observed rate will be manifest for $k_3 >> k_-$ and $k_2 >> k_+$, where one has the result:

$$k_{obs} \approx K_r k_+ \tag{84}$$

which, incidentally shows, in a clear manner, that the solvent dependency of the observed reaction may manifest itself via the equilibrium constant K_r as well as the quantum mechanical changes produced by the active precursor and successor complexes in their modulation by the solvent and vice-versa.

In practice, it may happen that the kinetics is fully determined by the association process, i.e. $k_2 << k_+$, and $k_{obs} \approx k_1$. This type of reaction is fully solvent dependent but the interconversion step is no longer rate limiting. Still, the heart of the chemistry is contained in the interconversion event.

The complexes E-$\tilde{S}$i and E-$\tilde{S}$f have a geometry not very different from the one characterizing the saddle point of index 1 for the same interconversion process in vacuum [96-98, 172]. This structure enforces a specific stereochemistry. For instance, in the hydrolysis of esters groups, the transition structure is almost tetrahedral around the carbon-center in the carboxyl moiety; in the reactants, the carboxyl moiety is planar, as it is in the product acid. If bulky groups arc hanging to the ester function, they ought to reorganize themselves in order to achieve a geometry of the saddle point of index 1. It is thcrcfore not surprising that the solvent E may play a central role during the kinetics of this process. Implicit in all this discussion is the fact that the environment (solvent) structure is influenced by the reacting species [201, 202]. At the interconversion step and within the APC-IQC-ASC system, solvent fluctuations may act as trapping devices to relax either forward to product or backwards to reactants. The recent work by Parrinello illustrate this point quite neatly [120]. Potential of mean force would fail to detect such dynamical effects.

For transition structures involving chiral centers, if the solvent has no chiral preferences, the reaction may take any of the chiral TS species [203].

5.2.CATALYSIS AS A SURROUNDING MEDIUM EFFECT

The use of the symbol E in 5.1 for the environment had a double objective. It stands there for general environments, and it also stands for the enzyme considered as a very specific environment to the chemical interconversion step [102, 172]. In the theory discussed above catalysis is produced if the energy levels of the quantum precursor and successor states are shifted below the energy value corresponding to the same species in a reference surrounding medium. Both the catalytic environment E and the substrates S are molded into complementary surface states to form the complex between the active precursor complex $\tilde{S}$i and the enzyme structure adapted to it: **E**--$\tilde{S}$i. In enzyme catalyzed reactions the special productive binding has been confussed with the possible mechanisms to attain it: lock-key represents a static view; while the induced fit concept

[204] stands for a dynamic description of how the enzyme-substrate system achieves complementarity. As discussed in previous sections, the geometry attained by the substrate would tend to resemble as much as possible to the geometry characteristic of the stationary intermediate Hamiltonian (leading to the QIC).

In Figure 3 a schematic view is presented of how primary catalysis is achieved. Besides this necessary and sufficient condition required to set up catalysis, there may be some other factors producing an enhancement of the catalytic event. General acid and general base catalytic groups, metal coordination sphere appropriately prepared are examples of catalytic subsidiary effects. The pure molding factor is usually achieved by catalytic antibodies techniques.

There is also a dynamical factor related to the coupling between the fluctuation pattern of the partners in the activated complex E--$\tilde{S}$i. They have to couple in phase so that vibrational energy could flow among these subsystems. The enzyme should not bind the transition state so tight that the reactive fluctuations can take place. Thus, for example, high pressure applied to the structure may deform the protein and perturb the surface complementarity. This idea makes sense if the geometry of the saddle point is invariant. And such invariance is a key element of the present approach. It is possible that with present computing schemes the quantum spectra is not well represented at the adiabatic level, but one may expect that the geometry is less sensitive [205] so that one get it correctly from quantum chemical calculations of stationary saddle points of index one. Fluctuations of electric fields in enzyme active sites have been suggested as an efficient source of reaction activation [206].

Thus, surface complementarity towards the SPi-1 (calculated in vacuum) is a necessary condition to produce catalysis. In many cases it may turn out to be sufficient. For instance, the results with a fully mutated Serine protease suggest that the enhancement can be about a factor of 10^3 with respect to the same reaction in solution [172] if the mutated protein binds the substrate with a geometry in a neighborhood of the characteristic geometry of the QIC of the wildtype. This idea has a counterpart in the transition state analogue [204, 207] akin to the standard transition state theory. The principal difference resides in the fact that our theory implies a molding of the substrates into a geometric setup compatible with the SPi-I. For us, the catalysts bind the substrates in specific activated geometries thereby opening the channels towards the interconversion quantum states. This process is general for the class of reaction using interconversion Hamiltonians.

The surface complementarity between the quantum activated complex and the catalytic surrounding media is the main idea of the present theory. The oscillating stereochemical control of the synthesis of thermoplastic elastomeric polypropylene recently reported by Coates and Waymouth [208] can be easily interpreted in terms of catalyst changing surface complementarity. Hill and Zhang have discovered a molecular catalyst that experiences a kinetic and thermodynamic drive for its own reassembly and repair under conditions of catalysis [209]. This is basically what an enzyme does when moving from the apo-structure towards the catalytically apt conformation.

In water, there are many reactions that are disfavoured. In terms of our scheme (Cf.Fig.3) the quantum activated complex may even have an energy above the one obtained in vacuum. In order to increase the rate of this process process, an environment is required that trap the complex with net free energy below the reference reaction (E+S in the figure). This is what Shabat et al., have accomplished by using catalytic antibodies [210] that help trap the reactants into active precursor-like geometries, thereby displacing the equilibrium towards the interconversion region. The reaction is not only catalyzed by the interconversion step protected from hydrolysis leading to unwanted side reactions otherwise. This is perhaps one of the most spectacular examples reported so far that can be interpreted as a trapping of the active precursor-like geometry, see also Danishefsky [211]. Lerner and coworkers [212] have provided with an example of control and catalysis in cationic cyclization reactions.

Figure 4 can be used to discuss solvent effects on the SN2 reactions. In the gas phase, the complexes may have an energy below the reference state. The reaction takes place via excited states of the QIC and active precursor and successor complexes. The reactant by passing over the quantum states generated at the bottom by the precursor, QIC and successor states must jump (resonance) into the precursor quantum states which in turn would open the product channel via the QIC-states. It is then apparent that relaxation (by photon emmission for instance) from the precursor and/or successor quantum states would produce such complexes in vibrationally excited states. If the energy of the product channel is below the entrance channel, the product may collect energy in one ot its vibrational states. Solvent effect on this reaction produces a high solvation of the ions in the ingoing and outgoing channels, while the species mediating the inter-conversion are less well solvated. This has been computationally illustrated in several occasions [213-215], and in particular, it was shown that under supercritical conditions the barrier is found to be intermediate between ambient water and gas phase in the Cl- and CH3Cl system [216].

6. Computer Simulations: An Overview

In the quantum mechanical continuum model, the solute is embedded in a cavity while the solvent, treated as a continuous medium having the same dielectric constant as the bulk liquid, is incorporated in the solute Hamiltonian as a perturbation. In this reaction field approach, which has its origin in Onsager′s work, the bulk medium is polarized by the solute molecules and subsequently back-polarizes the solute, etc. The continuum approach has been criticized for its neglect of the molecular structure of the solvent. Also, the higher-order moments of the charge distribution, which in general are not included in the calculations, may have important effects on the results. Another important limitation of the early implementations of this method was the lack of a realistic representation of the cavity form and size in relation to the shape of the solute.

These problems were partially solved through the inclusion of multipole expansions in ellipsoidal cavities [23] or through the use of the polarizable continuum method

(PCM) [217]. In the latter, the solute molecule is divided into atomic overlapping spheres, each of which has the dielectric polarization on its surface due to the electrostatic potential on the surface created by the charge distribution on that particular atom and the other atoms in the molecule. The electrostatic reaction field in this case is obtained by a direct numerical integration. In spite of the known deficiences of the continuum methods in many cases, thermo-dynamical properties of solutions, for instance ΔG_{sol} and related quantities, can be conveniently treated by this approach, both at the *ab initio* and semiempirical levels, yielding results that are within the range of experimental errors [8, 11, 12, 218, 219]

The alternative theoretical scheme for studying chemical reactivity in solution, the supermolecule approach, allows for the investigation of the solvation phenomena at a microscopic level. However, it does not enable the characterization of long-range bulk solvent forces; moreover, the number of solvent molecules required to properly represent bulk solvation for a given solute can be so large that to perform a quantum chemical calculation in such a system becomes prohibitively expensive .

Most of the theoretical works concerning dynamical aspects of chemical reactions are treated within the adiabatic approximation, which is based on the assumption that the solvent instantaneously adjusts itself to any change in the solute charge distribution. However, in certain conditions, such as sudden perturbations or long solvent relaxation times, the total polarization of the solvent is no longer equilibrated with the actual solute charge distribution and cannot be properly described by the adiabatic approximation. In such a case, the reacting system is better described by non-equilibrium dynamics.

Based on the continuum solvent model approach, a self-consistent reaction field model to calculate frequency-dependent molecular properties as well as electronic excitation energies and transition moments of solvated molecules was recently developed in terms of single-configuration self-consistent field (SCF) or multiconfiguration self-consistent field (MCSCF) electronic wave functions [220]. This method takes into account the response of the reference state to a time-dependent perturbation. Since in this case the energy is not stationary, the Frenkel's variation principle in the form of the Ehrenfcst's equation was used to derive the expressions for the time-depcndent response. In this model, the solute is enclosed in a spherical cavity embedded in the solvent, which is assumed to be a linear, polarizable, homogeneous, isotropic dielectric medium with a macroscopic frequency-dependent dielectric constant. The total polarization vector of the solvent is decomposed into two components: the optical polarization vector - which responds instantaneously to changes in the solute charge distribution inside the cavity - and the inertial polarization vector - which has a relaxation time, characteristic for the solvent, which describes how fast the inertial polarization vector changes as a consequence of sudden changes in the charge distribution within the cavity. To describe the response of the solute-solvent complex to a high frequency time-dependent perturbation, it is assumed that the electronic response of the solute molecule is slower than the optical polarization and faster than the relaxation time of the inertial

polarization. The system is described by a multiconfiguration self-consistent reaction field (MCSCRF) wave function, with a set of configuration state functions (CSF), which is fully optimized, thus satisfying the generalized Brillouin theorem. A time-dependent perturbation is applied to the system and the time evolution of the electronic wave function response is determined by requiring Ehrenfest's theorem to be satisfied through each order of the perturbation. The poles of the response function give the transition energies of the unperturbed system and the residues give the transition moment, thus allowing for the determination of the excitation energies and transition moments from the MCSCRF reference state to the excited states. This method has been applied to calculate electronic excitations, transition moments and frequency-dependent polarizabilities of a solute molecule in a series of dielectric media. The multipolar expansion of the solvent interaction energy was truncated at the seventh order multipole. The results showed that the properties of the outer dielectric medium can have a substantial effect on the solute molecular properties. Electron correlation was found to be important; also, the solvent effects cannot be described by correcting vacuum values with the aid of scalar factors [221].

The polarizable continuum model (PCM) of Miertus and Tomasi was recently modified to account for non-equilibrium effects due to the delay of solvent synchronism in a chemical reaction, through a proper representation of the boundary conditions associated with the solvent cavity [222]. Expressions to determine the nonequilibrium surface charge distribution were derived as a sum of the electronic (inertialess) polarization effects acting on the solvent molecules and the slower orientational and vibrational (inertial) motions of the molecular component of the medium. The continuous charge distributions were represented by a set of discrete point charges defined over the cavity surface; expressions were thereafter obtained to determine the nonequilibrium surface charge distribution required to derive the reaction potential, the solute wave function and the free energy of the system. This formalism was tested by studying the photoionization and electronic transition processes of ions and molecular solutes. Simplified models of the changes occurring in the orientational component of the solvent polarization during the characteristic time of an elementary reaction step were tested on the S_N2 reaction of fluoride ion with methylfluoride [222, 223].

The multicavity SCRF method developed by Karelson *et al* [114] was applied to calculate the hydration energies of the proton, hydroxyl ion and several inorganic ions [224]. Each hydrated complex was divided into five spheres, corresponding to the central atom and four water molecules of the first coordination sphere. The energy for cavity-formalion was accounted for by using scaled particle theory. The calculated total hydration energies, which includes both the quantum-chemical and the cavity formation contributions, was found to be in excellent agreement with experimental results. Studies were recently reported [225] on solvent reorganization and donor/acceptor coupling in electron-transfer processes. See also [226].

Based on the discrete solvent approach, a perturbed hard fluid model was developed to study dissociation reactions [227]. In this model, the solute-solvent interactions are

separated into repulsive hard sphere and mean field attractive contributions. Lennard-Jones potentials are used to represent the solute-solvent atoms and solvent-solvent interactions. Thermodynamics quantities can be computed within this scheme from the excess chemical potential change, which is related to the excess partial molar Gibbs free energy change, by using standard thermodynamics relations. The only adjustable parameters in this model, which represents the reactant and product attractive mean field coefficients, can be derived using simulation results at a single temperature and density. The hard fluid model was applied to quantitatively estimate repulsive contributions to solvation [228]. The excess solvation free energy of an atomic or molecular solute in a real liquid represents the reversible work required to introduce a fixed (zero kinetic energy) solute into solution. This energy for hard sphere solutes of various sizes and also the cavity size distributions in water and apolar organic solvents were calculated. The theoretical predictions were favorably compared, in most of the cases, with both computer simulation and rare gas solubility measurements. Some discrepancies were found when comparing hard fluid model predictions with simulation results, which may reflect details of the liquid structure arising from the nonspherical shape of real solvent molecules. The hard fluid model was also used to estimate the repulsive contributions to the excess free energy of solutions of atoms and molecules in water and *n*-hexane. The results indicated that the larger repulsive solvation energies in water than in *n*-hexane can be accounted for by the hard sphere model, which has no orientational order. According to the authors of this paper, this implies that hydrophobic hydration may have more to do with the translational order (or packing) than with the orientational order (or hydrogen bonding structure) of water around a solute.

6.1. SOLVENT EFFECTS AND CHEMICAL REACTIONS

Alternative approaches to simulate reactions in solution have been proposed by Warshel′s group [229], in which the system is partitioned into an inner region, which typically consists of solute molecules and is treated by quantum mechanical methods, and a surrounding region, corresponding to the solvent molecules, which is represented either by classical or by pseudopotentials at several levels of approximation. The replacement of the solvent classical potential by a pseudopotential is expected to provide an insight into the effects associated with the delocalization of the solute electrons on the solvent molecules. The calibration of the parameters in the potential can be achieved using results either from *ab initio* or density-functional calculations, or experimental data. The combined quantum/molecular mechanical potential and forces calculated at each step can be used in classical [60, 109] or free-energy perturbation molecular dynamics simulations [229].

Another similar approach applies an explicit density-functional theory treatment to the solute molecules, while representing the contribution of the solvent molecules as an effective potential [105].

An alternative reaction-field approach to the calculation of molecular electronic

structure, solvation energies and pK_a values was proposed [230]. In this work, the reaction potential is computed from a finite-difference solution to the Poisson-Boltzmann equation using an overrelaxation algorithm and numerical grids; the solute electronic structure is computed by density functional methods and self-consistency between the reaction potential and the electronic structure is iteratively achieved. The effective electron-electron interaction in the density functional approximation here considered is taken to be the Green function of the Poisson equation. This function is divided into a gas-phase-like Coulomb part and a remainder part, which represents the effect of the solvent. An iterative procedure brings the gas-phase and solvent parts of the calculation to self-consistency. Gradient corrections for the correlation and exchange functionals are added in the self-consistent cycle that determines the molecular electron density. Proton affinities, solvation energies, solvated dipole moments and absolute pK_a values were calculated for a variety of small organic molecules. The reported gas-phase results appear to be competitive with the best available *ab initio* ones, and the solvation energy estimates are comparable in quality with other models in which the solute is quantum-mechanically described.

The DFT approach has been applied to the study of small hydrated proton clusters [231]. The Perdew nonlocal potential for electron exchange and correlation was used in the calculations. The optimized structures of the clusters up to $H_{13}O_6^+$ were calculated; the corresponding harmonic vibrational frequencies and IR intensities were computed and compared with high resolution experimental data. A very good agreement with experience was obtained. Proton transfer barriers in clusters in aqueous solution were computed for a few model systems and the sensitivity of the calculations to the partial charges used was assessed. A combined *ab initio* density functional and molecular dynamics simulation was carried out to calculate the free energy of proton transfer. The barrier was found to be 3 kcal/mol higher than in the gas phase and very large solvent fluctuations were observed during the simulation.

Truhlar and coworkers [29, 232, 233] have proposed a quantum-mechanical-continuum dielectric model for aqueous solvation. This method is discussed by Truhlar and coworkers in Chapter I.

A combination of the quantum chemical PSGVB package (which performs *ab initio* quantum chemical calculations at the generalized valence bond/perfect pairing (GVB-PP) level) with the Delphi program (which yields a numerical solution to the Poisson-Boltzmann (PB) equation) has been recently proposed [234]. The continuous gas-phase charge distribution of the molecular solute obtained from the quantum chemical wave functions was replaced by atomic point charges at the atomic centers, obtained by fitting the former using a least-square criterion. These charges were passed to Delphi and then passed back to PSGVB, which solved the electronic structure equations in the electrostatic field of the point charges, i.e, in the presence of' the reaction field. The PSGVB and Delphi calculations were iterated until convergence was achieved. The electrostatic contribution to the solvation energy (E_{el}) was then obtained

as the difference between the gas-phase and solution-phase quantum chemical energies. Accurate gas-phase charge distributions for 29 small molecules representing a variety of functional groups were produced. Solvation energies that agree with experiment with an average error of 0.6 kcal/mol were also obtained, except for methylated and unmethylated primary amines and amides, which were systematically too low by 1-2.5 kcal/mol .

A combined quantum mechanical-configuration interaction and molecular mechanics (QM-CI/MM) method was developed [126, 235] to study solvatochromic shifts of electronic transitions. The condensed-phase system was partitioned as usual into distinct regions: quantum mechanical calculations were performed to treat the region consisting of solute molecules, while classical, empirical potentials in statistical mechanical simulations were used to represent the surrounding solvent molecules. Standard self-consistent field (SCF) Hartree-Fock (HF) equations were initially solved for the solute molecules and the HF wave-function was used as the reference state to build the CI (configuration interaction) wave function. The CI matrix was built and diagonalized, from which models of the ground-state and excited-state energies, as well as eigenvectors of the condensed-phase system, were obtained. The Monte Carlo Metropolis sampling was based on the ground-state CI potential energy; solute-solvent interaction energies for both the ground and excited states were determined by employing the corresponding one-particle density matrix of the CI wave function. A new configuration was then generated by randomly moving the solute, a solvent molecule or the volume and the procedure was repeated. Finally, the ensemble average and statistics were analyzed. This technique was applied to simulate solvent effects on the n-->π^* spectral shifts of acetone in water, methanol, acetonitrile, chloroform and carbon tetrachloride. The qualitative trend of solvent effects on the solvatochromic spectral shift of acetone in polar solvents was found to agree with experiments, while quantitative estimates were greater than the experimental values; however, the experimentally-observed red shift in the S_o->S_1 excitation of acetone in CC14 was not predicted because the mutual solute-solvent dispersion interactions were not included in this model.

The several theoretical and/or simulation methods developed for modelling the solvation phenomena can be applied to the treatment of solvent effects on chemical reactivity . A variety of systems - ranging from small molecules to very large ones, such as biomolecules [236-238], biological membranes [239] and polymers [240] – and problems – mechanism of organic reactions [25, 79, 223, 241-247], chemical reactions in supercritical fluids [216, 248-250], ultrafast spectroscopy [251-255], electrochemical processes [256, 257], proton transfer [74, 75, 231], electron transfer [76, 77, 104, 258-261], charge transfer reactions and complexes [262-264], molecular and ionic spectra and excited states [24, 265-268], solvent-induced polarizability [221, 269], reaction dynamics [28, 78, 270-276], isomerization [110, 277-279], tautomeric equilibrium [280-282], conformational changes [283], dissociation reactions [199, 200, 227], stability [284] - have been treated by these techniques. Some of these applications will now be reviewed.

6.2. ELECTRON AND CHARGE TRANSFER PROCESSES

Electron and charge transfer reactions play an important role in many chemical and biochemical processes. Dynamic solvation effects, among other factors, can largely contribute to determine the reaction rate of these processes and can be studied either by quantum mechanical or simulation methods.

Strong interactions are observed between the reacting solute and the medium in charge transfer reactions in polar solvents; in such a case, the solvent effects cannot be reduced to a simple modification of the adiabatic potential controlling the reactions, since the solvent nuclear motions may become decisive in the vicinity of the saddle point of the free energy surface (FES) controlling the reaction. Also, an explicit treatment of the medium coordinates may be required to evaluate the rate constant pre-exponential factor.

The reaction rate constant for the SN2 reaction of chloride ion with methylchloride in water was calculated within the SCRF framework by considering the FES cross section in the coordinate subspace including coordinates of both the reacting solute and the medium [79]. This approach allowed the subsequent evaluation of the transmission factor χ by the stochastic dynamical theory. The FES cross sections along the medium coordinate appeared to be single-well-shaped curves, even those obtained after the separation of the noninertial polarization. At the saddle point, all of the calculated cross-sections coincided; however, the cross-section in the total polarization space may differ from the latter by several kcal/mol when far away from the saddle point. A classification scheme for the mechanism of charge transfer reactions in polar solvents was proposed by the authors. According to this scheme, the reactions which proceed via a single-well shaped TS suffer little influence from the solvent molecules, the motion along the solute reaction coordinate being the driving force of the reaction. On the contrary, a double-well shaped TS is related to reactions which proceed through an electron-transfer mechanism.

The dynamics of carbon-halogen bond reductive cleavage in alkyl halides was studied by MP3 *ab initio* calculations, using pseudopotentials for the halogens and semidiffuse functions for the heavy atoms [104]. The effect of solvent was treated by means of the ellipsoidal cavity dielectric continuum model. Both a concerted (i.e., a one-step) and a stepwise mechanism (in which an anion radical is formed at first) were investigated, by calculating the energy of CH_3X and $CH_3X^{\cdot -}$ as a function of the distance carbon-halogen taken as the reaction coordinate. A comparison between the reductive cleavage of methyl- and perfluoromethyl chlorides was also performed; in this case, a full basis set was used, instead of a pseudopotential. The reaction profiles were quite similar to the preceding ones in the range of small and medium C-C1 distances. However, at large C-Cl distances, the CF_3C1 anion energy profile exhibited a clearly marked minimum, indicating a stepwise mechanism in the gas phase, in contrast with CH_3Cl, for which a transition state (TS) characteristic of a concerted mechanism was

determined. The effect of a polar solvent on the bond breaking profiles was also simulated; the results showed that these profiles remained almost unchanged in the case of the neutral molecules, whereas the anionic states were largely stabilized. The stabilization increased along the C-C1 distance, leading to an energy profile that decreases monotonically along the reaction coordinate. Thus, in the presence of a polar solvent, the carbon-halogen bond reductive cleavage of the perfluoromethyl chloride changes from a stepwise to a concerted mechanism, in agreement with previous electrochemical results.

6.3. ULTRAFAST SPECTROSCOPY

In this type of phenomena, electronic degrees of freedom are strongly coupled to the solvent instead of being completely delocalized as in the gas phase. This solute-solvent coupling results in an intense, broad electronic absorption, thus enabling the study of the dynamics of the solvation process involved in electron transfer and other chemical reactions. Different pictures concerning the nature of the solvent fluctuations coupled to the hydrated electron can be drawn from studies using different experimental techniques. Photoinjection of electrons into neat liquid water indicates that equilibrium solvated electrons are formed very rapidly (on the picosecond time scale); the equilibrium spectra is recovered nearly instantaneously upon nonadiabatic relaxation to the ground state [285-288]. However, in transient hole-burning spectroscopy (THB) experiments, in which the photoexcited electrons have the equilibrium solvation structure, spectral transients are found which persist for a few picoseconds [289, 290]. Nonadiabatic quantum molecular dynamics simulations of the excess electron solvation dynamics [291] and photoexcited equilibrium hydrated electrons [252, 253] have been performed in order to provide a better understanding of these phenomena. In the former work, the effects of molecular vibrations on the excited state lifetime of excess electrons, the relaxation dynamics and the influence on equilibrium spectroscopy were examined, while the latter works have addressed the problem of investigating the solvation dynamics following photoexcitation of the hydrated electron. In both cases, the hydrated electron-water interactions were modelled with a pseudopotential. The water-water interactions were represented by a simple point charge (SPC) model in which intramolecular flexibility was added to the standard SPC intermolecular potential. An algorithm including state-to-state transitions was used to represent the nonadiabatic transitions corresponding to a breakdown of the BO approximation. Nonadiabatic and ground state simulations were performed [291] and the relaxation from low lying excited states was followed. Two qualitatively different types of trajectories were found in this case, one of which cascaded quickly to the ground state, while the other trajectories were trapped for some period of the time in the lowest excited state. On the other hand, all of the calculated trajectories for the simulation of the dynamics of photoexcited equilibrium hydrated electrons, including those which were promoted to the second excited state upon excitation, presented qualitatively similar behavior, the solvent relaxation acting to raise

the energy of the ground state instead of lowering the energy of the excited states [252]. In this case, the strong coupling of the electronic eigenstates to aqueous solvent fluctuations made evident both by the fluctuations of the hydrated electron energy levels, which are comparable to the spacing between them, and by the enormous shift of the quantum energy gap (about 75% of the initial excitation energy) following excitation. Much of the local change in solvation structure was associated with a significant change in both size and shape of the electron upon excitation, as shown by the dynamic evolution of the solvent cavity containing the electron. These works have shown the relaxation of the quantum energy gap due to solvation to be directly related to the dynamics of non radiactive decay of the excited state electron, as well as to the differing relaxation pathways observed between electron photoinjection and transient hole-burning photoexcitation experiments. The results obtained in these simulations were further compared with available ultrafast laser experimental data [251]. The two-steps relaxation mechanism proposed to account for the simulation results has proved to be consistent with the experimental data. Moreover, alternative mechanisms proposed on the basis of the experimental results were shown to be accounted for in this mechanism.

6.4. ORGANIC REACTIONS

From a theoretical viewpoint, the effect of aqueous solvation in organic reactions has received considerable attention in recent years. These studies have gone a step beyond analysis of simple models to consider reactions such as SN1, SN2, cycloaddition reactions and CIaisen rearrangement, for instance, with more realistic models.

A coupled quantum mechanical/molecular dynamics scheme was used to examine the S_N1 splitting in water of the (neutral) tert-butyl chloride yielding two charged fragments [241]. In order to obtain the aqueous phase reaction profile for this reaction, potential of mean force calculations, using two different approaches to correct for the neglect of long-range electrostatic interactions, were performed. A good agreement with the experimental results was obtained when the Born correction for the generated ions was applied, except for the intimate ion pair formed in the first step of the proposed fragmentation mechanism, which appears to be too deep. At short C-C1 distances, the reaction profile obtained with the use of scaled charges correction also presented the expected behavior; however, as the reaction progressed to greater C-C1 separation, the energy of the system continued to drift downward, instead of rising as expected. Overall, the model using the Born correction seemed to be the most reasonable one. The solute and solvent structures along the MD trajectory have also been examined. Near the equilibrium C-C1 separation, little or no solvent structure around the solute was found. However, as the two product fragments are separated from each other, a very clear solvent structure became evident, the water molecules clustered about the chloride ion having their positively charged protons directed towards the anion. Specific interactions between the tert-butyl cation and the solvent were also observed.

The possible reaction paths of the cycloaddition reaction between ketenes and

aldehydes to form 2-oxetanones was studied by *ab initio* calculations [242] with the aim of understanding the origins of the abnormally low stereo-selectivity of this reaction, as well as the influence of the solvent and Lewis acid catalyst on the mechanism. The solvent effects were examined with the aid of the ellipsoidal cavity continuum model. A resonably synchronous transition state (TS) was located and characterized in the initial gas-phasc potential energy hypersurface. Two possible orientations (exo and endo) of the TS were examined and the authors arrived at the conclusion that monosubstituted ketenes should interact exclusively through exo TS's, at least in the gas phase. The catalytic effect of a Lewis acid on this cycloaddition reaction was investigated by using a formaldehyde-BH_3 complex. The calculated saddle point in the catalyzed reaction corresponded to a relatively early and asynchronous zwitterionic TS, in which the BH_3 moiety was bonded to the carbonyl oxygen of the aldehyde and adopted an exo disposition with respect to the 2-oxetanone ring being formed. A concerted two-steps reaction mechanism was therefore envisaged. A decrease in activation energy was found with respect to the non-catalyzed reaction. Upon introduction of the solvent effects using both the Onsager and the ellipsoidal cavity models, the activation and reaction energies did not vary significantly with respect to the gas-phase reaction. However, the main features of the exo TS differed significantly from the in vacuo results: this TS was slightly earlier and more synchronous than its gas-phase analog. The shape of the solvated TS explained the change in stereoselectivity observed in the catalyzed reaction, leading to the preferential formation of cis 2-oxetanoncs when bulky Lewis acid catalysts are used.

The Claisen rearrangement is an electrocyclic reaction which converts an allyl vinyl ether into a γ,δ-unsaturated aldehyde or ketone, via a (3.3) sigmatropic shift. The rate of this reaction can be largely increased in polar solvents. Several works have addressed the study of the reaction mechanism and the electronic structure of the transition state (TS) by examining substituent and solvent effects on the rate of this reaction.

The reaction coordinate of the Claisen rearrangement of allyl vinyl ether in the gas-phase and in aqueous solution was calculated in order to determine the effect of hydration on the free energy of activation for this reaction [292] and also the influence of multiple conformational states for the reactants [293]. *Ab initio* calculations at the RHF/6-31 G(d) level were used to locate the transition state(s) (TS) for the reaction and to obtain a minimum energy reaction path. The reactants partial charges along it, which are needed for the potential functions that describe the intermolecular interactions between the reacting system and the solvent molecules, were also calculated. Solvent structures were chosen along the gas-phase reaction coordinate and a Monte Carlo simulation with statistical perturbation theory was carried out to generate the aqueous reaction coordinate. Estimates of the relative free energies of hydration for the reactants, TS and products were obtained. The increased hydration of the TS as compared with the reactants was assumed to account for the rate increase by a factor of 664 over the gas-phase reaction. This observed hydration effect was related to an increase of the number and strength of the solvent hydrogen bonding to the ether oxygen in progressing from the reactants to

the transition state. This effect arose from an increased accessibility of the oxygen atom in the TS and also from an increase in its partial charge. The effect of including multiple conformational states for the reactant on the free energies of activation were found to be small and similar in the gas phase and in water.

The effect of solvation by water on the Meyer-Schuster reaction [202] and di-*n*-butyl ether-water on the Claisen rearrangement of allyl vinyl ether was studied by a number of variants of the continuum models combined with *ab initio* wave functions [244]. The gas phase barrier for this reaction was predicted via a density functional method including electron correlation, while both Hartree-Fock and DF wave functions were used to model solvation. In the latter case, the strategy of solvating stationary point structures determined for the gas phase reaction was followed, according to the same procedure followed previously by Severance & Jorgensen [292]. Three continuum models were used to predict solvent effects on the barrier height of the reaction: (i) a spherical solvent cavity, (ii) an ellipsoidal cavity and (iii) the polarizable continuum method (PCM) . At the Hartree-Fock level, the PCM approach was seen to give results closest to the experimental ones both for solvation in water and di-n-butyl ether; however, the experimental barrier height reduction may be somewhat underestimated for water solvation. Electron correlation was found to affect the transition state (TS) more than the ground state energy; such barrier lowering is reflected in the reduced polarity of the TS compared with that of the ground state and leads to a reduction in the calculated differential solvation energy.

A theoretical study at a HF/3-21G level of stationary structures in view of modeling the kinetic and thermodynamic controls by solvent effects was carried out by Andres and coworkers [294]. The reaction mechanism for the addition of azide anion to methyl 2,3-dideaoxy-2,3-epimino-α-L-erythrofuranoside, methyl 2,3-anhydro-α-L-crythrofuranoside and methyl 2,3-anhydro-β-L-erythrofuranoside were investigated. The reaction mechanism presents alternative pathways (with two saddle points of index 1) which act in a kinetically competitive way. The results indicate that the inclusion of solvent effects changes the order of stability of products and saddle points. From the structural point of view, the solvent affects the energy of the saddles but not their geometric parameters. Other stationary points geometries are also stable.

6.5. CHEMICAL REACTIONS IN SUPERCRITICAL FLUIDS

Supercritical water (SCW) presents a unique combination of aqueous and non-aqueous character, thus being able to replace an organic solvent in certain kinds of chemical synthesis. In order to allow for a better understanding of the particular properties of SCW and of its influence on the rate of chemical reactions, molecular dynamics computer simulations were used to determine the free energy of the S_N2 substitution reaction of Cl^- and CH_3Cl in SCW as a function of the reaction coordinate [216]. The free energy surface of this reaction was compared with that for the gas-phase and ambient water (AW) [248]. In the gas phase, an ion-dipole complex and a symmetric transition

state were found. In AW, the minima corresponding to the ion-dipole complex essentially disappeared as a consequence of the weakning of the nucleophile-water hydrogen bond interaction, which offsets the energy of ion-dipole interaction. The free energy barrier in SCW was found to be close to that in AW, in spite of the large differences in solvent density and dielectric constant among them; however, a slight minimum is present in SCW, corresponding to the ion-dipole complex. The activation barrier in SCW is only 1 kcal/mol higher than that between reactants and the transition state; therefore, there is an equilibrium between the reactants and the ion-dipole complex. The potential of mean force for this reaction in SCW was further compared with that for an organic polar solvent, dimethylformamide (DMF) [216]. The activation barrier and the well for the ion-dipole complex in SCW lie between those in AW and DMF, even if the dielectric constant is 9.7.5 for SCW, 78 for AW and 38 for DMF. Angle averaged cylindrical resolved distribution functions for the water molecule near the solutes at the geometries of the separated reactants, ion-dipole complex and transition state were calculated. The solvation is dominated by electrostatic forces, since a clear preference for the water molecules to solvate the ion versus the dipole was observed. Detailed structural information about the changes in coordination number and hydrogen bonding with both density and temperatures for solutes of varying charges was also obtained. Even though the coordination number remains high, the number of hydrogen bonds from AW to SCW decreases as the hydrogen bond strength increases for the solute series from Cl' and Cl in the transition state, to Cl^- in the ion-dipole complex and finally to free Cl^-.

Hu and Truhlar have recently reported a modeling transition state solvation at a single-water representation [295]. Recent experimental advances leading to the study of SN2 reactions of gas-phase microsolvated clusters which can advantageously been studied with ab initio electronic theory. These experiments and theoretical studies are quite relevant to chemical reactions in supercritical water.

Homogenous catalysis in supercritical fluids has recently been reviewed by Noyori and coworkers [250].

7. Discussion

The theory of solvent effects on standard solutes and on chemically reacting species has been developed in this chapter. Some shortcomings related to the Born-Oppenheimer view that are important at the interconversion domains have been discussed. A quantum theory of chemical interconversion in the gas-phase and in passive solvent media has been introduced. This is an extention of our earlier ideas [43].

By using an intcrconversion coordinate, it is shown that degeneracies of reacting states on the BO-scheme are only apparent crossings. The concept of electro-nuclear fluctuation has been used in connection with reactant quantum states at the energy degeneracy regions. The expectation values of the interconversion coordinate with the degenerate quantum states have values allowing for a differentiation (along this axis) of

these states. The chemical interconversion process appears to be a quantum jump between quasi degenerate states that have non-zero transition moments. The near zero-frequancy photon field created by the thermally equilibrated system acts as the coupling source among the quantum molecular states.

The theory goes beyond standard inolecular orbital and valence bond approaches. The stationary Hamiltonians having no ground state play a central role. Their energies are solvent dependents, while their geometries appears to be conserved within reasonable bounds. Calculations using ab initio and semi empirical methods and different model systems show that the geometries are a rather robust entity. Of course, in standard valence bond and molecular orbital approaches there is an apparent shift of the saddle point for results ploted along the reaction coordinate. Using the interconversion coordinate concept and active precursor and successor complexes the invariance aspect is more easily observable in actual calculations. Normally, the distance between donor and acceptor centers for precursor and successor complexes are different among themselves and they are different from the distance characteristic of the SPi-1. It is therefore logically inconsistent to directly compare precursor and succesors. The introduction of activated precursor and successor complexes built around the geometry of the SPi-1 solves the logical inconsistency and allows for the study of the quantum interconversion (in a region where there will be a minimal geometric deformation [167]). The standard approach leads to the classical concept of reaction path, while in the present view such an idea is foreign. The success in obtaining kinetic isotope effects with our approach is based on this new idea [94, 96, 174].

The theory of rates has been dominated by the transition state theory. Following Laidler and King [37], the essential features of this theory can be summarized as follows: (i) Rates can bc obtained by focussing attention on the activated complex, which lies at the saddle point of the potential energy surface; (ii) The activated complex is in a state of “quasi-equilibrium” with the reactants; (iii) the motion of the system at the saddle along the “reaction coordinate” can be treated as a free translational motion. In the present theory, point (iii) is completely rejected, while (i) and (ii) are modified. For unimolecular processes, the RRKM theory has played an important role in interpreting experimental data [296]. Being an statistical theory, there is no need for detailed information concerning the intramolecular dynamics. Most important is the assumption of a critical configuration separating internal states of the reactant from those of the products. Classically, this configuration represents a dividing surface parting the phase space of reactant and product. It is assumed then that a crossing of this surface occurs only once, the system thereafter proceeds towards products. In the theory presented in this paper, the concept of critical configuration is retained (it would correspond for a given R-region distance to the optimized geometries obtained along the interconversion axis, each one obtained from model wavefunctions of reactant and product), but the quantum jumping among states eliminate the classical view found in the RRKM approach. The interconversion process cannot be reduced to an adiabatic process. On the contrary, energy relaxation inside reactant or inside product channels can be modeled

with adiabatic procedures. This latter subject has extensively been analyzed in the literature [26, 38, 166, 297-300],

The introduction of at least one interconversion process (step) having a nature different from the activation-relaxation processes found along the reactant and product channels allows for a distinction between rate-related and mechanistic-related processes among quantum states. A simple reaction is defined by the existence of only one interconversion step. A real chemical reaction can, in principle, be decomposed in a series of simple reactions.

It is worth noticing that quantum reactive scattering theory, semiclassical scattering theory and reduced dimensionality theory of quantum reactive scattering treat this problem in a different manner [21, 159, 160, 163, 301, 302]. The BO scheme is used throughout. In our theory, the quantum states of the precursor and active precursor can be adiabatically related (in principle all those states belong to the same stationary Hamiltonian), while there is no adiabatic process leading to a change of quantum state (in particular at the QIC). In words of Polanyi and Zewail [303], " 'the transition state' ... illustrate the mystical event of trans-substantiation". In the present theory, this state is just the site where quantum mechanics reigns.

The present approach sets the chemical mechanism at focus. We have subscribed to a variant of the idea that the so called transition state is "a molecule like any other" [304]. But, at variance with Forst, the molecule in our view is characterized by a stationary Hamiltonian with no electronic ground state. It shares with any other molecule the fact that their excited states have finite lifetimes. Then, postulating the quantum interconversion complex is not entirely pointless exercise since it helps organize a good deal of general linear free energy relationships [172]. The invariance of its geometry and the principle of surface complementarity gives a simple explanation to enzyme evolution. The primary function of the enzyme would be to trap the substrates (reactants) by molding them into a geometry as similar as possible to any one the APC--ASC structures. As in normal molecules, there are "equilibrium" distances and angles that appear to be fairly invariant, and in this sense one can talk about standard geometrical parameters for transition structures in enzyme molecular mechanism. Since, for a given mechanism, the APC-IQC-ASC quantum region is unique, the enzyme via an adaptive process tend to deform the reactants into a zone as proximal as possible to this fundamental triad [43].

Acknowledgments. The authors are most grateful to V.Moliner for helping with the figures, JA acknowledges continued financial support from Conselleria de Educacio i Ciencia de la Generalitat Valenciana, Ministerio de Educacion y Ciencia y Ministerio de Asuntos Exteriores de España and Fundacio Universitat Jaume I-Bancaixa. OT is most grateful to NFR for financial support. FLMGS acknowleges a grant from the Swedish Institute.

References

1. Tapia, **O.** (1980) Local field representation of surrounding medium effects. From liquid solvent to protein core effects, in Daudel, R., Pullman, A., Salem, L. and Veillard, A.(eds.), *Quantum theory of chemical reactions*, Reidel, Dordrecht,pp.25-72.

2. Tapia, **O.** and Johannin, G.: An inhomogeneous self-consistent reaction field theory of protein core effects. Towards a quantum scheme for describing enzyme reactions, *J.Chem.Phys.,* 75 (1981), 3624-3635

3. Tapia, **O.** (1982) Quantum theories of solvent-effect representation: an overview of methods and results,in Ratajczack, H. and Orville-Thomas, W. J.(eds.), *Molecular. Interactions,* Wiley, Chichester,pp.47-117.

4. Tapia, **O.** (1989) An overview of the theory of chemical reactions and reactivity in enzymes and solution,in Maruani, J.(eds.), *Molecules in Physics, Chemistry and Biology,* Kluwer Academic Publishers, Dordrecht,pp.405-422.

5. Tapia, **O.** (1992) Theoretical evaluation of solvent effects,in Maksic, Z. B.(eds.), *Theoretical models of chemical bonding,* Spinger-Verlag, Berlin,pp.43.5-458.

6. Tapia, **O.:**Solvent effect theories : quantum and classical formalisms and their applications in chemistry and biochemistry, *J. Math. Chem.,* 10 (1992), 139-181

7. Angyan, J. G. and Jansen, G.: Arc direct reaction field methods appropriate for describing dispersion interactions?, *Chem.Phys.Lett.,* 175 (1990), 313-318

8. Tomasi, J., Bonaccorsi, R., Cammi, R. and Olivares del Valle, F. J.: Theoretical chemistry in solution. Some results and perspectives of the continuum methods and in particular of the polarizable continuurn model, .*J.Mol.Struct.,* 234 (1991), 401-424

9. Angyan, J.: Common theoretical framework for quantum chemical solvent effect theories, *J.Math.Chem.,* 10 (1992), 93-137

10. Dillet, V., Rinaldi, D., Angyan, J. and Rivail, J.-L.: Reaction field factors for the multipole distribution in a cavity surrounded by a continuum, *Chem.Phys.Lett.,* 202 (1993, 18-22

11. Tomasi, J. (1994) Application of continuurn solvation models based on a Quantum Mechanical Hamiltonian.,in Cramer, C. J. and Truhlar, D. G.(eds.), *Structure and Reactivity in Aqueous Solution,* American Chemical Society, Washington,pp. 10-23.

12. Tomasi, J. and Persico, M.: Molecular interactions in solution: An overview of methods based on continuous distributions of the solvent, *Chem.Rev.,* 94 (1994), 2027-2094

13. Jansen, G., Angyan, J. and Colonna, F., First European Conference on computational chemistry., (1994)

14. Warshel, A. and Levitt, H.: Theoretical studies of enzymatic reactions: dielectric, electrostatic and steric stabilization of the carbonium ion in the reaction of lysozyme, *J. Mol. Biol.,* 103 (1976), 227-249

15. Devanlt, D.: Quantum mechanical tunnelling in biological systems, *Quarterly Review of Biophysics,* 13 (1980), 387-564

16. Bash, P. A., Field, M. J. and Karplus, M.: Free energy perturbation method for chemical reactions in the condensed phase: a dynamical approach based on a combined quantum and molecular mechanics potential, *J.Am.Chem.Soc.,* 109 (1987), 8092-8096

17. Warshel, A., Chu, Z. T. and Parson, W. W.: Dispersed polaron simulations of electron transfer in photosynthetic reaction centers, *Science,* 246 (1989), 112-116

18. Äqvist, **J.** and Warshel, A.: Free energy relationship in metalloenzyme-catalyzed reactions. Calculations of the effects of metal ion substitutions in staphylococcal nuclease, *J.Am.Chem.Soc.,* 112 (1990), 2860-2868

19. Bolton, J. R. and Archer, M. D. (1991) Basic electron-transfer theory,in Bolton, J. R., Mataga, N. and McLendon, G.(eds.), *Electron Transfer* in *Inorganic, Organic and Biological Systems,* American Chemical Society, 7-23.

20. Bauschlicher, C. W. and Langhoff, S. R.: Quantum mechanical calculations to chemical accuracy, *Science,* 254 (1991), 394-398

21. Bowman, J. M.: Reduced dimensionality theory of quantum reactive scattering, *J.Phys. Chem.,* 95 (1991), 4960-4968
22. Daggett, V., Schröder, S. and Kollman, P.: Catalytic pathways of serine proteases : classical and quantum mechanical calculations, *J. Am. Chem.* Soc., 113 (1991), 8926-8935
23. Rivail, J. L., Loos, M. and Thery, V., Trends Ecol. Phys. Chem., Proc. Int. Workshop Ecol. Phys. Chem., 2nd (1992) 17-26
24. Zeng, J., Craw, J. S., Hush, N. S. and Reimers, J. R.: Medium effects on molecular and ionic electronic spectra. Application to the lowest 1(n,π*) state of dilute pyridine in water, *Chem.Phys.Lett.,* 206 (1993), 323-328
25. Jorgensen, W. L., Blake, J. F., Lim, D. and Severance, D. L.: Investigation of solvent effects on pericyclic reactions by computer simulations, *J. Chem.Soc., Faraday Trans.,* 90 (1994), 1727-1732
26. Jortner, J., Levine, R. D. and Pullman, B.(ed.), *The Jerusalem Symposia on Quantum Chemistry and Biochemistry,* Kluwer Acad.Pub., Dordrecht, 1994.
27. Knops-Gerrits, P.-P., De Vos, D., Thibault-Starzyk, F. and Jacobs, P. A.: Zeolite-encapsulated Mn(II) complexes as catalysts for alkene oxidation, *Nature,* 369 (1994), 543-546
28. Rasaiah, J. and Zhu, J. (1994) Solvent dynamics and electron transfer reactions,in Gauduel, Y. and Rossky, P. J.(eds.), *Ultrafast reaction dynamics and solvent effects,* AIP Press, New York,pp.421-434.
29. Storer, J. W., Giesen, D. J., Hawkins, G. D., Lynch, G. C., Cramer, C. J., Truhlar, D. G. and Liotard, D. A. (1994) Solvation modeling in aqueous and nonaqueous solvents.,in Cramer, C. J. and Truhlar, D. G.(eds.), *Structure and Reactivity in Aqueous Solution,* American Chemical Society, Washington,pp.24-49.
30. Spears, K. G.: Models for electron transfer with vibrational state resolution, *J.Phys. Chem.,* 99 (1995), 2469-2476
31. Luzhkov, V. and Warshel, A.: Microscopic models for quantum mechanical calculations of chemical processes in solutions: LD/AMPAC and SCAAS/AMPAC calculations of solvation energies, *J. Comp. Chem .,* 13 (1992), 199-213
32. Evans, M. G. and Polanyi, M.: Inertia and driving force of chemical reactions, *Disc.Faraday Soc.,* (1938), 11-24
33. Wigner, E.: The transition state method, *Trans.Faraday Soc,* 34 (1938), 29-41
34. Glasstone, K. J., Laidler, K. J. and Eyring, H.: *Theory of rate processes,* McGraw-Hill, New York, 1941
35. Garret, B. C. and Truhlar, D. G.: Generalized transition state theory. Classical mechanical theory and applications to collinear reactions of hydrogen molecules, *J.Phys.Chem.,* 83 (1979), 1052-1079
36. Garret, B. C. and Truhlar, D. G.: Generalized transition state theory. Quantum effects for collinear reactions of hydrogen molecules and isotopically substituted hydrogen molecules, *J.Phys. Chem.,* 83 (1979), 1079-1112
37. Laidler, K. J. and King, M. C.: The development of transition-state theory, *J. Phys. Chem.,* 87 (1983), 2657-2664
38. Fong. F. K.: A successor to transition-state theory, *Acc.Chem.Res.,* 9 (1976), 433-438
39. Miller, W. H.: Beyond transition state theory : a rigorous quantum theory of chemical reaction rates, *Acc. Chem. Res.,* 26 (1993), 174-181
40. Bolton, J. B., Mataga, N. and McLendon, G.: *Advances in Chemistry Series CSC Symposium Series 2,* 1991
41. Marcus, R. A.: Schrödinger equation for strongly interacting electron-transfer systems, *J.Phys.Chem.,* 96 (1992), 1753-1757
42. Pauling, L.: Nature of forces between large molecules of biological interest, *Nature,* 161 (1948), 707-709
43. Tapia, O. and Andres, J.: On a quantum theory of chemical reactions and the role of in vacuum transition structures. Primary and secondary sources of enzyme catalysis, *J. Mol.Str (THEOCHEM),* 335 (1995), 267-286
44. Feynman, R. P.: *Statistical mechanics,* Benjamin,Inc., Reading, 1972

45. Feynman, R. P.: *Quantum electrodynamics,* Benjamin, Inc., New York, 1961
46. Craig, D. P. and Thirunamachandran, T.: *Molecular quantum electrodynamics,* Academic Press, London, 1984
47. Sakurai, J. J.: *Modern Quantum Mechanics,* Benjamin/Cummings, Menlo Park, 1985
48. McQuarrie, D. A.: *Statistical mechanics,* Harper & Row, New York, USA, 1976
49. Baer, M.: Adiabatic and diabatic representations for atom-molecule collisions: Treatment of the collinear arrangement, *Chem.Phys.Lett.,* 35 (1975), 112-118
50. Baer, M.: Adiabatic and diabatic representations for atom-diatom collisions: Treatment of the three-dimensional case, *Chem.Phys.,* 15 (1976), 49-57
51. Chapuisat, X., Nauts, A. and Dehareng-Dao, D.: Adiabatic-to-diabatic electronic state transformation and curvilinear nuclear coordinates for molecular systems, *Chem.Phys.Lett.,* 95 (1983), 139-143
52. Naray-Szabo, G., Surjan, P. R. and Angyan, J. G.: *Applied Quantum Chemistry,* Reidel, Dordrecht, 1987
53. Park, D.: *Introduction to the quantum theory,* MacGraw-Hill, New York, 1974
54. Cortes, E., West, B. J. and Lindenberg, K.: On the generalized Langevin equation: classical and quantum mechanical, *J.Chem.Phys.,* 82 (1985), 2708-2717
55 . Deumens, E., Diz, A., Longo, R. and Öhrn, I.: Time-dependent theoretical treatments of the dynamics of electrons and nuclei in molecular systems, *Rev.Mod.Phys.,* 66 (1994), 917-983
56. Kroto, H. W.: *Molecular rotation spectra,* Dover Publications Inc., New York, 1992
57. Roos, B. J. (1992) The multiconfigurational (MC) self-consistent field (SCF) theory,in Roos, B. J.(eds.), *Lecture notes in quantum chemistry,* Springer-Verlag, Berlin,pp. 179-254.
58. Cohen-Tannoudji, C., Dupont-Roc, J. and Grynberg, G.: *Processus d'interaction entre photons et atomes,* InterEditions/Editions du CNRS, Paris, 1988
59. Park, *D.: Classical dynamics and its quantum analogues,* Springer-Verlag, Berlin, 1990
60. Gao, J. and Xia, X. (1994) Simulating solvent effects on reactivity and interactions in ambient and supercritical water,in Cramer, C. J. and Truhlar, D. G.(eds.), *Structure and Reactivity in Aqueous Solution,* American Chemical Society, Washington,pp.212-228.
61. Jansen, G., Colonna, F. and Angyan, J. G.: Mixed quantum-classical calculations on the water molecule in liquid phase: Influence of a polarizable environment on electronic properties, *Int.J.Quantum Chem,* in press (1995),
62. Carloni, P., Blöchl, P. E. and Parrinello, M.: Electronic structure of the Cu,Zn superoxide dismutase active site and its interactions with the substrate, *J.Phys.Chem.,* 99 (1995), 1338-1348
63. Eyring, H.: The activated complex in chemical reactions, *J. Chem. Phys.,* 3 (1935), 107-115
64. Eliason, M. A. and Hirschfelder, J. **O.:**General collision theory for the rate of bimolecular, gas phase reactions, .*J. Chem. Phys.,* 30 (1959), 1426.1436
65. Marcus, R. A.: Theoretical relations among rate constants, barriers, and Bronsted slopes of chemical reactions., *J. Phys. Chem.,* 72 (1968), 891
66. Laidler, K. J.: *Theories of chemical reaction rates,* McGraw-Hill, New York, 1969
67. Caldwell, D. and Eyring, H. (1971) Quantum-mechanical rate processes,in Yourgrau, W. and van der Merwe, A.(eds.), *Perpectives in quantum theory,* Dover Publications,Inc., New York,pp. 117-138.
68. Truhlar, D. G. and Garrett, B. C.: Variational transition-state *theory, Acc. Chem. Res.,* 13 (1980), 440-448
69. Cerjan, C. J. and Miller, W. H.: On finding transition states, *J.Chem.Phys.,* 75 (1981), 2800-2806
70. Pollak, E.: Theory of activated rate processes: a new derivation of Kramer's expression, *J. Chem.Phys.,* 85 (1986), 865-867
71. Miller, W. H.: *The theory of chemical reaction dynamics,* Reidel, Dordrecht, Netherlands, 1986
72. Truhlar, D. G. and Steckler, R.: Potential energy surfaces for polyatomic reaction dynamics, *Chem. Rev.,* 87 (1987), 217-236
73. Hwang, J. K., Chu, Z. T., Yadav, A. and Warshel, A.: Simulations of quantum mechanical corrections

for rate constants of hydride-transfer reactions in enzymes and solutions, *J. Phys. Chem.*, 95 (1991), 8445-8448

74. Lobaugh, J. and Voth, G. A.: Calculation of quantum activation free energies for proton transfer reactions in polarsolvents, *Chem. Phys. Lett.*, 198 (1992), 311-315

75. Borgis, D. (1992) Proton transfer reactions in solutions: a molecular approach,in *Electron Proton Transfer Chem. Biol.*, 345-362.

76. Marcus, R. A. and Siddarth, P.: Theory of electron transfer reactions and comparison with experiments, *NATO ASI Ser., Ser. C*, 376(Photoprocesses in Transition Metal Complexes, Biosystems and Other Molecules) (1992), 49-88

77. Tominaga, K., Kliner, D. A. V., Johnson, A. E., Levinger, N. E. and Barbara, P. E.: Femtosecond experiments and absolute rate calculations on intervalence electron transfer of mixed-valence compounds, *J.Chem.Phys.*, 98 (1993), 1228-1243

78. Borgis, D. and Hynes, J. T.: Dynamical theory of proton tunneling transfer rates in solution: general formulation, *Chem. Phys.*, 170 (1993), 315-346

79. Basilevsky, M. V., Chudinov, G. E. and Napolov, D. V.: Calculation of the rate constant for the reaction chloride + chloromethane ---> C1CH3 + C1- in the framework of the continuum medium model, *J. Phys Chem.*, 97 (1993), 3270-3277

80. Miller, W. H.: Quantum mechanical theory of collisional recombination rates, *J.Phys. Chem.*, 99 (1995), 12387-12390

81. Herring, C.: Critique of the Heitler-London method of calculating spin couplings at large distances, *Rev.Mod.Phys.*, 34 (1962), 631-645

82. Herring, C. and Flicker, M.: Asymptotic exchange coupling of two hydrogen atoms, *Phys.Rev.*, 134 (1964), A362-A366

83. Migdal, A. B. and Krainov, V. P.: *Approximation methods in quantum mechanics*, Benjamin,Inc., New York, 1969

84. Levine, R. D. and Bernstein, R. B.: *Molecular reaction dynamics and chemical reactivity*, Oxford University Press, New York, 1987

85. Shaik, S. S., Schlegel, H. B. and Wolfe, S.: *Theoretical aspects* of *physical organic chemistry*, Wiley, New York, 1992

86. Hase, W. L.: Simulation of gas-phase chemical reactions: Applications to SN2 nucleophilic substitution, *Science*, 266 (1994), 998-1002

87. Kearley, G. J., Fillaux, F., Baron, M.-H., Bennington, S. and Tomkinson, J.: A new look at proton dynamics along the hydrogen bonds in amides and peptides, *Science*, 264 (1994), 1285-1289

88. Mezey, P. G.: Catchment region partitioning of energy hypersurfaces,I., *Theoret.chim.Acta(Berl.)*, 58 (1981), 390-330

89. Mezey, P. G.: Topology of energy hypersurfaces, *Theoret.Chim.Acta (Berl.)*, 62 (1982), 133-161

90. Schrödinger, E. (1983) The present situation in quantum mechanics: A translation of Schrödinger's "Cat Paradox" paper,in Wheeler, J. A. and Zurek, W. H.(eds.), *Quantum theory and measurement*, Princeton University Press, Princeton,New Jersey,pp.152-167.

91. Zeilinger, A., Bernstein, H. J., Greenberger, D. M., Horne, M. A. and Zukowski, M. (1993) Controlling entanglement in quantum optics,in Esawa, H. and Murayama, Y.(eds.), *Quantum control and measurement*, Elsevier, Amsterdam,pp.9-22

92. Langbein, D.: *Theory of van der- Waals attraction*, Springer-Verlag, Berlin, 1974

93. Andres, J., Cárdenas, R., Silla, E. and Tapia, 0.: A theoretical study of the Meyer-Schuster reaction mechanism : minimum-energy profile and properties of transition-state structures, *J. Am. Chem. Soc.*, 110 (1988), 666-672

94. Tapia, O., Cardenas, R., Andres. J. and Colonna-Cesari, F.: Transition structure for hydride transfer to pyridinium cation from methanolate. Modeling of LADH catalyzed reaction, *J. Am. Chem. Soc.*, 110 (1988), 4046-4047

95. Tapia, O., Andres, J., Aullo, J. M. and Cardenas, R.: Electronic aspects of the hydride transfer

mechanism. Part 2. *Ab initio* analytical gradient studies of the pyridinium cation/l,4-dihydropyridine, ciclopropenyl-cation/cyclopropene and formaldehyde/methanolate model reactant system, *J. Mol. Struct. THEOCHEM.,* 167 (1988). 395-412

96. Andres, J., Moliner, V. and Safont, V. S.: Theoretical kinetic isotope effects for the hydride-transfer step in Lactate Dehydrogenase, *J. Chem. Soc . Faraday Trans.,* 90 (1994),

97. Andres, J., Safont, V. S., Martins, J. B. L., Beltran, A. and Moliner, V.: AMI and PM3 transition structure for the hydride transfer. A model of reaction catalyzed by dihydrofolate reductase, *J. Mol.Struct. THEOCHEM,* 330 (1995), 411-417

98. Cardenas, R., Andrés, J., Krechl, J., Campillo, M. and Tapia, O.: On a possible invariance of a transition structure to the effects produced by ancyllary H-bonding molecules:

Modelling the effects of Ser-48 in the hydride transfer step of liver alcohol dehydrogenase, *Int.J.Quantum Chem.,* in press (1995),

99. Yliniemela, A., Konschin, H., Neagu, C., Pajunen, A., Hase, T., Brunow, G. and Teleman, **O.:** Design and synsthesis of a transition state analog for the ene reaction between maleimide and 1-alkenes, *J.Am.Chem.Soc.,* 117 (1995), 5120-5126

100. Tapia, O., Jacob, **O.** and Colonna, F.: Transition structures for carbon dioxide and formaldehyde hydroxylation reactions in the coordinate sphere of zinc, *Theor. Chim. Acta,* 8.5 (1993), 217-230

101. Tapia, O., Andres, J. and Safont, V. S.: Theoretical study of transition structures for intramolecular hydrogen transfer in molecular models representing D-ribulose-1,s-bisphosphate. A possible molecular mechanism for the enolization step in Rubisco, *J.Phys.Chem.,* 98 (1994), 4821-4830

102. Tapia, O., Andres, J. and Safont, V. S.: Enzyme catalysis and transition structures in vacuo. Transition structures for the enolization, carboxylation and oxygenation reactions in ribulose- 1,5-bisphosphate carboxylase/oxygenase enzyme (Rubisco), *J. Chem.Soc.Faraday Trans.,* 90 (1994), 2365-2374

103. Tapia, O. and Andres, J.: A simple protocol to help calculate saddle points. Transition state structures for the Meyer-Schuster reaction in non-aqueous media : an *ab initio* MO study., *Chem. Phys. Letters,* 109 (1984), 471-477

104. Bertran, J., Gallardo, I., Moreno, M. and Saveant, J. M.: Dissociative electron transfer. *Ab initio* study of the carbon-halogen bond reductive cleavage in methyl and perfluoromethyl halides. Role of the solvent, *J.Am.Chem.Soc.,* 114 (1992), 9576-9583

105. Wesolowski, T. A. and Warshel, A.: Frozen density functional approach for ab initio calculations of solvated molecules, *J.Phys.Chem.,* 97 (1993), 8050-8053

106. Honig, B. and Nicholls, A.: Classical electrostatics in biology and chemistry, *Science,* 268 (1995), 1144.1149

107. Angyan, J. G.: Rayleigh-Schrödinger perturbation theory of non-linear Schrödinger equations with linear perturbation, *Int.J.Quantum Chem.,* 47 (1993), 469-483

108. Angyan, J. G.: Choosing between alternative MP2 algoritms in the selfconsistent reaction field (SCRF) theory of solvent effects, *Chem.Phys.Lett.,* in press (1995),

109. Gao, J.: Combined QM/MM simulation study of the Claisen rearrangement of allyl vinyl ether in aqueous solution, *J.Am.Chem.Soc.,* 116 (1994), 1563-1564

110. Pappalardo, R. R., Sanchez Marcos, E., Ruiz-Lopez, M. F., Rinaldi, D. and Rivail, J. L.: Solvent effects on molecular geometries and isomerization processes: A study of push-pull ethylenes in solution, *J.Am.Chem.Soc.,* 115 (1993), 3722-3730

111. Sánchez Marcos, E., Pappalardo, R. R. and Rinaldi, D.: Effects of the solvent reaction field on the geometrical structures of hexahydrate metallic cations, *J.Phys. Chem.,* 95 (1991), 8928-8932

112. Maran, U., Pakkanen, T. A. and Karelson, M.: A semiempirical study of the solvent effect on the Menshutkin reaction, *J.Chem.Soc.Perkin II,* submitted (1995).

113. Karelson, M. M. and Zerner, M. C.: Theoretical treatment of solvent effects on electronic spectroscopy, *J.Phys. Chem.,* 96 (1992), 6949-6957

114. Karelson, M., Tamm, T. and Zerner, M. C.: Multicavity reaction field method for the solvent effect

description in flexible molecular systems, *J.Phys.Chem.,* 97 (1993), 11901-11907
115. Zhao, X. G. and Cuckier, R. I.: Molecular dynamics and quantum chemistry study of a proton-coupled electron transfer reaction, *J.Phys. Chem.,* 99 (1995), 945-954
116. Glossman, M. D., Balbás, L. C., Rubio, A. and Alonso, J. A.: Nonlocal exchange and kinetic energy density functionals with correct asymptotic behavior for electronic systems, *Int.J. Quantum Chem.,* 49 (1994), 171-184
117. Bersuker, I. B.: On the limitations of the density functional theory in electronic structure calculations, *Int.J. Quantum Chem.,* submitted (1995),
118. Soirat, A., Flocco, M. and Massa, L.: Approximately N-representable density functionals density matrices, *Int.J.Quantum Chem.,* 49 (1994), 291-298
119. Marx, D. and Parrinello, M.: Structural quantum effects and three-centre two-electron bonding in CH5+, *Nature,* 375 (1995), 216-218
120. Tuckerman, M., Laasonen, K., Sprik, M. and Parrinello, M.: Ab initio molecular dynamics simulation of the solvation and transport of H3O+ and OH- ions in water, *J.Phys.Chem.,* 99 (1995), 5749-5752
121, Tuckerman, M., Laasonen, K., Sprik, M. and Parrinello, M.: Ab initio molecular dynamics simulation of the solvation and transport of hydronium and hydroxyl ions in water, *J.Chem.Phys.,* 103 (1995), 150-161
122. Porezag, D. and Pederson, M. R.: Density functional based studies of transition states and barriers for hydrogen exchange and abstraction reactions, *J.Chem.Phys.,* 102 (1993, 9345-9349
123. Tapia, O., Colonna, F. and Angyan, J. G.: Generalized self-consistent reaction field theory in multicenter-multipole ab initio LCGO framework. I. Electronic properties of the water molecule in a Monte Carlo sample of liquid water molecules studied with standard basis sets, *J.Chim.Phys.,* (1990), 875-903
124. Warshel, A.: Computer simulations of enzymatic reactions, *Curr. Op. in Struct. Biol,* 2 (1992), 230-236
125. Merz Jr., K. M.: Computer simulation of enzymatic reactions, *Curr Op. in Struct. Biol., 3* (1993), 234-240
126. Gao, J.: Monte Carlo quantum mechanical-configutration interaction and molecular mechanics simulations of solvent effects on the n-->π* blue shift in acetone, *J.Am.Chem.Soc.,* 116 (1994), 9324-9328
127. Kubo, R.: *The fluctuation-dissipation theorem,* Benjamin,Inc., New York, 1969
128. Wax, N.(ed.), Dover Publications, Inc., New York, 1954.
129. Adelman, S. A.: Generalized Langevin equations and many-body problems in chemical physics, *Adv.Chem.Phys.,* 44 (1980), 143-253
130. Risken, H.: *The Fokker-Planck equation,* Springer-Verlag, Berlin, 1989
131. Evans, M. W., Evans, G. T., Coffey, W. T. and Grigolini, P.: *Molecular dynamics and theory of broad band spectroscopy,* John Wiley & Sons, New York, 1982
132. Straat, R. M.: The instantaneous normal modes of liquids, *Acc.Chem.Res.,* 28 (1995), 201-207
133. Lindenberg, K. and West, B. J.: Statistical properties of quantum systems: The linear oscillator, *Phys.Rev.A,* 30 (1984), 568-582
134. Kittel, C.: *Introduction to solid state physics,* Wiley & Sons,Inc., New York, 1976
135. Skinner, J. L. and Trommsdorf, H. P.: Proton transfer in benzoic acid crystals: A chemical spin-boson problem. Theoretical analysis of nuclear magnetic resonance, neutron scattering, and optical experiments, *J.Chem.Phys.,* 89 (1988), 897-907
136. Blaizot, J.-P. and Ripka, G.: *Quantum theory of finite systems,* The MIT Press, Cambridge,Massachusetts, 1986
137. Zwanzig, R. W. (1961) Statistical mechanics of irreversibility,in Brittin, W. E., Downs, B. W. and Downs, J.(eds.), *Lectures in theoretical physics,* Interscience Pub.Inc., New York,pp.106-141.
138. West, B. J. and Lindenberg, K.: Energy transfer in condensed media. 1.Two-level systems, *J.Chem.Phys.,* 83 (1985), 4118-4135
139. Christov, S. G.: Two types of Kramers rate equations for reactions in condensed media, *Int.J.Quantum Chem.,* 52 (1994), 1219-1228
140. Pollak. E.: Quantuin theory of activated rate processes: a maximum free energy approach,

J.Chem.Phys., 103 (1995), 973-980
141. Brown, D. W., Lindenberg, K. and West, B. J.: Energy transfer in condensed media. II. Comparison of stochastic Liouville equations, *J.Chem.Phys.,* 83 (1985), 4136-4143
142. Brown, D. W., Lindenberg, K. and West, B. J.: On the dynamics of polaron formation in a deformable medium, *J.Chem.Phys.,* 84 (1986), 1574-1582
143. Leggett, A. J., Chakravarty, S., Dorsey, A. T., Fisher, M. P., Garg, A. and Zwerger, W.: Dynamics of the dissipative two-state system, *Rev.Mod.Phys.,* 59 (1987), 1-85
144. Smith, B. B., Staib, A. and Hynes, J. T.: Well and barrier dynamics and electron transfer rates. A molecular dynamics study, *Chem.Phys.,* 176 (1993), 521-537
145. Smith, B. B. and Hynes, J. T.: Electron friction and electron transfer rates at metallic electrodes, *J.Chem.Phys.,* 99 (1993), 6517-6530
146. Zewail, H. A.: *FEMTOCHEMISTRY. Ultrafast dynamics of the chemical bond,* World Scientific, Singapore, 1994
147. Jimenez, R., Fleming, G. R., Kumar, P. V. and Maroncelli, M.: Femtosecond solvation dynamics of water, *Nature,* 369 (1994), 471-473
148. Richter, W., Lee, S., Warren, W. S. and He, Q.: Imaging with intermolecular multiple-quantum coherences in solution nuclear magnetic resonance, *Science,* 267 (1995), 654-657
149. He, Q., Richter, W., Vathyam, S. and Warren, W. S.: Intermolecular multiple-quantum coherences and cross correlations in solution nuclear magnetic resonance, *J. Chem.Phys.,* 98 (1993), 6779-6800
150. Skrebkov, O. V.: Diffusional description of vibrational realaxation in a binary mixture of diatomic molecules-quantum oscillators, *Chem.Phys.,* 191 (1995), 87-99
151. Åberg, U., Åkesson, E., Alvarez, J.-L., Fedchenia, I. and Sundström, V.: Femtosecond spectral evolution monitoring the bond- twisting event in barrierless isomerization in solution, *Chem.Phys.,* 183 (1994), 269-288
152. Dirac, P. A. M.: *The principles of quantum mechanics,* Clarendon Press, Oxford, 1947
153. Loudon, R.: *The quantum theory of light,* Clarendon Press, Oxford, 1986
154. Ballentine, L. E.: *Quantum mechanics,* Prentice Hall, Englewood Cliffs, 1990
155. Mannervik, B. (1981) Design and analysis of kinetic experiment for discrimination between rival models,in Endrenyi, L.(eds.), *Kinetic data analysis,* Plenum Pub.Co., New York,pp.
156. Tapia, O., Poulain, E. and Sussman, F.: Hydrogen Bond. Environmental effects on proton potential curves. An SCRF MO CNDO/2 calculation of a water dimer, *Chem.Phys.Lett.,* 33 (1975), 65-70
157. Hemley, R. J., Soos, Z. G., Hanfland, M. and Mao, H.-k.: Charge-transfer states in dense hydrogen, *Nature,* 369 (1994), 384-387
158. Basché, T., Kummer, S. and Bräuchle, C.: Direct spectroscopic observation of quantum jumps of a single molecule, *Nature,* 373 (1995), 132-134
159. Pechukas, P.: Time-dependent semiclassical scattering theory. I. Potential scattering, *Phys.Rev.,* 181 (1969), 166-174
160. Pechukas, P.: Time-dependent semiclassical scattering theory. II. Atomic collisions, *Phys.Rev.,* 181 (1969), 174-185
161. Basilevsky, M. V. and Ryaboy, V. M.: Two approaches to the calculation of molecular resonance states: Solution of scattering equations and matrix diagonalization, *J.Comp.Chem.,* 8 (1987), 683-699
162. Lefebvre, R. and Moiseyev, N.: Artificial resonance procedure for the determination of quantum mechanical rate constants in the tunneling regime, *J. Chem. Phys.,* 93 (1990), 7173-7178
163. Clary, D. C.: Quantum scattering calculations on the OH + H2 (v =0.1), OH + D2, and OD + H2 reactions, *J. Chem. Phys.,* 96 (1992), 3656-3665
164. Ryaboy, V. and Lefebvre, R.: Flux-flux correlation function study of resonance effects in reactive collision, *J. Chem. Phys.,* 99 (1993), 9547-9552
165 Lefebvre, R., Ryaboy, V. and Moiseyev, N.: Resonance and reaction, *J. Mol. Struct.* (*THEOCHEM*), 332 (1995), 209-215

166. Davis, M. J.: Bottlenecks to intramolecular energy transfer and the calculation of relaxation rates, *J. Chem. Phys.*, 83 (1985), 1016-1031

167. Williams, I. H. and Maggiora, G. M.: Use and abuse of the distinguished-coordinate method for transition-state structure searching, *J. Mol. Struct.* (*THEOCHEM*), 89 (1982), 365-378

168. DePuy, C. H., Gronert, S., Mullin, A. and Bierbaum, V. M.: Gas-phase SN2 and E2 reactions of alkyl halides, *J.Am.Chem.Soc.*, 112 (1990), 8650-8655

169. Borman, S.: New insight gained on gas-phase SN2 reaction, *Chem.Eng.News*, (1992), 22-26

170. Cyr, D. M., Scarton, M. G. and Johnson, M. A.: Photoelectron spectroscopy of the gas-phase SN2 reaction intermediates I⁻.CH3I and I-.CD3I: Distorsion of the CH3I at the "ion-dipole" complex, *J.Chem.Phys.*, 99 (1993), 4869-4872

171. Wladkowski, B. D., Allen, W. D. and Brauman, J. I.: The SN2 identity reaction F-+CH3F -> FCH3 + F⁻, *J.Phys.Chem.*, 98 (1995), 13532-13540

172. Tapia, O., Paulino, M. and Stamato, F. M. L. G.: Computer assisted simulations and molecular graphics methods in molecular design. 1.Theory and applications to enzyme active-site directed drug design, *Mol.Eng.*, 3 (1994), 377-414

173. Tapia, **O.** and Andres, J.: Towards an explanation of carboxylation/oxygenation bifuinctionality in Rubisco. Transition structure for the carboxylation reaction of 2,3,4-pentanetriol., *Mol. Eng.*, 2 (1992), 37-41

174. Tapia, O., Andres, J. and Cardenas, R.: Transition structure for the hydride transfer reaction from formate anion to cyclopropenyl cation: a simple theoretical model for the reaction catalyzed by formate dehydrogenase, *Chem. Phys. Lett*, 189 (1992), 395-400

175. Mezey, P. G. (1981) Optimization and analysis of energy hypersurfaces,in Csizmadia, I. G. and Daudel, R.(eds.), *Computational theoretical organic chemistry*, 101-128.

176. Hu, W.-P. and Truhlar, D. G.: Structural distorsion of CH3I in an ion-dipole precursor complex, *J.Phys.Chem.*, 98 (1994), 1049-1052

177. Zewail, A. H.: *FEMTOCHEMISTRY. Ultrafast dynamics of the chemical bond*, World Scientific, Singapore, 1994

178. Zare, R. N.: Reactions a la mode, Nuture, 365 (1993), 105-106

179. Guettler, R. D., Jones Jr., G. C., Posey, L. A. and Zare, R. N.: Partial control of an ion-molecule reaction by selection of internal motion of the polyatomic reagent ion, *Science*, 266 (1994), 259-261

180. Gericke, K.-H.: Control of ion-molecule reactions in the gas phase, *Angew.Chem.Int.Ed.Engl.*, 34 (1995), 885-886

181. Tapia, O., Cardenas, R., Andres, J., Krechl, J., Campillo, M. and Colonna-Cesari, F.: Electronic aspects of LADH catalytic mechanism, *Int. J. Quantum. Chem.*, 39 (1991), 767-786

182. Andres, J., Safont, V. S., Queralt, J. and Tapia, O: A theoretical study of the singlet-triplet energy gap dependence upon rotation and pyramidalization for 1,2-dihydroxyethylene. A simple model to study the enediol moiety in rubisco's substrate., *J. Phys. Chem.*,97 (1993), 7888-7893

183. Andres, J., Moliner, V., Krechl, J. and Silla, E.: Comparison of several semiempirical and ab initio methods for transition state structure characterization. Addition of CO_2 to $CH_3NHCONH_2$, *J. Phys. Chem.*, 98 (1994), 3664-3668

184. Andres, J., Moliner, V., Krechl, J., Domingo, J. L. and Picher, M. T.: A theoretical study of the molecular mechanism for the methanol oxidation by PQQ, *J. Am. Chem.* Soc.,117 (1995), 8807-8815

185. Pritchard, H. O.: *The quantum theory* of *unimolecular reactions*, Cambridge University Press, Cambridge, 1984

186. Zhao, M. and Rice, S. A.: Resonance state approach to quantum transition state theory, *J. Phys. Chem.*, 98 (1994), 3444-2449

187. Truhlar, D. G. and Garrett, B. C.: Resonance state approach to quantum mechanical variational transition state theory, *J. Phys. Chem.*, 96 (1992), 6515-6518

188. Graul, S. T. and Bowers, M. T.: The nonstatical dissociation dynamics of Cl-(CH3Br) : evidence for

vibrational excitation in the products of gas-phase SN2 reactions, *J. Am. Chem. Soc.,* 113 (1991). 9696-9697

189. Viggiano, A. A., Morris, R. A., Paschkewitz, J. S. and Paulson, J. F.: Kinetics of the gas-phase reactions of CI- with CH3Br and CD3Br: experimental evidence for nonstatistical behavior, *J.Am. Chem.Soc*., 114 (1992), 10477-10482

190. Graul, S. T. and Bowers, M. T.: Vibrational excitation in products of nucleophilic substitution: the dissociation of metastable X-(CH3Y) in the gas phase, *J.Am.Chem.Soc,* 116 (1994), 3875-3883

191. Vande Linde, S. R. and Hase, W. L.: Trajectory studies of SN2 nucleophilic substitution. I. Dynamics of CI^- + CH3C1 reactive collisions, *J.Chem.Phys.,* 93 (1990),

192. Cho, Y. J., Vande Linde, S. R., Zhu, L. and Hase, W. L.: Trajectory studies of SN2 nucleophilic substitution. II. Nonstatistical central barrier recrossing in the CI- + CH3C1 system, *J. Chem.Phys.,* 96 (1992), 8275-8287

193. Viggiano, A. A., Morris, R. A., Su, T., Wladkowski, B. D., Craig, S. L., Zhong, M. and Brauman, J. **I.:** The SN2 identity exchange reaction ^{37}C1- + ^{35}CICH2CN -> $^{35}C1^-$ + ^{37}CICH2CN: Kinetic energy and temperature dependence, *J.Am.Chem.Soc.,* 116 (1994), 2213-2214

194. Morris, R. A. and Viggiano, A. A.: Kinetics of the reactions of F- with CF3Br and CF31 as a function of temperature, kinetic energy, internal temperature, and pressure, *J.Phys. Chem.,* 98 (1994), 3740-3746

195. Breen, J. J., Peng, L. W., Willberg, D. M., Heikal, A., Cong, P. and Zewail, A. H.: Real-time probing of reactions,in clusters, *J. Chem.Phys.,* 92 (I990), 805-807

196. Leggett, A. J.: Quantum tunneling in the presence of an arbitrary linear dissipation mechanism, *Phys.Rev.B* , 30 (1984), 1208-1218

197. Makri, N. and Miller, W. H.: Basis method for describing the quantum mechanics of a "system" interacting with a harmonic bath, *J.Chem.Phys.,* 86 (1987), 1451-1457

198. Kim, H. J. and Hynes, J. T.: Equilibrium and nonequilibrium solvation and solute electronic structure, *Int.J.Quantum Chem.,* 24 (1990), 821-833

199. Kim, H. J. and Hynes, J. T.: A theoretical model for SN1 ionic dissociation in solution. 1. Activation free energy and transition-state structure, *J.Am.Chem.Soc.,* 114 (1992), 10508-10528

200. Kim, H. J. and Hynes, J. T.: A theoretical model for SNI ionic dissociation in solution. 2. Nonequilibriurn solvation reaction path and reaction rate, *J.Am.Chem.Soc.,* 114 (1992), 10528-10537

201. Tapia, O. and Lluch, J. M.: Solvent effects on chemical reaction profiles.I. Monte Carlo simulation of hydration effects on quantum chemically calculated stationary structures, *J. Chem.Phys.,* 83 (1983, 3970-3982

202. Tapia, O., Lluch, J. M., Cardenas, R. and Andres, J.: Theoretical study of solvation effects in chemical reactions. A combined quantum chemical/Monte Carlo study of the Meyer-Schuster reaction mechanism in water, *J. Am. Chem. Soc.,* 111 (1989), 829-835

203. Gouverneur, V. E., Houk, K. N., Pascual-Teresa, B., Beno, B., Janda, K. D. and Lerner, R. A.: Control of the exo and endo pathways of the Diels-Alder reaction by antibody catalysis, *Science,* 262 (1993), 204-208

204. Fersht, A.: *Enzyme structure and mechanism,* W.H.Freeman &Co., New York, 1985

205. Levy, M. and Perdew, J. P.: Success of quantum mechanical approximations for molecular geometries and electron-nuclear attraction expectation values : gift of the Coulomb potential ?, *J. Chem. Phys.,* 84 (1986), 4519-4523

206. Sitnitsky, A. E.: Fluctuations of electric fields in enzyme active sites as an efficient source of reaction activation, *Chem.Phys.Lett.,* 240 (1995), 47-52

207. Mathews, C. K. and van Holde, K. E.: *Biochemistry,* Benjamin/Cummings, Redwood City, 1990

208. Coates, G. W. and Waymouth, R. M.: Oscillating stereocontrol: A strategy for the synthesis of thermoplastic elastomeric propylene, *Science,* 267 (1993, 217-219

209. Hill, C. L. and Zhang, X.: A 'smart' catalyst that self-assembles under turnover conditions, *Nature,* 373 (1995), 324-326

210. Shabat, D., Itzhaky, H., Reymond, J.-L. and Keinan, E.: Antibody catalysis of a reaction otherwise strongly disfavoured in water, *Nature*, 374 (1995), 143-146
211. Danishefsky, S.: Catalytic antibodies and disfavored reactions, *Science*, 259 (1993), 469-470
212. Li, T. L., Janda, K. D., Ashley, J. A. and Lerner, R. A.: Antibody catalyzed cationic cyclization, *Science*, 264 (1994), 1289–1293
213. Chandrasekhar, J., Smith, S. F. and Jorgensen, W. L.: SN2 reaction profiles in the gas phase and aqueous solution, *J.Am.Chem.Soc.*, 106 (1984), 3049-3050
214. Chandrasekhar, J., Smith, S. F. and Jorgensen, W. L.: Theoretical examination of the SN2 reaction involving chloride ion and methyl chloride in the gas phase and aqueous solution, *J. Am. Chem. Soc.*, 107 (1985), 154-163
215. Huston, S. E., Rossky, P. J. and Zichi, D. A.: Hydration effects on SN2 reaction: An integral equation study of free energy surface and corrections to transitiion-state theory, *J.Am.Chem.Soc.*, 111 (1989), 5680-5687
216. Balbuena, P. B., Johnston, K. P. and Rossky, P. J.: Computer simulation of an SN2 reaction in supercritical water, *J.Phys.Chem.*, 99 (1993, 1554-1565
217. Miertus, S., Scrocco, E. and Tomasi, J.: Electrostatic interaction of a solute with a continuum. A direct utilization of ab initio molecular potentials for the prevision of solvent effects., *Chem. Phys.*, 55 (1981), 117-129
218. Tunon, I., Silla, E. and Pascual-Ahuir, J. L.: Theoretical study of the inversion of the alcohol acidity scale in aqueous solution. Toward an interpretation of the acid-base behavior of organic compunds in solution, *J. Am. Chem. Soc.*, 115 (1993), 2226-2230
219. Tortonda, F. R., Pascual-Ahuir, J. L., Silla, E. and Tunon, I.: Solvent effects on the thermodynamics and kinetics of the proton transfer between hydronium ions and ammonia. A Theoretical study using the continuum and the discrete models, *J. Phys. Chem.*, 99 (1995), 12525-12531
220. Mikkelsen, K. V., Joergensen, P. and Aagard-Jensen, H. J.: A multiconfiguration self-consistent reaction field response method, *J. Chem.Phys.*, 100 (1994), 6597-6607
221. Mikkelsen, K., Luo, Y., Ågren, H. and Joergensen, P.: Solvent induced polarizabilities and hyperpolarizabilities of para-nitroaniline studied by reaction field linear response theory, *J.Chem.Phys.*, 100 (1994), 8240-8250
222. Aguilar, M. A., Olivares del Valle, F. J. and Tomasi, J.: Nonequilibrium solvation: an *ab initio* quantum-mechanical method in the continuum cavity model approximation, *J.Chem.Phys.*, 98 (1993), 7375-7384
223. Aguilar, M., Bianco, R., Miertus, S., Persico, M. and Tomasi, J.: Chemical reactions in solution: modeling of the delay of solvent synchronism (dielectric friction) along the reaction path of an SN2 reaction, *Chem. Phys.*, 174 (1993), 397-407
224. Diercksen, G. H. F., Karelson, M., Tamm, T. and Zerner, M. C.: Multicavity SCRF calculation of ion hydration energies, *Int.J. QuantumChem.:Quantum Chem.Symp.*, 28 (1994), 339-348
225. Liu, Y.-P. and Newton, M. D.: Solvent reorganization and donor/acceptor coupling in electron-transfer processes: self-consistent reaction field theory and ab initio applications, *J.Phys. Chem.*, 99 (1995), 12382-12386
226. Truong, T. N. and Stefanovich, E. V.: A new method for incorporating solvent effect into the classical ab initio molecular orbital and density functional theory frameworks for arbitrary shape cavity, *Chem.Phys.Lett.*, 240 (1995), 253-260
227. de Souza, L. E. S. and Ben-Amotz, D.: Solvent mean force perturbations of diatomic dissociation reactions. Comparison of perturbed hard fluid and computer simulation results, *J. Chem. Phys.*, 101 (1994), 41 17-4122
228. de Souza, L. E. S. and Ben-Amotz, D.: Hard fluid model for molecular solvation free energies, *J.Chem.Phys.*, 101 (1994), 9858-9863
229. Vaidehi, N., Wesolowski, T. A. and Warshel, A. J.: Quantum-mechanical calculations of solvation free energies. A combined ab initio pesudopotential free-energy perturbation approach, *J.Chem.Phys.*,97

(1992), 4264-4271
230. Chen, J. L., Noodleman, L., Case, D. A. and Bashford, D.: Incorporating solvation effects into density functional electronic structure calculations, *J. Phys. Chem.*, 98 (1994), 11059-11068
231. Wei, D. and Salahub, D. R.: Hydrated proton clusters and solvent effects on the proton transfer barrier: a density functional study, *J. Chem. Phys.*, 101 (1994), 7633-7642
232. Cramer, C. J. and Truhlar, D. G.: General parametrized SCF model for free energies of solvation in aqueous solution, *J. Am. Chem. Soc.*, 113 (1991), 8305-8311
233. Giesen, D. J., Storer, J., Cramer, C. J. and Truhlar, D. J.: General semiempirical quantum mechanical solvation model for nonpolar solvation free energies. n-hexadacane., *J.Am. Chem.Soc.*, 117 (1995), 1057-1068
234. Tannor, D. J., Marten, B., Murphy, R., Friesner, R. A., Sitkoff, D., Nicholls, A., Honig, B., Ringnalda, M. and Goddard, W. A., III: Accurate first principles calculation of molecular charge distributions and solvation energies from *ab initio* Quantum Mechanics and continuum dielectric theory., *J. Am. Chem. Soc.*, 116 (1994), 11875-11882
235. Orozco, M., Luque, F. J., Habibollahzadeh, D. and Gao, J.: The polarization contribution to the free energy of hydration, *J.Chem.Phys.*, 102 (1995), 6145-6152
236. Stouten, P. W., Froemmel, C., Nakamura, H. and Sander, C.: An effective solvation term based on atomic occupancies for use in protein simulations, *Mol. Simul.*, 10 (1993), 97-120
237. Fraga, S. and Thornton, S. E.: Theoretical studies of peptidic structures. Environmental effects, *Theor. Chim.* Acta, 85 (1993), 61-67
238. Collura, V. P., Greaney, P. J. and Robson, B.: A method for rapidly assessing and refining simple solvent treatments in molecular modeling. ExampIe studies on the antigen-combining loop H2 from FAB fragment McPC603, *Protein Eng.*, 7 (1994), 221-233
239. Guba, W. and Kessler, H.: A novel computational mimetic of biological membranes in molecular dynamics simulations, *J.Phys.Chem.*, 98 (1994). 23-27
240. Cifra, P. and Bleha, T.: Conformer populations and the excluded volume effect in lattice simulations of flexible chains in solutions, *Polymer*, 34 (1993). 3716-3722
241. Hartsough, D. S. and Merz Jr., K. M.: Potential of mean force calculations on the SN1 fragmentation of tert-butyl chloride, *J.Phys. Chem.*, 99 (1995), 384-390
242. Lecea, B., Arrieta, A., Roa, G., Ugalde, J. M. and Cossio, F. P.: Catalytic and solvent effects on the cycloaddition reaction between ketenes and carbonyl compounds to form 2-oxetanones, *J.Am. Chem.Soc.*, 116 (1994), 9613-9619
243. Pardo, L., Osman, R., Weinstein, H. and Rabinowitz, J. R.: Mechanisms of nucleophiIic addition to activated double bonds: 1,2- and l,4-Michael addition of ammonia, *J.Am.Chem.Soc.*, 115 (1993), 8263-8269
244. Davidson, M. M., Hillier, I. H., Hall, R. J. and Burton, N. A.: Effect of solvent on the Claisen rearrangement of allyl vinyl ether using *ab initio* continuum methods, *J.Am.Chem.Soc.*, 116 (1994), 9294-9297
245. Lim, D., Hrovat, D. A., Borden, W. T. and Jorgensen, W. L.: Solvent effects on the ring opening of cyclopropanones to oxyallyls: a combined ab initio and Monte Carlo study, *J.Am.Chem.Soc.*, 116 (1994), 3494-3499
246. Reguero, M., Pappalardo, R. R., Robb, M. A. and Rzepa, H. S.: An MCSCF study of the effect of substituents and solvent on the [2 + 2] cycloaddition of tert-butylcyanoketene to phenylethene, *J.Chem.Soc., Perkin Trans.* 2, (1993), 1499-1502
247. Dejaegere, A., Liang, X. and Karplus, M.: Phosphate ester hydrolysis: calculation of gas-phase reaction paths and solvation effects, *J.Chem.Soc., Faraday Trans.*, 90 (1994), 1763-1770
248. Balbuena, P. B., Johnston, K. P. and Rossky, P. J.: Molecular simulation of a chemical reaction in supercritical water, *J.Am.Chem.Soc.*, 116 (1994), 2689-2690
249. Gupta, R. B., Combes, J. R. and Johnston, K. P.: Solvent effect on hydrogen bonding in supercritical fluids, *J.Phys. Chem.*, 97. (1993), 707-715

250. Jessop, P. G., Ikariya, T. and Noyori, R.: Homogenous catalysis in supercritical fluids, *Science,* 269 (1995), 1065-1069
251. Keszei, E., Murphrey, T. H. and Rossky, P. J.: Electron hydration dynamics: simulation results compared to pump and probe experiments, *J.Phys.Chem.,* 99 (1995), 22-28
252. Schwartz, B. J. and Rossky, P. J.: Aqueous solvation dynamics with a quantum mechanical solute: computer simulation studies of the photoexcited hydrated electron, *J.Chem.Phys.,* 101 (1994), 6902-6916
253. Schwartz, B. J. and Rossky, P. J.: Pump-probe spectroscopy of the hydrated electron: a quantum molecular dynamics simulation, *J. Chem. Phys.,* 101 (1994), 6917- 6926
254. Schultz, K. E., Russel, D. H. and Harris, C. B.: The applicability of binary collision theories to complex molecules in simple liquids, *J.Chem.Phys.,* 97 (1992), 5431-5438
255. Cho, M. and Fleming, G. R.: Photon-echo measurements in liquids: numerical calculations with model systems, *J. Chem. Phys.,* 98 (1993), 2848-2859
256. Torrie, G. M. and Patey, G. N.: Molecular solvent model for an electrical double layer: asymmetric solvent effects, *J.Phys.Chem.,* 97 (1993). 12909-12918
257. Zhang, L., Davis, H. T. and White, H. S.: Simulations of solvent effects on confined electrolytes, *J.Chem.Phys.,* 98 (1993), 5793-5799
258. Scherer, P. L. J. and Fischer, S. F.: Theoretical analysis of the photoinduced electron transfer in porphyrin-quinone cyclophanes, *Chem.Phys.Lett.,* 190 (1992), 574-580
259. Burshtein, A. I.: Diffusional desaturation of electron transfer, *J.Chem.Phys.,* 98 (1993), 471 1-4717
260. Tachiya, M. and Hilczer, M. (1994) Solvent effect on the electron transfer rate and the energy gap law,in Gauduel, Y. and Rossky, P. J.(eds.), *Ultrafast reaction dynamics and solvent effects,* AIP Press, New York,pp.447-459.
261, Rauhut, G. and Clark, T.: Molecular orbital studies of electron-transfer reactions, *J.Chem.Soc., Faraday Trans.,* 90 (1994), 1783-1788
262. Marguet, S., Mialocq, J. C., Millie, P., Berthier, G. and Momicchioli, F.: Intramolecular charge transfer and trans-cis isomerization of the DCM styrene dye in polar solvents. A CS-INDO MRCI study, *Chem.Phys.,* 160 (1992), 265-279
263. Simon, J. D. and Doolen, R.: On the dimensionality of the reaction coordinate of intramolecular charge-transfer reactions in protic solvents, *J.Am.Chem.Soc.,* 114 (1992), 4861-4870
264. Gould, I., Young, R. H., Mueller, L. J., Albrecht, A. C. and Farid, S.: Electronic structures of exciplexes and excited charge-transfer complexes, *J. Am. Chem. Soc.,* 116 (1994), 8188-8199
265. Broo, A.: Electronic structure of donor-spacer-acceptor molecules of potential interest for molecular electronics. *I.* Donor-.pi. spacer-acceptor, *Chem. Phys.,* 169 (1993), 135-150
266. Marquez, F., Zabala, I. and Tomas, F.: Phosphorescence emission and polarization of 3-carboxyquinoline, *J.Lumin.,* 55 (1993). 25-30
267. Torri, H. and Tasumi, M.: Correlation between redshifts and widths of the 0-0 band in the absorption spectra of all-trans-β-carotene in solution, *J.Chem.Phys.,* 98 (1993), 3697-3702
268. Zeng, J., Craw, J. S., Hush, N. S. and Reimers, J. R.: Solvent effects on molecular and ionic spectra. 4. Photochemistry of Fe2+(H2O)6 in water revisited: possible mechanisms for the primacy absorption process leading to electron ejection, *J. Phys. Chem.,* 98 (1994), 11075-11088
269. Luhmer, M., Stein, M. L. and Reisse, J.: Relative polarity of 1,3-dioxane and 1,4-dioxane studied by the reaction field theory and via computer simulations, *Heterocycles,* 37 (1994), 1041-I051
270. Ben-Nun, M. and Levin, R. D.: Dynamics of bimolecular reactions in solution: a nonadiabatic activation mode, *J.Chem.Phys.,* 97 (1992), 8341-8356
271. Schenter, G. K., McRae, R. P. and Garrett, B. C.: Dynamic solvent effects on activated chemical reactions. I. Classical effects of reaction-path curvature, *J.Chem.Phys.,* 97 (1992), 9116-9137
272. Charutz, D. M. and Levine, R. D.: Dynamics of barrier crossing in solution: simulations and a hard-sphere model, *J.Chem.Phys.,* 98 (1993), 1979-1988
273. Hu, X. and Martens, C. C.: Classical-trajectory simulation of the cluster-atom association reaction

iodine-argon cluster (I-Am) + I ---> I2 + nAr. I. Capture of iodine by the I(Ar)12 cluster, *J.Chem.Phys.*, 98 (1993). 8551-8559
274. Maroncelli, M.: The dynamics of solvation in polar liquids, *J.Mol.Liq.*, 57 (1993), 1-37
275. Phelps, D. K., Weaver, M. J. and Ladanyi, B. M.: Solvent dynamic effects in electron transfer: molecular dynamics simulations of reactions in methanol, *Chem. Phys.*, 176 (1993), 575-588
276. Krause, J. L., Whitnell, R. M., Wilson, K. E. and Yan, Y. J. (1994) "Classical" quantum control with application to solution reaction dynamics,in Gauduel, Y. and Rossky, P. J.(eds.), *Ultrafast reaction dynamics and solvent effects*, AIP Press, New York,pp.3- 15.
277. Pappalardo, R. M., Martinez, J. M. and Sanchez Marcos, E.: Geometrical structure of the cis- and trans-isomers of 1,2-dihaloethylenes and the energetics of their chemical equilibrium in solution., *Chem.Phys.Lett.*, 225 (1994), 202-207
278. Depaepe, J. M., Ryckaert, J. P. and Bellemans, A.: Kinetics of the geometric isomerization of cyclohexene in a stochastic bath, *Mol. Phys.*, 78 (1993), 1575-1588
279. Weiss, S.: Molecular dynamics study of an isomerizing triatomic in solution, *Mol.Phys.*, 81 (1994), 1281-1288
280. Wiberg, K. B. and Wong, M. W.: Solvent effects. 4. Effect of solvent on the E/Z energy difference for methyl formate and methyl acetate, *J.Am.Chem.Soc.*, 115 (1993), 1078-1084
281. Contreras, J. G. and Alderete, J. B.: MO calculationsof solvent effects on the prototropic tautomerism of 6-thiopurine, *THEOCHEM*, 115 (1994), 137-141
282. Rodrigues Prieto, F., Rios Rodriguez, M. C., Mosquera Gonzalez, M. and Rios Fernandez, M. A.: Ground- and excited-state tautomerism in 2-(3'-Hydroxy-2'-pyridyl)benzimidazole, *J. Phys. Chem.*, 98 (1994), 8666-8672
283. El Tayar, N., Mark, A. E., Vallat, P., Brunne, R. A., Testa, B. and van Gunsteren, W. E.: Solvent-dependent conformation and hydrogen-bonding capacity of cyclosporin A: evidence from partition coefficients and molecular dynamics simulations, *J.Med. Chem.*, 36 (1993), 3757-3764
284. Alagona, G. and Ghio, C.: Stability and acidity of salicylic acid rotamersin aqueous solution. A continuous model study, *J. Mol. Liq.*, 61 (1994), 1-16
285. Migus, A., Gauduel, Y., Martin, J. L. and Antonetti, A.: Excess electrons in liquid water: first evidence of a prehydrated state with femtosecond lifetime., *Phys. Rev. Lett.*, 58 (1987), 1559-1562
286. Long, F. H., Lu, H. and Eisenthal, K. B.: Femtosecond studies of the presolvated electron: an excited state of the solvated electron?, *Phys.Rev.Lett.*, 64 (1990), 1469-1472
287. Long, F. H., Lu, H., Shi, X. and Eisenthal, K. B.: Intensity dependent geminate recombination in water., *Chem.Phys.Lett.*, 185 (1991), 47-52
288. Pommeret, S., Antonetti, A. and Gauduel, Y.: Electron hydration in pure liquid water. Existence of two nonequilibrium configuration in the near-IR region, *J.Am.Chem.Soc.*, 113 (1991). 9105-9111
289. Alfano, J. C., Walhout, P. K., Kimura, Y. and Barbara, P. F.: Ultrafast transient-absorption spectroscopy of the aqueous solvated electron, *J.Chem.Phys.*, 98 (1993), 5996-5998
290. Kimura, Y., Alfano, J. C., Walhout, P. K. and Barbara, P. F.: Ultrafast transient absorption spectroscopy of the solvated electron in water, *J.Phys. Chem.*, 98 (1994), 3450-3458
291. Murphrey, T. H. and Rossky, P. J.: The role of solvent intramolecular modes in excess electron solvation dynamics, *J.Chem.Phys.*, 99 (1993). 515-522
292. Severance, D. L. and Jorgensen, W. L.: Effects of hydration on the Claisen rearrangement of allyl vinyl ether from computer simulations, *J.Am.Chem.Soc.*, 114 (1992), 10966-10968
293. Severance, D. L. and Jorgensen, W. L. (1994) Claisen rearrangement of allyl vinyl ether,in Cramer, C. J. and Truhlar, D. G.(eds.), *Structure and Reactivity in Aqueous Solution*, American Chemical Society, Washington,pp.243-259.
294. Andres, J., Bohm, S., Moliner, V., Silla, E. and Tunon, I.: A theoretical study of stationary structures for the addition of azide anion to tetrafuranosides : modeling the kinetic and thermodynamic controls by solvent effects, *J. Phys. Chem.*, 98 (1994), 6955-6960

295. Hu, W.-P. and Truhlar, D. G.: Modeling transition state solvation at the single-molecule level: test of correlated ab initio predictions against experiment for the gas-phase SN2 reaction of microhydrated fluoride with methyl chloride, *J.Am.Chem.Soc.,* 116 (1994), 7797-7800

296. Hase, W. L.: Variational unimolecular rate theory, *Acc. Chem. Res.,* 16 (1983), 258-264

297. Fong, F. K.(ed.), *Radiationless processes. Topics in applied physics,* Springer-Verlag, Berlin, 1976.

298. Ulstrup, J.: *Charge transfer processes in condensed media,* Springer-Verlag, Berlin, 1979

299. Broeckhove, J. and Lathouwers, L.(ed.), *Time-dependent quantum molecular dynamics, NATO ASI Series B: Physics,* Plenum Press, New York, 1992.

300. Jortner, J. and Pullman, B.(ed.), *Intramolecular dynamics, The Jerusalem Symposia on Quantum Chemistry and Biochemistry,* Reidel, Dordrecht, 1982.

301. Schatz, G. C., Colton, M. C. and Grant, J. L.: A Quasiclassical trajectory of the state-to-state dynamics of H + H2O ↔ OH + H2, *J. Phys. Chem,* 88 (1984), 2971-2977

302. Wang, D. and Bowman, J. M.: Reduced dimensionality quantum calculations of mode specificity in OH+H2 ↔ H_2O+H, *J.Chem.Phys.,* 96 (1992), 8906-8913

303. Polanyi, J. C. and Zewail, A. H.: Direct obesrvation of the transition state, *Acc. Chem. Res.,* 28 (1995), 119-132

304. Forst, W.: Unimolecular rate theory test in thermal reactions, *J.Phys.Chem.,* 76 (1972), 342-348

This page intentionally left blank.

INDEX

A

B

C

F

G

H

J

K

L

M

N

S

T

This page intentionally left blank.

Understanding Chemical Reactivity

1. Z. Slanina: *Contemporary Theory of Chemical Isomerism.* 1986 ISBN 90-277-1 707-9
2. G. Náray-Szabó, P.R. Surján, J.G. Angyán: *Applied Quantum Chemistry.* 1987 ISBN 90-277-1901-2
3. V.I. Minkin, L.P. Olekhnovich and Yu. A. Zhdanov: *Molecular Design of Tautomeric Compounds.* 1988 ISBN 90-277-2478-4
4. E.S. Kryachko and E.V. Ludeña: *Energy Density Functional Theory of Many-Electron Systems.* 1990 ISBN 0-7923-0641-4
5. P.G. Mezey (ed.): *New Developments in Molecular Chirality.* 1991 ISBN 0-7923-1021-7
6. F. Ruette (ed.): *Quantum Chemistry Approaches to Chemisorption and Heterogeneous Catalysis.* 1992 ISBN 0-7923-1543-X
7. J.D. Simon (ed.): *Ultrafast Dynamics of Chemical Systems.* 1994 ISBN 0-7923-2489-7
8. R. Tycko (ed.): *Nuclear Magnetic Resonance Probes of Molecular Dynamics.* 1994 ISBN 0-7923-2795-0
9. D. Bonchev and O. Mekenyan (eds.): *Graph Theoretical Approaches to Chemical Reactivity.* 1994 ISBN 0-7923-2837-X
10. R. Kapral and K. Showalter (eds.): *Chemical Waves and Patterns.* 1995 ISBN 0-7923-2899-X
11. P. Talkner and P. Hänggi (eds.): *New Trends in Kramers' Reaction Rate Theory.* 1995 ISBN 0-7923-2940-6
12. D. Ellis (ed.): *Density functional Theory of Molecules, Clusters, and Solids.* 1995 ISBN 0-7923-3083-8
13. S.R. Langhoff (ed.): *Quantum Mechanical Electronic Structure Calculations with Chemical Accuracy.* 1995 ISBN 0-7923-3264-4
14. R. Carbó (ed.): *Molecular Similarity and Reactivity: From Quantum Chemical to Phenomenological Approaches.* 1995 ISBN 0-7923-3309-8
15. B.S. Freiser (ed.): *Organometallic Ion Chemistry.* 1996 ISBN 0-7923-3478-7
16. D. Heidrich (ed.): *The Reaction Path in Chemistry: Current Approaches and Perspectives.* 1995 ISBN 0-7923-3589-9
17. O. Tapia and J. Bertrán (eds.): *Solvent Effects and Chemical Reactivity.* 1996 ISBN 0-7923-3995-9

Kluwer Academic Publishers – Dordrecht / Boston / London